OMICS APPROACH TOWARDS UNDERSTANDING THE FUNCTION OF BIOACTIVE LIPIDS IN OSTEOSARCOMA

BY

JAHNABI ROY

DISSERTATION

Submitted in partial fulfillment of the requirements
for the degree of Doctor of Philosophy in Chemistry
in the Graduate College of the
University of Illinois at Urbana-Champaign, 2017

Urbana, Illinois

Doctoral Committee:

Assistant Professor Aditi Das, Research Director
Professor Wilfred van der Donk, Chair
Professor Timothy Fan
Assistant Professor Jefferson Chan

ABSTRACT

Osteosarcoma is the most common form of primary bone cancer in humans and well as dogs. The treatment options for OS include a multi-agent induction chemotherapy and radical excision of the tumor followed by adjuvant chemotherapy. Despite the aggressive treatment course, the survival rates are poor. In patients with localized disease, 5-year survival rates are approximately 65%. However, for metastatic disease at diagnosis or recurrence, the 5-year survival rates have plateaued to only 20%. Although progress has been made towards improving treatment options, the early detection and subsequent control of metastasis have been challenging in OS. This work is aimed at discovering the various proteomic and lipidomic biomarkers in metastatic and non-metastatic osteosarcoma as well as development of lipid mediators as potential therapeutics.

We take a high-throughput approach towards identifying specific membrane proteins and lipids that are differentially expressed in normal osteoblasts, non-metastatic and metastatic osteosarcoma. As described in chapter 2, a high throughput peptide fingerprinting enabled us to identify various membrane proteins that are differentially expressed in metastatic versus non-metastatic osteosarcoma. Membrane proteins are the largest class of drug targets and this study identifies proteins that can targets for drugs without having to overcome the delivery of drugs across the plasma membrane. However, the functional study of membrane proteins is complicated by the fact that they exist in an amphipathic environment and lose their structure in aqueous buffers. Thus we stabilize the membrane proteome of osteosarcoma cells in nanodiscs (chapter 3). Nanodiscs are lipid bilayers surrounded by membrane scaffold protein and provide the amphipathic environment for membrane proteins. In this study we showed that lipid composition affects the protein composition incorporated.

Since lipid composition affects protein incorporation and lipid-protein interactions are important for cell signaling processes, we investigated the global cellular lipidome of osteosarcoma and osteoblast cells through a high throughput lipidomics approach (chapter 4). We identified that several lipid classes and lipid species are differentially regulated in normal cells versus non-metastatic cells vs metastatic cells. These include both structural lipids as well as signaling lipids. Since signaling lipids play an important role in various physiological functions, we chose to further explore the role of a specific class of signaling lipids, known as endocannabinoid epoxides, in osteosarcoma (chapter 5). Endocannabinoid epoxides are metabolites of omega-3 fatty acids that arise from a cross-talk of phospholipase D and cytochrome P450 epoxygenase enzymes. They have previously been shown to have anti-inflammatory and anti-angiogenic

properties. In this study, we show that they also possess anti-tumorigenic activity. Furthermore, we synthesize novel analogs of specific endocannabinoid epoxides that show reduced susceptibility to biological enzymes, making them better therapeutic candidates.

Therefore, we have performed a thorough proteomic and lipidomic characterization of osteosarcoma that can serve as biomarkers as well as initiate the development of novel therapeutics. The lipid mediators synthesized in chapter 5 show promise in cellular studies and can be taken forward into mice models for osteosarcoma and bone cancer pain. These will likely show similar effects in other cancers and studies can be expanded to carcinomas and other cancers as well.

ACKNOWLEDGEMENTS

First of all I would like to thank my adviser Prof. Aditi Das, who has helped me become the person I am today. She supported me when I needed support the most and helped me rebuild my confidence scientifically. I would not have been able to complete my projects on my own if she did not show faith in my abilities and my decisions. I have learned a lot from her scientifically as well as in life lessons. I would also like to thank my co-adviser Dr. Timothy Fan, from whom I have learned tremendously. He is a true example of how one can be knowledgeable, assertive, as well as a nice person at the same time. I would like to thanks Mrs. Holly Pondenis who I have learned all my cell culture and other biological techniques from. She is also a joy to talk to about life in general. I would like to thank my other committee members Prof. Wilfred van der Donk, Prof. Jefferson Chan and Prof. Paul Hergenrother. Prof. van der Donk told me that students do not always realize that they have a choice in graduate school and they can also control their fate and this gave me the faith to continue. I would like to thank my Das lab mates past and present. John Krapf and Josephine Watson have been great friends in lab and a support system. Insup Hong has been a very hardworking undergraduate helping to push my project further. I want to thank my Fan lab mates. Dr. Wycislo is my favorite lab mate to talk to about books even though we never seem to like the same books. I would like to thank my collaborators at the University of Michigan, Dr. Michael Holinstat and Dr. Reheman Adili for their help with the platelet aggregation work. I would like to thank my collaborators Dr. Saurabh Sinha and Mr. Payam Diabeinia at UIUC for their help with statistics in the lipidomics work. I would like to thank the various facility managers at the UIUC campus: Dr. Peter Yau and Dr. Lucas Li at the Roy J Carver Biotechnology Center and Dr. Dean Olson at the NMR lab. I would like to thank the OCB office for helping me through various degree requirements, especially Ms. Lori Johnson and Ms. Gayle Adkisson. I would also like to thank Dr. Eric Woerly, Dr. Justin Struble and Dr. Stephen Davis for all the organic synthesis I know.

I would like to thank all the people without whom I would not have made it through graduate school. The late Mrs. Becky Duffield and Ms. Krista Smith were the people who watched me almost give up and told me that there is always a way and helped me pick myself up when I was at my worst. Dr. Ellen Wang Althaus is an amazing woman who helped me make important decisions for myself. I have had the opportunity to meet some wonderful people in graduate school who I hope to be friends with for life. Dr. Ellen Muehl and Dr. Jessie Peh are my best friends without whom this journey would not have had a good ending. I would like to thank my childhood best friend, Siddharth Gupta without whom I would've had no idea how to get started with applying to UIUC or had the strength to go through all the application

materials without feeling very overwhelmed. Dr. Adina Badea was an unexpected friend who suddenly turned my world around. Aditi Banerjee, Nidhi Kakkar, Ananya Sen and Pallavi Sharma have been wonderful friends. Dr. Iulia Strambeanu and Dr. Andrea Ambrosi are the two people I need if I want to have a fun night out and we had a lot of fun nights together.

My Illinois journey would not be complete without mentioning my husband Dr. Nicholas Clay who is the most kind, patient and humble man I know. He inspires me to be like him- a better person. If I can be half as nice as he is in my lifetime, I will consider that a job well done. I would like to thank his (and now my) family, for their support and encouragement. And finally, I would like to thank my parents Mrs. Santa and Mr. Joydeb Roy, who told me it was okay to fall when I was at my lowest and thus gave me the strength to rise up again, and to whom this thesis is dedicated.

TABLE OF CONTENTS

CHAPTER I: OSTEOSARCOMA INTRODUCTION AND DISSERTATION OVERVIEW

1.1 OSTEOSARCOMA OVERVIEW

Osteosarcoma is the most common form of primary bone cancer in pediatric patients as well as dogs (1, 2). Every year there are 3.1 incidences per million or 3-5% of all newly diagnosed childhood cancers, making it the most common malignancy in pediatric patients after leukemia and lymphoma (1). It occurs in the long bones of the limbs, near the metaphyseal growth plate. Common sites include the femur, the tibia and the humerus, and less commonly the skull, the jaw or the pelvis. Limb sparing surgeries are the most common treatment for OS. However, the survival rate with surgery alone is 15-17% (3, 4). Thus current therapeutic approaches incorporate surgical resection and combinational chemotherapy, which cures ~70% patients. In patients with localized disease, the response to chemotherapy before surgery is the strongest predictor of survival (5). However, in patients with metastatic disease, the 5- year survival rate has stagnated to about 20% in the past 30 years (4, 6). Therefore, there is a need for novel biomarkers for early diagnosis of metastasis, as well as development of therapeutics for these biomarkers.

1.2 PROTEIN BIOMARKERS IN OS

Biomarkers are measurable cellular, metabolic or molecular alterations in a diseased state that can be identified in tissues, blood or other biological media. The traditional approach towards biomarker discovery relied on discovery of dysregulated genetic factors (7) as well as differential transcriptomics (8). These discoveries have led to a deeper understanding of the underlying mechanisms of cancer pathways as well as drug discovery (9). Recently, various efforts have focused on the discovery of protein biomarkers. While proteins are traditionally more challenging to handle than their nucleic acid counterparts (REF), proteins are the final target of drugs, making them directly relevant to the process. Additionally, the fact that RNA levels do not always correspond to the protein levels, due to processes like post transcriptional degradation of mRNA (10), has made proteomic biomarkers very relevant.

Functional proteomics has provided a rapid route towards discovery of biomarkers associated with tumors. Various techniques have been employed in the discovery of proteomic biomarkers including 2D-SDS PAGE (11), LC-MS (12, 13), MALDI-TOF (14, 15), antibody arrays (16) and tissue microarrays (17, 18). While most of these techniques are rapid and often semi-quantitative,

LC-MS or liquid chromatography followed by mass spectrometry, has been shown to be a very high throughput technique, allowing analysis of hundreds of proteins in a given sample in a short amount of time (19). LC-MS has also been coupled with various other proteomic approaches, like SDS-PAGE (20), to identify specific proteins. Two different approaches have been taken towards LC-MS analysis of proteins- bottom up approach or peptide fingerprinting and top-down approach or intact protein analysis. In the top down approach, single proteins are separated and then intact proteins are identified using electrospray ionization (ESI) (21). Although top down proteomics has several advantages, including the ability to identify post-translational modifications (PTMs), it is a relatively new technique and has been largely restricted to model systems and availability of specialized instrumentations. In the bottom up approach, the protein mixture is initially digested by trypsin or similar enzymatic agent, and the peptide fragments are then analyzed by liquid chromatography (22). The LC-MS procedure generates a list of peptides, which can then be matched to existing databases to generate a list of proteins. Bottom up proteomics is well developed and is routinely performed in many laboratories.

As such, majority of the biomarker discovery processes in osteosarcoma and other cancers have relied on bottom up proteomics. Bottom up proteomics or simply referred to as proteomics from this point, has been utilized for whole cell (23) as well as for identifying the proteome of cellular fractions (24). The subcellular fractionation can be facilitated via various biochemical processes including sucrose gradients (25) or aqueous two phase extractions (26). Specifically, plasma membrane proteomics has been the focus of recent studies since the plasma membrane hosts the largest class of druggable targets as it is the first target presented to the drug and drugs do not have to cross the plasma membrane to perform their action (27). The plasma membrane hosts a variety of proteins including seven transmembrane receptors known as G-protein coupled receptors (GPCRs) and other transmembrane receptors. The plasma membrane is also associated with peripheral membrane proteins, both on the cytoplasmic side as well as the extracellular side that perform important cellular functions like signal transduction processes. Keeping these vast number of targetable proteins, several efforts have focused on osteosarcoma proteomics for identification of novel targets.

An LC/MS/MS based differential plasma membrane proteomics of human OS cell line MG63 and osteoblast cell line hFOB revealed 342 non-redundant proteins out of which 68 were differentially

expressed at a 1.5 fold difference (28). This work further revealed that CD151 was overexpressed in osteosarcoma by immunohistochemistry. In a separate work, using a combination of 2D SDS PAGE and LC/MS, it was shown that NDRG1 was a biomarker for osteosarcoma (29). Similarly, high throughout proteomics was also employed to show that EPHA2, an ephrin type receptor was a biomarker for OS (30). Proteomic profiling of OS cell lines MNNG/HOS, MG63, and U2OS and osteoblast cells hFOB also showed nine up-regulated proteins – FAS, CNOT1, ACACA, LRPPRC, FAK, ASNS, HMGCS1, PHGDH, and EFHD2 and two down-regulated proteins – MX1 and TAGLN (31). All these studies utilized a high throughput proteomic screening, followed by validation of target by biochemical methodologies like flow cytometry, western blotting and immunohistochemistry.

As mentioned above, several biomarkers for osteosarcoma have been identified using proteomics. However, a key challenge in OS is the metastasis of the disease. Thus, studies are required that focus on the proteomics of metastatic and non- metastatic osteosarcoma to understand the factors underlying metastasis as well as find markers specific to metastasis. Currently, only one such study exists comparing the proteomics profile of metastatic and non-metastatic canine osteosarcoma. This study utilized canine non-metastatic cell line POS, metastatic line HMPOS, and a normal canine osteoblast cell line CnOB to identify that thrombospondin-1, CD44, Plexin-B2, Notch-2 and CYR61 were differentially regulated (32).

Therefore, a study examining the plasma membrane proteomic profile of human metastatic and non-metastatic osteosarcoma is lacking. Additionally, since osteosarcoma affects pet dogs, it provides us a wonderful opportunity to extend the proteomic profiling to canine cell lines similar to the work by Milovancev and coworkers. It has been shown that human and canine osteosarcoma are genetically identical (33). Thus the identification of common proteomic profiles through comparative profiling of the human and canine membrane proteome will lead to the simultaneous development of therapies for both species and has been described in Chapter 2 of this thesis.

1.3 NANODISCS FOR STABILIZATION OF MEMBRANE PROTEOME

The utilization of membrane proteins for the drug development has faced several challenges. Membrane proteins are embedded in an amphipathic environment of lipids and proteins. Isolating them from their natural environment for biochemical studies, which are typically performed in aqueous buffer systems, results in denaturation of the protein. Thus, membrane proteins are

typically stabilized in a lipid based system for downstream assays. Detergents, liposomes, micelles and vesicles have all been used for incorporating a stabilizing membrane proteins (34). However, all these methodologies have major drawbacks. Detergents help solubilize membrane proteins but are often charged or zwitterionic and charged interactions are not favorable for many biochemical assays. This has been circumvented to an extent by utilizing uncharged detergents like β-maltoside. Furthermore, liposomes and micellar systems have to be prepared and used on the same day and all these systems do not provide long term stability to the protein.

In the light of these drawbacks, nanodiscs have emerged as model membrane systems which are stable over a longer period of time and can survive several freeze thaw cycles. Nanodiscs are lipid bilayers surround by membrane scaffold proteins (MSP), providing an amphipathic environment to the embedded protein (35). The assembly of nanodiscs is accomplished by equilibrating the desired lipids, MSP and detergent briefly before detergent removal by Bio-beads® or by dialysis (36). Typically, the choice of lipids is POPC (1-palmitoyl-2-oleoyl-sn-glycero-3-phosphocholine), a neutral lipid containing one unsaturated bond. However, as the technology has progressed, various different lipids including POPS (1-palmitoyl-2-oleoyl-sn-glycero-3-phospho-L-serine), an anionic lipid and even cholesterol have been incorporated (37). A major advantage of the nanodisc system is the ability to control the size using a different MSP variant (38). The two most commonly used nanodisc variants are MSP1D1 and MSP1E3D1, which generate nanodiscs of sizes 10nm and 13 nm respectively. However, MSP variants have been generated for nanodiscs as large as 50 nm (39) and as small as 7 nm (40). Additionally, nanodisc systems have been optimized to be compatible with many biochemical and biophysical assays including NMR, surface plasmon resonance, and others (41).

Typically, membrane proteins are overexpressed in simplified systems like bacteria or yeast, purified and then incorporated into nanodiscs (36). This is very useful for studying specific proteins for deducing their structure, specific known interactions as well as calculating binding to ligands. However, not all proteins are amenable to overexpression and purification. Additionally, this approach is not suitable for detecting novel protein-protein or protein-small molecule interactions. Therefore, a library approach to membrane protein stabilization is required for stabilizing and studying membrane proteins that have low expression.

The first effort towards the formation of a nanodisc library utilized bacterial protein in POPC based nanodiscs (42). The authors verified the incorporation by SDS PAGE analysis and specific proteins from the inner and outer membrane were identified by excising specific bands from the gel followed by peptide fingerprinting. In a separate work, the membrane proteome of synapses was incorporated into a nanodisc library (43). The incorporation was verified by SDS PAGE followed by western blotting of several specific proteins associated with the synaptic membrane. The incorporated proteins were then utilized for functional assays to identify binding sites for alzheimer's associated Aβ oligomers. The first fully characterized mammalian protein nanodisc library was established from osteosarcoma cells as described in chapter 3 of this dissertation (37). This work expanded the nanodisc library to incorporating various different lipids, which affected the population of incorporated nanodiscs as evidenced by peptide fingerprinting. Finally, the membrane proteome of HEK239 cells, erythrocytes and platelets was incorporated into PEG-PE discs (44).

1.4 LIPID BIOMARKERS IN OS

The other important component of the plasma membrane are the lipids. The plasma membrane consists 50% of lipids (45). Lipids also form a significant component of organellar membranes as well as vesicles trafficking pathways. Lipids serve various important functions in living systems. First, they are used for energy storage. Second, as they comprise of a hydrophobic and hydrophilic portion, they tend to self-assemble into amphipathic structures like the plasma membrane and form a barrier for the cell. Finally, they compartmentalize the various organelles to allow for discrete functional units in the cell (46).

Lipids show a large diversity in structure including their backbone, chain length, and number and position of unsaturated bonds. Based on their backbone, lipids are classified into phospholipids, glycolipids, sphingolipids and steroids. Phospholipids constitute of the largest class including neutral lipids like phosphatidylcholine, negatively charged phosphatidylserine and positively charged phosphatidylethanolamine among others. Sphingolipids comprise of sphingomyelins and ceramides. Steroids comprise of molecules like cholesterol with a steroid core. These molecules are differentially distributed in the various membranes and contribute to specific functions. Lipid rafts are a popular example of how lipids segregate into various functional domains (47). Specifically, lipid rafts are rich in cholesterol and sphingolipids and various receptors are known

to partition into lipid rafts for signaling activities. Thus, lipids and their synthesis and metabolism has emerged as a ripe area of exploration to be able to gain an integrated picture of the cellular physiology.

Historically, cellular lipids have been extracted using an organic extraction method. Bligh and Dyer devised a two-step organic extraction that is still in use today (48). However the separation and identification of lipids is a complicated process due to their structural diversity. Thin layer chromatography was initially used to separate out lipid classes and further analysis (49). This allows for separation of the various classes and analysis, but finer details like chain lengths and location of unsaturations, etc. are still not detectable by this method. With the development of mass spectrometry (MS), the separation and analysis of lipids has become more convenient and high-throughput (50). MS based lipidomics can be targeted, focusing on a single class of molecules or global where the aim is to quantify all lipids in the system. The application of liquid chromatography (LC) in combination with MS/MS has been a popular approach for high throughput untargeted lipidomics. Also known as shotgun lipidomics, the various lipid classes are first separated by their polarity, followed by ESI (electrospray ionization) of the individual components of the classes. A normal phase column is used to separate the various classes. However this is often coupled with a reverse phase column to separate minor molecular species. The spectral data obtain post ESI analysis is then processed by specific softwares to generate a list of lipids in the sample (51, 52).

This high-throughput shotgun lipidomics has been utilized to identify differentially regulated lipids as biomarkers in various diseases including cancer (53), cardiovascular health (54), neurodegenerative disease (55) and others. Specifically in cancer, recent work has focused on the differences in normal cells versus tumorigenic cells. Cancer cells are known to reprogram their lipid machinery to sustain their uncontrolled growth and proliferation (56). Early literature demonstrated that cancer cells increase their production of lipids significantly (57). This was further supported by studies that showed that fatty acid synthase is upregulated and is a biomarker in various cancers (58) and that increased fatty acid synthesis is an initial step in tumor development (59). Increased cholesterol biosynthesis has also been shown to be a biomarker for prostate cancer (60). While the role of increased lipid production in cancer is not fully understood,

there are various studies that provide interesting insight into their role beyond providing more lipids for the rapidly proliferating cells.

An increase in specific lipids can could result in increased formation of lipid rafts that result in higher signaling activity from cancer cells (61). Lipids are also involved in autophagy (62) and the mobilization of lipids from intracellular stores has consequently been termed macrolipophagy (63). This is interesting in light of the fact that autophagy is thought to be a pro-survival pathway in cancer (64). Lipid biosynthesis has also been linked to disruption of normal cellular architecture (65) as well as tumor cell dissemination (66). A difference in the pattern of lipid synthesis is also observed. The shift from lipid uptake in normal cells to *de novo* lipogenesis in cancer cells leads to increased lipid saturation, resulting in higher levels of saturated and monounsaturated phospholipids, potentially protecting cancer cells from oxidative damage by reducing lipid peroxidation (67). Increase lipid saturation has also been associated with increased membrane fluidity and has been associated with breast cancer cells (68). Therefore, a high throughput profiling of cancer cells and their comparison to non-tumorigenic cells has been pursued to identify lipid biomarkers as well as to identify specific lipid synthesis or metabolism pathways that are dysregulated in cancer cells.

A phospholipid analysis of breast cancer cell lines revealed that phosphatidylethanolamines (PE) was highest in non-malignant cells while phosphatidic acid was present with highest relative abundance in metastatic cells (69). A similar profiling of isogenic metastatic and non-metastatic adenocarcinoma cells showed increased PC and triglyceride lipid levels, decreased PE lipids, decreased C-16 containing sphingomyelin and ceramide lipid levels, and a dramatic increase in the abundances of total cholesterol ester and triglyceride lipids in the primary cells compared to their metastatic counterparts (70). In leukemia cell lines 14 classes of lipids- TG, DG, PS, PG, PI, PA, LPC, LPE, LPS, LPG, LPI, Cer, Sa, and Cer1P were upregulated and 3 classes- ChE, PC, and LPA were downregulated (71).

To gain a more holistic view of the tumorigenesis process, lipidomics has been correlated with transcriptomic data from the same cells or tissues. In renal cell carcinoma, lipidomic analysis of affected tissue versus normal surrounding tissue revealed that the cancerous tissue was distinguished by higher levels of ether-type phospholipids, cholesterol esters, and triacylglycerols, as well as by lower levels of phospholipids (except for phosphatidylcholines) and polyunsaturated

fatty acids (72). Furthermore, an mRNA analysis indicated that changes in the levels of mRNAs and metabolites suggested that the phosphatidylethanolamine (PE) synthesis pathway is suppressed in renal cell carcinoma and is therefore associated with cell proliferation. Analysis of prostate cancer tumor and non-tumor tissue showed that cholesteryl esters are most accumulated in the tumor samples and cholesteryl oleate as a biomarker for prostate cancer (73). Furthermore, it was shown that overexpressed scavenger receptor class B type I (SR-BI) may contribute to CEs accumulation. As evidenced by these examples, high throughput lipidomics has enabled the identification of various differentially regulated cancers including breast cancer, prostate cancer and adenocarcinoma. However, a similar study is lacking for cancers of mesenchymal origin like osteosarcoma. In light of the fact that the lipidome of the cell greatly affects the cellular polarization and the lipid composition (74), the lipidomics of osteosarcoma is an important area of research and is described in Chapter 4 of this dissertation.

1.5 LIPID MEDIATORS AS THERAPEUTICS IN OS

Beyond serving as structural components of cellular membranes, lipids also act as primary and secondary messengers in various signaling pathways. The omega-6 membrane lipid arachidonic acid (AA) gets metabolized to form various signaling molecules (75). The main pathways of AA metabolism are the cyclooxygenase (COX) pathway, the lipoxygenase (LOX) pathway and the epoxygenase (EPOX) pathway, collectively giving rise to eicosanoids. The COX pathway metabolizes AA into prostaglandins, which interact through prostaglandin receptors and affect various factors like cell growth, constriction of vasculature, platelet aggregation and others (76). The LOX pathway metabolizes AA into leukotrienes, which act through GPCRs and are responsible for inflammation and smooth muscle constriction (77). The EPOX pathway metabolizes AA into EETs or epoxyeicosatrienoic acids, which act through an unknown receptor, but also have roles in inflammation and other physiological effects (78). A fourth metabolite of AA is anandamide (AEA), which arises in a two-step synthesis (79). First AA converts to N-arachidonoyl phosphatidylethanolamine (NAPE). Furthermore, NAPE converts to AEA through cleavage by phospholipase D. Anandamide is an endocannabinoid, which acts through the cannabinoid receptors found throughout the human body. It has anti-cancer (80), anti-pain (81) and anti-inflammatory effects (82).

Similar to derivatives of omega-6 fatty acids, the body also metabolizes omega-3 fatty acids that are obtained through diet. Omega-3 fatty acid EPA (eicosapentaenoic acid) and DHA (docosahexaenoic acid) are found in fish, chicken eggs and various nuts and have been shown to have various beneficial (83). These molecules are similar to structure to arachidonic acid and are metabolized by similar classes of enzymes. The EPOX pathway enzymes, cytochrome P450s (CYPs) metabolize EPA and DHA into their corresponding epoxides (84). Additionally, both EPA and DHA are converted into the ethanolamide derivative DHEA and EPEA, which have been shown to be endocannabinoids. Both these metabolites have shown to have physiological activities including anti-cancer properties.

The epoxide derivatives of EPA and DHA will be referred to as EEQs and EDPs respectively. EEQs have shown to inhibit proliferation in endothelial cells by p28 MAP kinase activation and cyclin D1 downregulation (85). Furthermore, EDPs have also been shown to be anti-angiogenic, and restrict tumor growth and metastasis in mice (86). The ethanolamide derivatives also have anti-tumorigenic activity. It has been shown in prostate cancer cells that both EPEA and DHEA have anti-proliferative activity (87). It is hypothesized that the beneficial effects of DHA and EPA are due to their downstream metabolites including their epoxides and amide derivatives.

While the exact mechanism of action of these molecules I unknown, there are several hypotheses. The epoxide derivatives are thought to mediate their effects through a variety of receptor-mediated signaling pathways and ion channels including a putative GPCR (g-protein coupled protein receptor), whose identity remains unclear in the CYP450 epoxygenase literature (88). Additionally, their action maybe mediated through peroxisome proliferator-activated receptor gamma (PPARγ) (89) as well as transient vanilloid receptor 4 (TRPV4) (90). The receptor binding of endocannabinoids is better understood. Endocannabinoids like anandamide traditionally are thought to bind to the cannabinoid receptors 1 and 2 (CB1 and CB2) (91). CB1 and CB2 are also GPCRs which have relatively distinct distributions in the body. CB1 is mainly expressed in the central nervous system and CB2 is expressed on immune cells. However, the role of CB1 and CB2 in the anti-proliferative activity of DHEA and EPEA is not clear (87).

A new class of molecules known as endocannabinoid epoxides have recently been discovered (92). These molecules have both the ethanolamine conjugation as well as the epoxide moiety. Endocannabinoid epoxides of both EPA and DHA known as EEQ-EA and EDP-EA were found

to be endogenously expressed in rat organs. They were further shown to be anti-inflammatory, anti-angiogenic as well as anti-aggregatory in platelets. Finally, these molecules were shown to bind to both cannabinoid receptors. The literature precedence of epoxides and endocannabinoid derivatives of DHA being anti-tumorigenic, and the anti-inflammatory and anti-angiogenic activity of endocannabinoid epoxides (eCBs), taken together, indicate that eCBs could possess anti-tumorigenic activity against various cancers including osteosarcoma.

Furthermore, endocannabinoids also possess anti-nociceptive activity (93). Since bone cancer pain is one of the most debilitating side effects of OS as well as metastasis of other cancers to the bone, various pain management therapies have been employed to combat this. Cannabinoid receptor agonists, like the endocannabinoid anandamide and other synthetic agonists, have also been used for the attenuation of such pain (81). Therefore, the endocannabinoid epoxides provide promise that in addition to their anti-inflammatory effects, they could possess anti-tumorigenic and anti-nociceptive activity against OS.

However, these molecules contain two hydrolytically susceptible groups which reduce their endogenous effects. First, the epoxide group is susceptible to hydrolysis by soluble epoxide hydrolases (sEH). Additionally, the amide group is labile to fatty acid amide hydrolase (FAAH). Efforts to increase their biological activity has been made by employing inhibitors of sEH and FAAH (81, 86) in addition to the bioactive molecule. A second approach to increasing their biological lifetime has been to synthesize derivatives that retain biological function but due to steric and electronic factors have reduced hydrolytic susceptibility. Towards the epoxide functional group, substitution by heteroatoms like nitrogen and sulfur (94) as well as replacing it with bioisosteric groups has been employed (95). Towards attenuating the hydrolysis of the amide group, the 1’ position of the amide results in increased metabolic stability of AEA due to the steric bulk reducing hydrolysis, while affecting the CB1 binding ability (96). A variety of other functional groups have been conjugated to the nitrogen of the amide group including straight chains, saturated and unsaturated cyclic structures, heterocyclic groups and even bulky groups like adamantane (97). These groups affect hydrolysis by FAAH to varying degrees as well as receptor binding. Modest increase in steric bulk assists in FAAH inhibition and increasing CB1 binding. However, very large groups reduce both. Majority of the literature has focused on derivatives of

anandamide. It can be postulated that similar modifications can be employed for EPA and DHA metabolites to reduce their hydrolytic susceptibility.

Thus the anti-tumorigenic activity of these eCBs has been explored in Chapter 5 of this dissertation in cell models for OS. Additionally, since these molecules are labile to enzymatic hydrolysis, derivatives have been synthesized to reduce their hydrolytic susceptibility and also tested for their pro-apoptotic and anti-migratory activity.

1.6 SUMMARY

Osteosarcoma is the most common form of primary bone cancer in humans and dogs. Despite progress in biomarker discovery and personalized therapeutics in various other cancers like breast cancer and leukemia, including drugs like Herceptin and Imatinib, the approach for OS treatment remains traditional surgery including amputation. Therefore, there is a necessity for biomarker discovery in OS for the early discovery and development of therapeutics of OS. In this chapter are summarized the various efforts that have been directed towards proteomic and lipidomic investigations in biomarker discovery in OS and other cancers exhibiting the deficiency of preliminary work on OS biomarker discovery. Therefore the second and fourth chapters of this thesis focus on preliminary biomarker discovery in OS.

Furthermore, since this work focuses on the membrane proteome for biomarker discovery, we further attempt to stabilize the membrane proteome in nanodisc libraries in chapter three to avoid complications of unfolding and denaturation that is faced by membrane proteins in aqueous buffers. Finally, we explore the anti-tumorigenic activity of a novel class of bioactive lipids known as endocannabinoid epoxides towards therapeutics for OS.

1.7 FIGURES, TABLES AND LEGENDS

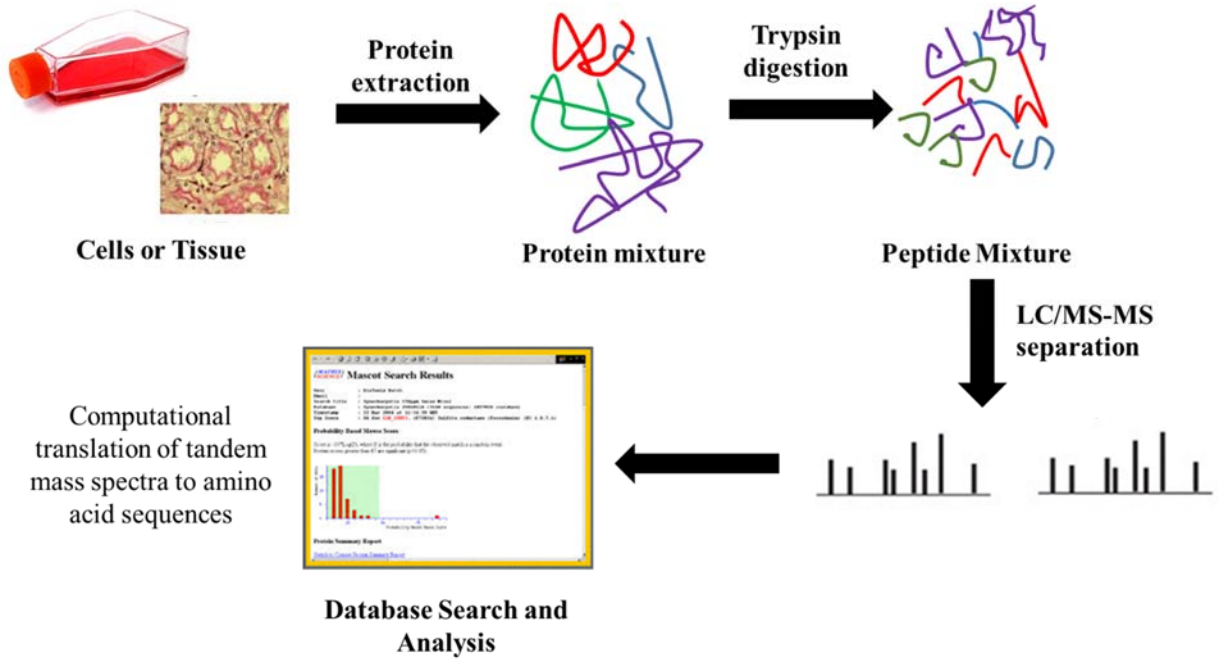

Figure 1.1: A representation of bottom up proteomics approach. Proteins extracted from cells or tissue are enzymatically digested and then subject to LC-MS/MS separation. The peptide spectra so generated is matched to protein databases to obtain a list of proteins in the mixture.

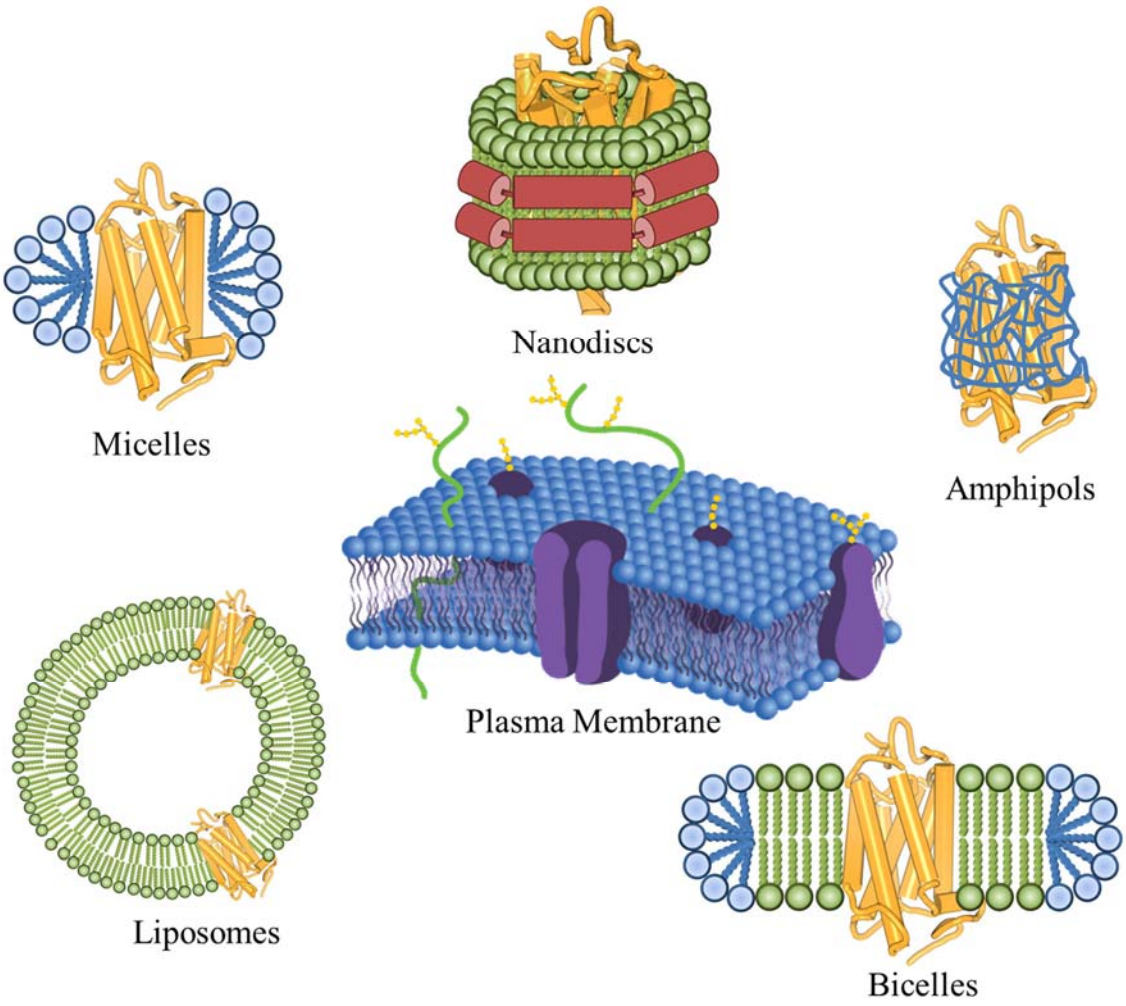

Figure 1.2: [1]Figure represents various model membrane systems utilized for stabilization of membrane proteome.

[1] Figure has been reproduced and modified from "Large-scale production and protein engineering of G protein-coupled receptors for structural studies" Dalibor Milic and Dmitry Veprintsev. *Front. Pharmacol.* 2015, *6*, 66. The work is allowed to be republished under the Creative Commons Attribution license (https://creativecommons.org/licenses/by/4.0/)

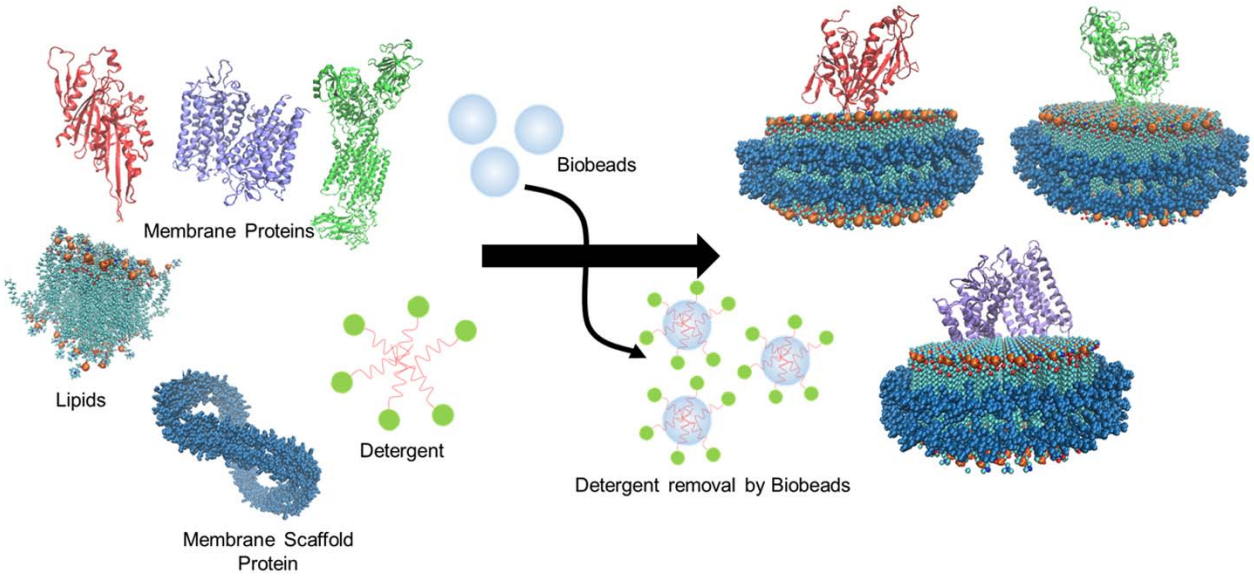

Figure 1.3[2]: Figure represents synthesis of a nanodisc library. Membrane proteins are equilibrated with lipids, membrane scaffold protein and detergent. In the presence of biobeads, the nanodisc self-assembly progresses.

[2] Figure has been reprinted with permission from John Wiley and Sons License. "Recent Advances in Nanodisc Technology for Membrane Protein Studies (2012-2017)" John Rouck, John Krapf, Jahnabi Roy, Hannah Huff, Aditi Das. *FEBS Lett.* 2017, *591*, 2057–2088.

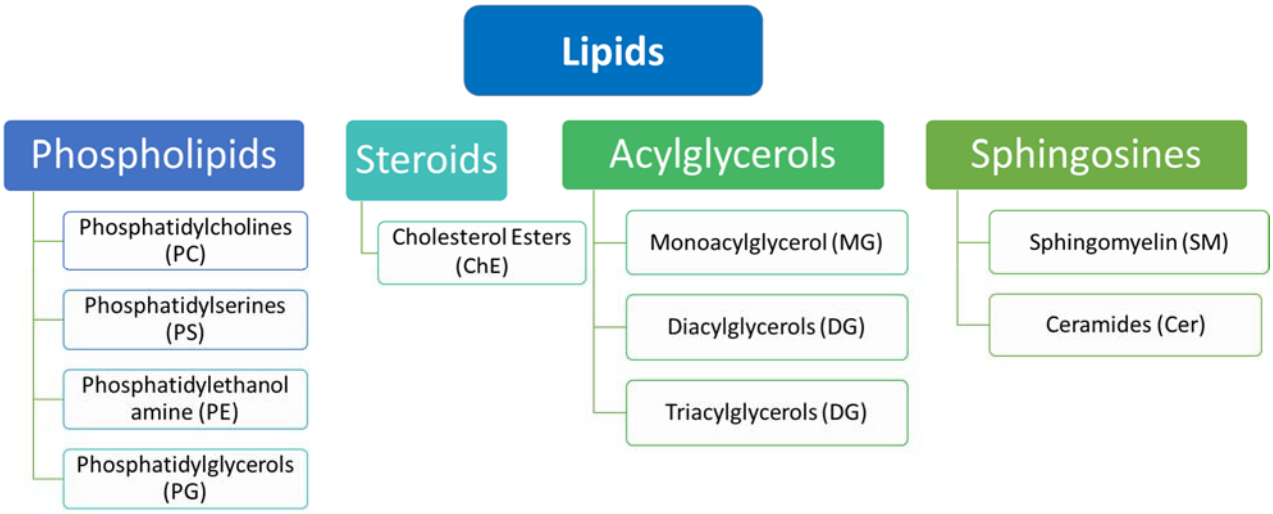

Figure 1.4: Figure represents the major classes of lipids in a mammalian cell line.

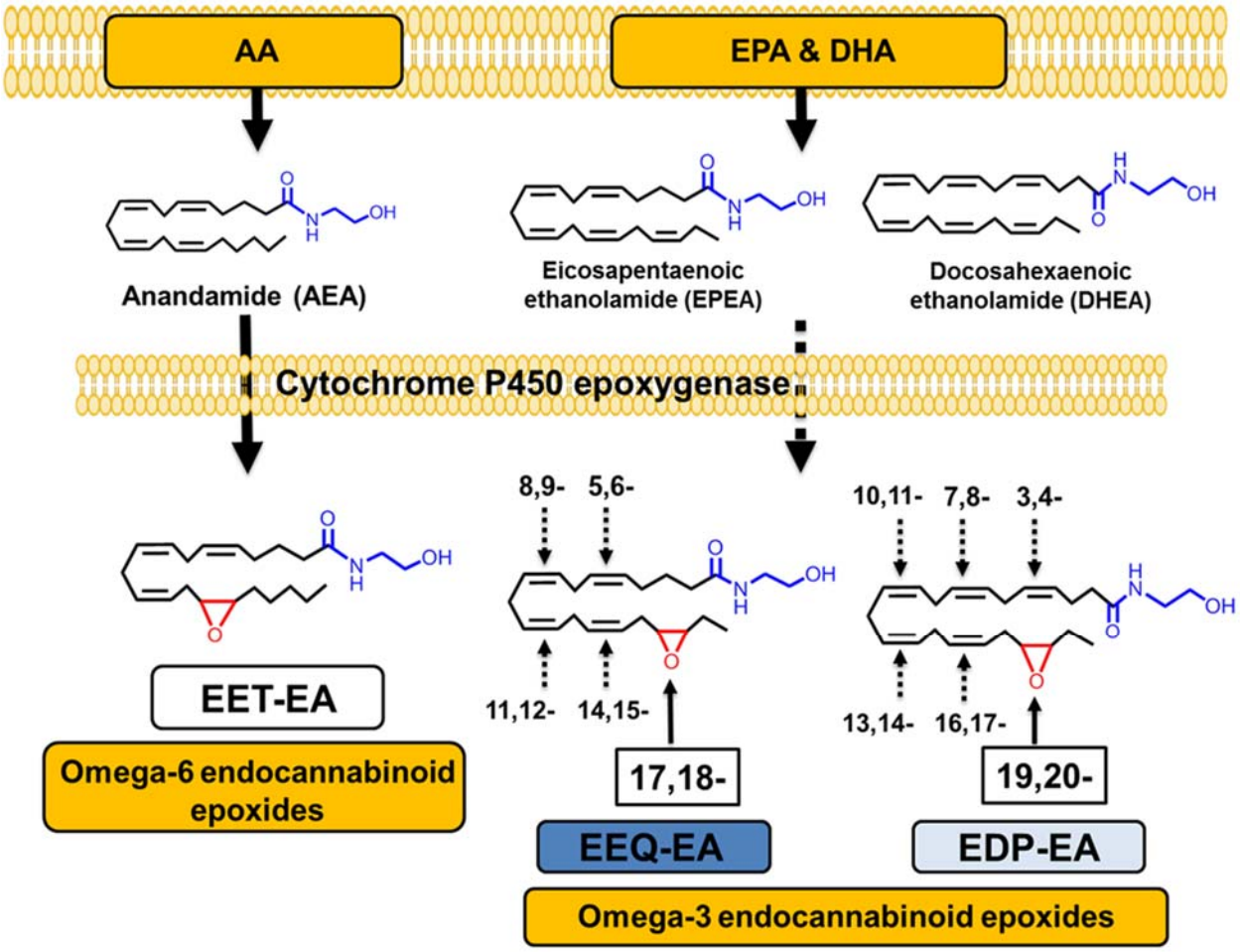

Figure 1.5[3]: Figure shows the various endocannabinoid epoxides originating from omega 6 membrane lipid arachidonic acid and the dietary omega 3 lipids EPA and DHA. The metabolites AEA, EPEA and DHEA, respectively get metabolized by cytochrome P450 epoxygenase enzymes to form EET-EAs, EEQ-EAs and EDP-EAs.

[3] Figure has been reprinted from "Anti-inflammatory ω-3 endocannabinoid epoxides" Daniel R. McDougle, Josephine E. Watson, Amr A. Abdeen, Reheman Adili, Megan P. Caputo, John E. Krapf, Rodney W. Johnson, Kristopher A. Kilian, Michael Holinstat, and Aditi Das. *Proc. Nat. Acad. Sci.* 2017, *114 (30),* E6034.

1.8 REFERENCES

1. Damron TA, Ward WG, Stewart A. Osteosarcoma, chondrosarcoma, and Ewing's sarcoma: National Cancer Data Base Report. Clinical orthopaedics and related research. 2007;459:40-7. doi: 10.1097/BLO.0b013e318059b8c9. PubMed PMID: 17414166.
2. Wycislo KL, Fan TM. The immunotherapy of canine osteosarcoma: a historical and systematic review. Journal of veterinary internal medicine. 2015;29(3):759-69. doi: 10.1111/jvim.12603. PubMed PMID: 25929293; PubMed Central PMCID: PMC4895426.
3. Bernthal NM, Federman N, Eilber FR, Nelson SD, Eckardt JJ, Eilber FC, Tap WD. Long-term results (>25 years) of a randomized, prospective clinical trial evaluating chemotherapy in patients with high-grade, operable osteosarcoma. Cancer. 2012;118(23):5888-93. doi: 10.1002/cncr.27651. PubMed PMID: 22648705.
4. Link MP, Goorin AM, Miser AW, Green AA, Pratt CB, Belasco JB, Pritchard J, Malpas JS, Baker AR, Kirkpatrick JA, et al. The effect of adjuvant chemotherapy on relapse-free survival in patients with osteosarcoma of the extremity. The New England journal of medicine. 1986;314(25):1600-6. doi: 10.1056/NEJM198606193142502. PubMed PMID: 3520317.
5. Collins M, Wilhelm M, Conyers R, Herschtal A, Whelan J, Bielack S, Kager L, Kuhne T, Sydes M, Gelderblom H, Ferrari S, Picci P, Smeland S, Eriksson M, Petrilli AS, Bleyer A, Thomas DM. Benefits and adverse events in younger versus older patients receiving neoadjuvant chemotherapy for osteosarcoma: findings from a meta-analysis. Journal of clinical oncology : official journal of the American Society of Clinical Oncology. 2013;31(18):2303-12. doi: 10.1200/JCO.2012.43.8598. PubMed PMID: 23669227.
6. Meyers PA, Healey JH, Chou AJ, Wexler LH, Merola PR, Morris CD, Laquaglia MP, Kellick MG, Abramson SJ, Gorlick R. Addition of pamidronate to chemotherapy for the treatment of osteosarcoma. Cancer. 2011;117(8):1736-44. doi: 10.1002/cncr.25744. PubMed PMID: 21472721; PubMed Central PMCID: PMC3059356.
7. Walsh MF, Nathanson KL, Couch FJ, Offit K. Genomic Biomarkers for Breast Cancer Risk. Advances in experimental medicine and biology. 2016;882:1-32. doi: 10.1007/978-3-319-22909-6_1. PubMed PMID: 26987529; PubMed Central PMCID: PMC5016023.
8. Brinkmann O, Wong DTW. Salivary Transcriptome Biomarkers in Oral Squamous Cell Cancer Detection. Adv Clin Chem. 2011;55:21-34. doi: 10.1016/B978-0-12-387042-1.00002-2. PubMed PMID: WOS:000295549100002.
9. Herceg Z, Hainaut P. Genetic and epigenetic alterations as biomarkers for cancer detection, diagnosis and prognosis. Mol Oncol. 2007;1(1):26-41. doi: 10.1016/j.molonc.2007.01.004. PubMed PMID: WOS:000263829000006.
10. Bevilacqua A, Ceriani MC, Capaccioli S, Nicolin A. Post-transcriptional regulation of gene expression by degradation of messenger RNAs. Journal of cellular physiology. 2003;195(3):356-72. doi: 10.1002/jcp.10272. PubMed PMID: 12704645.
11. Rabilloud T, Triboulet S. Two-dimensional SDS-PAGE fractionation of biological samples for biomarker discovery. Methods Mol Biol. 2013;1002:151-65. doi: 10.1007/978-1-62703-360-2_13. PubMed PMID: 23625402.
12. Ma H, Chen G, Guo M. Mass spectrometry based translational proteomics for biomarker discovery and application in colorectal cancer. Proteomics Clinical applications. 2016;10(4):503-15. doi: 10.1002/prca.201500082. PubMed PMID: 26616366.
13. Mermelekas G, Zoidakis J. Mass spectrometry-based membrane proteomics in cancer biomarker discovery. Expert review of molecular diagnostics. 2014;14(5):549-63. doi: 10.1586/14737159.2014.917965. PubMed PMID: 24820261.
14. Flatley B, Malone P, Cramer R. MALDI mass spectrometry in prostate cancer biomarker discovery. Biochimica et biophysica acta. 2014;1844(5):940-9. doi: 10.1016/j.bbapap.2013.06.015. PubMed PMID: 23831156.
15. Swiatly A, Horala A, Hajduk J, Matysiak J, Nowak-Markwitz E, Kokot ZJ. MALDI-TOF-MS analysis in discovery and identification of serum proteomic patterns of ovarian cancer. BMC cancer.

2017;17(1):472. doi: 10.1186/s12885-017-3467-2. PubMed PMID: 28683725; PubMed Central PMCID: PMC5501370.
16. Sanchez-Carbayo M. Antibody Microarrays as Tools for Biomarker Discovery. Methods Mol Biol. 2011;785:159-82. doi: 10.1007/978-1-61779-286-1_11. PubMed PMID: WOS:000294443400011.
17. Voduc D, Kenney C, Nielsen TO. Tissue microarrays in clinical oncology. Seminars in radiation oncology. 2008;18(2):89-97. doi: 10.1016/j.semradonc.2007.10.006. PubMed PMID: 18314063; PubMed Central PMCID: PMC2292098.
18. Wang Y, Savage K, Grills C, McCavigan A, James JA, Fennell DA, Hamilton PW. A TMA de-arraying method for high throughput biomarker discovery in tissue research. PloS one. 2011;6(10):e26007. doi: 10.1371/journal.pone.0026007. PubMed PMID: 22016800; PubMed Central PMCID: PMC3189244.
19. Xie F, Liu T, Qian WJ, Petyuk VA, Smith RD. Liquid chromatography-mass spectrometry-based quantitative proteomics. J Biol Chem. 2011;286(29):25443-9. doi: 10.1074/jbc.R110.199703. PubMed PMID: 21632532; PubMed Central PMCID: PMC3138289.
20. Hua YQ, Jia XF, Sun MX, Zheng LP, Yin L, Zhang LJ, Cai ZD. Plasma membrane proteomic analysis of human osteosarcoma and osteoblastic cells: revealing NDRG1 as a marker for osteosarcoma. Tumor Biol. 2011;32(5):1013-21. doi: 10.1007/s13277-011-0203-4. PubMed PMID: WOS:000293962800019.
21. Catherman AD, Skinner OS, Kelleher NL. Top Down proteomics: Facts and perspectives. Biochem Bioph Res Co. 2014;445(4):683-93. doi: 10.1016/j.bbrc.2014.02.041. PubMed PMID: WOS:000335095700002.
22. Zhang YY, Fonslow BR, Shan B, Baek MC, Yates JR. Protein Analysis by Shotgun/Bottom-up Proteomics. Chem Rev. 2013;113(4):2343-94. doi: 10.1021/cr3003533. PubMed PMID: WOS:000317548700004.
23. Kocher T, Pichler P, Swart R, Mechtler K. Analysis of protein mixtures from whole-cell extracts by single-run nanoLC-MS/MS using ultralong gradients. Nat Protoc. 2012;7(5):882-90. doi: 10.1038/nprot.2012.036. PubMed PMID: WOS:000303359300007.
24. Drissi R, Dubois ML, Boisvert FM. Proteomics methods for subcellular proteome analysis. Febs J. 2013;280(22):5626-34. doi: 10.1111/febs.12502. PubMed PMID: WOS:000327130900007.
25. Baghirova S, Hughes BG, Hendzel MJ, Schulz R. Sequential fractionation and isolation of subcellular proteins from tissue or cultured cells. MethodsX. 2015;2:440-5. doi: 10.1016/j.mex.2015.11.001. PubMed PMID: 26740924; PubMed Central PMCID: PMC4678309.
26. Iqbal M, Tao Y, Xie S, Zhu Y, Chen D, Wang X, Huang L, Peng D, Sattar A, Shabbir MA, Hussain HI, Ahmed S, Yuan Z. Aqueous two-phase system (ATPS): an overview and advances in its applications. Biological procedures online. 2016;18:18. doi: 10.1186/s12575-016-0048-8. PubMed PMID: 27807400; PubMed Central PMCID: PMC5084470.
27. Bakheet TM, Doig AJ. Properties and identification of human protein drug targets. Bioinformatics. 2009;25(4):451-7. doi: 10.1093/bioinformatics/btp002. PubMed PMID: WOS:000263406000006.
28. Zhang Z, Zhang L, Hua Y, Jia X, Li J, Hu S, Peng X, Yang P, Sun M, Ma F, Cai Z. Comparative proteomic analysis of plasma membrane proteins between human osteosarcoma and normal osteoblastic cell lines. BMC Cancer. 2010;10:206. Epub 2010/05/18. doi: 10.1186/1471-2407-10-206
1471-2407-10-206 [pii]. PubMed PMID: 20470422; PubMed Central PMCID: PMC2880991.
29. Hua Y, Jia X, Sun M, Zheng L, Yin L, Zhang L, Cai Z. Plasma membrane proteomic analysis of human osteosarcoma and osteoblastic cells: revealing NDRG1 as a marker for osteosarcoma. Tumour Biol. 2011;32(5):1013-21. Epub 2011/06/28. doi: 10.1007/s13277-011-0203-4. PubMed PMID: 21706236.
30. Posthumadeboer J, Piersma SR, Pham TV, van Egmond PW, Knol JC, Cleton-Jansen AM, van Geer MA, van Beusechem VW, Kaspers GJ, van Royen BJ, Jimenez CR, Helder MN. Surface proteomic analysis of osteosarcoma identifies EPHA2 as receptor for targeted drug delivery. British journal of cancer. 2013;109(8):2142-54. doi: 10.1038/bjc.2013.578. PubMed PMID: 24064975; PubMed Central PMCID: PMC3798973.

31. Cheng DD, Li J, Li SJ, Yang QC, Fan CY. CNOT1 cooperates with LMNA to aggravate osteosarcoma tumorigenesis through the Hedgehog signaling pathway. Mol Oncol. 2017;11(4):388-404. doi: 10.1002/1878-0261.12043. PubMed PMID: 28188704; PubMed Central PMCID: PMC5527480.
32. Milovancev M, Hilgart-Martiszus I, McNamara MJ, Goodall CP, Seguin B, Bracha S, Wickramasekara SI. Comparative analysis of the surface exposed proteome of two canine osteosarcoma cell lines and normal canine osteoblasts. BMC veterinary research. 2013;9:116. doi: 10.1186/1746-6148-9-116. PubMed PMID: 23758893; PubMed Central PMCID: PMC3684535.
33. Paoloni M, Davis S, Lana S, Withrow S, Sangiorgi L, Picci P, Hewitt S, Triche T, Meltzer P, Khanna C. Canine tumor cross-species genomics uncovers targets linked to osteosarcoma progression. BMC genomics. 2009;10:625. doi: 10.1186/1471-2164-10-625. PubMed PMID: 20028558; PubMed Central PMCID: PMC2803201.
34. Seddon AM, Curnow P, Booth PJ. Membrane proteins, lipids and detergents: not just a soap opera. Biochimica et biophysica acta. 2004;1666(1-2):105-17. doi: 10.1016/j.bbamem.2004.04.011. PubMed PMID: 15519311.
35. Denisov IG, Sligar SG. Nanodiscs in Membrane Biochemistry and Biophysics. Chem Rev. 2017;117(6):4669-713. doi: 10.1021/acs.chemrev.6b00690. PubMed PMID: 28177242.
36. Bayburt TH, Sligar SG. Membrane protein assembly into Nanodiscs. Febs Lett. 2010;584(9):1721-7. doi: 10.1016/j.febslet.2009.10.024. PubMed PMID: WOS:000276717600013.
37. Roy J, Pondenis H, Fan TM, Das A. Direct Capture of Functional Proteins from Mammalian Plasma Membranes into Nanodiscs. Biochemistry-Us. 2015;54(41):6299-302. doi: 10.1021/acs.biochem.5b00954. PubMed PMID: WOS:000363347600002.
38. Denisov IG, Sligari SG. Nanodiscs in Membrane Biochemistry and Biophysics. Chem Rev. 2017;117(6):4669-713. doi: 10.1021/acs.chemrev.6b00690. PubMed PMID: WOS:000397477600001.
39. Nasr ML, Baptista D, Strauss M, Sun ZYJ, Grigoriu S, Huser S, Pluckthun A, Hagn F, Walz T, Hogle JM, Wagner G. Covalently circularized nanodiscs for studying membrane proteins and viral entry. Nat Methods. 2017;14(1):49-52. doi: 10.1038/Nmeth.4079. PubMed PMID: WOS:000391162300023.
40. Hagn F, Etzkorn M, Raschle T, Wagner G. Optimized Phospholipid Bilayer Nanodiscs Facilitate High-Resolution Structure Determination of Membrane Proteins. J Am Chem Soc. 2013;135(5):1919-25. doi: 10.1021/ja310901f. PubMed PMID: WOS:000314794400047.
41. Rouck JE, Krapf JE, Roy J, Huff HC, Das A. Recent advances in nanodisc technology for membrane protein studies (2012-2017). Febs Lett. 2017;591(14):2057-88. doi: 10.1002/1873-3468.12706. PubMed PMID: WOS:000406240400003.
42. Marty MT, Wilcox KC, Klein WL, Sligar SG. Nanodisc-solubilized membrane protein library reflects the membrane proteome. Analytical and bioanalytical chemistry. 2013;405(12):4009-16. doi: 10.1007/s00216-013-6790-8. PubMed PMID: 23400332; PubMed Central PMCID: PMC3628400.
43. Wilcox KC, Marunde MR, Das A, Velasco PT, Kuhns BD, Marty MT, Jiang HM, Luan CH, Sligar SG, Klein WL. Nanoscale Synaptic Membrane Mimetic Allows Unbiased High Throughput Screen That Targets Binding Sites for Alzheimer's-Associated A beta Oligomers. PloS one. 2015;10(4). doi: UNSP e0125263
10.1371/journal.pone.0125263. PubMed PMID: WOS:000353713100074.
44. Mak S, Sun RY, Schmalenberg M, Peters C, Luppa PB. Express incorporation of membrane proteins from various human cell types into phospholipid bilayer nanodiscs. Biochem J. 2017;474(8):1361-71. doi: 10.1042/Bcj20161110. PubMed PMID: WOS:000405371400002.
45. Warnock DE, Roberts C, Lutz MS, Blackburn WA, Young WW, Baenziger JU. Determination of Plasma-Membrane Lipid Mass and Composition in Cultured Chinese-Hamster Ovary Cells Using High-Gradient Magnetic Affinity-Chromatography. J Biol Chem. 1993;268(14):10145-53. PubMed PMID: WOS:A1993LB80000033.
46. van Meer G, Voelker DR, Feigenson GW. Membrane lipids: where they are and how they behave. Nat Rev Mol Cell Bio. 2008;9(2):112-24. doi: 10.1038/nrm2330. PubMed PMID: WOS:000252676600012.

47. Pike LJ. Lipid rafts: bringing order to chaos. J Lipid Res. 2003;44(4):655-67. doi: 10.1194/jlr.R200021-JLR200. PubMed PMID: WOS:000182214500001.
48. Bligh EG, Dyer WJ. A Rapid Method of Total Lipid Extraction and Purification. Can J Biochem Phys. 1959;37(8):911-7. PubMed PMID: WOS:A1959WM52500001.
49. Mangold HK. Thin-Layer Chromatography of Lipids. J Am Oil Chem Soc. 1961;38(12):708-27. doi: Doi 10.1007/Bf02633061. PubMed PMID: WOS:A1961WW55700014.
50. Blanksby SJ, Mitchell TW. Advances in Mass Spectrometry for Lipidomics. Annu Rev Anal Chem. 2010;3:433-65. doi: 10.1146/annurev.anchem.111808.073705. PubMed PMID: WOS:000280599500020.
51. Katajamaa M, Miettinen J, Oresic M. MZmine: toolbox for processing and visualization of mass spectrometry based molecular profile data. Bioinformatics. 2006;22(5):634-6. doi: 10.1093/bioinformatics/btk039. PubMed PMID: 16403790.
52. Meng D, Zhang Q, Gao X, Wu S, Lin G. LipidMiner: a software for automated identification and quantification of lipids from multiple liquid chromatography/mass spectrometry data files. Rapid communications in mass spectrometry : RCM. 2014;28(8):981-5. doi: 10.1002/rcm.6865. PubMed PMID: 24623704; PubMed Central PMCID: PMC4000603.
53. Zhang Y, Baycin-Hizal D, Kumar A, Priola J, Bahri M, Heffner KM, Wang M, Han X, Bowen MA, Betenbaugh MJ. High-Throughput Lipidomic and Transcriptomic Analysis To Compare SP2/0, CHO, and HEK-293 Mammalian Cell Lines. Analytical chemistry. 2017;89(3):1477-85. doi: 10.1021/acs.analchem.6b02984. PubMed PMID: 27991764.
54. Fernandez C, Sandin M, Sampaio JL, Almgren P, Narkiewicz K, Hoffmann M, Hedner T, Wahlstrand B, Simons K, Shevchenko A, James P, Melander O. Plasma lipid composition and risk of developing cardiovascular disease. PloS one. 2013;8(8):e71846. doi: 10.1371/journal.pone.0071846. PubMed PMID: 23967253; PubMed Central PMCID: PMC3744469.
55. Wang M, Han X. Advanced Shotgun Lipidomics for Characterization of Altered Lipid Patterns in Neurodegenerative Diseases and Brain Injury. Methods Mol Biol. 2016;1303:405-22. doi: 10.1007/978-1-4939-2627-5_24. PubMed PMID: 26235081; PubMed Central PMCID: PMC4780753.
56. Baenke F, Peck B, Miess H, Schulze A. Hooked on fat: the role of lipid synthesis in cancer metabolism and tumour development. Dis Model Mech. 2013;6(6):1353-63. doi: 10.1242/dmm.011338. PubMed PMID: WOS:000329275000007.
57. Medes G, Thomas A, Weinhouse S. Metabolism of Neoplastic Tissue .4. A Study of Lipid Synthesis in Neoplastic Tissue Slices Invitro. Cancer Res. 1953;13(1):27-9. PubMed PMID: WOS:A1953UD93700005.
58. Kuhajda FP, Jenner K, Wood FD, Hennigar RA, Jacobs LB, Dick JD, Pasternack GR. Fatty-Acid Synthesis - a Potential Selective Target for Antineoplastic Therapy. Proceedings of the National Academy of Sciences of the United States of America. 1994;91(14):6379-83. doi: DOI 10.1073/pnas.91.14.6379. PubMed PMID: WOS:A1994NV42000029.
59. Menendez JA, Lupu R. Fatty acid synthase and the lipogenic phenotype in cancer pathogenesis. Nat Rev Cancer. 2007;7(10):763-77. doi: 10.1038/nrc2222. PubMed PMID: WOS:000249691700013.
60. Hager MH, Solomon KR, Freeman MR. The role of cholesterol in prostate cancer. Curr Opin Clin Nutr. 2006;9(4):379-85. doi: DOI 10.1097/01.mco.0000232896.66791.62. PubMed PMID: WOS:000239101600006.
61. Simons K, Gerl MJ. Revitalizing membrane rafts: new tools and insights. Nat Rev Mol Cell Bio. 2010;11(10):688-99. doi: 10.1038/nrm2977. PubMed PMID: WOS:000282152800012.
62. Dall'Armi C, Devereaux KA, Di Paolo G. The Role of Lipids in the Control of Autophagy. Current Biology. 2013;23(1):R33-R45. doi: 10.1016/j.cub.2012.10.041. PubMed PMID: WOS:000313383700015.
63. Singh R, Kaushik S, Wang YJ, Xiang YQ, Novak I, Komatsu M, Tanaka K, Cuervo AM, Czaja MJ. Autophagy regulates lipid metabolism. Nature. 2009;458(7242):1131-U64. doi: 10.1038/nature07976. PubMed PMID: WOS:000265754600039.
64. White E. Deconvoluting the context-dependent role for autophagy in cancer. Nat Rev Cancer. 2012;12(6):401-10. doi: 10.1038/nrc3262. PubMed PMID: WOS:000304437000012.

65. Willemarck N, Rysman E, Brusselmans K, Van Imschoot G, Vanderhoydonc F, Moerloose K, Lerut E, Verhoeven G, van Roy F, Vleminckx K, Swinnen JV. Aberrant Activation of Fatty Acid Synthesis Suppresses Primary Cilium Formation and Distorts Tissue Development. Cancer Res. 2010;70(22):9453-62. doi: 10.1158/0008-5472.CAN-10-2324. PubMed PMID: WOS:000284213300050.
66. Nieman KM, Kenny HA, Penicka CV, Ladanyi A, Buell-Gutbrod R, Zillhardt MR, Romero IL, Carey MS, Mills GB, Hotamisligil GS, Yamada SD, Peter ME, Gwin K, Lengyel E. Adipocytes promote ovarian cancer metastasis and provide energy for rapid tumor growth. Nat Med. 2011;17(11):1498-U207. doi: 10.1038/nm.2492. PubMed PMID: WOS:000296779300042.
67. Rysman E, Brusselmans K, Scheys K, Timmermans L, Derua R, Munck S, Van Veldhoven PP, Waltregny D, Daniels VW, Machiels J, Vanderhoydonc F, Smans K, Waelkens E, Verhoeven G, Swinnen JV. De novo Lipogenesis Protects Cancer Cells from Free Radicals and Chemotherapeutics by Promoting Membrane Lipid Saturation. Cancer Res. 2010;70(20):8117-26. doi: 10.1158/0008-5472.CAN-09-3871. PubMed PMID: WOS:000282879900038.
68. Hilvo M, Denkert C, Lehtinen L, Muller B, Brockmoller S, Seppanen-Laakso T, Budczies J, Bucher E, Yetukuri L, Castillo S, Berg E, Nygren H, Sysi-Aho M, Griffin JL, Fiehn O, Loibl S, Richter-Ehrenstein C, Radke C, Hyotylainen T, Kallioniemi O, Iljin K, Oresic M. Novel Theranostic Opportunities Offered by Characterization of Altered Membrane Lipid Metabolism in Breast Cancer Progression. Cancer research. 2011;71(9):3236-45. doi: 10.1158/0008-5472.CAN-10-3894. PubMed PMID: WOS:000290020400008.
69. Doria ML, Cotrim CZ, Simoes C, Macedo B, Domingues P, Domingues MR, Helguero LA. Lipidomic analysis of phospholipids from human mammary epithelial and breast cancer cell lines. Journal of cellular physiology. 2013;228(2):457-68. doi: 10.1002/jcp.24152. PubMed PMID: 22767159.
70. Fhaner CJ, Liu S, Ji H, Simpson RJ, Reid GE. Comprehensive lipidome profiling of isogenic primary and metastatic colon adenocarcinoma cell lines. Analytical chemistry. 2012;84(21):8917-26. doi: 10.1021/ac302154g. PubMed PMID: 23039336; PubMed Central PMCID: PMC3491142.
71. Lee JW, Shinohara H, Jung JH, Mok HJ, Akao Y, Kim KP. Detailed characterization of alterations in the lipid profiles during autophagic cell death of leukemia cells. Rsc Adv. 2016;6(35):29512-8. doi: 10.1039/c6ra01965j. PubMed PMID: WOS:000373029500058.
72. Saito K, Arai E, Maekawa K, Ishikawa M, Fujimoto H, Taguchi R, Matsumoto K, Kanai Y, Saito Y. Lipidomic Signatures and Associated Transcriptomic Profiles of Clear Cell Renal Cell Carcinoma. Scientific reports. 2016;6. doi: Artn 28932
10.1038/Srep28932. PubMed PMID: WOS:000378908300001.
73. Li J, Ren SC, Piao HL, Wang FB, Yin PY, Xu CL, Lu X, Ye GZ, Shao YP, Yan M, Zhao XJ, Sun YH, Xu GW. Integration of lipidomics and transcriptomics unravels aberrant lipid metabolism and defines cholesteryl oleate as potential biomarker of prostate cancer. Sci Rep-Uk. 2016;6. doi: Artn 20984
10.1038/Srep20984. PubMed PMID: WOS:000369923500001.
74. Sampaio JL, Gerl MJ, Klose C, Ejsing CS, Beug H, Simons K, Shevchenko A. Membrane lipidome of an epithelial cell line. Proceedings of the National Academy of Sciences of the United States of America. 2011;108(5):1903-7. doi: 10.1073/pnas.1019267108. PubMed PMID: WOS:000286804700031.
75. Samuelsson B. Arachidonic-Acid Metabolism - Role in Inflammation. Z Rheumatol. 1991;50:3-6. PubMed PMID: WOS:A1991FK88400002.
76. Ricciotti E, FitzGerald GA. Prostaglandins and Inflammation. Arterioscl Throm Vas. 2011;31(5):986-1000. doi: 10.1161/Atvbaha.110.207449. PubMed PMID: WOS:000289720800010.
77. Hammarstrom S. Leukotrienes. Annu Rev Biochem. 1983;52:355-77. doi: DOI 10.1146/annurev.bi.52.070183.002035. PubMed PMID: WOS:A1983QY55400014.
78. Spector AA, Fang X, Snyder GD, Weintraub NL. Epoxyeicosatrienoic acids (EETs): metabolism and biochemical function. Prog Lipid Res. 2004;43(1):55-90. doi: 10.1016/S0163-7827(03)00049-3. PubMed PMID: WOS:000187732300003.
79. Liu J, Wang L, Harvey-White J, Osei-Hyiaman D, Razdan R, Gong Q, Chan AC, Zhou ZF, Huang BX, Kim HY, Kunos G. A biosynthetic pathway for anandamide. Proceedings of the National Academy of Sciences of the United States of America. 2006;103(36):13345-50. doi: 10.1073/pnas.0601832103. PubMed PMID: WOS:000240512700018.

80. Laezza C, D'Alessandro A, Paladino S, Maria Malfitano A, Chiara Proto M, Gazzerro P, Pisanti S, Santoro A, Ciaglia E, Bifulco M, Endocannabinoid Research G. Anandamide inhibits the Wnt/beta-catenin signalling pathway in human breast cancer MDA MB 231 cells. European journal of cancer. 2012;48(16):3112-22. doi: 10.1016/j.ejca.2012.02.062. PubMed PMID: 22425263.
81. Khasabova IA, Khasabov SG, Harding-Rose C, Coicou LG, Seybold BA, Lindberg AE, Steevens CD, Simone DA, Seybold VS. A decrease in anandamide signaling contributes to the maintenance of cutaneous mechanical hyperalgesia in a model of bone cancer pain. The Journal of neuroscience : the official journal of the Society for Neuroscience. 2008;28(44):11141-52. doi: 10.1523/JNEUROSCI.2847-08.2008. PubMed PMID: 18971457; PubMed Central PMCID: PMC2628759.
82. Eljaschewitsch E, Witting A, Mawrin C, Lee T, Schmidt PM, Wolf S, Hoertnagl H, Raine CS, Schneider-Stock R, Nitsch R, Ullrich O. The endocannabinoid anandamide protects neurons during CNS inflammation by induction of MKP-1 in microglial cells. Neuron. 2006;49(1):67-79. doi: 10.1016/j.neuron.2005.11.027. PubMed PMID: 16387640.
83. Swanson D, Block R, Mousa SA. Omega-3 fatty acids EPA and DHA: health benefits throughout life. Advances in nutrition. 2012;3(1):1-7. doi: 10.3945/an.111.000893. PubMed PMID: 22332096; PubMed Central PMCID: PMC3262608.
84. Arnold C, Markovic M, Blossey K, Wallukat G, Fischer R, Dechend R, Konkel A, von Schacky C, Luft FC, Muller DN, Rothe M, Schunck WH. Arachidonic acid-metabolizing cytochrome P450 enzymes are targets of {omega}-3 fatty acids. J Biol Chem. 2010;285(43):32720-33. doi: 10.1074/jbc.M110.118406. PubMed PMID: 20732876; PubMed Central PMCID: PMC2963419.
85. Cui PH, Petrovic N, Murray M. The omega-3 epoxide of eicosapentaenoic acid inhibits endothelial cell proliferation by p38 MAP kinase activation and cyclin D1/CDK4 down-regulation. British journal of pharmacology. 2011;162(5):1143-55. doi: 10.1111/j.1476-5381.2010.01113.x. PubMed PMID: 21077851; PubMed Central PMCID: PMC3051386.
86. Zhang G, Panigrahy D, Mahakian LM, Yang J, Liu JY, Stephen Lee KS, Wettersten HI, Ulu A, Hu X, Tam S, Hwang SH, Ingham ES, Kieran MW, Weiss RH, Ferrara KW, Hammock BD. Epoxy metabolites of docosahexaenoic acid (DHA) inhibit angiogenesis, tumor growth, and metastasis. Proceedings of the National Academy of Sciences of the United States of America. 2013;110(16):6530-5. doi: 10.1073/pnas.1304321110. PubMed PMID: 23553837; PubMed Central PMCID: PMC3631682.
87. Brown I, Cascio MG, Wahle KW, Smoum R, Mechoulam R, Ross RA, Pertwee RG, Heys SD. Cannabinoid receptor-dependent and -independent anti-proliferative effects of omega-3 ethanolamides in androgen receptor-positive and -negative prostate cancer cell lines. Carcinogenesis. 2010;31(9):1584-91. doi: 10.1093/carcin/bgq151. PubMed PMID: 20660502; PubMed Central PMCID: PMC2930808.
88. Spector AA, Kim HY. Cytochrome P450 epoxygenase pathway of polyunsaturated fatty acid metabolism. Biochimica et biophysica acta. 2015;1851(4):356-65. doi: 10.1016/j.bbalip.2014.07.020. PubMed PMID: 25093613; PubMed Central PMCID: PMC4314516.
89. Liu Y, Zhang Y, Schmelzer K, Lee TS, Fang X, Zhu Y, Spector AA, Gill S, Morisseau C, Hammock BD, Shyy JY. The antiinflammatory effect of laminar flow: the role of PPARgamma, epoxyeicosatrienoic acids, and soluble epoxide hydrolase. Proc Natl Acad Sci U S A. 2005;102(46):16747-52. Epub 2005/11/04. doi: 0508081102 [pii]
10.1073/pnas.0508081102. PubMed PMID: 16267130; PubMed Central PMCID: PMC1276614.
90. Kotlikoff MI. EDHF redux: EETs, TRPV4, and Ca2+ sparks. Circulation Research. 2005;97(12):1209-10. Epub 2005/12/13. doi: 97/12/1209 [pii]
10.1161/01.RES.0000196741.99904.e4. PubMed PMID: 16339490.
91. Maccarrone M, Lorenzon T, Bari M, Melino G, Finazzi-Agro A. Anandamide induces apoptosis in human cells via vanilloid receptors. Evidence for a protective role of cannabinoid receptors. J Biol Chem. 2000;275(41):31938-45. doi: 10.1074/jbc.M005722200. PubMed PMID: 10913156.
92. McDougle DR, Watson JE, Abdeen AA, Adili R, Caputo MP, Krapf JE, Johnson RW, Kilian KA, Holinstat M, Das A. Anti-inflammatory omega-3 endocannabinoid epoxides. Proceedings of the National Academy of Sciences of the United States of America. 2017;114(30):E6034-E43. doi: 10.1073/pnas.1610325114. PubMed PMID: 28687674; PubMed Central PMCID: PMC5544256.

93. Schreiber AK, Neufeld M, Jesus CH, Cunha JM. Peripheral antinociceptive effect of anandamide and drugs that affect the endocannabinoid system on the formalin test in normal and streptozotocin-diabetic rats. Neuropharmacology. 2012;63(8):1286-97. doi: 10.1016/j.neuropharm.2012.08.009. PubMed PMID: 22959964.
94. Falck JR, Yadagiri P, Capdevila J. Synthesis of epoxyeicosatrienoic acids and heteroatom analogs. Methods in enzymology. 1990;187:357-64. PubMed PMID: 2233353.
95. Falck JR, Wallukat G, Puli N, Goli M, Arnold C, Konkel A, Rothe M, Fischer R, Muller DN, Schunck WH. 17(R),18(S)-epoxyeicosatetraenoic acid, a potent eicosapentaenoic acid (EPA) derived regulator of cardiomyocyte contraction: structure-activity relationships and stable analogues. Journal of medicinal chemistry. 2011;54(12):4109-18. doi: 10.1021/jm200132q. PubMed PMID: 21591683; PubMed Central PMCID: PMC3122156.
96. Abadji V, Lin SY, Taha G, Griffin G, Stevenson LA, Pertwee RG, Makriyannis A. (R)-Methanandamide - a Chiral Novel Anandamide Possessing Higher Potency and Metabolic Stability. J Med Chem. 1994;37(12):1889-93. doi: Doi 10.1021/Jm00038a020. PubMed PMID: WOS:A1994NR64700020.
97. Jarrahian A, Manna S, Edgemond WS, Campbell WB, Hillard CJ. Structure-activity relationships among N-arachidonylethanolamine (anandamide) head group analogues for the anandamide transporter. J Neurochem. 2000;74(6):2597-606. doi: DOI 10.1046/j.1471-4159.2000.0742597.x. PubMed PMID: WOS:000086968800042.

CHAPTER II: HIGH-THROUGHPUT PROTEOMICS TO IDENTIFY MEMBRANE PROTEIN BIOMARKERS IN OSTEOSARCOMA[4]

2.1 ABSTRACT

Osteosarcoma is the most common bone cancer in dogs and people. In order to improve clinical outcomes, it is necessary to identify proteins that are differentially expressed by metastatic cells. Membrane bound proteins are responsible for multiple pro-metastatic functions. Therefore characterizing the differential expression of membranous proteins between metastatic and non-metastatic clonal variants will allow the discovery of druggable targets and consequently improve treatment methodology. The objective of this investigation was to systemically identify the membrane-associated proteomics of metastatic and non-metastatic variants of human and canine origin. Two clonal variants of divergent in vivo metastatic potential from human and canine origins were used. The plasma membranes were isolated and peptide fingerprinting was used to identify differentially expressed proteins. Selected proteins were further validated using western blotting, flow cytometry, confocal microscopy and immunohistochemistry. Over 500 proteins were identified for each cell line with nearly 40% of the proteins differentially regulated. Conserved between both species, metastatic variants demonstrated significant differences in expression of membrane proteins that are responsible for pro-metastatic functions. Additionally, CD147, CD44 and vimentin were validated using various biochemical techniques. Taken together, through a comparative proteomic approach we have identified several differentially expressed cell membrane proteins that will help in the development of future therapeutics.

2.2 INTRODUCTION

Osteosarcoma (OS) is the most common form of primary bone cancer among children and young adults. The treatment options for OS include a combination of multi-agent induction chemotherapy, and radical excision of the tumor followed by adjuvant chemotherapy. Despite the aggressive treatment course, the survival rates are poor. For instance, in patients with localized disease, 5-year survival rates are approximately 65%; however, in the case of metastatic disease at

[4] This work has been previously published as "Comparative proteomic investigation of metastatic and non-metastatic osteosarcoma cells of human and canine origin." Jahnabi Roy, Kathryn L. Wycislo, Holly Pondenis, Timothy M. Fan and Aditi Das. *PlosOne,* 2017, *12(9),* e0183930.

diagnosis or recurrence, the 5-year survival rates are only 20% [1,2]. Although progress has been made towards improving treatment options, the early detection and subsequent control of metastasis have been challenging in OS.

The current approach towards the discovery of drug targets has focused on using high throughput peptide fingerprinting techniques to identify plasma membrane (PM) biomarkers in various cancers. Cell membranes are a dynamic and selective gatekeeper that controls the influx and efflux of multiple signaling molecules, and is responsible for multiple functions including adhesion, proliferation, migration and intercellular communication. Given their key roles in diverse, yet critical cellular functions, perturbations in plasma membrane proteins are associated with pathological states including cancer. Hence, the characterization of the membrane proteins in the cell surface of tumor cells can aid not only in early diagnosis, but also lead to the development of novel therapeutics. Recent evidence demonstrates the fluidity of cancer cell proteomic profiles with distinct classes of proteins being differentially expressed by tumor cells during metastatic progression [3]. Therefore, the current approach in this work is to identify and characterize the differential PM biomarkers of metastatic OS. This will be facilitated through the use of high throughput peptide fingerprinting that has been employed to identify targetable receptors in various cancers [4,5] as well as to identify differentially regulated markers in OS [6,7]. The thorough annotation of PM proteins differentially expressed by metastatic and non-metastatic OS cells holds promise to identify surrogate biomarkers of aggressive OS leading to earlier disease detection, as well as illuminate the biochemistry of metastasis.

A major limiting factor in the development of novel therapeutics in OS is the lack of suitable comparative animal models. While mouse models are commonly used for studying OS, they lack the degree of genetic heterogeneity as humans, making the study of OS oversimplified. Dogs are companion animals, which share the same environment with their human counterparts and have a greater genetic diversity than mice bred for research. Importantly, pet dogs also spontaneously develop OS that is genetically indistinguishable from human OS [8]. Hence dogs are more reliable comparative animal models that can aid in the discovery of novel OS therapeutics that can benefit both human and dogs. Currently there are no studies that show the correlation in cell surface receptors between human and canine OS. The identification of receptors that are upregulated in

both humans as well as dogs, will allow for the development of novel therapeutics for both species in a parallel manner.

This will provide an opportunity to employ high throughput peptide fingerprinting to profile the global membrane proteome of human and canine OS and perform a cross-species analysis. For our study, we chose isogenic human and canine metastatic and non-metastatic cells. The availability of these cell lines allowed us to examine the differences in proteomic profiles that affect a metastatic phenotype without a significant genetic difference. Additionally, the comparison of metastatic versus non-metastatic cells, as opposed to tumorigenic and non-tumorigenic species, provides additional insight into factors that not only promote initial tumor formation but also those that promote metastasis.

Herein, we isolated the plasma membrane proteins and characterized the proteins by high-throughput peptide fingerprinting. We identified membrane proteins that were differentially regulated in both canine and human OS cell lines. We validated several targetable receptors using biochemical methodologies and immunohistochemistry studies in paired canine primary and metastatic tissues. Finally, overall changes in GPCR activity were measured that corroborated with the changes in the GPCR distribution in metastatic and non-metastatic samples as identified from the peptide fingerprinting data. Taken together, in this work we identify cross-species trends in expression of cell surface receptors between metastatic and non-metastatic OS that were consistent between both human and canine species. Several of these receptors are known targets in various cancer types and therefore drugs targeting of these receptors can be repurposed to develop OS therapeutics.

2.3 MATERIALS AND METHODS

Materials: Antibodies- CD44 (Santa Cruz Biotechnology sc-18849), Vimentin (Abcam ab16700) and CD147 (Abcam ab108317). Secondary antibodies for confocal microscopy and flow cytometry- Goat anti-Rabbit IgG (H+L) Secondary Antibody, Alexa Fluor® 488 conjugate (ThermoFischer Scientific A-11034) and Goat anti rat (Santa Cruz Biotechnology sc-2011). Image IT Fx Signal Enhancer (R37107), ProLong Gold Antifade Mount (P10144), 4', 6-diamidino-2-phenylindoleg (DAPI) were obtained from Thermo Fischer Scientific. IHC- all IHC reagents, except primary antibodies and 61-9520 are from Biocare Medical (biocare.net). 61-9520 is from Fisher Scientific (thermofisher.com)

Cell culture: Human cell lines HOS and 143B and canine cells POS and HMPOS were cultured in DMEM (Gibco, Invitrogen, Carlsbad, CA, USA) supplemented with 10% fetal bovine serum (FBS) and 1mgml–1 penicillin–streptomycin (Gibco, Invitrogen) at 37 °C and 5% CO2 in a humidified incubator. All cell lines were verified via STR analysis. The human cell lines HOS and 143B were verified at The University of Arizona Genetics Core and the canine cell lines POS and HMPOS were verified at Colorado State University Flint Animal Cancer Center.

Extraction of plasma membranes: Membrane extraction was done as previously published (7, 58). All steps were carried out at 4°C. Briefly, about 60 million adherent cells were washed with phosphate-buffered saline (PBS), scraped using a plastic cell lifter, and lysed in 1 mL solution containing 0.2 mM EDTA and 1 mM NaHCO3 and 20 µL protease inhibitor (Nacalai USA, Inc.), using a glass homogenizer. The nuclear and unbroken cells were removed through centrifugation a 200×g, and the supernatant was collected and centrifuged for 30 min at 25,000 rpm. The cell pellets were resuspended in 1 mM NaHCO3 in an approximate ratio of 1 mL per 5×108 cells and used for PM separation by two-phase systems. Suspended cell pellets were added to the top of 14 g of the dextran–poly (ethylene glycol) mixture (6.6% Dextran T500, 6.6% PEG 3350, 0.1 M sucrose, 5 mM K3PO4, pH= 7.2). After mixing up and down for 40 times, the tube was centrifuged for 5 min at 750×g. The PM-enriched up phase was collected and purified again as described above. The up phase was diluted with 1 mM sodium bicarbonate and centrifuged at 100,000×g for 2 h in a SW32 rotor.

Peptide fingerprinting:

Protein Identifications using CID mass spectrometry:

Sample preparation: Sample cleanup was done using G-Biosciences (St. Louis, MO) Perfect Focus according to manufacturer's instruction. 1-100µl of protein solution (containing 10µg protein per sample) was transferred into a 1.5ml microfuge tube. 300µl of reagent UPPA-I was added and mixed well. This was incubated at 4°C for 15 minutes. 300µl of reagent UPPA-II was added to the protein mixture and the tube was vortexed. The tube was then centrifuged at 15,000x g for 5 minutes to form a protein pellet. Carefully, without disturbing the pellet, a pipette tip was used to remove & discard the entire supernatant. The tube was centrifuged again for 30 seconds. A pipette tip was used to remove the remaining supernatant. 40µl of FOCUS-Wash was added on top of the pellet. The tube was centrifuged again for 5 minutes and the wash was discarded. 25µl of milliQ

water was added on top of the pellet and the tube was vortexed. 1ml OrgoSol Buffer, pre-chilled at –20°C, was added to the tube containing protein suspension. The tube was vortexed to suspend the pellet. The tube was incubated at –20°C for 30 minutes. Periodically the tube was vortexed for 20-30 seconds. The tube was centrifuged at 15,000xg for 5 minutes to form a pellet and the supernatant was removed and discarded. The pellet was air dried and the white pellet turned translucent on air drying.

Digestion with trypsin: Sample was digested with MSG-Trypsin (G-Biosciences, St. Louis, MO) at a w/w ratio of 1:10 using a CEM Discover Microwave Digestor (Mathews, SC) at 55 ˚C and maximum power of 60 watts for 30 minutes. Digested peptides were lyophilized in a Virtis -55 lyophilizer to dryness. The digested peptides were dissolved in 5% acetonitrile + 0.1% formic acid for LC/MS.

LC/MS: LC/MS was performed using a Thermo Dionex Ultimate RSLC3000 operating in nano mode at 300 microliters/min with a gradient from 0.1% formic acid to 100% acetonitrile + 0.1% formic acid in 120 minutes. The trap column used was a Thermo Acclaim PepMap 100 (100 µm x 2 cm) and the analytical column was a Thermo Acclaim PepMap RSLC (75 µm x 15 cm). 2 micrograms of the digested peptides were loaded per injection.

Mass spectrometry was performed on a Thermo LTQ Velos ETD Pro Mass spectrometer using data dependent MS/MS analysis on the top five most intense ions detected in the precursor scan mode. Previously detected ions were automatically excluded for 60 seconds to allow deeper coverage of the less abundant ions.

Data Analysis: The Xcalibur raw file was converted by Mascot Distiller into peaklists that were submitted to an in-house Mascot Server and searched against specific NCBI-NR protein databases. The list of proteins obtained was filtered by a $p < 0.05$ for a 95% confidence value. Additional data about peptide fingerprinting parameters can be found in SI. The peak lists have been uploaded into external repository as indicated at the end of this section. This list of proteins was then classified by their subcellular location (to filter out non- membrane contaminants) and plasma membrane candidates were classified into various functional classes. The emPAI values were normalized to the total emPAI value and compared as a percentage to the overall composition.

Quantitation: emPAI protocol: The Exponentially Modified Protein Abundance Index (emPAI) offers approximate, label-free, relative quantitation of the proteins in a mixture based on protein coverage by the peptide matches in a database search result. Developed by Ishihama and colleagues, Exponentially modified protein abundance index (emPAI) is a quantification unit for estimation of absolute protein amount in proteomics as calculated from the number of sequenced peptides per protein [9].

Unlike the other quantitation protocols, the information required for emPAI is always present in a search result, and there are no parameter settings, as long as the MS/MS search contains at least 100 spectra.

emPAI= 〖10〗^(Nobserved/Nobservable)-1

Where Nobserved is the number of experimentally observed peptides and Nobservable is the calculated number of observable peptides for each protein. The tricky bit is deciding what to include and what to exclude in these two counts.

Western Blot: Based on protein concentration measurements, equal amounts of plasma membrane preparations generated from all cells were resolved by 4–20% SDS-PAGE (Pierce) and transferred onto a PVDF membrane. The membranes were blocked in PBS, 0.1% Tween 20, 5% nonfat dry milk powder for 1 h at room temperature and incubated with primary antibody for 16 h at 4 °C followed by washing and incubation with HRP-conjugated secondary antibody for 1 h at room temperature. All antibody incubations and washing steps were carried out in PBS, 0.1% Tween 20. The immunoreactive bands were visualized using an ECL Western blot kit (Amersham Biosciences). The western blots were normalized by Ponceau staining [10].

Confocal Microscopy: Cells were grown in 8 well chamber slides (Ibidi, Verona, WI), overnight. The cells were washed with warm phenol red free DMEM free of FBS. The cells were fixed with warm phenol red free DMEM free of FBS containing 4% methanol free paraformaldehyde at room temperature for 10 minutes. The wells were washed 3X with PBS, and permeabilized with 0.1% Triton-X 100 in PBS for 5 minutes. The cells were then blocked with 5- drops of IT signal FX solution (SFX kit, Invitrogen) for 30 min. at room temperature. After 3 washes with PBS, the slides were blocked with 3% BSA in PBS for 30 min at room temperature. The primary antibody, which was diluted in PBS containing 3% BSA (1:100), was added to the cells, and samples were

incubated overnight at 4 °C. Cells were rinsed 3X with PBS, secondary antibody was added in PBS containing 3% BSA (1:200), and cultures were incubated for 1 hour at room temperature. After 3 washes with PBS, nuclei were counterstained with DAPI for 15 minutes at room temperature, samples were washed 3X with PBS, and cells were mounted with 5 drops of ProLong Gold solution and allowed to dry in a chemical fume hood for 24 hours before imaging. Imaging was performed through the bottom of the chamber slides in a Nikon A1R confocal laser microscope system. The data was analyzed using ImageJ and NIS Elements Confocal Microscope Imaging Software. Laser power and other parameters indicated in Supporting Information.

GPCR activity assay: Intracellular cAMP levels were measured as an indicator of GPCR activity by a competitive immunoassay based on time-resolved fluorescence resonance energy transfer (TR-FRET) between the fluorescent reporter cAMP-d2 and anti-cAMP-cryptate using a cAMP dynamic 2 kit (Cisbio Bioassays). Cells were cultured in 96-well cell culture plates with a concentration at 26000 cells/well overnight at 37 °C with forskolin or with DMSO control. The medium was removed and lysis buffer (50 µl/well) supplied in the kit was added to lyse cells in the presence of 3-isobutyl-1-methylxanthine (IBMX- phosphodiesterase inhibitor). Then, 10 µl cell lysate/well was transferred to 384-well microplates followed by the addition of cAMP-d2 and anti cAMP- cryptate (5 µl each). Each cell line was measured in triplicate to account for variability as well as two separate experiments weeks apart to ensure no batch-to-batch variability. Incubation for 1 h at room temperature was followed by a read out with Analyst HT (Molecular Devices, LLC). Data processing and quantification of cAMP were performed according to the manufacturer's instructions.

Flow cytometry: Cells were washed with PBS, scraped and pelleted at 2000 RPM for 5 min and divided into flow cytometry tubes. 0.1 mL of Fixation/ Permeabilization solution was added to the cells (BD Bioscience Fixation/Permeabilization Solution Kit catalog no. 554714) and pulse vortexed. The cells were incubated for 1h at room temperature. Cells were washed with 0.1 mL of Permeabilization/Wash Buffer followed by centrifugation and decanting of supernatant. Cells were suspended in 0.2 mL of Permeabilization/Wash Buffer and the primary antibody was incubated (1:100) overnight at 4 °C. The cells were pelleted and washed 3X with 0.2 mL of Permeabilization/Wash Buffer and secondary antibody was incubated (1:200) at room temperature in the dark for 1h. The cells were pelleted and washed 3X with 0.2 mL of Permeabilization/Wash

Buffer and resuspended in Permeabilization/Wash Buffer for flow cytometry in Accuri C6 instrument.

Immunohistochemistry in cell pellets: Confluent cell cultures were collected, washed in PBS, and pelleted by centrifugation. Supernatant PBS was discarded and the washed cells were suspended in 1 mL of 10% formalin for 1 hour, followed by centrifugation and formalin removal. 1 mL 4% melted agarose gel was then added to the fixed, pelleted cells, which were immediately vortexed to create a uniform cell suspension and then briefly centrifuged to create an agarose-embedded cell pellet.

Canine tumor samples: Immunohistochemistry in paired metastatic and primary canine tumor samples: All tissue controls for antibody optimization and specificity of staining were obtained from canine necropsy specimens at the Veterinary Diagnostic Lab at the College of Veterinary Medicine, University of Illinois, Urbana-Champaign. The skin samples (negative control) were taken from a necropsy specimen without skin disease. The kidney samples (positive control) were taken from a necropsy specimen without kidney disease. Canine appendicular OS tissue blocks and their corresponding lung metastases tissue blocks were also retrieved from the University of Illinois Veterinary Diagnostic Laboratory for immunohistochemistry (IHC). Formalin-fixed, agarose-embedded cell pellets from the previously utilized cell lines were also processed into paraffin-embedded tissue blocks for IHC. Slides cut from the tissue blocks were deparaffinized in xylene and rehydrated in ethanol. Antigen retrieval was performed using Diva Decloacker (DV2004). Endogenous peroxidase activity was blocked using Peroxidazed 1 (PX968) for 5 minutes, followed by blocking of non-specific background staining using Background Punisher (BP974) for 10 minutes. Blocked slides were incubated with either anti-human CD147 (ab108317) for 1 hour and 15 minutes or anti-mouse CD44 (sc-18849) for 1 hour at dilutions of 1:100 and 1:50, respectively. CD147 slides were then incubated with a rabbit-on-canine horseradish peroxidase (HRP) secondary antibody (RC542) for 30 minutes and CD44 slides were incubated with a rabbit-on-rat HRP secondary antibody (61-9520) for 30 minutes at 1:100. The chromogen 3-3'-diaminobenzidine (DAB) (IPK5010) was applied for 5 minutes to develop slides, followed by counterstaining with Cat hematoxylin (CATHE). All steps were followed by washing in either wash buffer or DI water, as appropriate. Negative controls for the samples were processed

identically in the absence of primary antibody. Using ImageJ software, immunohistochemical-staining positivity was expressed as normalized pixel intensity per positive cell.

2.4 RESULTS

We chose two human and two canine isogenic cell lines for proteomic profiling. The human cell lines HOS (non-metastatic) and 143B (metastatic) have been established as clinically relevant orthotopic models for human OS [11]. Both HOS and 143B cells were derived from parent TE-85 cells through methylnitronitrosoguanidine (MNNG) or Ki-ras transformation respectively. The canine cells POS (non-metastatic) was derived from spontaneous canine osteosarcoma and HMPOS (metastatic) were established from five subcutaneous implantation cycles of lung tumor deposits [12]. We choose cell lines over tumor tissue in order to avoid heterogeneity in tissue samples obtained from tumor tissue [13]. The cell lines chosen here have been previously shown to be appropriate models for OS [11,12]. Additionally, since the cell lines are isogenic, it reduces the possibility of differential proteomic patterns arising due to different cellular origins. Finally, to avoid differences due to nutritional treatment, all cells were harvested at 80-90% confluency, and the samples utilized for different methods of detection as described below.

The overall workflow is outlined in Figure 2.A. Briefly, the cells were scraped instead of trypsinizing to maintain the integrity of cell surface proteins. The plasma membrane fraction was enriched by aqueous two phase extraction protocol in order to remove cytoplasmic contaminants that may overwhelm the signal from low-population PM proteins. Subsequently peptide fingerprinting was done that provided a list of proteins that was then classified by function to identify global proteomic changes (Table ST1- ST4 in Appendix II).

Proteomic profiles from peptide fingerprinting:

Peptide fingerprinting is a high throughput method that provides a list of proteins and their relative abundances. For each sample set, 10 µg of protein from each set was taken to analyze as indicated in the materials and methods section to remove any differences that may arise due to different quantities of proteins used for each sample. This is the first control towards standardizing the protein abundance. Peptide fingerprinting provided a list of over ~500 proteins per cell line. It is a semi-quantitative technique and provides the relative amount of specific proteins in a given mixture through a measure of the exponentially modified protein abundance index (emPAI) [9] as explained in the materials and methods section. Other similar measures include spectral counts

and peptide counts. The emPAI value can help understand the overall protein composition of the membrane. However, it is not a consistent measure across various samples. Thus, two different methods were used for standardizing the emPAI aside from loading the same amount of protein initially. Each proteins individual emPAI was normalized to the total emPAI of that set. Furthermore, trends of proteomic distribution can be compared in the human and canine sets across the two species. It is important to note that many proteins were undetectable as they present in low abundance and is below p value of 0.05, which was set as a significance cut-off for matching the peptide fingerprinting results to the MASCOT database. The analysis of the peptide fingerprinting data, as seen in Figure 2.1, revealed various interesting trends that are discussed below. The corresponding calculations are represented in Table 2.1. The peptide fingerprinting protocol was used only to generate a list of potential candidates and therefore not replicated. Statistical significance from peptide fingerprinting was only utilized to filter out targets that have questionable peptide match and therefore may not be valid targets. The candidates of interest were taken forward for downstream validations where each biochemical validation was replicated for at least n=3.

Structural proteins: The structural proteins form the largest class of proteins in the membrane proteome (1 and Table 2.1). They play various roles including maintenance of cell shape, adhesion, and migration. In our proteomic data, we observed several different structural proteins that are differentially regulated as discussed below.

Intermediate filaments: We observe a significant increase in the total content of intermediate filaments (Figure 2.2 and Table 2.1), which comprises of mainly keratins and vimentin. Vimentin is a marker for the epithelial to mesenchymal transition in various epithelial cancers and has been discussed in further detail in the validation of targets section below.

Collagens: Collagens are important constituents of the extracellular matrix. The increase of collagen expression in the tumor microenvironment has been correlated with tumor progression [14]. We observed an overall increase in the amount of collagens in both metastatic cell lines as compared to the non-metastatic cell lines. In human cells, there was a 48% increase in the collagen content of metastatic cells versus non-metastatic cells. Likewise, in the canine cell lines, the metastatic cells expressed 46% more collagen than the non-metastatic cells (Figure 2.2).

Annexins: Annexins A1, A2 and A5 have been found on the cell surface and are involved in membrane scaffolding and are responsible for anchoring several membrane proteins. In our studies, in both cell lines the metastatic cells produce only about half the annexin A1 as the non-metastatic (Table 2.2). This agrees with previous literature where reduced Annexin A1 expression was significantly associated with advanced breast cancer [15].

Annexin A2 is a calcium-dependent, phospholipid-binding protein. It plays multiple roles in regulating cellular functions, including angiogenesis, proliferation, apoptosis, cell migration, invasion and adhesion. It has been implicated in several cancers [16-19]. The upregulation of annexin A2 in various cancers is 5.74, the metastatic HMPOS show values of 8.63 (Table 2.2). However, with the human cell lines, a reverse trend is observed. The non-metastatic HOS line has an emPAI value of 36.85, whereas the metastatic 143B cells show 17.11 emPAI (Table 2.2).

Immune markers: Immunological eradication of cancer is an important function of the immune system. This is evident from literature that indicates that cancer cells downregulate their immune markers to evade this response [20]. The major histocompatibilty complex (MHC) is a key component of the immune system. Our findings through peptide-fingerprinting mass spectrometry show a significant change in the expression levels of MHCs and immunoglobulins within the metastatic and non-metastatic human cells. The overall expression of immune-related proteins reduces approximately 80% in human metastatic cell line and about 50% in the canine metastatic cell line (Figure 2.3B). A much lower density of MHC class I is also observed in the metastatic versus the non-metastatic cells. In the human lines, 143B expresses only 0.10 times MHC Class I than HOS, and in the canine lines the expression of MHC Class I in HMPOS was not detectable for $p<0.05$ whereas POS expression was detected. The down regulation of MHC class of molecules has been intrinsically linked to cancer as it assists in tumor immune escape [21]. Specifically in OS, the down regulation of MHC class I has been shown in patient samples and it is suggested that it restricts cytotoxic T lymphocyte pathway, which plays a major role in immune surveillance of patients with OS [22].

G proteins and GPCRs: G-protein coupled receptors (GPCRs) are a large family of cell-surface receptors that are responsible for signal transduction in a large number of cellular processes. Malignant cancer cells are known to hijack the normal physiological functions of GPCRs to survive, proliferate autonomously, evade the immune system, increase blood supply, invade their

surrounding tissues and disseminate to other organs. Increased GPCR expression has been observed in various cancers including breast cancer [23]. Herein we observe an overall increase in percentage of GPCRs from 7% of total proteins identified in HOS cells to 18% of total in the human metastatic143B cells (Figure 2.3A). A similar trend, albeit of smaller magnitude, is observed for the canine lines, where 11% of total proteins identified are GPCRs in POS cells and 13% of total identified in HMPOS (expression difference in the human lines and canine lines is depicted in Figure 2.3A).

A class of small G-proteins, the RAS family, has also been implicated in several oncogenic processes [24] and is the most common gene mutation observed in various cancers [25]. This is supported by our proteomics results where a significant overexpression of KRAS is observed in the metastatic cells versus the non-metastatic cells in both human and canine lines (Table 2.2). KRAS expression was also validated for the four cell lines by western blotting (Figure 2.4), which shows significant overexpression in the 143B cells versus the HOS cells. However, the differences between the canine cell lines in KRAS by western blotting were not significant.

Finally, a specific class of GPCRs that has been aberrantly been linked to cancer are olfactory receptors (ORs). Initially thought to be an anomaly, genes responsible for ORs showing significant mutation have been observed in various cancers [26-28]. Our findings also suggest an increase in the overall expression of ORs in the metastatic cell line as compared to the non-metastatic cell lines... In our peptide fingerprinting results OR7D2 and OR4N4 were observed in the 143B cell membrane proteome and OR4C11 and OR4C16 were identified in HMPOS membrane proteome. There were no ORs identified in the corresponding non-metastatic cells HOS and POS at $p<0.05$, which was set for our peptide fingerprinting data.

GPCR activity assay: Peptide fingerprinting indicated that GPCR levels are overall upregulated in metastatic vs. non-metastatic cells. To investigate whether the expression levels correspond with a concomitant increase in activity, a GPCR activity assay was performed. Cyclic AMP (cAMP) is a secondary messenger of several GPCR pathways- the Gi and Gs, and thus cAMP levels were measured as an indicator of GPCR activity. Briefly, cells were stimulated with forskolin (stimulates Gs class of G-proteins) or DMSO and then lysed, and cAMP was measured by a TR-FRET-based method. As seen in Fig 2.5, the overall levels of cAMP were significantly higher in

143B and HMPOS cells as compared to their non-metastatic counterparts, HOS and POS, respectively, indicating higher metastatic activity is accompanied by increase in GPCR activity.

Receptors and Transporters:

Integrin β1: Integrins are a family of transmembrane glycoprotein receptors that mediate cell-matrix and intercellular interactions [29]. Integrins play a key role in the invasion process by inducing various matrix metalloproteinases (MMPs) and lead to the breakdown of extracellular matrix (ECM). We observed an increase in integrin β1 expression in the metastatic human cell line by nearly 1.5 times as compared to the non-metastatic line (Table 2.2). No integrin β1 was observed in the canine lines at $p< 0.05$ in the peptide fingerprinting data. CD98 is known to associate with integrin signaling and thereby increase cell growth and proliferation [30,31].

CD147: Tumors interact with their microenvironment through enzymes known as matrix metalloproteinases (MMP). CD147, also known as Basigin, is an MMP inducer that is overexpressed and promotes tumor progression, invasion, and metastasis by stimulating MMP secretion [32,33]. Due to the pivotal role of CD147 in cancer, this molecule has been termed a cancer-associated biomarker [34] and serves as a target for cancer therapy [35]. In our studies we also observed an increase in CD147 expression in the metastatic lines for both species. In the human cells, there was a 1.6-fold increase in CD147 expression, whereas in the canine cells there was a greater than twofold increase in expression which was further validated by western blotting and confocal microscopy. Interestingly, CD147 is known to be associated with increased expression of monocarboxylate transporter (MCT) expression in various cancers including cervical carcinoma [33,36]. Our results corroborate this, with the increased expression of MCT1 by over twofold for the human lines. In the canine lines, POS expression of MCT1 was not detectable for $p<0.05$; however, the metastatic HMPOS line shows expression. These insights can lead towards targeting not only specific proteins but also cellular pathways that are involved in increasing the metastatic potential of the cells. Due to potential implication of CD147 in therapy, this target was further validated by biochemical methods as indicated in the validation section.

CD44: CD44 is a multifunctional cell surface glycoprotein involved in cell proliferation, cell differentiation and cell migration. The crucial involvement of this protein in cell processes makes it highly important in the pathologic state of cancer cells. In our studies, we observed CD44 to be upregulated in metastatic cell lines. In human cells, it was 1.3 times in 143B cells versus HOS

cells. In canine cells, while no CD44 was detected for POS at $p<0.05$, a value of 0.16 was observed for HMPOS cells. Previously in OS, a higher level of CD44 has been shown to correlate with poor prognosis (42).

CD98: CD98 or 4F2 antigen is a large neutral amino acid transport protein that has been implicated in various cancers [37,38]. In our results, we observed a 1.2-fold increase in the metastatic human cell line for CD98 expression. In the canine lines, CD98 was not detected in the non-metastatic line but it was detected in the metastatic line indicating an increase. In OS, increased expression of CD98 has been observed in patient samples [39].

Validation of selected targets using western blots and confocal microscopy: Several differentially regulated targets were further validated as seen in Table 2. Three targets that were validated by western blotting and confocal microscopy are: CD44, CD147 and vimentin. These targets were chosen due to their implications in various other cancers. For western blotting samples, since the samples are membrane fractions and not whole cells, housekeeping proteins like GADPH and beta-actin do not present themselves as ideal controls. Thus Ponceau staining was used as a loading control as has been indicated in materials and methods. In general 5 µg of total protein was loaded for CD44 and CD147 in each trial and 1 µg was loaded for vimentin in each trial. A total of n=3 was performed for all western blotting samples and n=2 was performed for confocal microscopy. The quantification for confocal microscopy images is shown in Figure 2.8.

CD44: In our studies, we observed CD44 to be upregulated in metastatic cell lines. In human cells, it was 1.89 times in 143B cells versus HOS cells. In canine cells, while no CD44 was detected for POS at $p<0.05$, a value of 0.12 was observed for HMPOS cells. We validated CD44 in both human and canine cells by western blotting and confocal microscopy. As observed in Figs 2.6A and 2.7A, a strong upregulation of CD44 is observed when evaluated using the two detection methods.

CD147: In our peptide fingerprinting data we observed an increase in CD147 expression in the metastatic lines for both species. In the human cells, there was a 1.6-fold increase in CD147 expression, whereas in the canine cells there was a greater than twofold increase in expression which was further validated by western blotting and confocal microscopy. As seen in Figs 2.6B and 2.7B, an increased expression of CD147 is observed in the metastatic versus non-metastatic cell lines.

Vimentin: Vimentin is an intermediate filament expressed in mesenchymal cells and is responsible for maintenance of cell shape and integrity, migration, and adhesion. In our results, we observed a 1.2-fold increase in vimentin expression in the human cell lines and an over threefold increase in vimentin expression in canine metastatic cell lines. This target was validated by western blotting and confocal microscopy and as shown in Figs 2.6C and 2.7C, these results corroborate our findings from peptide fingerprinting analysis.

Validation of selected targets using immunohistochemistry in paired primary and metastatic canine tumor samples: Using western blots and confocal microscopy, we validated the upregulation of three targets that can also observed to be upregulated-using peptide fingerprinting. Two of these targets, CD44 and CD147, were further investigated, as they are potential druggable targets. First, flow cytometry was performed. For each sample, flow cytometry was performed in triplicates for n=3. As observed from Figs 2.9A and 2.9B, in both human and canine cell lines, the metastatic cells showed higher levels of CD44 and CD147 as compared to the non-metastatic counterparts. Furthermore, immunohistochemical (IHC) analysis was performed for both CD44 and CD147 on formalin fixed cells for n=3. As observed in Fig 2.9C and 2.9D, the staining of CD44 and CD147 is greater on the metastatic cell lines 143B and HMPOS as compared to their non-metastatic counterparts. This is in agreement with our western blotting, confocal microscopy and flow cytometry data. The quantification is shown in Figure 2.10. This also indicates that no changes in staining trends are observed due to formalin fixation, which was done for cell pellets in immunohistochemistry (IHC) but not for other biochemical techniques.

The expression of these proteins was finally tested in paired primary and metastatic OS canine tissue samples to investigate whether the findings in cell lines corresponds with spontaneously-arising osteosarcoma tumors in pet dogs. For each antibody to be tested two distinct sets of paired primary and metastatic tissue samples were evaluated for PM protein expressions. Furthermore, five sections of each tissue were stained to account for tissue heterogeneity. As observed in Figs 2.11 A-B, for CD44 all the metastatic samples showed significantly higher staining intensity than their primary counterparts (A and B: $p < 0.05$). For CD147, the staining intensities in the patient samples also followed the trend as that of the cell lines. While samples from patient C did show higher CD147 expression in the metastatic ($p<0.01$), samples D showed metastatic staining greater than non-metastatic with $p=0.01$. The quantification is shown in Figure 2.12.

2.5 DISCUSSION

The discovery of biomarkers and targetable receptors in osteosarcoma is key to improving therapeutic outcomes of metastatic OS disease. Herein we use high throughput peptide fingerprinting to identify potential protein level differences between metastatic and non-metastatic OS. While traditional investigations in biomarker discovery have focused on the comparison of tumorigenic versus non-tumorigenic samples, this study investigates the more subtle differences between metastatic and non-metastatic samples. Metastasis is a major challenge in OS therapy since non-metastatic OS can be treated by limb-sparing surgeries but metastatic disease has poor five-year survival rates and is often fatal. Thus, identifying metastasis biomarkers for potential therapeutics is of great importance. Additionally, the subtle changes in protein expression profile between metastatic and non-metastatic cells, provides a deeper insights into the factors that are responsible for promoting the metastasis of OS.

Furthermore, we investigated the proteome of metastatic and non-metastatic canine OS cellular membrane and compared it to the proteome of human OS cellar membrane. Canine OS is spontaneously arising and could serve as closer animal model for human OS than mice in which the disease has to be induced. Additionally, a similar trend in metastasis biomarkers for both species can help advance parallel development of therapeutics. Furthermore, our cross-species study lends more support to the differentially regulated protein species that are identified through the peptide fingerprinting studies.

The high-throughput capacity of proteomics method allows analysis of targets more rapidly than traditional biochemical methods like western blotting and flow cytometry. Herein, the semi-quantitative peptide fingerprinting method provided us with several protein candidates that were differentially expressed in the metastatic versus non-metastatic OS cell lines. While, proteomic approaches have been utilized for biomarker discovery in various cancers, its use has been limited in OS due to difficulty in protein collection from bone tissues. To circumvent this problem, a few studies have performed peptide fingerprinting on cell lines, comparing tumor cells versus osteoblasts [6,7,40]. These studies have provided valuable insight into the membrane proteome of OS cells and identified key biomarkers including NDRG1 and EPHA2. In this study, the membrane proteome of metastatic and non-metastatic OS cells were subject to peptide fingerprinting.

There are several important steps in metastasis including uncontrolled proliferation, motility, invasion and survival in vasculature that are mediated by interaction of signaling molecules with membrane proteins. Membrane proteins are known to be differentially regulated in cancerous states [41]. Membrane proteins are important components of the cell and form the largest class of drug targets. They form the gateway of the cells and control the influx and efflux of multiple signaling molecules. They are responsible for multiple functions including adhesion, cellular remodeling, proliferation and migration, several of which are significantly altered between normal and tumorigenic cells. Membrane proteins can be classified into various major classes including structural proteins, GPCRs, receptors (not including GPCRs), transport proteins, proteins responsible for immune responses and other smaller classes like enzymes.

GPCRs are a large class of PM receptors. The aberrant overexpression of GPCRs and their autocrine and paracrine activation by agonists released by tumor cells is one of the most frequent strategies used by cancer cells to develop and maintain their metastatic phenotype. While GPCRs constitute over 50% of current drug targets [42], the GPCRs targeted for cancer therapy are very few [43]. Various GPCRs including KRAS have shown to dysregulate the MAPK pathway and result in uncontrolled proliferation [44]. In our studies, in both species the metastatic cell lines showed an overall increase in GPCR content and this was also reflected in our GPCR activity assay. In this assay, the Gs class of receptors when stimulated by forskolin showed heightened cAMP production for both metastatic cell lines as compared to the non-metastatic cells.

Furthermore, proteins that formed an essential component of the ECM such as collagen were found to be differentially regulated, as degradation of the ECM and cell motility is a key step in the metastatic process. Overall collagens increased in both metastatic cell lines. Collagen regulates extracellular martrix (ECM) remodeling through matrix metalloproteinases (MMPs) [45]. It has been shown that in OS, the synthesis and activation of MMP-2 is affected by interactions between OS cells and collagen I. Proteins that promote the invasion of the vasculature, for example integrin β1, were also identified as upregulated. Interestingly, in OS, integrin α2β1 has shown to be correlated with increased invasion through its interaction with collagen 1 [46]. In the same study, cells forced to overexpress the α2 subunit was not sufficient to increase tumorigenesis implicating the involvement of the β1 subunit [46].

Proteins involved in the degradation of ECM, CD147 and MCT1, were also found to be upregulated in the metastatic cell lines. CD147 expression in the various cell lines was also validated through downstream biochemical techniques. Although no drugs are clinically available for targeting CD147, progress has been made towards the use of siRNA in targeting CD147 in human malignant melanoma [47].

Finally, a downregulation of immune complexes was observed in the metastatic cell lines as compared to the non-metastatic cell lines was also observed in our results. As cancerous cells try to evade the immune response, there is downregulation of the major histocompatibility complex. Lower expressions of MHCs, specifically MHC class I, have indicated less-favorable prognoses of various cancers [48].

In this work, we validated three proteins from different functional classes, by western blotting, flow cytometry, confocal microscopy and cell pellet IHC, as a representative set to show that results from proteomics hold true in low-throughput biochemical methods. CD147 has been discussed with respect to its importance in the metastatic process as well as possible therapeutic routes. CD44 and vimentin were the other two proteins which were significantly upregulated in both human and canine metastatic cells as compared to their non-metastatic counterparts. CD44 is a cell surface glycoprotein that has been implicated in various cancers. It is hypothesized that the poor prognosis to increased chemoresistance as mediated with its interaction with its ligand hyaluronic acid. However, the correlation of CD44 expression to prognosis and disease outcome has not been clearly established. Whereas in renal cell carcinoma a high expression level of CD44 is related to poor outcome [49], in ovarian cancer overexpression of CD44 is related to favorable prognosis [50]. Moreover, in breast cancer CD44 has been related to both tumor suppression and promotion [51]. Vimentin overexpression, on the other hand, is a marker of epithelial to mesenchymal transition in cancers of epithelial origin, like breast cancer. However, in sarcomas, the role of vimentin as a tumor marker has not been explored deeply due to its ubiquitous expression. Recent work has shown that Withaferin A targets vimentin in soft tissue sarcomas resulting in vimentin cleavage and apoptosis [52], increasing the promise for vimentin as a target in cancers of mesenchymal origin.

Finally, the results were validated in spontaneously arising osteosarcoma tumors in dog. For these studies, paired primary and lung metastasized samples from canine patients were utilized. The

importance of using paired samples is to avoid any differences due to genetic differences in results. The results obtained show that in vitro cell culture proteomic studies followed by validation did correspond with the expression levels in canine patient samples. The CD44 results agreed very well with our small set of patient samples, the staining of CD147 in patient samples was not as intense as that in cell lines, although it was upregulated in the metastatic tumor as compared to the primary tumor.

This work is a proteomic profiling of human and canine membrane proteome and indicates that the upregulation of specific proteins follows the same trend. This has been verified in a limited number of canine paired primary and metastatic samples. However future work will focus on the verification of these targets, and other targets in a greater number of paired primary and metastatic canine tissues as well as human tissue samples. While it is anticipated that the upregulation will not be the same fold across all samples, the trends are expected to remain constant.

While cell lines only represent one part of the tumor microenvironment, tumors themselves present a significant level of heterogeneity. This microenvironment is also responsible for tumor development and progression through the interaction of the ECM, signaling molecules, immune system and other cell populations. The modeling of such environments to investigate their effects on the proteomic signature of cancer cells has been a subject of recent interest [53]. It is likely that these interaction will alter the proteomic profile of the tumor cells in both primary as well as metastatic tumors. Conversely, the presence of the tumor will also affect the environment and biomarker discovery from tumor microenvironment has also been explored [54].

To further explore the proteomic profile of cancer cells in orthotopic models, the study can be extended to animal models of the disease. While murine models are not the best models for osteosarcoma, since they do not develop spontaneous tumor and tumors have to be induced, they do provide a platform for testing out preliminary hypotheses. The cell lines used in this study have been previously shown to be a clinically relevant orthotopic model for human osteosarcoma because their tumor progression and metastasis development in mice, mimic the clinical scenario [11]. These studies will provide more evidence for the studies to be extended tocompanion animals that show more similar proteomic profile as humans, such as dogs, and will allow for a parallel development of therapeutics for both species.

2.6 CONCLUSIONS

This study describes a cross-species comparison of PM proteins of metastatic and non-metastatic OS. We have shown that the global membrane proteomes of canine and human OS show significant preferential regulation of various proteins, which agrees with results in genetic expression levels. Furthermore, the cross-species comparison allows greater confirmation that dogs can be utilized as a model for human OS. It also offers a platform for the development of therapeutics for both species. We identified various differentially regulated proteins that were validated downstream by biochemical techniques including western blotting, flow cytometry and confocal microscopy. CD44, CD147 and vimentin were identified as significantly upregulated in both human and canine OS. The results were also confirmed by IHC in spontaneously arising osteosarcoma tumors samples.

2.7 ACKNOWLEDGEMENTS

We thank Dr. Peter Yau and the Roy J. Carver Biotechnology Center, Protein Sciences Facility, for assistance with peptide fingerprinting.

2.8 FIGURES, TABLES AND LEGENDS

Table 2.1: Table shows the percentage of proteins in each category in each cell membrane. Table 1 represents the calculations reflected in Fig 1. HOS and POS are the non-metastatic human and canine cell lines and 143B and HMPOS are the metastatic human and canine cell lines respectively.

	HOS	**143B**	**POS**	**HMPOS**
Structure	63.48	56.68	49.11	56.01
Transport	3.41	2.46	14.82	6.59
Immune Complexes	15.69	11.09	2.26	0.62
G protein and GPCRs	6.74	18.3	10.99	13.02
Chaperones	1.6	1.47	3.61	5.89
Receptors	3.19	4.88	2.57	3.24
Enzymes	4.23	1.35	8.52	9.4
Others	1.66	3.77	8.11	5.24
Total	100	100	100	100

Table 2.2: Table shows the relative emPAI of selected differentially regulated proteins in the human and canine osteosarcoma cells. HOS and POS are the non-metastatic human and canine cell lines and 143B and HMPOS are the metastatic human and canine cell lines respectively. emPAI of each protein is normalized to total emPAI. The ratios 143B/HOS and HMPOS/POS show fold change in expression.

Protein	**HOS**	**143B**	**143B/ HOS**	**POS**	**HMPOS**	**HMPOS/ POS**
Keratin Type 1	2.31	4.31	1.87	2.99	3.80	1.27
Keratin Type 2	0.30	2.48	8.30	2.48	3.41	1.38
Vimentin	6.06	7.20	1.19	4.34	13.69	3.16
Annexin A1	0.86	0.45	0.52	1.91	1.01	0.53
Annexin A2	36.85	17.11	0.46	5.74	8.63	1.50
MHC Class I	2.73	0.28	0.10	0.15	0.00	0.00
KRAS	0.40	1.53	3.80	0.05	0.24	4.48
CD44	0.17	0.33	1.30	0.00	0.16	
CD 147 (Basigin)	0.42	0.67	1.6	0.22	0.46	2.12
Monocarboxylate transporter I	0.07	0.11	1.46	0.00	0.09	
CD 98	0.15	0.18	1.20	0.00	0.07	
Integrin β1	0.21	0.30	1.47	0.00	0.00	0.00

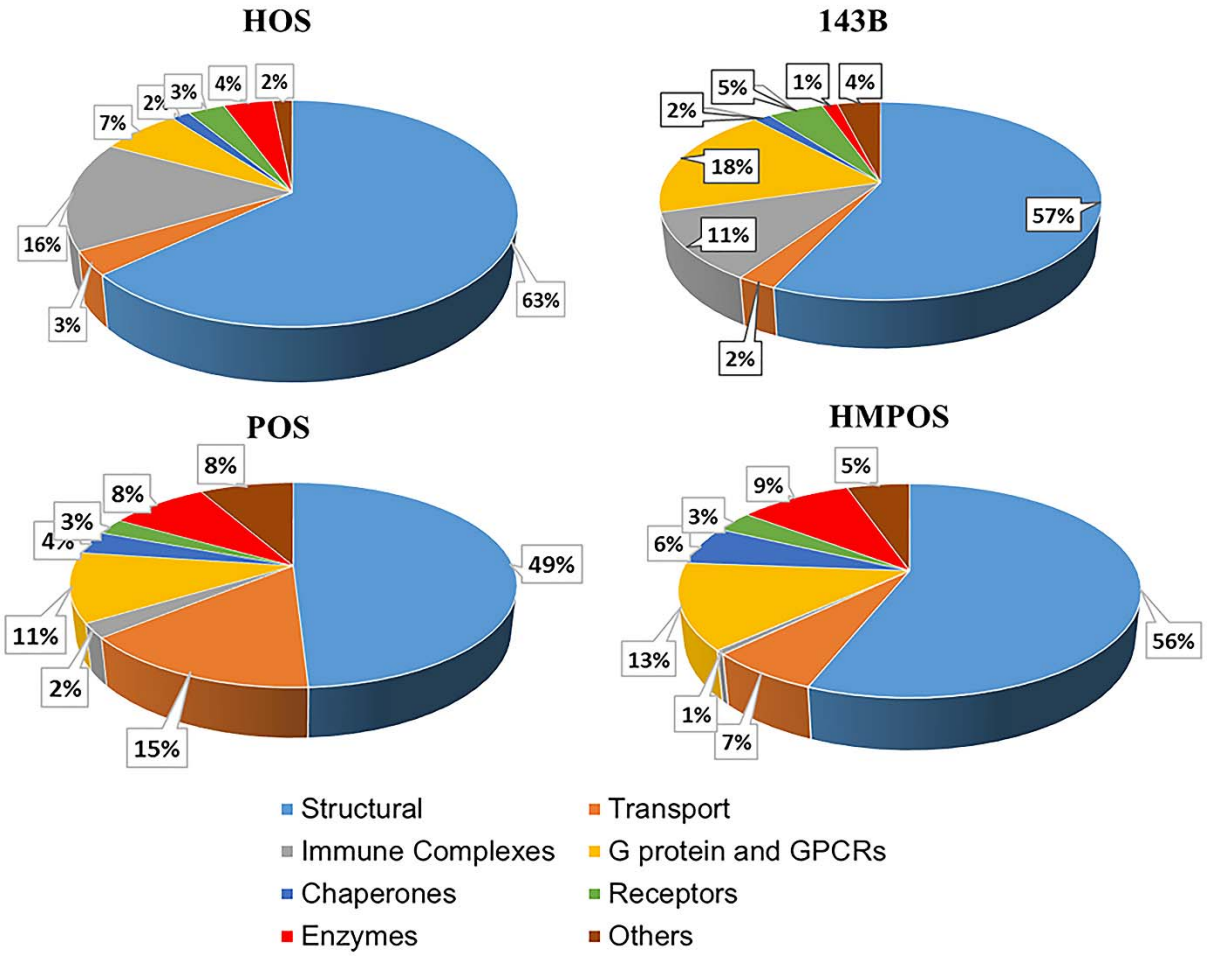

Figure 2.1: Figure shows global membrane proteomic composition across various cell lines classified according to function. The colors are as mentioned in the key. HOS and POS are the non- metastatic human and canine cell lines and 143B and HMPOS are the metastatic human and canine cell lines respectively.

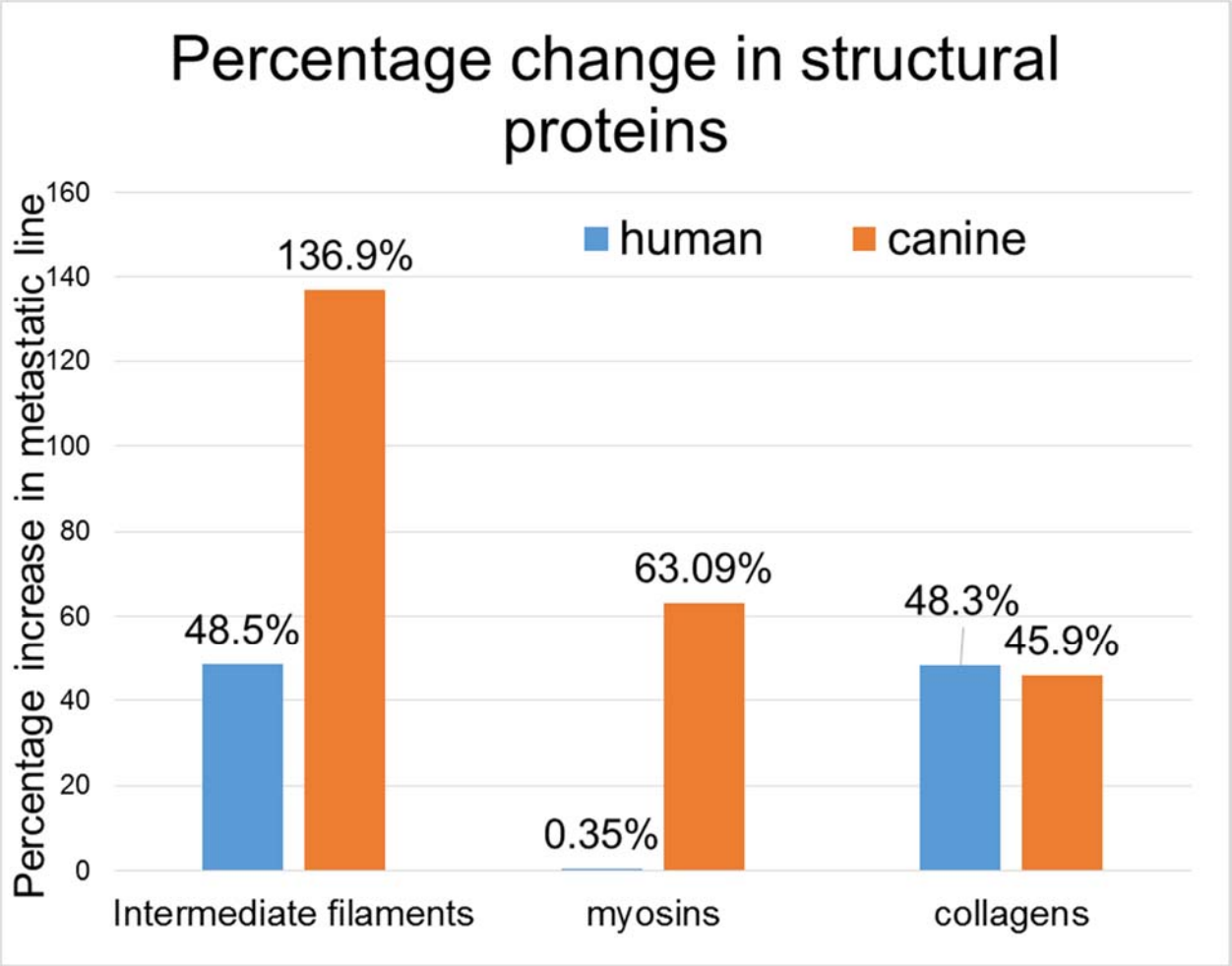

Figure 2.2: Relative expression of structural proteins in metastatic versus non- metastatic cells as observed by peptide fingerprinting. The percentage increase in the expression in the metastatic cells as compared to the corresponding non-metastatic cells is represented.

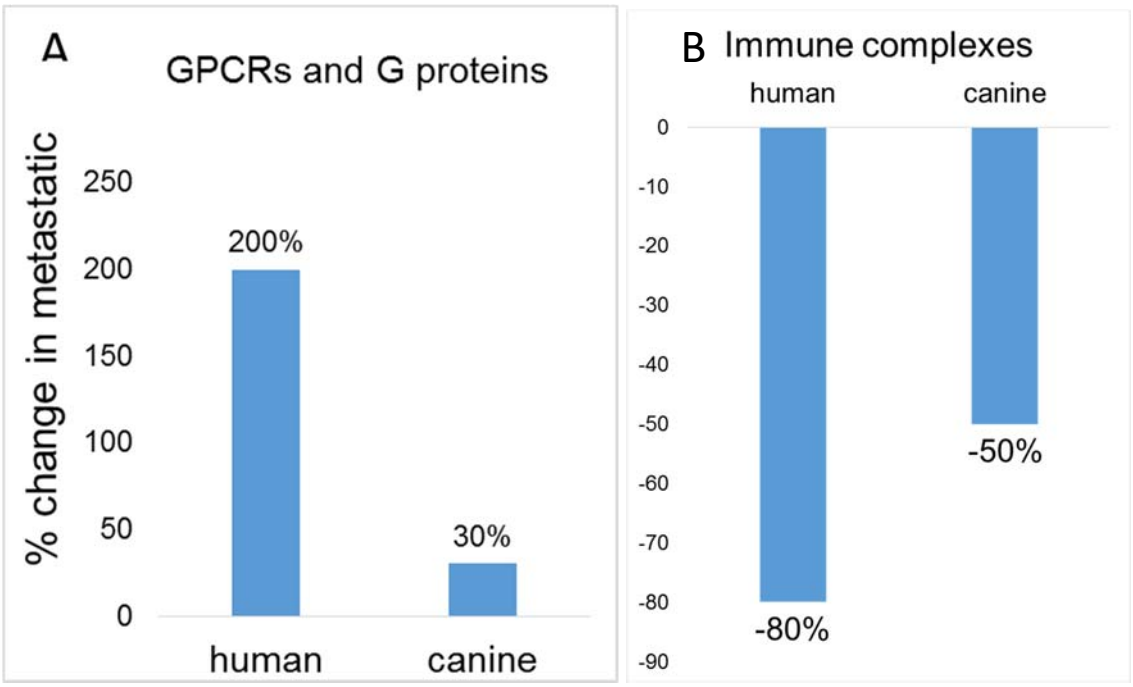

Figure 2.3: Change in expression of (A) Immune complexes and (B) GPCRs in metastatic versus corresponding non-metastatic cells

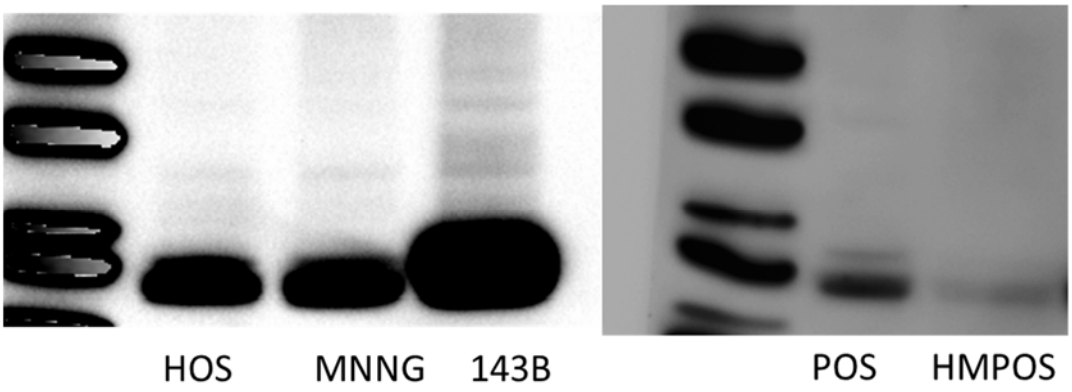

Figure 2.4: Western blot showing overexpression of KRAS in 143B vs HOS. 143B shows greater expression of KRAS than HOS and MNNG (non-metastatic human OS cell line).

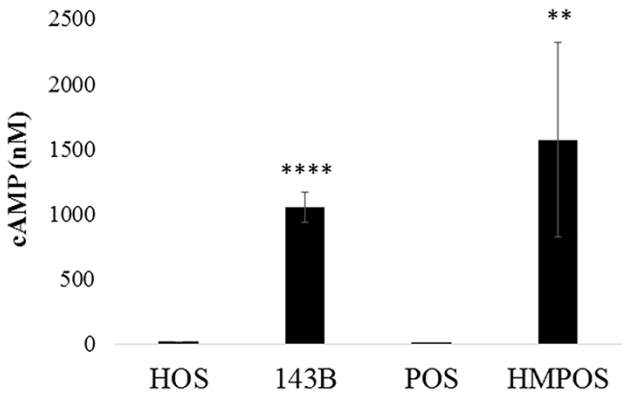

Figure 2.5: Figure shows the relative GPCR activity as measured by cAMP concentration. The experiment was performed in biological triplicates (and technical duplicates) with n=2 (total separate trials). **** $p < 0.0001$ and ** $p < 0.01$

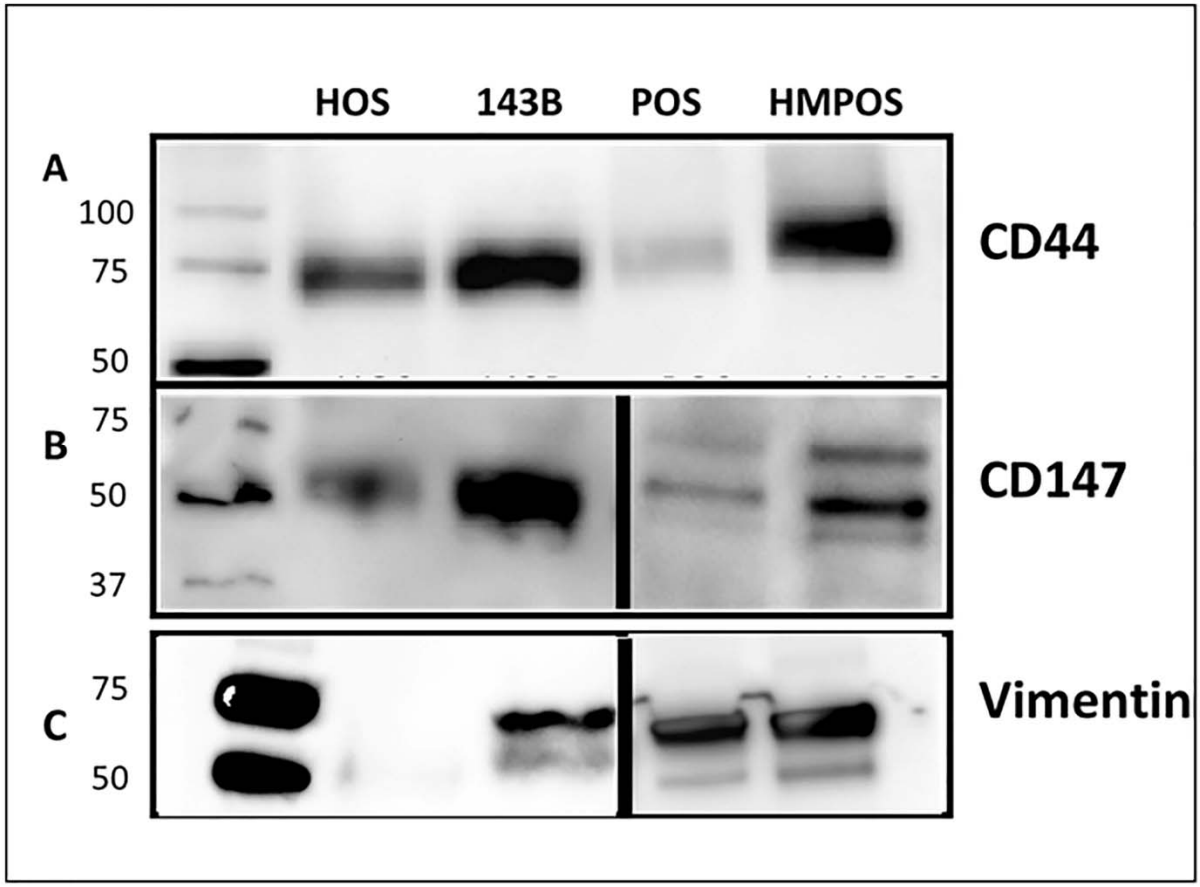

Figure 2.6: Western blot showing the expression of (A) CD44, (B) CD147 and (C) Vimentin. Lanes from left to right: ladder, HOS, 143B, POS and HMPOS. HOS and POS are the non-metastatic human and canine cell lines and 143B and HMPOS are the metastatic human and canine cell lines respectively.

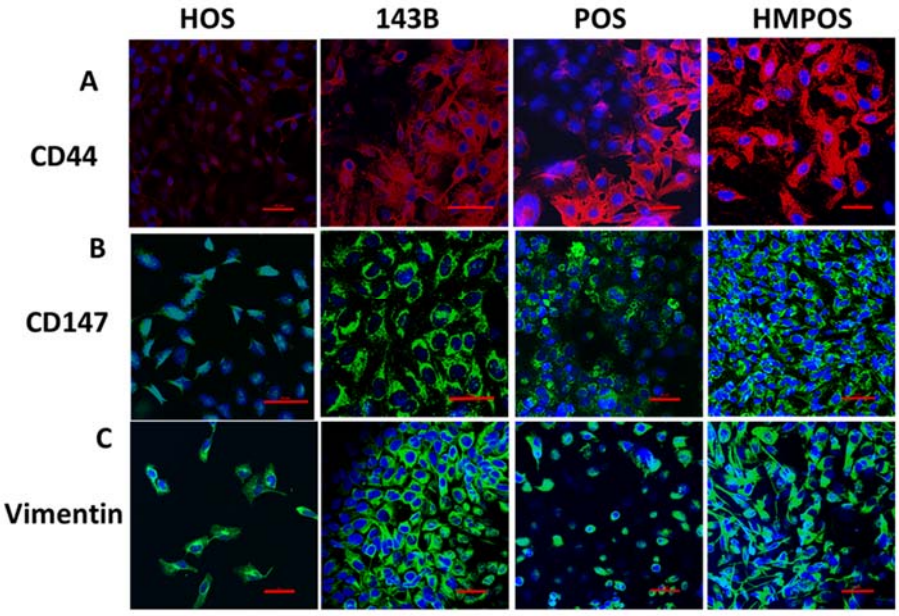

Figure 2.7: Confocal microscopy images showing the expression of (A) CD44, (B) CD147 and (C) Vimentin. HOS and POS are the non- metastatic human and canine cell lines and 143B and HMPOS are the metastatic human and canine cell lines respectively. Blue staining of nuclei with DAPI and red staining of CD44 with phycoerythrin secondary and green staining of Alexa Fluor 488 for CD147 and vimentin. Red bar in each section corresponds to 50 μm.

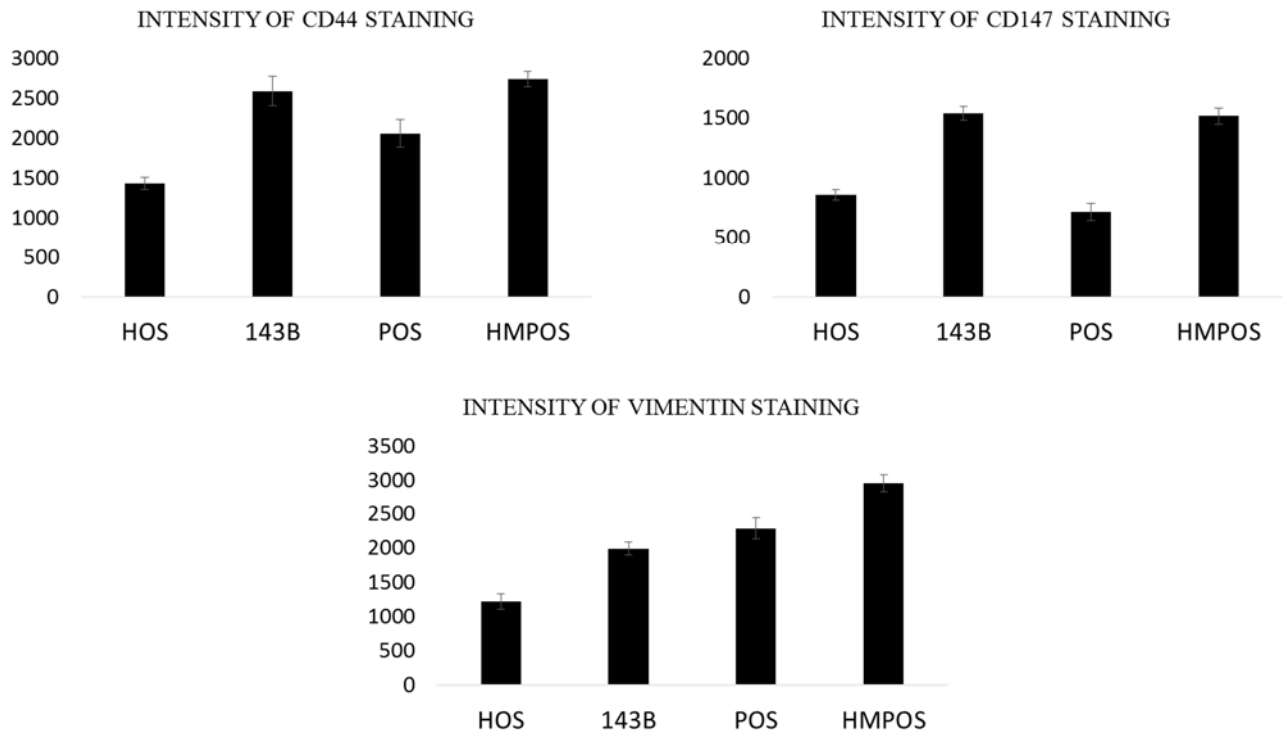

Figure 2.8: Fig shows the ImageJ quantification of confocal microscopy images. Quantification was performed by measuring staining intensity of 20 random cells each in 2 different slides. The images are Fig 4.

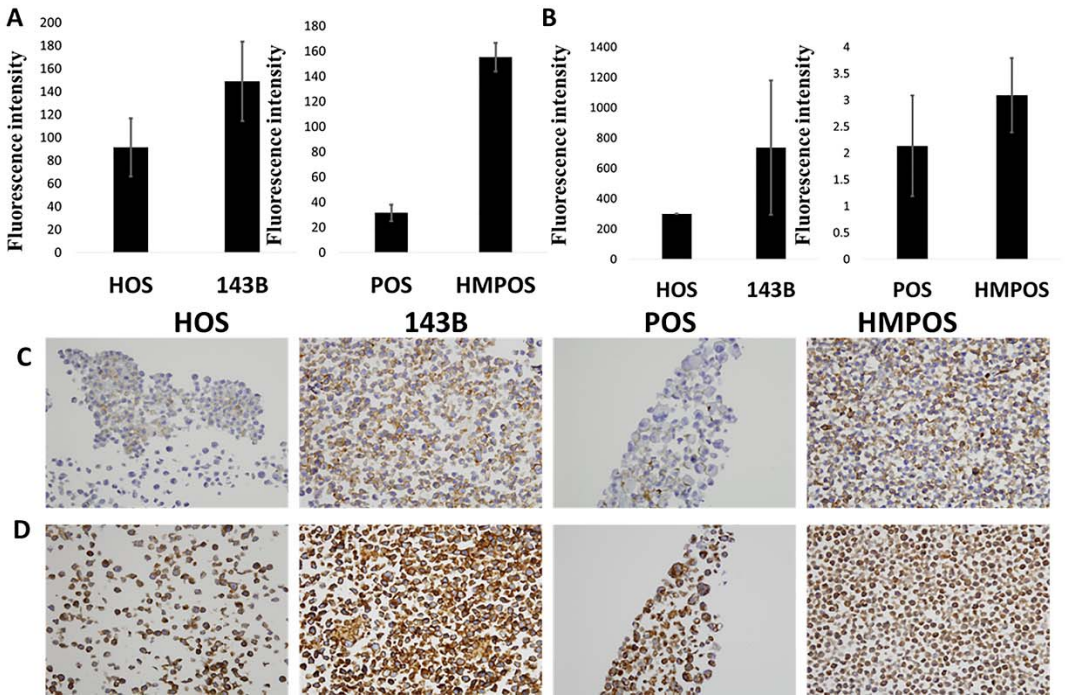

Figure 2.9: Flow cytometry fluorescence levels showing the expression of (A) CD44 and (B) CD147. Cell pellet immunohistochemistry showing the expression of (C) CD44 and (D) CD147. HOS and POS are the non- metastatic human and canine cell lines and 143B and HMPOS are the metastatic human and canine cell lines respectively.

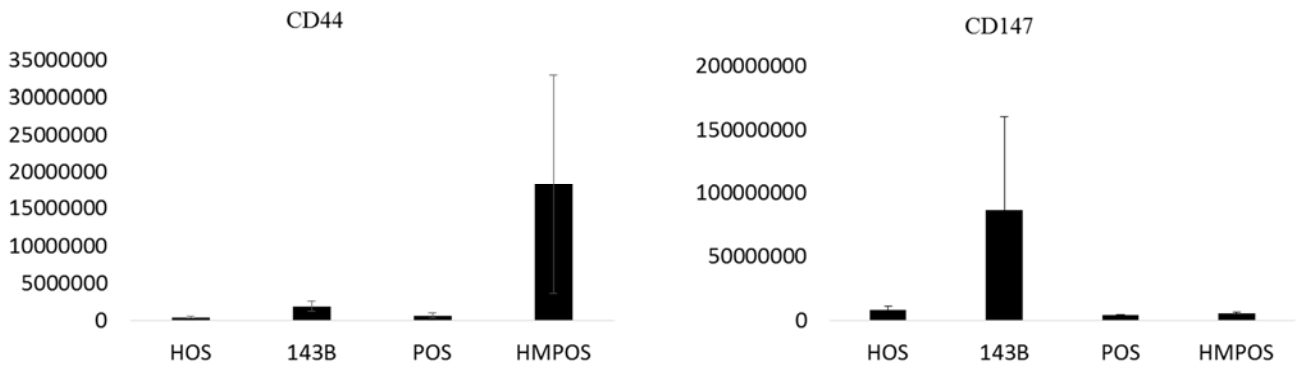

Figure 2.10: Image shows quantification of cell pellet immunohistochemistry. Images were quantified by using ImageJ and Adobe Photoshop. The images corresponding are Fig 5C and D. p values are as follows: CD44 human (HOS and 143B) p=0.07, canine (POS and HMPOS) p=0.17. CD147 human (HOS and 143B) p=0.2, canine (POS and HMPOS) p=0.17.

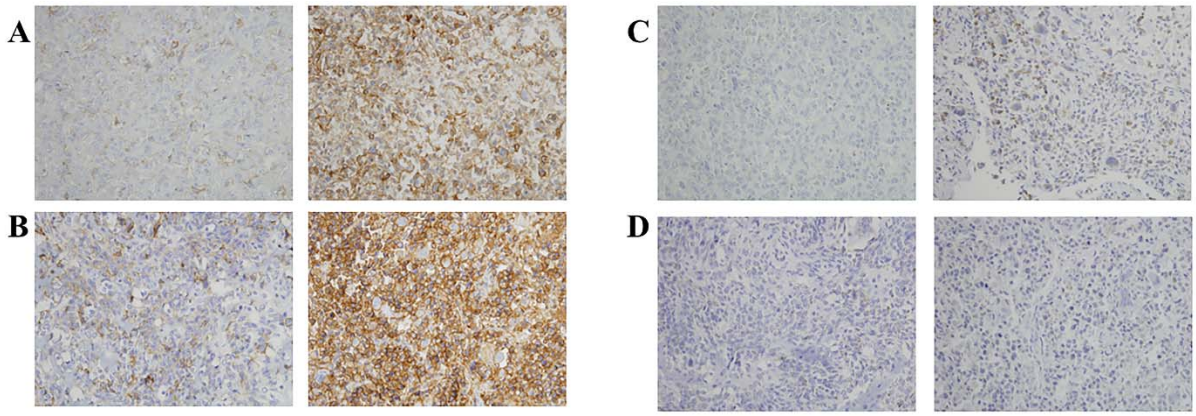

Figure 2.11: Immunohistochemistry of paired canine primary (left) and metastatic (right) in two different patient samples showing the expression of (A-B) CD44 and (C-D) CD147. p values for A and B $p < 0.05$ with metastatic > primary. p values for C $p < 0.01$ with metastatic > primary.

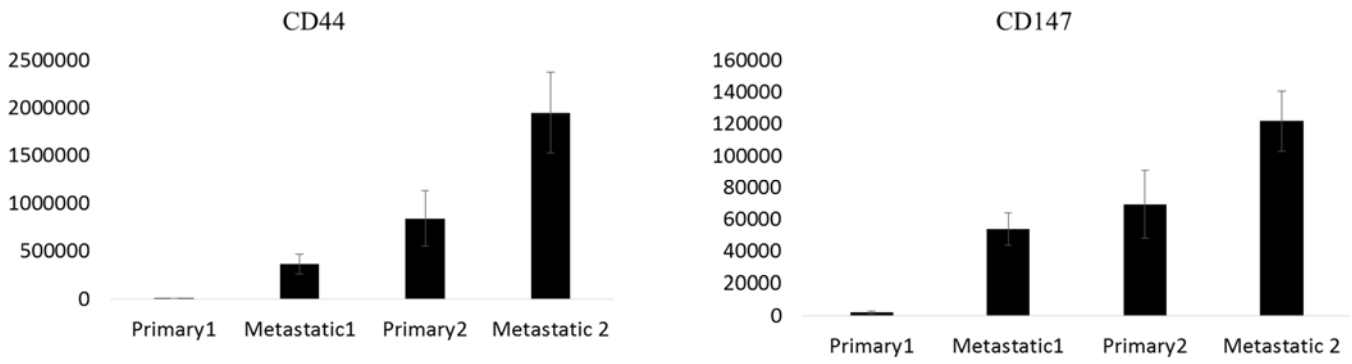

Fig 2.12: Image shows quantification of paired primary and metastatic tissue immunohistochemistry. Images were quantified by using ImageJ and Adobe Photoshop. The images corresponding are Fig 6. p values are as follows: CD44 primary and metastatic 1 p=0.01, primary and metastatic 2 p=0.03. CD147 primary and metastatic 1 p=0.003, canine primary and metastatic 2 p=0.01.

2.9 REFERENCES

1. Bielack SS, Kempf-Bielack B, Delling G, Exner GU, Flege S, Helmke K, Kotz R, Salzer-Kuntschik M, Werner M, Winkelmann W, Zoubek A, Jurgens H, Winkler K. Prognostic factors in high-grade osteosarcoma of the extremities or trunk: an analysis of 1,702 patients treated on neoadjuvant cooperative osteosarcoma study group protocols. Journal of clinical oncology : official journal of the American Society of Clinical Oncology. 2002;20(3):776-90. doi: 10.1200/jco.2002.20.3.776. PubMed PMID: 11821461.
2. Hughes DP. Strategies for the targeted delivery of therapeutics for osteosarcoma. Expert opinion on drug delivery. 2009;6(12):1311-21. doi: 10.1517/17425240903280422. PubMed PMID: 19761419; PubMed Central PMCID: PMC4163784.
3. Leth-Larsen R, Lund RR, Ditzel HJ. Plasma membrane proteomics and its application in clinical cancer biomarker discovery. Molecular & cellular proteomics : MCP. 2010;9(7):1369-82. Epub 2010/04/13. doi: 10.1074/mcp.R900006-MCP200
R900006-MCP200 [pii]. PubMed PMID: 20382631; PubMed Central PMCID: PMC2938092.
4. Kischel P, Guillonneau F, Dumont B, Bellahcene A, Stresing V, Clezardin P, De Pauw EA, Castronovo V. Cell membrane proteomic analysis identifies proteins differentially expressed in osteotropic human breast cancer cells. Neoplasia. 2008;10(9):1014-20. Epub 2008/08/21. PubMed PMID: 18714363; PubMed Central PMCID: PMC2517647.
5. Liu X, Zhang M, Go VL, Hu S. Membrane proteomic analysis of pancreatic cancer cells. J Biomed Sci. 2010;17:74. Epub 2010/09/14. doi: 10.1186/1423-0127-17-74
1423-0127-17-74 [pii]. PubMed PMID: 20831833; PubMed Central PMCID: PMC2949717.
6. Posthumadeboer J, Piersma SR, Pham TV, van Egmond PW, Knol JC, Cleton-Jansen AM, van Geer MA, van Beusechem VW, Kaspers GJ, van Royen BJ, Jimenez CR, Helder MN. Surface proteomic analysis of osteosarcoma identifies EPHA2 as receptor for targeted drug delivery. Br J Cancer. 2013;109(8):2142-54. Epub 2013/09/26. doi: 10.1038/bjc.2013.578
bjc2013578 [pii]. PubMed PMID: 24064975; PubMed Central PMCID: PMC3798973.
7. Zhang Z, Zhang L, Hua Y, Jia X, Li J, Hu S, Peng X, Yang P, Sun M, Ma F, Cai Z. Comparative proteomic analysis of plasma membrane proteins between human osteosarcoma and normal osteoblastic cell lines. BMC Cancer. 2010;10:206. Epub 2010/05/18. doi: 10.1186/1471-2407-10-206
1471-2407-10-206 [pii]. PubMed PMID: 20470422; PubMed Central PMCID: PMC2880991.
8. Paoloni M, Davis S, Lana S, Withrow S, Sangiorgi L, Picci P, Hewitt S, Triche T, Meltzer P, Khanna C. Canine tumor cross-species genomics uncovers targets linked to osteosarcoma progression. BMC genomics. 2009;10:625. doi: 10.1186/1471-2164-10-625. PubMed PMID: 20028558; PubMed Central PMCID: PMC2803201.
9. Ishihama Y, Oda Y, Tabata T, Sato T, Nagasu T, Rappsilber J, Mann M. Exponentially modified protein abundance index (emPAI) for estimation of absolute protein amount in proteomics by the number of sequenced peptides per protein. Mol Cell Proteomics. 2005;4(9):1265-72. Epub 2005/06/17. doi: M500061-MCP200 [pii]
10.1074/mcp.M500061-MCP200. PubMed PMID: 15958392.
10. Romero-Calvo I, Ocon B, Martinez-Moya P, Suarez MD, Zarzuelo A, Martinez-Augustin O, de Medina FS. Reversible Ponceau staining as a loading control alternative to actin in Western blots. Analytical Biochemistry. 2010;401(2):318-20. doi: Doi 10.1016/J.Ab.2010.02.036. PubMed PMID: ISI:000277397400021.
11. Luu HH, Kang Q, Park JK, Si W, Luo Q, Jiang W, Yin H, Montag AG, Simon MA, Peabody TD, Haydon RC, Rinker-Schaeffer CW, He TC. An orthotopic model of human osteosarcoma growth and spontaneous pulmonary metastasis. Clinical & experimental metastasis. 2005;22(4):319-29. doi: 10.1007/s10585-005-0365-9. PubMed PMID: 16170668.
12. Barroga EF, Kadosawa T, Okumura M, Fujinaga T. Establishment and characterization of the growth and pulmonary metastasis of a highly lung metastasizing cell line from canine osteosarcoma in nude mice. J Vet Med Sci. 1999;61(4):361-7. Epub 1999/05/26. PubMed PMID: 10342286.

13. Domcke S, Sinha R, Levine DA, Sander C, Schultz N. Evaluating cell lines as tumour models by comparison of genomic profiles. Nat Commun. 2013;4. doi: Artn 2126
10.1038/Ncomms3126. PubMed PMID: ISI:000323715900006.
14. Provenzano PP, Inman DR, Eliceiri KW, Knittel JG, Yan L, Rueden CT, White JG, Keely PJ. Collagen density promotes mammary tumor initiation and progression. BMC Med. 2008;6:11. Epub 2008/04/30. doi: 10.1186/1741-7015-6-11
1741-7015-6-11 [pii]. PubMed PMID: 18442412; PubMed Central PMCID: PMC2386807.
15. Wang LP, Bi J, Yao C, Xu XD, Li XX, Wang SM, Li ZL, Zhang DY, Wang M, Chang GQ. Annexin A1 expression and its prognostic significance in human breast cancer. Neoplasma. 2010;57(3):253-9. Epub 2010/04/01. PubMed PMID: 20353277.
16. Vishwanatha JK, Chiang Y, Kumble KD, Hollingsworth MA, Pour PM. Enhanced expression of annexin II in human pancreatic carcinoma cells and primary pancreatic cancers. Carcinogenesis. 1993;14(12):2575-9. Epub 1993/12/01. PubMed PMID: 8269629.
17. Sharma MR, Koltowski L, Ownbey RT, Tuszynski GP, Sharma MC. Angiogenesis-associated protein annexin II in breast cancer: selective expression in invasive breast cancer and contribution to tumor invasion and progression. Exp Mol Pathol. 2006;81(2):146-56. Epub 2006/04/29. doi: S0014-4800(06)00025-6 [pii]
10.1016/j.yexmp.2006.03.003. PubMed PMID: 16643892.
18. Mohammad HS, Kurokohchi K, Yoneyama H, Tokuda M, Morishita A, Jian G, Shi L, Murota M, Tani J, Kato K, Miyoshi H, Deguchi A, Himoto T, Usuki H, Wakabayashi H, Izuishi K, Suzuki Y, Iwama H, Deguchi K, Uchida N, Sabet EA, Arafa UA, Hassan AT, El-Sayed AA, Masaki T. Annexin A2 expression and phosphorylation are up-regulated in hepatocellular carcinoma. Int J Oncol. 2008;33(6):1157-63. Epub 2008/11/21. PubMed PMID: 19020748.
19. Inokuchi J, Narula N, Yee DS, Skarecky DW, Lau A, Ornstein DK, Tyson DR. Annexin A2 positively contributes to the malignant phenotype and secretion of IL-6 in DU145 prostate cancer cells. Int J Cancer. 2009;124(1):68-74. Epub 2008/10/17. doi: 10.1002/ijc.23928. PubMed PMID: 18924133.
20. Corthay A. Does the immune system naturally protect against cancer? Front Immunol. 2014;5. doi: Artn 197
10.3389/Fimmu.2014.00197. PubMed PMID: WOS:000354219200001.
21. Poschke I, Mougiakakos D, Kiessling R. Camouflage and sabotage: tumor escape from the immune system. Cancer Immunol Immunother. 2011;60(8):1161-71. Epub 2011/06/01. doi: 10.1007/s00262-011-1012-8. PubMed PMID: 21626032.
22. Tsukahara T, Kawaguchi S, Torigoe T, Asanuma H, Nakazawa E, Shimozawa K, Nabeta Y, Kimura S, Kaya M, Nagoya S, Wada T, Yamashita T, Sato N. Prognostic significance of HLA class I expression in osteosarcoma defined by anti-pan HLA class I monoclonal antibody, EMR8-5. Cancer Sci. 2006;97(12):1374-80. Epub 2006/09/26. doi: CAS317 [pii]
10.1111/j.1349-7006.2006.00317.x. PubMed PMID: 16995877.
23. Singh A, Nunes JJ, Ateeq B. Role and therapeutic potential of G-protein coupled receptors in breast cancer progression and metastases. Eur J Pharmacol. 2015;763(Pt B):178-83. Epub 2015/05/20. doi: 10.1016/j.ejphar.2015.05.011
S0014-2999(15)30008-X [pii]. PubMed PMID: 25981295; PubMed Central PMCID: PMC4784721.
24. Goodsell DS. The molecular perspective: the ras oncogene. Oncologist. 1999;4(3):263-4. Epub 1999/07/08. PubMed PMID: 10394594.
25. Downward J. Targeting RAS signalling pathways in cancer therapy. Nat Rev Cancer. 2003;3(1):11-22. Epub 2003/01/02. doi: 10.1038/nrc969
nrc969 [pii]. PubMed PMID: 12509763.
26. Lawrence MS, Stojanov P, Polak P, Kryukov GV, Cibulskis K, Sivachenko A, Carter SL, Stewart C, Mermel CH, Roberts SA, Kiezun A, Hammerman PS, McKenna A, Drier Y, Zou L, Ramos AH, Pugh TJ, Stransky N, Helman E, Kim J, Sougnez C, Ambrogio L, Nickerson E, Shefler E, Cortes ML, Auclair D, Saksena G, Voet D, Noble M, DiCara D, Lin P, Lichtenstein L, Heiman DI, Fennell T, Imielinski M, Hernandez B, Hodis E, Baca S, Dulak AM, Lohr J, Landau DA, Wu CJ, Melendez-Zajgla J, Hidalgo-

Miranda A, Koren A, McCarroll SA, Mora J, Lee RS, Crompton B, Onofrio R, Parkin M, Winckler W, Ardlie K, Gabriel SB, Roberts CW, Biegel JA, Stegmaier K, Bass AJ, Garraway LA, Meyerson M, Golub TR, Gordenin DA, Sunyaev S, Lander ES, Getz G. Mutational heterogeneity in cancer and the search for new cancer-associated genes. Nature. 2013;499(7457):214-8. Epub 2013/06/19. doi: 10.1038/nature12213 nature12213 [pii]. PubMed PMID: 23770567; PubMed Central PMCID: PMC3919509.
27. Flegel C, Manteniotis S, Osthold S, Hatt H, Gisselmann G. Expression profile of ectopic olfactory receptors determined by deep sequencing. PloS one. 2013;8(2):e55368. Epub 2013/02/14. doi: 10.1371/journal.pone.0055368
PONE-D-12-28987 [pii]. PubMed PMID: 23405139; PubMed Central PMCID: PMC3566163.
28. Sanz G, Leray I, Dewaele A, Sobilo J, Lerondel S, Bouet S, Grebert D, Monnerie R, Pajot-Augy E, Mir LM. Promotion of cancer cell invasiveness and metastasis emergence caused by olfactory receptor stimulation. PloS one. 2014;9(1):e85110. Epub 2014/01/15. doi: 10.1371/journal.pone.0085110
PONE-D-13-17161 [pii]. PubMed PMID: 24416348; PubMed Central PMCID: PMC3885679.
29. Hynes RO. Integrins: versatility, modulation, and signaling in cell adhesion. Cell. 1992;69(1):11-25. Epub 1992/04/03. doi: 0092-8674(92)90115-S [pii]. PubMed PMID: 1555235.
30. Fenczik CA, Sethi T, Ramos JW, Hughes PE, Ginsberg MH. Complementation of dominant suppression implicates CD98 in integrin activation. Nature. 1997;390(6655):81-5. Epub 1997/11/18. doi: 10.1038/36349. PubMed PMID: 9363894.
31. Feral CC, Nishiya N, Fenczik CA, Stuhlmann H, Slepak M, Ginsberg MH. CD98hc (SLC3A2) mediates integrin signaling. Proc Natl Acad Sci U S A. 2005;102(2):355-60. Epub 2004/12/31. doi: 0404852102 [pii]
10.1073/pnas.0404852102. PubMed PMID: 15625115; PubMed Central PMCID: PMC544283.
32. Jemal A, Siegel R, Ward E, Hao Y, Xu J, Thun MJ. Cancer statistics, 2009. CA Cancer J Clin. 2009;59(4):225-49. Epub 2009/05/29. doi: 10.3322/caac.20006
caac.20006 [pii]. PubMed PMID: 19474385.
33. Lu Q, Lv G, Kim A, Ha JM, Kim S. Expression and clinical significance of extracellular matrix metalloproteinase inducer, EMMPRIN/CD147, in human osteosarcoma. Oncol Lett. 2013;5(1):201-7. Epub 2012/12/21. doi: 10.3892/ol.2012.981
ol-05-01-0201 [pii]. PubMed PMID: 23255920; PubMed Central PMCID: PMC3525466.
34. Li Y, Xu J, Chen L, Zhong WD, Zhang Z, Mi L, Zhang Y, Liao CG, Bian HJ, Jiang JL, Yang XM, Li XY, Fan CM, Zhu P, Fu L, Chen ZN. HAb18G (CD147), a cancer-associated biomarker and its role in cancer detection. Histopathology. 2009;54(6):677-87. Epub 2009/05/15. doi: 10.1111/j.1365-2559.2009.03280.x
HIS3280 [pii]. PubMed PMID: 19438743.
35. Xu J, Shen ZY, Chen XG, Zhang Q, Bian HJ, Zhu P, Xu HY, Song F, Yang XM, Mi L, Zhao QC, Tian R, Feng Q, Zhang SH, Li Y, Jiang JL, Li L, Yu XL, Zhang Z, Chen ZN. A randomized controlled trial of Licartin for preventing hepatoma recurrence after liver transplantation. Hepatology. 2007;45(2):269-76. Epub 2007/01/30. doi: 10.1002/hep.21465. PubMed PMID: 17256759.
36. Pinheiro C, Longatto-Filho A, Pereira SM, Etlinger D, Moreira MA, Jube LF, Queiroz GS, Schmitt F, Baltazar F. Monocarboxylate transporters 1 and 4 are associated with CD147 in cervical carcinoma. Dis Markers. 2009;26(3):97-103. Epub 2009/07/15. doi: 10.3233/DMA-2009-0596
TX61467X4308U036 [pii]. PubMed PMID: 19597291; PubMed Central PMCID: PMC3833680.
37. Dixon WT, Sikora LK, Demetrick DJ, Jerry LM. Isolation and characterization of a heterodimeric surface antigen on human melanoma cells and evidence that it is the 4F2 cell activation/proliferation molecule. Int J Cancer. 1990;45(1):59-68. Epub 1990/01/15. PubMed PMID: 2404879.
38. Garber ME, Troyanskaya OG, Schluens K, Petersen S, Thaesler Z, Pacyna-Gengelbach M, van de Rijn M, Rosen GD, Perou CM, Whyte RI, Altman RB, Brown PO, Botstein D, Petersen I. Diversity of gene expression in adenocarcinoma of the lung. Proc Natl Acad Sci U S A. 2001;98(24):13784-9. Epub 2001/11/15. doi: 10.1073/pnas.241500798
241500798 [pii]. PubMed PMID: 11707590; PubMed Central PMCID: PMC61119.

39. Koshi H, Sano T, Handa T, Yanagawa T, Saitou K, Nagamori S, Kanai Y, Takagishi K, Oyama T. L-type amino acid transporter-1 and CD98 expression in bone and soft tissue tumors. Pathol Int. 2015;65(9):460-7. Epub 2015/07/03. doi: 10.1111/pin.12323. PubMed PMID: 26134029.
40. Hua Y, Jia X, Sun M, Zheng L, Yin L, Zhang L, Cai Z. Plasma membrane proteomic analysis of human osteosarcoma and osteoblastic cells: revealing NDRG1 as a marker for osteosarcoma. Tumour Biol. 2011;32(5):1013-21. Epub 2011/06/28. doi: 10.1007/s13277-011-0203-4. PubMed PMID: 21706236.
41. Roy J, Pondenis H, Fan TM, Das A. Direct Capture of Functional Proteins from Mammalian Plasma Membranes into Nanodiscs. Biochemistry. 2015;54(41):6299-302. Epub 2015/09/29. doi: 10.1021/acs.biochem.5b00954. PubMed PMID: 26415091.
42. Dorsam RT, Gutkind JS. G-protein-coupled receptors and cancer. Nat Rev Cancer. 2007;7(2):79-94. Epub 2007/01/26. doi: nrc2069 [pii]
10.1038/nrc2069. PubMed PMID: 17251915.
43. Hutchings CJ, Koglin M, Marshall FH. Therapeutic antibodies directed at G protein-coupled receptors. MAbs. 2010;2(6):594-606. Epub 2010/09/25. doi: 10.4161/mabs.2.6.13420
13420 [pii]. PubMed PMID: 20864805; PubMed Central PMCID: PMC3011214.
44. Shapiro P. Ras-MAP kinase signaling pathways and control of cell proliferation: relevance to cancer therapy. Critical reviews in clinical laboratory sciences. 2002;39(4-5):285-330. PubMed PMID: 12385501.
45. Elenjord R, Allen JB, Johansen HT, Kildalsen H, Svineng G, Maelandsmo GM, Loennechen T, Winberg JO. Collagen I regulates matrix metalloproteinase-2 activation in osteosarcoma cells independent of S100A4. FEBS J. 2009;276(18):5275-86. Epub 2009/08/18. doi: 10.1111/j.1742-4658.2009.07223.x
EJB7223 [pii]. PubMed PMID: 19682073.
46. Vihinen P, Riikonen T, Laine A, Heino J. Integrin alpha 2 beta 1 in tumorigenic human osteosarcoma cell lines regulates cell adhesion, migration, and invasion by interaction with type I collagen. Cell Growth Differ. 1996;7(4):439-47. Epub 1996/04/01. PubMed PMID: 9052985.
47. Su J, Chen X, Kanekura T. A CD147-targeting siRNA inhibits the proliferation, invasiveness, and VEGF production of human malignant melanoma cells by down-regulating glycolysis. Cancer Lett. 2009;273(1):140-7. Epub 2008/09/10. doi: 10.1016/j.canlet.2008.07.034
S0304-3835(08)00616-2 [pii]. PubMed PMID: 18778892.
48. Zeestraten EC, Reimers MS, Saadatmand S, Dekker JW, Liefers GJ, van den Elsen PJ, van de Velde CJ, Kuppen PJ. Combined analysis of HLA class I, HLA-E and HLA-G predicts prognosis in colon cancer patients. Br J Cancer. 2014;110(2):459-68. Epub 2013/11/08. doi: 10.1038/bjc.2013.696
bjc2013696 [pii]. PubMed PMID: 24196788; PubMed Central PMCID: PMC3899753.
49. Mikami S, Mizuno R, Kosaka T, Saya H, Oya M, Okada Y. Expression of TNF-alpha and CD44 is implicated in poor prognosis, cancer cell invasion, metastasis and resistance to the sunitinib treatment in clear cell renal cell carcinomas. Int J Cancer. 2014. Epub 2014/08/16. doi: 10.1002/ijc.29137. PubMed PMID: 25123505.
50. Sillanpaa S, Anttila MA, Voutilainen K, Tammi RH, Tammi MI, Saarikoski SV, Kosma VM. CD44 expression indicates favorable prognosis in epithelial ovarian cancer. Clin Cancer Res. 2003;9(14):5318-24. Epub 2003/11/14. PubMed PMID: 14614016.
51. Louderbough JM, Schroeder JA. Understanding the dual nature of CD44 in breast cancer progression. Mol Cancer Res. 2011;9(12):1573-86. Epub 2011/10/06. doi: 10.1158/1541-7786.MCR-11-0156
1541-7786.MCR-11-0156 [pii]. PubMed PMID: 21970856.
52. Lahat G, Zhu QS, Huang KL, Wang S, Bolshakov S, Liu J, Torres K, Langley RR, Lazar AJ, Hung MC, Lev D. Vimentin is a novel anti-cancer therapeutic target; insights from in vitro and in vivo mice xenograft studies. PloS one. 2010;5(4):e10105. Epub 2010/04/27. doi: 10.1371/journal.pone.0010105. PubMed PMID: 20419128; PubMed Central PMCID: PMC2855704.
53. Werbeck JL, Thudi NK, Martin CK, Premanandan C, Yu L, Ostrowksi MC, Rosol TJ. Tumor microenvironment regulates metastasis and metastasis genes of mouse MMTV-PymT mammary cancer

cells in vivo. Veterinary pathology. 2014;51(4):868-81. doi: 10.1177/0300985813505116. PubMed PMID: 24091811; PubMed Central PMCID: PMC4291313.
54. Hanash S, Schliekelman M. Proteomic profiling of the tumor microenvironment: recent insights and the search for biomarkers. Genome medicine. 2014;6(2):12. doi: 10.1186/gm529. PubMed PMID: 24713112; PubMed Central PMCID: PMC3978437.

CHAPTER III: DIRECT CAPTURE OF FUNCTIONAL PROTEINS FROM MAMMALIAN PLASMA MEMBRANES INTO NANODISCS[5]

3.1 ABSTRACT

Mammalian plasma membrane proteins are the largest class of drug targets yet are difficult to study in a cell free system due to their intransigent nature. Herein, we perform direct encapsulation of plasma membrane proteins derived from mammalian cells into a functional nanodisc library. Peptide fingerprinting was used to analyze the proteome of the incorporated proteins in nanodiscs and to further demonstrate that lipid composition of the nanodiscs directly affects the class of protein that is incorporated. Furthermore, the functionality of the incorporated membrane proteome was evaluated by measuring the activity of membrane proteins – Na+/K+-ATPase and receptor tyrosine kinases. This work is the first report of successful establishment and characterization of a cell free functional library of mammalian mem-brane proteins into nanodiscs

3.2 INTRODUCTION

Plasma membranes (PMs) serve as a protective bilayer for cells by forming a permeability barrier for trafficking molecules into and out of the cell. These membranes are comprised of a diverse array of proteins and lipids that interact to form a complex superstructure with capacity to regulate various cellular processes. PM proteins are involved in cellular signaling, regulation, and homeostasis and serve as the largest class of druggable targets (1). These proteins can be classified into various functional groups, including receptors, transporters, and enzymes (2). Additionally, these membranes also contain various lipid components consisting primarily of different types of phospholipids, including POPC (1-palmitoyl-2-oleoyl-sn-glycero-3-phosphocholine), POPS (1-palmitoyl-2-oleoyl-sn-glycero- 3-phospho-L-serine), and sphingomyelin, and other lipids, including cholesterol (3-6). Furthermore, the PM contains microdomains such as lipid rafts that contain a percentage of cholesterol and sphingomyelin significantly higher than that of the regular plasma membrane that aid in protein signaling (4, 7). Taken together, the plasma membranes are highly ordered, and their complexity arises from the intricate interplay between membrane proteins

[5] Reprinted with permission of the American Chemical Society Permissions. "Direct Capture of Functional Proteins from Mammalian Plasma Membranes into Nanodiscs." Jahnabi Roy, Holly Pondenis, Timothy Fan and Aditi Das. *Biochemistry* 2015, *54*, 6299−6302.

and a variety of lipids. The involvement of plasma membrane proteins in signaling processes and their importance in therapeutic development necessitate the discovery of innovative methods for interrogation of membrane proteins in a cell free medium (1). Here we use nanodiscs to efficiently capture membrane proteins directly from the mammalian cellular membranes (Figure 3.1). Previous studies show that nanodiscs can be used to preserve the structural and functional integrity of membrane proteins, including cytochrome P450s, G protein-coupled receptors (GPCRs), and other receptors (8-10). Additionally, they can be coupled to various downstream detection methodologies and assays such as SILAC and MALDI, nuclear magnetic resonance, and fluorescence microscopy (11). The application of nanodiscs has been predominantly limited to the incorporation of single purified proteins (8-10, 12-14). Recently, there have been studies to prepare membrane protein nanodisc libraries (MPNLs) by directly encapsulating proteins from the membranes of simpler organisms such as bacteria (15) and yeast (16). This work is the first report of a mammalian membrane protein nanodisc library with detailed characterization of the incorporated proteome. Furthermore, we demonstrate that the incorporated proteins also retain functional activity. The capacity to stably incorporate membrane proteins as a library in nanodiscs provides a cell free platform suitable for facile downstream functional analysis and drug binding studies.

3.3 MATERIALS AND METHODS

Materials: β- octylglucoside, imidazole, ethylenediaminetetraacetic acid (EDTA), and Amberlite XAD-2 beads were purchased from Sigma-Aldrich (St. Louis, MO). Phenylmethanesulfonyl fluoride (PMSF) was obtained from Fisher Scientific (Pittsburgh, PA). Ni- NTA resin was purchased from Gold Biotechnology (St. Louis, MO). Sodium Cholate as obtained from Affymetrix (Maumee, OH). 1-palmitoyl-2-oleoyl-sn-glycero-3-phosphocholine (POPC) and 1-palmitoyl-2-oleoyl-sn-glycero-3-phospho-L-serine (POPS) were obtained from Avanti Polar Lipids (Alabaster, AL). MHC Class I antibody was obtained from Abcam (ab134189). Ras antibody was obtained from Upstate Cell Signalling (05-516). Kinase assay kit was obtained from R&D system (EA004). Ouabain was kindly gifted by Mr. Carl Malmgren University of Illinois, Urbana- Champaign.

Cell culture: Human cell line 143B was cultured in DMEM (Gibco, Invitrogen, Carlsbad, CA, USA) supplemented with 10% fetal bovine serum (FBS) and 1mg ml–1 penicillin–streptomycin (Gibco, Invitrogen) at 37 °C and 5% CO2 in a humidified incubator.

Extraction of plasma membranes: Membrane extraction was done as previously published(17, 18). All steps were carried out at 4°C. Briefly, about 60 million adherent cells were washed with phosphate-buffered saline (PBS), scraped using a plastic cell lifter, and broken in 1 mL solution containing 0.2 mM EDTA and 1 mM NaHCO3 and 20 µL protease inhibitor (Nacalai USA, Inc.), using a glass homogenizer. The nuclear and unbroken cells were removed through centrifugation a 200×g, and the supernatant was collected and centrifuged for 30 min at 25,000 rpm. The cell pellets were resuspended in 1 mM NaHCO3 in an approximate ratio of 1 mL per 5×108 cells and used for PM separation by two-phase systems. Suspended cell pellets were added to the top of 14 g of the dextran–poly (ethylene glycol) mixture (6.6% Dextran T500, 6.6% PEG 3350, 0.1 M sucrose, 5 mM K3PO4, pH= 7.2). After mixing up and down for 40 times, the tube was centrifuged for 5 min at 750×g. The PM-enriched up phase was collected and purified again as described above. The up phase was diluted with 1 mM sodium bicarbonate and centrifuged at 100,000×g for 2 h in a SW32 rotor.

Assembly of 143B nanodisc: All steps were done at 4 °C unless otherwise mentioned. Expression and purification of MSP1E3D1 was performed as previously described(19, 20). MSP from stock concentration of 75 µM was added in 1:132 ratio in POPC, dried under nitrogen and solubilized in 25% β- octyl glucoside and 0.1mM sodium cholate. Although solubilization of lipids in typically performed in 50 mM sodium cholate, precaution was taken to reduce the amount of total cholate to prevent any denaturation of mammalian proteins. The MSP and POPC mixture was equilibrated for 30 min. Simultaneously, the membrane protein (ratio of 1:10- MP: MSP) was equilibrated with 2% β- octyl glucoside for 15 min. The MP was then added to the MSP- POPC mixture and 6 mL of 0.1 M phosphate buffer (pH 7.4) was added to dilute salts in the protein buffer and DTT to final concentration of 0.1 mM was added. The mixture was allowed to equilibrate for 30 min and Amberlite ® biobeads were added to the mixture to remove detergents and allow nanodisc formation. The biobeads were filtered off after 2.5 h and the nanodisc solution was loaded onto a Ni- NTA column (1.5 mL). The column was washed with 1.5 mL of 20 mM imidazole in 0.1 M

tris buffer (pH 7.4). The nanodisc was then eluted with 200 mM imidazole in 0.1 M tris buffer (pH 7.4).

Size exclusion chromatography: Size exclusion chromatography (SEC) was performed with a calibrated Superdex HR 200 10/300 size exclusion column (Amersham-Pharmacia Biotech, Piscataway, NJ) by a Waters Alliance System. Samples were filtered prior to analysis and injected using a 500 µL sample loop and a flow rate of 0.5 mL/min with 0.1 M phosphate buffer (pH 7.4).

Disassembly of nanodiscs for peptide fingerprinting: The nanodisc preparation was loaded on to Ni-NTA column (1.5mL) and the flow through was removed. A solution of 200 mM sodium cholate (2 mL) was added to the column and pipetted up and down to mix. The column was allowed to stand in sodium cholate solution for 30 min and the sodium cholate solution was eluted containing the proteins liberated due to nanodisc dis-assembly. The MSP remained attached to the column due to its His-tag.

Peptide fingerprinting:

Sample preparation: Sample cleanup was done using G-Biosciences (St. Louis, MO) Perfect Focus according to manufacturer's instruction.

Digestion with trypsin: Sample was digested with MSG-Trypsin (G-Biosciences, St. Louis, MO) at a ratio of 1:10 – 1:50 using a CEM Discover Microwave Digestor (Mathews, SC) at 55 ˚C and maximum power of 60 watts for 15 minutes. Digested peptides were lyophilized and resuspended in 5% acetonitrile + 0.1% formic acid for LC/MS.

LC/MS: LC/MS was performed using a Thermo Dionex Ultimate RSLC3000 operating in nano mode at 300 microliters/min with a gradient from 0.1% formic acid to 100% acetonitrile + 0.1% formic acid in 120 minutes. The trap column used was a Thermo Acclaim PepMap 100 (100 µm x 2 cm) and the analytical column was a Thermo Acclaim PepMap RSLC (75 µm x 15 cm).

Data Analysis: The peptide fingerprinting Xcalibur raw file was converted by Mascot Distiller into peaklists that were submitted to an in-house Mascot Server and searched against specific NCBI-NR protein databases. The list of proteins obtained was filtered by a $p < 0.05$ for a 95% confidence value. This list of proteins was then classified by their subcellular location (to filter out non-membrane contaminants) and plasma membrane candidates were classified into various functional

classes. The emPAI values were normalized to the total emPAI value and compared as a percentage to the overall composition.

Western Blot: Based on protein concentration measurements, equal amounts of plasma membrane preparations generated from all cells were resolved by 4–20% SDS-PAGE (Pierce) and transferred onto a PVDF membrane. The membranes were blocked in PBS, 0.1% Tween 20, 5% nonfat dry milk powder for 1 h at room temperature and incubated with primary antibody for 16 h at 4 °C followed by washing and incubation with HRP-conjugated secondary antibody for 1 h at room temperature. All antibody incubations and washing steps were carried out in PBS, 0.1% Tween 20. The immunoreactive bands were visualized using an ECL Western blot kit (Amersham Biosciences). The western blots were normalized by Ponceau staining(21).

Na+/K+ ATPase assay: Samples were incubated at various mentioned temperatures for different periods of time, as mentioned for the assay. For freeze thaw samples, the freezing was done as a flash freeze in liquid nitrogen for 1 min. The samples were thawed on ice for analysis before flash freezing again. The total Na+/K+-ATPase activity was assayed at 37°C in an incubation mixture containing 30 mmol/L Tris-HCl, pH 7.4, 0.1 mmol/L EDTA, 50 mmol/L NaCl, 5 mmol/L KCl, 6 mmol/L MgCl2, and 1 mmol/L ATP in the presence or absence of ouabain (0.5 mM), as described previously (22, 23). Briefly, after preincubating the isolated membranes or nanodisc preparation, for 10 min at 37°C, the reaction was started by the addition of ATP and stopped with 55 μL of ammonium molybdate in sulfuric acid after 20 min. The amount of inorganic phosphate released was determined by reduction of phosphomolybdate complex by 10% ascorbic acid solution and measuring absorbance at 820 nm. The Na+/K+-ATPase activity was calculated as the difference between the presence or absence of ouabain-sensitive Na+/K+-ATPase activity. Experiments were performed in triplicates.

Kinase assay: The assay was performed according to manufacturer's instruction. Briefly, the nanodisc preparation was incubated with imatinib (20 μM) or DMSO (control) for 10 min. To this ATP and coupling phosphatase were added and incubated for 10 min. The reaction was quenched with Malachite reagent A, water and Malachite reagent B and readout was measured at 620 nm. The absorbance of nanodisc incubated with imatinib was subtracted from that with DMSO control for final phosphate calculations and the readings were adjusted for total protein used in each preparation. Assay was performed in triplicates.

3.4 RESULTS AND DISCUSSION

For the preparation of the MPNL, we utilized metastatic human osteosarcoma 143B cells17 in the study presented here to serve as a model of mammalian plasma membranes for the preparation of the mammalian protein nanodisc library (MPNL). The immortalized 143B cell line originates from the malignant osteoblast lineage and is characterized by a short doubling time in vitro and a spontaneous metastatic potential in vivo (24). The potential discovery of membrane biomarkers of osteosarcoma and drug discovery against identified receptor targets permit 143B cells to serve as a relevant and suitable mammalian cell model for this study. To capture the membrane proteins into nanodiscs, first, the membrane fraction from 143B cells was isolated using an aqueous two-phase partitioning system (ATPS) (17, 25). This was followed by equilibration with mild, nonionic detergent, β-octyl glucoside, to extract the proteins from the membrane. Use of β-octyl glucoside has been previously shown to maintain the functional integrity of membrane proteins as compared to that of cholate or sodium dodecyl sulfate (26, 27). Detergent-solubilized lipids and membrane scaffold protein (MSP1E3D1) were added followed by removal of the detergents by Amberlite Biobeads to initiate nanodisc self-assembly (Figure 3.1). The ratio of these components was optimized and verified by using size exclusion chromatography (Figure 3.2). The following lipid compositions were chosen to make nanodiscs (NDs): 100% POPC (ND1), 20% POPS and 80% POPC (ND2), 20% cholesterol and 80% POPC (ND3), and 20% POPS, 72% POPC, and 8% cholesterol (ND4). Interestingly, the nanodiscs prepared from different lipid compositions had similar sizes except for the cholesterol nanodiscs that show a later elution time, indicating a smaller size (Figure 3.2). The rigid structure of cholesterol possibly increases the fluidity of the nanodisc as it disrupts the phospholipid packing (28). A similar reduction in size upon incorporation of cholesterol has been observed in molecular dynamics (MD) simulations of bilayers (29). For peptide fingerprinting analysis of the MPNL, the protein content of the nanodiscs was further characterized using peptide fingerprinting by mass spectrometry (30, 31). Prior to proteomic analysis, the MPNL nanodiscs were disassembled using sodium cholate followed by use of a Ni-NTA to remove His-tagged MSP1E3D1 as the presence of MSP1E3D1 overwhelms the ion signal from the other membrane proteins. The proteins identified in the nanodiscs using proteomics were classified into the following functional categories: structural, GPCRs, enzymes, transporters, chaperones, immune complexes, and other receptors (Figure 3.3 and Appendix III). Herein, we use two parameters for data analysis. Figure 3.3 and Table 3.1 represent the percentage of a

particular functional class of membrane protein in the protein mixture. The second parameter is the incorporation of proteins into nanodiscs as compared to the initial membrane (Table 3.2) indicating the percentage incorporation Peptide fingerprinting of POPC nanodisc ND1 revealed that ∼55% of membrane protein species in the initial membrane fraction were incorporated into nanodiscs (Table 3.2). Although a majority of the protein categories were conserved in these nanodiscs, the percentage of structural proteins was only 19% in ND1 as compared to 56% in MP (Table 3.1). An important class of structural proteins, annexins, was completely absent in ND1 (Appendix III), indicating that the protein−lipid electrostatic interaction that is important for annexin binding is lacking in the zwitterionic POPC lipid bilayer (15, 32). Typically, the plasma membrane of cells consists of ∼20% anionic lipids such as phosphatidylserine (6). Various proteins, including phospholipases and annexins that contain positively charged residues, preferentially associate with anionic lipids to perform their biological activities (33-35). Therefore, ND2 containing 20% POPS (Appendix III) was prepared. In these nanodiscs, the protein content recapitulated the initial membrane composition (Table 3.1) and achieved an overall incorporation of 70% of the initial mixture of membrane proteins into nanodiscs (Table 3.2). Unlike ND1, the structural proteins constituted the largest class of proteins in ND2 (Figure 3.3C and Table 3.1) as seen for the original MP fraction (Figure 3.3A and Table 3.1). Next we incorporated cholesterol into nanodiscs. Cholesterol is the primary lipid component of lipid raft domains in the plasma membranes that have been implicated in clustering of GPCRs and other signaling proteins (36, 37). In vivo, these rafts contain a percentage of cholesterol (∼30%) significantly higher than that of the plasma membrane (8−14%) (4). Because of the rigid nature of the sterol group, cholesterol partitions preferentially into the lipid rafts where acyl chains of the phospholipids tend to be more rigid and in a less fluid state. The proteomic analysis of 20% cholesterol-containing nanodiscs, ND3 (Appendix III), surprisingly showed an incorporation efficiency of 15% (Table 3.1), and only a few protein classes were detected (Table 3.2 and Figure 3.3D). Similar to ND1, cholesterol nanodiscs demonstrated a lack of proteins binding preferentially to anionic lipids. Interestingly, the percentage of enzymes incorporated into ND3 was higher than in ND1 and ND2 (Table 3.1). However, the overall incorporation of membrane proteins in cholesterol ND3 was poor. MD simulation studies show that the volume of a bilayer decreases with an increase in cholesterol content (29). The smaller size is also evident from our size exclusion chromatography, which showed that ND3 was smaller than other nanodiscs (Figure 3.2). The smaller volume of the

nanodisc due to a high cholesterol concentration possibly results in a lower incorporation efficiency. Finally, ND4 nanodiscs that closely mimicked the composition of the plasma membrane [POPC (72%), POPS (20%), and cholesterol (8%)] were prepared. Results from peptide fingerprinting show that ND4 achieved >75% incorporation of proteins, the highest incorporation efficiency among the different nanodisc classes (Table 3.2). There was a dramatic enrichment of GPCRs and G proteins (Figure 3.3E and Tables 3.1 and Appendix III). ND4 contains significantly less cholesterol than ND3 and therefore an overall greater nanodisc size as evidenced by size exclusion chromatography (SEC). Additionally, the presence of cholesterol has been linked to GPCR signaling either directly by binding to the GPCR33 or by altering membrane physical properties (38, 39), or both. The significant enrichment of GPCRs in ND4 is probably due to favorable interactions of cholesterol with GPCRs. For the enrichment of selective membrane proteins in the MPNL, all the nanodisc libraries show enrichment of the membrane protein population (Appendix III). This led to identification of several low-abundance membrane proteins not originally detected in the membrane proteome. Therefore, nanodiscs preferentially capture and enrich membrane proteins and remove the soluble proteins and other cellular contaminants. For Western blot validation of selected membrane proteins in the MPNL, we further validated the incorporation of two specific membrane protein targets into nanodiscs using Western blot analysis. It was determined that both GTPase KRAS, a peripheral membrane protein, and major histocompatibility complex (MHC) class I, an integral membrane protein, identified via peptide fingerprinting were present in Western blot analysis in all the different nanodisc preparations (ND1− ND4) (Figure 3.4 A,B). For the functional assay of proteins in the MPNL, from the proteomics data, we see that ND4, which most closely resembles the lipid composition of the native plasma membrane, is able to capture more than 75% of the initial membrane proteins (Table 3.2). The primary advantage of incorporation of proteins into nanodiscs as compared to detergent-solubilized membrane preparations is the preservation of their function (10, 12). From the peptide fingerprinting analysis, we chose two representative classes of proteins to demonstrate that proteins are functionally active in nanodiscs: Na+ /K+ -ATPase and receptor tyrosine kinases (RTKs). The Na+ /K+ -ATPase transports sodium and potassium ions across their concentration gradient by hydrolyzing one molecule of ATP to ADP and inorganic phosphate (Pi). Ouabain is a specific inhibitor of Na+ /K+ -ATPase. The protein activity was measured by phosphate liberated in the absence and presence of ouabain (22, 23) (Figure 3.4C). It can be seen that Na+ /K+ -ATPase

incorporated into the MPNL retains functionality over 7 days at 37 °C. Furthermore, the functional assay was conducted at a variety of temperatures [4 °C and room temperature (23 °C)] over different periods of time (days 1−7) and using freeze−thaw conditions (Figure 3.5). Under all tested conditions, Na+ /K+ -ATPase activity was retained in nanodiscs over a broad range of storage durations and temperatures. Phosphorylation of proteins is a key process for signal transduction in enzymatic regulation. A major class of kinases is receptor tyrosine kinases (RTKs), which are involved in cancer, and there are various inhibitors that currently are available to target them (40). We measured the activity of RTKs in nanodiscs by using malachite green-dependent detection of phosphate released from kinase activity (41) in the presence and absence of imatinib. This inhibitor inhibits multiple RTKs, including platelet-derived growth factor (PDGF) receptor, an overexpressed receptor in osteosarcoma (42, 43). All four nanodisc preparations retained RTK activity as evidenced by the decrease in activity in the presence of imatinib, indicating functional kinases that are inhibited by imatinib (Figure 3.4D). Interestingly, the highest RTK activity was identified in POPC/POPS/cholesterol ND4. The activity of RTKs was lowest in the 20% cholesterol nanodisc, correlating with the absence of PDGF receptor and small amounts of RTKs detected by peptide fingerprinting. This demonstrates that the MPNL can be used for screening small molecules against a large variety of kinases in a model library.

3.5 CONCLUSION

In conclusion, this work establishes the formation of a functional mammalian nanodisc library from human osteosarcoma 143B cells and is the first to report a detailed analysis of Figure 3. (A and B) Western blot showing incorporation of MHC-1 and KRAS protein into the different nanodiscs: (1) ladder, (2) 143B membrane, (3) 100% POPC ND1, (4) 20% POPS ND2, (5) 20% cholesterol ND3, and (6) 8% cholesterol and 20% POPS ND4. (C) Na+ /K+ -ATPase activity in nanodiscs monitored at 37 °C by measuring phosphate produced in the presence and absence of ouabain (Na+ /K+ -ATPase blocker) relative to day 1. (D) Net kinase activity measured in the nanodiscs in the presence and absence of imatinib (RTK inhibitor) showing active RTK in nanodiscs is inhibited. Furthermore, it is shown that the change in lipid composition strongly influences the subpopulation of proteins incorporated into the nanodisc. This study can be further extended to other lipid compositions, including sphingomyelin, cardiolipin, etc. In ND4 containing both anionic lipids and cholesterol, there was more than 75% incorporation of membrane protein, including enrichment of certain GPCRs and G proteins. These MPNLs are functionally active as

shown by measuring Na+ /K+ -ATPase activity and RTK activity as proof-of-concept protein classes. This approach of using functional nanodisc libraries provides promise for stabilizing entire membrane proteomes in a cell free system that can be further utilized for evaluating protein interactions and drug binding studies. Notably, the methods used to prepare a functional MPNL from 143B cells can be broadly applied to other cell lines, including cancerous and noncancerous cells.

3.6 ACKNOWLEDGEMENTS

We thank Dr. Peter Yau and the Roy J. Carver Biotechnology Center, Protein Sciences Facility for assistance in peptide fingerprinting. We thank Mr. Javier Baylon for assistance with figures. We thank Sligar Lab for providing the gene for MSP1E3D1. We thank Mr. Daniel McDougle and Mr. John Rouck for editing the manuscript. We grate-fully acknowledge the financial support provided by the Campus Research Board, American Heart Association, and Office of the Provost, University of Illinois at Urbana-Champaign).

3.7 TABLES AND FIGURES

Table 3.1: Percentage abundance of proteins of each class in membrane fraction or nanodiscs as identified by peptide fingerprinting (individual data in Appendix III). Abundance does not directly correlate with number of species in each class. emPAI or exponentially modified protein abundance index is a parameter indicating relative abundance of proteins in the mixture.

	Membrane	**ND1**	**ND2**	**ND3**	**ND4**
Structure	56.3	19.3	63.6	31.4	25.9
Transport	2.4	10.0	2.9	7.6	3.2
Immune complexes	11.0	38.0	16.2	23.3	20.0
G proteins and GPCRs	18.1	20.2	10.8	1.2	43.8
Chaperones	1.4	4.4	0.3	0.0	0.7
Receptors	4.8	4.0	2.9	1.6	2.7
Enzymes	1.9	3.8	2.2	22.5	2.3
Others	3.7	0.0	0.8	12.0	1.0

Table 3.2: Number of individual proteins identified in each class (data in Appendix III). Number of proteins identified in nanodisc can be higher than those identified in initial membrane due to improved signal to noise ratio on removal of non- membrane contaminant proteins.

	Membrane	ND1	ND2	ND3	ND4
Structural	56	35	52	9	41
Transport	20	13	14	4	13
Immune Complexes	15	18	19	2	22
G- proteins and GPCRs	34	18	23	1	38
Chaperones	8	5	2	0	4
Other Receptors	17	10	14	2	12
Enzymes	20	11	8	7	11
Others	31	0	8	4	9
	201	110	140	29	150

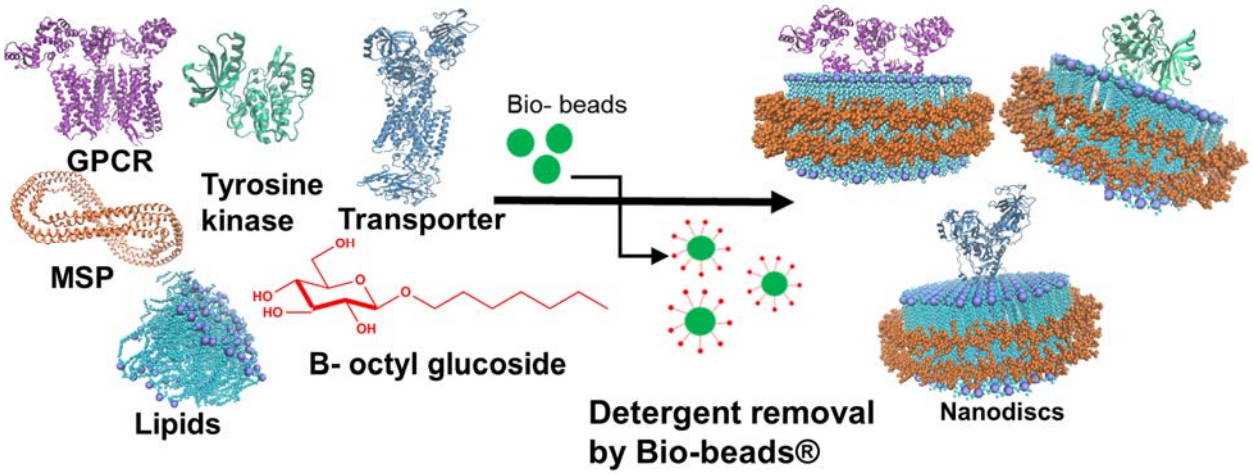

Figure 3.1: Schematic of nanodisc assembly. Membrane proteins in membranes were mixed with membrane scaffold protein (MSP), β- octyl glucoside, and lipids of choice. The detergent was removed bybiobeads, leading to the onset of the assembly of the membraneprotein nanodisc library (MPNL).

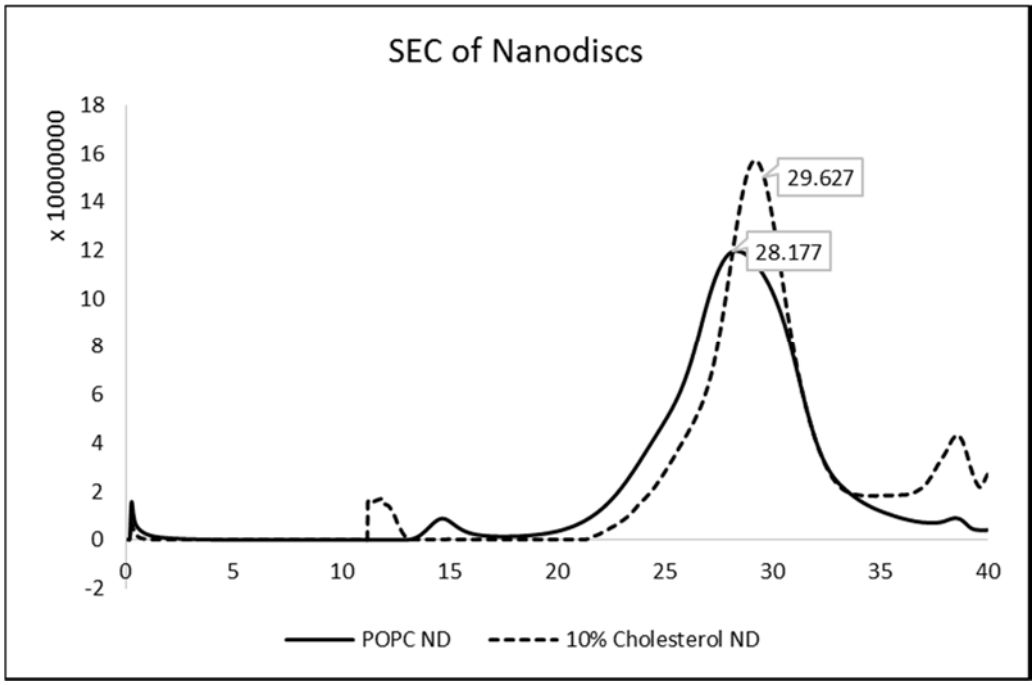

Figure 3.2: Size exclusion chromatogram of various nanodiscs showing the formation of symmetrical nanodiscs. POPC (ND1) SEC is also representative of POPS (ND2) and 8% cholesterol+ 20% POPS + 72% POPC disc (ND4). 20% Cholesterol nanodiscs (ND3) formed are slightly smaller than POPC and other nanodiscs.

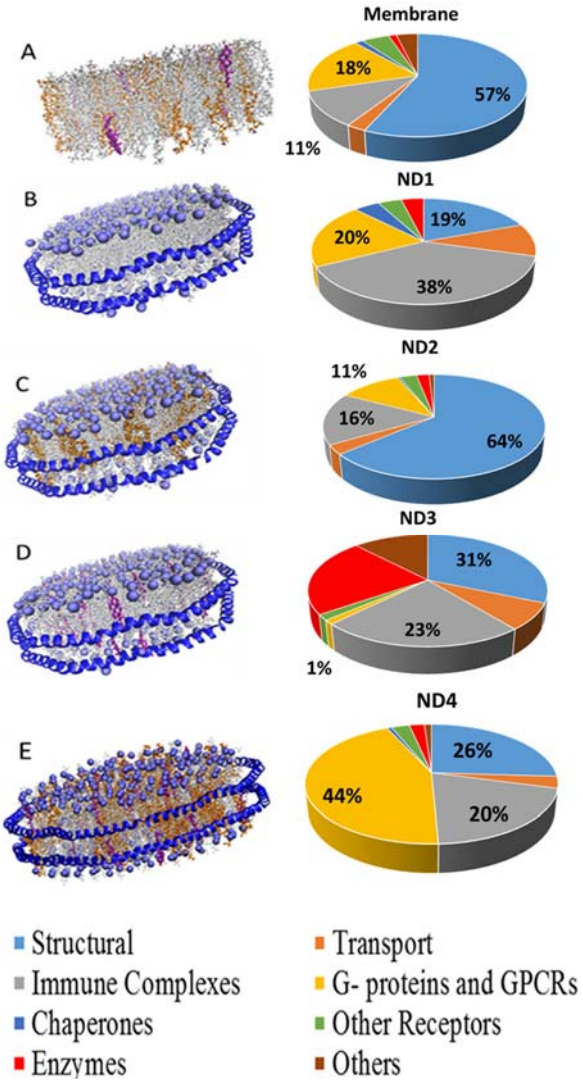

Figure 3.3: Schematics (left) of nanodiscs containing different lipid compositions. POPC lipids are colored white and POPS lipids orange, and cholesterol is colored pink. Phospholipid headgroups are colored purple, and membrane scaffold protein is colored blue: (A) MP, (B) ND1 (100% POPC), (C) ND2 (20% POPS and 80% POPC), (D) ND3 (20% cholesterol and 80% POPC), and (E) ND4 (20% POPS, 8% cholesterol, and 72% POPC). Functional classification (right) of the membrane proteome. The percentage represents the ratio of one particular class of membrane protein in the mixture. The percentages of structural proteins (blue), immune complexes (gray), and GPCRs (yellow) are indicated.

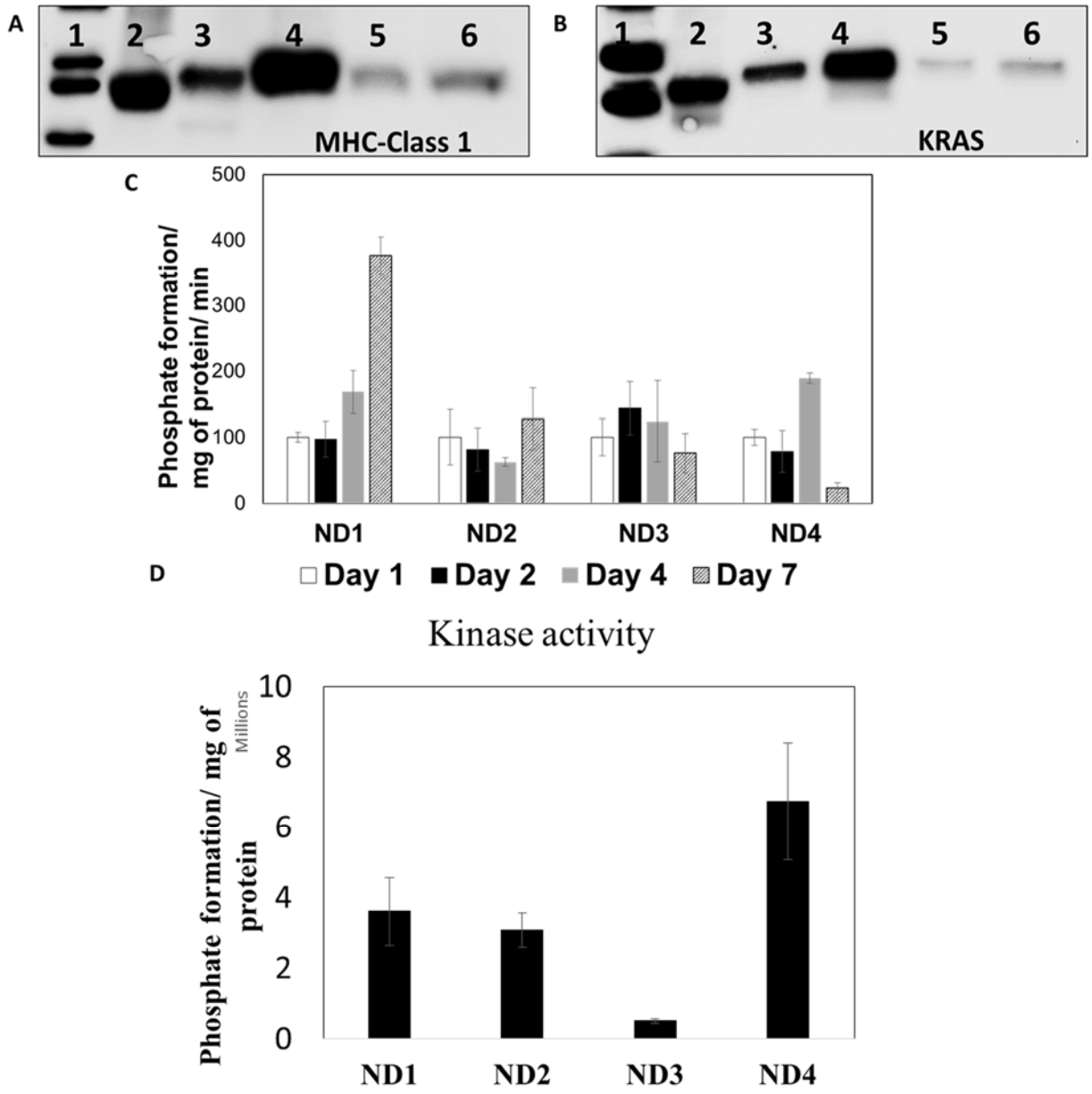

Figure 3.4: (A and B) Western blot showing incorporation of MHC-1 and KRAS protein into the different nanodiscs: (1) ladder, (2) 143B membrane, (3) 100% POPC ND1, (4) 20% POPS ND2, (5) 20% cholesterol ND3, and (6) 8% cholesterol and 20% POPS ND4. (C)Na+/K+ -ATPase activity in nanodiscs monitored at 37 °C by measuring phosphate produced in the presence and absence of ouabain (Na+ /K+ -ATPase blocker) relative to day 1 (details in Table ST8). (D) Net kinase activity measured in the nanodiscs in the presence and absence of imatinib (RTK inhibitor) showing active RTK in nanodiscs is inhibited.

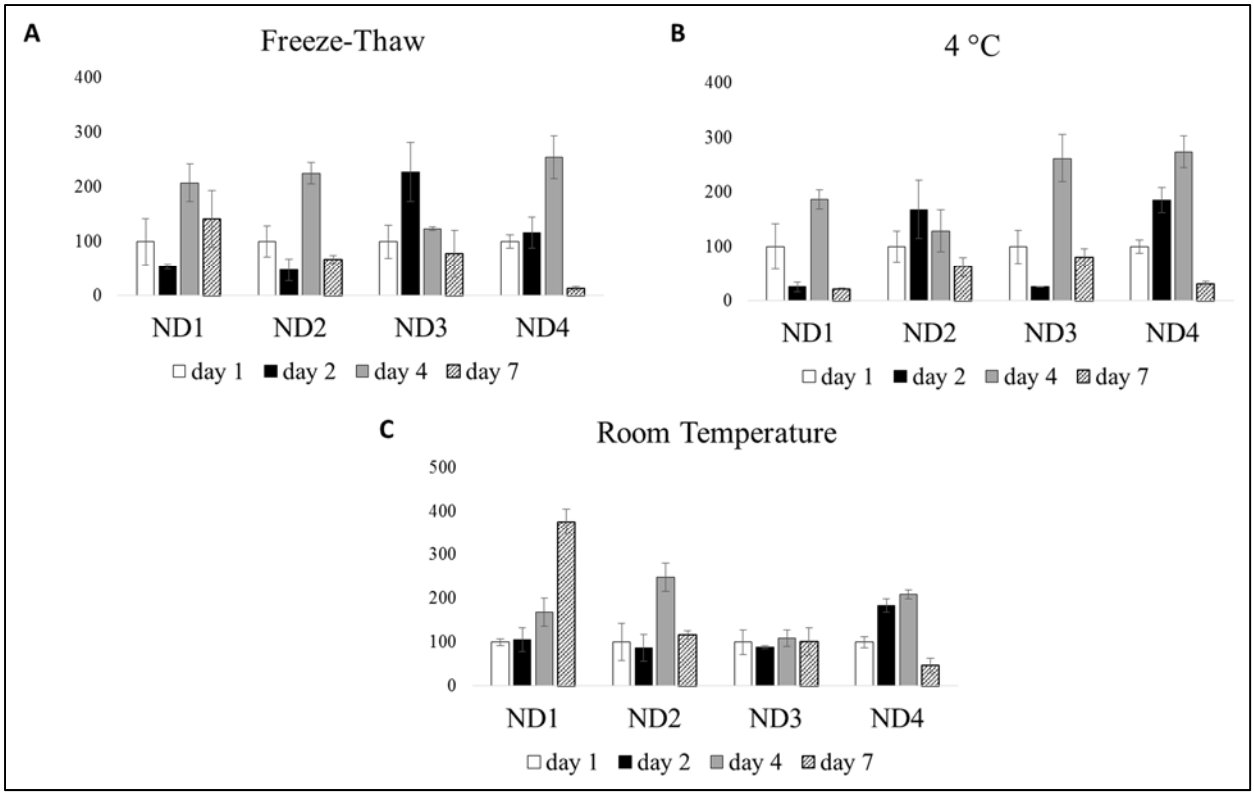

Figure 3.5: Sodium potassium ATPase activity by measuring total phosphate produced in the presence and absence of ouabain over different temperature conditions over 7 days. (A) Freeze thaw cycles, (B) 4 °C and (C) room temperature (23 °C). Data shows no appreciable change in phosphate produced at any temperature over a period of 7 days. Data is average of three replicates. (ND1 (100% POPC); ND2 (20% POPS-80% POPC); ND3 (20% cholesterol- 80% POPC); ND4 (20% POPS, 8 % cholesterol and 72% POPC)).

3.8 REFERENCES

1. Bakheet TM, Doig AJ. Properties and identification of human protein drug targets. Bioinformatics. 2009;25(4):451-7. doi: 10.1093/bioinformatics/btp002. PubMed PMID: 19164304.
2. Almen MS, Nordstrom KJ, Fredriksson R, Schioth HB. Mapping the human membrane proteome: a majority of the human membrane proteins can be classified according to function and evolutionary origin. BMC biology. 2009;7:50. doi: 10.1186/1741-7007-7-50. PubMed PMID: 19678920; PubMed Central PMCID: PMC2739160.
3. Maldonado RL, Blough HA. A comparative study of the lipids of plasma membranes of normal cells and those infected and transformed by Rous sarcoma virus. Virology. 1980;102(1):62-70. PubMed PMID: 6245508.
4. Pike LJ, Han X, Chung KN, Gross RW. Lipid rafts are enriched in arachidonic acid and plasmenylethanolamine and their composition is independent of caveolin-1 expression: a quantitative electrospray ionization/mass spectrometric analysis. Biochemistry-Us. 2002;41(6):2075-88. PubMed PMID: 11827555.
5. van Meer G, Voelker DR, Feigenson GW. Membrane lipids: where they are and how they behave. Nature reviews Molecular cell biology. 2008;9(2):112-24. doi: 10.1038/nrm2330. PubMed PMID: 18216768; PubMed Central PMCID: PMC2642958.
6. Zachowski A. Phospholipids in animal eukaryotic membranes: transverse asymmetry and movement. Biochem J. 1993;294 (Pt 1):1-14. PubMed PMID: 8363559; PubMed Central PMCID: PMC1134557.
7. Resh MD. Membrane targeting of lipid modified signal transduction proteins. Sub-cellular biochemistry. 2004;37:217-32. PubMed PMID: 15376622.
8. Denisov IG, Sligar SG. Cytochromes P450 in nanodiscs. Biochimica et biophysica acta. 2011;1814(1):223-9. doi: 10.1016/j.bbapap.2010.05.017. PubMed PMID: 20685623; PubMed Central PMCID: PMC2974961.
9. Borch J, Torta F, Sligar SG, Roepstorff P. Nanodiscs for immobilization of lipid bilayers and membrane receptors: kinetic analysis of cholera toxin binding to a glycolipid receptor. Analytical chemistry. 2008;80(16):6245-52. doi: 10.1021/ac8000644. PubMed PMID: 18616345.
10. Leitz AJ, Bayburt TH, Barnakov AN, Springer BA, Sligar SG. Functional reconstitution of Beta2-adrenergic receptors utilizing self-assembling Nanodisc technology. BioTechniques. 2006;40(5):601-2, 4, 6, passim. PubMed PMID: 16708760.
11. Leney AC, Fan X, Kitova EN, Klassen JS. Nanodiscs and electrospray ionization mass spectrometry: a tool for screening glycolipids against proteins. Analytical chemistry. 2014;86(11):5271-7. doi: 10.1021/ac4041179. PubMed PMID: 24779922.
12. Das A, Varma SS, Mularczyk C, Meling DD. Functional investigations of thromboxane synthase (CYP5A1) in lipid bilayers of nanodiscs. Chembiochem : a European journal of chemical biology. 2014;15(6):892-9. doi: 10.1002/cbic.201300646. PubMed PMID: 24623680.
13. McDougle DR, Kambalyal A, Meling DD, Das A. Endocannabinoids anandamide and 2-arachidonoylglycerol are substrates for human CYP2J2 epoxygenase. The Journal of pharmacology and experimental therapeutics. 2014;351(3):616-27. doi: 10.1124/jpet.114.216598. PubMed PMID: 25277139; PubMed Central PMCID: PMC4244587.
14. Meling DD, McDougle DR, Das A. CYP2J2 epoxygenase membrane anchor plays an important role in facilitating electron transfer from CPR. Journal of inorganic biochemistry. 2015;142:47-53. doi: 10.1016/j.jinorgbio.2014.09.016. PubMed PMID: 25450017.
15. Marty MT, Wilcox KC, Klein WL, Sligar SG. Nanodisc-solubilized membrane protein library reflects the membrane proteome. Analytical and bioanalytical chemistry. 2013;405(12):4009-16. doi: 10.1007/s00216-013-6790-8. PubMed PMID: 23400332; PubMed Central PMCID: PMC3628400.
16. Long AR, O'Brien CC, Malhotra K, Schwall CT, Albert AD, Watts A, Alder NN. A detergent-free strategy for the reconstitution of active enzyme complexes from native biological membranes into

nanoscale discs. BMC biotechnology. 2013;13:41. doi: 10.1186/1472-6750-13-41. PubMed PMID: 23663692; PubMed Central PMCID: PMC3702409.
17. Zhang Z, Zhang L, Hua Y, Jia X, Li J, Hu S, Peng X, Yang P, Sun M, Ma F, Cai Z. Comparative proteomic analysis of plasma membrane proteins between human osteosarcoma and normal osteoblastic cell lines. BMC cancer. 2010;10:206. doi: 10.1186/1471-2407-10-206. PubMed PMID: 20470422; PubMed Central PMCID: PMC2880991.
18. Cao R, Li X, Liu Z, Peng X, Hu W, Wang X, Chen P, Xie J, Liang S. Integration of a two-phase partition method into proteomics research on rat liver plasma membrane proteins. J Proteome Res. 2006;5(3):634-42. Epub 2006/03/04. doi: 10.1021/pr050387a. PubMed PMID: 16512679.
19. Bayburt TH, Grinkova YV, Sligar SG. Self-assembly of discoidal phospholipid bilayer nanoparticles with membrane scaffold proteins. Nano Letters. 2002;2(8):853-6. doi: Doi 10.1021/Nl025623k. PubMed PMID: ISI:000177485500013.
20. Denisov IG, Grinkova YV, Lazarides AA, Sligar SG. Directed self-assembly of monodisperse phospholipid bilayer Nanodiscs with controlled size. J Am Chem Soc. 2004;126(11):3477-87. Epub 2004/03/18. doi: 10.1021/ja0393574. PubMed PMID: 15025475.
21. Romero-Calvo I, Ocon B, Martinez-Moya P, Suarez MD, Zarzuelo A, Martinez-Augustin O, de Medina FS. Reversible Ponceau staining as a loading control alternative to actin in Western blots. Analytical Biochemistry. 2010;401(2):318-20. doi: Doi 10.1016/J.Ab.2010.02.036. PubMed PMID: ISI:000277397400021.
22. Reinila M, MacDonald E, Salem N, Jr., Linnoila M, Trams EG. Standardized method for the determination of human erythrocyte membrane adenosine triphosphatases. Analytical biochemistry. 1982;124(1):19-26. PubMed PMID: 6214964.
23. Sarkar PK. A quick assay for Na+-K+-AtPase specific activity. Zeitschrift fur Naturforschung C, Journal of biosciences. 2002;57(5-6):562-4. PubMed PMID: 12132703.
24. Luu HH, Kang Q, Park JK, Si W, Luo Q, Jiang W, Yin H, Montag AG, Simon MA, Peabody TD, Haydon RC, Rinker-Schaeffer CW, He TC. An orthotopic model of human osteosarcoma growth and spontaneous pulmonary metastasis. Clin Exp Metastasis. 2005;22(4):319-29. doi: 10.1007/s10585-005-0365-9. PubMed PMID: 16170668.
25. Seddon AM, Curnow P, Booth PJ. Membrane proteins, lipids and detergents: not just a soap opera. Biochimica et biophysica acta. 2004;1666(1-2):105-17. doi: 10.1016/j.bbamem.2004.04.011. PubMed PMID: 15519311.
26. Kunimoto M, Shibata K, Miura T. Comparison of the cytoskeleton fractions of rat red blood cells prepared with non-ionic detergents. Journal of biochemistry. 1989;105(2):190-5. PubMed PMID: 2722765.
27. Nakamura S, Rodbell M. Octyl glucoside extracts GTP-binding regulatory proteins from rat brain "synaptoneurosomes" as large, polydisperse structures devoid of beta gamma complexes and sensitive to disaggregation by guanine nucleotides. Proceedings of the National Academy of Sciences of the United States of America. 1990;87(16):6413-7. PubMed PMID: 2117281; PubMed Central PMCID: PMC54544.
28. Coderch L, Fonollosa J, De Pera M, Estelrich J, De La Maza A, Parra JL. Influence of cholesterol on liposome fluidity by EPR. Relationship with percutaneous absorption. Journal of controlled release : official journal of the Controlled Release Society. 2000;68(1):85-95. PubMed PMID: 10884582.
29. Hofsass C, Lindahl E, Edholm O. Molecular dynamics simulations of phospholipid bilayers with cholesterol. Biophysical journal. 2003;84(4):2192-206. doi: 10.1016/S0006-3495(03)75025-5. PubMed PMID: 12668428; PubMed Central PMCID: PMC1302786.
30. Zhang Y, Fonslow BR, Shan B, Baek MC, Yates JR, 3rd. Protein analysis by shotgun/bottom-up proteomics. Chem Rev. 2013;113(4):2343-94. doi: 10.1021/cr3003533. PubMed PMID: 23438204; PubMed Central PMCID: PMC3751594.
31. Ishihama Y, Oda Y, Tabata T, Sato T, Nagasu T, Rappsilber J, Mann M. Exponentially modified protein abundance index (emPAI) for estimation of absolute protein amount in proteomics by the number of sequenced peptides per protein. Mol Cell Proteomics. 2005;4(9):1265-72. doi: 10.1074/mcp.M500061-MCP200. PubMed PMID: 15958392.

32. Goluch ED, Shaw AW, Sligar SG, Liu C. Microfluidic patterning of nanodisc lipid bilayers and multiplexed analysis of protein interaction. Lab on a chip. 2008;8(10):1723-8. doi: 10.1039/b806733c. PubMed PMID: 18813396.
33. Mulgrew-Nesbitt A, Diraviyam K, Wang J, Singh S, Murray P, Li Z, Rogers L, Mirkovic N, Murray D. The role of electrostatics in protein-membrane interactions. Biochimica et biophysica acta. 2006;1761(8):812-26. doi: 10.1016/j.bbalip.2006.07.002. PubMed PMID: 16928468.
34. Dowhan W. Molecular basis for membrane phospholipid diversity: why are there so many lipids? Annu Rev Biochem. 1997;66:199-232. doi: 10.1146/annurev.biochem.66.1.199. PubMed PMID: 9242906.
35. Bezzine S, Bollinger JG, Singer AG, Veatch SL, Keller SL, Gelb MH. On the binding preference of human groups IIA and X phospholipases A2 for membranes with anionic phospholipids. J Biol Chem. 2002;277(50):48523-34. doi: 10.1074/jbc.M203137200. PubMed PMID: 12244093.
36. Simons K, Toomre D. Lipid rafts and signal transduction. Nature reviews Molecular cell biology. 2000;1(1):31-9. doi: 10.1038/35036052. PubMed PMID: 11413487.
37. Sheets ED, Holowka D, Baird B. Membrane organization in immunoglobulin E receptor signaling. Current opinion in chemical biology. 1999;3(1):95-9. PubMed PMID: 10021405.
38. Wydro P. The interactions between cholesterol and phospholipids located in the inner leaflet of human erythrocytes membrane (DPPE and DPPS) in binary and ternary films--the effect of sodium and calcium ions. Colloids and surfaces B, Biointerfaces. 2011;82(1):209-16. doi: 10.1016/j.colsurfb.2010.08.041. PubMed PMID: 20864321.
39. Lee AG. How lipids affect the activities of integral membrane proteins. Biochimica et biophysica acta. 2004;1666(1-2):62-87. doi: 10.1016/j.bbamem.2004.05.012. PubMed PMID: 15519309.
40. Takeuchi K, Ito F. Receptor tyrosine kinases and targeted cancer therapeutics. Biological & pharmaceutical bulletin. 2011;34(12):1774-80. PubMed PMID: 22130229.
41. Wu ZL. Phosphatase-coupled universal kinase assay and kinetics for first-order-rate coupling reaction. PloS one. 2011;6(8):e23172. doi: 10.1371/journal.pone.0023172. PubMed PMID: 21853082; PubMed Central PMCID: PMC3154929.
42. Kubo T, Piperdi S, Rosenblum J, Antonescu CR, Chen W, Kim HS, Huvos AG, Sowers R, Meyers PA, Healey JH, Gorlick R. Platelet-derived growth factor receptor as a prognostic marker and a therapeutic target for imatinib mesylate therapy in osteosarcoma. Cancer. 2008;112(10):2119-29. doi: 10.1002/cncr.23437. PubMed PMID: 18338812.
43. Arora A, Scholar EM. Role of tyrosine kinase inhibitors in cancer therapy. The Journal of pharmacology and experimental therapeutics. 2005;315(3):971-9. doi: 10.1124/jpet.105.084145. PubMed PMID: 16002463.

CHAPTER IV: DIFFERENTIAL LIPID PROFILE OF METASTATIC OSTEOSARCOMA CELLS VIA LIPIDOMICS

4.1 ABSTRACT

Osteosarcoma (OS) is the most common form of primary bone cancer in humans. The early detection and subsequent control of metastasis has been challenging in OS. Lipids are important constituents of cells that act as signaling molecules, maintaining structural integrity as well as storage of energy, and are reprogrammed in cancerous states. Herein, we investigate the global lipidomic differences in metastatic (143B) and non-metastatic (HOS) human OS cells as compared to normal fetal osteoblast cells (FOB) using lipidomics. We detect fifteen distinct lipid classes in all the three cell lines that included ~1500 lipid species across various classes including phospholipids, sphingolipids and ceramides, glycolipids and cholesterol. The statistical significance in the class wise differences was ascertained using ANOVA and the individual species were analyzed using the non-parametric Wilcoxon rank sum test and the comparison was corrected by Benjamini-Hochberg false discovery rate (FDR). Finally, we identify a key class of lipids, diacylglycerols are overexpressed in metastatic OS cells as compared to their non-metastatic or non-tumorigenic counterparts. We show that blocking diacyglycerol synthesis reduces cellular viability and reduce cell migration in metastatic osteosarcoma cells. Thus, the differentially regulated lipids in this study can be targets for biomarker development and the synthesis and metabolism of specific lipids can be targeted for therapeutic development.

4.2 INTRODUCTION

Osteosarcoma (OS) is the most common form of primary bone cancer in humans. The treatment options for OS consists of multi-agent induction chemotherapy, and tumor excision and adjuvant chemotherapy. The survival rates remain poor despite aggressive treatment. In patients with localized disease, 5-year survival rates are approximately 65%; however, in the case of metastatic disease, the 5-year survival rates have plateaued to about 20% (98, 99). Although progress has been made towards improving treatment options in OS, the early detection and subsequent control of metastasis has been challenging. Lipids are important constituents of cells that act as signaling molecules, maintaining structural integrity as well as storage of energy, and are often reprogrammed in cancerous states (185). The discovery of metabolically altered pathways

especially those related to lipid synthesis can aid in understanding the mechanism of tumor formation and metastasis and can aid in the development of novel OS therapeutics.

Lipids are an important component of the cellular machinery. They encompass a large class of biomolecules including diversity in backbone, chain length as well as number and position of unsaturated bonds (186, 187). While the functional consequences of lipid diversity are not fully understood, it is well characterized that lipids help regulate a variety of cellular functions including protein signaling in the membrane as well as homeostasis (188, 189). Thus, the dysregulation in lipid metabolism is linked to a variety of pathological conditions including immune disorders and cancer (190).

Cancer cells are metabolically reprogrammed to sustain their uncontrolled growth and proliferation. An increased production of lipids, nucleic acids and proteins is required to drive downstream oncogenic processes (185). While significant research has delved into the transcriptomics and proteomics of various cancers, the lipidomic profiles of most cancers remain poorly understood Lipids form a major component of the plasma membrane and various cellular membranes, as well as in vesicles for inter- and intra-cellular transport. Altered lipid composition leads to changes in membrane fluidity and cellular polarization (191). Thus the lipidomic profiles of cancer cells can lead to the development of biomarkers, identify potential therapeutic targets and help understand the underlying mechanisms of the diseased state.

Various analytical approaches have been taken towards understanding lipid profiles of cancer cells. The expression level and activity profiling of various lipid synthesis enzymes have been performed to identify increased fatty acid synthase activity and ATP citrate lyase activity in tumors (192, 193). Microarray profiling of metabolic genes has revealed altered cholesterol metabolism and LDL profile (194). Raman spectroscopy has also been employed for understanding cellular lipid profiles at the single cell level (195) as well as 31P NMR spectroscopy has been employed towards lipidomic profiling (196).

The complexity in study of lipids arises from the similarity in structures of lipids accompanied with overlapping mass. Lipids are classified in various ways including classifications based on their chain length, backbone or saturation levels. Based on their backbone, lipids are classified mainly into phospholipids, glycolipids, sphingolipids and sterols (Figure 1). The saponifiable part of phospholipids, glycolipids and sphingolipids are free fatty acids. Thus mixtures of lipids are

highly diverse and numerous, based on combinations of fatty acids and the backbone. The development of mass spectrometric techniques has enabled the separation and identification of complex lipid mixtures. Soft ionization techniques including ESI and MALDI allow lipids to remain intact for mass spectrometric analyses. These techniques, in combination with highly specialized softwares, are also quantitative allowing a thorough and high-throughput analysis of the lipid mixtures.

The use of mass spectrometry to study cancer lipidomics has precedence in breast cancer, prostate cancer and adenocarcinoma among others (69, 70, 197). Phospholipids are the largest class of structural lipids and have been widely explored in various cancers. It has been observed that lysophosphatidylcholine (LPC) levels are increased in aggressive breast cancer cell lines (198). Individual lipid species including palmitate-containing phosphatidylcholines are overexpressed in malignant cancers (68). Furthermore, data obtained from lipidomics has been compared to transcriptomic data to discover specific lipid markers like cholesteryl oleate (CE) for prostate cancer and correspondingly overexpressed scavenger receptor class B type I resulting in CE accumulation (73).

Although, there are several examples of lipidomics in cancer types of epithelial origin, the lipidomic profiles of cancers of mesenchymal origin such as osteosarcoma (OS), has remained unexplored. In this work, we investigate the global lipidomic differences in metastatic and non-metastatic OS cells as compared to normal fetal osteoblast cells in a high throughout manner. We identified over 1500 lipid species across various classes including phospholipids, sphingolipids and ceramides, glycolipids and cholesterol. Differences in lipid profiles between the classes as well as difference between specific lipids were observed in all the classes of lipid that were examined. The statistical significance in the class wise differences was ascertained using ANOVA and the individual species were analyzed using the non-parametric Wilcoxon rank sum test (199) and the comparison was corrected by Benjamini-Hochberg false discovery rate (FDR) in MATLAB, accounting for false discovery rates. Furthermore, the lipidomic signature of each class was identified using principal component analysis. Finally, we identify a key class of lipids, diacylglycerols as being preferentially upregulated in the tumorigenic cell lines as compared to the non-cancerous control cell line. We block the pathway of diacylglycerol synthesis and show that it induces apoptosis as compared to non-treatment control as well as reduces migratory potential

of the metastatic cells. Taken together, in this work we compare the global lipidomic profile of osteoblasts, and non-metastatic and metastatic osteosarcoma cell lines. We further identify several differentially regulated pathways including diacylglycerols, which can serve as biomarkers and targeted for potential therapeutics.

4.3 MATERIALS AND METHODS

Materials: Amplex red kit was obtained from Thermo Scientific catalog no. A12216. PLC inhibitor U73122 was obtained from Enzo catalog no. BML-ST391-0005. U73122 was obtained from Santa Cruz Biotechnology (sc-3574).

Cell culture: Human cell lines FOB, HOS and 143B were cultured in DMEM (Gibco, Invitrogen, Carlsbad, CA, USA) supplemented with 10% fetal bovine serum (FBS) and 1mgml–1 penicillin–streptomycin (Gibco, Invitrogen) at 37 °C and 5% CO2 in a humidified incubator. FOB cells were kindly provided by Dr. Avudaiappan Maran at Mayo Clinic, Rochester, Minnesota.

Extraction of Lipids: Cells were grown to 80-90% confluency. Cells were detached using scraping and cell count was performed. The cell suspension was immediately diluted with PBS (1:1) and centrifuged 5 min at 1700 rpm. The cell pellet was washed three times with 1ml PBS, followed by centrifugation at 1700 rpm for 5 min, and cells resuspended in 1ml PBS. The cells were lysed using 6 freeze thaw cycles rapidly. Total lipids from all cell lines were extracted with the Bligh and Dyer method (200). Briefly, 3.75 ml chloroform/methanol 1:2 (v/v) was added to 1ml of cell sample, vortexed well for 15 min, and incubated on ice for 5 min. An additional volume of 1.25 ml chloroform and 1.25 ml dH2O were added. Finally, following vigorous vortex for 5 min, samples were centrifuged at 1,000 rpm for 5 min at room temperature to obtain a two-phase system: aqueous top phase and organic bottom phase from which lipids were obtained. This was dried down and submitted for MS.

Lipidomics Analysis:

Sample preparation: 200 uL methanol, 100 uL chloroform, and 30 uL water were added into the dried sample. After centrifugation, 150 uL of aliquot from aforementioned solution was spiked with 5 uL 50 ug/mL internal mixture (Cer 18:1/12:0; PC 12:0/12:0; PE 14:0/14:0; PG 14:0/14:0;PS 14:0/14:0) before instrument injection.

Instrument analysis: The samples were analyzed by using the Thermo Q-Exactive MS system (Bremen, Germany) in the Metabolomics Laboratory of Roy J. Carver Biotechnology Center, University of Illinois at Urbana-Champaign. Software Xcalibur 3.0.63 was used for data acquisition and analysis. The Dionex Ultimate 3000 series HPLC system (Thermo, Germering, Germany) used includes a degasser, an autosampler, and a binary pump. The LC separation was performed on an Thermo Accucore C18 column (2.1 x 150 mm, 2.6 μm) with mobile phase A (60% acetonitrile: 40% H2O with 10 mM ammonium formate and 0.1% formic acid) and mobile phase B (90% isopropanol : 10% aceontrile with with 10 mM ammonium formate and 0.1% formic acid). The flow rate was 0.4 mL/min. The linear gradient was as follows: 0 min, 70% A; 4 min, 55% A; 12 min, 35% A; 18 min, 15% A; 20 -25 min, 0% A; 26-33 min, 70% A. The autosampler was set to 15°C and the column was kept at 45°C. The injection volume was 10 μL. Mass spectra were acquired under both positive (sheath gas flow rate, 50; aux gas flow rate: 13; sweep gas flow rate, 3; spray voltage, 3.5 kV; capillary temp, 263 °C; Aux gas heater temp, 425 °C) and negative electrospray ionization (sheath gas flow rate, 50; aux gas flow rate: 13; sweep gas flow rate, 3; spray voltage, -2.5 kV; capillary temp, 263 °C; Aux gas heater temp, 425 °C). The full scan mass spectrum resolution was set to 70,000 with the scan range of m/z 230 ~ m/z 1,600, and the AGC target was 1E6 with a maximum injection time of 200 ms. For MS/MS scan, the mass spectrum resolution was set to 17,500. AGC target was 5E4 with a maximum injection time of 50 ms. Loop count was 10. Isolation window was 1.0 m/z with NCE of 25 and 30 eV.

Data analysis: Thermo software LipidSearch (v.4.1.30) was used for lipid identification. The lipid signal responses were normalized to sample dry weight and the corresponding internal standard signal response (for those lipid classes without corresponding internal standard, positive lipid ion signals were normalized with the signal of internal standard Cer 18:1/12:0 and negative ion signals were normalized with the signal of internal standard PG 14:0/14:0.

Statistical Analysis: The high dimensional lipidomic data of three cell lines with their three replicates were orthogonally transformed to a lower dimensional eigenspace using principal component analysis (PCA) in MATLAB. The lower dimensional space is formed by three principal components (PC) that contain more than 85% of the data.

In order to identify the details of separation in lipid profiles of three cell lines, a two sample statistical test was used to compare a cell line versus each of the other two, resulted in a total of

three comparisons. The non-parametric Wilcoxon rank sum test (199) implemented in MATLAB was used to calculate the p-values. The comparison was corrected by Benjamini-Hochberg false discovery rate (FDR) control [2] and FDR values were calculated in MATLAB. Moreover, fold-change was jointly used with p-values to compare different levels in lipidomic profiles and determine significant regulations.

This procedure of statistical testing was executed in a global analysis among 17 lipid classes as well as an analysis of individual lipid profiles. Moreover, a third analysis was accomplished to characterize different lipid levels in treated versus untreated 143B cell lines. The global lipid profile is presented by lipid levels for all the 16 lipid classes in three cell lines with 3 replicates for each cell line. Therefore, a global lipid level value assigned to a lipid class in a replicate of one of the cell line is attained by adding up the profiles of all lipids belonging to that class and measured in the same replicate of the corresponding cell line. Finally, the global lipid profile is fed to the statistical testing procedure to identify significantly regulated lipids. In all three lipidomic analyses, the significance is assigned if fold-change > 2-fold or fold-change < 0.5-fold. Moreover, as a second measure in global and individual lipid analyses, significance is assigned if FDR < 0.15 and FDR < 0.13 respectively. For the third analysis between treated and untreated 143B cell lines, FDR < 0.07 was used to assign significance.

Identification of differentially expressed genes (DEGs) was carried by same statistical testing explained above. For gene expression analysis, significance is assigned if fold-change > 2-fold or fold-change < 0.5-fold and p-value < 0.05 (No significantly regulated genes were found for FDR < 0.35).

Amplex red cholesterol assay: Lipids were extracted as outlined in the Bligh and Dyer protocol above. The lipids were suspended in reaction buffer and the protocol was followed as outlined for Amplex red cholesterol assay (Thermo Scientific catalog no. A12216). Briefly, 50 µL of lipid extract and 50 µL of the Amplex® Red reagent/HRP/cholesterol oxidase/cholesterol esterase working solution or working solution without esterase was added to the appropriate well and incubated in the dark at 37° C for 90 minutes. The plate was read using a spectramax II with excitation at 534 nm and emission at 590 nm. The samples were compared to cholesterol standard and normalized to cell number.

Cell titer blue assay: 20,000 cells were plated per well in 96 well plates and allowed to adhere overnight. In the morning, the cell media was aspirated and replaced with fresh 100 µL of cell media and incubated with compound or DMSO vehicle control (1 µL) and allowed to incubate at 37 °C and 5% CO2 in a humidified incubator for 4 hours. 20 µL of cell titer blue reagent was added and the plate was incubated for 1 hour before the fluorescence was read using a plate reader with excitation at 534 nm and emission at 590 nm.

Wound healing assay: Cells were grown to a confluent monolayer in 12 well plates and a scratch was made across the center of the plate with a pipette tip and images were taken. The media was replaced with fresh media and treatment or vehicle control was added to the wells. The cells were maintained at 37 °C and 5% CO2 in a humidified incubator and images were taken every two hours. The images were processed using ImageJ via the wound healing plugin and normalized to 100% area at time 0.

4.4 RESULTS

Global lipidomics profile of osteosarcoma cells: To evaluate the lipidomic differences in osteosarcoma as compared to non-tumorigenic cells, we compared human osteoblast cells (FOB) to HOS osteosarcoma cells which are non-metastatic and with 143B cells which are highly metastatic (105). The total lipid was extracted from roughly 90% confluent cell plates using Bligh and Dyer method (200) for three separate experiments (n=3). Total lipid extract was subjected to LC-MS/MS analysis by Thermo Q-Exactive Hybrid Quadrupole-Orbitrap Mass Spectrometer and the data was searched against LIPIDSEARCHTM (Thermo Scientific) software to identify specific lipid species. The lipids were then normalized to respective internal standards and cell count from that sample to avoid instrument errors as well as errors due to different amounts of cells in each sample.

Greater than 1000 species of lipids were identified in each of the cell lines (Appendix IV). The highest number of species was identified in phosphatidylcholines (PC) followed by phosphatidylethanolamines (PE) and cardiolipin (CL). The global data was statistically analyzed using single factor ANOVA and Tuckey post-hoc test. Figure 4.2 shows the global lipidomic changes by ANOVA. Furthermore, to gain more rigorous and specific information, the different classes as well as single lipid species were tested by the non-parametric Wilcoxon rank sum test (199) and the comparison was corrected by Benjamini-Hochberg false discovery rate (FDR)

control in MATLAB. A secondary analysis yielded finer details of what specific species within a class were upregulated and downregulated. The various class wise differences are represented in figure 4.3. A similar treatment of individual species is represented in figure 4.4 which shows the significantly upregulated species in each class. The data corresponding to figure 4.4 is given in Appendix IV. We note that in classes with low number of individual species, the results typically appear amplified and therefore results for MG (7 species), Pet (7), PA (6) and LPE (4) are not very as reliable as classes with higher totals species. Therefore, we focus on the lipid classes that are significantly upregulated or downregulated and discuss them further.

Finally, a principal component analysis (PCA) was performed on the lipidomes of the different OS cell types (FOB, HOS, 143B) to distinguish the normal osteoblast cells (FOB) as compared to the non-metastatic and metastatic cells (HOS, 143B). As seen in figure 4.5A, in the PCA score plot, the OS cells (HOS and 143B) are separated in a different ellipsoid space from the normal osteoblast cells. This is also reflected in the two dimensional plot in figure 4.5B. The various classes and the specific species that were differentially regulated have been discussed below. We have discussed both total lipid content in each class and the type of lipid species in each class.

Phosphatidylcholines (PCs) and Lysophosphatidylcholine (LPCs)

Phosphatidylcholines (PCs) are the largest class of membrane phospholipids. LPC are phosphatidylcholines that arise from partial hydrolysis of PCs. PCs and LPCs were analyzed in positive ion mode. 130 species of PCs and 21 species of LPCs were detected (Appendix IV). Overall, similar levels of PC species were found in all three cell lines. The levels of PC in normal osteoblast FOB cells was slightly higher than HOS and 143B cells albeit insignificantly as analyzed by ANOVA and Wilcoxon tests.

Figure 4.4 represents the upregulation in specific species. As indicated in the labels, the three different colors represent the differential regulation in a class versus another. As seen in figure 4.4, about 20% species are differentially regulated in FOB vs HOS, about 60% between HOS and 143B and about 50% species are differentially regulated between FOB and 143B. PC (34:1) was the most abundant species in all three cell lines

As PCs form a large class of structural lipids, significant alteration in PC levels is not expected. However, lysophosphatidylcholine (LPCs) and sub-class of PCs have been correlated with various

cancers (201, 202). Herein, we observed that the amount of LPC was significantly higher in FOB cells than in 143B cells (p= 0.015) by ANOVA. This corresponds to the non-parametric global analysis test where LPC is downregulated in 143B with respect to both HOS and FOB cells as shown in figures 4.2 and 4.3. The amount of saturated LPCs was higher in all three cell lines as compared to the unsaturated LPC counterparts. However, both saturated and unsaturated LPCs were significantly higher in FOB cells as compared to the tumorigenic cell lines

Among specific LPC species higher plasma levels of LPC (18:0) have been related to lower risk of cancer (203). This was corroborated in our results where FOB cells had the highest amount of LPC (18:0) and was significantly higher than 143B cells (p= 0.014) and modestly higher than HOS (p= 0.099). Figure 4.4 shows the comparison of individual species in all cell lines. About 20% species were different among FOB and HOS and about 30% differential regulation was seen between HOS vs 143B and FOB vs 143B.

Phosphatidylethanolamines (PE) and Lysophophatidylethanolamines (LPEs)

PEs are positively charged phospholipids that account for 25% of all phospholipids. LPEs are derived from partial hydrolysis of PEs similar to LPCs (from PCs). Both PEs and LPEs were measured in negative ion mode. 117 PE species and 4 LPE species were detected (Appendix IV). Overall, no significant changes were observed in PE levels among the three cell lines by ANOVA and Wilcoxon test (Figure 4.2 and 4.3). There was a slight gradient decrease on going from osteoblasts to non-metastatic to metastatic cells, but these differences were not statistically significant. These results are in agreement with literature in breast cancer cell lines where MCF-10A non-malignant cell lines had higher abundance of PE than the corresponding cancerous cells (69).

The most abundant species was PE (18:0) in HOS and FOB cells. However, PE (18:1) was the most abundant in 143B metastatic cells. As observed in figure 4.4, under 30% of the PE individual species were differentially regulated in FOB vs HOS, 60% between HOS vs 143B and about 40% between FOB and 143B.

Similar to the trend observed in LPCs, the levels of LPEs were significantly higher in FOB versus 143B cells (p= 0.009). LPEs were highest in FOB cells, followed by HOS and least in 143B cells (Figure 4.2). A moderate change in LPE levels was also observed on going from non-metastatic

HOS to metastatic 143B cells (p=0.072). Due to low number of LPE species detected, the statistical data for individual species as seen in figure 4.4 is unreliable for LPE>

Phosphatidylserines (PS)

Phosphatidylserines are negatively charged membrane proteins that are typically present in the inner cell membranes (204). However, in cells undergoing apoptosis they flip out to the outer membrane in cells undergoing apoptosis (205). 43 species of PS were detected in our studies in negative ion mode (Appendix IV). The differences between the three cell lines were not significant by ANOVA and Wilcoxon tests (Figure 4.2 and 4.3).

However, specific lipid species were differently expressed. As seen in figure 4.4, there was less than 10% difference in the individual species between FOB and HOS. However, over 50% species were differentially regulated in HOS vs 143B and 30% species between FOB and 143B potentially suggesting a role for specific PS species in the metastatic process.

Sphingolipids- Ceramides (Cer) and Sphingomyelins (SM)

Sphingomyelins and ceramides are lipids with a sphingosine backbone. Ceramides were analyzed in positive ion mode and total of 124 individual ceramide species were detected (Appendix IV). Among these 20 CerG1, 14 CerG2 and 9 CerG3 ceramides of the simple Glc series (neutral glycosphingolipids) were detected. Overall ceramides were found to be significantly downregulated in HOS vs FOB cells by Wilcoxon test (figure 4.3). The tumorigenic cells showed slightly less amount of total ceramides than their osteoblast counterpart. Specifically, HOS cells had the least amount of ceramides followed by 143B with FOB exhibiting the highest amount (figure 4.2).

Comparing the individual species in the three cell lines, as seen in figure 4.4, there is about a 45% difference between FOB and HOS, HOS and 143B and FOB and 143B.

Sphingomyelins were analyzed in positive ion mode. 101 SM species were detected (Appendix IV) and overall the differences in SM content in all 3 lines remained relatively consistent (figure 4.2). However, the levels of SM were slightly less in the metastatic 143B cells as compared to the osteoblast FOB cells and non-metastatic HOS cells (figure 4.2).

Specifically, several SM species were significantly lower in 143B cell lines and sometimes below the threshold of detection. These were SM(d18:1/19:0), (d40:4), (d42:5), (d44:4), (d44:7), (d46:7) and (d48:2). As seen in figure 4.4, all classes showed several differentially regulated species. A 50-60% difference in individual species was observed in all three comparisons FOB vs HOS, HOS vs 143B and FOB vs 143B.

Cardiolipins (CL)

Cardiolipin is an inner mitochondrial membrane phospholipid constituting 20% of the membrane lipid composition (206). 142 CL species were detected in negative ion mode (Appendix IV). As seen from figures 4.2 and 4.3, CL expression in HOS cells is significantly more than in FOB and 143B cell lines.

As shown in figure 4.4, there is a 45% difference in individual species in FOB vs HOS, about 65% between HOS and 143B and about 30% between FOB and 143B.

Cholesteryl Esters (ChE)

Cholesteryl esters are fatty acid esters of cholesterol through the hydroxyl group of cholesterol. They are a biologically inert form of cholesterol storage and liberate cholesterol when it is required for membrane and lipoprotein formation (207). In our data, 38 distinct species of cholesteryl esters were detected in positive ion mode (Appendix IV). While the levels of ChE in FOB and HOS cells was relatively similar, the amount of ChE in 143B cells was significantly lesser ($p= 0.045$ HOS vs 143B and $p= 0.068$ FOB vs 143B) by ANOVA (Figure 4.2). This is reflected in the non-parametric global analysis in figure 4.3 where 143B is downregulated as compared to both HOS and FOB cells.

Several distinct species of ChE were downregulated in 143B vs HOS and FOB. These include 18:1, 18:2, 20:3, 20:4, 20:5, 22:3, 22:4, 22:5, 22:6 and 24:4, 24:5, 24:6, 26:0, 28:1, 30:1 and 30:5 (Figure 4.6B). Conversely however, three species were significantly higher in 143B vs FOB and HOS cells. These were 28:1, 30:1 and 30:3. As observed in figure 4.4, HOS and FOB have only 10% species differentially regulated. However there are greater than 60% difference in species when 143B is compared to FOB or HOS.

Total cholesterol was not measured in our studies via high throughput lipidomics since the ESI-MS platform is not well suited for detection of free cholesterol. However, as the interest in cholesterol and cholesterol metabolism and their correlation with cancer has increased in literature, we measured both total cholesterol as well as cholesteryl esters in our cells through amplex red measurement (208). The assay is based on the oxidation of cholesterol in the presence of cholesterol oxidase. The hydrogen peroxide so generated converts the amplex red to resorufin, which is a fluorescent molecule. The assay is further modified to convert cholesterol esters to free cholesterol first by using cholesterol esterase and thus gives a measurement of total cholesterol in the cells. In our assay, we performed the experiment with all three cell lines with and without cholesterol esterase to examine the amount of free cholesterol, cholesterol esters and total cholesterol in each cell line. As observed in figure 4.6A, the total cholesterol levels were greatest in FOB cells, followed by 143B cells and then HOS cells. However, none of these differences were significant. The amount of free cholesterol also followed the same pattern in levels. Finally, the difference between total cholesterol and free cholesterol was calculated to determine the amount of cholesteryl esters. As observed in figure 4.6A, the amount of ChE was greatest in FOB followed by HOS and very low in 143B, although these differences were not statistically significant. These values indicate that the levels of esterified cholesterol are lower in 143B cells as compared to FOB and HOS cells thereby confirming results found in our lipidomics data.

MonoacylGlycerols (MG)

Monoacylglycerols contain one glycerol moiety connected to a fatty acid through an ester bond. MGs are catabolized by monoacylglycerol lipase (MAGL) to form free fatty acid and glycerol and the overexpression of MAGL in cancers has generated recent interest in this pathway. In our studies we detected seven MG species in positive ion mode with four saturated and three monounsaturated species (Appendix IV). A significant overexpression of MG was observed in 143B metastatic cells as compared to both non-metastatic HOS ($p=0.0105$) and osteoblast FOB ($p=0.0069$) cells by ANOVA and is also reflected by the results of the non-parametric global analysis (figure 4.2 and 4.3). However the difference between HOS and FOB cells was not significant. The low number of MG species makes the species differences in figure 4.4 statistically not reliable.

DiacylGlycerols (DG)

Diacylglycerols contain two glycerol units esterified with a fatty acid backbone. DG levels in cancer cells has been shown to be dysregulated, signaling through the protein kinase C pathway (209). Additionally, the levels of DG have been shown to affect the effectivity of drugs such as fatty acid synthase inhibitors in cancer cells (210). In our studies, 54 DG species were detected in positive ion mode (Appendix IV).

Different regulation of DG species was observed in 143B cells as compared to HOS cells ($p=0.029$) and FOB cells ($p=0.07$) by ANOVA (figure 4.2). Although the latter is not significant by ANOVA, both are reflected in the global Wilcoxon test as significant regulations (figure 4.3).

As seen in figure 4.4, over 60% species were differentially regulated in 143B as compared to FOB and HOS, making this class one of the hallmark characteristics of the 143B cell line. There was only a 30% difference between FOB and HOS.

Phosphatidic Acids (PA)

Phosphatidic acids are components of the membrane and generate DAGs as mentioned previously. DAG itself converts to PA in the presence of DAG kinases that are also targets for cancer drugs (211). In our studies six PA species were detected in negative ion mode (Appendix IV). While ANOVA indicated the differences in PA levels to be not significant (figure 4.2), global Wilcoxon test revealed that PA is downregulated in HOS as compared to FOB cells (figure 4.3).

TriAcylGlycerols (TG)

Triacylglycerols contain three esterified glycerols on a fatty acid backbone. Similar to MG and DG, TGs are also implicated in various cancerous pathways. Particularly, increased levels of TG are associated with enhanced apoptosis (212, 213). Our results show a similar trend. 163 species of TG were identified in positive ion mode (Appendix IV) and the levels of TG were most in FOB cells, followed by HOS and least in 143B cells (Figure 4.2). The difference between FOB and 143B was significant with $p=0.03$ by ANOVA and was also reflected in the global Wilcoxon test (figure 4.3).

Specific species that were higher in FOB versus 143B cells were As observed in figure 4.4, there is a 20% difference in individual species levels in FOB vs HOS, 35% between HOS and 143B and about 50% between 143B and FOB.

DG inhibition results in reduced cell viability and migration

As identified in the previous section, diacylglycerols are a significantly upregulated population in the lipidome of 143B vs HOS and FOB cells. Therefore, we wanted to investigate if the inhibition of DG synthesis will result in reduced cell viability and migration. There are several different synthetic pathways for the formation of DGs. The chief pathway of synthesis is through the phospholipase C (PLC) catalyzed hydrolysis of phosphatidylinositol 4,5-bisphosphate (PIP2) in the membrane to form DG, which remains in the membrane and inositol-triphosphate (IP3), which acts as an intracellular signal transduction molecule. Alternately, DG can be produced from MGs by monoacylglycerol transferase and from phosphatidic acid through phosphatidic acid phosphatase (PAP). The inhibition of PLC to inhibit DG synthesis and its effects on various diseased states has been investigated (214, 215). In our studies, we used PLC inhibitor U73122 to block diacylglycerol synthesis and investigate its effects on metastatic 143B cells. First, 143B cells were incubated with 1 μM U73122 for four hours and lipids were extracted by the Bligh and Dyer method and analyzed by high-throughput lipidomics. As seen from figure 4.7A, the levels of DG were reduced in the treated samples as compared to the controls. Surprisingly, TG levels went up significantly after inhibitor treatment. We further looked at what percentage of individual species were affected by the inhibitor treatment. As seen in figure 4.7B, most classes of lipids were affected. This is expected, since DG synthesis is directly linked to most phospholipid synthesis (216).

Furthermore, as seen from figure 4.8A, the cell viability is reduced in all three cell lines, but the change is greatest in 143B cells, the presence of 0.1 μM, 0.5 μM and 1 μM of U73122 using the cell titer blue assay (217). Finally, a reduction in cell migration is also observed in 143B cells in the presence of U73122 as indicated by the wound healing assay (218) in figure 4.8B-D but the effect is not observed in HOS cells (figure 4.6D). While a PLC inhibitor affects various pathways in the cancer cell, this study exhibits that the reduction of DAG levels is a contributor towards reducing cell viability and reduction of cell migration, two hallmarks of cancer cells.

Finally, we wanted to explore if the gene expressions for the synthesis and metabolism of diacylglycerols concur with our data. We studied a published microarray gene expression data (219) available in GEO database (accession number: GSE66673) containing the gene expression during the early and late passages of HOS and 143B cells with three replicates (n=3) for all cell lines (219). This dataset contained 42545 probe sets that were mapped to either a known or a model RefSeq accession number and were grouped into 20724 unique genes. We used the data to identify differentially expressed genes in late passage 143B versus late passage HOS cells. Among all of the 20724 genes, 1415 genes passed our significance thresholds that gives a differentially expressed gene ratio of 0.068. In order to identify the differentially expressed genes in DG metabolism, we used KEGG database to obtain DG metabolic pathway. We identified 3 differentially identified genes in DG metabolism that were found to be upregulated in 143B versus the HOS cells- AGPAT9, PPAP2C and MGLL as shown in figure 4.9.

4.5 DISCUSSION

The lipidomic profiling of cancer cells has become an important area of research that has been facilitated by the improvement of mass spectrometric techniques that can identify as quantify very small quantities of lipids in mixtures of hundreds of species. While the investigation of the lipidome of breast cancer and prostate cancer cells has been recently explored, the investigation of lipidomic profiles of bone cancers has remained unexplored. In this work, we investigate the lipidomic profile of human osteosarcoma cell lines and compared them to a human osteoblast cell line. We perform high throughput lipidomics of osteoblasts (FOB), non-metastatic (HOS) and metastatic (143B) cells. Various classes and hundreds of individual species in each class were identified in our results and several of them were found to be differentially regulated.

Among the chief lipid classes, we found cholesteryl esters, cardiolipins, mono-, di- and triacylglycerols, lysophosphatidylcholines, lysophosphatidylethanolamines, as well as various individual lipid species to be significantly differentially regulated. In general, various patterns can be drawn from the global lipidomic changes represented in figures 4.2 and 4.3. Lipids that are differentially regulated in HOS or 143B vs FOB can be correlated with the process of tumorigenesis. Additionally, lipids that are differentially regulated in 143B vs HOS can be correlated with the metastatic process. As seen in figure 4.2 and 4.3, ceramides are downregulated in HOS cells and cardiolipins are upregulated in HOS cells as compared to FOB cells. Furthermore,

mono and diacylglycerols are upregulated in 143B vs HOS and LPC and LPE are downregulated in 143B vs HOS.

Ceramides are bioactive sphingolipids that have come to the forefront of cancer research. However, the various ceramide species, depending on the fatty acid conjugated to them have shown various properties including their roles in cellular proliferation or cancer cell death (220). For instance, C18-ceramide treatment suppresses tumor growth in head and neck cancer cells (221), however, the C16- ceramides induce head and neck squamous cell carcinoma tumor proliferation (222). Thus, a cumulative evaluation of ceramide species will not be accurate in representing the correlation of lipid with osteosarcoma. In our results, the levels of C18 ceramides was significantly less in 143B and HOS cells as compared to the FOB cells, which is in agreement with literature results. C-18 ceramide has been recognized as a serum biomarker for monitoring chemotherapy response as its levels increase with improvement in diseased state for HNSCC (223).

Conversely, cardiolipins (CL) maybe implicated in tumorigenesis. Indeed, CL has been found to impact prostate cancer cell proliferation (224). Specifically, C16 rich cardiolipin was found to stimulate proliferation and C18 cells were found to reduce proliferation. As observed from table ST1, C18 rich CL appear to have a higher expression in FOB cells as compared to 143B cells and C16 rich CL have a higher expression in 143B cells, therefore in agreement with literature observation. For example, CL(16:0/16:0/16:0/16:0) is not detected in FOB cells but is detected in both 143B and HOS cells and CL(18:4/18:2/18:2/18:2) is much lower in 143B cells as compared to FOB cells.

The abundance of LPCs in non-tumorigenic cell line as compared to the tumorigenic OS cell lines, indicates a faster metabolism of LPCs in OS cells as compared to the normal cells. Indeed, in human colorectal cancer, it has been shown that lysophosphatidylcholine acyltransferase 1 (LPCAT1), the enzyme that converts LPC to PC is overexpressed (225) and LPCAT1 expression has been investigated as a biomarker in prostate cancer as well (226). However, as the levels of LPC reduces in 143B cells as compared to HOS cells indicating that while they promote tumorigenesis, they may not be completely implicated in the process of metastasis.

Cholesterol and cholesterol metabolism have been found to be highly dysregulated in cancer (227). However, the underlying mechanism of this is not very well understood. The accumulation of

cholesterol is usually correlated with higher cancer progression and metastasis. However, in our studies we observed that the level of cholesteryl esters in metastatic OS cell line 143B was significantly less than the osteoblast and the non-metastatic cell lines. On exploring this further via an Amplex red detection of total cholesterol as well as cholesteryl esters in all three cell lines we found that the levels of cholesterol, both free and esterified, were higher, albeit not significantly, in normal osteoblast cells than tumorigenic osteosarcoma cells.

The other lipid signaling pathway of interest are acylglycerols. Mono-, di- and tri-acyl glycerols are important lipid components of the cell and all three were identified in our studies. While MGs and DGs increased in metastatic cells as compared to their non-metastatic counterparts, TGs reduced. While all three moieties are synthesized through various pathways, they also interconvert through various enzymatically facilitated pathways. Since the DG levels increase but no increase but the reverse trend is seen for TGs, it can be hypothesized that diacylglycerol transferase (DGAT), the enzyme responsible for the conversion of DG to TG is expressed less in metastatic cells. Conversely, it is possible that the lipase responsible for TG to DG conversion is overexpressed. Additionally, phosphatidic acid (PA) is converted to DAG by PAP (phosphatidic acid phosphatase) and it is possible that PAP is overexpressed resulting in high levels of DAG but similar levels of PA in the osteoblast versus osteosarcoma cells.

In our work, we show that inhibiting PLC and therefore inhibiting the DG synthesis pathway results in reduced cell viability and migration. DG is an important membrane lipid and acts as a secondary messenger. DG is known to bind directly to protein kinase C and D family, as well as to the Ras family (228, 229). The DG related activation of PKC and PKD plays an important role in cancer as they signal through multiple pathways and control the expression of genes controlling cell cycle progression, tumorigenesis and metastasis (230). Therefore, it is not surprising that the reduction of DG accumulation in cells reduces the cellular viability. Finally, we identify genes associated with the DG pathway that are differentially regulated. AGPAT9 encodes for glycerol-3-phosphate acyltransferase 3 (GPAT3). It catalyzes the conversion of glycerol-3-phosphate (G3P) to lysophosphatidic acid (LPA), which converts to phosphatidic acid and subsequently to diacylglycerol (231). The genetic upregulation of AGPAT9 in 143B therefore corresponds to the increased synthesis of diacylglycerol and thus higher levels of DGs in 143B cells than HOS. Interestingly, AGPAT9 is also known as metastasis associated gene 1 and activates the mTOR

pathway (232). PPAP2C gene encodes for lipid phosphate phosphohydrolase 2, which catalyzes the conversion of phosphatidic acid to diacylglycerol (233) and hence increases levels of DG overall. PPAP2C has been shown to be a potential anti-cancer drug target by genomic screening in transformed adult mesenchymal stem cells (234). Furthermore the knockdown of PPAP2C impaired anchorage-dependent in vitro growth of cancer cell lines and impaired the in vitro growth of primary mesenchymal stem cells but not differentiated human fibroblasts by delaying entry into S phase of the cell cycle and is transcriptionally regulated by p53.

4.6 CONCLUSION

This work compares the global lipidomic profile of normal osteoblast cells to non-metastatic and metastatic osteosarcoma cell lines. We show that various different lipid pathways and specific lipid species are differentially regulated in the diseased state. Furthermore, we identify that diacylglycerols are significantly upregulated in metastatic 143B cells as compared to HOS and FOB cells. We block the synthesis of DG though PLOC inhibition and exhibit that this reduces cell viability as well as cell migration in 143B cells. Finally, we identify 2 genes involved in DG synthesis pathway that are significantly upregulated and therefore can be potential therapeutic targets in osteosarcoma.

4.7 ACKNOWLEDGEMENTS

I would like to thank Mr. Payam Dibaeinia for his help with the statistical analysis in this work. I would also like to thank Dr. Lucas Li at the Roy J Carver Biotechnology Center for generating the lipidomic data.

4.8 FIGURES, TABLES AND LEGENDS

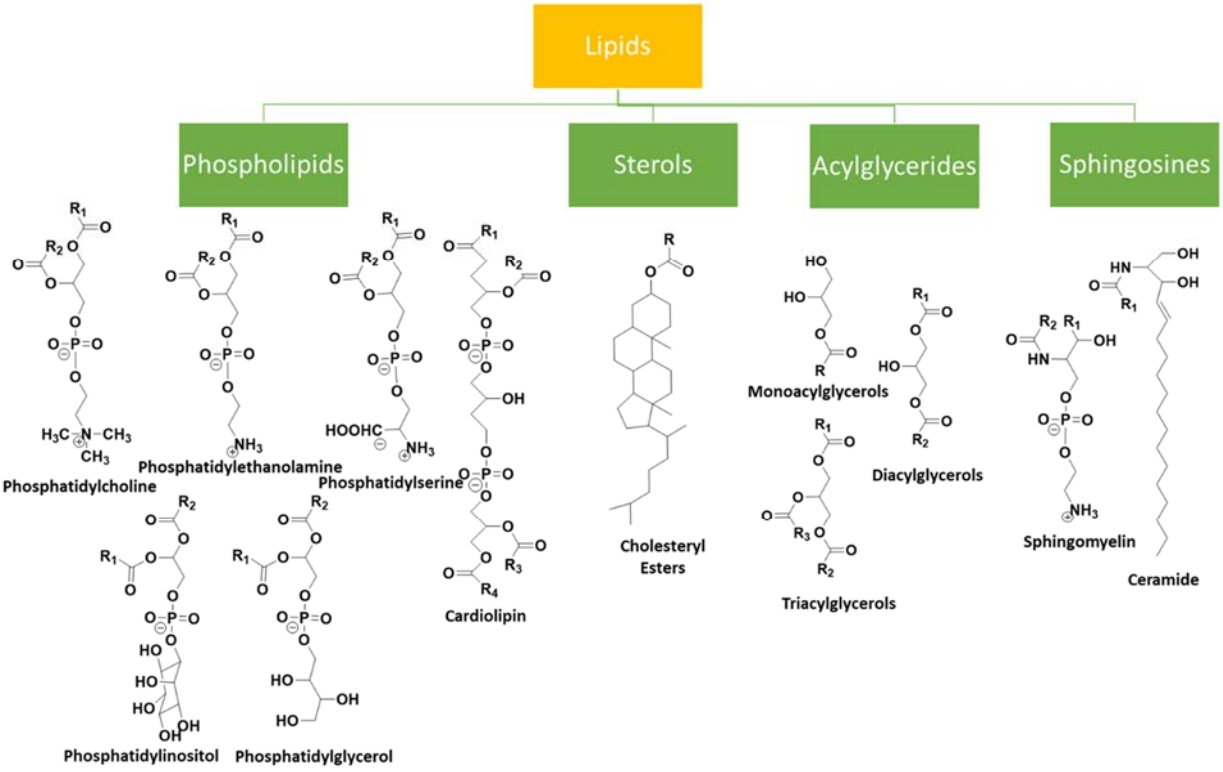

Figure 4.1: Figure shows the various classes of lipids. The major classes of biological lipids are phospholipids, sterols, acylglycerides and sphingolipids. Phospholipids are further classified into phosphatidylcholines (PC), phosphatidylethanolamines (PE), phosphatidylserines (PS), phosphatidylglycerols (PG), cardiolipin (CL) and phosphatidylinositols (PI). The major human sterol is cholesterol which is often stored as cholesteryl ester (ChE). Acylglycerols can be monoacylglycerols (MG), diacylglycerols (DG) and triacylglycerols (TG) based on the number of acyl groups attached. Sphingolipids are mainly classified into sphingomyelins and ceramides.

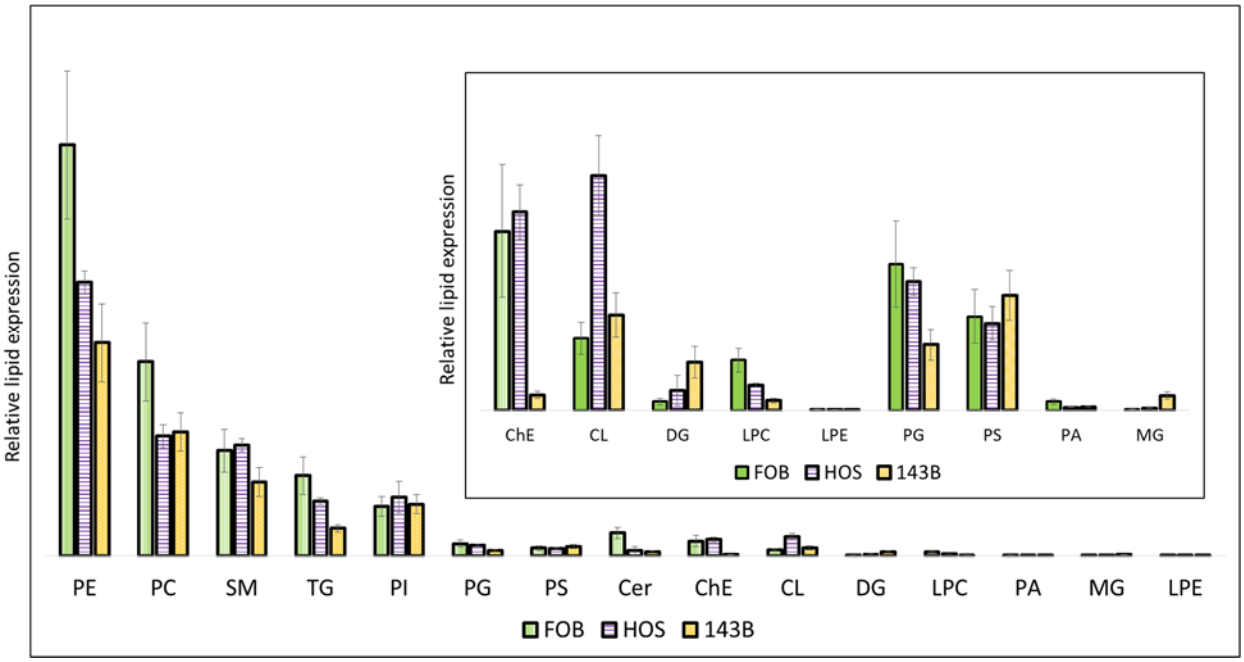

Figure 4.2: Figure represents the fifteen major classes of lipids detected in three cell lines- osteoblast FOB (green vertical striped), non-metastatic HOS (purple horizontal striped) and metastatic 143B (yellow dots) as analyzed by ANOVA. The various lipid classes are phosphatidylcholines (PC), phosphatidylethanolamines (PE), phosphatidylserines (PS), phosphatidylglycerols (PG), phosphatidylinositols (PI), cardiolipin (CL), cholesteryl ester (ChE), monoacylglycerols (MG), diacylglycerols (DG), triacylglycerols (TG), sphingomyelins (SM) and ceramides (Cer), lysophosphatidylcholines (LPC) and lysophosphatidylethanolamines (LPE). All experiments were performed in three biological replicates (n=3).

B

Lipid Class	log10(Fold Change)		
	HOS vs FOB	143B vs HOS	FOB vs 143B
Cer	0.58481	-0.15094	-0.43387
ChE	-0.044246	1.1086	-1.0644
CL	-0.51201	0.38973	0.12228
DG	0.15607	-0.48649	0.33041
LPC	0.29598	0.40937	-0.70535
PC	0.21053	-0.01504	-0.19549
PE	0.17574	0.10912	-0.28485
LPE	0.16934	0.5566	-0.72595
Pet	-0.031667	0.041763	-0.010096
PI	-0.075866	0.054902	0.020964
PG	0.054521	0.29447	-0.34899
PS	0.032501	-0.12202	0.089524
SM	-0.022243	0.17534	-0.15309
TG	0.16666	0.29795	-0.46461
PA	0.47663	-0.10977	-0.36686
MG	-0.27296	-0.78615	1.0591

Figure 4.3: (A) Figure shows the global analysis of lipid classes by Wilcoxon rank sum test and comparison correction by Benjamini-Hochberg false discovery rate. The heat map represents classes that are upregulated (green), downregulated (red) and those where no significant differences were found (grey) in each lipid class for HOS when compared to FOB (left panel), 143B when compared to HOS (middle panel) and FOB when compared to 143B (right panel). (B) Table shows the log fold change in lipid classes in all three cell lines.

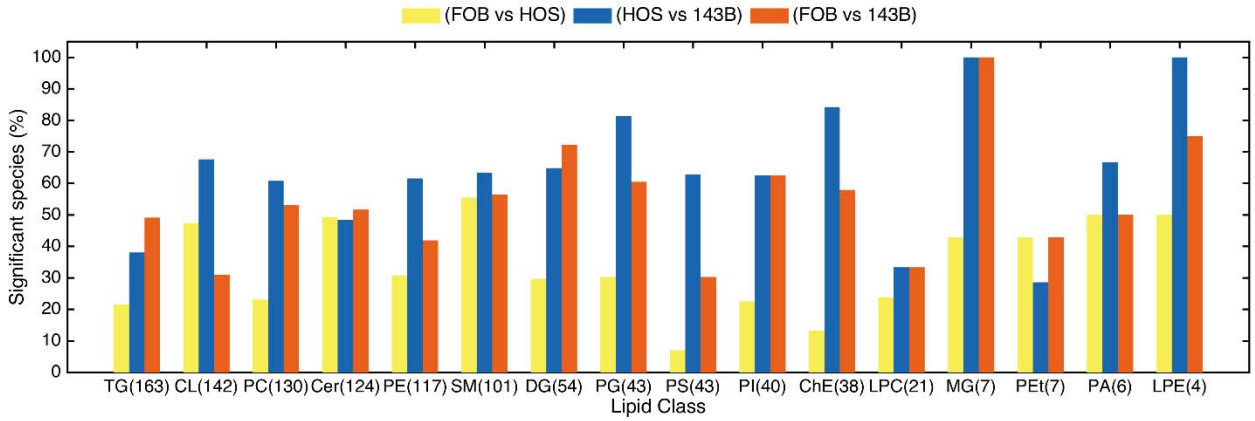

Figure 4.4: Figure shows the number of individual species that are significantly different among the three cell lines. Differences between FOB and HOS represents differences in lipids between normal and non-metastatic state (yellow). Differences between 143B and HOS represents differences in lipids between non-metastatic and metastatic state (blue). Differences between FOB and 143B represents differences in lipids between normal and metastatic state (orange).

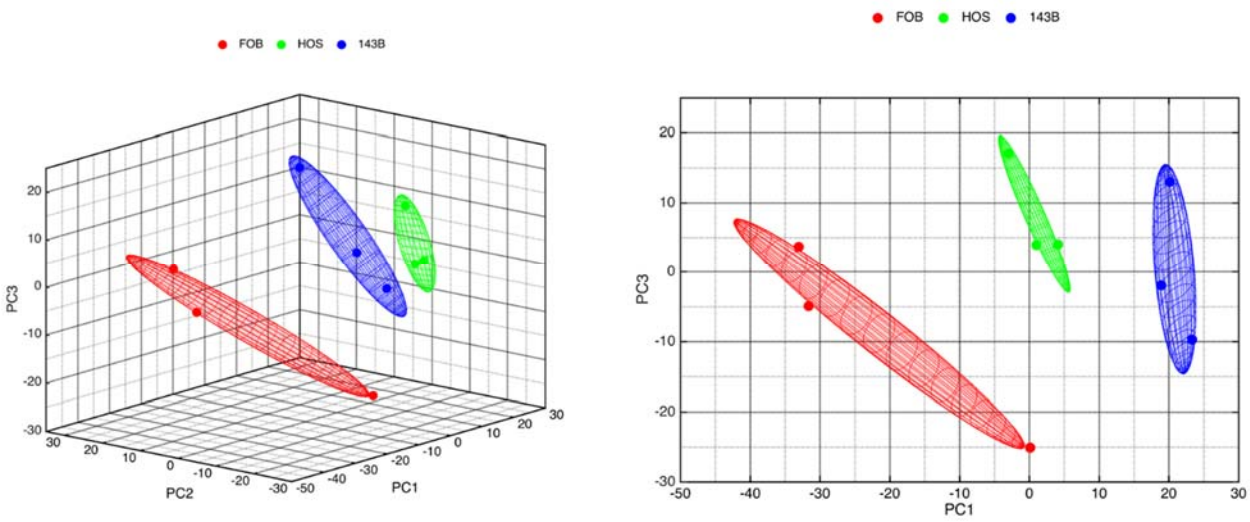

Figure 4.5: (A) Figure shows principal component analysis on all three cell lines, osteoblast FOB (red), non-metastatic (green) and metastatic 143B (blue) cells as represented in a three dimensional space. (B) The same PCA plot with osteoblast FOB (red), non-metastatic (green) and metastatic 143B (blue) cells as represented in a two dimensional space. As seen in figure, all three cell lines occupy a different space in the plot.

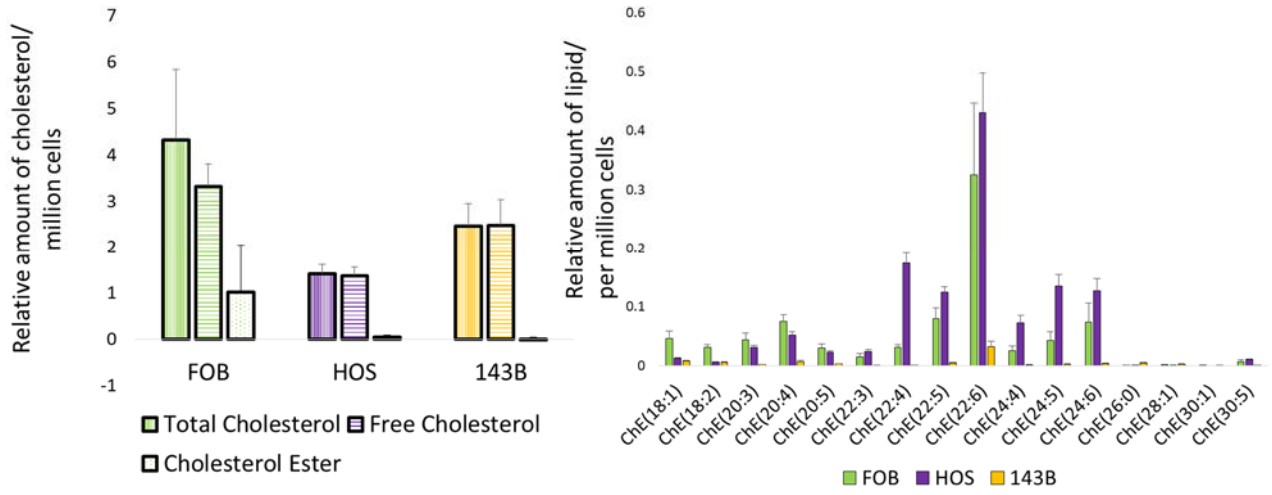

Figure 4.6: (A) Figure shows the levels of total cholesterol (vertical lines), free cholesterol (horizontal bars) and cholesteryl ester (dots) in FOB (green), HOS (purple) and 143B (yellow) cells as measured by the Amplex red detection methodology. (B) Figure shows shows specific cholesteryl ester species significantly differentially regulated in the three cell lines FOB (green), HOS (purple) and 143B (yellow).

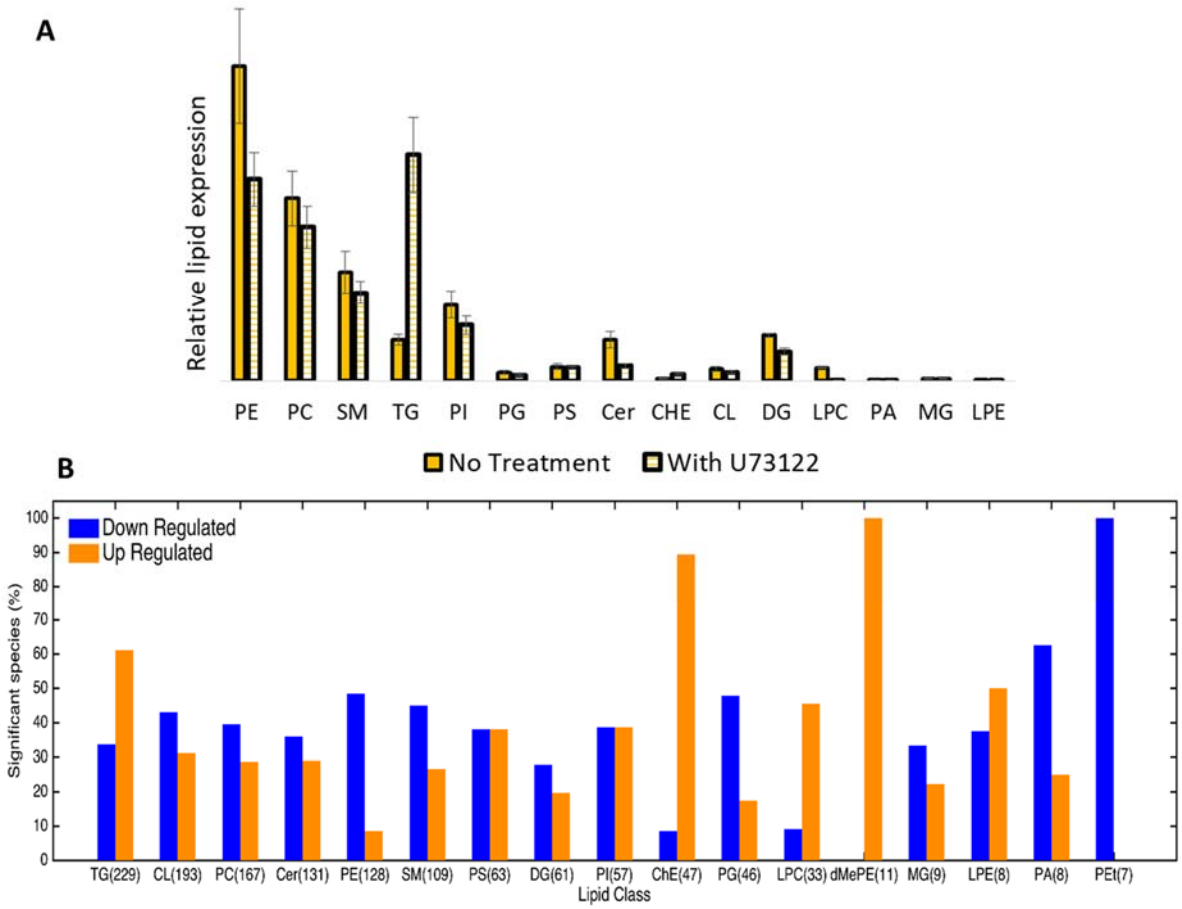

Figure 4.7: (A) Figure represents differences in total lipidomic content of 143B cells on treatment with PLC inhibitor U73122. Solid bars represent the lipidomic composition before treatment and striped bars represent composition after treatment with PLC inhibitor. (B) Figure represents percentage changes in individual lipid species in treated vs untreated cells that are downregulated (blue) and upregulated (orange).

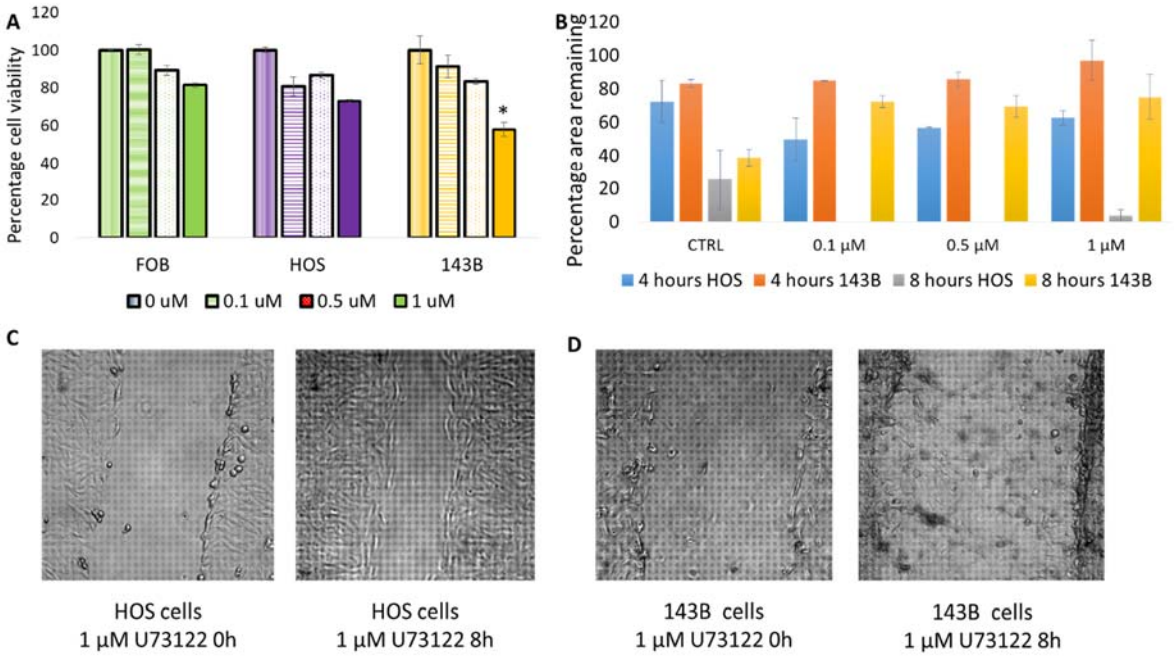

Figure 4.8: (A) Figure represents reduction in cell viability in all three cell lines on treatment with PLC inhibitor as measured by cell titer blue assay. (B) Figure represents cell migration in 143B and HOS cells over time at different concentrations of PLC inhibitor U73122. (C) Figure represents cell migration in HOS cells at 0 and 8h time points with 1 µM concentration of U73122. (D) Figure represents cell migration in 143B cells at 0 and 8h time points with 1 µM concentration of U73122.

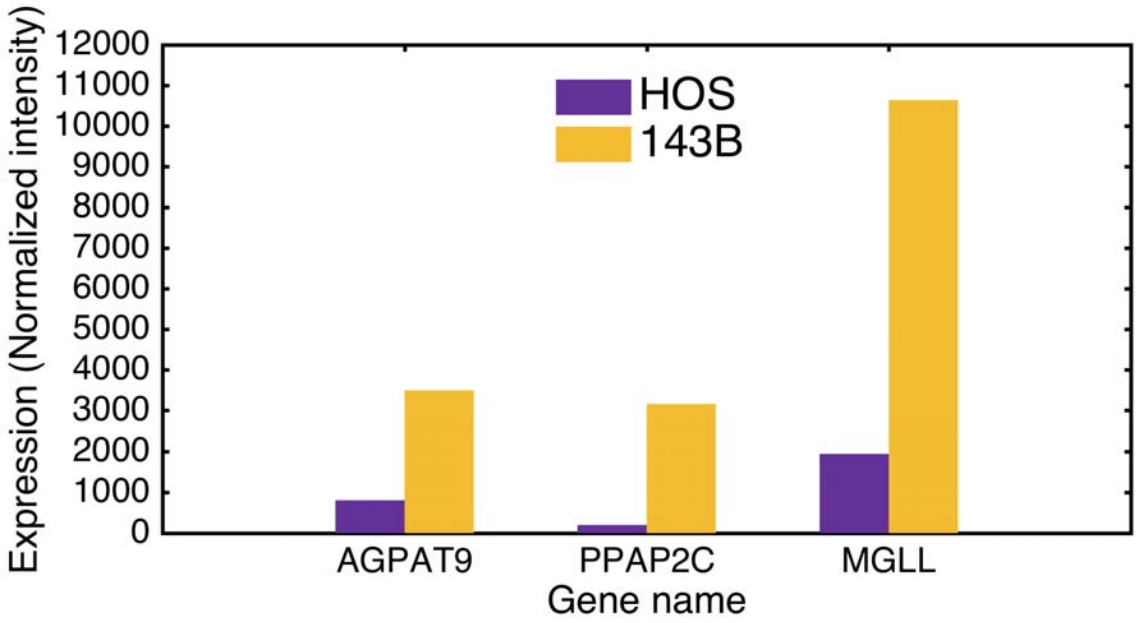

Figure 4.9: Figure shows differentially regulated genes associated with the diacylglycerol synthesis and metabolism pathway in 143B (purple) vs HOS cells (yellow).

4.9 REFERENCES

1. Bielack SS, Kempf-Bielack B, Delling G, Exner GU, Flege S, Helmke K, Kotz R, Salzer-Kuntschik M, Werner M, Winkelmann W, Zoubek A, Jurgens H, Winkler K. Prognostic factors in high-grade osteosarcoma of the extremities or trunk: an analysis of 1,702 patients treated on neoadjuvant cooperative osteosarcoma study group protocols. Journal of clinical oncology : official journal of the American Society of Clinical Oncology. 2002;20(3):776-90. doi: 10.1200/jco.2002.20.3.776. PubMed PMID: 11821461.
2. Hughes DP. Strategies for the targeted delivery of therapeutics for osteosarcoma. Expert opinion on drug delivery. 2009;6(12):1311-21. doi: 10.1517/17425240903280422. PubMed PMID: 19761419; PubMed Central PMCID: PMC4163784.
3. Baenke F, Peck B, Miess H, Schulze A. Hooked on fat: the role of lipid synthesis in cancer metabolism and tumour development. Disease models & mechanisms. 2013;6(6):1353-63. doi: 10.1242/dmm.011338. PubMed PMID: 24203995; PubMed Central PMCID: PMC3820259.
4. Dopico AM, Tigyi GJ. A glance at the structural and functional diversity of membrane lipids. Methods in molecular biology. 2007;400:1-13. doi: 10.1007/978-1-59745-519-0_1. PubMed PMID: 17951723.
5. Shevchenko A, Simons K. Lipidomics: coming to grips with lipid diversity. Nature reviews Molecular cell biology. 2010;11(8):593-8. doi: 10.1038/nrm2934. PubMed PMID: 20606693.
6. Escriba PV, Wedegaertner PB, Goni FM, Vogler O. Lipid-protein interactions in GPCR-associated signaling. Biochimica et biophysica acta. 2007;1768(4):836-52. doi: 10.1016/j.bbamem.2006.09.001. PubMed PMID: 17067547.
7. Stordeur C, Puth K, Saenz JP, Ernst R. Crosstalk of lipid and protein homeostasis to maintain membrane function. Biological chemistry. 2014;395(3):313-26. doi: 10.1515/hsz-2013-0235. PubMed PMID: 24152902.
8. Corda D, De Matteis MA. Lipid signalling in health and disease. The FEBS journal. 2013;280(24):6280. doi: 10.1111/febs.12604. PubMed PMID: 24286187.
9. Sampaio JL, Gerl MJ, Klose C, Ejsing CS, Beug H, Simons K, Shevchenko A. Membrane lipidome of an epithelial cell line. Proceedings of the National Academy of Sciences of the United States of America. 2011;108(5):1903-7. doi: 10.1073/pnas.1019267108. PubMed PMID: 21245337; PubMed Central PMCID: PMC3033259.
10. Zaidi N, Swinnen JV, Smans K. ATP-citrate lyase: a key player in cancer metabolism. Cancer research. 2012;72(15):3709-14. doi: 10.1158/0008-5472.CAN-11-4112. PubMed PMID: 22787121.
11. Menendez JA, Lupu R. Fatty acid synthase and the lipogenic phenotype in cancer pathogenesis. Nature reviews Cancer. 2007;7(10):763-77. doi: 10.1038/nrc2222. PubMed PMID: 17882277.
12. Guillaumond F, Bidaut G, Ouaissi M, Servais S, Gouirand V, Olivares O, Lac S, Borge L, Roques J, Gayet O, Pinault M, Guimaraes C, Nigri J, Loncle C, Lavaut MN, Garcia S, Tailleux A, Staels B, Calvo E, Tomasini R, Iovanna JL, Vasseur S. Cholesterol uptake disruption, in association with chemotherapy, is a promising combined metabolic therapy for pancreatic adenocarcinoma. Proceedings of the National Academy of Sciences of the United States of America. 2015;112(8):2473-8. doi: 10.1073/pnas.1421601112. PubMed PMID: 25675507; PubMed Central PMCID: PMC4345573.
13. Wu HW, Volponi JV, Oliver AE, Parikh AN, Simmons BA, Singh S. In vivo lipidomics using single-cell Raman spectroscopy. Proceedings of the National Academy of Sciences of the United States of America. 2011;108(9):3809-14. doi: 10.1073/pnas.1009043108. PubMed PMID: WOS:000287844400067.
14. Sterin M, Cohen JS, Ringel I. Hormone sensitivity is reflected in the phospholipid profiles of breast cancer cell lines. Breast Cancer Res Tr. 2004;87(1):1-11. doi: Doi 10.1023/B:Brea.0000041572.07837.Ec. PubMed PMID: WOS:000223914600001.
15. Doria ML, Cotrim CZ, Simoes C, Macedo B, Domingues P, Domingues MR, Helguero LA. Lipidomic analysis of phospholipids from human mammary epithelial and breast cancer cell lines. Journal of cellular physiology. 2013;228(2):457-68. doi: 10.1002/jcp.24152. PubMed PMID: 22767159.

16. Fhaner CJ, Liu S, Ji H, Simpson RJ, Reid GE. Comprehensive lipidome profiling of isogenic primary and metastatic colon adenocarcinoma cell lines. Analytical chemistry. 2012;84(21):8917-26. doi: 10.1021/ac302154g. PubMed PMID: 23039336; PubMed Central PMCID: PMC3491142.
17. Zhou X, Mao J, Ai J, Deng Y, Roth MR, Pound C, Henegar J, Welti R, Bigler SA. Identification of plasma lipid biomarkers for prostate cancer by lipidomics and bioinformatics. PloS one. 2012;7(11):e48889. doi: 10.1371/journal.pone.0048889. PubMed PMID: 23152813; PubMed Central PMCID: PMC3495963.
18. Doria ML, Cotrim Z, Macedo B, Simoes C, Domingues P, Helguero L, Domingues MR. Lipidomic approach to identify patterns in phospholipid profiles and define class differences in mammary epithelial and breast cancer cells. Breast Cancer Res Tr. 2012;133(2):635-48. doi: 10.1007/s10549-011-1823-5. PubMed PMID: WOS:000304610600022.
19. Hilvo M, Denkert C, Lehtinen L, Muller B, Brockmoller S, Seppanen-Laakso T, Budczies J, Bucher E, Yetukuri L, Castillo S, Berg E, Nygren H, Sysi-Aho M, Griffin JL, Fiehn O, Loibl S, Richter-Ehrenstein C, Radke C, Hyotylainen T, Kallioniemi O, Iljin K, Oresic M. Novel Theranostic Opportunities Offered by Characterization of Altered Membrane Lipid Metabolism in Breast Cancer Progression. Cancer Res. 2011;71(9):3236-45. doi: 10.1158/0008-5472.CAN-10-3894. PubMed PMID: WOS:000290020400008.
20. Li J, Ren SC, Piao HL, Wang FB, Yin PY, Xu CL, Lu X, Ye GZ, Shao YP, Yan M, Zhao XJ, Sun YH, Xu GW. Integration of lipidomics and transcriptomics unravels aberrant lipid metabolism and defines cholesteryl oleate as potential biomarker of prostate cancer. Scientific reports. 2016;6. doi: Artn 20984 10.1038/Srep20984. PubMed PMID: WOS:000369923500001.
21. Wilcoxon F. Individual comparisons of grouped data by ranking methods. Journal of economic entomology. 1946;39:269. PubMed PMID: 20983181.
22. Bligh EG, Dyer WJ. A rapid method of total lipid extraction and purification. Can J Biochem Physiol. 1959;37(8):911-7. Epub 1959/08/01. doi: 10.1139/o59-099. PubMed PMID: 13671378.
23. Luu HH, Kang Q, Park JK, Si W, Luo Q, Jiang W, Yin H, Montag AG, Simon MA, Peabody TD, Haydon RC, Rinker-Schaeffer CW, He TC. An orthotopic model of human osteosarcoma growth and spontaneous pulmonary metastasis. Clin Exp Metastasis. 2005;22(4):319-29. doi: 10.1007/s10585-005-0365-9. PubMed PMID: 16170668.
24. Kuliszkiewicz-Janus M, Tuz MA, Baczynski S. Application of 31P MRS to the analysis of phospholipid changes in plasma of patients with acute leukemia. Biochimica et biophysica acta. 2005;1737(1):11-5. doi: 10.1016/j.bbalip.2005.08.019. PubMed PMID: 16213190.
25. Cvetkovic B, Vucic V, Cvetkovic Z, Popovic T, Glibetic M. Systemic alterations in concentrations and distribution of plasma phospholipids in prostate cancer patients. Medical oncology. 2012;29(2):809-14. doi: 10.1007/s12032-011-9914-z. PubMed PMID: 21442313.
26. Kuhn T, Floegel A, Sookthai D, Johnson T, Rolle-Kampczyk U, Otto W, von Bergen M, Boeing H, Kaaks R. Higher plasma levels of lysophosphatidylcholine 18:0 are related to a lower risk of common cancers in a prospective metabolomics study. BMC medicine. 2016;14:13. doi: 10.1186/s12916-016-0552-3. PubMed PMID: 26817443; PubMed Central PMCID: PMC4730724.
27. Leventis PA, Grinstein S. The distribution and function of phosphatidylserine in cellular membranes. Annual review of biophysics. 2010;39:407-27. doi: 10.1146/annurev.biophys.093008.131234. PubMed PMID: 20192774.
28. Marino G, Kroemer G. Mechanisms of apoptotic phosphatidylserine exposure. Cell research. 2013;23(11):1247-8. doi: 10.1038/cr.2013.115. PubMed PMID: 23979019; PubMed Central PMCID: PMC3817543.
29. Schlame M, Ren M. The role of cardiolipin in the structural organization of mitochondrial membranes. Biochimica et biophysica acta. 2009;1788(10):2080-3. doi: 10.1016/j.bbamem.2009.04.019. PubMed PMID: 19413994; PubMed Central PMCID: PMC2757492.
30. Ginsburg GS, Atkinson D, Small DM. Physical properties of cholesteryl esters. Progress in lipid research. 1984;23(3):135-67. PubMed PMID: 6399750.

31. Robinet P, Wang Z, Hazen SL, Smith JD. A simple and sensitive enzymatic method for cholesterol quantification in macrophages and foam cells. Journal of lipid research. 2010;51(11):3364-9. doi: 10.1194/jlr.D007336. PubMed PMID: 20688754; PubMed Central PMCID: PMC2952578.
32. Griner EM, Kazanietz MG. Protein kinase C and other diacylglycerol effectors in cancer. Nature reviews Cancer. 2007;7(4):281-94. doi: 10.1038/nrc2110. PubMed PMID: 17384583.
33. Benjamin DI, Li DS, Lowe W, Heuer T, Kemble G, Nomura DK. Diacylglycerol Metabolism and Signaling Is a Driving Force Underlying FASN Inhibitor Sensitivity in Cancer Cells. ACS chemical biology. 2015;10(7):1616-23. doi: 10.1021/acschembio.5b00240. PubMed PMID: 25871544; PubMed Central PMCID: PMC4701379.
34. Merida I, Torres-Ayuso P, Avila-Flores A, Arranz-Nicolas J, Andrada E, Tello-Lafoz M, Liebana R, Arcos R. Diacylglycerol kinases in cancer. Advances in biological regulation. 2017;63:22-31. doi: 10.1016/j.jbior.2016.09.005. PubMed PMID: 27697466.
35. Al-Saffar NM, Titley JC, Robertson D, Clarke PA, Jackson LE, Leach MO, Ronen SM. Apoptosis is associated with triacylglycerol accumulation in Jurkat T-cells. British journal of cancer. 2002;86(6):963-70. doi: 10.1038/sj.bjc.6600188. PubMed PMID: 11953830; PubMed Central PMCID: PMC2364152.
36. Finstad HS, Dyrendal H, Myhrstad MC, Heimli H, Drevon CA. Uptake and activation of eicosapentaenoic acid are related to accumulation of triacylglycerol in Ramos cells dying from apoptosis. Journal of lipid research. 2000;41(4):554-63. PubMed PMID: 10744776.
37. Tsai FC, Seki A, Yang HW, Hayer A, Carrasco S, Malmersjo S, Meyer T. A polarized Ca2+, diacylglycerol and STIM1 signalling system regulates directed cell migration. Nature cell biology. 2014;16(2):133-44. doi: 10.1038/ncb2906. PubMed PMID: 24463606; PubMed Central PMCID: PMC3953390.
38. Stella N, Schweitzer P, Piomelli D. A second endogenous cannabinoid that modulates long-term potentiation. Nature. 1997;388(6644):773-8. doi: 10.1038/42015. PubMed PMID: 9285589.
39. Stapleton CM, Mashek DG, Wang S, Nagle CA, Cline GW, Thuillier P, Leesnitzer LM, Li LO, Stimmel JB, Shulman GI, Coleman RA. Lysophosphatidic acid activates peroxisome proliferator activated receptor-gamma in CHO cells that over-express glycerol 3-phosphate acyltransferase-1. PloS one. 2011;6(4):e18932. doi: 10.1371/journal.pone.0018932. PubMed PMID: 21533082; PubMed Central PMCID: PMC3080373.
40. Ahmed SA, Gogal RM, Jr., Walsh JE. A new rapid and simple non-radioactive assay to monitor and determine the proliferation of lymphocytes: an alternative to [3H]thymidine incorporation assay. Journal of immunological methods. 1994;170(2):211-24. PubMed PMID: 8157999.
41. Liang CC, Park AY, Guan JL. In vitro scratch assay: a convenient and inexpensive method for analysis of cell migration in vitro. Nature protocols. 2007;2(2):329-33. doi: 10.1038/nprot.2007.30. PubMed PMID: 17406593.
42. Muff R, Rath P, Ram Kumar RM, Husmann K, Born W, Baudis M, Fuchs B. Genomic instability of osteosarcoma cell lines in culture: impact on the prediction of metastasis relevant genes. PloS one. 2015;10(5):e0125611. doi: 10.1371/journal.pone.0125611. PubMed PMID: 25992885; PubMed Central PMCID: PMC4438062.
43. Saddoughi SA, Ogretmen B. Diverse functions of ceramide in cancer cell death and proliferation. Advances in cancer research. 2013;117:37-58. doi: 10.1016/B978-0-12-394274-6.00002-9. PubMed PMID: 23290776.
44. Koybasi S, Senkal CE, Sundararaj K, Spassieva S, Bielawski J, Osta W, Day TA, Jiang JC, Jazwinski SM, Hannun YA, Obeid LM, Ogretmen B. Defects in cell growth regulation by C18:0-ceramide and longevity assurance gene 1 in human head and neck squamous cell carcinomas. The Journal of biological chemistry. 2004;279(43):44311-9. doi: 10.1074/jbc.M406920200. PubMed PMID: 15317812.
45. Senkal CE, Ponnusamy S, Bielawski J, Hannun YA, Ogretmen B. Antiapoptotic roles of ceramide-synthase-6-generated C16-ceramide via selective regulation of the ATF6/CHOP arm of ER-stress-response pathways. FASEB journal : official publication of the Federation of American Societies for Experimental Biology. 2010;24(1):296-308. doi: 10.1096/fj.09-135087. PubMed PMID: 19723703; PubMed Central PMCID: PMC2797032.

46. Saddoughi SA, Garrett-Mayer E, Chaudhary U, O'Brien PE, Afrin LB, Day TA, Gillespie MB, Sharma AK, Wilhoit CS, Bostick R, Senkal CE, Hannun YA, Bielawski J, Simon GR, Shirai K, Ogretmen B. Results of a phase II trial of gemcitabine plus doxorubicin in patients with recurrent head and neck cancers: serum C(1)(8)-ceramide as a novel biomarker for monitoring response. Clinical cancer research : an official journal of the American Association for Cancer Research. 2011;17(18):6097-105. doi: 10.1158/1078-0432.CCR-11-0930. PubMed PMID: 21791630; PubMed Central PMCID: PMC3176980.
47. Sapandowski A, Stope M, Evert K, Evert M, Zimmermann U, Peter D, Page I, Burchardt M, Schild L. Cardiolipin composition correlates with prostate cancer cell proliferation. Molecular and cellular biochemistry. 2015;410(1-2):175-85. doi: 10.1007/s11010-015-2549-1. PubMed PMID: 26314254.
48. Mansilla F, da Costa KA, Wang S, Kruhoffer M, Lewin TM, Orntoft TF, Coleman RA, Birkenkamp-Demtroder K. Lysophosphatidylcholine acyltransferase 1 (LPCAT1) overexpression in human colorectal cancer. Journal of molecular medicine. 2009;87(1):85-97. doi: 10.1007/s00109-008-0409-0. PubMed PMID: 18974965; PubMed Central PMCID: PMC2614561.
49. Zhou X, Lawrence TJ, He Z, Pound CR, Mao J, Bigler SA. The expression level of lysophosphatidylcholine acyltransferase 1 (LPCAT1) correlates to the progression of prostate cancer. Experimental and molecular pathology. 2012;92(1):105-10. doi: 10.1016/j.yexmp.2011.11.001. PubMed PMID: 22101258; PubMed Central PMCID: PMC3294031.
50. Kuzu OF, Noory MA, Robertson GP. The Role of Cholesterol in Cancer. Cancer research. 2016;76(8):2063-70. doi: 10.1158/0008-5472.CAN-15-2613. PubMed PMID: 27197250.
51. Carrasco S, Merida I. Diacylglycerol-dependent binding recruits PKCtheta and RasGRP1 C1 domains to specific subcellular localizations in living T lymphocytes. Molecular biology of the cell. 2004;15(6):2932-42. doi: 10.1091/mbc.E03-11-0844. PubMed PMID: 15064353; PubMed Central PMCID: PMC420115.
52. Ebinu JO, Stang SL, Teixeira C, Bottorff DA, Hooton J, Blumberg PM, Barry M, Bleakley RC, Ostergaard HL, Stone JC. RasGRP links T-cell receptor signaling to Ras. Blood. 2000;95(10):3199-203. PubMed PMID: 10807788.
53. Garg R, Benedetti LG, Abera MB, Wang H, Abba M, Kazanietz MG. Protein kinase C and cancer: what we know and what we do not. Oncogene. 2014;33(45):5225-37. doi: 10.1038/onc.2013.524. PubMed PMID: 24336328; PubMed Central PMCID: PMC4435965.
54. Cao J, Li JL, Li D, Tobin JF, Gimeno RE. Molecular identification of microsomal acyl-CoA:glycerol-3-phosphate acyltransferase, a key enzyme in de novo triacylglycerol synthesis. Proceedings of the National Academy of Sciences of the United States of America. 2006;103(52):19695-700. doi: 10.1073/pnas.0609140103. PubMed PMID: 17170135; PubMed Central PMCID: PMC1702318.
55. Wang Y, Jia H, Lin H, Tan X, Du Z, Chen H, Xu Y, Han X, Zhang J, Zhao S, Yu X, Lu Y. Metastasis-associated gene, mag-1 improves tumour microenvironmental adaptation and potentiates tumour metastasis. Journal of cellular and molecular medicine. 2012;16(12):3037-51. doi: 10.1111/j.1582-4934.2012.01633.x. PubMed PMID: 22985252; PubMed Central PMCID: PMC4393732.
56. Leung DW, Tompkins CK, White T. Molecular cloning of two alternatively spliced forms of human phosphatidic acid phosphatase cDNAs that are differentially expressed in normal and tumor cells. DNA and cell biology. 1998;17(4):377-85. doi: 10.1089/dna.1998.17.377. PubMed PMID: 9570154.
57. Flanagan JM, Funes JM, Henderson S, Wild L, Carey N, Boshoff C. Genomics screen in transformed stem cells reveals RNASEH2A, PPAP2C, and ADARB1 as putative anticancer drug targets. Molecular cancer therapeutics. 2009;8(1):249-60. doi: 10.1158/1535-7163.MCT-08-0636. PubMed PMID: 19139135.

CHAPTER V: ANTI-TUMORIGENIC PROPERTIES OF OMEGA-3 ENDOCANNABINOID EPOXIDES

5.1 ABSTRACT

Dietary omega-3 fatty acids such as eicosapentaenoic acid (EPA) and docosahexaenoic acid (DHA) have been shown to suppress tumor growth and progression as they are converted into downstream lipid metabolites that exert anti-inflammatory, pro-resolving and anti-tumorigenic effects. Recently, a new class of omega-3 lipid metabolites known as endocannabinoid epoxides (eCB epoxides) were found to have potent anti-inflammatory and anti-angiogenic properties. Herein, we show that a novel class of omega-3 eCB epoxides and their stable derivatives exhibit anti-inflammatory (28), anti-angiogenic, anti-tumorigenic and anti-migratory properties in osteosarcoma, the most common bone cancer in human. We find these molecules are 80% more in osteosarcoma metastatic lungs. We synthesized more stable analogs of these molecules, which are less hydrolytically susceptible to fatty acid amide hydrolase (FAAH) while retaining their anti-tumorigenic activity. Furthermore, we investigated whether the endogenous molecules as well as the synthetic analogs affect the cell cycle of osteosarcoma cells as well as whether they have an effect on the angiogenic properties of endothelial cells. Taken together, we show that a new class of biological metabolites of omega-3 fatty acids have beneficial anti-cancer effects and have therapeutic potential with respect to bone cancer pain and inflammation.

5.2 INTRODUCTION

Recent studies in cancer have focused on understanding the role of inflammation in tumor initiation and malignant progression. It has been shown previously that inflammatory conditions can promote oncogenic transformation, and in turn the carcinogenic environment can also generate an inflammatory microenvironment that can further support tumor progression (1-3). Dietary omega-3 fatty acids such as eicosapentaenoic acid (EPA) and docosahexaenoic acid (DHA) have been shown to suppress tumor growth and progression as they are converted into downstream lipid metabolites that exert anti-inflammatory, pro-resolving (4) and anti-tumorigenic effects (5) (6) (7). As inflammation dictates tumor initiation, progression and growth, it is hypothesized that omega-3 fatty acid derived lipid metabolites will contribute towards preventing tumor formation and metastasis (5). Hence, it is necessary to discover potential omega-3 fatty acids based lipid metabolites that possess anti-tumorigenic and anti-inflammatory properties.

In one particular physiological pathway, omega-3 fatty acids such as EPA and DHA are converted to their corresponding epoxides by cytochrome P450 (CYP) epoxygenase that have shown to exhibit have anti-cancer properties. The epoxide derivative of EPA known has been shown to be anti-proliferative (8). It was observed that the terminal epoxide of EPA, 17,18-EEQ (epoxyeicosatetraenoic acids), decreased endothelial cell proliferation, interrupted the cell cycle in S-phase and down-regulated the cyclin D1/cyclin-dependent kinase (CDK)-4 complex. The corresponding DHA epoxide, epoxydocosapentaenoic (EDP) inhibits metastasis and tumor growth (9). Furthermore, the action of the DHA and EPA epoxides are attenuated in the absence of a soluble epoxide hydrolase (sEH) inhibitor, indicating that the functional epoxide moiety is key for their anti-tumorigenic properties.

Omega-3 fatty acids such as DHA and EPA are also converted non-oxidatively into docosahexaenoyl ethanolamide (DHEA) and eicosapentaenoyl ethanolamide (EPEA) through the N-acyl ethanolamine synthesis pathway similar to the conversion of arachidonic acid to arachidonoyl ethanolamide (AEA, anandamide) (10, 11). These ethanolamide derivatives are collectively termed as endocannabinoids (eCB) as they elicit similar physiological effects as cannabinoids found in marijuana. The endocannabinoid system consists of the eCBs and cannabinoids receptors 1 and 2 (CB1 & CB2) (12, 13). While, CB1 is predominantly found in the central nervous system (CNS), CB2 is found in immune cells (14). These receptors interact with various eCBs to exert their physiological activities (15). Interestingly, these receptors also interact with the active ingredients in cannabis, or marijuana and are responsible for their psychoactive and anti-inflammatory properties. Phytocannabinoids, Δ-9-THC and cannabidiol (CBD), are major components of marijuana has been shown to induce apoptosis in hepatocellular carcinoma, breast cancer as well as colon cancer (16). Phytocannabinoids and eCBs have been shown to play an important role in cancer cell proliferation, apoptosis, inflammation and immunomodulation and form the basis of medical marijuana use in cancer (17, 18).

The most studied eCBs in the human body are AEA and 2-arachidonylglycerol (2-AG) that are derived from the omega-6 fatty acid arachidonic acid (AA). Anandamide was shown to be anti-tumorigenic in breast cancer, colorectal cancer as well as osteosarcoma (19-21). 2-AG has been shown to induce apoptosis in prostate cancer (22). Omega-3 derived eCBs, DHEA and EPEA have shown greater anti-proliferative efficiency than their parent counterparts in prostate cancer cells

(11). Additionally, it was also shown that the activity of eCBs in cancer cell was increased in the presence of a fatty acid amide hydrolase (FAAH) inhibitor, indicating that the ethanolamide endocannabinoids, AEA DHEA and EPEA contributes to the increased pro-apoptotic and anti-proliferative activity.

Recently, we showed that a novel class of eCB epoxides are generated from the cross-talk of the NAPE-PLD pathway and CYP epoxygenase pathways that are anti-inflammatory in nature and were found in multiple tissues (23) (Figure 5.1A). As separately both the endocannabinoid and epoxyeicosanoid pathway have been implicated in cancer as described above (8, 9) we wanted to evaluate their anti-tumorigenic properties of dual functional eCB epoxides in a cancer model. These lipid metabolites termed as EPEA epoxide (a.k.a. epoxyeicosatetraenoic-ethanolamide (EEQ-EA)) and DHEA epoxide (a.k.a. epoxydocosapentaenoic-ethanolamide (EDP-EA)) are synthesized from EPEA and DHEA by cytochrome P450s. More importantly, our analysis of the metastatic lung tissues show that there is almost ~77% increase in these eCB epoxides in metastatic lungs (Figure 5.1B and Appendix V) as compared to normal lungs of mice indicating that they play a physiological role in cancer metastasis.

Herein, we investigate the anti-tumorigenic role of the different regioisomers of omega-3 eCB epoxides of DHEA on osteosarcoma. Osteosarcoma (OS) is the most prevalent primary bone cancer in humans and presents high rates of invasion and metastasis. The cannabinoid receptor agonist WIN-55212 has been shown to potentiate the anti-tumorigenic properties of drugs like Adriamycin in OS (24). Additionally, the administration of cannabinoid receptor agonists have shown to reduce bone loss in bone tumor model and cannabinoid receptor mediated nociceptive pain (25, 26). Taken together, herein we test our hypothesis that DHEA epoxide regioisomers and their stable derivatives will exhibit anti-tumorigenic activities in osteosarcoma and will potentially reduce bone cancer pain through receptor selective activation.

In order to examine the anti-tumorigenic properties of DHEA epoxides, we first tested the apoptotic potential of the different regioisomers of DHEA epoxides using annexin V staining assay in three different OS cell lines - metastatic OS cell lines MG63 and 143B and the non-metastatic cell line HOS, and identified the most potent DHEA epoxide regioisomer. We further tested the anti-migratory potential of the DHEA epoxides via a wound healing assay in all three cell lines (27). Interestingly, we observed significant differences between the different DHEA epoxide

regioisomers tested with respect to their pro-apoptotic and anti-migratory properties that were uniform across the different cell lines chosen for the studies. This indicates common signaling pathways being triggered in the different cell lines by specific isomers of these lipid metabolites.

Furthermore, we synthesized stable derivatives of the most pro-apoptotic regioisomer of DHEA epoxide (10,11-EDP-EA) to reduce its hydrolytic susceptibility to fatty acid-amide hydrolase (FAAH) and increase binding to cannabinoid receptor 1 (CB1). The action of the most potent regioisomer and its stable derivatives were further tested towards their anti-tumorigenic, anti-migratory and FAAH hydrolysis.

Herein, we report a novel class of eCB epoxides and their stable derivatives that exhibit anti-inflammatory (28), anti-angiogenic, anti-tumorigenic and anti-migratory properties and by virtue of their ability to bind cannabinoid receptors will also exhibit anti-nociceptive bone pain activities. As osteosarcoma is accompanied by inflammation and pain, these molecules will aid in alleviating both. Moreover, as they are naturally occurring increasing their levels using FAAH and sEH dual inhibition will be effective adjuvant therapy for osteosarcoma (29, 30).

5.3 MATERIALS AND METHODS

Materials: Annein V/ PI kit was obtained from BD biosciences (556547). HUVEC cells were obtained from ThermoFisher (C0035C) and endothelial cell media was obtained from Lonza (EGM2 bullet kit CC-3162). Angiogenesis kit was obtained from Abcam (ab204726).

Isolation of endocannabinoids from tissue samples: K7M2 Experimental Metastasis Tumor Models. All animal experimental procedures were reviewed and approved by the University of Illinois Institutional Animal Care and Use Committee (Protocol 15120). 1,000,000 K7M2 cells were prepared in HBSS and intravenously injected into the tail vein of 6−8 week old female BALB/c mice (day 0) in a 200 μL volume. After x days the mice were sacrificed and lung tissue was isolated, weighted and total endocannabinoids were extracted. The tissue was mechanically homogenized on ice with a BioHomogenizer (BioSpec) in a 1:1 ratio with PBS supplemented with sEH inhibitor 12-(3-adamantan-1-yl-ureido)-dodecanoic acid (AUDA) (Cayman Chemical) (30 μm) and FAAH inhibitor PMSF (1 mM) till a homogenous slurry was formed. For 1 g of each tissue was homogenized, 40 mL of ethyl acetate/hexane (9:1) was employed with a BioHomogenizer (BioSpec) at room temperature and then was sonicated for 1 min. The resulting solution was washed with a 30% volume of water and centrifuged for the layers to separate. The

organic layer was removed, and the aqueous layer was extracted with an equal volume of ethyl acetate/hexane (9:1) twice. The total organic layer was concentrated in vacuo using a Buchi 120 rotary evaporator and was reconstituted in 1 mL of chloroform. The metabolites of interest were isolated by solid-phase extraction (SPE) using a 1-mL silica gel column (no. 214477; Sigma). The reconstituted samples were added to the silica column and washed in three column volumes of chloroform, and consequently eluted with four column volumes of methanol/chloroform (1:9). The eluent was dried, and samples were reconstituted in ethanol for analysis via LC-MS/MS.

Liquid chromatography mass spectrometry analysis. The LC separation was performed on an Agilent Eclipse XDB-C18 (4.6 x 150mm, 5µm) with mobile phase A (0.1% formic acid in water) and mobile phase B (0.1% formic acid in acetontrile). The flow rate was 0.4 mL/min. The linear gradient was as follows: 0-2min, 90%A; 8min, 55%A; 13-25min, 40%A; 30min, 30%A; 35min, 25%A; 40-47min, 20%A; 47.5-54min, 90%A. The autosampler was set at 5°C. The injection volume was 10 µL. Positive mass spectra were acquired with the ion spray voltage of 5500 V under electrospray ionization (ESI). The source temperature was 450°C. The curtain gas, ion source gas 1, and ion source gas 2 were 32 psi, 60 psi, and 60 psi, respectively. Multiple reaction monitoring (MRM) was used for quantitation: 19,20-EDP-EA and 7,8-EDP-EA m/z 388.1 → m/z 62.1; 16,17-EDP-EA, 13,14-EDP-EA, and 10,11-EDP-EA m/z 388.1 → m/z 370.1; DHEA 372.4 à m/z 62.1; Anandamide m/z 348.3 à m/z 62.1. Internal standards were monitored at: m/z 376.4 → m/z 66.1 for DHEA-d4.

Cell culture: Human cell lines HOS, MG63 and 143B were cultured in DMEM (Gibco, Invitrogen, Carlsbad, CA, USA) supplemented with 10% fetal bovine serum (FBS) and 1mgml–1 penicillin–streptomycin (Gibco, Invitrogen) at 37 °C and 5% CO2 in a humidified incubator.

CTB assay: 20,000 cells were plated per well in 96 well plates and allowed to adhere overnight. In the morning, the cell media was aspirated and replaced with fresh 100 µL of cell media and incubated with compound or DMSO vehicle control (1 µL) and allowed to incubate at 37 °C and 5% CO2 in a humidified incubator for 4 hours. 20 µL of cell titer blue reagent was added and the plate was incubated for 1 hour before the fluorescence was read using a plate reader with excitation at 534 nm and emission at 590 nm

Annexin V assay: Annexin V kit from BD biosciences -San Diego, CA) was used. Briefly, cells were scraped and collected with the dead cells. They were washed with ice cold 2X PBS twice and

resuspended in 1X binding buffer and incubated with annexin V-FITC and propidium iodide for 15 mins, followed by flow cytometry by BD Accuri C6 instrument. Annexin V/PI assay was performed as per manufacturer's instructions. Briefly, cells were trypsinized and collected for analysis. Dead cells in the media were collected for testing along with the rest of the sample. The total cell sample was washed twice with cold PBS and then resuspended in 100 µL of binding buffer. 5 µL of each annexin V and PI were added and the cells were vortexed and incubated in the dark for 15 mins. The cells were then diluted with 400 µL of binding buffer and analyzed by BD Accuri flow cytometer within an hour. The treated samples were compared with negative and positive stained samples both with vehicle control.

Wound healing assay: Cells were grown to a confluent monolayer in 12 well plates and a scratch was made across the center of the plate with a pipette tip and images were taken. The media was replaced with fresh media and treatment or vehicle control was added to the wells. The cells were maintained at 37 °C and 5% CO2 in a humidified incubator and images were taken every two hours. The images were processed using ImageJ via the wound healing plugin and normalized to 100% area at time 0.

Synthesis of amine EDP-EAs and analogs: To a solution of epoxide in acetonitrile, we will add a solution of 1-Ethyl-3-(3-dimethylaminopropyl) carbodiimide (EDC) (10 mg/mL in acetonitrile) and N-hydroxysuccinimide (NHS) (10 mg/mL in acetonitrile) in the ratio of (1:50:50) and incubate at 37 °C for 20 mins. To this is we will add a solution of amine (2 mg/mL in acetonitrile) in the ratio of 1:50 with epoxide and this will be stirred at room temperature overnight. The acetonitrile will be removed under reduced pressure and the residue will be dissolved in ethanol before purification via HPLC. Purification of 10,11-EDP derivatives will be performed using a reversed phase high-performance liquid chromatography (RP-HPLC), Sun Fire Prep C18 5 µm 19 x 50 mm (Waters, PN 186002566) and a mobile system composed of solvent A (H20/acetonitrile/acetic acid 95:5:0.1) and solvent B (H20/acetonitrile/acetic acid 5:95:0.1) and a linear gradient from 50% A to 0% A in 50 minutes.

Cell cycle analysis: 80% confluent cells in a 12 well plate were treated for 24 hours with appropriate treatment and harvested. Cells were washed twice with PBS and fixed with 70% ethanol in ice for 30 mins by vortexing to prevent clumping. The cells were washed twice with PBS and were incubated with a 50 µL of a 100 µg/ mL RNase solution for 30 mins on ice followed

by addition of 200 µL of 50 µg/mL propidium iodide solution before analysis by BD LSR II flow cytometer and analyzed by FCS software.

FAAH hydrolysis: The preparation of pig forebrain membranes was achieved using dounce homogenization in buffer (50 mM Tris pH 7.4, 1 mM EDTA and 3 mM MgCl2) and membrane pelleting as previously described (31). Incubations contained 5 µg forebrain protein in a 0.5 mL reaction containing 50 mM Tris (pH 7.4), 1 mM EDTA, 3 mM MgCl2, and amide at 20 µM. At 40 min reactions were quenched with methanol containing 1 mM PMSF and and centrifuged to pellet protein (10,000 g x 10 min). The supernatant was collected and analyzed via LC-MS/MS as outlined below.

Analysis of 10,11-EDP by LC-MS/MS: LC-MS/MS method for quantitation of 17,18-EEQ and 19,20-EDP. Analyses were performed using the 5500 QTRAP LC/MS/MS system (AB Sciex, Foster City, CA) in Metabolomics Lab of Roy J. Carver Biotechnology Center, University of Illinois at Urbana-Champaign. The 1200 series HPLC system (Agilent Technologies, Santa Clara, CA) includes a degasser, an autosampler, and a binary pump, and this system was used to separate the metabolites. LC separation was performed on an Agilent Eclipse XDB-C18 (4.6 x 150mm, 5µm) with mobile phase A (0.1% formic acid in 20 water) and mobile phase B (0.1% formic acid in acetonitrile) at a flow rate was 0.4 mL/min. The linear gradient was as follows: 0-2min, 90%A; 8min, 55%A; 13-25min, 40%A; 30min, 30%A; 35min, 25%A; 40min, 20%A; 45-47min, 15%A; 48-54min, 90%A. The autosampler was set at 5°C. The injection volume was 10 µL. Negative mass spectra were acquired with the ion spray voltage of -4500 V under electrospray ionization (ESI). The source temperature was 450 °C. The curtain gas, ion source gas 1, and ion source gas 2 were 32 psi, 50 psi, and 55 psi, respectively. Multiple reaction monitoring (MRM) was used for quantitation: 10,11-EDP m/z 343.0.

Angiogenesis Assay: Angiogenesis in endothelial HUVEC cells was measured using abcam angiogenesis kit (ab204726). Briefly, HUVEC cells at passage 2 (p=2) were grown to 80% confluency. The matrigel provided was thawed overnight and 50 µL was put into each well of a 96 well plate that had been chilled overnight in a -20 °C freezer. The plate was rocked slightly and then allowed to incubate at 37 °C for 1 hour. 15,000 HUVEC cells were then plated into the wells and were treated with vehicle control or 0.5 µM or 1 µM compound. A no matrix control and a control with vinblastine (inhibitor of angiogenesis) was also performed. All wells were performed

in duplicates. The plates were then incubated for 5 hours at 37 °C. The incubation medium was removed and cells were washed with 100 µL of wash buffer. 100 µL of staining dye was added to each well and incubated for 30 mins at 37 °C. The wells were imaged using a fluorescent microscope and analyzed using ImageJ with Angiogenesis Analyzer Plugin.

Synthesis of 10,11-cyclopropylamideaziridine: To a stirred solution of sodium azide (2 equivalents) and ammonium chloride (3 equiv) in water at room temperature a solution of ethanolamine epoxide (1 equiv) was added in MeOH and then the reaction was stirred at 80 °C for 3 h. After the solution is cooled to room temperature, the excess of MeOH will be removed under reduced pressure and the residue will be diluted with EtOAc, washed with water, dried over anhydrous sodium sulfate and concentrated under reduced pressure to give a brown oil. Filtration on a pad of silica gel (hexane/EtOAc 4:1) gave the nitrile that is taken forward for the next reaction. A solution of nitrile in anhydrous acetonitrile was heated to reflux under nitrogen atmosphere. Next, triphenylphosphine (20 equiv), was added immediately and the reaction will be stirred under reflux for 3 h. After cooling to room temperature, the mixture was concentrated under reduced pressure and purified by column chromatography on silica gel (hexane/EtOAc 7:3).

Synthesis of 10,11-cyclopropylamidethiirane: To a solution of 10,11-cyclopropylamine in methanol was added KSCN and oxalic acid and heated in a commercial microwave at power 1 for 10 mins. The reaction mixture was cooled and concentrated in vacuo. The mixture was purified using normal phase HPLC using 90% hexane 10% isopropanol as the eluent.

5.4 RESULTS

DHEA epoxides are endogenously produced in osteosarcoma metastatic lung tissues. We have developed a targeted lipidomics method in the multiple reaction monitoring (MRM) mode to identify and quantitate DHEA epoxides (EDP-EA) regioisomers (19,20-, 16,17-, 13,14-, 10,11-, and 7,8-) (28). In order to estimate the basal levels of the endogenous EDP-EA regioisomers in metastatic and non-metastatic lungs, we measured the metabolites on osteosarcoma tumor in mice. Towards this, an experimental metastasis tumor model was prepared. 1,000,000 K7M2 cells (murine OS cells) were prepared in HBSS and intravenously injected into the tail vein of 6−8 week old female BALB/c mice in a 200 µL volume. Lungs from ten mice, five nude mice with lungs free of tumor and five with lung metastasized osteosarcoma tumors were isolated and the total endocannabinoids were extracted and quantified by LC-MS/MS as described in materials and

methods. As indicated in figure 5.1B and Appendix V, we can observe that both tumor-free lungs and lungs with tumors produced eCB epoxides with several fold difference compared to DHEA, the parent molecule. There was ~87% increase in the terminal DHEA epoxide (19,20-EDP-EA), 66% increase in 16,17-EDP-EA, 72% increase 13,14-EDP-EA, 49% 10,11-EDP-EA and DHEA essentially decreases in lungs with metastasized tumors as compared to healthy lungs with no tumors. The high increase of these metabolites in the metastasized lungs warranted further investigation of their anti-tumorigenic properties.

In order to investigate the effects of eCB epoxides on osteosarcoma, all five regioisomers were synthesized as described previously (23). Briefly, DHA was reacted with mCPBA, followed by separation using reverse phase HPLC and normal phase HPLC to separate the different regioisomers. The individual regioisomers were further coupled to ethanolamine and purified by reverse phase chromatography. The compounds were quantified and used for further studies.

Effect of DHEA epoxides (EDP-EA) regioisomers on cell viability.

To evaluate the effect of EDP-EA isomers on cellular viability of osteosarcoma cells, cell titer blue assay was performed on 143B metastatic OS cells at 5 μM concentration. As seen in Appendix V, only 13,14-, 10,11- and 7,8- EDP-EA reduced total cell viability. However, no change effect on cell viability was seen by action of similar concentration of 19,20-EDP-EA and 16,17-EDP-EA and no further studies were performed with these regioisomers. Next, we measured the cell viability as a function of the variable concentration of 13,14-, 10,11- and 7,8- EDP-EA. As seen in figure 5.1C, all three regioisomers reduced cell viability in a dose dependent fashion. In order to evaluate if the decrease in cell viability of the three different DHEA epoxide regioisomers is due to cell death or check in cell migration, we performed apoptosis and cell migration assay.

Induction of apoptosis in metastatic OS cells by DHEA epoxides (EDP-EA) regioisomers

The apoptotic potential of 7,8-EDP-EA, 10,11- EDP-EA and 13,14-EDP-EA were tested in three different cell lines - HOS, 143B and MG63 cells using the Annexin V/ PI staining assay at 12.5 μM concentration. This concentration was chosen to reflect a point in the CTB assay where cell viability is reduced but not completely diminished. As seen in Figure 5.1D, all three regioisomers induced apoptosis in all the cell lines at a concentration of 12.5 μM. Specifically, in 143B cell line (Table ST1), 7,8-EDP-EA induced 8.75 ±0.145% apoptosis. 10,11-EDP-EA induced 17.92 ±

3.32% apoptosis and 13,14- EDP-EA induced 9.95 ± 1.88% apoptosis. Similar to these results, in MG63 cells (Table ST2), 7,8-EDP-EA induced 16.4 ±1.4% apoptosis. 10,11-EDP-EA induced 26.6 ± 3.5% apoptosis and 13,14- EDP-EA induced 16.9 ± 2.3% apoptosis. In HOS cells (Table ST3), the trend followed and 7,8-EDP-EA 17.1± 0.5% apoptosis. 10,11-EDP-EA induced 31.1 ± 2.3% apoptosis (p=) and 13,14- EDP-EA induced 19.6 ± 3.5% apoptosis.

In contrast to these results (Table ST4), treatment of all three different cell lines with AA, AEA, DHA and DHEA at 12.5 μM concentration showed little to no suppression of apoptosis as compared to no treatment control.

DHEA epoxides inhibit cell migration of cancer cells determined using wound healing assay

A wound healing assay or scratch assay has been shown to be an effective measure for directional migration of cells in vivo (32). A wound healing assay was performed for 7,8-EDP-EA, 10,11-EDP-EA and 13,14-EDP-EA at 5 μM . This concentration was chosen to reflect a concentration where the compounds are not significantly pro-apoptotic and the reduction in wound healing is because of the compound's anti-migratory properties. Figure 5.1E shows the effects of 7,8-EDP-EA, 10,11- EDP-EA and 13,14-EDP-EA on the wound closure in 143B cells as a representation. As seen from the data in Figure 5.1F, in HOS cells, all three compounds inhibit cell migration. However, for 7,8-EDP-EA and 13,14-EDP-EA the difference in wound closure at 10 hours is not significant. For 10,11-EDPEA, the wound closure at 10 hours tends to significance (p=0.08). In 143B cells, Figure 5.1F (ii), 7,8-EDPEA and 13,14-EDPEA do not inhibit wound healing at 10 hours. However 10,11-EDPEA inhibit wound closure significantly (p=0.05). In MG63 cell lines, Figure 5.1F, all three isomers restrict wound healing and at 10 hours and 10,11-EDP-EA prevented wound closure. Thus, while all three isomers are able to restrict wound healing and thereby show anti-migratory potential, the effect is greatest in 10,11-EDP-EA.

Taken together, we found from the apoptosis assay and cell migration assay that 10,11-EDP-EA was the most potent regioisomer and this was partly mediated through cannabinoid receptor 1 as using CB1 receptor antagonist, the reduction of cell migration by 10,11-EDP-EA was completely abolished (Appendix V).

Synthesis of amide derivatives of 10,11-DHEA epoxide (10,11-EDP-EA)

The eCB epoxides are dual functional molecules. As the amide bond is susceptible to fatty acid amide hydrolase (FAAH), we designed more stable analogs of 10,11-EDP-EA, which shows highest efficacy amongst the various epoxide derivatives of DHA. First, derivatives were made at the carboxylate end for different amide modifications, to reduce susceptibility to FAAH as well as better receptor binding to CB1 and CB2, which are the purported receptors for apoptotic activity (33-35).

The current literature has mainly focused on anandamide or arachidonylethanolamine (AEA) derivatives, since AEA is the biological ligand of CB1 and CB2 receptors and thus is likely to be the receptor binding to DHEA and its analogs. It has been previously shown that introduction of a methyl group at the 1' position of the amide results in increased metabolic stability of AEA, while affecting the CB1 binding ability (33). It was shown that the R isomer shows 4-fold higher CB1 binding and the S isomers shows 2-fold lower binding as compared to AEA. Thus the R-1'-methyl isomer was the first modification made to 10,11-EDP (figure 5.2). Next, the cyclopropyl derivative of AEA has been shown to have modest FAAH inhibition with an IC50 value of 4.1 ±2.0 μM, with significantly increased CB1 binding (34). Finally, the n-propyl derivative was made to assess the effect of acyl chain length on FAAH hydrolysis. It has also been shown to have better affinity for CB1 than AEA (35, 36).

The synthesis of these analogs is outlined in the materials and methods section similar to the synthesis of 10,11-EDP-EA. Briefly, 10,11-EDP was incubated with NHS and EDC in acetonitrile for 20 mins at 37 °C, followed by additional of the amine and stirring overnight at room temperature. The amines were purified by reverse phase HPLC chromatography and quantified similar to 10,11-EDP-EA.

Susceptibility to FAAH hydrolysis of 10,11-DHEA epoxides and its amide derivatives

Fatty acid amide hydrolase (FAAH) is a ubiquitously expressed protein in various mammals and the sequence of the protein has shown to be highly conserved in humans (36), mouse (36) and pig (37). For our studies, we used pig brain membrane preparations to analyze the effect of FAAH on 10,11-EDP-EA as well as the three amino derived modifications. The details of membrane preparation from pig brains are mentioned in materials and methods. As observed from figure 5.2B, there was significant reduction of hydrolytic potential in all three derivatives as compared to 10,11-EDP-EA. While 10,11-EDP formed from 10,11-EDP-EA was 1121.2 ± 11.2 ng min-1

mg protein-1, the same for 10,11-EDP-NA, 10,11-EDP-IA and 10,11-EDP-CA was 3.7 ± 2.3, ng min-1 mg protein-1 39.8 ± 1.7 ng min-1 mg protein-1and 198.6 ± 2.3 ng min-1 mg protein-1 respectively. Since the three derivatives show significantly reduced hydrolytic susceptibility, they could have higher bioavailability and thus their apoptotic and anti-migratory potential was further evaluated.

Apoptosis induced by amino modified derivatives of 10,11 DHEA epoxide (10,11-EDP-EA)

All three amino-modified derivatives of 10,11-EDP were tested for their apoptotic activity. All three compounds showed increased apoptotic potential as compared to the no treatment control with variation in different cell lines. The cyclopropyl analog seemed to have the highest pro-apoptotic potential among the three derivatives that were synthesized for the study. In HOS, MG63 and 143B cells, it increased apoptosis to 27.19 ± 4.05%, 17.09 ± 4.4% and 21.3 ± 1.9% respectively. The iso-propyl analog seemed to be the second most effective in HOS and MG63 cells with apoptotic potentials of 20.15± 1.75% and 17.48 ± 2.8% respectively. In 143B cells it was only 18.8 ± 0.3% for the iso-propyl derivative as compared to 25.7 ± 0.4% for the n-propyl derivative. However, the n-propyl derivative was least effective in HOS and MG63 cells with only 17.05 ± 1.4% and 15.15 ± 3.28% respectively. Overall, all the derivatives showed similar pro-apoptotic potential to the parent compound without discernable differences.

Would healing assay to determine the potential to inhibit cell migration by amino modified derivatives of 10,11 DHEA epoxide (10,11-EDP-EA)

A scratch assay was performed to analyze the anti-migratory properties of the three derivatives. The data in Figure 5.2 D is represented as a ratio of the percentage area remaining in the wound by compound and the control. As seen in Figure 5.2D, in all the cell lines, all the 10,11-EDP derivatives restrict wound migration at 10 hours. Among the derivatives, the 10,11-cyclopropyl derivative shows significantly greater potency at the 8 and 10 hour time points inhibiting migration by 4.5- 6 times more than vehicle control.

Similarly as seen in figure 5.2D, in the 143B cells, restriction in wound migration was 1- 1.9 times by 10,11-EDP-EA, 1- 1.47 times by n-propyl derivative, 1- 3.9 times by isopropyl derivative and 1 to nearly 10 fold by the cyclopropyl derivative as compared to the control. Finally, in the MG63 cell line (figure 5.2D), the restriction in wound healing was 1-2 times by 10,11-EDP-EA as

compared to the control. The 10,11-EDP-NA and 10,11-EDP-IA were slightly poorer than the control in restricting wound migration. And the 10,11-EDP-CA was comparable to 10,11-EDP-EA for the MG63 cell line in restricting wound migration.

As observed from the various results, it was concluded that the 10,11-EDP-CA was the most potent in inhibiting wound migration in 143B and HOS cells and comparable to the parent molecule in MG63 cells. It is interesting to note that the rate of wound closure is not constant in all the cases.

Cell cycle analysis of 10,11-EDP-EA and its analogs

The effects of 10,11-EDP-EA and its analogs was tested on cell cycle progression by treating cells with the compound for 24 hours, staining with propidium iodide and then analyzing with flow cytometry. As seen in Table 5.1, in 143B cells there does not appear to be a significant effect on the cell cycle except a slight suppression in the S phase with 10,11-EDP-NA. However, with the HOS cell lines there is an increase in G1 phase with all compounds but a suppression in the S phase with all the compounds. Finally, with MG63 there is an increase in the G1 phase and suppression in S phase with the 10,11-EDPIA.

10,11-EDPEA and its analogs prevent angiogenesis in HUVEC cells

Increased angiogenesis is one of the hallmarks of cancer. The development of neo-vascularization is key for the adequate supply of nutrients and oxygen to the site of metastasis (38). Endothelial tube formation on matrix has been established as a cellular model for angiogenesis (39). Briefly, endothelial HUVEC cells were grown on matrix and treated with vehicle control, 0.5 μM compound or 1 μM compound. The tube formation was assessed by Image J analysis. As seen in figure 5.3, 0.5 μM restricts tube formation significantly as compared to the vehicle control but does not completely restrict it. However, at 1 μM concentration, the tube formation is completely restricted. It was also verified that 1 μM concentration of treatment did not reduce cell viability in HUVEC cells as seen in appendix V.

Expression of CB1 and CB2 receptors in model cell lines

Literature evidence suggest that DHEA is an agonist of CB1 and CB2 receptors (11). Therefore, we investigated whether the effect of DHEA is through CB1/ CB2 pathway mediated. Additionally, CB receptors have been shown to be overexpressed in various cancers including osteosarcoma (40). We first determined the expression of CB1 and CB2 receptors in all three cell lines HOS, 143B and MG63. Additionally, the expression of CB1 and CB2 was also significantly higher in 143B cells as compared to HOS cells.

Apoptotic effect of DHEA epoxides in the presence of CB1 and CB2 antagonists

As an initial investigation into the mechanism of action for these endocannabinoids, we assessed their apoptotic activity in the presence of CB1 and CB2 antagonists, rimonabant and AM 630 respectively. As seen from Appendix V, rimonabant and AM 630 exhibit very limited apoptotic activity as compared to control. When CB1 and CB2 antagonist were incubated with 7,8-EDP-EA, a slight increase in apoptotic activity with 14.60 ± 1.82% and 10.12 ± 1.36% respectively. A similar result was seen for 13,14-EDP-EA where the treatment plus CB1 antagonist showed 13.03 ± 3.63%. The treatment plus CB2 antagonist showed no difference in apoptosis as compared to treatment alone at 9.2 ± 0.80%. The slight increase in apoptosis might be as a combinatorial effect of the treatment with the antagonist. Alternatively, since the molecules have two different reactive centers, the epoxide as well as the amide, they likely act through two different receptor classes- the cannabinoid receptor and the unknown epoxide receptor. It is possible that the blocking of the CB1 or CB2 receptors shuttle the molecule to the second epoxide receptor pathway thereby increasing the apoptotic activity. Finally, 10,11-EDP-EA showed a decrease in apoptotic potential with CB1 and CB2 antagonist at 7.44 ± 2.19% and 10.9 ± 0.08% indicating that this molecule mainly goes through the CB1 and CB2 receptors.

5.5 DISCUSSION

Lipid metabolites that are generated from omega-3 fatty acids such as DHA have been shown to exert anti-inflammatory, pro-resolving (4) and anti-tumorigenic effects through various mechanisms (5) (6) (7). In one mechanism, DHA is converted to DHA epoxides (EDPs) by CYP epoxygenase that have shown to exhibit have anti-tumorigenic properties. Alternatively, DHA is converted to DHEA, an endocannabinoid that have shown anti-proliferative efficiency in prostate cancer cells (11). Previously, we have shown that CYPs convert DHEA into DHEA epoxides (EDP-EA) that have both ethanolamide and epoxide moiety (23) (Figure 5.1A). Herein we

evaluated the anti-tumorigenic properties of all the different regioisomers of DHEA epoxides as both the endocannabinoid and epoxyeicosanoid pathway have been separately implicated in cancer (8, 9) and the terminal DHEA epoxide was shown to exhibit anti-inflammatory properties (23).

In order to execute our studies, we induced tumor in mice by injecting metastatic K7M2 intravenously into the tail vein. The mice were sacrificed and lung tissues were collected and the endocannabinoids were extracted. We showed that the DHEA epoxides were increased 20-80% depending on the regioisomers (Figure 5.1B) in the metastatic mice with osteosarcoma tumors as compared to the normal lungs. We further show that the EDP-EAs show a reduction of migratory potential of the cancer cells and moderately increased apoptosis in osteosarcoma cell lines. We hypothesized that the increase production of DHEA epoxides (EDP-EA) in the metastasized lungs are due to the immune response that is trying to reduce inflammation, cell migration and angiogenesis and promote apoptosis.

We tested all the five epoxide regioisomers of EDP-EAs towards their ability to do apoptosis in three human osteosarcoma cell lines- 143B and MG63, which are metastatic and HOS, which is a non-metastatic cell line. In all the three cell lines, the various regioisomers show an apoptotic effect and an anti-migratory affect. However, this effect is differential among the various EDP-EA regioisomers. For instance, 10,11-EDP-EA emerges as the most potent regioisomers in reducing cell migration. Interestingly, this effect was mediated via the CB1 receptor as using a CB1 antagonist, the anti-migratory potential of 10,11-EDP-EA was significantly reduced (Appendix V).

Since 10,11-EDP-EA showed the greatest potency in our assays, we wanted to characterize the molecule and explore its therapeutic potential in vivo. However, EDP-EAs has two hydrolytically susceptible groups. The amide functionality is hydrolyzed by fatty acid amide hydrolase. And the epoxide group is hydrolyzed by soluble epoxide hydrolases. Thus, the approach was to modify the molecules such that they retain their efficacy while being less susceptible to hydrolysis. Based on literature, modifications at the amide end of anandamide can reduce hydrolytic susceptibility as well as increase cannabinoid receptor binding (96). Thus, the R-1'-methyl isomer was the first modification made to 10,11-EDP. Next, the cyclopropyl derivative of AEA has been shown to have modest FAAH inhibition, with significantly increased CB1 binding (97). Finally, the n-propyl derivative was chosen for examination to assess the effect of acyl chain length on FAAH

hydrolysis. It has also been shown to have better affinity for CB1 than AEA (235, 236). We made similar analogs of 10,11-EDP-EA. All the analogs demonstrated similar apoptotic potential (Figure 5.2C) as compared to parent 10,11-EDP-EA, but markedly reduced susceptibility to FAAH hydrolysis (Figure 5.2B). Next, we performed a cell cycle analysis of 10,11-EDP-EA and analogs in all three cell lines. The data suggests that there is an increase in the G1 phase and a lowering of the S phase thus implying that the G1 to S phase transition is being blocked.

Next, we wanted to ascertain whether these molecules are acting through the cannabinoid receptors 1 and 2. We show that all three cell lines express both CB1 and CB2 (Appendix V). From the apoptosis assay in the presence of CB receptor antagonists, we conclude that the apoptosis is not mediated through cannabinoid receptor. However, the reduction of cell migration by 10,11-EDP-EA was abolished using CB1 antagonist. Taken together, these results suggest that in addition to CB1, 10,11-EDP-EA mediates its effect through other receptors including the uncharacterized epoxide receptor, PPAR and TRPV as their anti-tumorigenic effects cannot be completely abolished using CB1 agonists.

Thus, we show that a novel class of eCB epoxides and their stable derivatives exhibit anti-inflammatory (28), anti-angiogenic, anti-tumorigenic and anti-migratory properties. By virtue of their ability to bind CB receptors, these molecules will also exhibit anti-nociceptive bone pain activities. As osteosarcoma is accompanied by inflammation and pain, these molecules will aid in alleviating both conditions. As pointed out in the introduction, as these molecules are naturally occurring and their levels increase ~80% in osteosarcoma metastatic lungs, increasing their levels in vivo using FAAH and sEH dual inhibition will be effective adjuvant therapy for osteosarcoma (29, 30).

5.6 CONCLUSIONS

Omega-3 fatty acids and their biological metabolites have numerous physiological activities. In this work we show that a new class of omega-3 fatty acid metabolites known as endocannabinoid epoxides (eCBs) exert pro-apoptotic and anti-migratory effects in osteosarcoma cell lines. We show that the various regioisomers of eCBs have differential effects on the anti-tumorigenic effects. Furthermore, we develop synthetic analogs that are more hydrolytically stable to fatty acid amide hydrolase while maintaining their anti-apoptotic and anti-migratory effects. Thus, we show that a new class of omega-3 metabolites have potential anti-cancer therapeutic effect.

5.7 ACKNOWLEDGEMENTS

I would like to thank Dr. Zhong Li at the Roy J Carver Biotechnology institute for help with LC/MS detection of endocannabinoids and their degradation products. I would like to thank Ms. Josephine Watson for helpful discussions and Mr. Insup Hong for help with synthesis of endocannabinoid epoxides and their derivatives. I would like to thank Mrs. Holly Pondenis for helpful discussions of the biological assays.

5.8 FIGURE, TABLES AND LEGENDS

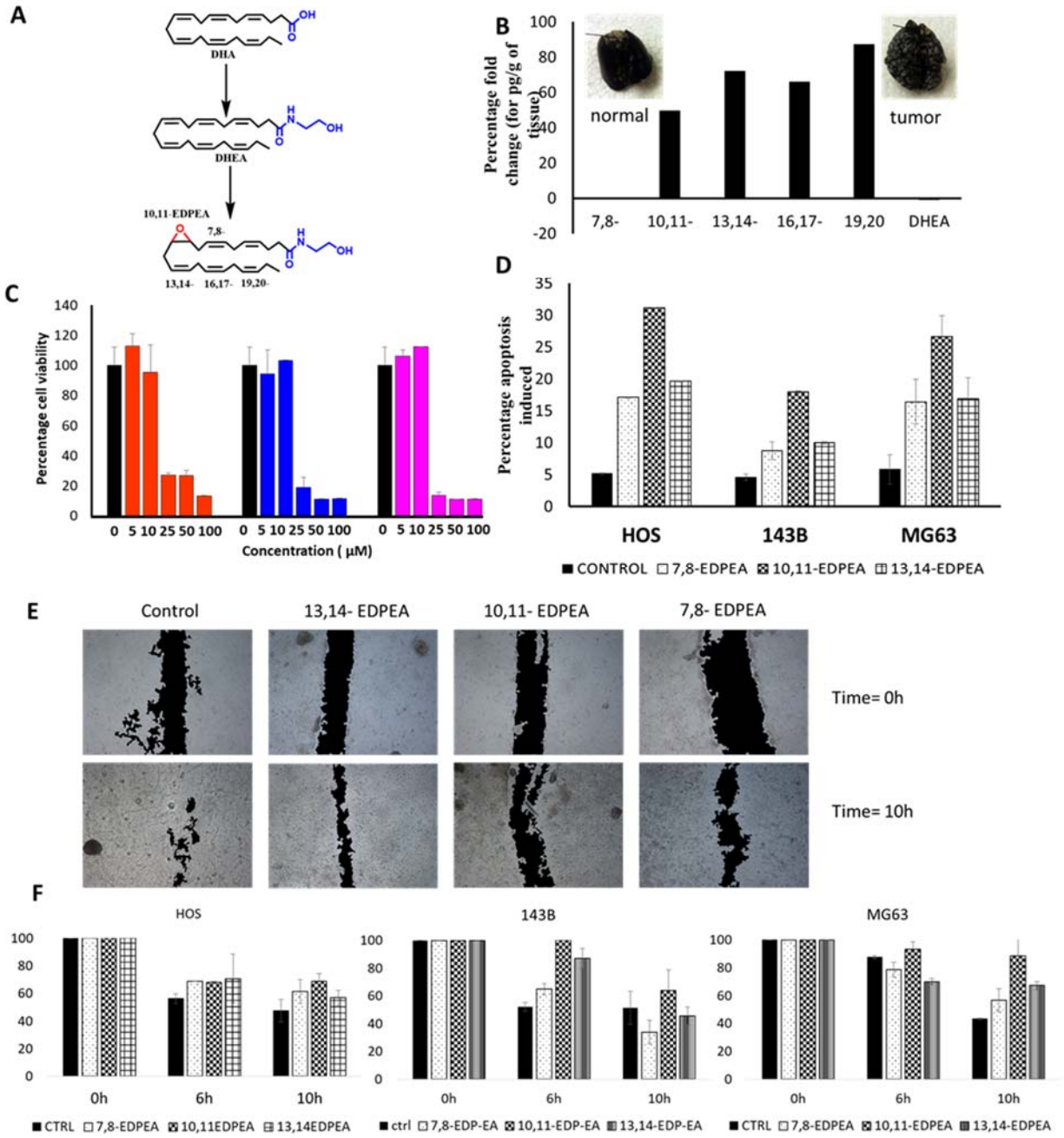

Figure 5.1: (A) Figure shows the synthesis of five structural isomers of DHEA-epoxide- 19,20-, 16,17-, 13,14-, 10,11- and 7,8- EDPEA from DHA and DHEA. (B) Figure shows the percentage fold change in endocannabinoid epoxides synthesized found in normal lung tissue and lung tissue with metastasized OS tumor. (C) Figure shows percentage cell viability as measured by cell titer

blue assay at 5 different concentrations of 13,14-EDPEA (orange), 10,11- EDPEA (blue) and 7.8-EDPEA (pink). (D) Apoptosis induced in HOS, 143B and MG63 cells at 12.5 μM concentration of 13,14-EDPEA (criss-cross), 10,11- EDPEA (checkered) and 7,8- EDPEA (dots). (E) Wound healing scratch shown at 0h and 10h in 143B cell lines by 13,14-EDPEA 10,11- EDPEA and 7,8-EDPEA at 5 μM concentration. (F) Wound healing represented as a percentage of original wound over 10 hours in three cell lines (i) HOS, (ii) 143B and (iii) MG63 by 5 μM concentration of 13,14-EDPEA (criss-cross), 10,11- EDPEA (checkered) and 7,8- EDPEA (dots).

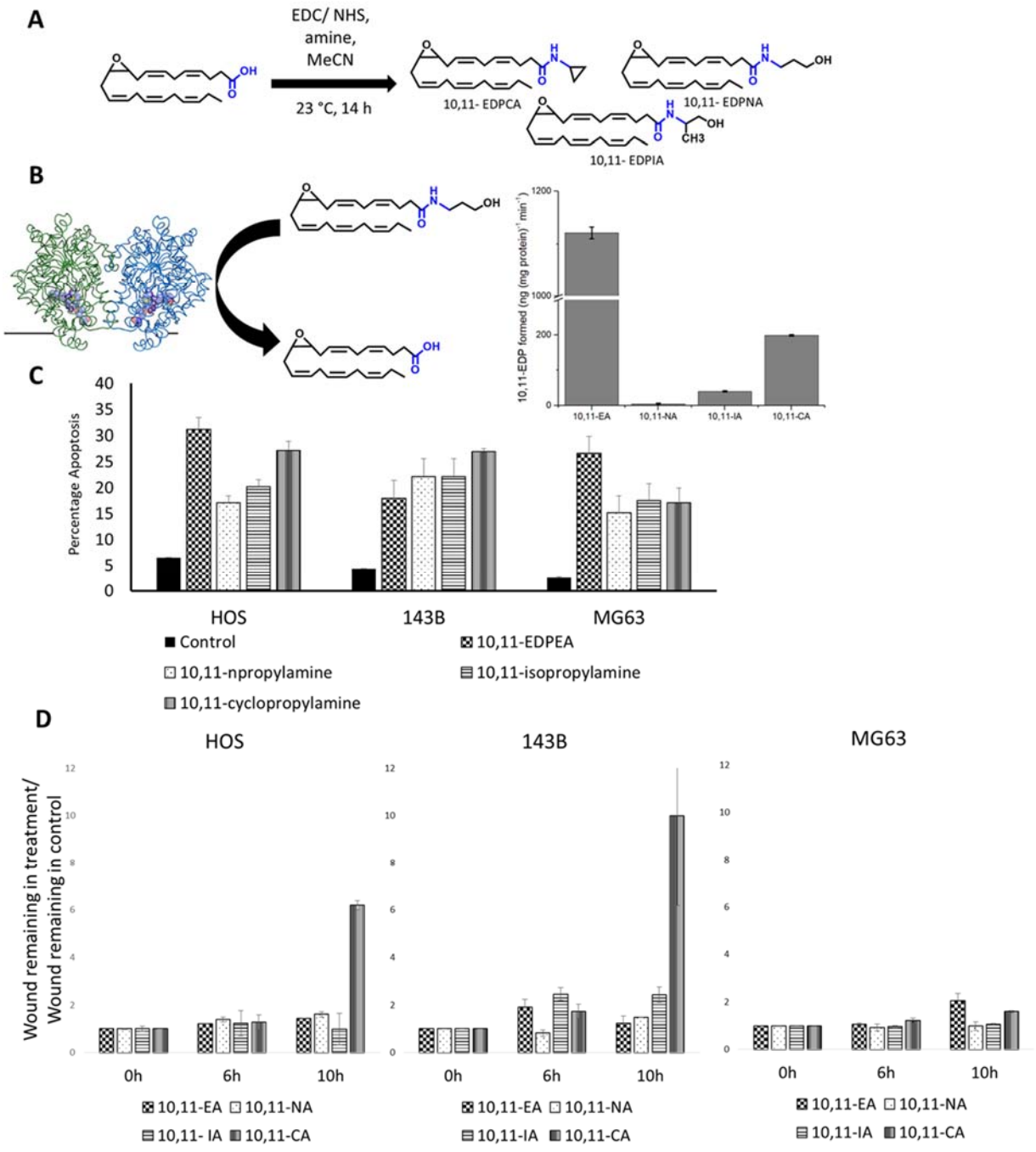

Figure 5.2: (A) Figure shows synthetic scheme for EDP-EA analogs. (B) Figure shows the Fatty Acid Amide Hydrolase (FAAH) dependent hydrolysis of amide derivatives. (C) Figure shows the apoptotic potential as shown by 10,11-EDPEA, 10,11-EDPNA, 10,11-EDPIA and 10,11EDPCA as compared to control as measured by Annexin V apoptosis assay. (D) Figure shows the anti-migratory properties of 10,11-EDPEA, 10,11-EDPNA, 10,11-EDPIA and 10,11EDPCA as

compared to control as measured by wound healing scratch assay on HOS, 143B and MG63 cell lines.

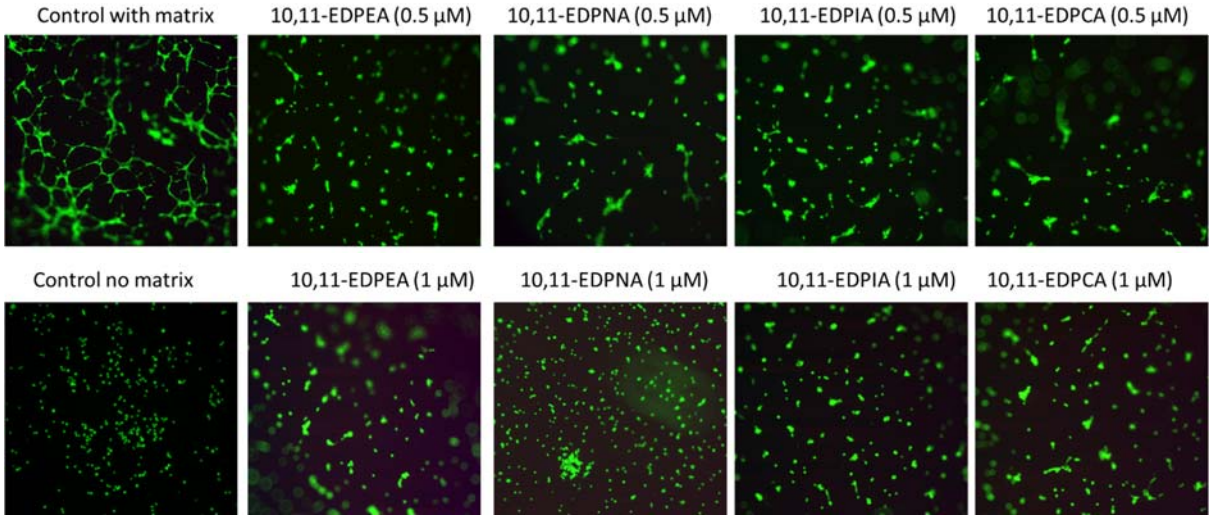

Figure 5.3: Figure shows the restriction of tube formation in endothelial HUVEC cells on matrigel by 10,11-EDPEA, 10,11-EDPNA, 10,11-EDPIA and 10,11EDPCA at 0.5 µM and 1 µM.

Table 5.1: Table shows cell cycle analysis of 10,11-EDPEA, 10,11-EDPNA, 10,11-EDPIA and 10,11-EDPCA as monitored by propidium iodide staining in all three cell lines. All experiments were done in triplicates. * $p<0.05$, **$p<0.01$ as compared to untreated, # $p<0.05$, ##$p<0.01$ as compares to EA.

Cell line	**untreated**	**10,11-EDPEA**	**10,11-EDPNA**	**10,11-EDPIA**	**10,11-EDPCA**
143B					
G1	56.17 ± 2.67	50.74 ± 2.03	52.21 ± 0.13	50.09 ± 0.03	54.23 ± 0.75
S	26.61 ± 0.42	28.18 ± 3.90	24.04 ± 0.28*	41.84 ± 3.74	22.87 ± 0.32
G2	17.22 ± 2.25	21.08 ± 1.87	23.74 ± 0.41	8.07 ± 3.70	22.85 ± 0.42
HOS					
G1	47.81 ± 0.66	67.23 ± 0.62**#	62.17 ± 0.42**	55.75 ± 5.03	54.37 ± 1.41*#
S	37.08 ± 1.62	20.33 ± 0.88*	20.73 ± 2.07*	24.28 ± 1.36*	30.49 ± 1.76#
G2	15.11 ± 0.97	12.44 ± 0.25	17.09 ± 1.65	19.96 ± 3.66	15.13 ± 0.35#
MG63					
G1	62.91 ± 1.75	67.71 ± 2.23	63.46 ± 0.81	76.71 ± 0.06*	59.61 ± 0.25
S	20.17 ± 1.76	17.89 ± 2.07	19.00 ± 0.42	10.84 ± 0.28*	23.05 ± 0.39
G2	16.92 ± 0.01	14.4 ± 0.15**	17.54 ± 0.4#	12.45 ± 0.35**#	16.88 ± 0.14##

5.9 REFERENCES

1. Mantovani A, Allavena P, Sica A, Balkwill F. Cancer-related inflammation. Nature. 2008;454(7203):436-44. Epub 2008/07/25. doi: 10.1038/nature07205. PubMed PMID: 18650914.
2. Sica A, Allavena P, Mantovani A. Cancer related inflammation: the macrophage connection. Cancer letters. 2008;267(2):204-15. Epub 2008/05/02. doi: 10.1016/j.canlet.2008.03.028. PubMed PMID: 18448242.
3. Yu H, Pardoll D, Jove R. STATs in cancer inflammation and immunity: a leading role for STAT3. Nature reviews Cancer. 2009;9(11):798-809. Epub 2009/10/24. doi: 10.1038/nrc2734. PubMed PMID: 19851315; PubMed Central PMCID: PMC4856025.
4. Jaudszus A, Gruen M, Watzl B, Ness C, Roth A, Lochner A, Barz D, Gabriel H, Rothe M, Jahreis G. Evaluation of suppressive and pro-resolving effects of EPA and DHA in human primary monocytes and T-helper cells. Journal of lipid research. 2013;54(4):923-35. doi: 10.1194/jlr.P031260. PubMed PMID: 23349208; PubMed Central PMCID: PMC3605999.
5. Laviano A, Rianda S, Molfino A, Rossi Fanelli F. Omega-3 fatty acids in cancer. Current opinion in clinical nutrition and metabolic care. 2013;16(2):156-61. doi: 10.1097/MCO.0b013e32835d2d99. PubMed PMID: 23299701.
6. Rose DP, Connolly JM. Omega-3 fatty acids as cancer chemopreventive agents. Pharmacol Therapeut. 1999;83(3):217-44. doi: Doi 10.1016/S0163-7258(99)00026-1. PubMed PMID: ISI:000082606600003.
7. D'Eliseo D, Velotti F. Omega-3 Fatty Acids and Cancer Cell Cytotoxicity: Implications for Multi-Targeted Cancer Therapy. Journal of clinical medicine. 2016;5(2). doi: 10.3390/jcm5020015. PubMed PMID: 26821053; PubMed Central PMCID: PMC4773771.
8. Cui PH, Petrovic N, Murray M. The omega-3 epoxide of eicosapentaenoic acid inhibits endothelial cell proliferation by p38 MAP kinase activation and cyclin D1/CDK4 down-regulation. British journal of pharmacology. 2011;162(5):1143-55. Epub 2010/11/17. doi: 10.1111/j.1476-5381.2010.01113.x. PubMed PMID: 21077851; PubMed Central PMCID: PMC3051386.
9. Zhang G, Panigrahy D, Mahakian LM, Yang J, Liu JY, Stephen Lee KS, Wettersten HI, Ulu A, Hu X, Tam S, Hwang SH, Ingham ES, Kieran MW, Weiss RH, Ferrara KW, Hammock BD. Epoxy metabolites of docosahexaenoic acid (DHA) inhibit angiogenesis, tumor growth, and metastasis. Proc Natl Acad Sci U S A. 2013;110(16):6530-5. Epub 2013/04/05. doi: 10.1073/pnas.1304321110
1304321110 [pii]. PubMed PMID: 23553837; PubMed Central PMCID: PMC3631682.
10. Brown I, Cascio MG, Rotondo D, Pertwee RG, Heys SD, Wahle KW. Cannabinoids and omega-3/6 endocannabinoids as cell death and anticancer modulators. Prog Lipid Res. 2013;52(1):80-109. Epub 2012/10/30. doi: 10.1016/j.plipres.2012.10.001
S0163-7827(12)00053-7 [pii]. PubMed PMID: 23103355.
11. Brown I, Cascio MG, Wahle KW, Smoum R, Mechoulam R, Ross RA, Pertwee RG, Heys SD. Cannabinoid receptor-dependent and -independent anti-proliferative effects of omega-3 ethanolamides in androgen receptor-positive and -negative prostate cancer cell lines. Carcinogenesis. 2010;31(9):1584-91. doi: 10.1093/carcin/bgq151. PubMed PMID: 20660502; PubMed Central PMCID: PMC2930808.
12. Skaper SD, Di Marzo V. Endocannabinoids in nervous system health and disease: the big picture in a nutshell. Philos Trans R Soc Lond B Biol Sci. 2012;367(1607):3193-200. Epub 2012/10/31. doi: 10.1098/rstb.2012.0313
rstb.2012.0313 [pii]. PubMed PMID: 23108539; PubMed Central PMCID: PMC3481537.
13. Fonseca BM, Costa MA, Almada M, Correia-da-Silva G, Teixeira NA. Endogenous cannabinoids revisited: a biochemistry perspective. Prostaglandins Other Lipid Mediat. 2013;102-103:13-30. Epub 2013/03/12. doi: 10.1016/j.prostaglandins.2013.02.002
S1098-8823(13)00008-7 [pii]. PubMed PMID: 23474290.
14. Ashton JC, Glass M. The cannabinoid CB2 receptor as a target for inflammation-dependent neurodegeneration. Curr Neuropharmacol. 2007;5(2):73-80. doi: Doi 10.2174/157015907780866884. PubMed PMID: ISI:000247022800001.

15. Onaivi ES. Cannabinoid receptors in brain: pharmacogenetics, neuropharmacology, neurotoxicology, and potential therapeutic applications. International review of neurobiology. 2009;88:335-69. doi: 10.1016/S0074-7742(09)88012-4. PubMed PMID: 19897083.
16. Vara D, Salazar M, Olea-Herrero N, Guzman M, Velasco G, Diaz-Laviada I. Anti-tumoral action of cannabinoids on hepatocellular carcinoma: role of AMPK-dependent activation of autophagy. Cell death and differentiation. 2011;18(7):1099-111. doi: 10.1038/cdd.2011.32. PubMed PMID: 21475304; PubMed Central PMCID: PMC3131949.
17. Ladin DA, Soliman E, Griffin L, Van Dross R. Preclinical and Clinical Assessment of Cannabinoids as Anti-Cancer Agents. Front Pharmacol. 2016;7. doi: Artn 361
10.3389/Fphar.2016.00361. PubMed PMID: ISI:000385058800001.
18. Guindon J, Hohmann AG. The endocannabinoid system and cancer: therapeutic implication. British journal of pharmacology. 2011;163(7):1447-63. doi: 10.1111/j.1476-5381.2011.01327.x. PubMed PMID: 21410463; PubMed Central PMCID: PMC3165955.
19. Hsu SS, Huang CJ, Cheng HH, Chou CT, Lee HY, Wang JL, Chen IS, Liu SI, Lu YC, Chang HT, Huang JK, Chen JS, Jan CR. Anandamide-induced Ca2+ elevation leading to p38 MAPK phosphorylation and subsequent cell death via apoptosis in human osteosarcoma cells. Toxicology. 2007;231(1):21-9. doi: 10.1016/j.tox.2006.11.005. PubMed PMID: 17222495.
20. De Petrocellis L, Melck D, Palmisano A, Bisogno T, Laezza C, Bifulco M, Di Marzo V. The endogenous cannabinoid anandamide inhibits human breast cancer cell proliferation. Proc Natl Acad Sci U S A. 1998;95(14):8375-80. PubMed PMID: 9653194; PubMed Central PMCID: PMC20983.
21. Patsos HA, Hicks DJ, Dobson RR, Greenhough A, Woodman N, Lane JD, Williams AC, Paraskeva C. The endogenous cannabinoid, anandamide, induces cell death in colorectal carcinoma cells: a possible role for cyclooxygenase 2. Gut. 2005;54(12):1741-50. doi: 10.1136/gut.2005.073403. PubMed PMID: 16099783; PubMed Central PMCID: PMC1774787.
22. Nithipatikom K, Endsley MP, Isbell MA, Falck JR, Iwamoto Y, Hillard CJ, Campbell WB. 2-arachidonoylglycerol: a novel inhibitor of androgen-independent prostate cancer cell invasion. Cancer research. 2004;64(24):8826-30. doi: 10.1158/0008-5472.CAN-04-3136. PubMed PMID: 15604240.
23. McDougle DR, Watson JE, Abdeen AA, Adili R, Caputo MP, Krapf JE, Johnson RW, Kilian KA, Holinstat M, Das A. Anti-inflammatory omega-3 endocannabinoid epoxides. Proc Natl Acad Sci U S A. 2017. doi: 10.1073/pnas.1610325114. PubMed PMID: 28687674.
24. Niu F, Zhao S, Xu CY, Sha H, Bi GB, Chen L, Ye L, Gong P, Nie TH. Potentiation of the antitumor activity of adriamycin against osteosarcoma by cannabinoid WIN-55,212-2. Oncology letters. 2015;10(4):2415-21. doi: 10.3892/ol.2015.3525. PubMed PMID: 26622862; PubMed Central PMCID: PMC4580018.
25. Hald A, Ding M, Egerod K, Hansen RR, Konradsen D, Jorgensen SG, Atalay B, Nasser A, Bjerrum OJ, Heegaard AM. Differential effects of repeated low dose treatment with the cannabinoid agonist WIN 55,212-2 in experimental models of bone cancer pain and neuropathic pain. Pharmacology, biochemistry, and behavior. 2008;91(1):38-46. doi: 10.1016/j.pbb.2008.04.021. PubMed PMID: 18611408.
26. Lozano-Ondoua AN, Wright C, Vardanyan A, King T, Largent-Milnes TM, Nelson M, Jimenez-Andrade JM, Mantyh PW, Vanderah TW. A cannabinoid 2 receptor agonist attenuates bone cancer-induced pain and bone loss. Life sciences. 2010;86(17-18):646-53. doi: 10.1016/j.lfs.2010.02.014. PubMed PMID: 20176037; PubMed Central PMCID: PMC2871326.
27. Luu HH, Kang Q, Park JK, Si W, Luo Q, Jiang W, Yin H, Montag AG, Simon MA, Peabody TD, Haydon RC, Rinker-Schaeffer CW, He TC. An orthotopic model of human osteosarcoma growth and spontaneous pulmonary metastasis. Clinical & experimental metastasis. 2005;22(4):319-29. doi: 10.1007/s10585-005-0365-9. PubMed PMID: 16170668.
28. McDougle DR, Watson JE, Abdeen AA, Adili R, Caputo MP, Krapf JE, Johnson RW, Kilian KA, Holinstat M, Das A. Anti-inflammatory omega-3 endocannabinoid epoxides. Proc Natl Acad Sci U S A. 2017;114(30):E6034-E43. doi: 10.1073/pnas.1610325114. PubMed PMID: 28687674; PubMed Central PMCID: PMC5544256.

29. Zhang G, Panigrahy D, Hwang SH, Yang J, Mahakian LM, Wettersten HI, Liu JY, Wang Y, Ingham ES, Tam S, Kieran MW, Weiss RH, Ferrara KW, Hammock BD. Dual inhibition of cyclooxygenase-2 and soluble epoxide hydrolase synergistically suppresses primary tumor growth and metastasis. Proc Natl Acad Sci U S A. 2014;111(30):11127-32. doi: 10.1073/pnas.1410432111. PubMed PMID: 25024195; PubMed Central PMCID: PMC4121808.
30. Winkler K, Ramer R, Dithmer S, Ivanov I, Merkord J, Hinz B. Fatty acid amide hydrolase inhibitors confer anti-invasive and antimetastatic effects on lung cancer cells. Oncotarget. 2016;7(12):15047-64. doi: 10.18632/oncotarget.7592. PubMed PMID: 26930716; PubMed Central PMCID: PMC4924770.
31. Hillard CJ, Wilkison DM, Edgemond WS, Campbell WB. Characterization of the kinetics and distribution of N-arachidonylethanolamine (anandamide) hydrolysis by rat brain. Biochimica et biophysica acta. 1995;1257(3):249-56. PubMed PMID: 7647100.
32. Liang CC, Park AY, Guan JL. In vitro scratch assay: a convenient and inexpensive method for analysis of cell migration in vitro. Nature protocols. 2007;2(2):329-33. doi: 10.1038/nprot.2007.30. PubMed PMID: 17406593.
33. Abadji V, Lin SY, Taha G, Griffin G, Stevenson LA, Pertwee RG, Makriyannis A. (R)-Methanandamide - a Chiral Novel Anandamide Possessing Higher Potency and Metabolic Stability. J Med Chem. 1994;37(12):1889-93. doi: Doi 10.1021/Jm00038a020. PubMed PMID: WOS:A1994NR64700020.
34. Jarrahian A, Manna S, Edgemond WS, Campbell WB, Hillard CJ. Structure-activity relationships among N-arachidonylethanolamine (anandamide) head group analogues for the anandamide transporter. J Neurochem. 2000;74(6):2597-606. doi: DOI 10.1046/j.1471-4159.2000.0742597.x. PubMed PMID: WOS:000086968800042.
35. Pinto JC, Potie F, Rice KC, Boring D, Johnson MR, Evans DM, Wilken GH, Cantrell CH, Howlett AC. Cannabinoid Receptor-Binding and Agonist Activity of Amides and Esters of Arachidonic-Acid. Mol Pharmacol. 1994;46(3):516-22. PubMed PMID: WOS:A1994PJ60100016.
36. Sheskin T, Hanus L, Slager J, Vogel Z, Mechoulam R. Structural requirements for binding of anandamide-type compounds to the brain cannabinoid receptor. J Med Chem. 1997;40(5):659-67. doi: Doi 10.1021/Jm960752x. PubMed PMID: WOS:A1997WK72600004.
37. Giang DK, Cravatt BF. Molecular characterization of human and mouse fatty acid amide hydrolases. P Natl Acad Sci USA. 1997;94(6):2238-42. doi: DOI 10.1073/pnas.94.6.2238. PubMed PMID: WOS:A1997WP33400029.
38. Goparaju SK, Kurahashi Y, Suzuki H, Ueda N, Yamamoto S. Anandamide amidohydrolase of porcine brain: cDNA cloning, functional expression and site-directed mutagenesis. Bba-Mol Cell Biol L. 1999;1441(1):77-84. doi: Doi 10.1016/S1388-1981(99)00143-2. PubMed PMID: WOS:000083281400009.
39. Nishida N, Yano H, Nishida T, Kamura T, Kojiro M. Angiogenesis in cancer. Vascular health and risk management. 2006;2(3):213-9. PubMed PMID: 17326328; PubMed Central PMCID: PMC1993983.
40. Arnaoutova I, Kleinman HK. In vitro angiogenesis: endothelial cell tube formation on gelled basement membrane extract. Nature protocols. 2010;5(4):628-35. doi: 10.1038/nprot.2010.6. PubMed PMID: 20224563.
41. Chakravarti B, Ravi J, Ganju RK. Cannabinoids as therapeutic agents in cancer: current status and future implications. Oncotarget. 2014;5(15):5852-72. PubMed PMID: WOS:000347919500003.

CHAPTER VI: CONCLUSIONS AND FUTURE WORK

6.1 SUMMARY

In summary, this work investigates various proteomic and lipidomic profiles in osteosarcoma. The second chapter performed a comparative proteomic profiling of the membrane proteome of metastatic and non-metastatic osteosarcoma in human and canine cell lines by peptide fingerprinting. While several proteins were identified as differentially regulated, three proteins- CD44, CD147 and vimentin were taken forward for biochemical validation by western blotting, flow cytometry, confocal microscopy and immunohistochemistry in cell pellets and paired primary and metastatic samples from canine patients. The results from biochemical validation confirmed those from peptide fingerprinting. A major conclusion of this work was that canine and human OS cell lines show similar proteomic profiles. Thus, dogs are an appropriate model for human OS and there can be development of parallel therapeutics for metastatic disease in both species.

Furthermore, we established the first fully characterized mammalian membrane protein nanodisc library. This allows stabilization of membrane proteins that cannot be overexpressed as well as to preserve protein-protein interactions. A major finding in this study was that lipid composition affects the proteomic incorporation and this could be exploited to the user's goal. Furthermore, we showed that the activity of the incorporated proteome is preserved in all nanodisc compositions by two different activity assays.

Next, a lipidomics composition change was investigated in normal osteoblasts, non-metastatic OS as well as metastatic human OS cells. Several different lipids were found to be differentially regulated in the three cell lines. Most notably diacylglycerols were upregulated in metastatic vs non-metastatic or normal cells and cholesteryl esters followed the reverse trend.

Finally, we investigated the anti-tumorigenic effects of endogenous lipids known as endocannabinoid epoxides (eCBs). We determined that endogenous eCBs show modest pro-apoptotic and anti-migratory activity in OS cell lines. This was followed by synthesis of analogs designed to reduce the hydrolytic susceptibility of the endogenous molecules. These molecules showed slight reduction in hydrolytic susceptibility as well as similar anti-migratory and pro-apoptotic activity as the endogenous molecules making them better targets for therapeutic delivery since they are likely to have longer bioavailability, while retaining similar activity.

6.2 FUTURE DIRECTIONS

As summarized in the previous section, four aspects relating to biomarkers and therapeutics in osteosarcoma. Each aspect has its own future direction. In the first section, several different biomarkers were identified in OS. The next steps towards this would be to evaluate if these proteomic profiles are conserved in tissue samples beyond what has been shown in our work with immunohistochemistry of tissue samples. This is especially in light of the fact that processing the primary tissue sample of bone cancers involves several steps including decalcification and fixing. These steps can significantly alter the epitopes exposed on the tissue surface and a better picture of the protein expression can be obtained by peptide fingerprinting. Furthermore, the proteomic study can be extended both in cell lines by employing top-down proteomics (1). Top-down proteomics will allow differentiation in post translational modifications that in themselves can be targets for therapeutics. The ultimate goal of this project is to develop therapeutics towards the differentially regulated proteins identified. For CD44, various peptides that affect hyaluronic acid binding to CD44 (2) as well as antibody conjugates (3) have been explored in various cancers. These could provide a starting point towards exploration of anti-CD44 therapy. Towards CD147, limited efforts have been with antibodies (4). Therefore there is potential for peptide as well as small molecule therapeutic development for CD147.

Towards the stabilization of the membrane proteome in nanodisc libraries, there are two main areas of exploration following the work described in chapter three. First, a systematic study of varying lipid composition instead of a few discrete compositions can be performed to see how the changing lipid profile affects the incorporated proteome. This would be beneficial towards optimizing the incorporation of proteins in the desired ratios. This could be furthered to incorporating other lipids including sphingomyelin, as well as lipids like DOPC (1,2-Dioleoyl-sn-glycero-3-phosphocholine) and DPPC (1,2-dipalmitoyl-sn-glycero-3-phosphocholine). The second direction is the biophysical characterization of the synthesized nanodiscs by techniques like small angle X-ray scattering (SAXS) (5). Techniques like SAXS could help understand why cholesterol results in smaller disc size as well as how the lipid distribution changes in the disc- whether they have a uniform distribution or form discrete units. Towards this I have performed some initial phase transition studies by incorporating fluorescent molecule laurdan in the nanodisc and measuring the change in fluorescence polarization with increase in temperature.

The lipidomics study for OS is the first study deciphering the lipidomic composition for OS and identifies the diacylglycerols as an upregulated class in the lipidome. While in this study, the DG synthesis is blocked by a PLC inhibitor in a proof of concept study to show that DG reduction lowers the cell viability as well as migration in metastatic OS cells. However, PLC inhibition affects a variety of lipid syntheses and is not a viable therapeutic approach for specifically blocking DG synthesis. Therefore, more specific pathways need to be identified for inhibiting DG synthesis. One probable pathway could be from monoacylglycerol (MG) to DG synthesis through MGAT (monoacylglycerol tansferase) (6-8). Furthermore, an interesting find was the lowering of cholesteryl esters in the metastatic cells. It is known that cells store energy as esterified cholesterol (9) and since cholesterol is known to increase in metastasized disease in various cancers (10), it would be interesting to investigate what factors are lowering the conversion of free cholesterol to esterified cholesterol, and if this is specific to osteosarcoma or prevalent in all cancers.

Finally, in chapter five we have shown that endocannabinoid epoxides are moderately anti-tumorigenic in osteosarcoma cell lines. This study should be followed by pharmacokinetic studies in mice and mice models of osteosarcoma to see the effects of the eCBs on the tumor size in lung metastasized tumors (11). Finally, these compounds can be employed to measure reduction in inflammatory pain in animal models (12).

6.3 REFERENCES

1. Whitelegge J. Intact protein mass spectrometry and top-down proteomics. Expert review of proteomics. 2013;10(2):127-9. doi: 10.1586/Epr.13.10. PubMed PMID: WOS:000318189900008.
2. Orian-Rousseau V. CD44, a therapeutic target for metastasising tumours. European journal of cancer. 2010;46(7):1271-7. doi: 10.1016/j.ejca.2010.02.024. PubMed PMID: WOS:000277906900012.
3. Sahin IH, Klostergaard J. CD44 as a drug delivery target in human cancers: where are we now? Expert Opin Ther Tar. 2015;19(12):1587-91. doi: 10.1517/14728222.2015.1088834. PubMed PMID: WOS:000366980400001.
4. Wang Y, Yuan L, Yang XM, Wei D, Wang B, Sun XX, Feng F, Nan G, Wang Y, Chen ZN, Bian HJ. A chimeric antibody targeting CD147 inhibits hepatocellular carcinoma cell motility via FAK-PI3K-Akt-Girdin signaling pathway. Clin Exp Metastas. 2015;32(1):39-53. doi: 10.1007/s10585-014-9689-7. PubMed PMID: WOS:000348977000005.
5. Skar-Gislinge N, Arleth L. Small-angle scattering from phospholipid nanodiscs: derivation and refinement of a molecular constrained analytical model form factor. Phys Chem Chem Phys. 2011;13(8):3161-70. doi: 10.1039/c0cp01074j. PubMed PMID: WOS:000287041700019.
6. Take K, Mochida T, Maki T, Satomi Y, Hirayama M, Nakakariya M, Amano N, Adachi R, Sato K, Kitazaki T, Takekawa S. Pharmacological Inhibition of Monoacylglycerol O-Acyltransferase 2 Improves Hyperlipidemia, Obesity, and Diabetes by Change in Intestinal Fat Utilization. PloS one. 2016;11(3). doi: ARTN e0150976
10.1371/journal.pone.0150976. PubMed PMID: WOS:000371735200160.
7. Huard K, Londregan AT, Tesz G, Bahnck KB, Magee TV, Hepworth D, Polivkova J, Coffey SB, Pabst BA, Gosset JR, Nigam A, Kou K, Sun H, Lee K, Herr M, Boehm M, Carpino PA, Goodwin B, Perreault C, Li QF, Jorgensen CC, Tkalcevic GT, Subashi TA, Ahn K. Discovery of Selective Small Molecule Inhibitors of Monoacylglycerol Acyltransferase 3. Journal of medicinal chemistry. 2015;58(18):7164-72. doi: 10.1021/acs.jmedchem.5b01008. PubMed PMID: WOS:000361921800006.
8. Ma ZP, Chao HGJ, Turdi H, Hangeland JJ, Friends T, Kopcho LM, Lawrence RM, Cheng D. Characterization of monoacylglycerol acyltransferase 2 inhibitors by a novel probe in binding assays. Analytical biochemistry. 2016;501:48-55. doi: 10.1016/j.ab.2016.02.012. PubMed PMID: WOS:000374204300008.
9. Ikonen E. Cellular cholesterol trafficking and compartmentalization. Nat Rev Mol Cell Bio. 2008;9(2):125-38. doi: 10.1038/nrm2336. PubMed PMID: WOS:000252676600013.
10. Kuzu OF, Noory MA, Robertson GP. The Role of Cholesterol in Cancer. Cancer Res. 2016;76(8):2063-70. doi: 10.1158/0008-5472.CAN-15-2613. PubMed PMID: WOS:000374170700003.
11. Botham RC, Roth HS, Book AP, Roady PJ, Fan TM, Hergenrother PJ. Small-Molecule Procaspase-3 Activation Sensitizes Cancer to Treatment with Diverse Chemotherapeutics. ACS central science. 2016;2(8):545-59. doi: 10.1021/acscentsci.6b00165. PubMed PMID: 27610416; PubMed Central PMCID: PMC4999974.
12. Inceoglu B, Jinks SL, Ulu A, Hegedus CM, Georgi K, Schmelzer KR, Wagner K, Jones PD, Morisseau C, Hammock BD. Soluble epoxide hydrolase and epoxyeicosatrienoic acids modulate two distinct analgesic pathways. Proceedings of the National Academy of Sciences of the United States of America. 2008;105(48):18901-6. doi: 10.1073/pnas.0809765105. PubMed PMID: 19028872; PubMed Central PMCID: PMC2596245.

APPENDIX A: DEVELOPMENT OF POLY UNSATURATED FATTY ACID DERIVATIVES OF ASPIRIN FOR INHIBITION OF PLATELET FUNCTION[6]

A.1 ABSTRACT

The inhibition of platelet function is a key step in prevention of myocardial infarction and ischemic stroke. Aspirin is the most widely used drug for the inhibition of platelet aggregation. However, it suffers from several key drawbacks including its poor permeability across biological membranes due to its ionic state at physiological pH. In this work, we propose new aspirin anhydride molecules for the inhibition of platelet function where aspirin is conjugated to dietary omega-3 and omega-6 fatty acids. Omega-3 fatty acids themselves have shown inhibitory effects on platelet function and thus this approach employs a "hybrid-drug" strategy of combining selected unsaturated fatty acids with aspirin. The molecules are tested for their effectiveness towards inhibiting platelet aggregation in washed platelets and platelet-rich plasma. Furthermore, they are examined biochemically for their effect on the COX-1 thromboxane synthase pathway for platelet aggregation, as well as COX-1 activity. Finally, hydrolysis studies on these molecules indicate release of aspirin and free fatty acids from these conjugates at a controlled rate in both buffer and plasma.

A.2 INTRODUCTION

Platelet adhesion and aggregation is important for maintaining normal hemostasis and is an essential component in the morbidity and mortality associated with cardiovascular disease including myocardial infarction and ischemic stroke. Therefore, the ability to modulate platelet function is of significant clinical importance. Aspirin is currently the most widely used therapeutic for inhibition of platelet activation. Aspirin functions via irreversible acetylation of platelet COX-1, resulting in inhibition of platelet-derived TXA2 formation. It has poor permeability across biological membranes at physiological pH due to the presence of free carboxylic acid, which is significantly ionized at physiological pH. The result is poor absorption of drugs with carboxylic acid moieties through lipid membrane barriers. Typically, NSAIDs also cause gastric toxicity as

[6] Reprinted with permission of the American Society for Pharmacology and Experimental Therapeutics. Development of poly unsaturated fatty acid derivatives of aspirin for inhibition of platelet function. Jahnabi Roy, Reheman Adili, Richard Kulmacz, Michael Holinstat, and Aditi Das. *J Pharm Exp Ther* 2016, *359(1),* 134-141.

they inhibit COX-1 which is involved in maintaining the integrity of gastrointestinal epithelium. The general approach to solve these side effects is to esterify the carboxylic acid to produce lipophilic pro-drug forms. However, several aliphatic or aromatic esters of carboxylic acid drugs are not sufficiently labile in vivo to ensure a suitably high rate and extent of conversion from the esterified form. Additionally, esters are highly susceptible to enzymatic hydrolysis in plasma and thus have differential rates of aspirin liberation in different individuals. Moreover, aspirin has two major functional groups, the carboxylate end and the O-acetyl end. As the O-acetyl end is the pharmacophore for the activity of aspirin, for an aspirin ester derivative pro-drug to be effective, it must hydrolyze at the carboxylate end faster than the O-acetyl end (238). Therefore in this work, we synthesize aspirin anhydride derivatives with lipids and evaluate their platelet aggregation function.

Recent work has focused on the modification of drug molecules with lipids or lipid derivatives as a means to overcome their side effects as well as to facilitate their delivery. Specifically, addition of a hydrophobic lipid tail allows the drug molecule to cross the hydrophobic plasma membrane and enter the cell (239). Herein we combine the two approaches of derivatizing aspirin with poly-unsaturated fatty acids in order to keep aspirin in a unionized form so as to achieve facile transport across the plasma membrane. The “hybrid-drug” approach of combining two drugs with similar therapeutic properties but different mechanisms has been gaining interest (240). For instance, there are several reports in literature indicating the inhibition of platelet aggregation by dietary fatty acids, chiefly omega-3 fatty acids EPA and DHA and omega-6 fatty acid linoleic acid (LA) (241). The action of these lipids is thought to be through competitive inhibition of COX-1-mediated arachidonic acid metabolism. The metabolism of EPA and DHA by COX-1 leads to the formation of alternative thromboxane-like molecule that are less potent than TXA2 with regard to platelet aggregation.

In our studies, we synthesize anhydride conjugates of dietary fatty acids- LA, EPA and DHA with aspirin for the inhibition of platelet aggregation. We hypothesized that if the omega-3 fatty acids and aspirin are reducing platelet aggregation separately then the conjugated moiety itself will have anti-platelet aggregatory properties through a synergistic or co-drug effect. Additionally these aspirin-lipid conjugates will prevent the deleterious effects of the free aspirin carboxylate group. The aspirin-lipid anhydride bond will be more susceptible to hydrolysis compared to O-acetyl end.

Therefore the compound will decompose to its carboxylic acid counterpart at a predictable rate and pattern depending on the conjugated molecule, as shown previously with related compounds (242). Furthermore, anhydrides are typically less sensitive to enzymatic cleavage than esters or amides (243). Thus the use of lipid anhydride conjugation is likely to increase bio-availability, be released in a controlled manner, and reduce gastric and mucosal toxicity.

In summary, this work is the first report on application of aspirin anhydride using polyunsaturated fatty acids– LA, EPA and DHA for reduction in platelet aggregation. We demonstrate that anhydride conjugates of aspirin with dietary omega-3 fatty acids are potent inhibitors of platelet aggregation. Furthermore, we biochemically examine their effect on the COX-1 mediated TXA2 formation since the focus of current literature in dietary lipids has focused on dietary supplementation in controlled trial groups (241). Finally, we exhibit through hydrolysis studies, that the conjugates release aspirin and free fatty acids at a controlled rate in both buffer and plasma.

A.3 MATERIALS AND METHODS

Materials: Human TXAS gene was obtained from Origene. Ampicillin, arabinose, chloramphenicol, isopropyl β-D-1-thiogalactopyranoside (IPTG) and Ni-NTA resin were bought from Gold Biotechnology. δ-Aminolevulinic acid (δ-ALA) and hematin were obtained from Frontier Scientific. 1-palmitoyl-2-oleoyl-sn-glycero-3-phosphocholine (POPC) was purchased from Avanti Polar Lipids. Aspirin was purchased from Sigma Aldrich. Arachidonic acid, EPA, DHA and LA were obtained from Cayman Chemicals. PAR4-AP (AYPGKF) and PAR1-AP (SFLLRN) were purchased from GL Biochem (Shanghai, China). Thrombin was purchased from Enzyme Research Laboratories (South Bend, IN). Collagen and ristocetin was purchased from Chorology Cooperation. U46619 and ADP were purchased from Sigma Aldrich. University of Michigan Review Board approved studies and written informed consent was obtained from all participants prior to blood collection.

Synthesis of aspirin chloride: Aspirin chloride was synthesized as previously mentioned (244). Briefly, to a 250 mL round bottom flask charged with stir bar was added aspirin (500mg, 2.77 mmole) and dissolved in benzene (69.5 mL, 0.04 M in aspirin) and thinoyl chloride (805 μL, 11.1 mmoles) was added. The mixture was refluxed for 8 h and the resulting solution was cooled down. The solution was concentrated in vacuo to yield a white solid that was taken into future reactions without further purification. Yield: 435 mg, 79%.

Synthesis of anhydrides: To a 7 mL vial charged with stir bar was added aspirin chloride (10 mg, 0.05 mmoles) and fatty acid (DHA- 16 mg, 0.05 mmole, EPA- 15 mg, 0.05 mmole, 14 mg, 0.05 mmole) and dissolved in DCM (1 mL, 0.04 M). To this was added pyridine (4 µL, 0.075 mmole) and the solution was stirred at room temperature for 4 h. The reaction was then quenched with 1 mL of 1 N HCl solution and vortexed. The organic layer was removed and the aqueous layer was re-extracted with 1 mL DCM. The combined organic layers were dried over sodium sulfate and concentrated in vacuo. The residual solid was recrystallized in diethyl ether to yield a white solid. Yields: DHA anhydride- 3.5 mg, 20%, EPA anhydride- 6 mg, 26%, LA anhydride- 17.5 mg, 79%.

Platelet purification: Human whole blood was drawn from the antecubital vein of healthy donors. PRP was obtained from whole blood by centrifugation at 200g for 10 minutes. Leftover blood samples were centrifuged at 200g for 10 minutes to obtain Platelet-poor-plasma (PPP). Washed human platelets were isolated from whole blood and platelet aggregation studies were performed as previously described (245). Whole Blood was drawn from the antecubital vein of untreated healthy donors or healthy donors who were orally given 81mg/day aspirin for 7 days. Platelets were pelleted from PRP in the presence of ACD (2.5%) and apyrase (0.02 U/mL) by centrifugation at 2000g for 10 minutes then resuspended in Tyrodes buffer (12 mM NaHCO3, 127 mM NaCl, 5 mM KCl, 0.5 mM NaH2PO4, 1 mM MgCl2, 5 mM glucose, 10 mM HEPES) to a final concentration of 3.0 x 108 platelets/mL. Washed platelets (250µL) were separately incubated with 2.5, 5, 10 µM or with same volume of DMSO for 5 minutes.

Washed human platelet aggregation: platelet aggregation was induced by 5 µM AA, Thrombin (1nM), PAR4-AP, PAR1-AP (SFLLRN), ADP (1µM) or U46619 (1µM) and change in light transmission was recorded by eight channel platelet aggregometer (Chronolog) under stirring at 1200 rpm at 37°C.

Platelet aggregation in PRP: Platelet concentration in PRP was adjusted to 3.0 x 108 platelets/mL using PPP from same donor. 10 µM of C1, C2, C3 compounds or DMSO in same volume was separately incubated with 250uL of PRP for 5 minutes. Platelet aggregation was induced by adding AA (5 µM) ADP (1 µM), collagen (2 µg/mL), Ristocetin (1 µM) or U46619 (1 µM) and change in light transmission were recorded by platelet aggregometer as described above.

Expression and purification of cyclooxygenase 1 (COX-1)

An 8- 10 g of Sf9 cell pellet from a 2L cell culture expression COX-1 was suspended in 40-45 ml of Buffer A (25 mM NaPO4 / 20 mM imidazole, pH 7.4 / 1 mM phenol) and 5 ml of 10x Sigma protease inhibitor (P2714) was added. Cell clumps were resuspended by magnetic stirring. This resuspension was homogenized by sonication and centrifuged at 100,000 × g for 1 hr and supernatant was removed. The pellet was resuspended in ~45 ml of Buffer B (25 mM NaPO4 / 100 mM NaCl / 20 mM imidazole / 0.1 mM phenol, pH 7.4) using with a Dounce homogenizer. 10% Tween 20 solution was added to a 1.5% final concentration and stirred for 1-2 hr followed by centrifugation at 100,000 x g for 1 hr. The supernatant (S1) was removed and the pellet was resuspended in ~20 ml Buffer B. S1 was mixed with 2.5-3 ml of Ni-NTA Agarose (Qiagen) prewashed with Buffer C (25 mM NaPO4 / 100 mM NaCl / 20 mM imidazole / 0.1 mM phenol, pH 7.4 / 0.1% Tween 20) and rocked in cold room for 2 hours. The mixture was poured into column (~1.5 x 10 cm) and the flow though was allowed to drain out. The column was washed with 10-15 mL of Buffer C and then with 10-15 ml of Buffer D (25 mM NaPO4 / 300 mM NaCl / 20 mM imidazole / 0.1 mM phenol, pH 7.4 / 0.1% Tween 20). The protein was eluted with 10 x 0.75 ml aliquots of Buffer E (25 mM NaPO4 / 100 mM NaCl / 200 mM imidazole / 0.1 mM phenol, pH 7.4 / 0.1% Tween 20). The active fractions were pooled and concentrated.The buffer was exchanged on a 10DG column eluted with 50 mM KPi, pH 7.2 / 50 mM NaCl / 0.01% NaN3 / 0.1% Tween 20 and collect 0.25 ml fractions. COX- 1 activity each fraction was assayed and active fractions were pooled. Protein was stored at -80 °C with ¼ vol of glycerol.

Expression and purification of thromboxane synthase: TXAS was expressed and purified as previously mentioned (159). Briefly, the cells were grown in terrific Broth (TB) and were induced with 1 mM IPTG and 0.5 mM δ-ALA and 4 mg/L arabinose at O.D 1.2. They were grown for 44 hours at 26°C and 160 rpm. The harvested cells were resuspended in Buffer A (0.1 M potassium phosphate pH 7.4, 10% glycerol, 0.1 M sodium chloride) containing 2 mM magnesium chloride, 1 mM PMSF, 1 mg each of DNase and RNase for 1 hour and lysed 5 times for 1 min each using a sonicator. The solution was then centrifuged at 35 K rpm for 1 hour and the pellet was resuspended in Buffer A containing 2% Lubrol to solubilize TXAS. The re-suspended sample was centrifuged at 35 K rpm for 1 hour and the supernatant was loaded onto a Ni-NTA column. The column was incubated for 2 hours with 5X column volume of buffer A containing 10 mM Histidine, 5 mM ATP, 10 mM MgCl2 and 150 mM KCl to separate any co-purifying GroEL (246). TXAS was eluted using Buffer A containing 0.2% Lubrol and 100 mM Histidine.

Assembly of TXAS -Nanodiscs: TXAS-Nanodiscs were assembled from a mixture of TXAS, membrane scaffold protein (MSP1D1), cholate and POPC lipids by removing the detergents using Amberlite (164). MSP1D1 was added to POPC (solubilized using sodium cholate) in a ratio of 65:1 (lipids: MSP1D1) and the solution was incubated at 4oC for 1 hour on a shaker. We thank Sligar laboratories for giving the MSP1D1 gene. TXAS was then added in a ratio of 1:15 (TXAS : MSP1D1) and incubated another 1 hour. Amberlite was added to remove detergents and initiate the formation of Nanodiscs. The TXAS-Nanodiscs were then purified using size exclusion chromatography as previously mentioned (159).

Coupled assay with secondary lipids: TXAS converts PGH2 into TXA2, and HHT (12(L)-hydroxy-5,8,10-heptadecatrienoic acid) and MDA (malondialdehyde) as a side reaction (247). To measure overall effect of a secondary lipid on the metabolization of AA, a coupled enzymatic assay was performed. Briefly, to COX-1 (10 nM) incubated with hematin (0.5 μM) in tris buffer (0.1 M, pH= 7.4) was added TXAS (50 nM). To this was added AA (20 μM) and secondary substrate (20 μM) and rate of MDA formation was monitored over 3 minutes at 268 nm and HHT at 234 nm. Absorbance was then measured and the reaction mixture was quenched in 300 μL of ethyl acetate. The amount of TXB2 formed was determined using TXB2 EIA ELISA Kit (Cayman).

A.4 RESULTS

Synthesis of aspirin anhydride derivatives: The synthesis of the fatty acid-aspirin derivatives was performed as shown in Scheme A.1. The free carboxylic acid in aspirin was first converted to its corresponding acid chloride by reacting with thionyl chloride in the presence of amine base by refluxing in benzene for 8h. The activated acid chloride was taken, without further purification, to react with the carboxylic acid in EPA, DHA and LA to form a mixed anhydride. The mixed anhydride was purified by recrystallization in diethylether to give >99% purity by 1H- NMR and HR-ESI mass spectrometry (Figure A.1-A.3).

Lipid- aspirin conjugates inhibit AA induced platelet aggregation: The effect of fatty acid- aspirin derivatives compounds C1, C2 and C3 on platelet function was studied in vitro using platelet aggregation at differing concentrations from 2.5μM to 10 μM. As shown in Figure A.4, arachidonic acid-induced (5 μM) platelet aggregation was inhibited by all three compounds in a dose-dependent manner. However, these compounds varied in potency of inhibition with C3 being

the most potent followed by C2 and C1. As seen from the aggregation curves, as compared to the DMSO control, compound C1, LA anhydride, shows a slight decrease in platelet aggregation with a significant decrease at 10 μM concentration ($p= 0.0158$). In contrast C2, the EPA anhydride, shows a greater inhibition at lower concentrations with a significant decrease at 5 μM ($p= 0.0176$) and a further decrease at 10 μM ($p \leq 0.0001$). Compound C3, DHA anhydride, shows most significant inhibition of platelet aggregation with a significant inhibition at 2.5 μM ($p= 0.0049$) and 5 μM ($p= 0.0011$) and almost complete inhibition of aggregation at 10 μM ($p= 0.0002$). Similar results were observed for platelet rich plasma (PRP) (Figure A.5). As seen in Figures A.5A and A.5B, at 10 μM concentration, compounds C2 and C3 show a significant decrease in platelet aggregation ($p= 0.1006$ for C2 and $p= 0.0003$ for C3). However, C1 did not show a significant decrease in aggregation in PRP.

In addition to AA, compounds C1, C2 and C3 attenuated platelet aggregation induced by various platelet agonists including thrombin, PAR4-AP, PAR1-AP, ADP or 46619. As seen in Figure A.6 and 7 a slight allbeit insignificant decrease was observed in platelet aggregation induced by thrombin, PAR4-AP and PAR1-AP for all three compounds at 10 μM concentration. No notable inhibition in platelet aggregation was observed in PRP stimulated with ADP, collagen, ristocetin, or U46619 (Figure A.6 (D), (E) and 7 (B), (C), (D)). Collectively, these observations indicated that the aspirin-lipid conjugates are acting through the inhibition of the COX- thromboxane synthase pathway.

In order to understand the potency of inhibitory effects of fatty acid-aspirin derivatives compounds on human platelet function, we compared the effectiveness of compound C3 against aspirin treated controls. As seen in figure A.5C, washed platelets with AA induced aggregation, as compared to DMSO controls, with 20 μM of compound C3 shows a similar level of inhibition as aspirin treated controls, of platelet function in response to AA ($p< 0.0001$). The inhibition values are similar to aspirin treated controls where a treatment of 81 mg/day of aspirin was administered for 7 days. Thus, compound C3 at 20 μM concentration displays similar effectiveness to aspirin

Inhibition of COX-1-thromboxane synthase activity by lipid-aspirin conjugates: Platelet aggregometry data shows that the inhibition by these compounds is effective only when induced by AA. Thus, the mechanism of action of the derivatives is likely through the COX-1-TXAS pathway. To confirm the effects of the derivatives and their parent compounds on the COX-1-

TXAS enzyme system, a coupled activity assay was performed. In this assay, COX-1 converts AA to prostaglandin H2 that is further converted by TXAS to thromboxane A2. TXA2 is a pro-aggregatory molecule that initiates platelet aggregation. However, TXA2 is quickly converted to TXB2 by hydrolysis of the endoperoxide bond to the diol form. TXB2 can be subsequently measured.

We utilized nanodiscs to stabilize TXAS is a membrane protein, which tends to lose functionality in aqueous buffers typically used for protein assays. Therefore it was incorporated into nanodiscs, lipid bilayers surrounded by membrane scaffold protein (MSP) (Figure A.8A). Previously we have shown that TXAS facilitates robust biophysical studies in nanodiscs as compared to naked protein in detergent solution (248).

The anhydrides and their parent molecules were subjected to the coupled activity assay in a 1:1 ratio with the substrate molecule AA. As observed in Figure A.9A, the EPA and DHA anhydrides were potent in inhibiting the thromboxane formed in a coupled assay system to a similar extent. The perceived reduction in TXA2 formation in both cases was about 30-35% of the control. However, the LA anhydride did not show any significant decrease in the formation of thromboxane. These observations are in agreement with the results obtained in the aggregometry studies that LA did not reduce platelet aggregation in washed platelets (Figure A.1).

Furthermore, the parent molecules- LA, EPA and DHA, by themselves did not show any decrease in TXA2 formation (Figure A.8B). It is hypothesized that LA, EPA, and DHA compete with AA for metabolism by COX-1 and thereby reduce the ability of AA to be converted to TXA2, inducing aggregation. EPA is metabolized to PGH3 and subsequently TXA3 (249). However, our results indicate that the rate of metabolism of any of these fatty acids is not sufficient to result in competitive inhibition of AA metabolism by COX-1-CYP5A1. Therefore, it is evident that the effect of dietary unsaturated fatty acids on the COX pathway of platelet aggregation is not significant.

Direct inhibition of COX-1-thromboxane synthase activity by lipid-aspirin conjugates: Observations in the coupled assay indicated that the EPA and DHA anhydride conjugates reduce platelet aggregation by inhibiting the COX-1 -TXAS pathway. Since both aspirin and PUFAs are thought to affect COX-1 directly, we wanted to test the effects of these anhydrides on COX-1 activity. COX-1 converts AA into PGH2, which as previously stated is highly unstable and

decomposes to PGF2α. Thus a second reaction converting PGH2 into PGF2α, via action of tin (II) chloride was performed to completely convert it to PGF2α, a more stable species, and was subsequently measured by ELISA to determine the inhibition of COX activity by reduction in product formation. The inhibition of product formation by COX was measured at concentrations from 0-50 μM and the product formation relative to a no inhibitor control was fitted using non-linear regression analysis. As seen in Figure A.9B, all three anhydrides show a dose-dependent decrease in PGF2α formation, showing less than 10% product formation, as compared to the absence of inhibitor at 50 μM. However, the trend in decline of product formation varied for the three derivatives. While for the LA anhydride the decrease in product formation was gradual, it was more dramatic initially for the EPA ad DHA anhydrides. The EPA anhydride shows an initial decline to 50% activity at 2.5 μM and then gradually declines to >10% at 25 μM concentration. The DHA anhydride shows an initial drop to less than 40% of total activity at 2.5μM and then slowly declines to ~10% at 25 μM. Interestingly, both EPA and DHA anhydrides show similar effects above 10 μM concentrations. The IC50 values for the compounds were calculated to be 7.5 μM, 5.8 μM and 2.1 μM respectively for the LA anhydride, EPA anhydride and DHA anhydride.

Direct buffer hydrolysis of the lipid-aspirin conjugates: To test the lability of the anhydrides in buffer, the rate of hydrolysis was measured by analyzing the remaining anhydride in PBS at 37°C at different time intervals. In all three cases, HPLC analysis of the aliquot indicated the presence of the original parent compound, aspirin and the corresponding fatty acid, indicating the release of the aspirin active moiety and not of salicylic acid. As observed in Figure A.10A, all three compounds show pseudo-first order kinetics of decomposition. The LA-aspirin anhydride shows a gradual decomposition over 30 mins, leading to decomposition of about 60% of the drug species into its individual components. In contrast, the EPA-aspirin anhydride shows a sharp decomposition in the first 5 mins and plateaus around 60% decomposition after the initial hydrolysis. This provides an explanation to the significant differences in the activities of EPA and LA anhydrides in the COX activity assay as well as the COX-thromboxane synthase coupled activity assays that are carried out over shorter incubation times. The LA anhydride being liberated more slowly has a lesser effect on the inhibition of COX-1 than the EPA anhydride, which releases the active species much faster. The DHA anhydride shows hydrolysis trends similar to LA anhydride whereby it is more gradual over the initial 5 mins and plateaus to about 55% at 60 mins.

Plasma hydrolysis studies: To investigate the release of aspirin from the aspirin-fatty acid mixed anhydride in plasma, plasma buffered with phosphate buffer (pH=7.4) was equilibrated at 37°C and the anhydride was added. At various time points aliquots were withdrawn and the extracted products were analyzed by HPLC. Figure A.10B represents the plasma hydrolysis patterns of all three anhydrides. Similar to the buffer hydrolysis, pseudo-first order kinetics can be observed in all three cases. All three compounds show a gradual decomposition over 2 hours plateauing to about 35- 40% decomposition. Note that the plasma hydrolysis of DHA is at a comparable range as EPA.

A.5 DISCUSSION

Platelet aggregation is triggered by a number of primary activators leading to positive feedback and potentiation of the activation signal. The Cyclooxygenase-1 (COX-1)-thromboxane synthase (TXAS) pathway is a well-established positive feedback signal in the platelet. In this pathway, arachidonic acid (AA) is metabolized by COX-1 to prostaglandin H2 (PGH2) followed by conversion of PGH2 to thromboxane A2 (TXA2), which is a pro-aggregatory molecule (250). Activation of the platelet either through primary activation or feedback activation via COX-1 leads to activation of the integrin GPIIb/IIIa resulting in platelet clot formation. The inhibition of platelet aggregation both ex vivo and in vivo can be aided by molecules inhibiting the COX-1-dependent feedback pathway as well as by directly blocking GPIIb/IIIa integrins (245) .

Aspirin is the most popular NSAID for reducing pain, fever and inhibition of platelet function. The free carboxylate group in aspirin stays as an ionized species at physiological pH, which is poorly absorbed across lipid bilayers. Hence, the derivatization of the free carboxylic acid, to form more lipophilic species can facilitate transport across bio-membranes. Herein, we have derivatized the carboxylate end of aspirin through anhydride formation with dietary fatty acids including EPA and DHA (omega-3 fatty acids) as well as LA (omega-6 fatty acid) that have been shown to reduce platelet aggregation through dietary supplementation in platelet aggregometry studies. As compared to esters, anhydrides show more controlled patterns of hydrolysis and decomposition that are not enzyme dependent. Therefore we report the design of aspirin-poly unsaturated fatty acid mixed anhydrides that would exist in a unionized, lipophilic state as well as allow for a facile, more controlled release of the active species in plasma. Additionally, recent studies on polyanhydrides as drug carriers show that anhydrides degrade in a controlled fashion and are

biocompatible with human body tissues, including the brain (251). One of the rationale for the design of the hybrid co-drug is that the aspirin-fatty acid-anhydride pro-drug would hydrolyze to release not one but two active species, which could both inhibit the enzyme.

The synthesis of the mixed anhydrides were tested in platelet aggregometry studies to analyze their anti-aggregatory effects. All three compounds displayed a concentration dependent decrease in platelet aggregation. However, the DHA anhydride was most potent, almost completely inhibiting aggregation at 10 μM concentration, followed by EPA anhydride and, finally, LA anhydride, which showed marginal decrease in the inhibition of aggregation. As expected from the mechanism of inhibition of platelet aggregation studies, the decrease was only observed in AA-induced platelet aggregation and not observed for ADP, collagen, U46619 or thrombin, indicating that these molecules did not affect those pathways for platelet aggregation. Furthermore, comparing the inhibition of the DHA anhydride with aspirin-treated species showed comparable inhibition potentials.

To understand the biochemical mechanism of action of these molecules, an activity assay was performed on the COX-1 -thromboxane synthase system. It was observed that while the reduction in TXA2 for EPA and DHA anhydride was significant, LA anhydride did not show significant reduction, thereby following the similar trend of the platelet aggregometry studies. More interestingly, however, the parent fatty acids showed no inhibition in thromboxane formation (Figure A.8). Thus, it appears that while LA, EPA, and DHA may be able to compete for metabolism against AA, this is likely not the chief mechanism of their action to prevent platelet aggregation. Literature reports have suggested that omega-3 fatty acids reduce platelet aggregation by signaling through other pathways (252). Furthermore, a meta- analysis of the effect of omega-3 fatty acids on the inhibition of platelet aggregation suggests that the effect is sufficiently short-term to hinder significant changes in plasma lipid or lipoprotein composition (253, 254). Additionally it is possible that this inhibition is mediated through collagen induced pathways (255).

Next, we determined the effect of the compounds on COX-1 activity and derived IC50 values for the anhydrides. The values for the LA, EPA, and DHA anhydrides were obtained to be 7.1, 5.8 and 2.1 μM respectively. Literature reports suggest that the IC50 values of COX-1 inhibition for linolenic acid, EPA, and DHA are 93 μM, 13 μM and 15 μM, respectively. Furthermore, the IC50

value of aspirin on COX-1 in purified enzyme system is 8 μM (256). The culmination of these results suggests a greater effect of the mixed anhydrides in comparison to their parent molecules.

Finally, the molecules were characterized by their hydrolytic decomposition patterns as it is the key step in releasing both the species. It was observed that the only species resulting from the hydrolysis of the fatty acid- aspirin anhydride were aspirin and the corresponding fatty acid. This is important since in several aspirin formulations it has been observed that the O-acetyl group of aspirin hydrolyzes before the aspirin moiety is released from the pro-drug thereby only being as effective as salicylic acid and not aspirin. Furthermore, we observed that all three molecules show pseudo-first order decomposition kinetics in both buffer and plasma. Additionally, the extents of hydrolysis in buffer and plasma were comparable, indicating that enzyme hydrolysis is not a significant pathway for the release of aspirin. It appears that EPA hydrolyzes faster than DHA, which hydrolyzes more rapidly than LA. This can be partly explained by the hydrophobicity of the species attached to the aspirin moiety. It is known that LA > DHA > EPA in terms of hydrophobicity. In general, the more hydrophobic a species, the slower the rate of hydrolysis. This observation can be further extended to control the rate of hydrolyses of these species by carefully tuning the anhydride partner.

A.6 CONCLUSION

We have synthesized anhydrides of aspirin and dietary fatty acids to explore a “hybrid- drug” approach. Both aspirin and the fatty acids in this study are inhibitors of platelet aggregation and this conjugation addresses the side effects of aspirin in addition to the synergism between the two species. We observed that all three compounds individually inhibit platelet aggregation in a dose-dependent manner in the effectiveness order of C3, C2 then C1. Additionally, we show that C3 is comparable to aspirin-treated samples. Furthermore, we show that while all three molecules act through the COX-thromboxane synthase pathway by inhibiting COX-1, the parent fatty acids do not act via that pathway. Finally, hydrolysis studies of the drugs in buffer as well as plasma conditions confirm the release of aspirin and fatty acid separately, instead of the salicylate moiety as is the case with several aspirin pro-drugs.

A.7 ACKNOWLEDGEMENT

We acknowledge Ms. Susan Zelasko for initial literature review, Mr. Daniel McDougle and Ms. Navroop Gill for providing helpful comments on the manuscript. This work was supported by

American Heart Association (AHA) Scientist Development grant[15SDG25760064], GM105671 and HL114405. We thank Graduate College Travel Award and Department of Chemistry Graduate Fellowship (JR). Authorship contributions: JR and AD conceived the project. JR performed the synthesis, NMR characterization, coupled and direct assays and hydrolysis studies. JR and AD analyzed corresponding data. RA performed the platelet aggregometry experiments. RA and MH analyzed corresponding data. RK contributed COX-1. JR, RA, MH and AD wrote the paper.

A.8 FIGURES, TABLES AND LEGENDS

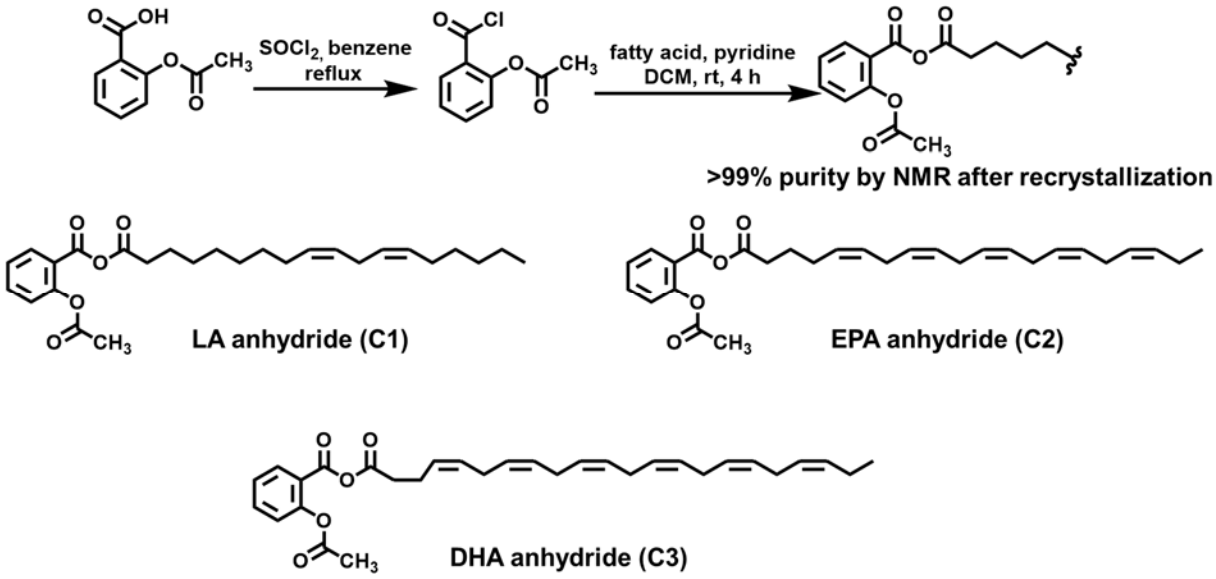

Scheme A.1: Synthesis of anhydrides. Aspirin (acetylsalicylic acid) is first converted to the activated acyl chloride by refluxing with thionyl chloride ($SOCl_2$) in benzene. This further reacts with the carboxylate on dietary fatty acids in the presence of pyridine in DCM to give LA anhydride (C1) EPA anhydride (C2) and DHA anhydride (C3).

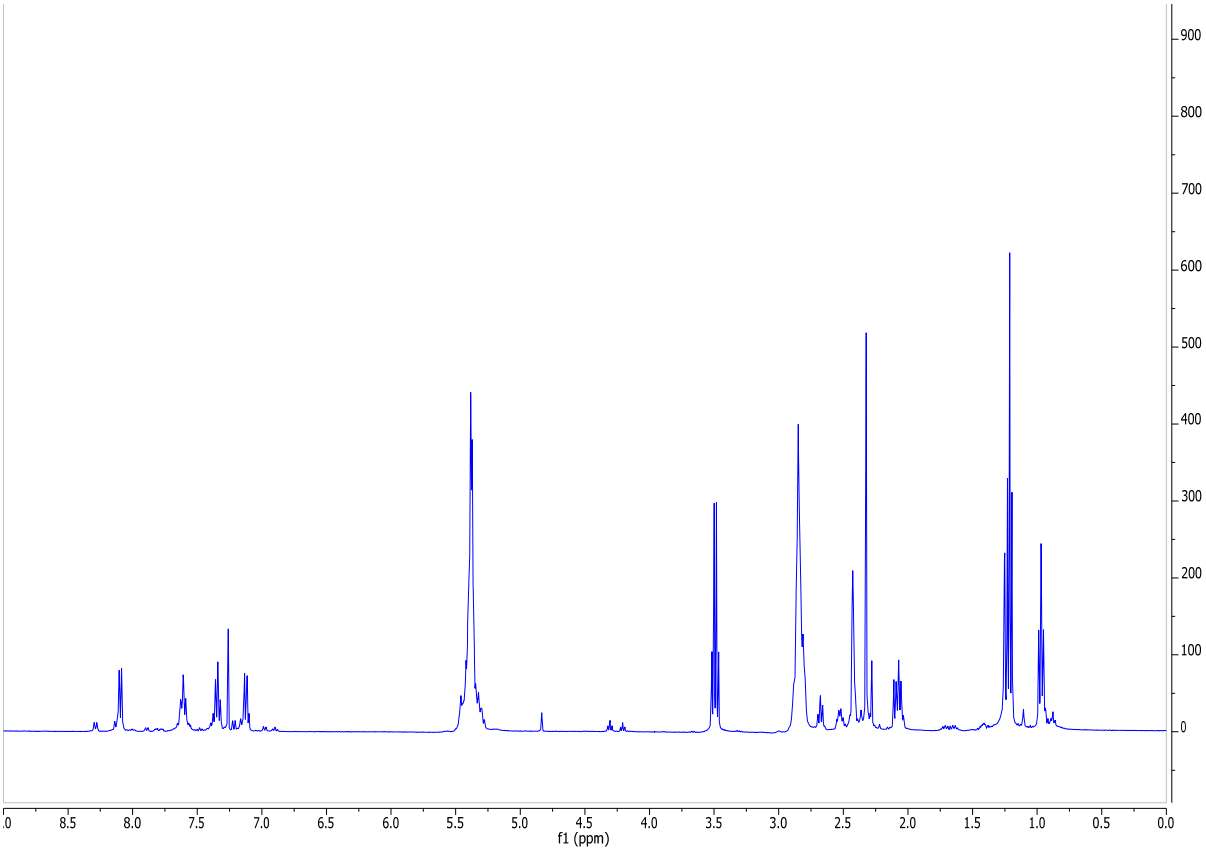

Figure A.1: ^{1}H NMR of DHA- aspirin anhydride in $CDCl_3$

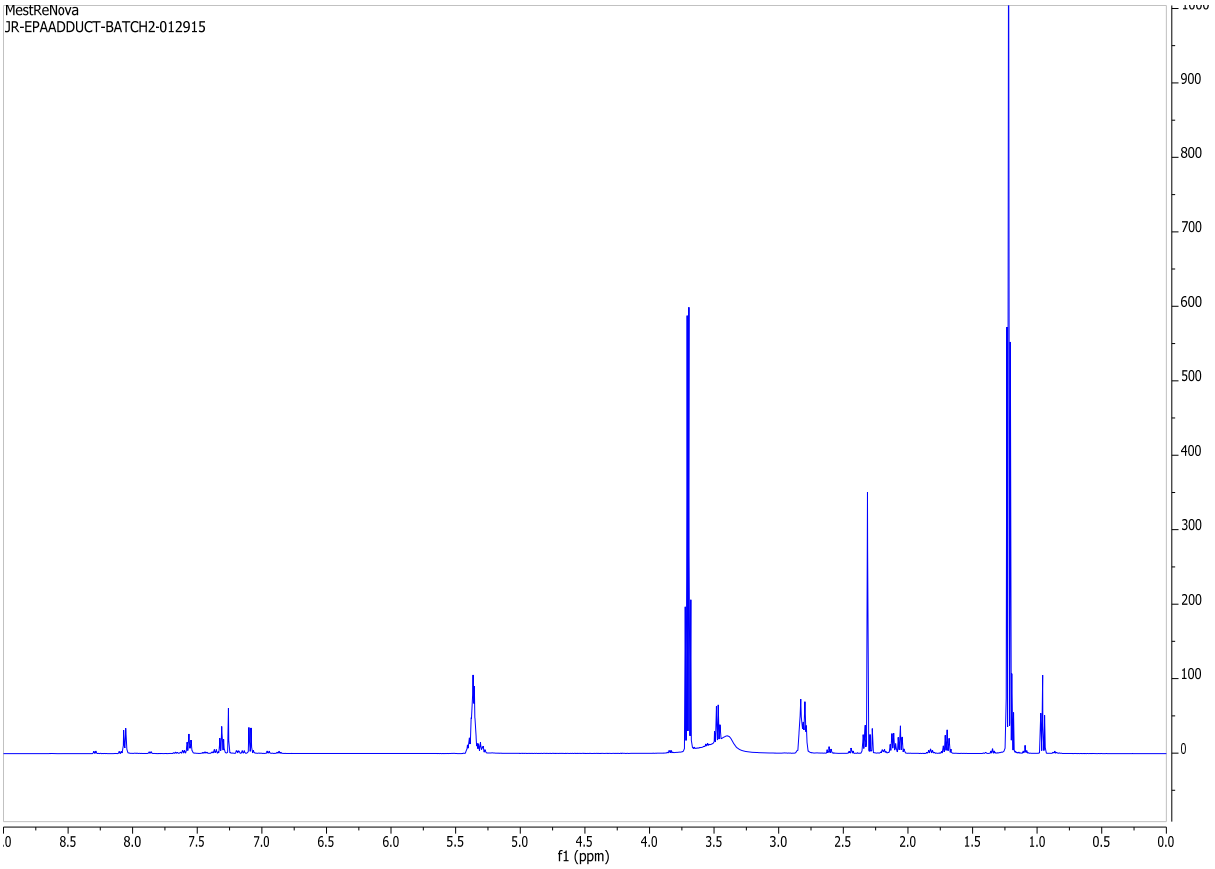

Figure A.2: ^{1}H NMR of EPA- aspirin anhydride in $CDCl_3$

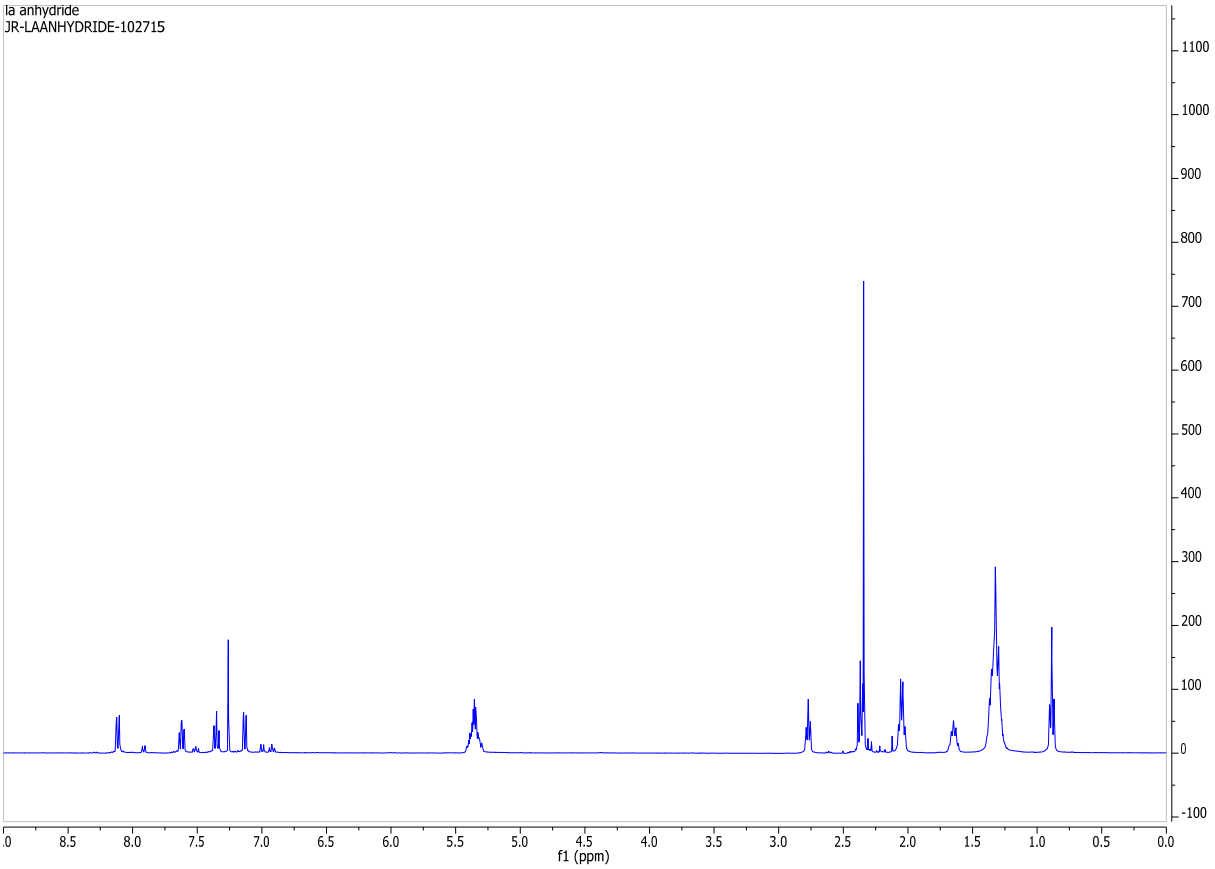

Figure A.3: ^{1}H NMR of LA- aspirin anhydride in $CDCl_3$

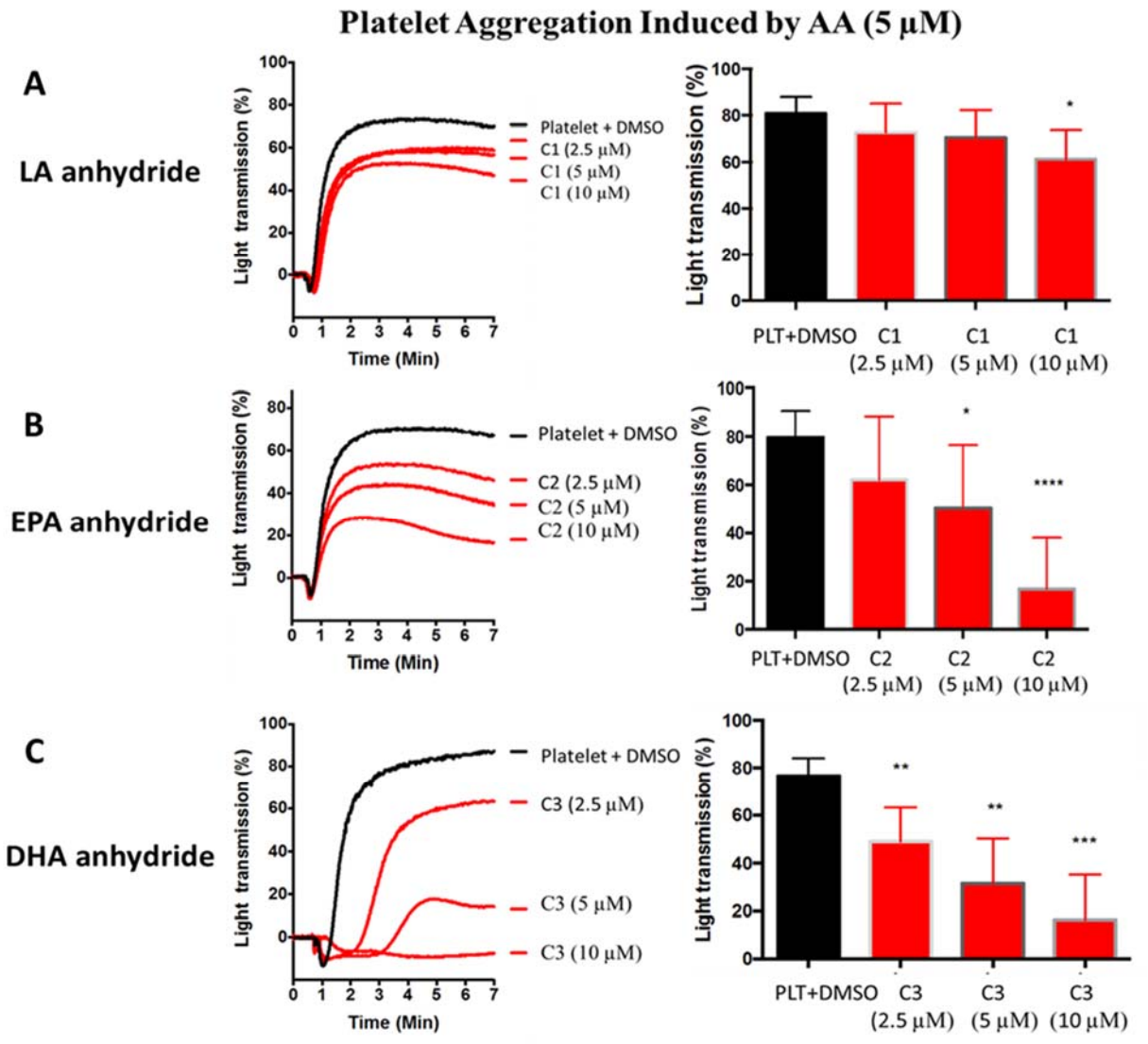

Figure A.4: Effect of anhydrides on platelet aggregation in washed platelets by arachidonic acid. The plots show the transmission of light versus time for various concentrations (2.5 µM, 5 µM and 10 µM) of (A) LA anhydride (C1) (B) EPA anhydride (C2) and (C) DHA anhydride (C3), and DMSO control. The reduction of light transmission indicates the inhibition of aggregation. All compounds show a concentration dependent decrease in aggregation in the order of effectivity LA anhydride<EPA anhydride<DHA anhydride. The results show data from n=5. (* p< 0.05, ** p < 0.01, *** p < 0.001, **** p <0.0001)

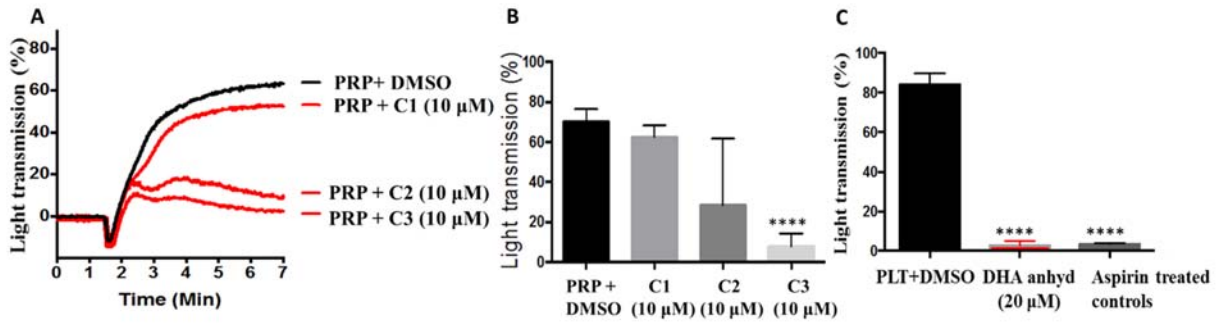

Figure A.5: (A) Effect of 10 µM anhydrides on platelet aggregation as indicated by light transmission in platelet rich plasma by 5 µM arachidonic acid. (B) All compounds show a concentration dependent decrease in aggregation in the order of effectivity LA anhydride (C1) < EPA anhydride (C2) < DHA anhydride (C3). The results show data from n=5. (C) Comparison of the inhibitory effect of C3 compound with Aspirin. 20 µM C3 compound completely inhibited the washed human platelet aggregation similar to Aspirin treated (81mg/day X 7days) tested by 5 µM AA.

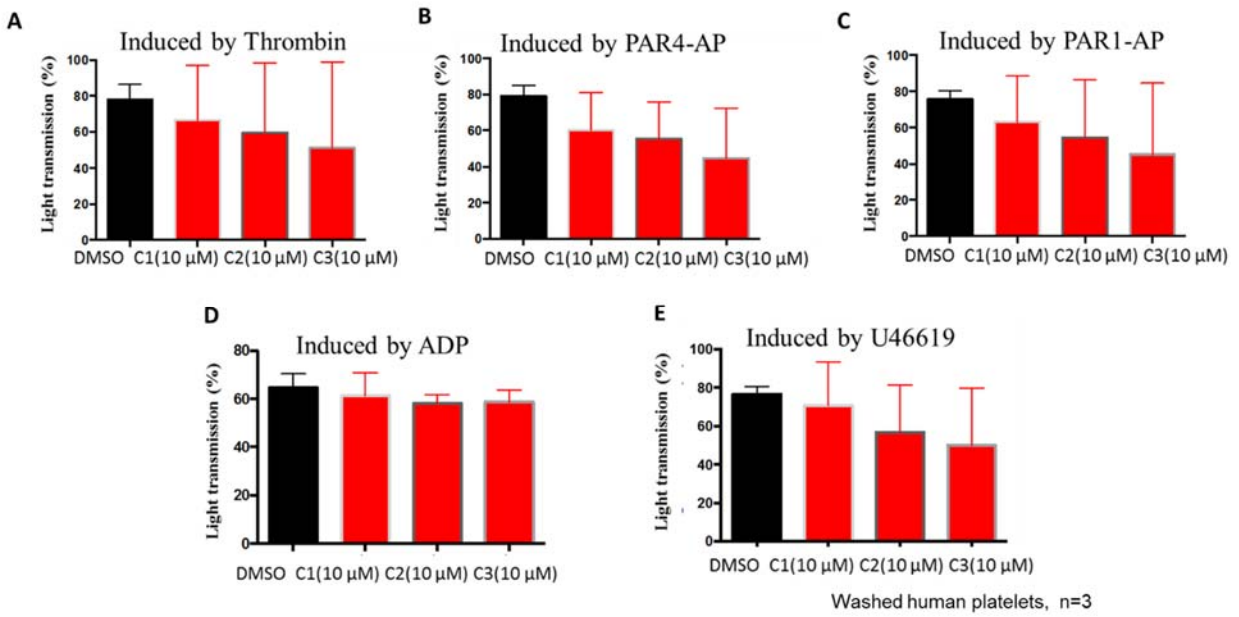

Figure A.6: Inhibition of platelet aggregation in washed platelets by anhydrides (10 uM) in the presence of (A) 1nM Thrombin (B) 50 µM PAR4-AP (C) 1 µM PAR1- AP (D) 1 µM ADP (E) 1 µM U46619 (thromboxane analog). Results show no significant decrease in platelet aggregation using alternate agonists. The results show data from n=3.

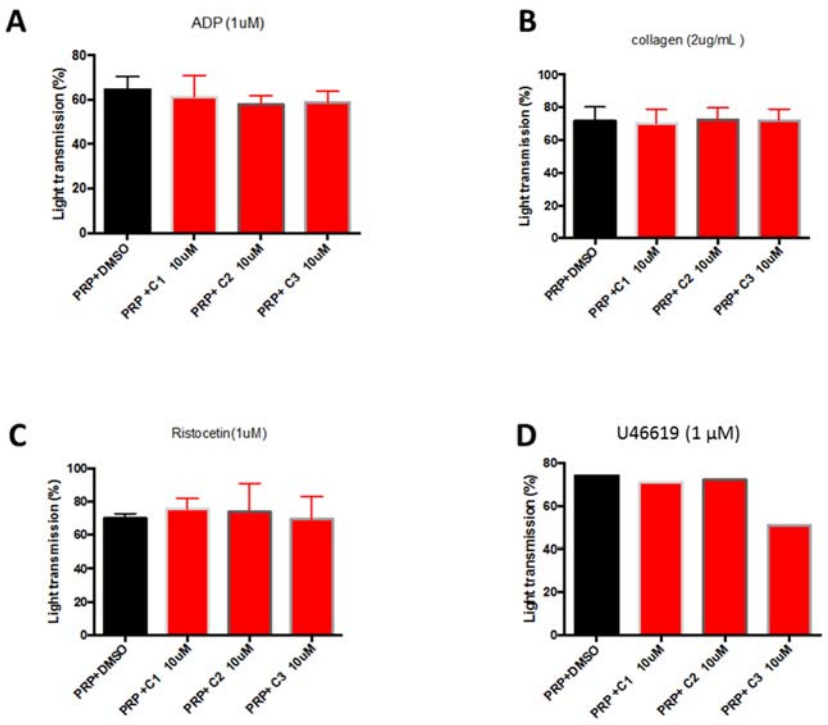

Figure A.7: Inhibition of platelet aggregation in platelet rich plasma by anhydrides (10 uM) in the presence of (A) 1 uM ADP (B) 2 µg/mL Collagen (C) 1 µM ristocetin (D) 1 µM U46619 (thromboxane analog). Results show no significant decrease in platelet aggregation using alternate agonists. Results show no significant decrease in platelet aggregation. The results show data from n=3 for ADP, collagen and ristocetin and n=2 for U46619.

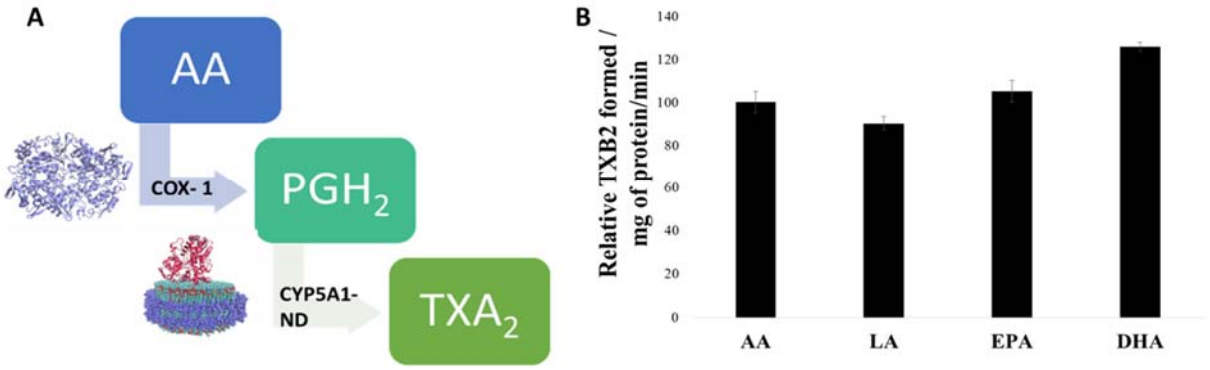

Figure A.8: (A) Schematic of coupled assay. Arachidonic acid (AA) converts to Prostaglandin H_2 (PGH_2) in the presence of enzyme COX-1 (cyclooxygenase-1). PGH_2 converts to Thromboxane A_2 (TXA_2) in the presence of TXAS (thromboxane synthase) that is stabilized in nanodiscs. (B) Thromboxane formed in the presence of LA, EPA and DHA in a coupled assay and AA control with no inhibitor. Results show that while no significant reduction in thromboxane formation is observed in the presence of any of the dietary unsaturated fatty acids LA, EPA or DHA.

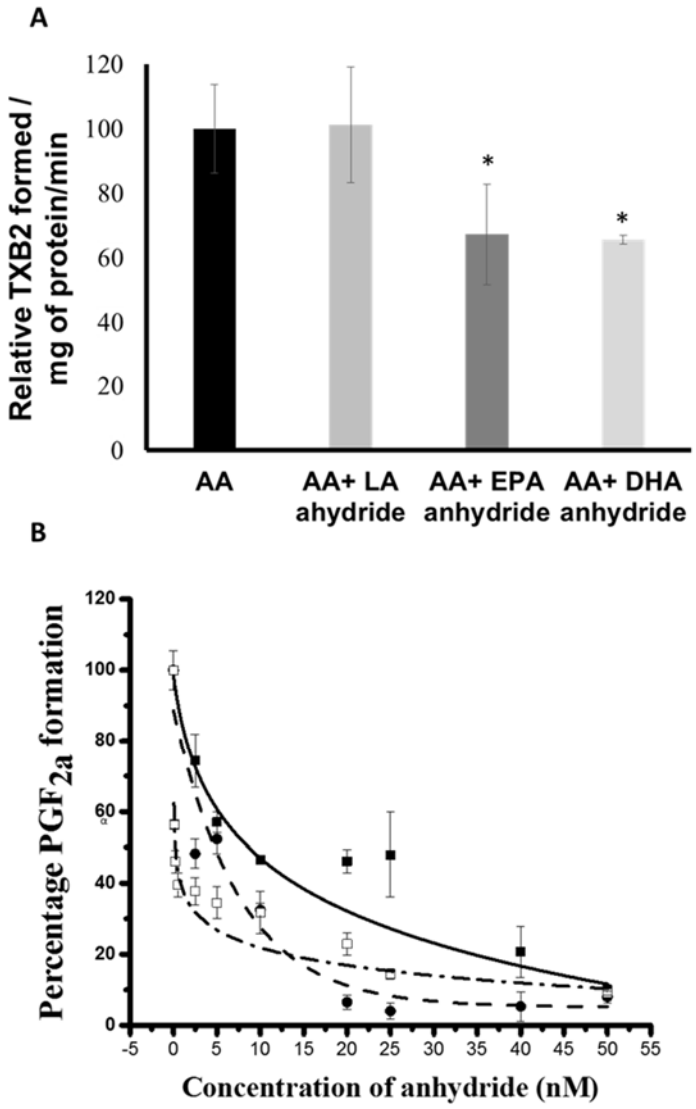

Figure A.9: (A) Thromboxane formed in the presence of LA anhydride, EPA anhydride and DHA anhydride in a coupled assay and AA control with no inhibitor. Results show that while no significant reduction in thromboxane formation is observed in the presence of LA anhydride, significant thromboxane reduction is seen in the presence of EPA anhydride and DHA anhydride. (B) Effect of LA anhydride (solid square, solid line), EPA anhydride (solid circle, dashed line) and DHA anhydride (open square, dashed and dotted line) on COX activity from 0- 50μM. All anhydrides show a concentration dependent inhibition of COX-1. (* $p < 0.05$)

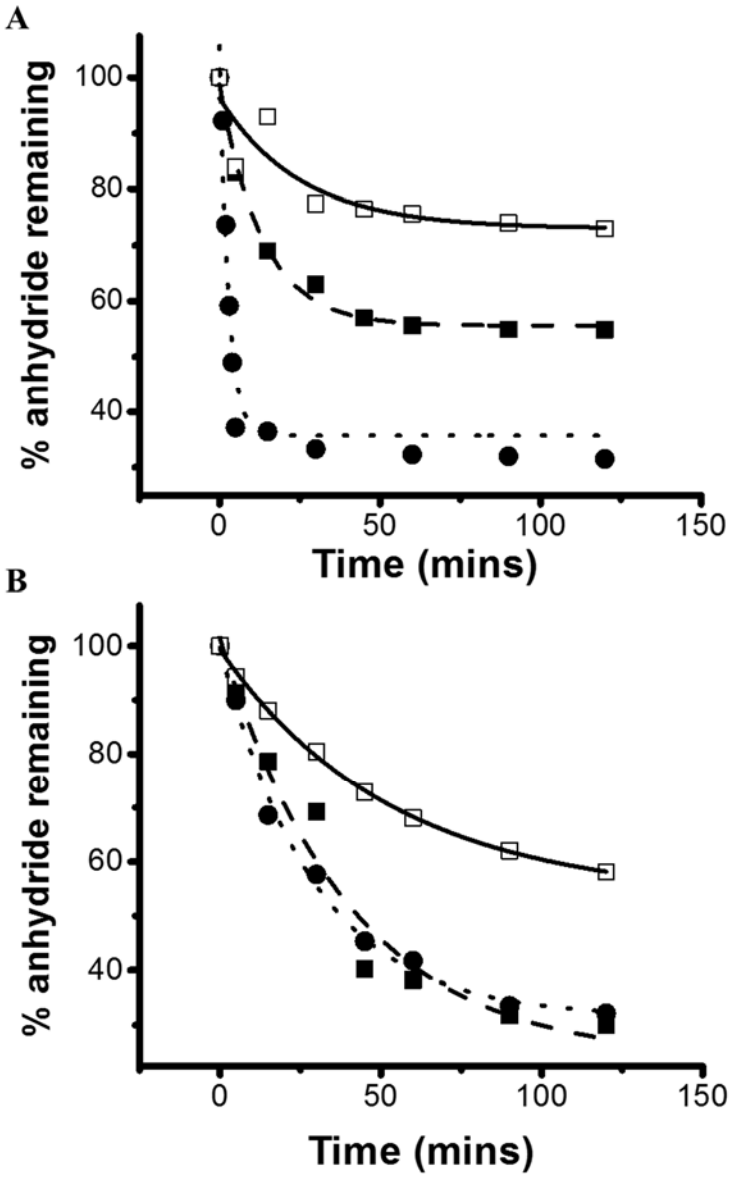

Figure A.10: (A) Buffer hydrolysis of anhydrides. (B) Plasma hydrolysis of anhydrides: DHA anhydride (dashed line, solid squares), EPA anhydride (dotted line, solid circle) and LA anhydride (solid line, open square). The extent of hydrolysis is in the order EPA anhydride > DHA anhydride > LA anhydride. All compounds achieve a plateau after an hour of hydrolysis.

A.9 REFERENCES

1. Gilmer JF, Moriarty LM, Lally MN, Clancy JM. Isosorbide-based aspirin prodrugs. II. Hydrolysis kinetics of isosorbide diaspirinate. Eur J Pharm Sci. 2002;16(4-5):297-304. Epub 2002/09/05. doi: S0928098702001240 [pii]. PubMed PMID: 12208460.
2. Bradley MO, Swindell CS, Anthony FH, Witman PA, Devanesan P, Webb NL, Baker SD, Wolff AC, Donehower RC. Tumor targeting by conjugation of DHA to paclitaxel. J Control Release. 2001;74(1-3):233-6. Epub 2001/08/08. doi: S0168365901003212 [pii]. PubMed PMID: 11489499.
3. Sparatore A, Santus G, Giustarini D, Rossi R, Del Soldato P. Therapeutic potential of new hydrogen sulfide-releasing hybrids. Expert Rev Clin Pharmacol. 2011;4(1):109-21. Epub 2011/11/26. doi: 10.1586/ecp.10.122. PubMed PMID: 22115352.
4. Phang M, Lincz LF, Garg ML. Eicosapentaenoic and docosahexaenoic acid supplementations reduce platelet aggregation and hemostatic markers differentially in men and women. J Nutr. 2013;143(4):457-63. Epub 2013/02/08. doi: 10.3945/jn.112.171249
jn.112.171249 [pii]. PubMed PMID: 23390192.
5. Mizrahi B, Domb AJ. Anhydride prodrug of ibuprofen and acrylic polymers. AAPS PharmSciTech. 2009;10(2):453-8. Epub 2009/04/22. doi: 10.1208/s12249-009-9228-z. PubMed PMID: 19381828; PubMed Central PMCID: PMC2690791.
6. Kumar N, Langer RS, Domb AJ. Polyanhydrides: an overview. Adv Drug Deliv Rev. 2002;54(7):889-910. Epub 2002/10/18. doi: S0169409X02000509 [pii]. PubMed PMID: 12384314.
7. Abdellatif KR, Chowdhury MA, Dong Y, Das D, Yu G, Velazquez CA, Suresh MR, Knaus EE. Dinitroglyceryl and diazen-1-ium-1,2-diolated nitric oxide donor ester prodrugs of aspirin, indomethacin and ibuprofen: synthesis, biological evaluation and nitric oxide release studies. Bioorg Med Chem Lett. 2009;19(11):3014-8. Epub 2009/05/08. doi: 10.1016/j.bmcl.2009.04.059
S0960-894X(09)00515-0 [pii]. PubMed PMID: 19419861.
8. Yeung J, Holinstat M. Newer agents in antiplatelet therapy: a review. J Blood Med. 2012;3:33-42. Epub 2012/07/14. doi: 10.2147/JBM.S25421
jbm-3-033 [pii]. PubMed PMID: 22792011; PubMed Central PMCID: PMC3393068.
9. Das A, Varma SS, Mularczyk C, Meling DD. Functional investigations of thromboxane synthase (CYP5A1) in lipid bilayers of nanodiscs. Chembiochem. 2014;15(6):892-9. Epub 2014/03/14. doi: 10.1002/cbic.201300646. PubMed PMID: 24623680.
10. Joseph RE, Andreotti AH. Bacterial expression and purification of interleukin-2 tyrosine kinase: single step separation of the chaperonin impurity. Protein Expr Purif. 2008;60(2):194-7. Epub 2008/05/23. doi: 10.1016/j.pep.2008.04.001
S1046-5928(08)00099-5 [pii]. PubMed PMID: 18495488; PubMed Central PMCID: PMC2581883.
11. Bayburt TH, Grinkova YV, Sligar SG. Self-assembly of discoidal phospholipid bilayer nanoparticles with membrane scaffold proteins. Nano Letters. 2002;2(8):853-6. doi: Doi 10.1021/Nl025623k. PubMed PMID: ISI:000177485500013.
12. Diczfalusy U, Falardeau P, Hammarstrom S. Conversion of prostaglandin endoperoxides to C17-hydroxy acids catalyzed by human platelet thromboxane synthase. FEBS Lett. 1977;84(2):271-4. Epub 1977/12/15. doi: 0014-5793(77)80704-7 [pii]. PubMed PMID: 598509.
13. Das A, Varma SS, Mularczyk C, Meling DD. Functional Investigations of Thromboxane Synthase (CYP5A1) in Lipid Bilayers of Nanodiscs. Chembiochem. 2014;15(6):892-9. doi: 10.1002/cbic.201300646. PubMed PMID: ISI:000333966100018.
14. Fischer S, Weber PC. Thromboxane A3 (TXA3) is formed in human platelets after dietary eicosapentaenoic acid (C20:5 omega 3). Biochem Biophys Res Commun. 1983;116(3):1091-9. Epub 1983/11/15. doi: S0006-291X(83)80254-X [pii]. PubMed PMID: 6316965.
15. Paul BZ, Jin J, Kunapuli SP. Molecular mechanism of thromboxane A(2)-induced platelet aggregation. Essential role for p2t(ac) and alpha(2a) receptors. J Biol Chem. 1999;274(41):29108-14. Epub 1999/10/03. PubMed PMID: 10506165.

16. Domb AJ, Israel ZH, Elmalak O, Teomim D, Bentolila A. Preparation and characterization of carmustine loaded polyanhydride wafers for treating brain tumors. Pharm Res. 1999;16(5):762-5. Epub 1999/06/01. PubMed PMID: 10350022.
17. Abeywardena MY, Head RJ. Longchain n-3 polyunsaturated fatty acids and blood vessel function. Cardiovasc Res. 2001;52(3):361-71. Epub 2001/12/12. doi: S0008636301004060 [pii]. PubMed PMID: 11738053.
18. Driss F, Vericel E, Lagarde M, Dechavanne M, Darcet P. Inhibition of platelet aggregation and thromboxane synthesis after intake of small amount of icosapentaenoic acid. Thromb Res. 1984;36(5):389-96. Epub 1984/12/01. doi: 0049-3848(84)90295-0 [pii]. PubMed PMID: 6098051.
19. Gao LG, Cao J, Mao QX, Lu XC, Zhou XL, Fan L. Influence of omega-3 polyunsaturated fatty acid-supplementation on platelet aggregation in humans: a meta-analysis of randomized controlled trials. Atherosclerosis. 2013;226(2):328-34. Epub 2012/11/17. doi: 10.1016/j.atherosclerosis.2012.10.056 S0021-9150(12)00742-3 [pii]. PubMed PMID: 23153623.
20. Tremoli E, Maderna P, Marangoni F, Colli S, Eligini S, Catalano I, Angeli MT, Pazzucconi F, Gianfranceschi G, Davi G, et al. Prolonged inhibition of platelet aggregation after n-3 fatty acid ethyl ester ingestion by healthy volunteers. Am J Clin Nutr. 1995;61(3):607-13. Epub 1995/03/01. PubMed PMID: 7872228.
21. Mitchell JA, Akarasereenont P, Thiemermann C, Flower RJ, Vane JR. Selectivity of nonsteroidal antiinflammatory drugs as inhibitors of constitutive and inducible cyclooxygenase. Proc Natl Acad Sci U S A. 1993;90(24):11693-7. Epub 1993/12/15. PubMed PMID: 8265610; PubMed Central PMCID: PMC48050.

APPENDIX B: TABLES OF PROTEINS IDENTIFIED BY PEPTIDE FINGERPRINTING OF HOS, 143B, POS AND HMPOS CELL LINES

Parameters for Proteomics Classifications

Taxonomy	Homo sapiens (human) (287,757 sequences)
Type of search	MS/MS Ion Search
Enzyme	Trypsin
Variable modifications	Oxidation (M)
Mass values	Monoisotopic
Protein mass	Unrestricted
Peptide mass tolerance	0.3 Da
Fragment mass tolerance	0.3 Da
Max missed cleavages	3
Instrument type	ESI-TRAP
Number of queries	8,371
Significance threshold p<	0.05
Max. number of families	AUTO

Ions score or expect cut-off	0

emPAI or exponentially modified protein abundance index is a parameter indicating relative abundance of proteins in the mixture

ST1: Proteomics data of plasma membrane protein from HOS

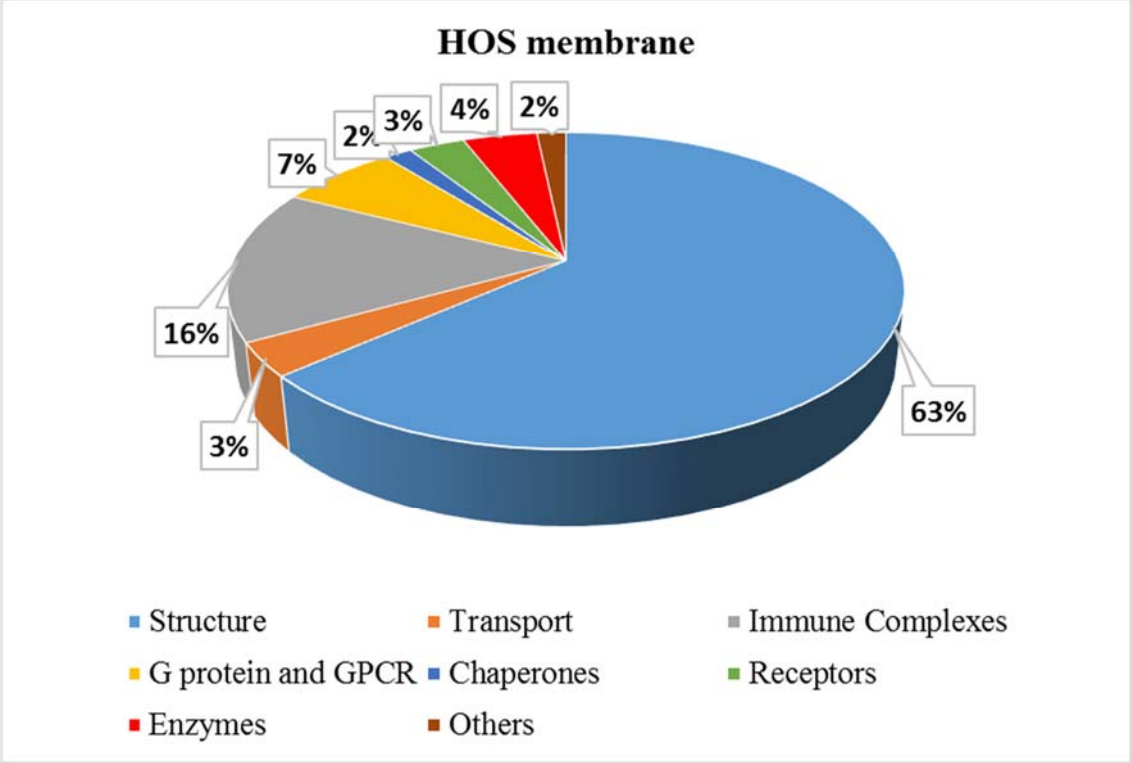

ST1-1. Overall proteomic profile

	emPAI	Percentage
Structure	67.86	63.48
Transport	3.65	3.41

Immune Complexes	16.77	15.69
G protein and GPCR	7.21	6.74
Chaperones	1.71	1.60
Receptors	3.41	3.19
Enzymes	4.52	4.23
Others	1.77	1.66
Total	106.9	100

ST1-2: Structural Proteins Identified

Accession	Mass	emPAI	Description
gi|11935049	66027	2.07	keratin 1 [Homo sapiens]
gi|119617057	57772	0.83	keratin 8, isoform CRA_a [Homo sapiens]
gi|119617032	59874	0.44	keratin 6B, isoform CRA_a [Homo sapiens]
gi|119395754	62340	0.32	keratin, type II cytoskeletal 5 [Homo sapiens]
gi|119581148	57526	1.3	keratin 9 (epidermolytic palmoplantar keratoderma) [Homo sapiens]
gi|12653819	48003	1.26	Keratin 18 [Homo sapiens]
gi|1195531	51206	0.4	type I keratin 16 [Homo sapiens]
gi|181402	65825	0.7	epidermal cytokeratin 2 [Homo sapiens]

gi|7106439	49639	1.2	tubulin beta-5 chain [Mus musculus]
gi|119608775	48794	1.04	tubulin, beta 2C, isoform CRA_b [Homo sapiens]
gi|340021	50120	0.68	alpha-tubulin [Homo sapiens]
gi|62421087	11517	0.44	actin-like protein [Homo sapiens]
gi|4501885	41710	9.89	actin, cytoplasmic 1 [Homo sapiens]
gi|63055057	41976	1.53	beta-actin-like protein 2 [Homo sapiens]
gi|24119203	29015	0.56	tropomyosin alpha-3 chain isoform 2 [Homo sapiens]
gi|17986258	16919	1.13	myosin light polypeptide 6 isoform 1 [Homo sapiens]
gi|5031573	47341	0.2	actin-related protein 3 isoform 1 [Homo sapiens]
gi|2605594	19694	0.55	myosin regulatory light chain [Homo sapiens]
gi|5031595	19654	0.55	actin-related protein 2/3 complex subunit 4 isoform a [Homo sapiens]
gi|4826659	30609	0.15	F-actin-capping protein subunit beta isoform 1 [Homo sapiens]
gi|530417302	104260	0.23	PREDICTED: alpha-actinin-4 isoform X1 [Homo sapiens]
gi|194097350	105502	0.23	alpha-actinin-1 isoform a [Homo sapiens]
gi|167887751	49623	6.48	vimentin variant 3 [Homo sapiens]
gi|12667788	226392	0.02	myosin-9 [Homo sapiens]
gi|4757756	38580	19.39	annexin A2 isoform 2 [Homo sapiens]

gi|157833780	35984	3.78	Chain A, Human Annexin V With Proline Substitution By Thioproline
gi|71773329	75826	0.99	annexin A6 isoform 1 [Homo sapiens]
gi|119582952	40057	0.72	annexin A1, isoform CRA_c [Homo sapiens]
gi|53791219	277332	0.21	filamin A [Homo sapiens]
gi|105990514	277990	0.07	filamin-B isoform 2 [Homo sapiens]
gi|34234	31774	0.5	laminin-binding protein, partial [Homo sapiens]
gi|187609338	20107	1.34	Chain A, Crystal Structure Of The Extracellular Portion Of Hab18gCD147
gi|119625804	66564	0.92	moesin, isoform CRA_b [Homo sapiens]
gi|16974825	8483	0.63	Chain A, Solution Structure Of Calcium-calmodulin N-terminal Domain
gi|7656991	53215	0.18	coronin-1C isoform b [Homo sapiens]
gi|19920317	65983	0.3	cytoskeleton-associated protein 4 [Homo sapiens]
gi|4826898	15045	1.32	profilin-1 [Homo sapiens]
gi|3212355	11064	3.53	Chain A, P11 (s100a10), Ligand Of Annexin Ii
gi|641958	228798	0.02	non-muscle myosin B [Homo sapiens]
gi|15778914	42189	0.11	Parvin, alpha [Homo sapiens]
gi|5031601	40923	0.11	actin-related protein 2/3 complex subunit 1B [Homo sapiens]

gi|3676059	231477	0.02	envoplakin [Homo sapiens]
gi|578798330	64316	0.07	PREDICTED: afadin- and alpha-actinin-binding protein isoform X6 [Homo sapiens]
gi|44889481	124872	0.04	unconventional myosin-Ib isoform 2 [Homo sapiens]
gi|1846005	332987	0.01	collagen type XII alpha-1 [Homo sapiens]
gi|119585235	84713	0.05	SWI/SNF related, matrix associated, actin dependent regulator of chromatin, subfamily c, member 1, isoform CRA_a [Homo sapiens]
gi|4235275	269661	0.02	talin [Homo sapiens]
gi|306896	57790	0.08	intercellular adhesion molecule-1 precursor [Homo sapiens]
gi|119584665	9744	0.53	ankyrin repeat domain 28, isoform CRA_d [Homo sapiens]
gi|119587605	119373	0.04	neural cell adhesion molecule 1, isoform CRA_a [Homo sapiens]
gi|530421342	193067	0.02	PREDICTED: FERM and PDZ domain-containing protein 4 isoform X1 [Homo sapiens]
gi|6912534	29088	0.16	BMP and activin membrane-bound inhibitor homolog precursor [Homo sapiens]
gi|50897294	51245	0.09	POTE ankyrin domain family member A isoform 1 [Homo sapiens]
gi|14149805	38735	0.12	enkurin domain-containing protein 1 [Homo sapiens]

gi|4503375	56594	0.08	dihydropyrimidinase [Homo sapiens]
gi|29801	53563	0.18	CD44E (epithelial form) [Homo sapiens]
gi|119598259	132309	0.03	uveal autoantigen with coiled-coil domains and ankyrin repeats, isoform CRA_a [Homo sapiens]

ST 1-2: Transport Proteins Identified

Accession	Mass	emPAI	Description
gi|530396432	69258	0.06	PREDICTED: two pore calcium channel protein 2 isoform X4 [Homo sapiens]
gi|62088088	85811	0.94	transferrin receptor variant [Homo sapiens]
gi|119574954	34459	0.65	voltage-dependent anion channel 2, isoform CRA_a [Homo sapiens]
gi|190133	134625	0.07	plasma membrane Ca2+ pumping ATPase [Homo sapiens]
gi|1478281	56585	0.17	neutral amino acid transporter B [Homo sapiens]
gi|119595679	95691	0.05	potassium voltage-gated channel, KQT-like subfamily, member 2, isoform CRA_c [Homo sapiens]
gi|115583685	53909	0.08	monocarboxylate transporter 1 [Homo sapiens]
gi|119626956	136757	0.03	cache domain containing 1 [Homo sapiens]
gi|98986321	58920	0.08	gliomedin [Homo sapiens]

gi|238427	30623	0.15	Porin 31HM [human, skeletal muscle membranes, Peptide, 282 aa]
gi|222143239	13223	0.38	Chain A, Crystal Structure Of The Px Domain Of Sorting Nexin-17 (Snx17)
gi|15012080	17190	0.28	ACAT1 protein [Homo sapiens]
gi|549988	81597	0.05	sulfate transporter [Homo sapiens]
gi|347948492	8529	0.62	Chain A, Complex Of Cambr And Cam
gi|3882215	119783	0.04	KIAA0747 protein [Homo sapiens]

ST 1-4: Immune Complexes Identified

Accession	Mass	emPAI	Description
gi|161376703	31480	0.51	MHC class I antigen [Homo sapiens]
gi|47564005	31489	0.73	MHC class I antigen [Homo sapiens]
gi|358423242	21090	0.84	MHC class I antigen [Homo sapiens]
gi|333036593	21139	0.84	MHC class I antigen [Homo sapiens]
gi|34222512	40410	0.54	RecName: Full=HLA class I histocompatibility antigen, B-73 alpha chain; AltName: Full=MHC class I antigen B*73; Flags: Precursor
gi|55415712	10828	0.47	MHC class II antigen [Homo sapiens]
gi|371448219	14569	0.34	immunoglobulin G heavy chain variable region, partial [Homo sapiens]
gi|26801098	8458	0.63	immunoglobulin heavy chain variable region [Homo sapiens]

gi|371447513	13673	0.36	immunoglobulin G heavy chain variable region, partial [Homo sapiens]
gi|62871150	17043	0.28	immunoglobulin alpha heavy chain variable region [Homo sapiens]
gi|304562592	13044	0.38	immunoglobulin gamma 1 heavy chain variable region [Homo sapiens]
gi|388777938	13723	0.36	immunoglobulin heavy chain variable region, partial [Homo sapiens]
gi|177216	58041	0.16	4F2 heavy chain antigen [Homo sapiens]
gi|179531	26172	0.18	IgE-binding protein [Homo sapiens]
gi|220702506	54199	0.9	Chain A, TapasinERP57 HETERODIMER
gi|7161035	10423	0.49	immunoglobulin heavy chain [Homo sapiens]
gi|886258	65091	0.07	alcam [Homo sapiens]
gi|19909527	38169	0.57	DERP12 (dermal papilla derived protein 12) [Homo sapiens]
gi|19747283	12346	0.41	X antigen family member 2 [Homo sapiens]
gi|627493	2788	2.82	interferon alpha (component g) - human (fragment)
gi|70913399	2021	4.89	T cell receptor alpha variable 7 [Homo sapiens]

ST 1-5: GPCRs and G proteins

Accession	Mass	emPAI	Description
gi|4504041	40425	0.38	guanine nucleotide-binding protein G(i) subunit alpha-2 isoform 1 [Homo sapiens]

gi|119574084	39680	0.39	guanine nucleotide binding protein (G protein), beta polypeptide 2-like 1, isoform CRA_h [Homo sapiens]
gi|297660220	16459	0.3	Rho GTPase activating protein 26 variant 3 [Homo sapiens]
gi|1770396	42266	0.11	G-protein coupled receptor (putative) [Homo sapiens]
gi|6680045	37353	0.12	guanine nucleotide-binding protein G(I)/G(S)/G(T) subunit beta-1 [Mus musculus]
gi|1174072	42116	0.23	G alpha-q [Homo sapiens]
gi|52353947	34995	0.13	olfactory receptor 51F1 [Homo sapiens]
gi|187281	77555	0.4	M4 protein [Homo sapiens]
gi|540344584	37576	0.12	guanine nucleotide-binding protein subunit alpha-12 isoform 3 [Homo sapiens]
gi|62088744	29577	0.16	regulator of G-protein signalling 11 isoform 1 variant [Homo sapiens]
gi|4758796	40517	0.11	developmentally-regulated GTP-binding protein 1 [Homo sapiens]
gi|119626208	51201	0.09	septin 11, isoform CRA_a [Homo sapiens]
gi|58257741	171369	0.03	KIAA1219 protein [Homo sapiens]
gi|4505675	68448	0.07	high affinity cGMP-specific 3',5'-cyclic phosphodiesterase 9A isoform a [Homo sapiens]
gi|4456467	77101	0.06	TM7XN1 protein [Homo sapiens]
gi|3002951	15512	0.31	breakpoint cluster region protein 1 [Homo sapiens]
gi|71296783	76213	0.06	RAP1GAP protein [Homo sapiens]

gi|119608392	123307	0.04	Rap guanine nucleotide exchange factor (GEF) 1, isoform CRA_b [Homo sapiens]
gi|21928311	35019	0.13	seven transmembrane helix receptor [Homo sapiens]
gi|13569962	22157	1.17	ras-related protein Rab-1B [Homo sapiens]
gi|119620329	28129	0.85	RAB1A, member RAS oncogene family, isoform CRA_f [Homo sapiens]
gi|4506413	20974	0.5	ras-related protein Rap-1A precursor [Homo sapiens]
gi|20147713	23971	0.43	Ras family small GTP binding protein RALA [Homo sapiens]
gi|5031703	52132	0.09	ras GTPase-activating protein-binding protein 1 [Homo sapiens]
gi|141797011	189162	0.07	IQ motif containing GTPase activating protein 1 [Homo sapiens]
gi|508285	23553	0.44	Rab5c-like protein, similar to Canis familiaris Rab5c protein, PIR Accession Number S38625 [Homo sapiens]
gi|763130	24559	0.19	YPT3 [Homo sapiens]
gi|359807059	20502	0.23	TBC1 domain family member 1 isoform 4 [Homo sapiens]

ST 1-6: Chaperone Proteins Identified

ACCESSION	MASS	EMPAI	DESCRIPTION
GI|431822408	82269	0.89	heat shock protein HSP 90-beta isoform c [Homo sapiens]
GI|153792590	98099	0.43	heat shock protein HSP 90-alpha isoform 1 [Homo sapiens]

GI|4502643	57988	0.08	T-complex protein 1 subunit zeta isoform a [Homo sapiens]
GI|5453603	57452	0.08	T-complex protein 1 subunit beta isoform 1 [Homo sapiens]
GI|48762932	59583	0.08	T-complex protein 1 subunit theta isoform 1 [Homo sapiens]
GI|48145555	59291	0.08	CCT7 [Homo sapiens]
GI|671527	60292	0.07	gamma subunit of CCT chaperonin [Homo sapiens]

ST 1-7: Receptors Identifed

ACCESSION	MASS	EMPAI	DESCRIPTION
GI|19743813	88357	0.22	integrin beta-1 isoform 1A precursor [Homo sapiens]
GI|119581591	46372	0.45	basigin (Ok blood group), isoform CRA_g [Homo sapiens]
GI|119610286	18642	1.5	progesterone receptor membrane component 1, isoform CRA_b [Homo sapiens]
GI|62897779	62485	0.07	thyroid hormone receptor interactor 10 variant [Homo sapiens]
GI|291621647	26154	0.18	membrane-associated progesterone receptor component 2 [Homo sapiens]
GI|62089372	30214	0.15	FK506 binding protein 5 variant [Homo sapiens]
GI|483831	303844	0.01	type 3 inositol 1,4,5-trisphosphate receptor [Homo sapiens]
GI|472848	22094	0.21	N-methyl-D-aspartate receptor subunit, partial [Homo sapiens]

GI|703110	17307	0.28	thyroid receptor interactor, partial [Homo sapiens]
GI|62088916	265943	0.02	Insulin-like growth factor 2 receptor variant [Homo sapiens]
GI|62089376	70414	0.06	complement component 1, q subcomponent, receptor 1 variant [Homo sapiens]
GI|15192139	19666	0.24	porimin [Homo sapiens]
GI|578831638	204161	0.02	PREDICTED: peripheral-type benzodiazepine receptor-associated protein 1 isoform X3 [Homo sapiens]

ST 1-8: Enzymes Identified

ACCESSION	MASS	EMPAI	DESCRIPTION
GI|33946291	59113	0.08	lysophosphatidylcholine acyltransferase 1 [Homo sapiens]
GI|291463382	17983	1.58	Chain A, Free Acetyl-Cypa Trigonal Form
GI|181250	22597	1.13	cyclophilin, partial [Homo sapiens]
GI|33946291	59113	0.08	lysophosphatidylcholine acyltransferase 1 [Homo sapiens]
GI|6331328	115103	0.08	KIAA1280 protein [Homo sapiens]
GI|530390528	71082	0.06	PREDICTED: carnitine O-acetyltransferase isoform X1 [Homo sapiens]

GI|119596301	24546	0.42	tyrosine 3-monooxygenase/tryptophan 5-monooxygenase activation protein, beta polypeptide, isoform CRA_b [Homo sapiens]
GI|693933	47079	0.32	2-phosphopyruvate-hydratase alpha-enolase [Homo sapiens]
GI|605604525	9922	0.53	Chain A, Crystal Structure Of Phospholipase C Beta 3 In Complex With Pdz1 Of Nherf1
GI|38202211	143531	0.03	N-acetylglucosamine-1-phosphotransferase subunits alpha/beta precursor [Homo sapiens]
GI|570359824	37730	0.12	Chain A, Crystal Structure Of The Human Cyclin G Associated Kinase (gak)
GI|68051721	49031	0.09	neutral cholesterol ester hydrolase 1 isoform b [Homo sapiens]

ST 1-9: Other Proteins Identified

ACCESSION	MASS	EMPAI	DESCRIPTION
GI|1665773	78230	0.06	KIAA0253 [Homo sapiens]
GI|178775	28944	1.1	proapolipoprotein, partial [Homo sapiens]
GI|4505893	16680	0.29	proteolipid protein 2 [Homo sapiens]
GI|1374813	23368	0.2	SNAP-23 [Homo sapiens]
GI|28376621	46614	0.1	SEC14-like protein 4 isoform a [Homo sapiens]
GI|530393410	236464	0.02	PREDICTED: myoferlin isoform X1 [Homo sapiens]

ST2: Proteomics data of plasma membrane protein from 143B

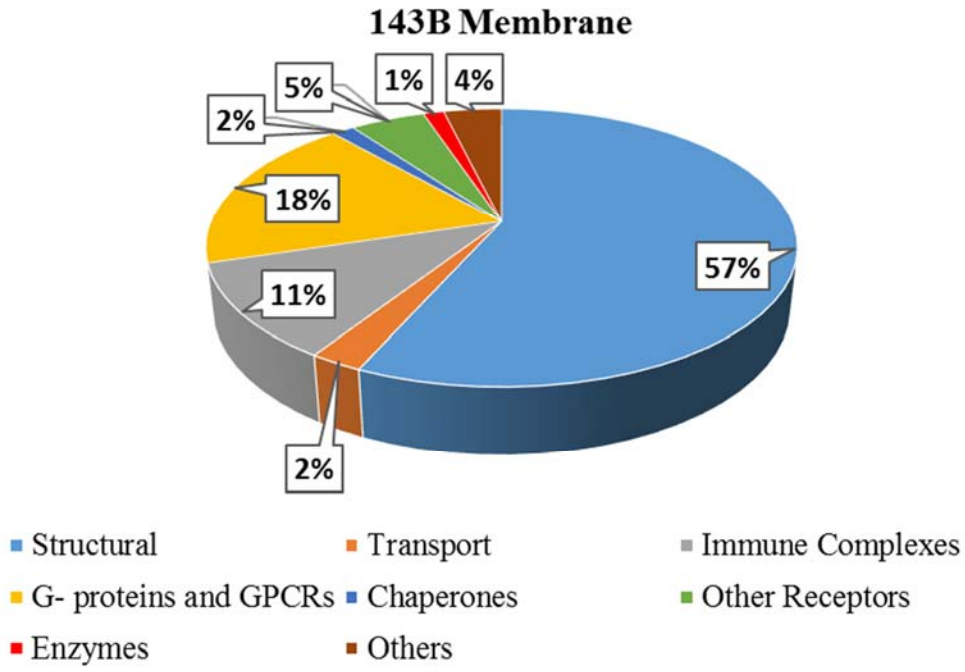

ST2-1. Overall proteomic profile

	emPAI	Percentage (Equation SE-1)
Structural	87.73	56.68
Transport	3.81	2.46
Immune Complexes	17.16	11.09
G- proteins and GPCRs	28.33	18.30
Chaperones	2.27	1.47
Other Receptors	7.55	4.88
Enzymes	2.09	1.35

Others	5.84	3.77
Total	154.78	100

ST2-2. Structural proteins detected

Accession	Mass	emPAI	Description
gi|435476	62092	2.89	cytokeratin 9 [Homo sapiens]
gi|12803709	51619	1.26	Keratin 14 [Homo sapiens]
gi|12653819	48003	0.3	Keratin 18 [Homo sapiens]
gi|11935049	66027	6.72	keratin 1 [Homo sapiens]
gi|62414289	53619	9.57	vimentin [Homo sapiens]
gi|47132620	65393	2.88	keratin, type II cytoskeletal 2 epidermal [Homo sapiens]
gi|119617032	59874	0.76	keratin 6B, isoform CRA_a [Homo sapiens]
gi|119395754	62340	0.84	keratin, type II cytoskeletal 5 [Homo sapiens]
gi|119617057	57772	0.79	keratin 8, isoform CRA_a [Homo sapiens]
gi|28173564	58887	0.15	keratin, type II cytoskeletal 73 [Homo sapiens]
gi|73909156	40503	26.66	Annexin A2 [Homo sapiens]
gi|62897671	41694	8.17	beta actin variant [Homo sapiens]
gi|7106439	49639	1.77	tubulin beta-5 chain [Mus musculus]
gi|119608775	48794	1.81	tubulin, beta 2C, isoform CRA_b [Homo sapiens]
gi|157833780	35984	1.54	Chain A, Human Annexin V With Proline Substitution By Thioproline

gi|34234	31774	0.7	laminin-binding protein, partial [Homo sapiens]
gi|16974825	8483	10.06	Chain A, Solution Structure Of Calcium-calmodulin N-terminal Domain
gi|5031635	18491	2.07	cofilin-1 [Homo sapiens]
gi|4502101	38690	0.92	annexin A1 [Homo sapiens]
gi|12667788	226392	0.18	myosin-9 [Homo sapiens]
gi|24119203	29015	1.06	tropomyosin alpha-3 chain isoform 2 [Homo sapiens]
gi|17986258	16919	1.67	myosin light polypeptide 6 isoform 1 [Homo sapiens]
gi|179976	75857	0.48	calelectrin [Homo sapiens]
gi|37492	50126	0.52	alpha-tubulin [Homo sapiens]
gi|321400138	46537	0.31	CD44 antigen isoform 6 precursor [Homo sapiens]
gi|119593154	263754	0.08	filamin A, alpha (actin binding protein 280), isoform CRA_e [Homo sapiens]
gi|530393410	236464	0.07	PREDICTED: myoferlin isoform X1 [Homo sapiens]
gi|7656991	53215	0.08	coronin-1C isoform b [Homo sapiens]
gi|3282771	278018	0.06	actin-binding protein homolog ABP-278 [Homo sapiens]
gi|4826898	15045	0.73	profilin-1 [Homo sapiens]
gi|119584665	9744	0.52	ankyrin repeat domain 28, isoform CRA_d [Homo sapiens]
gi|186837	197937	0.02	laminin B1 [Homo sapiens]
gi|41322910	512292	0.03	plectin isoform 1d [Homo sapiens]

gi|205831092	68253	0.06	RecName: Full=Putative IQ motif and ankyrin repeat domain-containing protein LOC642574
gi|641958	228798	0.02	non-muscle myosin B [Homo sapiens]
gi|3287188	127296	0.03	ankyrin-like protein [Homo sapiens]
gi|120660098	163133	0.03	CAMSAP1 protein [Homo sapiens]
gi|444738793	5129	1.16	alternative protein CEP350 [Homo sapiens]
gi|8885790	287292	0.03	filamin 2 [Homo sapiens]
gi|762885	81583	0.05	Plakoglobin [Homo sapiens]
gi|578821687	271519	0.02	PREDICTED: spectrin beta chain, non-erythrocytic 2 isoform X3 [Homo sapiens]
gi|438056	342550	0.01	laminin M chain (merosin) [Homo sapiens]
gi|4507115	54496	0.08	fascin [Homo sapiens]
gi|119576069	394840	0.01	myosin XVA, isoform CRA_c [Homo sapiens]
gi|6563228	43212	0.1	rap2 interacting protein x [Homo sapiens]
gi|4757944	25792	0.18	CD81 antigen [Homo sapiens]
gi|1107687	505963	0.02	homologue of Drosophila Fat protein [Homo sapiens]
gi|578837838	423562	0.01	PREDICTED: dystrophin isoform X5 [Homo sapiens]
gi|578823153	93390	0.05	PREDICTED: tastin isoform X1 [Homo sapiens]
gi|119574344	91877	0.05	ankyrin repeat domain 30B, partial [Homo sapiens]
gi|2996006	70660	0.06	outer dense fiber protein 2/2 [Homo sapiens]
gi|34226	288131	0.01	laminin A chain [Homo sapiens]
gi|530370381	134263	0.03	PREDICTED: unconventional myosin-Ib isoform X2 [Homo sapiens]

gi|186964	177492	0.02	laminin B2 chain [Homo sapiens]
gi|578819318	310817	0.01	PREDICTED: ankyrin-3 isoform X17 [Homo sapiens]
gi|55743096	193394	0.02	collagen alpha-1(XIV) chain precursor [Homo sapiens]

ST 2-3: Transport Proteins detected

Accession	Mass	emPAI	Description
gi|119574954	34459	0.84	voltage-dependent anion channel 2, isoform CRA_a [Homo sapiens]
gi|198443050	31818	0.3	Chain A, Solution Structure Of Human Vdac-1 In Ldao Micelles
gi|61744477	68059	0.28	4F2 cell-surface antigen heavy chain isoform b [Homo sapiens]
gi|4505893	16680	0.28	proteolipid protein 2 [Homo sapiens]
gi|51094709	102523	0.04	tweety homolog 3 (Drosophila) [Homo sapiens]
gi|48255951	136789	0.03	plasma membrane calcium-transporting ATPase 2 isoform 1 [Homo sapiens]
gi|5733504	27630	0.16	voltage-dependent anion channel VDAC3 [Homo sapiens]
gi|1478281	56585	0.16	neutral amino acid transporter B [Homo sapiens]
gi|5730102	106258	0.04	short transient receptor potential channel 6 [Homo sapiens]
gi|4502281	31492	0.14	sodium/potassium-transporting ATPase subunit beta-3 [Homo sapiens]
gi|115583685	53909	0.17	monocarboxylate transporter 1 [Homo sapiens]

gi|9957467	269786	0.02	ATP-binding cassette sub-family A member 2 [Homo sapiens]
gi|38516	20468	0.23	caveolin [Homo sapiens]
gi|347948492	8529	0.61	Chain A, Complex Of Cambr And Cam
gi|62087606	50068	0.09	sorting nexin 1 isoform a variant [Homo sapiens]
gi|2337920	29827	0.15	syntaxin 7 [Homo sapiens]
gi|25777643	59949	0.07	small conductance calcium-activated potassium channel protein 1 [Homo sapiens]
gi|51339295	126843	0.07	cation channel sperm-associated protein subunit beta precursor [Homo sapiens]
gi|4507297	68692	0.06	syntaxin-binding protein 1 isoform a [Homo sapiens]
gi|169790839	59534	0.07	excitatory amino acid transporter 1 isoform 1 [Homo sapiens]

ST 2-4 : Immune Complex proteins detected

Accession	Mass	emPAI	Description
gi|432139040	12890	0.38	immunoglobulin heavy chain variable region, partial [Homo sapiens]
gi|290560013	11815	3.04	Chain B, Crystal Structure Of Mhc Class I Hla-A2.1 Bound To A Photocleavable Peptide
gi|4324088	10594	0.47	immunoglobulin lambda light chain variable region [Homo sapiens]
gi|307496	1390	9.07	T cell receptor beta chain [Homo sapiens]
gi|333036593	21139	0.22	MHC class I antigen [Homo sapiens]

gi|151188217	40719	0.11	killer-cell Ig-like receptor [Homo sapiens]
gi|17986005	29943	0.15	major histocompatibility complex, class II, DR beta 3 precursor [Homo sapiens]
gi|611962048	10753	0.46	immunoglobulin heavy chain variable region, partial [Homo sapiens]
gi|247425243	13679	0.35	immunoglobulin heavy chain variable region [Homo sapiens]
gi|15680023	27975	0.16	B-cell receptor-associated protein 31 [Homo sapiens]
gi|4038122	4086	1.57	T-cell receptor beta chain [Homo sapiens]
gi|226316189	21056	0.22	MHC class I antigen [Homo sapiens]
gi|224962016	21226	0.48	MHC class II antigen [Homo sapiens]
gi|119573139	39827	0.11	SLAM family member 9, isoform CRA_a [Homo sapiens]
gi|26985944	13046	0.37	immunoglobulin IgG1 heavy chain [Homo sapiens]

ST 2- 5: GPCRs and G- proteins detected

Accession	Mass	emPAI	Description
gi|4506413	20974	0.81	ras-related protein Rap-1A precursor [Homo sapiens]
gi|327195100	33961	0.45	UBE2L3/KRAS fusion protein [Homo sapiens]
gi|119574084	39680	0.53	guanine nucleotide binding protein (G protein), beta polypeptide 2-like 1, isoform CRA_h [Homo sapiens]
gi|508285	23553	0.43	Rab5c-like protein, similar to Canis familiaris Rab5c protein, PIR Accession Number S38625 [Homo sapiens]
gi|13569962	22157	1.56	ras-related protein Rab-1B [Homo sapiens]

gi|33946329	23552	0.43	ras-related protein Ral-A precursor [Homo sapiens]
gi|1174149	23447	1.04	small GTP binding protein Rab7 [Homo sapiens]
gi|14249144	24473	0.67	ras-related protein Rab-11B [Rattus norvegicus]
gi|5729850	40506	0.37	guanine nucleotide-binding protein G(k) subunit alpha [Homo sapiens]
gi|21361884	24199	0.19	ras-related protein Rab-2B isoform 1 [Homo sapiens]
gi|5031703	52132	0.18	ras GTPase-activating protein-binding protein 1 [Homo sapiens]
gi|5031703	52132	0.18	ras GTPase-activating protein-binding protein 1 [Homo sapiens]
gi|297660220	16459	0.29	Rho GTPase activating protein 26 variant 3 [Homo sapiens]
gi|311697329	3564	1.93	KRAS protein [Homo sapiens]
gi|4885287	7314	0.73	guanine nucleotide-binding protein G(I)/G(S)/G(O) subunit gamma-5 precursor [Homo sapiens]
gi|540344584	37576	0.12	guanine nucleotide-binding protein subunit alpha-12 isoform 3 [Homo sapiens]
gi|3292965	1071	15.8	m1 muscarinic acetylcholine receptor protein [Homo sapiens]
gi|53828729	34724	0.13	olfactory receptor 7D2 [Homo sapiens]
gi|334278900	35700	0.12	olfactory receptor 4N4 [Homo sapiens]
gi|19338916	36399	0.12	G protein-coupled receptor SNSR5 [Homo sapiens]
gi|2500069	21555	0.21	RecName: Full=Ras-related protein Rab-31; AltName: Full=Ras-related protein Rab-22B [Homo sapiens]
gi|3327062	221821	0.02	KIAA0624 protein [Homo sapiens]
gi|4139784	24393	0.19	Chain A, Canine Gdp-Ran Q69l Mutant

gi|390635651	110782	0.04	ras-related protein Rab-44 [Homo sapiens]
gi|21928341	34874	0.13	seven transmembrane helix receptor [Homo sapiens]
gi|530416765	113467	0.04	PREDICTED: ras-interacting protein 1 isoform X1 [Homo sapiens]
gi|62088744	29577	0.15	regulator of G-protein signalling 11 isoform 1 variant [Homo sapiens]
gi|359807059	20502	0.22	TBC1 domain family member 1 isoform 4 [Homo sapiens]
gi|4836765	77704	0.06	G-protein-coupled receptor [Homo sapiens]
gi|13122463	37605	0.12	G protein-coupled receptor [Homo sapiens]
gi|9625037	21295	0.22	rho-related GTP-binding protein RhoG precursor [Mus musculus]
gi|51036603	8001	0.66	guanine nucleotide-binding protein G(I)/G(S)/G(O) subunit gamma-12 precursor [Homo sapiens]
gi|15293749	23836	0.19	olfactory receptor [Homo sapiens]

ST 2-6: Chaperone proteins detected

Accession	Mass	emPAI	Description
gi|431822408	82269	0.95	heat shock protein HSP 90-beta isoform c [Homo sapiens]
gi|153792590	98099	0.47	heat shock protein HSP 90-alpha isoform 1 [Homo sapiens]
gi|62089036	57725	0.16	chaperonin containing TCP1, subunit 6A isoform a variant [Homo sapiens]
gi|5453603	57452	0.16	T-complex protein 1 subunit beta isoform 1 [Homo sapiens]

gi|1136741	58465	0.16	KIAA0002 [Homo sapiens]
gi|5453607	59329	0.15	T-complex protein 1 subunit eta isoform a [Homo sapiens]
gi|671527	60292	0.07	gamma subunit of CCT chaperonin [Homo sapiens]
gi|36796	60356	0.15	t-complex polypeptide 1 [Homo sapiens]

ST 2-7: Other Receptor proteins detected

Accession	Mass	emPAI	Description
gi|1477388	132282	0.07	metabotropic glutamate receptor 1 alpha [Homo sapiens]
gi|119581591	46372	0.2	basigin (Ok blood group), isoform CRA_g [Homo sapiens]
gi|187609338	20107	0.51	Chain A, Crystal Structure Of The Extracellular Portion Of Hab18gCD147
gi|19743813	88357	0.47	integrin beta-1 isoform 1A precursor [Homo sapiens]
gi|124942	129214	0.14	RecName: Full=Integrin alpha-2; AltName: Full=CD49 antigen-like family member B; AltName: Full=Collagen receptor; AltName: Full=Platelet membrane glycoprotein Ia; Short=GPIa; AltName: Full=VLA-2 subunit alpha; AltName: CD_antigen=CD49b; Flags: Precu
gi|6424942	96019	0.05	ALG-2 interacting protein 1 [Homo sapiens]
gi|5729875	21658	0.21	membrane-associated progesterone receptor component 1 isoform 1 [Homo sapiens]
gi|4530577	65546	0.07	LISCH protein [Homo sapiens]
gi|21928311	35019	0.13	seven transmembrane helix receptor [Homo sapiens]

gi|62089376	70414	0.06	complement component 1, q subcomponent, receptor 1 variant [Homo sapiens]
gi|119611708	110644	0.04	protein tyrosine phosphatase, receptor type, C, isoform CRA_c [Homo sapiens]
gi|47077659	72805	0.06	FLJ00268 protein [Homo sapiens]
gi|1374813	23368	0.43	SNAP-23 [Homo sapiens]
gi|20072835	59945	0.07	ACSL1 protein, partial [Homo sapiens]
gi|5360115	89012	0.05	NY-REN-45 antigen [Homo sapiens]
gi|257743046	43424	0.1	C-C chemokine receptor type 3 isoform 2 [Homo sapiens]
gi|70913399	2021	4.89	T cell receptor alpha variable 7 [Homo sapiens]

ST 2-8: Enzymes detected

ACCESSION	MASS	EMPAI	DESCRIPTION
GI|189095938	11754	0.42	Chain A, Crystal Structure Of E60a Mutant Of Fkbp12
GI|530375065	51152	0.09	PREDICTED: neutral cholesterol ester hydrolase 1 isoform X1 [Homo sapiens]
GI|22209028	31786	0.3	Thioredoxin-related transmembrane protein 1 [Homo sapiens]
GI|4505977	32553	0.14	lipid phosphate phosphohydrolase 2 isoform 1 [Homo sapiens]
GI|530405604	56246	0.08	PREDICTED: death-associated protein kinase 2 isoform X1 [Homo sapiens]

GI|4505783	124805	0.03	phosphorylase b kinase regulatory subunit beta isoform a [Homo sapiens]
GI|1666423	161493	0.03	FMI protein [Homo sapiens]
GI|1486363	41988	0.11	extracellular signal regulated kinase [Homo sapiens]
GI|35360	65350	0.07	PDC-E2 precursor (AA -54 to 561) [Homo sapiens]
GI|516516	117320	0.04	neuronal kinesin heavy chain [Homo sapiens]
GI|181944	108185	0.04	protein-tyrosine kinase [Homo sapiens]
GI|16306598	153533	0.03	von Willebrand factor-cleaving protease precursor [Homo sapiens]
GI|5031697	143634	0.03	probable phospholipid-transporting ATPase IC [Homo sapiens]
GI|282847398	147344	0.03	mitogen-activated protein kinase kinase kinase 15 [Homo sapiens]
GI|134104091	31726	0.14	Chain A, Crystal Structure Of Human Pyridoxal 5'-Phosphate Phosphatase
GI|837261	88581	0.05	ERK5 [Homo sapiens]
GI|62897321	34328	0.13	steroid dehydrogenase homolog [Homo sapiens]
GI|3450828	33499	0.13	retinal short-chain dehydrogenase/reductase retSDR1 [Homo sapiens]
GI|124007195	73247	0.06	RecName: Full=Heparan-alpha-glucosaminide N-acetyltransferase; AltName: Full=Transmembrane protein 76 [Homo sapiens]

GI|13242866	31413	0.14	type 3 iodothyronine deiodinase [Homo sapiens]

ST 2-9: Other membrane proteins detected

Accession	Mass	emPAI	Description
gi|13129092	26194	0.38	transmembrane protein 109 precursor [Homo sapiens]
gi|5821140	40308	0.37	ASY [Homo sapiens]
gi|345198270	23750	0.69	tumor protein D54 isoform j [Homo sapiens]
gi|337930	27386	0.84	scar protein [Homo sapiens]
gi|23712	45220	0.32	myoblast antigen 24.1D5 [Homo sapiens]
gi|1160963	83616	0.29	transmembrane protein [Homo sapiens]
gi|662994	72707	0.06	GPI-anchored protein p137 [Homo sapiens]
gi|5729718	46003	0.1	trophoblast glycoprotein precursor [Homo sapiens]
gi|578830259	58187	0.08	PREDICTED: brain-specific angiogenesis inhibitor 1-associated protein 2 isoform X11 [Homo sapiens]
gi|7767178	19180	0.24	Chain A, Apolipoprotein E3 (Apoe3) Truncation Mutant 165
gi|6912582	30361	0.15	peflin [Homo sapiens]
gi|6002678	45242	0.1	colon carcinoma related protein [Homo sapiens]
gi|19923969	25820	0.18	coiled-coil domain-containing protein 124 [Homo sapiens]
gi|39725636	27260	0.17	transmembrane emp24 domain-containing protein 9 precursor [Homo sapiens]
gi|19920317	65983	0.14	cytoskeleton-associated protein 4 [Homo sapiens]
gi|1161384	384046	0.01	BRCA2 [Homo sapiens]
gi|40789001	108477	0.04	KIAA0964 protein [Homo sapiens]

gi|4240313	149996	0.03	KIAA0912 protein [Homo sapiens]
gi|30089664	575806	0.01	ABC A13 [Homo sapiens]
gi|27735113	50114	0.09	EF-hand calcium-binding domain-containing protein 3 isoform b [Homo sapiens]
gi|28680	21594	0.21	amphiglycan [Homo sapiens]
gi|235397	24680	0.18	HMFG, partial [Homo sapiens]
gi|15012003	17359	0.27	Family with sequence similarity 162, member A [Homo sapiens]
gi|1616918	46323	0.1	membrane protein with histidine rich charge clusters [Homo sapiens]
gi|6331328	115103	0.04	KIAA1280 protein [Homo sapiens]
gi|29648540	14892	0.32	MLL5 [Homo sapiens]
gi|20521880	198894	0.02	KIAA1305 protein [Homo sapiens]
gi|7706322	28051	0.16	UPF0568 protein C14orf166 [Homo sapiens]
gi|471270576	23424	0.2	Chain L, Crystal Structure Of Tnf-alpha In Complex With Infliximab Fab Fragment
gi|71891687	139575	0.03	KIAA0931 protein [Homo sapiens]
gi|223462187	266458	0.02	SPG11 protein [Homo sapiens]

ST3: Proteomics data of plasma membrane protein from POS

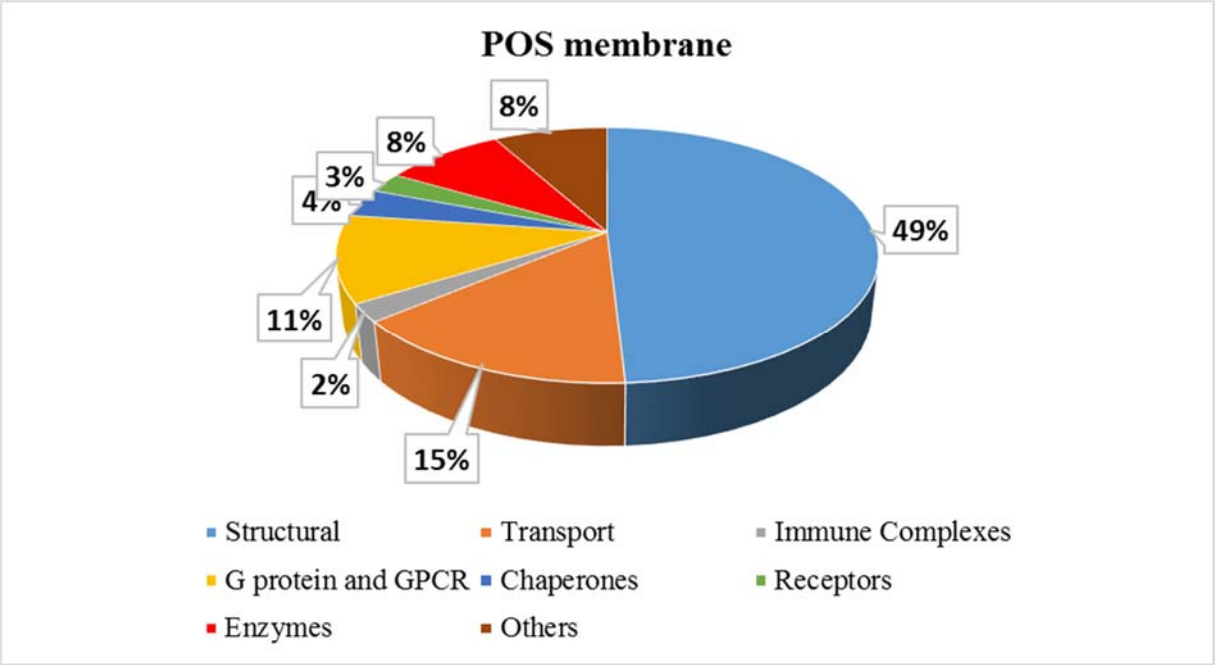

ST3-1. Overall proteomic profile

	emPAI	Percentage
Structural	36.45	49.11
Transport	11.00	14.82
Immune Complexes	1.68	2.26
G protein and GPCR	8.16	10.99
Chaperones	2.68	3.61
Receptors	1.91	2.57
Enzymes	6.32	8.52
Others	6.02	8.11

Total	74.22	100

ST 3-2 Structural Proteins Identified

Accession	Mass	emPAI	Description
gi|4501885	41710	6.01	actin, cytoplasmic 1 [Homo sapiens]
gi|6755901	50104	1.56	tubulin alpha-1A chain [Mus musculus]
gi|73997851	49990	0.54	PREDICTED: tubulin alpha-8 chain [Canis lupus familiaris]
gi|61740600	57676	1.83	keratin, type I cytoskeletal 10 [Canis lupus familiaris]
gi|545510666	54047	0.27	PREDICTED: keratin, type I cytoskeletal 42 [Canis lupus familiaris]
gi|62122767	76308	0.12	keratin, type I cytoskeletal 9 [Canis lupus familiaris]
gi|50950177	38630	4.26	annexin A2 [Canis lupus familiaris]
gi|7106439	49639	2.65	tubulin beta-5 chain [Mus musculus]
gi|5174735	49799	2.06	tubulin beta-4B chain [Homo sapiens]
gi|345803407	49835	0.54	PREDICTED: tubulin beta-6 chain isoform 3 [Canis lupus familiaris]
gi|50979272	63751	1.4	keratin, type II cytoskeletal 1 [Canis lupus familiaris]
gi|345791904	62778	0.41	PREDICTED: keratin, type II cytoskeletal 5 isoform X1 [Canis lupus familiaris]
gi|545545102	63592	0.5	PREDICTED: keratin, type II cytoskeletal 2 epidermal isoform X1 [Canis lupus familiaris]

gi|359323093	54684	0.48	PREDICTED: keratin, type II cytoskeletal 8 [Canis lupus familiaris]
gi|345791839	62832	0.23	PREDICTED: keratin, type II cytoskeletal 6A isoformX2 [Canis lupus familiaris]
gi|545545370	63946	0.22	PREDICTED: keratin, type II cytoskeletal 73 isoform X1 [Canis lupus familiaris]
gi|74008809	280450	0.26	PREDICTED: filamin-A isoform 2 [Canis lupus familiaris]
gi|559098393	53565	3.22	vimentin [Canis lupus familiaris]
gi|558695394	38602	1.42	annexin A1 [Canis lupus familiaris]
gi|73953627	75842	0.87	PREDICTED: annexin A6 isoformX2 [Canis lupus familiaris]
gi|160425231	226328	0.23	myosin-9 [Canis lupus familiaris]
gi|345802274	223986	0.04	PREDICTED: myosin-11 isoformX29 [Canis lupus familiaris]
gi|5031635	18491	0.98	cofilin-1 [Homo sapiens]
gi|545558304	69724	0.54	PREDICTED: moesin isoform X3 [Canis lupus familiaris]
gi|74005014	131810	0.14	PREDICTED: unconventional myosin-Ib isoformX2 [Canis lupus familiaris]
gi|50978940	129321	0.14	collagen alpha-2(I) chain precursor [Canis lupus familiaris]
gi|73947726	104337	0.09	PREDICTED: alpha-actinin-4 isoformX6 [Canis lupus familiaris]
gi|74005014	131810	0.14	PREDICTED: unconventional myosin-Ib isoformX2 [Canis lupus familiaris]

gi|73969959	65382	0.58	PREDICTED: cytoskeleton-associated protein 4 [Canis lupus familiaris]
gi|545494454	47490	0.72	PREDICTED: lactadherin [Canis lupus familiaris]
gi|55742853	35790	0.13	annexin A4 [Canis lupus familiaris]
gi|57106334	48209	0.09	PREDICTED: keratin, type I cytoskeletal 18 isoform 1 [Canis lupus familiaris]
gi|17986258	16919	0.28	myosin light polypeptide 6 isoform 1 [Homo sapiens]
gi|359320831	269595	0.07	PREDICTED: talin-1 isoform X1 [Canis lupus familiaris]
gi|157151714	342453	0.01	collagen alpha-3(VI) chain precursor [Canis lupus familiaris]
gi|460417294	41977	0.11	actin-related protein 3 isoform 2 [Homo sapiens]
gi|13937393	46861	0.1	actin-like protein 6B [Mus musculus]
gi|545552032	114397	0.04	PREDICTED: SWI/SNF-related matrix-associated actin-dependent regulator of chromatin subfamily A containing DEAD/H box 1 isoform X7 [Canis lupus familiaris]
gi|545530710	68641	0.13	PREDICTED: LOW QUALITY PROTEIN: kinesin light chain 2 [Canis lupus familiaris]
gi|545507020	59610	0.07	PREDICTED: cochlin [Canis lupus familiaris]
gi|73997258	106132	0.04	PREDICTED: calsyntenin-3 isoform 1 [Canis lupus familiaris]
gi|545551547	78081	0.06	PREDICTED: collagen alpha-2(VI) chain [Canis lupus familiaris]
gi|545517725	149690	0.03	PREDICTED: collagen alpha-1(XV) chain isoform X1 [Canis lupus familiaris]

gi|545529126	126396	0.03	PREDICTED: collagen alpha-1(I) chain [Canis lupus familiaris]
gi|545499057	41024	0.23	PREDICTED: ankyrin repeat domain-containing protein 65 isoform X2 [Canis lupus familiaris]
gi|545519655	339256	0.03	PREDICTED: collagen alpha-1(XII) chain isoform X2 [Canis lupus familiaris]
gi|545550190	52694	0.08	PREDICTED: ankyrin repeat and death domain-containing protein 1A isoform X2 [Canis lupus familiaris]
gi|73966959	53672	0.08	PREDICTED: vitronectin isoform 2 [Canis lupus familiaris]
gi|545521155	534043	0.04	PREDICTED: plectin isoform X9 [Canis lupus familiaris]
gi|73961895	20485	0.23	PREDICTED: myosin regulatory light polypeptide 9-like isoformX1 [Canis lupus familiaris]
gi|73986060	243902	0.02	PREDICTED: unconventional myosin-IXb isoform 1 [Canis lupus familiaris]
gi|345778515	114475	0.04	PREDICTED: collagen alpha-1(XIX) chain isoform X4 [Canis lupus familiaris]
gi|73953207	36599	0.12	PREDICTED: annexin A8 isoformX1 [Canis lupus familiaris]
gi|545503404	174479	0.03	PREDICTED: collagen alpha-1(XXIV) chain isoform X2 [Canis lupus familiaris]
gi|73994333	117807	0.04	PREDICTED: FERM, RhoGEF and pleckstrin domain-containing protein 2 isoform X3 [Canis lupus familiaris]
gi|545531759	99866	0.04	PREDICTED: protein inturned isoform X3 [Canis lupus familiaris]

gi|57095096	80886	0.05	PREDICTED: lebercilin isoform X11 [Canis lupus familiaris]
gi|545519914	632508	0.01	PREDICTED: midasin isoform X1 [Canis lupus familiaris]
gi|73981496	32964	0.14	PREDICTED: F-actin-capping protein subunit alpha-1 isoform 2 [Canis lupus familiaris]
gi|359322210	111999	0.08	PREDICTED: microtubule-associated protein 1S isoform X1 [Canis lupus familiaris]
gi|545492158	195634	0.02	PREDICTED: LOW QUALITY PROTEIN: protocadherin gamma-A12 [Canis lupus familiaris]
gi|359322609	151053	0.03	PREDICTED: nephrocystin-3 [Canis lupus familiaris]
gi|345789814	142795	0.03	PREDICTED: collagen alpha-1(XX) chain [Canis lupus familiaris]
gi|545501026	56949	0.08	PREDICTED: BAI1-associated protein 2-like 1 isoformX1 [Canis lupus familiaris]
gi|545533749	203686	0.02	PREDICTED: laminin subunit beta-2 isoform X1 [Canis lupus familiaris]
gi|545539045	144440	0.03	PREDICTED: cohesin subunit SA-1 [Canis lupus familiaris]
gi|545529816	113484	0.04	PREDICTED: ankyrin repeat and BTB/POZ domain-containing protein 2 isoformX2 [Canis lupus familiaris]
gi|545541617	77260	0.06	PREDICTED: cytoskeleton-associated protein 2 isoform X2 [Canis lupus familiaris]
gi|73949468	130850	0.03	PREDICTED: protocadherin-12 [Canis lupus familiaris]

gi|545492234	473796	0.02	PREDICTED: LOW QUALITY PROTEIN: basement membrane-specific heparan sulfate proteoglycan core protein [Canis lupus familiaris]
gi|73957734	84663	0.05	PREDICTED: procollagen-lysine,2-oxoglutarate 5-dioxygenase 3 isoform 1 [Canis lupus familiaris]
gi|545529571	85651	0.05	PREDICTED: CD44 antigen isoform X1 [Canis lupus familiaris]
gi|545489377	58668	0.16	PREDICTED: collagen alpha-1(III) chain-like [Canis lupus familiaris]
gi|545530382	45606	0.1	PREDICTED: lymphocyte-specific protein 1 isoform X1 [Canis lupus familiaris]
gi|73954163	480212	0.01	PREDICTED: protocadherin Fat 2 [Canis lupus familiaris]
gi|545486940	78614	0.06	PREDICTED: extracellular matrix protein 2 isoform X1 [Canis lupus familiaris]
gi|545549404	39867	0.11	PREDICTED: ankyrin repeat domain-containing protein 63 [Canis lupus familiaris]
gi|165973990	222838	0.04	myosin-7 [Canis lupus familiaris]
gi|545503105	61681	0.07	PREDICTED: palmdelphin [Canis lupus familiaris]
gi|307938297	78906	0.06	nephrocystin-1 [Canis lupus familiaris]
gi|95925865	87375	0.05	pinin 1 [Canis lupus familiaris]
gi|545531227	579498	0.01	PREDICTED: LOW QUALITY PROTEIN: neuroblast differentiation-associated protein AHNAK [Canis lupus familiaris]

gi|545551689	208083	0.02	PREDICTED: protein Shroom3 isoform X1 [Canis lupus familiaris]
gi|545525131	310349	0.01	PREDICTED: LOW QUALITY PROTEIN: protocadherin-23-like [Canis lupus familiaris]
gi|345796528	46416	0.1	PREDICTED: neuroserpin isoform X3 [Canis lupus familiaris]
gi|4757952	21245	0.22	cell division control protein 42 homolog isoform 1 precursor [Homo sapiens]
gi|304376314	240303	0.02	tenascin precursor [Canis lupus familiaris]
gi|345801801	172246	0.03	PREDICTED: leucine-rich repeat-containing protein 7 isoform X2 [Canis lupus familiaris]
gi|74000367	271428	0.02	PREDICTED: talin-2 isoformX1 [Canis lupus familiaris]

ST 3-3: Transport Proteins Identified

Accession	Mass	emPAI	Description
gi|545528359	112738	0.64	PREDICTED: sodium/potassium-transporting ATPase subunit alpha-1 isoform X1 [Canis lupus familiaris]
gi|345797872	114359	0.08	PREDICTED: sodium/potassium-transporting ATPase subunit alpha-4 isoform X2 [Canis lupus familiaris]
gi|73953093	31559	0.52	PREDICTED: voltage-dependent anion-selective channel protein 2 isoform 2 [Canis lupus familiaris]
gi|345807347	134128	0.03	PREDICTED: plasma membrane calcium-transporting ATPase 3 isoform X36 [Canis lupus familiaris]

gi|126723018	30722	2.38	voltage-dependent anion-selective channel protein 1 [Oryctolagus cuniculus]
gi|74008194	32996	1.47	PREDICTED: ADP/ATP translocase 2 isoform 2 [Canis lupus familiaris]
gi|545559996	32512	1.5	PREDICTED: ADP/ATP translocase 3 [Canis lupus familiaris]
gi|73965153	83507	0.05	PREDICTED: vesicle-fusing ATPase isoformX1 [Canis lupus familiaris]
gi|325301273	18932	0.95	translocon-associated protein subunit delta precursor [Canis lupus familiaris]
gi|545560056	17447	0.27	PREDICTED: proteolipid protein 2 [Canis lupus familiaris]
gi|73963665	24765	0.19	PREDICTED: transmembrane emp24 domain-containing protein 10 isoform 1 [Canis lupus familiaris]
gi|6002950	66639	0.07	triadin isoform 3 [Canis lupus familiaris]
gi|545504506	278817	0.02	PREDICTED: voltage-dependent R-type calcium channel subunit alpha-1E isoformX3 [Canis lupus familiaris]
gi|73959904	61702	0.07	PREDICTED: potassium voltage-gated channel subfamily A member 10 [Canis lupus familiaris]
gi|545489180	93799	0.05	PREDICTED: transmembrane channel-like 1 [Canis lupus familiaris]
gi|30410788	39650	0.11	tumor suppressor candidate 3 isoform a precursor [Homo sapiens]
gi|73967844	94035	0.05	PREDICTED: leucine-rich repeat-containing protein 8A isoformX1 [Canis lupus familiaris]

gi|545516959	73609	0.12	PREDICTED: polycystic kidney disease 2-like 2 protein isoform X2 [Canis lupus familiaris]
gi|4557469	104486	0.04	AP-2 complex subunit beta isoform b [Homo sapiens]
gi|345781116	111392	0.04	PREDICTED: anoctamin-4 isoformX1 [Canis lupus familiaris]
gi|73998421	94181	0.05	PREDICTED: metal transporter CNNM2 isoformX4 [Canis lupus familiaris]
gi|545547011	22720	0.2	PREDICTED: V-type proton ATPase subunit E 1 isoform X2 [Canis lupus familiaris]
gi|22759019	141456	0.03	multidrug resistance p-glycoprotein [Canis lupus familiaris]
gi|73979747	43639	0.1	PREDICTED: V-type proton ATPase subunit C 2 isoformX1 [Canis lupus familiaris]
gi|545531548	121210	0.04	PREDICTED: anoctamin-1 [Canis lupus familiaris]
gi|345801671	26040	0.18	PREDICTED: transmembrane emp24 domain-containing protein 5 isoform 2 [Canis lupus familiaris]
gi|359321467	136023	0.03	PREDICTED: anion exchange protein 2 isoform 1 [Canis lupus familiaris]
gi|345782667	11210	0.45	PREDICTED: protein S100-A10 isoform 1 [Canis lupus familiaris]
gi|73997059	47923	0.09	PREDICTED: ATP-sensitive inward rectifier potassium channel 8 isoformX1 [Canis lupus familiaris]
gi|545537221	52108	0.09	PREDICTED: synaptotagmin-9 [Canis lupus familiaris]

gi|6753074	49623	0.09	AP-2 complex subunit mu [Mus musculus]
gi|345800844	45731	0.1	PREDICTED: vesicle amine transport protein 1 homolog (T. californica)-like [Canis lupus familiaris]
gi|545491848	44646	0.1	PREDICTED: NIPA-like protein 3 isoform X1 [Canis lupus familiaris]
gi|73983332	61656	0.07	PREDICTED: solute carrier family 22 member 9 isoformX1 [Canis lupus familiaris]
gi|73953291	36136	0.13	PREDICTED: graves disease carrier protein isoform X2 [Canis lupus familiaris]
gi|559098415	90911	0.05	sodium/hydrogen exchanger 1 [Canis lupus familiaris]
gi|270288810	107786	0.04	anoctamin-5 precursor [Canis lupus familiaris]
gi|6755588	23300	0.2	synaptosomal-associated protein 25 isoform a [Mus musculus]
gi|345795474	141471	0.03	PREDICTED: trafficking protein particle complex subunit 10 isoform X2 [Canis lupus familiaris]
gi|545494271	78141	0.06	PREDICTED: sodium-dependent phosphate transport protein 2B isoform X2 [Canis lupus familiaris]
gi|55741729	220559	0.02	sodium channel protein type 10 subunit alpha [Canis lupus familiaris]
gi|73979590	128727	0.03	PREDICTED: trafficking protein particle complex subunit 11 [Canis lupus familiaris]
gi|73979536	31206	0.15	PREDICTED: neuronal membrane glycoprotein M6-a isoform 1 [Canis lupus familiaris]

gi|545510114	184849	0.02	PREDICTED: ATP-binding cassette sub-family A member 6 [Canis lupus familiaris]

ST 3-4: Immune Complex Proteins Identified

Accession	Mass	emPAI	Description
gi|122135	40437	0.11	RecName: Full=DLA class I histocompatibility antigen, A9/A9 alpha chain; Flags: Precursor
gi|208342202	15306	0.32	immunoglobulin heavy chain variable region, partial [Canis lupus familiaris]
gi|545493610	148085	0.03	PREDICTED: pro-interleukin-16 isoform X2 [Canis lupus familiaris]
gi|350543372	10740	0.47	MHC class II antigen [Canis lupus familiaris]
gi|345783307	72501	0.06	PREDICTED: T-cell differentiation antigen CD6 isoform X4 [Canis lupus familiaris]
gi|545509559	20851	0.22	PREDICTED: CMRF35-like molecule 7-like [Canis lupus familiaris]
gi|74007037	64149	0.07	PREDICTED: melanoma-associated antigen D2 isoformX2 [Canis lupus familiaris]
gi|6572519	32245	0.14	truncated B7-2 protein [Canis lupus familiaris]
gi|57112869	28042	0.16	PREDICTED: B-cell receptor-associated protein 31 isoform X3 [Canis lupus familiaris]
gi|545514193	87364	0.05	PREDICTED: interleukin-1 receptor-associated kinase 3 [Canis lupus familiaris]

gi|70794790	96206	0.05	interleukin-12 receptor subunit beta-2 precursor [Canis lupus familiaris]

ST 3-5: GPCRs and G proteins identified

Accession	Mass	emPAI	Description
gi|5174447	35055	1.08	guanine nucleotide-binding protein subunit beta-2-like 1 [Homo sapiens]
gi|50979222	40520	0.37	guanine nucleotide-binding protein G(i) subunit alpha-2 [Canis lupus familiaris]
gi|545506467	50860	0.18	PREDICTED: LOW QUALITY PROTEIN: guanine nucleotide-binding protein G(olf) subunit alpha [Canis lupus familiaris]
gi|55742672	37120	0.12	guanine nucleotide-binding protein G(I)/G(S)/G(T) subunit beta-3 [Canis lupus familiaris]
gi|345777861	36294	0.12	PREDICTED: olfactory receptor 13F1-like [Canis lupus familiaris]
gi|545510010	33160	0.14	PREDICTED: guanine nucleotide-binding protein subunit alpha-13 isoform X1 [Canis lupus familiaris]
gi|74009012	328348	0.01	PREDICTED: probable G-protein coupled receptor 112 [Canis lupus familiaris]
gi|545523201	34864	0.13	PREDICTED: olfactory receptor 2T27-like [Canis lupus familiaris]
gi|73985077	21585	0.48	PREDICTED: PRA1 family protein 3 [Canis lupus familiaris]

gi|72535184	20414	0.23	ADP-ribosylation factor-like protein 1 [Sus scrofa]
gi|545509639	71038	0.06	PREDICTED: septin-9 [Canis lupus familiaris]
gi|77736007	20515	0.23	ADP-ribosylation factor 4 [Bos taurus]
gi|545545958	144009	0.03	PREDICTED: DENN domain-containing protein 5B [Canis lupus familiaris]
gi|73985028	124393	0.04	PREDICTED: SLIT-ROBO Rho GTPase-activating protein 3 isoformX2 [Canis lupus familiaris]
gi|73966150	257794	0.02	PREDICTED: probable G-protein coupled receptor 179 isoform X3 [Canis lupus familiaris]
gi|511914243	26132	0.18	PREDICTED: GTPase KRas isoform X1 [Mustela putorius furo]
gi|6981476	20467	0.23	GTP-binding protein Rheb precursor [Rattus norvegicus]
gi|345793806	46359	0.1	PREDICTED: probable G-protein coupled receptor 151 [Canis lupus familiaris]
gi|545539728	215508	0.02	PREDICTED: ral GTPase-activating protein subunit alpha-2 isoform X1 [Canis lupus familiaris]
gi|345807071	38241	0.12	PREDICTED: probable G-protein coupled receptor 82 [Canis lupus familiaris]
gi|359320566	51114	0.09	PREDICTED: rab-3A-interacting protein isoform X6 [Canis lupus familiaris]
gi|73983774	58829	0.08	PREDICTED: atlastin-3 isoform X4 [Canis lupus familiaris]
gi|345788827	38635	0.12	PREDICTED: growth hormone-regulated TBC protein 1 [Canis lupus familiaris]

gi|545522667	101092	0.04	PREDICTED: rap guanine nucleotide exchange factor 5 isoform X2 [Canis lupus familiaris]
gi|545529658	59449	0.07	PREDICTED: synembryn-A [Canis lupus familiaris]
gi|545541279	45440	0.1	PREDICTED: histamine H3 receptor, partial [Canis lupus familiaris]
gi|545497487	129263	0.03	PREDICTED: rho GTPase-activating protein 20 isoform X1 [Canis lupus familiaris]
gi|545516132	139898	0.03	PREDICTED: TBC1 domain family member 9B isoform X1 [Canis lupus familiaris]
gi|545555224	101745	0.04	PREDICTED: rap guanine nucleotide exchange factor 4 isoform X1 [Canis lupus familiaris]
gi|545548334	71664	0.06	PREDICTED: rho GTPase-activating protein 22 [Canis lupus familiaris]
gi|194339213	9761	0.53	dynanmin 1 protein [Canis lupus familiaris]
gi|345793422	139573	0.03	PREDICTED: LOW QUALITY PROTEIN: probable G-protein coupled receptor 158 [Canis lupus familiaris]
gi|73971093	54255	0.08	PREDICTED: protein C9orf72 isoformX2 [Canis lupus familiaris]
gi|545516757	51263	0.09	PREDICTED: septin-8 isoform X1 [Canis lupus familiaris]
gi|545543197	53123	0.08	PREDICTED: septin-2 isoform X1 [Canis lupus familiaris]
gi|8926588	48722	0.09	endothelin B receptor [Canis lupus familiaris]
gi|131804	22555	0.76	RecName: Full=Ras-related protein Rab-10 [Canis lupus familiaris]
gi|13569962	22157	0.77	ras-related protein Rab-1B [Homo sapiens]

gi|50979156	23505	0.2	ras-related protein Rab-7a [Canis lupus familiaris]
gi|50979062	23441	0.2	ras-related protein Rab-5C [Canis lupus familiaris]
gi|4506413	20974	0.22	ras-related protein Rap-1A precursor [Homo sapiens]
gi|4758984	24378	0.19	ras-related protein Rab-11A isoform 1 [Homo sapiens]
gi|345785574	103197	0.04	PREDICTED: ras-interacting protein 1 isoform 1 [Canis lupus familiaris]
gi|545548447	143013	0.03	PREDICTED: LOW QUALITY PROTEIN: protein very KIND [Canis lupus familiaris]
gi|545525085	55435	0.08	PREDICTED: ras association domain-containing protein 9 [Canis lupus familiaris]
gi|9845511	21436	0.22	ras-related C3 botulinum toxin substrate 1 isoform Rac1 [Homo sapiens]

ST 3-6: Chaperone proteins identified

Accession	Mass	emPAI	Description
gi|545508859	72881	0.42	PREDICTED: heat shock protein HSP 90-alpha, partial [Canis lupus familiaris]
gi|545500762	58230	0.25	PREDICTED: T-complex protein 1 subunit zeta [Canis lupus familiaris]
gi|359323746	59559	0.24	PREDICTED: LOW QUALITY PROTEIN: T-complex protein 1 subunit epsilon isoform 1 [Canis lupus familiaris]
gi|159794954	76432	0.66	Chain A, Structure Of Full Length Grp94 With Amp-Pnp Bound
gi|545550950	77756	0.06	PREDICTED: T-complex protein 1 subunit theta isoform X2 [Canis lupus familiaris]

gi|345802573	60589	0.07	PREDICTED: T-complex protein 1 subunit gamma isoform 1 [Canis lupus familiaris]
gi|73980527	59383	0.07	PREDICTED: T-complex protein 1 subunit eta isoform 2 [Canis lupus familiaris]
gi|57032236	60216	0.07	PREDICTED: T-complex protein 1 subunit alpha isoformX1 [Canis lupus familiaris]
gi|73968673	57395	0.16	PREDICTED: T-complex protein 1 subunit beta isoformX1 [Canis lupus familiaris]

ST- Receptors identified

Accession	Mass	emPAI	Description
gi|3641357	11736	0.42	interferon gamma precursor [Canis lupus familiaris]
gi|545534382	88794	0.05	PREDICTED: EGF-like module-containing mucin-like hormone receptor-like 2-like isoform X1 [Canis lupus familiaris]
gi|73970497	114071	0.04	PREDICTED: semaphorin-6A isoformX2 [Canis lupus familiaris]
gi|73998651	92273	0.05	PREDICTED: semaphorin-4G isoform X4 [Canis lupus familiaris]
gi|545536637	36244	0.12	PREDICTED: LOW QUALITY PROTEIN: gastrin/cholecystokinin type B receptor, partial [Canis lupus familiaris]
gi|73993667	53592	0.08	PREDICTED: scavenger receptor class A member 5 isoformX1 [Canis lupus familiaris]

gi|545518755	96015	0.05	PREDICTED: metabotropic glutamate receptor 4 [Canis lupus familiaris]
gi|50979238	39187	0.12	C5a anaphylatoxin chemotactic receptor 1 [Canis lupus familiaris]
gi|545552715	125167	0.07	PREDICTED: ephrin type-A receptor 3 [Canis lupus familiaris]
gi|73962317	227388	0.02	PREDICTED: thyroid receptor-interacting protein 11 isoform X2 [Canis lupus familiaris]
gi|359322039	312091	0.01	PREDICTED: inositol 1,4,5-trisphosphate receptor type 1 isoform X1 [Canis lupus familiaris]
gi|73966275	63426	0.07	PREDICTED: insulin-like growth factor 2 mRNA binding protein 1 isoformX2 [Canis lupus familiaris]
gi|545543633	51208	0.09	PREDICTED: LOW QUALITY PROTEIN: hydroxycarboxylic acid receptor 3 [Canis lupus familiaris]
gi|545517466	222263	0.02	PREDICTED: protein unc-13 homolog B isoform X2 [Canis lupus familiaris]
gi|545548378	118345	0.04	PREDICTED: VPS10 domain-containing receptor SorCS1 [Canis lupus familiaris]
gi|545522902	50679	0.09	PREDICTED: corticotropin-releasing factor receptor 2 isoform X3 [Canis lupus familiaris]
gi|359318678	564218	0.01	PREDICTED: ryanodine receptor 1 isoform 1 [Canis lupus familiaris]
gi|359319428	107139	0.04	PREDICTED: glutamate receptor ionotropic, kainate 4 [Canis lupus familiaris]
gi|73959181	165177	0.03	PREDICTED: glutamate receptor ionotropic, NMDA 2A isoform X3 [Canis lupus familiaris]

gi|545506274	81668	0.11	PREDICTED: collectin-12 [Canis lupus familiaris]
gi|545555520	130753	0.03	PREDICTED: sperm-specific antigen 2, partial [Canis lupus familiaris]
gi|73987612	29284	0.16	PREDICTED: basigin [Canis lupus familiaris]
gi|345796108	87112	0.1	PREDICTED: integrin beta-5 [Canis lupus familiaris]
gi|545555528	118416	0.04	PREDICTED: integrin alpha-V isoform 2 [Canis lupus familiaris]

ST- 3-8 : Enzymes identified

Accession	Mass	emPAI	Description
gi|73958481	39478	1.65	PREDICTED: fructose-bisphosphate aldolase A isoformX2 [Canis lupus familiaris]
gi|73947982	62798	0.07	PREDICTED: glucose-6-phosphate isomerase isoformX1 [Canis lupus familiaris]
gi|308082020	26698	0.17	triosephosphate isomerase [Canis lupus familiaris]
gi|345800677	48956	0.19	PREDICTED: LOW QUALITY PROTEIN: alpha-enolase isoform 1 [Canis lupus familiaris]
gi|359321459	72351	0.06	PREDICTED: protein disulfide-isomerase A4 isoform 3 [Canis lupus familiaris]
gi|73980965	92301	0.05	PREDICTED: mannosyl-oligosaccharide glucosidase [Canis lupus familiaris]
gi|71043798	44292	0.21	cathepsin D precursor [Canis lupus familiaris]
gi|73965482	56737	0.08	PREDICTED: glycylpeptide N-tetradecanoyltransferase 1 isoformX1 [Canis lupus familiaris]

gi|545505244	76224	0.06	PREDICTED: calpain-2 catalytic subunit [Canis lupus familiaris]
gi|545529547	134832	0.03	PREDICTED: membrane-associated guanylate kinase, WW and PDZ domain-containing protein 2 [Canis lupus familiaris]
gi|359319350	34044	0.28	PREDICTED: cyclin-dependent kinase 1 isoformX1 [Canis lupus familiaris]
gi|11345462	20301	0.23	signal peptidase complex subunit 3 [Homo sapiens]
gi|73973859	150034	0.06	PREDICTED: inhibitor of Bruton tyrosine kinase isoform X5 [Canis lupus familiaris]
gi|5002350	42651	0.11	alkaline phosphatase [Canis lupus familiaris]
gi|73949883	123762	0.07	PREDICTED: phosphorylase b kinase regulatory subunit beta isoformX2 [Canis lupus familiaris]
gi|545552304	61205	0.07	PREDICTED: calcium/calmodulin-dependent protein kinase type II subunit delta isoform X2 [Canis lupus familiaris]
gi|359323733	239523	0.02	PREDICTED: basic helix-loop-helix domain-containing protein KIAA2018 homolog isoform X1 [Canis lupus familiaris]
gi|545513543	77724	0.06	PREDICTED: sulfhydryl oxidase 2 [Canis lupus familiaris]
gi|74007716	136827	0.03	PREDICTED: phosphorylase b kinase regulatory subunit alpha, skeletal muscle isoform isoformX5 [Canis lupus familiaris]
gi|73975797	40015	0.11	PREDICTED: serum paraoxonase/arylesterase 1 isoform 2 [Canis lupus familiaris]

gi|545486104	155818	0.03	PREDICTED: PH domain leucine-rich repeat-containing protein phosphatase 1 [Canis lupus familiaris]
gi|545507539	169948	0.03	PREDICTED: leucine-rich repeat-containing protein 9-like isoform X1 [Canis lupus familiaris]
gi|345780013	101930	0.04	PREDICTED: staphylococcal nuclease domain-containing protein 1 [Canis lupus familiaris]
gi|73950291	573081	0.02	PREDICTED: E3 ubiquitin-protein ligase UBR4 isoformX2 [Canis lupus familiaris]
gi|545508966	50665	0.09	PREDICTED: casein kinase I isoform delta isoform X1 [Canis lupus familiaris]
gi|545559938	63644	0.07	PREDICTED: glucose-6-phosphate 1-dehydrogenase isoform X1 [Canis lupus familiaris]
gi|74005468	104700	0.04	PREDICTED: GPI inositol-deacylase isoform X2 [Canis lupus familiaris]
gi|73979309	29068	0.16	PREDICTED: phosphatidate phosphatase PPAPDC1B isoform X2 [Canis lupus familiaris]
gi|345777094	88480	0.05	PREDICTED: transmembrane protease serine 6 isoform 2 [Canis lupus familiaris]
gi|345782357	87215	0.05	PREDICTED: vitamin K-dependent gamma-carboxylase isoform X2 [Canis lupus familiaris]
gi|545492172	215322	0.02	PREDICTED: microtubule-associated serine/threonine-protein kinase 4 [Canis lupus familiaris]
gi|545486178	181384	0.02	PREDICTED: mitogen-activated protein kinase kinase kinase 4 [Canis lupus familiaris]
gi|345782971	16804	0.29	PREDICTED: oligosaccharyltransferase complex subunit OSTC-like [Canis lupus familiaris]

gi|312283574	45486	0.1	hydroxysteroid dehydrogenase-like protein 2 [Canis lupus familiaris]
gi|73986266	36011	0.13	PREDICTED: very-long-chain enoyl-CoA reductase isoform 2 [Canis lupus familiaris]
gi|359322989	107203	0.04	PREDICTED: serine/threonine-protein kinase ULK1 isoform X2 [Canis lupus familiaris]
gi|545541538	29373	0.16	PREDICTED: cathepsin Z, partial [Canis lupus familiaris]
gi|73976741	51421	0.09	PREDICTED: adenylyl cyclase-associated protein 1 isoformX2 [Canis lupus familiaris]
gi|545550634	60860	0.07	PREDICTED: carbohydrate sulfotransferase 14 [Canis lupus familiaris]
gi|73969530	83522	0.05	PREDICTED: protein kinase C epsilon type isoformX1 [Canis lupus familiaris]
gi|545528333	523742	0.01	PREDICTED: baculoviral IAP repeat-containing protein 6 [Canis lupus familiaris]
gi|545531571	84382	0.05	PREDICTED: N-acetylated alpha-linked acidic dipeptidase-like 1 [Canis lupus familiaris]
gi|545535937	45964	0.1	PREDICTED: endonuclease domain-containing 1 protein, partial [Canis lupus familiaris]
gi|545511447	81119	0.05	PREDICTED: myeloperoxidase [Canis lupus familiaris]
gi|74005739	132463	0.03	PREDICTED: tubulin polyglutamylase TTLL4 isoform X3 [Canis lupus familiaris]
gi|545532775	97866	0.04	PREDICTED: LOW QUALITY PROTEIN: tubulin monoglycylase TTLL3 [Canis lupus familiaris]

gi|73990288	42108	0.11	PREDICTED: caspase-14-like [Canis lupus familiaris]
gi|399317	130240	0.03	RecName: Full=Adenylate cyclase type 6; AltName: Full=ATP pyrophosphate-lyase 6; AltName: Full=Adenylate cyclase type VI; AltName: Full=Adenylyl cyclase 6; AltName: Full=Ca(2+)-inhibitable adenylyl cyclase
gi|545512439	160241	0.03	PREDICTED: patatin-like phospholipase domain containing 7 isoformX1 [Canis lupus familiaris]
gi|545554163	127509	0.03	PREDICTED: phospholipase D1 [Canis lupus familiaris]
gi|74006997	27138	0.37	PREDICTED: 3-hydroxyacyl-CoA dehydrogenase type-2 isoform 1 [Canis lupus familiaris]
gi|558515998	88111	0.05	carnitine O-palmitoyltransferase 1, liver isoform [Canis lupus familiaris]
gi|73983265	138671	0.03	PREDICTED: 1-phosphatidylinositol 4,5-bisphosphate phosphodiesterase beta-3 isoformX2 [Canis lupus familiaris]
gi|212276080	258715	0.02	1-phosphatidylinositol-4,5-bisphosphate phosphodiesterase epsilon-1 [Canis lupus familiaris]
gi|545510617	49679	0.09	PREDICTED: 2',3'-cyclic-nucleotide 3'-phosphodiesterase isoform X1 [Canis lupus familiaris]
gi|545529305	88247	0.05	PREDICTED: calcium-independent phospholipase A2-gamma isoform X2 [Canis lupus familiaris]
gi|359320296	61456	0.07	PREDICTED: GPI transamidase component PIG-S [Canis lupus familiaris]

ST- 3-9: Other Proteins Identified

Accession	Mass	emPAI	Description
gi|345806081	72238	1.59	PREDICTED: 78 kDa glucose-regulated protein isoform 5 [Canis lupus familiaris]
gi|73971240	38546	0.74	PREDICTED: stomatin (EPB72)-like 2 isoform 1 [Canis lupus familiaris]
gi|345800374	42267	0.22	PREDICTED: plasminogen activator inhibitor 1 RNA-binding protein isoform 1 [Canis lupus familiaris]
gi|335286672	22363	0.46	PREDICTED: transgelin-2 isoformX1 [Sus scrofa]
gi|73968397	20542	0.23	PREDICTED: protein canopy homolog 2 isoformX1 [Canis lupus familiaris]
gi|545543609	46653	0.1	PREDICTED: LOW QUALITY PROTEIN: ADP-ribosylation-like factor 6 interacting protein 4 [Canis lupus familiaris]
gi|73994424	154240	0.03	PREDICTED: protein strawberry notch homolog 1 isoformX2 [Canis lupus familiaris]
gi|134031952	60903	0.07	suppressor of tumorigenicity 7 protein isoform 1 [Mus musculus]
gi|50979076	31956	0.14	translocon-associated protein subunit alpha precursor [Canis lupus familiaris]
gi|73945930	58023	0.25	PREDICTED: protein ERGIC-53 isoform X2 [Canis lupus familiaris]
gi|73989504	44247	0.34	PREDICTED: lysosome-associated membrane glycoprotein 1 isoformX1 [Canis lupus familiaris]

gi|57096757	103880	0.04	PREDICTED: transmembrane and TPR repeat-containing protein 3 isoform X2 [Canis lupus familiaris]
gi|345793179	35777	0.13	PREDICTED: regulator of microtubule dynamics protein 1 isoform X3 [Canis lupus familiaris]
gi|545511167	43137	0.1	PREDICTED: alpha-sarcoglycan isoform X1 [Canis lupus familiaris]
gi|545536806	98933	0.04	PREDICTED: protein MRVI1 isoform X1 [Canis lupus familiaris]
gi|545492524	75786	0.06	PREDICTED: erythrocyte membrane protein band 4.1 like 4A isoform X1 [Canis lupus familiaris]
gi|545526766	385163	0.01	PREDICTED: CUB and sushi domain-containing protein 1 [Canis lupus familiaris]
gi|73996813	73879	0.06	PREDICTED: dendrin isoform X4 [Canis lupus familiaris]
gi|345791006	137207	0.03	PREDICTED: LOW QUALITY PROTEIN: probable tumor suppressor protein MN1 [Canis lupus familiaris]
gi|359319183	44586	0.1	PREDICTED: arrestin domain-containing protein 4 [Canis lupus familiaris]
gi|345780090	451207	0.01	PREDICTED: A-kinase anchor protein 9 isoform X3 [Canis lupus familiaris]
gi|545549726	278230	0.02	PREDICTED: spatacsin isoform X1 [Canis lupus familiaris]
gi|545489348	274118	0.03	PREDICTED: WD repeat-containing protein 87 [Canis lupus familiaris]
gi|73982258	34069	0.13	PREDICTED: thioredoxin-related transmembrane protein 2 isoform 1 [Canis lupus familiaris]

gi|73968452	55145	0.08	PREDICTED: transmembrane protein 194A [Canis lupus familiaris]
gi|545503669	129290	0.07	PREDICTED: nodal modulator 1 [Canis lupus familiaris]
gi|545520844	125995	0.03	PREDICTED: arf-GAP with SH3 domain, ANK repeat and PH domain-containing protein 1 isoform X1 [Canis lupus familiaris]
gi|545537743	75354	0.12	PREDICTED: sciellin isoform X9 [Canis lupus familiaris]
gi|545540568	101633	0.04	PREDICTED: disks large-associated protein 4 isoform X10 [Canis lupus familiaris]
gi|545555959	122466	0.04	PREDICTED: partitioning defective 3 homolog B isoform X6 [Canis lupus familiaris]
gi|545491435	63031	0.07	PREDICTED: alpha-taxilin [Canis lupus familiaris]
gi|545486029	53932	0.08	PREDICTED: transmembrane protein 200A [Canis lupus familiaris]
gi|57104550	55115	0.08	PREDICTED: growth/differentiation factor 5 [Canis lupus familiaris]
gi|545511186	111858	0.04	PREDICTED: LOW QUALITY PROTEIN: MYCBP-associated protein [Canis lupus familiaris]
gi|73950747	27566	0.17	PREDICTED: transmembrane protein 51 isoform X6 [Canis lupus familiaris]
gi|545534941	120365	0.04	PREDICTED: A disintegrin and metalloproteinase with thrombospondin motifs 10 isoform X2 [Canis lupus familiaris]
gi|73969963	74150	0.06	PREDICTED: DCC-interacting protein 13-beta isoformX2 [Canis lupus familiaris]

gi|545495448	29205	0.16	PREDICTED: surfactant protein A1 isoform 1 [Canis lupus familiaris]
gi|545551868	400894	0.01	PREDICTED: WD repeat and FYVE domain-containing protein 3 isoformX1 [Canis lupus familiaris]

ST4: Proteomics data of plasma membrane protein from HMPOS

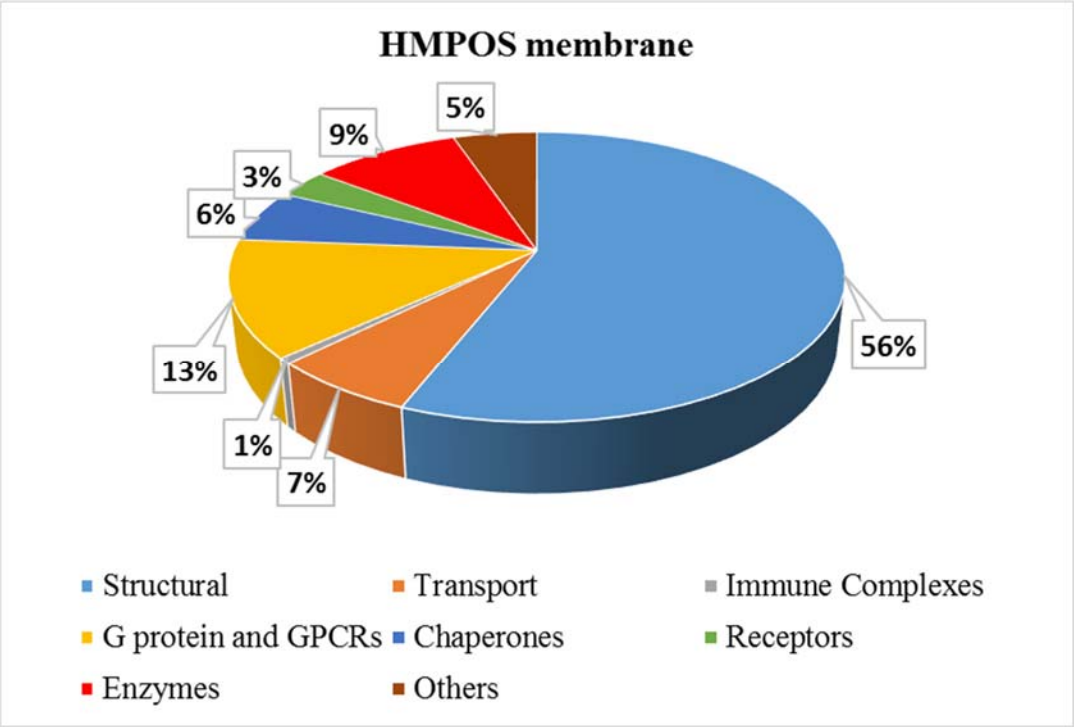

ST4-1. Overall proteomic profile

	emPAI	Percentage
Structural	41.72	56.01
Transport	4.91	6.59
Immune Complexes	0.46	0.62
G protein and GPCRs	9.7	13.02

Chaperones	4.39	5.89
Receptors	2.41	3.24
Enzymes	7	9.40
Others	3.9	5.24
Total	74.49	100

ST4-2: Structural Proteins Identified

Accession	Mass	emPAI	Description
gi|50950177	38630	6.43	annexin A2 [Canis lupus familiaris]
gi|61740600	57676	1.46	keratin, type I cytoskeletal 10 [Canis lupus familiaris]
gi|545510666	54047	0.89	PREDICTED: keratin, type I cytoskeletal 42 [Canis lupus familiaris]
gi|359279911	52279	0.94	keratin 14 [Canis lupus familiaris]
gi|73965817	51649	0.95	PREDICTED: keratin, type I cytoskeletal 16 [Canis lupus familiaris]
gi|359279916	43858	0.48	keratin, type I cytoskeletal 19 [Canis lupus familiaris]
gi|545538333	96812	0.09	PREDICTED: programmed cell death 6-interacting protein isoform X2 [Canis lupus familiaris]
gi|73974726	532579	0.21	PREDICTED: plectin isoformX1 [Canis lupus familiaris]
gi|4501885	41710	2.82	actin, cytoplasmic 1 [Homo sapiens]
gi|4501883	41982	1.05	actin, aortic smooth muscle [Homo sapiens]

gi|545490700	37169	1	PREDICTED: actin, beta-like 2 isoform X1 [Canis lupus familiaris]
gi|73973308	332597	0.44	PREDICTED: collagen alpha-1(XII) chain isoformX1 [Canis lupus familiaris]
gi|7106439	49639	1.84	tubulin beta-5 chain [Mus musculus]
gi|21361322	49554	1.39	tubulin beta-4A chain isoform 3 [Homo sapiens]
gi|21746161	49921	1.18	tubulin beta-2B chain [Mus musculus]
gi|50979272	63751	0.72	keratin, type II cytoskeletal 1 [Canis lupus familiaris]
gi|345791904	62778	0.41	PREDICTED: keratin, type II cytoskeletal 5 isoform X1 [Canis lupus familiaris]
gi|359323093	54684	0.37	PREDICTED: keratin, type II cytoskeletal 8 [Canis lupus familiaris]
gi|345791839	62832	0.41	PREDICTED: keratin, type II cytoskeletal 6A isoformX2 [Canis lupus familiaris]
gi|50979264	64527	0.31	keratin, type II cytoskeletal 2 epidermal [Canis lupus familiaris]
gi|545545402	51588	0.18	PREDICTED: keratin, type II cytoskeletal 7 [Canis lupus familiaris]
gi|545545370	63946	0.14	PREDICTED: keratin, type II cytoskeletal 73 isoform X1 [Canis lupus familiaris]
gi|34740335	50120	1.17	tubulin alpha-1B chain [Mus musculus]
gi|160425231	226328	0.21	myosin-9 [Canis lupus familiaris]
gi|558695394	38602	0.75	annexin A1 [Canis lupus familiaris]
gi|57100553	35921	0.82	PREDICTED: annexin A5 [Canis lupus familiaris]

gi|74004777	138356	0.21	PREDICTED: collagen alpha-1(III) chain isoform 2 [Canis lupus familiaris]
gi|359320831	269595	0.07	PREDICTED: talin-1 isoform X1 [Canis lupus familiaris]
gi|5031635	18491	0.58	cofilin-1 [Homo sapiens]
gi|74005014	131810	0.03	PREDICTED: unconventional myosin-Ib isoformX2 [Canis lupus familiaris]
gi|545558304	69724	0.06	PREDICTED: moesin isoform X3 [Canis lupus familiaris]
gi|460417294	41977	0.11	actin-related protein 3 isoform 2 [Homo sapiens]
gi|545497795	19402	0.24	PREDICTED: profilin-1 [Canis lupus familiaris]
gi|301774268	33202	0.14	PREDICTED: tropomyosin alpha-3 chain-like isoform 1 [Ailuropoda melanoleuca]
gi|74008809	280450	0.06	PREDICTED: filamin-A isoform 2 [Canis lupus familiaris]
gi|545494454	47490	0.1	PREDICTED: lactadherin [Canis lupus familiaris]
gi|345782840	191681	0.02	PREDICTED: laminin subunit beta-4 [Canis lupus familiaris]
gi|345799205	288872	0.02	PREDICTED: LOW QUALITY PROTEIN: PDZ domain-containing protein 2 [Canis lupus familiaris]
gi|545497238	45641	0.1	PREDICTED: LOW QUALITY PROTEIN: adhesion molecule, interacts with CXADR antigen 1 [Canis lupus familiaris]
gi|115947174	222863	0.02	myosin-4 [Canis lupus familiaris]

gi|545510084	21109	0.22	PREDICTED: myosin heavy chain IB-like [Canis lupus familiaris]
gi|17986258	16919	0.65	myosin light polypeptide 6 isoform 1 [Homo sapiens]
gi|73969653	212837	0.04	PREDICTED: girdin isoformX2 [Canis lupus familiaris]
gi|545533702	55298	0.08	PREDICTED: amphoterin-induced protein 3 [Canis lupus familiaris]
gi|545557020	109812	0.04	PREDICTED: contactin-2 [Canis lupus familiaris]
gi|545531544	208611	0.02	PREDICTED: LOW QUALITY PROTEIN: SH3 and multiple ankyrin repeat domains protein 2 [Canis lupus familiaris]
gi|359322210	111999	0.04	PREDICTED: microtubule-associated protein 1S isoform X1 [Canis lupus familiaris]
gi|73968528	44390	0.1	PREDICTED: dynactin subunit 2 isoformX3 [Canis lupus familiaris]
gi|73987361	33365	0.14	PREDICTED: calponin-2 isoformX1 [Canis lupus familiaris]
gi|545555092	390848	0.01	PREDICTED: xin actin-binding repeat-containing protein 2 isoform X1 [Canis lupus familiaris]
gi|545544126	120433	0.04	PREDICTED: unconventional myosin-Ih [Canis lupus familiaris]
gi|5031571	44732	0.1	actin-related protein 2 isoform b [Homo sapiens]
gi|73947726	104337	0.04	PREDICTED: alpha-actinin-4 isoformX6 [Canis lupus familiaris]

gi|545502948	55287	0.08	PREDICTED: amphoterin-induced protein 1 [Canis lupus familiaris]
gi|545520371	200465	0.02	PREDICTED: laminin subunit alpha-4 [Canis lupus familiaris]
gi|545493680	57725	0.08	PREDICTED: ankyrin repeat domain-containing protein 34C [Canis lupus familiaris]
gi|545541615	77347	0.06	PREDICTED: cytoskeleton-associated protein 2 isoform X1 [Canis lupus familiaris]
gi|545550658	214431	0.02	PREDICTED: unconventional myosin-Vc [Canis lupus familiaris]
gi|345784082	555378	0.01	PREDICTED: uncharacterized protein KIAA1109 [Canis lupus familiaris]
gi|545508415	106733	0.04	PREDICTED: LOW QUALITY PROTEIN: nesprin-3 [Canis lupus familiaris]
gi|62122767	76308	0.06	keratin, type I cytoskeletal 9 [Canis lupus familiaris]
gi|545485411	134816	0.03	PREDICTED: jouberin isoform X1 [Canis lupus familiaris]
gi|356640238	43975	0.1	CKLF-like MARVEL transmembrane domain-containing protein 1 [Canis lupus familiaris]
gi|345788489	345423	0.01	PREDICTED: LOW QUALITY PROTEIN: protocadherin-16 [Canis lupus familiaris]
gi|545510084	21109	0.22	PREDICTED: myosin heavy chain IB-like [Canis lupus familiaris]
gi|359323649	117106	0.04	PREDICTED: SWI/SNF-related matrix-associated actin-dependent regulator of chromatin subfamily A containing DEAD/H box 1 isoform X1 [Canis lupus familiaris]

gi|545489749	257974	0.02	PREDICTED: supervillin isoform X3 [Canis lupus familiaris]
gi|95925865	87375	0.05	pinin 1 [Canis lupus familiaris]
gi|73953627	75842	0.33	PREDICTED: annexin A6 isoformX2 [Canis lupus familiaris]
gi|545490274	16537	0.29	PREDICTED: endothelial cell surface expressed chemotaxis and apoptosis regulator isoform X2 [Canis lupus familiaris]
gi|2499844	38043	0.12	RecName: Full=CD44 antigen; AltName: Full=Extracellular matrix receptor-III; Short=ECMR-III; AltName: Full=GP90 lymphocyte homing/adhesion receptor; AltName: Full=HUTCH-I; AltName: Full=Hermes antigen; AltName: Full=Hyaluronate receptor; AltName: Fu

ST 4-3: Transport Proteins Identified

Accession	Mass	emPAI	Description
gi|73953093	31559	1.26	PREDICTED: voltage-dependent anion-selective channel protein 2 isoform 2 [Canis lupus familiaris]
gi|126723018	30722	0.32	voltage-dependent anion-selective channel protein 1 [Oryctolagus cuniculus]
gi|345805068	90259	0.05	PREDICTED: transient receptor potential cation channel subfamily V member 3 isoform X2 [Canis lupus familiaris]

gi|73997059	47923	0.09	PREDICTED: ATP-sensitive inward rectifier potassium channel 8 isoformX1 [Canis lupus familiaris]
gi|545528359	112738	0.47	PREDICTED: sodium/potassium-transporting ATPase subunit alpha-1 isoform X1 [Canis lupus familiaris]
gi|73963665	24765	0.68	PREDICTED: transmembrane emp24 domain-containing protein 10 isoform 1 [Canis lupus familiaris]
gi|354459073	30749	0.15	voltage-dependent anion-selective channel protein 3 isoform 1 [Canis lupus familiaris]
gi|345787913	67489	0.07	PREDICTED: sodium-coupled monocarboxylate transporter 2 isoform 1 [Canis lupus familiaris]
gi|545495952	43843	0.1	PREDICTED: magnesium transporter NIPA4 [Canis lupus familiaris]
gi|73997059	47923	0.09	PREDICTED: ATP-sensitive inward rectifier potassium channel 8 isoformX1 [Canis lupus familiaris]
gi|545495894	175252	0.05	PREDICTED: probable phospholipid-transporting ATPase VB isoform X1 [Canis lupus familiaris]
gi|5031569	42587	0.11	alpha-centractin [Homo sapiens]
gi|74008791	71836	0.06	PREDICTED: sodium- and chloride-dependent neutral and basic amino acid transporter B(0+) [Canis lupus familiaris]
gi|73945930	58023	0.08	PREDICTED: protein ERGIC-53 isoform X2 [Canis lupus familiaris]
gi|545560056	17447	0.28	PREDICTED: proteolipid protein 2 [Canis lupus familiaris]
gi|545497820	149551	0.03	PREDICTED: LOW QUALITY PROTEIN: misshapen-like kinase 1 [Canis lupus familiaris]

gi|345792321	15429	0.31	PREDICTED: vesicle transport protein GOT1B [Canis lupus familiaris]
gi|345805068	90259	0.05	PREDICTED: transient receptor potential cation channel subfamily V member 3 isoform X2 [Canis lupus familiaris]
gi|545531227	579498	0.02	PREDICTED: LOW QUALITY PROTEIN: neuroblast differentiation-associated protein AHNAK [Canis lupus familiaris]
gi|73983713	85720	0.05	PREDICTED: vacuolar protein sorting-associated protein 51 homolog [Canis lupus familiaris]
gi|73979536	31206	0.15	PREDICTED: neuronal membrane glycoprotein M6-a isoform 1 [Canis lupus familiaris]
gi|545522646	121825	0.04	PREDICTED: LOW QUALITY PROTEIN: multidrug resistance protein 1 [Canis lupus familiaris]
gi|50978854	61427	0.07	excitatory amino acid transporter 4 [Canis lupus familiaris]
gi|50979327	50151	0.09	equilibrative nucleoside transporter 1 [Canis lupus familiaris]
gi|545539571	29641	0.16	PREDICTED: sodium/potassium-transporting ATPase subunit beta-3, partial [Canis lupus familiaris]
gi|73956324	58186	0.08	PREDICTED: non-specific lipid-transfer protein isoformX3 [Canis lupus familiaris]

ST 4-3: Immune Complexes identified

Accession	Mass	emPAI	Description
gi|345807015	79859	0.06	PREDICTED: interleukin 1 receptor accessory protein-like 1 [Canis lupus familiaris]

gi|3334903	47844	0.09	endothelin receptor B [Canis lupus familiaris]
gi|545548378	118345	0.04	PREDICTED: VPS10 domain-containing receptor SorCS1 [Canis lupus familiaris]
gi|345787413	66034	0.07	PREDICTED: coiled-coil domain-containing protein 36 isoform X1 [Canis lupus familiaris]
gi|345797884	43717	0.1	PREDICTED: V-set and immunoglobulin domain-containing protein 8 isoform X1 [Canis lupus familiaris]
gi|545515158	45807	0.1	PREDICTED: LIM and senescent cell antigen-like domains 1 isoform X5 [Canis lupus familiaris]

ST- 4-5: GPCRs and G proteins identified

Accession	Mass	emPAI	Description
gi|74009012	328348	0.03	PREDICTED: probable G-protein coupled receptor 112 [Canis lupus familiaris]
gi|545546307	47526	0.1	PREDICTED: probable G-protein coupled receptor 19 isoform X2 [Canis lupus familiaris]
gi|345807071	38241	0.12	PREDICTED: probable G-protein coupled receptor 82 [Canis lupus familiaris]
gi|345783859	35013	0.13	PREDICTED: olfactory receptor 4C11-like [Canis lupus familiaris]
gi|54607157	52344	0.09	5-hydroxytryptamine receptor 2A [Canis lupus familiaris]
gi|305410870	21597	0.48	membrane-associated progesterone receptor component 1 [Canis lupus familiaris]

gi|545531462	41785	0.11	PREDICTED: LOW QUALITY PROTEIN: olfactory receptor 5AK2 [Canis lupus familiaris]
gi|345783868	35060	0.13	PREDICTED: olfactory receptor 4C16-like [Canis lupus familiaris]
gi|545525474	51582	0.09	PREDICTED: muscarinic acetylcholine receptor M2 isoform X1 [Canis lupus familiaris]
gi|545506467	50860	0.09	PREDICTED: LOW QUALITY PROTEIN: guanine nucleotide-binding protein G(olf) subunit alpha [Canis lupus familiaris]
gi|5174447	35055	0.44	guanine nucleotide-binding protein subunit beta-2-like 1 [Homo sapiens]
gi|6680045	37353	0.12	guanine nucleotide-binding protein G(I)/G(S)/G(T) subunit beta-1 [Mus musculus]
gi|5174447	35055	0.44	guanine nucleotide-binding protein subunit beta-2-like 1 [Homo sapiens]
gi|73985077	21585	0.22	PREDICTED: PRA1 family protein 3 [Canis lupus familiaris]
gi|4506365	23531	0.2	ras-related protein Rab-2A isoform a [Homo sapiens]
gi|4502201	20684	0.51	ADP-ribosylation factor 1 [Homo sapiens]
gi|6680045	37353	0.12	guanine nucleotide-binding protein G(I)/G(S)/G(T) subunit beta-1 [Mus musculus]
gi|545532122	103408	0.04	PREDICTED: rab3 GTPase-activating protein catalytic subunit isoform X7 [Canis lupus familiaris]
gi|359322679	79430	0.06	PREDICTED: LOW QUALITY PROTEIN: rho GTPase-activating protein 40 [Canis lupus familiaris]

gi|345783868	35060	0.13	PREDICTED: olfactory receptor 4C16-like [Canis lupus familiaris]
gi|4758796	40517	0.11	developmentally-regulated GTP-binding protein 1 [Homo sapiens]
gi|73964747	23379	0.2	PREDICTED: rho GDP-dissociation inhibitor 1 isoform 2 [Canis lupus familiaris]
gi|545514178	82795	0.05	PREDICTED: arf-GAP with GTPase, ANK repeat and PH domain-containing protein 2 [Canis lupus familiaris]
gi|345783859	35013	0.13	PREDICTED: olfactory receptor 4C11-like [Canis lupus familiaris]
gi|545546307	47526	0.1	PREDICTED: probable G-protein coupled receptor 19 isoform X2 [Canis lupus familiaris]
gi|73991970	166752	0.03	PREDICTED: ral GTPase-activating protein subunit beta isoformX1 [Canis lupus familiaris]
gi|345807071	38241	0.12	PREDICTED: probable G-protein coupled receptor 82 [Canis lupus familiaris]
gi|545531462	41785	0.11	PREDICTED: LOW QUALITY PROTEIN: olfactory receptor 5AK2 [Canis lupus familiaris]
gi|545506467	50860	0.09	PREDICTED: LOW QUALITY PROTEIN: guanine nucleotide-binding protein G(olf) subunit alpha [Canis lupus familiaris]
gi|73997540	127936	0.03	PREDICTED: ELKS/Rab6-interacting/CAST family member 1 isoformX1 [Canis lupus familiaris]
gi|345780300	53816	0.08	PREDICTED: beta-chimaerin isoform 2 [Canis lupus familiaris]

gi|545546746	51893	0.09	PREDICTED: tubby-related protein 3 isoform X4 [Canis lupus familiaris]
gi|545516757	51263	0.09	PREDICTED: septin-8 isoform X1 [Canis lupus familiaris]
gi|545545931	101735	0.04	PREDICTED: FYVE, RhoGEF and PH domain-containing protein 4 isoform X2 [Canis lupus familiaris]
gi|73951551	189049	0.02	PREDICTED: IQ motif containing GTPase activating protein 1 [Canis lupus familiaris]
gi|73965285	93254	0.05	PREDICTED: axin-2 isoformX1 [Canis lupus familiaris]
gi|545509639	71038	0.06	PREDICTED: septin-9 [Canis lupus familiaris]
gi|3334903	47844	0.09	endothelin receptor B [Canis lupus familiaris]
gi|131804	22555	0.76	RecName: Full=Ras-related protein Rab-10 [Canis lupus familiaris]
gi|4506413	20974	0.5	ras-related protein Rap-1A precursor [Homo sapiens]
gi|50979062	23441	0.2	ras-related protein Rab-5C [Canis lupus familiaris]
gi|50979156	23505	0.72	ras-related protein Rab-7a [Canis lupus familiaris]
gi|345799503	52039	0.18	PREDICTED: ras GTPase-activating protein-binding protein 1 isoform 4 [Canis lupus familiaris]
gi|50979150	23644	0.2	ras-related protein Rab-5A [Canis lupus familiaris]
gi|545489193	52983	0.08	PREDICTED: SHC-transforming protein 3 [Canis lupus familiaris]

ST 3-6 Chaperone Proteins Identified

Accession	Mass	emPAI	Description
gi|57032236	60216	0.54	PREDICTED: T-complex protein 1 subunit alpha isoformX1 [Canis lupus familiaris]
gi|359320591	58002	0.45	PREDICTED: T-complex protein 1 subunit delta isoform X1 [Canis lupus familiaris]
gi|545500762	58230	0.45	PREDICTED: T-complex protein 1 subunit zeta [Canis lupus familiaris]
gi|345805760	53551	0.38	PREDICTED: T-complex protein 1 subunit zeta-2 isoform X3 [Canis lupus familiaris]
gi|345802573	60589	0.33	PREDICTED: T-complex protein 1 subunit gamma isoform 1 [Canis lupus familiaris]
gi|545550950	77756	0.18	PREDICTED: T-complex protein 1 subunit theta isoform X2 [Canis lupus familiaris]
gi|73968673	57395	0.35	PREDICTED: T-complex protein 1 subunit beta isoformX1 [Canis lupus familiaris]
gi|359323746	59559	0.16	PREDICTED: LOW QUALITY PROTEIN: T-complex protein 1 subunit epsilon isoform 1 [Canis lupus familiaris]
gi|545558786	48739	0.09	PREDICTED: LOW QUALITY PROTEIN: t-complex 11 family, X-linked 2 [Canis lupus familiaris]
gi|126352614	83185	0.6	heat shock protein HSP 90-beta [Equus caballus]
gi|545508859	72881	0.52	PREDICTED: heat shock protein HSP 90-alpha, partial [Canis lupus familiaris]

ST 4-7 Receptors Identified

Accession	Mass	emPAI	Description
gi|50978812	86594	0.11	transferrin receptor protein 1 [Canis lupus familiaris]
gi|50979256	122944	0.04	platelet-derived growth factor receptor beta precursor [Canis lupus familiaris]
gi|345806764	118927	0.04	PREDICTED: toll-like receptor 8 isoform X1 [Canis lupus familiaris]
gi|50979256	122944	0.04	platelet-derived growth factor receptor beta precursor [Canis lupus familiaris]
gi|73987612	29284	0.34	PREDICTED: basigin [Canis lupus familiaris]
gi|545509559	20851	0.23	PREDICTED: CMRF35-like molecule 7-like [Canis lupus familiaris]
gi|73979339	56856	0.08	PREDICTED: TELO2-interacting protein 2 isoform X2 [Canis lupus familiaris]
gi|545548378	118345	0.04	PREDICTED: VPS10 domain-containing receptor SorCS1 [Canis lupus familiaris]
gi|305410870	21597	0.48	membrane-associated progesterone receptor component 1 [Canis lupus familiaris]
gi|545501026	56949	0.08	PREDICTED: BAI1-associated protein 2-like 1 isoformX1 [Canis lupus familiaris]
gi|54607157	52344	0.09	5-hydroxytryptamine receptor 2A [Canis lupus familiaris]
gi|545546046	64112	0.07	PREDICTED: transmembrane 7 superfamily member 3 isoform X1 [Canis lupus familiaris]

gi|545528700	27220	0.17	PREDICTED: hemojuvelin isoform X3 [Canis lupus familiaris]
gi|345777328	131191	0.03	PREDICTED: LOW QUALITY PROTEIN: reticulon-4 isoform 1 [Canis lupus familiaris]
gi|545507543	165246	0.03	PREDICTED: leucine-rich repeat-containing protein 9-like isoform X3 [Canis lupus familiaris]
gi|57089795	32521	0.14	PREDICTED: vesicle-associated membrane protein-associated protein A isoform 1 [Canis lupus familiaris]
gi|74008133	117410	0.04	PREDICTED: angiomotin isoformX1 [Canis lupus familiaris]
gi|545518973	88005	0.05	PREDICTED: leucine-rich repeat and fibronectin type-III domain-containing protein 2 [Canis lupus familiaris]
gi|73966275	63426	0.07	PREDICTED: insulin-like growth factor 2 mRNA binding protein 1 isoformX2 [Canis lupus familiaris]
gi|545514112	60102	0.07	PREDICTED: receptor-type tyrosine-protein phosphatase R isoform X1 [Canis lupus familiaris]
gi|545548312	89310	0.05	PREDICTED: receptor-type tyrosine-protein phosphatase epsilon isoform X5 [Canis lupus familiaris]
gi|359318678	564218	0.01	PREDICTED: ryanodine receptor 1 isoform 1 [Canis lupus familiaris]
gi|545531508	146992	0.03	PREDICTED: receptor-type tyrosine-protein phosphatase eta [Canis lupus familiaris]
gi|545531508	146992	0.03	PREDICTED: receptor-type tyrosine-protein phosphatase eta [Canis lupus familiaris]
gi|345796108	87112	0.05	PREDICTED: integrin beta-5 [Canis lupus familiaris]

ST 4-8 Enzymes Identified

Accession	Mass	emPAI	Description
gi|545535631	133147	0.03	PREDICTED: LOW QUALITY PROTEIN: non-receptor tyrosine-protein kinase TYK2 [Canis lupus familiaris]
gi|73980394	48268	0.87	PREDICTED: protein disulfide-isomerase A6 [Canis lupus familiaris]
gi|73964749	57381	1.12	PREDICTED: protein disulfide-isomerase [Canis lupus familiaris]
gi|345800677	48956	0.55	PREDICTED: LOW QUALITY PROTEIN: alpha-enolase isoform 1 [Canis lupus familiaris]
gi|545547462	87343	0.22	PREDICTED: delta-1-pyrroline-5-carboxylate synthase isoform X3 [Canis lupus familiaris]
gi|74000476	23761	0.43	PREDICTED: peptidyl-prolyl cis-trans isomerase B isoform 2 [Canis lupus familiaris]
gi|545539262	87576	0.22	PREDICTED: procollagen-lysine,2-oxoglutarate 5-dioxygenase 2 isoform X2 [Canis lupus familiaris]
gi|359321459	72351	0.13	PREDICTED: protein disulfide-isomerase A4 isoform 3 [Canis lupus familiaris]
gi|545512792	124956	0.04	PREDICTED: protein phosphatase 1 regulatory subunit 26 isoform X1 [Canis lupus familiaris]
gi|345802152	68262	0.07	PREDICTED: serine/threonine-protein kinase PLK1 [Canis lupus familiaris]
gi|345799467	71888	0.06	PREDICTED: tyrosine-protein kinase ITK/TSK [Canis lupus familiaris]

gi|73954910	52795	0.09	PREDICTED: serine/threonine-protein kinase Chk1 [Canis lupus familiaris]
gi|545548312	89310	0.05	PREDICTED: receptor-type tyrosine-protein phosphatase epsilon isoform X5 [Canis lupus familiaris]
gi|545557037	116529	0.04	PREDICTED: serine/threonine-protein kinase MARK1 [Canis lupus familiaris]
gi|545555517	3901076	0	PREDICTED: LOW QUALITY PROTEIN: titin [Canis lupus familiaris]
gi|73980965	92301	0.05	PREDICTED: mannosyl-oligosaccharide glucosidase [Canis lupus familiaris]
gi|6755588	23300	0.2	synaptosomal-associated protein 25 isoform a [Mus musculus]
gi|545521006	120316	0.04	PREDICTED: focal adhesion kinase 1 isoform X3 [Canis lupus familiaris]
gi|308082020	26698	0.17	triosephosphate isomerase [Canis lupus familiaris]
gi|345803586	35294	0.13	PREDICTED: retinol dehydrogenase 11 isoform X3 [Canis lupus familiaris]
gi|345804359	31495	0.15	PREDICTED: thioredoxin-related transmembrane protein 1 [Canis lupus familiaris]
gi|345782889	204305	0.02	PREDICTED: LOW QUALITY PROTEIN: histone-lysine N-methyltransferase 2E isoform 1 [Canis lupus familiaris]
gi|545489174	204718	0.02	PREDICTED: proprotein convertase subtilisin/kexin type 5 [Canis lupus familiaris]

gi|545535534	158607	0.03	PREDICTED: membrane-associated guanylate kinase, WW and PDZ domain-containing protein 1 [Canis lupus familiaris]
gi|57110216	43734	0.1	PREDICTED: p21-activated protein kinase-interacting protein 1 [Canis lupus familiaris]
gi|74006997	27138	0.17	PREDICTED: 3-hydroxyacyl-CoA dehydrogenase type-2 isoform 1 [Canis lupus familiaris]
gi|545514789	72610	0.06	PREDICTED: TGF-beta-activated kinase 1 and MAP3K7-binding protein 1 isoformX1 [Canis lupus familiaris]
gi|73966592	133435	0.03	PREDICTED: myotubularin-related protein 4 isoformX1 [Canis lupus familiaris]
gi|73958481	39478	0.12	PREDICTED: fructose-bisphosphate aldolase A isoformX2 [Canis lupus familiaris]
gi|545544113	42798	0.11	PREDICTED: mevalonate kinase isoform X1 [Canis lupus familiaris]
gi|532164718	54008	0.08	serine/threonine-protein phosphatase 2A 56 kDa regulatory subunit epsilon isoform isoform b [Homo sapiens]
gi|73967304	152838	0.03	PREDICTED: carboxypeptidase D isoform 2 [Canis lupus familiaris]
gi|347889344	97560	0.05	thyrotropin-releasing hormone-degrading ectoenzyme [Canis lupus familiaris]
gi|545497443	77070	0.06	PREDICTED: serine/threonine-protein phosphatase 2A 65 kDa regulatory subunit A beta isoform isoform X4 [Canis lupus familiaris]

gi|545535631	133147	0.03	PREDICTED: LOW QUALITY PROTEIN: non-receptor tyrosine-protein kinase TYK2 [Canis lupus familiaris]
gi|74002818	57933	0.08	PREDICTED: serine/threonine-protein kinase PAK 2 isoform 1 [Canis lupus familiaris]
gi|73975797	40015	0.11	PREDICTED: serum paraoxonase/arylesterase 1 isoform 2 [Canis lupus familiaris]
gi|73978267	40232	0.11	PREDICTED: glycosyltransferase 8 domain-containing protein 2 isoform X4 [Canis lupus familiaris]
gi|345790993	51995	0.09	PREDICTED: adenosine monophosphate-protein transferase FICD isoform X3 [Canis lupus familiaris]
gi|545511519	105714	0.04	PREDICTED: E3 ubiquitin-protein ligase TRIM37 isoform X3 [Canis lupus familiaris]
gi|545508117	148451	0.03	PREDICTED: tubulin polyglutamylase TTLL5 isoform X1 [Canis lupus familiaris]
gi|545516121	77140	0.06	PREDICTED: glutamine--fructose-6-phosphate aminotransferase [isomerizing] 2 [Canis lupus familiaris]
gi|73970573	45905	0.1	PREDICTED: protein-lysine 6-oxidase isoformX1 [Canis lupus familiaris]
gi|73983265	138671	0.03	PREDICTED: 1-phosphatidylinositol 4,5-bisphosphate phosphodiesterase beta-3 isoformX2 [Canis lupus familiaris]
gi|74008407	40859	0.11	PREDICTED: palmitoyltransferase ZDHHC9 isoform 2 [Canis lupus familiaris]
gi|57098955	44852	0.1	PREDICTED: ceramide synthase 2 isoform 1 [Canis lupus familiaris]

gi|545546189	73137	0.06	PREDICTED: 1-phosphatidylinositol 4,5-bisphosphate phosphodiesterase zeta-1 isoform X1 [Canis lupus familiaris]
gi|359323381	134236	0.07	PREDICTED: 1-phosphatidylinositol 4,5-bisphosphate phosphodiesterase beta-2 isoform X1 [Canis lupus familiaris]
gi|171184453	17118	0.28	prostaglandin E synthase [Canis lupus familiaris]
gi|545558971	77661	0.06	PREDICTED: long-chain-fatty-acid--CoA ligase 4 isoform X5 [Canis lupus familiaris]
gi|545529305	88247	0.05	PREDICTED: calcium-independent phospholipase A2-gamma isoform X2 [Canis lupus familiaris]
gi|359323612	82513	0.05	PREDICTED: lanosterol synthase isoform 2 [Canis lupus familiaris]

ST 4-9: Other Proteins Identified

Accession	Mass	emPAI	Description
gi|73969959	65382	1.52	PREDICTED: cytoskeleton-associated protein 4 [Canis lupus familiaris]
gi|345779293	27846	0.17	PREDICTED: transmembrane protein 51 [Canis lupus familiaris]
gi|73971240	38546	0.25	PREDICTED: stomatin (EPB72)-like 2 isoform 1 [Canis lupus familiaris]
gi|73983875	26187	0.18	PREDICTED: transmembrane protein 109 isoform X4 [Canis lupus familiaris]

gi|73972968	114692	0.04	PREDICTED: GLTSCR1-like isoform X3 [Canis lupus familiaris]
gi|345792510	118933	0.04	PREDICTED: LOW QUALITY PROTEIN: kinesin family member 11 [Canis lupus familiaris]
gi|71043798	44292	0.1	cathepsin D precursor [Canis lupus familiaris]
gi|545497651	120425	0.04	PREDICTED: myb-binding protein 1A [Canis lupus familiaris]
gi|73984530	44862	0.21	PREDICTED: transmembrane protein 43 isoform 1 [Canis lupus familiaris]
gi|545508686	36342	0.13	PREDICTED: inverted formin-2 isoform X1 [Canis lupus familiaris]
gi|345777168	195291	0.02	PREDICTED: GRIP and coiled-coil domain-containing protein 2 [Canis lupus familiaris]
gi|4502549	16827	0.29	calmodulin [Homo sapiens]
gi|1353187	47337	0.1	RecName: Full=Zona pellucida sperm-binding protein 3; AltName: Full=Sperm receptor; AltName: Full=Zona pellucida glycoprotein 3; Short=Zp-3; AltName: Full=Zona pellucida protein C; Contains: RecName: Full=Processed zona pellucida sperm-binding prote
gi|545492234	473796	0.01	PREDICTED: LOW QUALITY PROTEIN: basement membrane-specific heparan sulfate proteoglycan core protein [Canis lupus familiaris]
gi|345800374	42267	0.11	PREDICTED: plasminogen activator inhibitor 1 RNA-binding protein isoform 1 [Canis lupus familiaris]
gi|545511186	111858	0.04	PREDICTED: LOW QUALITY PROTEIN: MYCBP-associated protein [Canis lupus familiaris]

gi|545502406	43027	0.11	PREDICTED: clusterin-associated protein 1 isoform X2 [Canis lupus familiaris]
gi|73977162	78669	0.06	PREDICTED: neurochondrin isoform 2 [Canis lupus familiaris]
gi|359321386	149095	0.03	PREDICTED: LOW QUALITY PROTEIN: WD repeat-containing protein 65 [Canis lupus familiaris]
gi|73972924	37815	0.12	PREDICTED: protein YIPF3 isoform 1 [Canis lupus familiaris]
gi|545488074	63561	0.07	PREDICTED: coiled-coil domain-containing protein 61 isoform X1 [Canis lupus familiaris]
gi|545489280	127559	0.03	PREDICTED: LOW QUALITY PROTEIN: liprin-alpha-3 [Canis lupus familiaris]
gi|545520271	61863	0.07	PREDICTED: butyrophilin subfamily 1 member A1-like [Canis lupus familiaris]
gi|345786928	153318	0.03	PREDICTED: LOW QUALITY PROTEIN: calcium-dependent secretion activator 1 isoform 3 [Canis lupus familiaris]
gi|73998896	129755	0.03	PREDICTED: PDZ domain-containing protein 8 isoform X1 [Canis lupus familiaris]

APPENDIX C: TABLES OF PROTEINS IDENTIFIED BY PEPTIDE FINGERPRINTING OF 143B MEMBRANE AND PROTEINS INCORPORATED IN NANODISC 1- 4

ST1: Proteomics data of plasma membrane protein from 143B

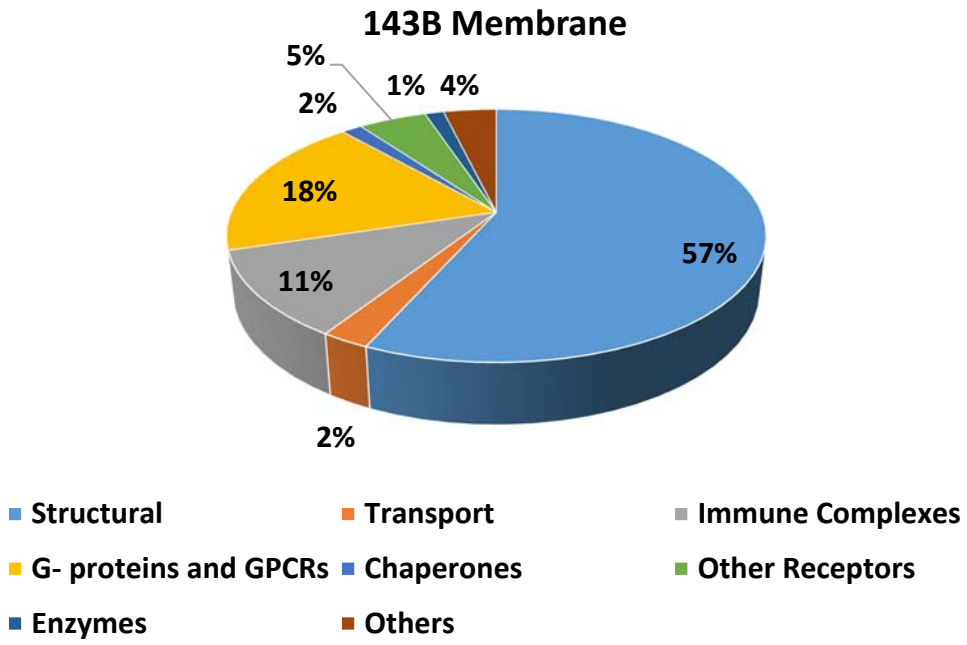

ST1-1. Overall proteomic profile

	emPAI	Percentage
Structural	87.73	56.68
Transport	3.81	2.46
Immune Complexes	17.16	11.09
G- proteins and GPCRs	28.33	18.30
Chaperones	2.27	1.47
Other Receptors	7.55	4.88

Enzymes	2.09	1.35
Others	5.84	3.77

ST1-2. Structural proteins detected

Accession	Mass	emPAI	Description
gi|435476	62092	2.89	cytokeratin 9 [Homo sapiens]
gi|12803709	51619	1.26	Keratin 14 [Homo sapiens]
gi|12653819	48003	0.3	Keratin 18 [Homo sapiens]
gi|11935049	66027	6.72	keratin 1 [Homo sapiens]
gi|62414289	53619	9.57	vimentin [Homo sapiens]
gi|47132620	65393	2.88	keratin, type II cytoskeletal 2 epidermal [Homo sapiens]
gi|119617032	59874	0.76	keratin 6B, isoform CRA_a [Homo sapiens]
gi|119395754	62340	0.84	keratin, type II cytoskeletal 5 [Homo sapiens]
gi|119617057	57772	0.79	keratin 8, isoform CRA_a [Homo sapiens]
gi|28173564	58887	0.15	keratin, type II cytoskeletal 73 [Homo sapiens]
gi|73909156	40503	26.66	Annexin A2 [Homo sapiens]
gi|62897671	41694	8.17	beta actin variant [Homo sapiens]
gi|7106439	49639	1.77	tubulin beta-5 chain [Mus musculus]
gi|119608775	48794	1.81	tubulin, beta 2C, isoform CRA_b [Homo sapiens]
gi|157833780	35984	1.54	Chain A, Human Annexin V With Proline Substitution By Thioproline
gi|34234	31774	0.7	laminin-binding protein, partial [Homo sapiens]

gi|16974825	8483	10.06	Chain A, Solution Structure Of Calcium-calmodulin N-terminal Domain
gi|5031635	18491	2.07	cofilin-1 [Homo sapiens]
gi|4502101	38690	0.92	annexin A1 [Homo sapiens]
gi|12667788	226392	0.18	myosin-9 [Homo sapiens]
gi|24119203	29015	1.06	tropomyosin alpha-3 chain isoform 2 [Homo sapiens]
gi|17986258	16919	1.67	myosin light polypeptide 6 isoform 1 [Homo sapiens]
gi|179976	75857	0.48	calelectrin [Homo sapiens]
gi|37492	50126	0.52	alpha-tubulin [Homo sapiens]
gi|321400138	46537	0.31	CD44 antigen isoform 6 precursor [Homo sapiens]
gi|119593154	263754	0.08	filamin A, alpha (actin binding protein 280), isoform CRA_e [Homo sapiens]
gi|530393410	236464	0.07	PREDICTED: myoferlin isoform X1 [Homo sapiens]
gi|7656991	53215	0.08	coronin-1C isoform b [Homo sapiens]
gi|3282771	278018	0.06	actin-binding protein homolog ABP-278 [Homo sapiens]
gi|4826898	15045	0.73	profilin-1 [Homo sapiens]
gi|119584665	9744	0.52	ankyrin repeat domain 28, isoform CRA_d [Homo sapiens]
gi|186837	197937	0.02	laminin B1 [Homo sapiens]
gi|41322910	512292	0.03	plectin isoform 1d [Homo sapiens]
gi|205831092	68253	0.06	RecName: Full=Putative IQ motif and ankyrin repeat domain-containing protein LOC642574
gi|641958	228798	0.02	non-muscle myosin B [Homo sapiens]

gi|3287188	127296	0.03	ankyrin-like protein [Homo sapiens]
gi|120660098	163133	0.03	CAMSAP1 protein [Homo sapiens]
gi|444738793	5129	1.16	alternative protein CEP350 [Homo sapiens]
gi|8885790	287292	0.03	filamin 2 [Homo sapiens]
gi|762885	81583	0.05	Plakoglobin [Homo sapiens]
gi|578821687	271519	0.02	PREDICTED: spectrin beta chain, non-erythrocytic 2 isoform X3 [Homo sapiens]
gi|438056	342550	0.01	laminin M chain (merosin) [Homo sapiens]
gi|4507115	54496	0.08	fascin [Homo sapiens]
gi|119576069	394840	0.01	myosin XVA, isoform CRA_c [Homo sapiens]
gi|6563228	43212	0.1	rap2 interacting protein x [Homo sapiens]
gi|4757944	25792	0.18	CD81 antigen [Homo sapiens]
gi|1107687	505963	0.02	homologue of Drosophila Fat protein [Homo sapiens]
gi|578837838	423562	0.01	PREDICTED: dystrophin isoform X5 [Homo sapiens]
gi|578823153	93390	0.05	PREDICTED: tastin isoform X1 [Homo sapiens]
gi|119574344	91877	0.05	ankyrin repeat domain 30B, partial [Homo sapiens]
gi|2996006	70660	0.06	outer dense fiber protein 2/2 [Homo sapiens]
gi|34226	288131	0.01	laminin A chain [Homo sapiens]
gi|530370381	134263	0.03	PREDICTED: unconventional myosin-Ib isoform X2 [Homo sapiens]
gi|186964	177492	0.02	laminin B2 chain [Homo sapiens]
gi|578819318	310817	0.01	PREDICTED: ankyrin-3 isoform X17 [Homo sapiens]
gi|55743096	193394	0.02	collagen alpha-1(XIV) chain precursor [Homo sapiens]

ST 1-3: Transport Proteins detected

Accession	Mass	emPAI	Description
gi|119574954	34459	0.84	voltage-dependent anion channel 2, isoform CRA_a [Homo sapiens]
gi|198443050	31818	0.3	Chain A, Solution Structure Of Human Vdac-1 In Ldao Micelles
gi|61744477	68059	0.28	4F2 cell-surface antigen heavy chain isoform b [Homo sapiens]
gi|4505893	16680	0.28	proteolipid protein 2 [Homo sapiens]
gi|51094709	102523	0.04	tweety homolog 3 (Drosophila) [Homo sapiens]
gi|48255951	136789	0.03	plasma membrane calcium-transporting ATPase 2 isoform 1 [Homo sapiens]
gi|5733504	27630	0.16	voltage-dependent anion channel VDAC3 [Homo sapiens]
gi|1478281	56585	0.16	neutral amino acid transporter B [Homo sapiens]
gi|5730102	106258	0.04	short transient receptor potential channel 6 [Homo sapiens]
gi|4502281	31492	0.14	sodium/potassium-transporting ATPase subunit beta-3 [Homo sapiens]
gi|115583685	53909	0.17	monocarboxylate transporter 1 [Homo sapiens]
gi|9957467	269786	0.02	ATP-binding cassette sub-family A member 2 [Homo sapiens]
gi|38516	20468	0.23	caveolin [Homo sapiens]

gi|347948492	8529	0.61	Chain A, Complex Of Cambr And Cam
gi|62087606	50068	0.09	sorting nexin 1 isoform a variant [Homo sapiens]
gi|2337920	29827	0.15	syntaxin 7 [Homo sapiens]
gi|25777643	59949	0.07	small conductance calcium-activated potassium channel protein 1 [Homo sapiens]
gi|51339295	126843	0.07	cation channel sperm-associated protein subunit beta precursor [Homo sapiens]
gi|4507297	68692	0.06	syntaxin-binding protein 1 isoform a [Homo sapiens]
gi|169790839	59534	0.07	excitatory amino acid transporter 1 isoform 1 [Homo sapiens]

ST 1-4 : Immune Complex proteins detected

Accession	Mass	emPAI	Description
gi|432139040	12890	0.38	immunoglobulin heavy chain variable region, partial [Homo sapiens]
gi|290560013	11815	3.04	Chain B, Crystal Structure Of Mhc Class I Hla-A2.1 Bound To A Photocleavable Peptide
gi|4324088	10594	0.47	immunoglobulin lambda light chain variable region [Homo sapiens]
gi|307496	1390	9.07	T cell receptor beta chain [Homo sapiens]
gi|333036593	21139	0.22	MHC class I antigen [Homo sapiens]
gi|151188217	40719	0.11	killer-cell Ig-like receptor [Homo sapiens]
gi|17986005	29943	0.15	major histocompatibility complex, class II, DR beta 3 precursor [Homo sapiens]

gi|611962048	10753	0.46	immunoglobulin heavy chain variable region, partial [Homo sapiens]
gi|247425243	13679	0.35	immunoglobulin heavy chain variable region [Homo sapiens]
gi|15680023	27975	0.16	B-cell receptor-associated protein 31 [Homo sapiens]
gi|4038122	4086	1.57	T-cell receptor beta chain [Homo sapiens]
gi|226316189	21056	0.22	MHC class I antigen [Homo sapiens]
gi|224962016	21226	0.48	MHC class II antigen [Homo sapiens]
gi|119573139	39827	0.11	SLAM family member 9, isoform CRA_a [Homo sapiens]
gi|26985944	13046	0.37	immunoglobulin IgG1 heavy chain [Homo sapiens]

ST 1- 5: GPCRs and G- proteins detected

Accession	Mass	emPAI	Description
gi|4506413	20974	0.81	ras-related protein Rap-1A precursor [Homo sapiens]
gi|327195100	33961	0.45	UBE2L3/KRAS fusion protein [Homo sapiens]
gi|119574084	39680	0.53	guanine nucleotide binding protein (G protein), beta polypeptide 2-like 1, isoform CRA_h [Homo sapiens]
gi|508285	23553	0.43	Rab5c-like protein, similar to Canis familiaris Rab5c protein, PIR Accession Number S38625 [Homo sapiens]
gi|13569962	22157	1.56	ras-related protein Rab-1B [Homo sapiens]
gi|33946329	23552	0.43	ras-related protein Ral-A precursor [Homo sapiens]
gi|1174149	23447	1.04	small GTP binding protein Rab7 [Homo sapiens]
gi|14249144	24473	0.67	ras-related protein Rab-11B [Rattus norvegicus]

gi|5729850	40506	0.37	guanine nucleotide-binding protein G(k) subunit alpha [Homo sapiens]
gi|21361884	24199	0.19	ras-related protein Rab-2B isoform 1 [Homo sapiens]
gi|5031703	52132	0.18	ras GTPase-activating protein-binding protein 1 [Homo sapiens]
gi|5031703	52132	0.18	ras GTPase-activating protein-binding protein 1 [Homo sapiens]
gi|297660220	16459	0.29	Rho GTPase activating protein 26 variant 3 [Homo sapiens]
gi|311697329	3564	1.93	KRAS protein [Homo sapiens]
gi|4885287	7314	0.73	guanine nucleotide-binding protein G(I)/G(S)/G(O) subunit gamma-5 precursor [Homo sapiens]
gi|540344584	37576	0.12	guanine nucleotide-binding protein subunit alpha-12 isoform 3 [Homo sapiens]
gi|3292965	1071	15.8	m1 muscarinic acetylcholine receptor protein [Homo sapiens]
gi|53828729	34724	0.13	olfactory receptor 7D2 [Homo sapiens]
gi|334278900	35700	0.12	olfactory receptor 4N4 [Homo sapiens]
gi|19338916	36399	0.12	G protein-coupled receptor SNSR5 [Homo sapiens]
gi|2500069	21555	0.21	RecName: Full=Ras-related protein Rab-31; AltName: Full=Ras-related protein Rab-22B [Homo sapiens]
gi|3327062	221821	0.02	KIAA0624 protein [Homo sapiens]
gi|4139784	24393	0.19	Chain A, Canine Gdp-Ran Q69l Mutant
gi|390635651	110782	0.04	ras-related protein Rab-44 [Homo sapiens]
gi|21928341	34874	0.13	seven transmembrane helix receptor [Homo sapiens]

gi|530416765	113467	0.04	PREDICTED: ras-interacting protein 1 isoform X1 [Homo sapiens]
gi|62088744	29577	0.15	regulator of G-protein signalling 11 isoform 1 variant [Homo sapiens]
gi|359807059	20502	0.22	TBC1 domain family member 1 isoform 4 [Homo sapiens]
gi|4836765	77704	0.06	G-protein-coupled receptor [Homo sapiens]
gi|13122463	37605	0.12	G protein-coupled receptor [Homo sapiens]
gi|9625037	21295	0.22	rho-related GTP-binding protein RhoG precursor [Mus musculus]
gi|51036603	8001	0.66	guanine nucleotide-binding protein G(I)/G(S)/G(O) subunit gamma-12 precursor [Homo sapiens]
gi|15293749	23836	0.19	olfactory receptor [Homo sapiens]

ST 1-6: Chaperone proteins detected

Accession	Mass	emPAI	Description
gi|431822408	82269	0.95	heat shock protein HSP 90-beta isoform c [Homo sapiens]
gi|153792590	98099	0.47	heat shock protein HSP 90-alpha isoform 1 [Homo sapiens]
gi|62089036	57725	0.16	chaperonin containing TCP1, subunit 6A isoform a variant [Homo sapiens]
gi|5453603	57452	0.16	T-complex protein 1 subunit beta isoform 1 [Homo sapiens]
gi|1136741	58465	0.16	KIAA0002 [Homo sapiens]
gi|5453607	59329	0.15	T-complex protein 1 subunit eta isoform a [Homo sapiens]
gi|671527	60292	0.07	gamma subunit of CCT chaperonin [Homo sapiens]
gi|36796	60356	0.15	t-complex polypeptide 1 [Homo sapiens]

ST 1-7: Other Receptor proteins detected

Accession	Mass	emPAI	Description
gi|1477388	132282	0.07	metabotropic glutamate receptor 1 alpha [Homo sapiens]
gi|119581591	46372	0.2	basigin (Ok blood group), isoform CRA_g [Homo sapiens]
gi|187609338	20107	0.51	Chain A, Crystal Structure Of The Extracellular Portion Of Hab18gCD147
gi|19743813	88357	0.47	integrin beta-1 isoform 1A precursor [Homo sapiens]
gi|124942	129214	0.14	RecName: Full=Integrin alpha-2; AltName: Full=CD49 antigen-like family member B; AltName: Full=Collagen receptor; AltName: Full=Platelet membrane glycoprotein Ia; Short=GPIa; AltName: Full=VLA-2 subunit alpha; AltName: CD_antigen=CD49b; Flags: Precu
gi|6424942	96019	0.05	ALG-2 interacting protein 1 [Homo sapiens]
gi|5729875	21658	0.21	membrane-associated progesterone receptor component 1 isoform 1 [Homo sapiens]
gi|4530577	65546	0.07	LISCH protein [Homo sapiens]
gi|21928311	35019	0.13	seven transmembrane helix receptor [Homo sapiens]
gi|62089376	70414	0.06	complement component 1, q subcomponent, receptor 1 variant [Homo sapiens]
gi|119611708	110644	0.04	protein tyrosine phosphatase, receptor type, C, isoform CRA_c [Homo sapiens]
gi|47077659	72805	0.06	FLJ00268 protein [Homo sapiens]
gi|1374813	23368	0.43	SNAP-23 [Homo sapiens]

gi|20072835	59945	0.07	ACSL1 protein, partial [Homo sapiens]
gi|5360115	89012	0.05	NY-REN-45 antigen [Homo sapiens]
gi|257743046	43424	0.1	C-C chemokine receptor type 3 isoform 2 [Homo sapiens]
gi|70913399	2021	4.89	T cell receptor alpha variable 7 [Homo sapiens]

ST 1-8: Enzymes detected

Accession	Mass	emPAI	Description
gi|189095938	11754	0.42	Chain A, Crystal Structure Of E60a Mutant Of Fkbp12
gi|530375065	51152	0.09	PREDICTED: neutral cholesterol ester hydrolase 1 isoform X1 [Homo sapiens]
gi|22209028	31786	0.3	Thioredoxin-related transmembrane protein 1 [Homo sapiens]
gi|4505977	32553	0.14	lipid phosphate phosphohydrolase 2 isoform 1 [Homo sapiens]
gi|530405604	56246	0.08	PREDICTED: death-associated protein kinase 2 isoform X1 [Homo sapiens]
gi|4505783	124805	0.03	phosphorylase b kinase regulatory subunit beta isoform a [Homo sapiens]
gi|1666423	161493	0.03	FMI protein [Homo sapiens]
gi|1486363	41988	0.11	extracellular signal regulated kinase [Homo sapiens]
gi|35360	65350	0.07	PDC-E2 precursor (AA -54 to 561) [Homo sapiens]

gi|516516	117320	0.04	neuronal kinesin heavy chain [Homo sapiens]
gi|181944	108185	0.04	protein-tyrosine kinase [Homo sapiens]
gi|16306598	153533	0.03	von Willebrand factor-cleaving protease precursor [Homo sapiens]
gi|5031697	143634	0.03	probable phospholipid-transporting ATPase IC [Homo sapiens]
gi|282847398	147344	0.03	mitogen-activated protein kinase kinase kinase 15 [Homo sapiens]
gi|134104091	31726	0.14	Chain A, Crystal Structure Of Human Pyridoxal 5'-Phosphate Phosphatase
gi|837261	88581	0.05	ERK5 [Homo sapiens]
gi|62897321	34328	0.13	steroid dehydrogenase homolog [Homo sapiens]
gi|3450828	33499	0.13	retinal short-chain dehydrogenase/reductase retSDR1 [Homo sapiens]
gi|124007195	73247	0.06	RecName: Full=Heparan-alpha-glucosaminide N-acetyltransferase; AltName: Full=Transmembrane protein 76 [Homo sapiens]
gi|13242866	31413	0.14	type 3 iodothyronine deiodinase [Homo sapiens]

ST 1-9: Other membrane proteins detected

Accession	Mass	emPAI	Description
gi|13129092	26194	0.38	transmembrane protein 109 precursor [Homo sapiens]
gi|5821140	40308	0.37	ASY [Homo sapiens]

gi|345198270	23750	0.69	tumor protein D54 isoform j [Homo sapiens]
gi|337930	27386	0.84	scar protein [Homo sapiens]
gi|23712	45220	0.32	myoblast antigen 24.1D5 [Homo sapiens]
gi|1160963	83616	0.29	transmembrane protein [Homo sapiens]
gi|662994	72707	0.06	GPI-anchored protein p137 [Homo sapiens]
gi|5729718	46003	0.1	trophoblast glycoprotein precursor [Homo sapiens]
gi|578830259	58187	0.08	PREDICTED: brain-specific angiogenesis inhibitor 1-associated protein 2 isoform X11 [Homo sapiens]
gi|7767178	19180	0.24	Chain A, Apolipoprotein E3 (Apoe3) Truncation Mutant 165
gi|6912582	30361	0.15	peflin [Homo sapiens]
gi|6002678	45242	0.1	colon carcinoma related protein [Homo sapiens]
gi|19923969	25820	0.18	coiled-coil domain-containing protein 124 [Homo sapiens]
gi|39725636	27260	0.17	transmembrane emp24 domain-containing protein 9 precursor [Homo sapiens]
gi|19920317	65983	0.14	cytoskeleton-associated protein 4 [Homo sapiens]
gi|1161384	384046	0.01	BRCA2 [Homo sapiens]
gi|40789001	108477	0.04	KIAA0964 protein [Homo sapiens]
gi|4240313	149996	0.03	KIAA0912 protein [Homo sapiens]
gi|30089664	575806	0.01	ABC A13 [Homo sapiens]
gi|27735113	50114	0.09	EF-hand calcium-binding domain-containing protein 3 isoform b [Homo sapiens]
gi|28680	21594	0.21	amphiglycan [Homo sapiens]
gi|235397	24680	0.18	HMFG, partial [Homo sapiens]

gi|15012003	17359	0.27	Family with sequence similarity 162, member A [Homo sapiens]
gi|1616918	46323	0.1	membrane protein with histidine rich charge clusters [Homo sapiens]
gi|6331328	115103	0.04	KIAA1280 protein [Homo sapiens]
gi|29648540	14892	0.32	MLL5 [Homo sapiens]
gi|20521880	198894	0.02	KIAA1305 protein [Homo sapiens]
gi|7706322	28051	0.16	UPF0568 protein C14orf166 [Homo sapiens]
gi|471270576	23424	0.2	Chain L, Crystal Structure Of Tnf-alpha In Complex With Infliximab Fab Fragment
gi|71891687	139575	0.03	KIAA0931 protein [Homo sapiens]
gi|223462187	266458	0.02	SPG11 protein [Homo sapiens]

ST2: Proteomics data of plasma membrane protein from POPC nanodiscs

ST- 2-1: Total Proteomic Profile

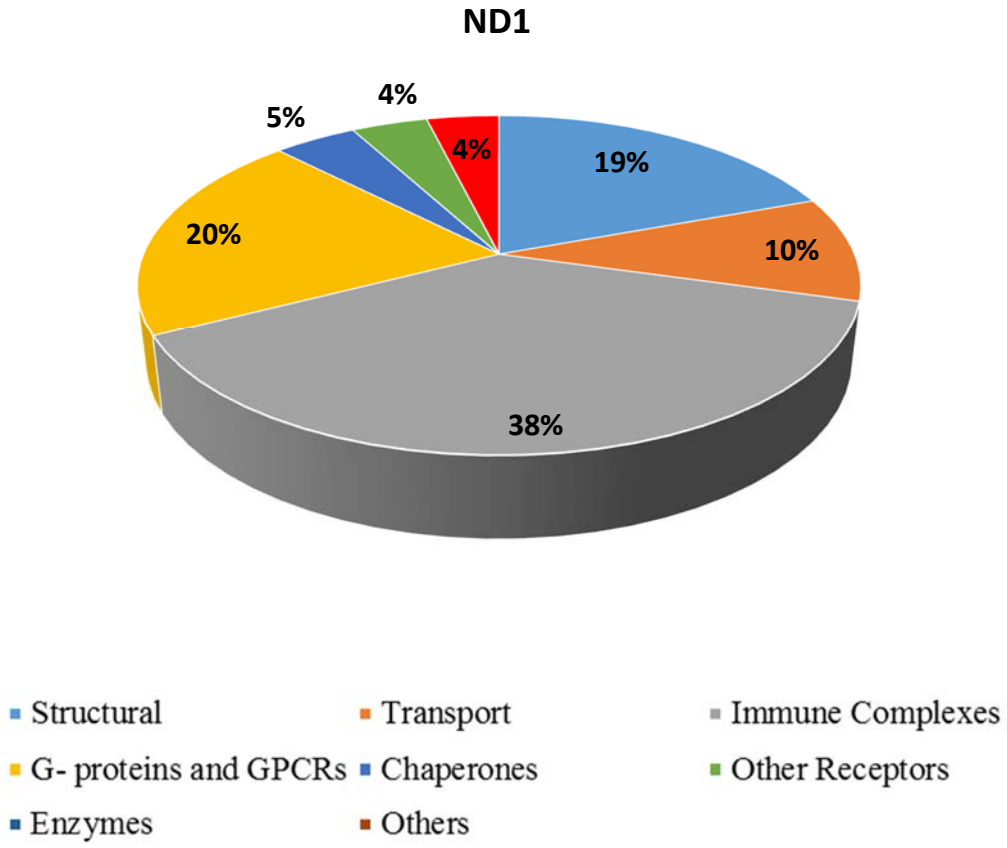

	emPAI	Percentage
Structure	6.73	19.39
Transport	3.47	10.00
Immune complexes	13.2	38.04
GPCRs and G-proteins	7.01	20.20
Chaperones	1.54	4.44

Other Receptors	1.41	4.06
Enzymes	1.34	3.86

ST 2-2: Structural proteins detected

Accession	Mass	emPAI	Description
gi|47132620	65393	0.69	keratin, type II cytoskeletal 2 epidermal [Homo sapiens]
gi|11935049	66027	0.79	keratin 1 [Homo sapiens]
gi|111600321	148955	0.06	Cingulin-like 1 [Homo sapiens]
gi|119581148	57526	0.45	keratin 9 (epidermolytic palmoplantar keratoderma) [Homo sapiens]
gi|124942	129214	0.18	RecName: Full=Integrin alpha-2; AltName: Full=CD49 antigen-like family member B; AltName: Full=Collagen receptor; AltName: Full=Platelet membrane glycoprotein Ia; Short=GPIa; AltName: Full=VLA-2 subunit alpha; AltName: CD_antigen=CD49b; Flags: Precu
gi|4757756	38580	0.93	annexin A2 isoform 2 [Homo sapiens]
gi|35959	49599	0.09	tubulin 5-beta [Homo sapiens]
gi|119606366	87389	0.05	integrin, beta 1 (fibronectin receptor, beta polypeptide, antigen CD29 includes MDF2, MSK12), isoform CRA_f [Homo sapiens]
gi|187609338	20107	0.23	Chain A, Crystal Structure Of The Extracellular Portion Of Hab18gCD147
gi|63055057	41976	0.36	beta-actin-like protein 2 [Homo sapiens]
gi|14250401	40978	0.51	actin, beta, partial [Homo sapiens]

gi|3043578	82629	0.05	KIAA0527 protein [Homo sapiens]
gi|1335273	131387	0.03	pm5 protein [Homo sapiens]
gi|29801	53563	0.08	CD44E (epithelial form) [Homo sapiens]
gi|4757944	25792	0.18	CD81 antigen isoform 1 [Homo sapiens]
gi|6755973	21820	0.21	protein lin-7 homolog C [Mus musculus]
gi|11602890	242566	0.02	betaIV spectrin isoform sigma4 [Homo sapiens]
gi|6331294	130203	0.03	KIAA1275 protein [Homo sapiens]
gi|996057	25106	0.18	gp25l2 [Homo sapiens]
gi|38194229	69830	0.06	kelch-like protein 17 [Homo sapiens]
gi|4502101	38690	0.12	annexin A1 [Homo sapiens]
gi|578832133	171296	0.03	PREDICTED: ankyrin repeat domain-containing protein 30B isoform X1 [Homo sapiens]
gi|17223624	184249	0.02	ATP-binding cassette A9 [Homo sapiens]
gi|47115317	53547	0.08	VIM [Homo sapiens]
gi|119623210	109613	0.04	protocadherin 19, isoform CRA_b [Homo sapiens]
gi|642945631	3992165	0	titin isoform IC [Homo sapiens]
gi|588293041	5873	0.97	Chain A, Crystal Structure Of Human Striatin-3 Coiled Coil Domain
gi|578828592	465974	0.01	PREDICTED: dynein heavy chain 3, axonemal isoform X1 [Homo sapiens]
gi|109627650	52955	0.08	coronin-6 [Homo sapiens]
gi|15395290	520649	0.01	axonemal beta heavy chain dynein type 11 [Homo sapiens]
gi|530355911	185529	0.02	PREDICTED: filaggrin-like isoform X1 [Homo sapiens]

gi|578800534	106620	0.04	PREDICTED: axonemal dynein light chain domain-containing protein 1 isoform X4 [Homo sapiens]
gi|35046	102386	0.04	NF-M [Homo sapiens]
gi|530383617	82734	0.05	PREDICTED: discoidin, CUB and LCCL domain-containing protein 1 isoform X1 [Homo sapiens]
gi|11128029	100981	0.04	protocadherin gamma-B6 isoform 1 precursor [Homo sapiens]

ST 2-2: Transport proteins detected

Accession	Mass	emPAI	Description
gi|21361181	112824	0.16	sodium/potassium-transporting ATPase subunit alpha-1 isoform a [Homo sapiens]
gi|340201	31575	0.5	voltage-dependent anion channel [Homo sapiens]
gi|5803165	9968	1.28	protein transport protein Sec61 subunit beta [Homo sapiens]
gi|4505893	16680	0.29	proteolipid protein 2 [Homo sapiens]
gi|238427	30623	0.32	Porin 31HM [human, skeletal muscle membranes, Peptide, 282 aa]
gi|15216171	55958	0.08	putative 40-9-1 protein [Homo sapiens]
gi|177207	57935	0.08	4F2 antigen heavy chain [Homo sapiens]
gi|1478281	56585	0.08	neutral amino acid transporter B [Homo sapiens]
gi|184039	227015	0.02	sodium channel alpha subunit [Homo sapiens]
gi|2337920	29827	0.15	syntaxin 7 [Homo sapiens]
gi|7243235	47877	0.09	KIAA1427 protein [Homo sapiens]

gi|18148873	62056	0.07	hUST3 [Homo sapiens]
gi|62088660	13888	0.35	solute carrier family 19, member 2 variant [Homo sapiens]

ST 2-3: Immune complex proteins identified

Accession	Mass	emPAI	Description
gi|303398863	31635	0.31	MHC class I antigen [Homo sapiens]
gi|695942218	11632	0.43	immunoglobulin G heavy chain variable region, partial [Homo sapiens]
gi|307751150	21033	0.22	MHC class I antigen [Homo sapiens]
gi|290560013	11815	0.42	Chain B, Crystal Structure Of Mhc Class I Hla-A2.1 Bound To A Photocleavable Peptide
gi|2654661	1795	6.07	T cell receptor beta chain, partial [Homo sapiens]
gi|63003901	44057	0.1	lymphocyte transmembrane adapter 1 isoform a [Homo sapiens]
gi|499592	12814	0.38	immunoglobulin heavy chain, partial [Homo sapiens]
gi|1835715	8609	0.6	T cell receptor alpha chain [Homo sapiens]
gi|304563130	13060	0.37	immunoglobulin gamma 1 heavy chain variable region [Homo sapiens]
gi|432139159	12229	0.4	immunoglobulin heavy chain variable region, partial [Homo sapiens]
gi|519672532	13596	0.36	immunoglobulin A heavy chain variable region, partial [Homo sapiens]
gi|106638	24733	0.19	Ig lambda chain - human

gi|674841392	12150	0.41	immunoglobulin heavy chain variable region, partial [Homo sapiens]
gi|7161029	10258	0.5	immunoglobulin heavy chain [Homo sapiens]
gi|371446172	13557	0.36	immunoglobulin G heavy chain variable region, partial [Homo sapiens]
gi|444738217	5338	1.1	alternative protein LY75 [Homo sapiens]
gi|11137273	8448	0.62	immunoglobulin heavy chain variable region [Homo sapiens]
gi|371447513	13673	0.36	immunoglobulin G heavy chain variable region, partial [Homo sapiens]

ST 2-4: GPCRs and G-proteins detected

Accession	Mass	emPAI	Description
gi|15718763	21642	2.21	GTPase KRas isoform a [Homo sapiens]
gi|183182	40437	0.37	guanine nucleotide-binding regulatory protein alpha-inhibitory subunit [Homo sapiens]
gi|126031531	40084	0.53	Chain A, Crystal Structure Of The Heterodimeric Complex Of Human Rgs8 And Activated Gi Alpha 3
gi|508285	23553	0.43	Rab5c-like protein, similar to Canis familiaris Rab5c protein, PIR Accession Number S38625 [Homo sapiens]
gi|13569962	22157	0.46	ras-related protein Rab-1B [Homo sapiens]
gi|1174149	23447	0.2	small GTP binding protein Rab7 [Homo sapiens]
gi|20147713	23971	0.19	Ras family small GTP binding protein RALA [Homo sapiens]
gi|4885287	7314	0.74	guanine nucleotide-binding protein G(I)/G(S)/G(O) subunit gamma-5 precursor [Homo sapiens]

gi|93279476	22431	0.21	Chain A, 3d Structure Of Inactive Human Rab11b Gtpase
gi|306785	37320	0.12	G protein beta subunit [Homo sapiens]
gi|4758988	22663	0.2	ras-related protein Rab-1A isoform 1 [Homo sapiens]
gi|119603524	83659	0.05	pleckstrin homology domain containing, family G (with RhoGef domain) member 4, isoform CRA_b [Homo sapiens]
gi|7710086	22527	0.21	ras-related protein Rab-10 [Mus musculus]
gi|38493105	7058	0.77	Chain B, Structure Of A Complex Of The Golgin-245 Grip Domain With Arl1
gi|452085171	98705	0.04	NACHT, LRR and PYD domains-containing protein 6 isoform 1 [Homo sapiens]
gi|14276193	26949	0.17	rho GTPase activating protein 8 isoform 2 [Homo sapiens]
gi|119590272	720673	0.01	obscurin, cytoskeletal calmodulin and titin-interacting RhoGEF, isoform CRA_a [Homo sapiens]
gi|33341670	44729	0.1	FP2461 [Homo sapiens]

ST 2-5: Chaperone proteins detected

Accession	Mass	emPAI	Description
gi|5729877	70854	0.06	heat shock cognate 71 kDa protein isoform 1 [Homo sapiens]
gi|74722493	47682	0.09	RecName: Full=Putative heat shock protein HSP 90-alpha A4; AltName: Full=Heat shock 90 kDa protein 1 alpha-like 2; AltName: Full=Heat shock protein 90-alpha D; Short=Heat shock protein 90Ad [Homo sapiens]
gi|635576870	15314	0.31	Chain A, Pih1d1/phospho-tel2 Complex

gi|165761148	20167	0.23	Chain A, Structure Of E163k Dj-1
gi|119590562	6589	0.85	heat shock 10kDa protein 1 (chaperonin 10), isoform CRA_c [Homo sapiens]

ST 2-6: Other receptors detected

Accession	Mass	emPAI	Description
gi|7243270	102932	0.04	KIAA1436 protein [Homo sapiens]
gi|4507685	87560	0.05	short transient receptor potential channel 1 isoform 2 [Homo sapiens]
gi|46107962	308295	0.01	inositol 1,4,5-trisphosphate receptor type 1 [Homo sapiens]
gi|66267488	38155	0.12	Trace amine associated receptor 5 [Homo sapiens]
gi|4504237	74776	0.06	semaphorin-7A isoform 1 preproprotein [Homo sapiens]
gi|371502087	40860	0.11	protein Wnt-5a isoform 2 precursor [Homo sapiens]
gi|182403	22199	0.21	TB2, partial [Homo sapiens]
gi|545719854	7768	0.69	Chain A, Crystal Structure Of Bap31 Vded At Acidic Ph
gi|1502343	160126	0.03	receptor phosphatase PCP-2 [Homo sapiens]
gi|578804728	50295	0.09	PREDICTED: secretin receptor isoform X2 [Homo sapiens]

ST 2-7: Enzymes detected

Accession	Mass	emPAI	Description
gi|73909094	48513	0.09	AADACL1 protein, partial [Homo sapiens]
gi|30348954	110066	0.04	E3 ubiquitin-protein ligase MIB1 [Homo sapiens]

gi|145579851	47479	0.09	Chain A, Structure Of The Mat Domain Of Human Fas With Malonyl-Coa
gi|338827653	9574	0.54	elongation of very long chain fatty acids protein 5 isoform 4 [Homo sapiens]
gi|33150814	123549	0.04	adenylyl cyclase type II [Homo sapiens]
gi|119601999	55892	0.08	serpin peptidase inhibitor, clade A (alpha-1 antiproteinase, antitrypsin), member 13, partial [Homo sapiens]
gi|1916935	34849	0.13	9-cis-retinol specific dehydrogenase [Homo sapiens]
gi|62897163	53507	0.08	complement component 1, r subcomponent-like precursor variant [Homo sapiens]
gi|30823	82619	0.05	diacylglycerol kinase [Homo sapiens]
gi|530370531	115588	0.04	PREDICTED: inactive phospholipase C-like protein 1 isoform X1 [Homo sapiens]
gi|4504235	28864	0.16	granzyme K precursor [Homo sapiens]

ST 2-8: Other membrane proteins detected

Accession	Mass	emPAI	Description
gi|213512168	148003	0.03	protein FAM205A [Homo sapiens]
gi|4929553	53130	0.08	CGI-41 protein [Homo sapiens]
gi|298351848	542265	0.01	RecName: Full=Hemicentin-2; Flags: Precursor [Homo sapiens]
gi|4929220	69777	0.06	colon cancer-associated protein Mic1 [Homo sapiens]
gi|299578	1653	6.85	urinary gonadotrophin peptide, UGP {N-terminal, PEAK 1} [human, urine, Peptide Partial, 15 aa]
gi|116283709	20830	0.22	TCTN1 protein [Homo sapiens]

gi|28204822	45420	0.1	EMI domain containing 1 [Homo sapiens]
gi|13540563	64377	0.07	complement factor H-related protein 5 precursor [Homo sapiens]

ST 3: Proteomics data of plasma membrane protein from 20% POPS nanodiscs

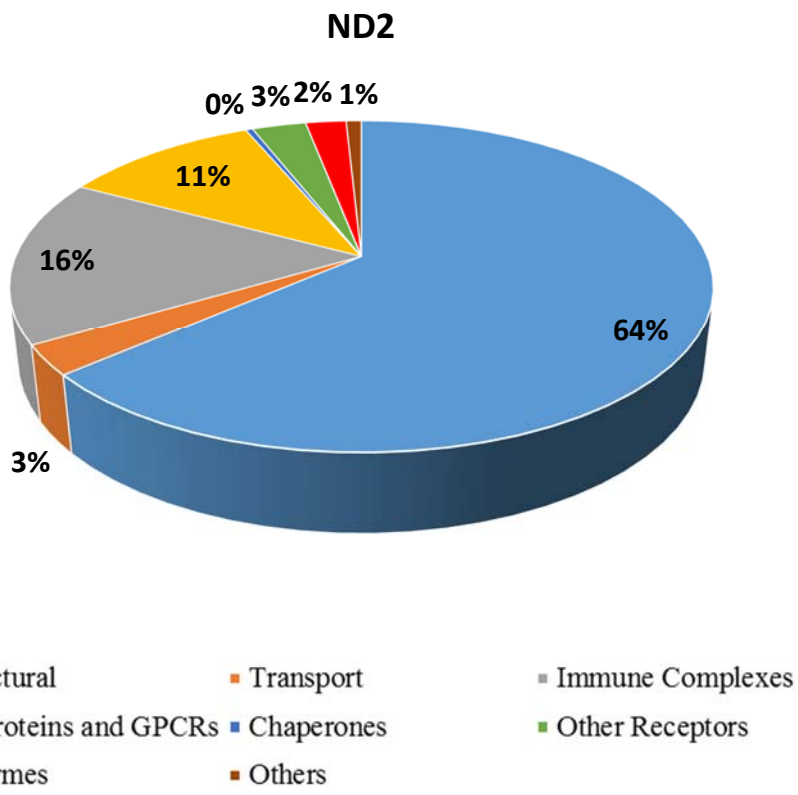

ST 3-1: Total Proteomic Composition

	emPAI	Percentage
Structure	44.16	63.65
Transport	2.03	2.93

Immune complexes	11.24	16.20
GPCRs and g-proteins	7.51	10.82
Chaperones	0.27	0.39
Other Receptors	2.05	2.95
Enzymes	1.54	2.22
Others	0.58	0.84

ST 3-2: Structural proteins detected

Accession	Mass	emPAI	Description
gi|11935049	66027	5.55	keratin 1 [Homo sapiens]
gi|119617035	59859	3.18	keratin 6E, isoform CRA_b [Homo sapiens]
gi|908790	59962	2.88	keratin type II [Homo sapiens]
gi|47132620	65393	1.19	keratin, type II cytoskeletal 2 epidermal [Homo sapiens]
gi|119395754	62340	2.68	keratin, type II cytoskeletal 5 [Homo sapiens]
gi|167887751	49623	1.17	vimentin variant 3 [Homo sapiens]
gi|55956899	62027	2.97	keratin, type I cytoskeletal 9 [Homo sapiens]
gi|1195531	51206	5.27	type I keratin 16 [Homo sapiens]
gi|119581150	44694	5.12	keratin 14 (epidermolysis bullosa simplex, Dowling-Meara, Koebner), isoform CRA_b [Homo sapiens]
gi|118835468	49555	0.54	Keratin 13 [Homo sapiens]

gi|119581154	47947	1.23	keratin 17, isoform CRA_a [Homo sapiens]
gi|4757756	38580	3.19	annexin A2 isoform 2 [Homo sapiens]
gi|4502101	38690	0.93	annexin A1 [Homo sapiens]
gi|28336	41786	1.78	mutant beta-actin (beta'-actin) [Homo sapiens]
gi|63055057	41976	0.66	beta-actin-like protein 2 [Homo sapiens]
gi|62420916	11548	1.05	actin-like protein [Homo sapiens]
gi|7656991	53215	0.08	coronin-1C isoform b [Homo sapiens]
gi|30506	113644	0.12	desmoglein type 1 [Homo sapiens]
gi|4507729	49875	0.09	tubulin beta-2A chain [Homo sapiens]
gi|119607750	48591	0.09	fascin homolog 1, actin-bundling protein (Strongylocentrotus purpuratus), isoform CRA_a [Homo sapiens]
gi|18652859	216528	0.02	Shroom-related protein [Homo sapiens]
gi|1020320	14066	0.81	CDM protein [Homo sapiens]
gi|3891470	14935	0.32	Chain A, Crystal Structure Of Human Galectin-7 In Complex With Galactosamine
gi|10047357	108677	0.04	KIAA1640 protein [Homo sapiens]
gi|4757944	25792	0.18	CD81 antigen isoform 1 [Homo sapiens]
gi|5031635	18491	0.25	cofilin-1 [Homo sapiens]
gi|3560124	162768	0.03	LGMD2B protein [Homo sapiens]
gi|29801	53563	0.08	CD44E (epithelial form) [Homo sapiens]
gi|509806	176506	0.02	laminin A3 [Homo sapiens]

gi|19923497	108835	0.04	echinoderm microtubule-associated protein-like 4 isoform a [Homo sapiens]
gi|3212355	11064	1.11	Chain A, P11 (s100a10), Ligand Of Annexin Ii
gi|684936	34017	0.13	peptide with resemblance to the actin family; the actual start of the coding region has not been determined, partial [Homo sapiens]
gi|5803106	55361	0.08	myotilin isoform a [Homo sapiens]
gi|33870359	38753	0.12	RADIL protein [Homo sapiens]
gi|8926617	86994	0.05	protocadherin beta 9 [Homo sapiens]
gi|208435559	15686	0.31	Chain A, Structure Of C-Terminal Actin Depolymerizing Factor Homology (Adf-H) Domain Of Human Twinfilin-2
gi|179106	284107	0.02	nonerythroid alpha-spectrin [Homo sapiens]
gi|4507869	39805	0.11	vasodilator-stimulated phosphoprotein [Homo sapiens]
gi|14009465	64812	0.07	protocadherin-psi1 [Homo sapiens]
gi|530377585	446623	0.01	PREDICTED: ankyrin-2 isoform X5 [Homo sapiens]
gi|20521772	228253	0.02	KIAA1132 protein [Homo sapiens]
gi|530367826	153588	0.03	PREDICTED: girdin isoform X9 [Homo sapiens]
gi|257467636	336007	0.01	TPR and ankyrin repeat-containing protein 1 [Homo sapiens]
gi|18032008	174823	0.02	scribble [Homo sapiens]
gi|190461797	21336	0.22	RecName: Full=Putative ankyrin repeat domain-containing protein ENSP00000383069 [Homo sapiens]
gi|7243015	49905	0.09	KIAA1317 protein [Homo sapiens]

gi|38683807	274088	0.02	ankyrin repeat domain-containing protein 17 isoform a [Homo sapiens]
gi|83404899	93103	0.05	KIF19 protein, partial [Homo sapiens]
gi|19115954	528684	0.01	dynein heavy chain 5, axonemal [Homo sapiens]
gi|20338988	285056	0.02	myosin heavy chain [Homo sapiens]
gi|34526505	65730	0.07	FLJ00279 protein [Homo sapiens]
gi|256222280	217331	0.02	ankyrin repeat domain-containing protein 36A [Homo sapiens]
gi|119631904	739985	0.01	nebulin, isoform CRA_a [Homo sapiens]

ST 3-3: Transport proteins detected

Accession	Mass	emPAI	Description
gi|21361181	112824	0.26	sodium/potassium-transporting ATPase subunit alpha-1 isoform a [Homo sapiens]
gi|119573123	114151	0.12	ATPase, Na+/K+ transporting, alpha 4 polypeptide, isoform CRA_b [Homo sapiens]
gi|23397696	59022	0.16	copine-1 isoform a [Homo sapiens]
gi|62087554	56981	0.08	solute carrier family 2 (facilitated glucose transporter), member 1 variant [Homo sapiens]
gi|4505893	16680	0.29	proteolipid protein 2 [Homo sapiens]
gi|996057	25106	0.18	gp25l2 [Homo sapiens]
gi|115583685	53909	0.08	monocarboxylate transporter 1 [Homo sapiens]
gi|5803165	9968	0.51	protein transport protein Sec61 subunit beta [Homo sapiens]

gi|40789265	116441	0.04	N-acetyl-beta-glucosaminyl-glycoprotein 4-beta-N-acetylgalactosaminyltransferase 1 [Homo sapiens]
gi|61744477	68059	0.13	4F2 cell-surface antigen heavy chain isoform b [Homo sapiens]
gi|578822063	221581	0.02	PREDICTED: exophilin-5 isoform X1 [Homo sapiens]
gi|14133203	85249	0.05	KIAA0420 [Homo sapiens]
gi|50083277	135782	0.03	probable phospholipid-transporting ATPase IM [Homo sapiens]
gi|5870893	55736	0.08	sodium-coupled neutral amino acid transporter 3 [Homo sapiens]

ST 3-4: Immune complex proteins detected

Accession	Mass	emPAI	Description
gi|187609338	20107	0.52	Chain A, Crystal Structure Of The Extracellular Portion Of Hab18gCD147
gi|4768677	25839	0.18	kappa 1 immunoglobulin light chain [Homo sapiens]
gi|732549066	8537	0.61	immunoglobulin heavy chain variable region, partial [Homo sapiens]
gi|969030	13557	0.36	HLA-drb5, partial [Homo sapiens]
gi|630868148	7893	0.68	immunoglobulin heavy chain variable region, partial [Homo sapiens]
gi|21956310	7087	0.77	immunoglobulin heavy chain variable region [Homo sapiens]
gi|16076230	8826	0.59	immunoglobulin heavy chain variable region [Homo sapiens]

gi|149673883	23520	0.2	immunoglobulin heavy chain [Homo sapiens]
gi|1235763	13564	0.36	immunoglobulin heavy chain V-D-J region [Homo sapiens]
gi|2895915	5313	1.11	T cell receptor beta chain [Homo sapiens]
gi|47600789	9215	0.56	immunoglobulin kappa light chain [Homo sapiens]
gi|46254169	12798	0.39	immunoglobulin heavy chain [Homo sapiens]
gi|5080756	301609	0.01	Fc gamma BP, partial [Homo sapiens]
gi|674841392	12150	0.41	immunoglobulin heavy chain variable region, partial [Homo sapiens]
gi|118406063	12843	0.38	immunoglobulin heavy chain variable region [Homo sapiens]
gi|293629988	20840	0.22	MHC class I antigen [Homo sapiens]
gi|40255157	123355	0.04	leucine-rich repeats and immunoglobulin-like domains protein 3 isoform 2 precursor [Homo sapiens]
gi|298465	2412	3.47	myelin basic protein specific T-cell receptor V beta-D beta-J beta, MBP reactive TCR VDJ beta {CDR3 region, clone JO(3)}v [human, normal peripheral blood lymphocytes, Peptide Partial, 23 aa]
gi|270053250	12941	0.38	immunoglobulin heavy chain variable region [Homo sapiens]

ST 3-5 GPCRs and G-proteins detected

Accession	Mass	emPAI	Description
gi|51036603	8001	1.77	guanine nucleotide-binding protein G(I)/G(S)/G(O) subunit gamma-12 precursor [Homo sapiens]

gi|18204869	37194	0.12	TUBA1B protein [Homo sapiens]
gi|183182	40437	0.23	guanine nucleotide-binding regulatory protein alpha-inhibitory subunit [Homo sapiens]
gi|327195100	33961	0.28	UBE2L3/KRAS fusion protein [Homo sapiens]
gi|332205939	17648	0.27	ras-related protein Rab-11A isoform 2 [Homo sapiens]
gi|550545552	21215	0.49	Chain A, Crystal Structure Of Gdp-bound Rab8:grab
gi|119620329	28129	0.35	RAB1A, member RAS oncogene family, isoform CRA_f [Homo sapiens]
gi|187281	77555	0.12	M4 protein [Homo sapiens]
gi|311697329	3564	1.93	KRAS protein [Homo sapiens]
gi|508285	23553	0.2	Rab5c-like protein, similar to Canis familiaris Rab5c protein, PIR Accession Number S38625 [Homo sapiens]
gi|1174149	23447	0.43	small GTP binding protein Rab7 [Homo sapiens]
gi|54114933	69033	0.06	DIS3 mitotic control homolog (S. cerevisiae)-like 2 [Homo sapiens]
gi|2921705	23947	0.19	olfactory receptor [Homo sapiens]
gi|4506405	23394	0.2	ras-related protein Ral-B [Homo sapiens]
gi|7363439	35230	0.13	olfactory receptor 10H1 [Homo sapiens]
gi|1839517	25621	0.18	RhoE [Homo sapiens]
gi|434765	74466	0.06	ORF [Homo sapiens]
gi|5803145	76016	0.06	ralA-binding protein 1 [Homo sapiens]
gi|40255080	61626	0.07	rho GTPase-activating protein 36 isoform 1 precursor [Homo sapiens]

gi|46094081	125420	0.03	arf-GAP with SH3 domain, ANK repeat and PH domain-containing protein 1 isoform 1 [Homo sapiens]
gi|20147765	21767	0.21	regulator of G protein signalling 14 short variant [Homo sapiens]
gi|14249174	49431	0.09	pleckstrin homology domain-containing family A member 8 isoform 3 [Homo sapiens]
gi|5174617	107622	0.04	nucleotide-binding oligomerization domain-containing protein 1 [Homo sapiens]

ST 3-6: Chaperone proteins detected

Accession	Mass	emPAI	Description
gi|5729877	70854	0.2	heat shock cognate 71 kDa protein isoform 1 [Homo sapiens]
gi|36796	60356	0.07	t-complex polypeptide 1 [Homo sapiens]

ST 3-7: Other receptors detected

Accession	Mass	emPAI	Description
gi|578815882	94485	0.05	PREDICTED: t-SNARE domain-containing protein 1 isoform X2 [Homo sapiens]
gi|19743813	88357	0.21	integrin beta-1 isoform 1A precursor [Homo sapiens]
gi|119610286	18642	0.25	progesterone receptor membrane component 1, isoform CRA_b [Homo sapiens]
gi|116295258	129215	0.1	integrin alpha-2 precursor [Homo sapiens]
gi|4504533	43540	0.1	5-hydroxytryptamine receptor 1B [Homo sapiens]

gi|2655006	99504	0.04	thyroid hormone receptor coactivating protein [Homo sapiens]
gi|440575811	11638	0.43	alternative protein CSF2RB [Homo sapiens]
gi|1200235	207530	0.02	SEX protein [Homo sapiens]
gi|182740	38376	0.12	N-formyl peptide receptor [Homo sapiens]
gi|4894663	35921	0.13	estrogen receptor beta2 splice variant [Homo sapiens]
gi|5032223	175630	0.02	plexin-C1 precursor [Homo sapiens]
gi|119626971	10488	0.49	integrin beta 3 binding protein (beta3-endonexin), isoform CRA_c [Homo sapiens]
gi|22651773	87487	0.05	vanilloid receptor like 3 protein splice variant b [Homo sapiens]
gi|338502	123290	0.04	heat-stable enterotoxin receptor [Homo sapiens]

ST 3-8: Enzymes detected

Accession	Mass	emPAI	Description
gi|28614	39307	1.14	aldolase A [Homo sapiens]
gi|181944	108185	0.04	protein-tyrosine kinase [Homo sapiens]
gi|49457448	47850	0.09	STK24 [Homo sapiens]
gi|5689457	100533	0.04	KIAA1060 protein [Homo sapiens]
gi|7019561	116926	0.04	thyrotropin-releasing hormone-degrading ectoenzyme [Homo sapiens]
gi|21361088	43916	0.1	sphingosine kinase 1 isoform 1 [Homo sapiens]
gi|1730288	67879	0.07	acetolactate synthase homolog [Homo sapiens]

gi|2326227	231143	0.02	phosphatidylinositol 4-kinase 230 [Homo sapiens]

ST 3-9: Other membrane proteins detected

Accession	Mass	emPAI	Description
gi|119607125	183296	0.05	RB1-inducible coiled-coil 1, isoform CRA_a [Homo sapiens]
gi|15055535	49142	0.09	BPI fold-containing family B member 2 precursor [Homo sapiens]
gi|119585838	186945	0.02	ADAM metallopeptidase with thrombospondin type 1 motif, 9, isoform CRA_a [Homo sapiens]
gi|14250417	21874	0.21	TMEM223 protein, partial [Homo sapiens]
gi|28204822	45420	0.1	EMI domain containing 1 [Homo sapiens]
gi|257153467	75487	0.06	disrupted in schizophrenia 1 protein isoform e [Homo sapiens]
gi|27368080	255664	0.02	retinitis pigmentosa 1-like 1 protein [Homo sapiens]
gi|187954537	164636	0.03	Coiled-coil domain containing 88B [Homo sapiens]

ST4: Proteomics data of plasma membrane protein from 20% cholesterol nanodiscs

ST- 4-1: Total Proteomic Profile

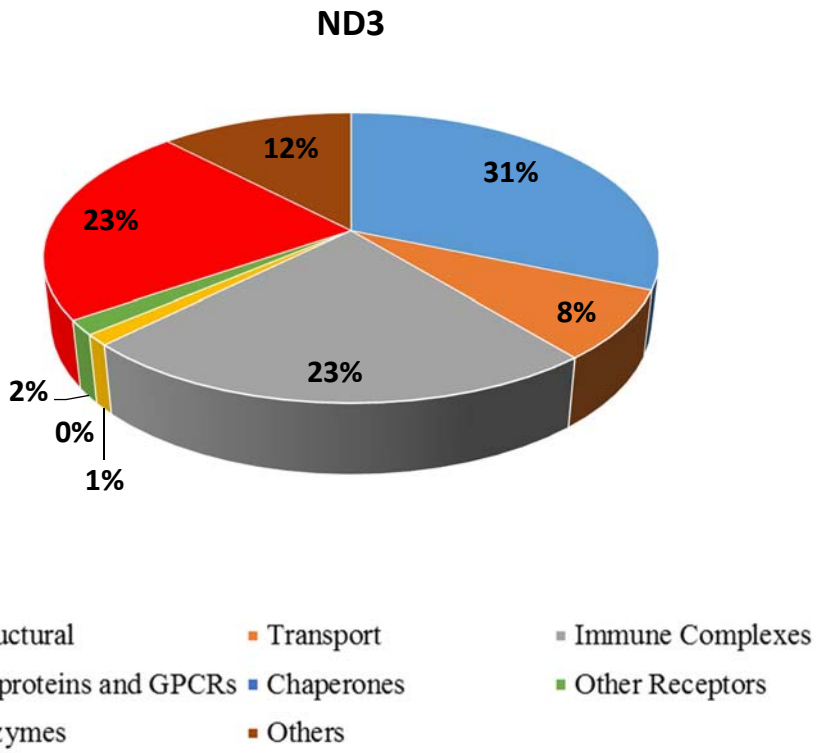

	emPAI	Percentage
Structure	0.78	31.45
Transport	0.19	7.66
Immune complexes	0.58	23.39
GPCRs and G proteins	0.03	1.21
Chaperones	0	0.00
Other Receptors	0.04	1.61

Enzymes	0.56	22.58
Others	0.3	12.10

ST 4-2: Structural proteins detected

Accession	Mass	emPAI	Description
gi|530372454	247138	0.02	PREDICTED: microtubule-associated protein 4 isoform X1 [Homo sapiens]
gi|226437606	58220	0.08	ankyrin repeat domain-containing protein 34C [Homo sapiens]
gi|40788231	180085	0.02	KIAA0373 [Homo sapiens]
gi|22477169	111219	0.04	CP110 protein [Homo sapiens]
gi|119621503	18928	0.25	transmembrane protein 18, isoform CRA_b, partial [Homo sapiens]
gi|1763665	21704	0.22	Snk interacting protein 2-28 [Homo sapiens]
gi|18606111	86511	0.05	Ankyrin repeat domain 5 [Homo sapiens]
gi|18650666	285075	0.02	myosin-like protein [Homo sapiens]
gi|87578394	58919	0.08	microtubule-associated protein 2 isoform 5 [Homo sapiens]

ST 4-3: Transport proteins detected

Accession	Mass	emPAI	Description
gi|179212	81680	0.05	Na+ K+ ATPase alpha subunit, partial [Homo sapiens]
gi|46409260	66508	0.07	EF-hand calcium-binding domain-containing protein 12 [Homo sapiens]

gi|17511944	118239	0.04	SEC24 family, member C (S. cerevisiae) [Homo sapiens]
gi|530393639	149887	0.03	PREDICTED: WASH complex subunit FAM21A isoform X2 [Homo sapiens]

ST 4-4: Immune complexes detected

Accession	Mass	emPAI	Description
gi|323433023	17228	0.28	immunoglobulin variable region [Homo sapiens]
gi|323431585	15902	0.3	immunoglobulin variable region [Homo sapiens]

ST 4-5: GPCRs and G proteins detected

Accession	Mass	emPAI	Description
gi|27529961	151481	0.03	KIAA1938 protein [Homo sapiens]

ST 4-6: Other receptor proteins detected

Accession	Mass	emPAI	Description
gi|119588279	129185	0.03	protein tyrosine phosphatase, receptor type, J, isoform CRA_a [Homo sapiens]
gi|2696015	550722	0.01	brain ryanodine receptor [Homo sapiens]

ST 4-7: Enzymes detected

Accession	Mass	emPAI	Description

gi|4885349	67743	0.07	G protein-coupled receptor kinase 5 [Homo sapiens]
gi|8101079	133254	0.03	FYVE domain-containing dual specificity protein phosphatase FYVE-DSP2 [Homo sapiens]
gi|1109782	65799	0.07	protein-tyrosine phosphatase [Homo sapiens]
gi|119617002	113726	0.04	ovochymase 1, isoform CRA_b, partial [Homo sapiens]
gi|5453906	23523	0.2	CDP-diacylglycerol--inositol 3-phosphatidyltransferase isoform 1 [Homo sapiens]
gi|119619352	57781	0.08	protein phosphatase, EF-hand calcium binding domain 1, isoform CRA_c [Homo sapiens]
gi|33186804	63999	0.07	TPA: type II transmembrane serine protease 7 precursor [Homo sapiens]

ST 4-8: Other membrane proteins detected

Accession	Mass	emPAI	Description
gi|94721250	32593	0.14	vesicle-associated membrane protein-associated protein A isoform 1 [Homo sapiens]
gi|10047317	148334	0.03	KIAA1620 protein [Homo sapiens]
gi|28204822	45420	0.1	EMI domain containing 1 [Homo sapiens]
gi|119620818	169460	0.03	KIAA1414 protein, isoform CRA_b [Homo sapiens]

ST5: Proteomics data of plasma membrane protein from 20% POPS+ 8% cholesterol nanodiscs

ST- 5-1: Total Proteomic Profile

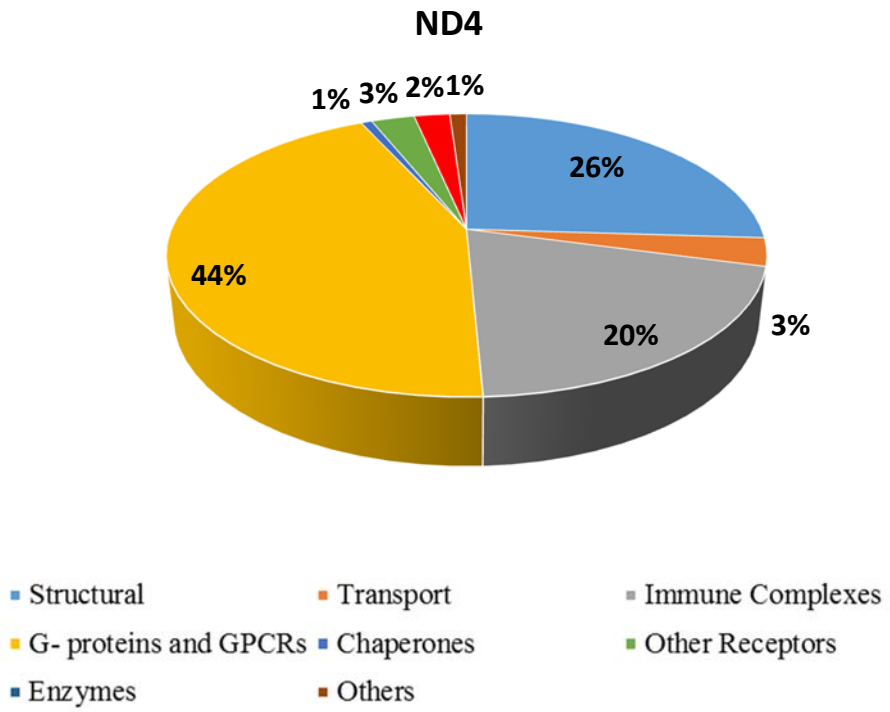

	emPAI	Percentage
Structure	21.79	25.98
Transport	2.69	3.21
Immune Complexes	16.84	20.08
GPCRs and G-proteins	36.81	43.89
Chaperones	0.59	0.70
Other receptors	2.32	2.77
Enzymes	1.93	2.30

Others	0.9	1.07

ST 5-2: Structural proteins identified

Accession	Mass	emPAI	Description
gi|62414289	53619	6.71	vimentin [Homo sapiens]
gi|11935049	66027	2.53	keratin 1 [Homo sapiens]
gi|181402	65825	1.08	epidermal cytokeratin 2 [Homo sapiens]
gi|119395754	62340	0.42	keratin, type II cytoskeletal 5 [Homo sapiens]
gi|119617057	57772	0.46	keratin 8, isoform CRA_a [Homo sapiens]
gi|435476	62092	2.57	cytokeratin 9 [Homo sapiens]
gi|114431246	50536	0.41	keratin, type I cytoskeletal 28 [Homo sapiens]
gi|119581150	44694	0.48	keratin 14 (epidermolysis bullosa simplex, Dowling-Meara, Koebner), isoform CRA_b [Homo sapiens]
gi|12653819	48003	0.2	Keratin 18 [Homo sapiens]
gi|114794644	35277	2.44	Chain A, Human Annexin A2 With Heparin Tetrasaccharide Bound
gi|28336	41786	0.69	mutant beta-actin (beta'-actin) [Homo sapiens]
gi|530421753	67936	0.68	PREDICTED: moesin isoform X2 [Homo sapiens]
gi|2773160	22941	0.76	neuronal tissue-enriched acidic protein [Homo sapiens]
gi|5031635	18491	0.26	cofilin-1 [Homo sapiens]
gi|338695	49727	0.3	beta-tubulin [Homo sapiens]
gi|6755901	50104	0.09	tubulin alpha-1A chain [Mus musculus]

gi|34234	31774	0.15	laminin-binding protein, partial [Homo sapiens]
gi|62088416	208278	0.02	ankyrin 1 isoform 4 variant [Homo sapiens]
gi|21281675	96460	0.05	GAS2-like protein 2 [Homo sapiens]
gi|29801	53563	0.09	CD44E (epithelial form) [Homo sapiens]
gi|197100396	20444	0.24	myosin regulatory light chain 12A [Pongo abelii]
gi|6731237	229553	0.02	myoferlin [Homo sapiens]
gi|530372502	102492	0.04	PREDICTED: microtubule-associated protein 4 isoform X23 [Homo sapiens]
gi|642945631	3992165	0	titin isoform IC [Homo sapiens]
gi|45331339	29608	0.16	BCR [Homo sapiens]
gi|4502719	78238	0.06	cadherin-13 isoform 1 preproprotein [Homo sapiens]
gi|608025	480107	0.01	ankyrin G [Homo sapiens]
gi|7239696	210642	0.02	myosin light chain kinase [Homo sapiens]
gi|182258028	45280	0.1	RHD [Homo sapiens]
gi|3323440	24479	0.19	myosin-IXb splice variant [Homo sapiens]
gi|32526901	79696	0.06	intraflagellar transport protein 81 homolog isoform 1 [Homo sapiens]
gi|528082092	55788	0.08	Chain A, Crystal Structure Of Human Catenin-beta-like 1 56 Kda Fragment
gi|5419655	287177	0.02	filamin, muscle isoform [Homo sapiens]
gi|1790878	306045	0.01	microtubule-associated protein 1a [Homo sapiens]
gi|7274242	109974	0.04	novel retinal pigment epithelial cell protein [Homo sapiens]

gi|767918801	36581	0.13	PREDICTED: LIM and senescent cell antigen-like-containing domain protein 2 isoform X2 [Homo sapiens]
gi|188219549	120972	0.04	ankyrin repeat domain-containing protein 32 [Homo sapiens]
gi|578825426	80723	0.06	PREDICTED: fermitin family homolog 2 isoform X1 [Homo sapiens]
gi|1000745	162108	0.03	Pro-a2(XI), partial [Homo sapiens]
gi|119577699	76618	0.06	basal cell adhesion molecule (Lutheran blood group), isoform CRA_b [Homo sapiens]
gi|767984060	150004	0.03	PREDICTED: kinesin-like protein KIF7 isoform X6 [Homo sapiens]

ST 5-3: Transport proteins identified

Accession	Mass	emPAI	Description
gi|21361181	112824	0.12	sodium/potassium-transporting ATPase subunit alpha-1 isoform a [Homo sapiens]
gi|1478281	56585	0.26	neutral amino acid transporter B [Homo sapiens]
gi|5803165	9968	1.32	protein transport protein Sec61 subunit beta [Homo sapiens]
gi|4505893	16680	0.29	proteolipid protein 2 [Homo sapiens]
gi|177207	57935	0.08	4F2 antigen heavy chain [Homo sapiens]
gi|5803040	25190	0.19	transmembrane emp24 domain-containing protein 1 precursor [Homo sapiens]
gi|119573492	28411	0.17	metaxin 1, isoform CRA_c [Homo sapiens]

gi|457879	227770	0.02	voltage-gated sodium channel [Homo sapiens]
gi|767944882	547785	0.01	PREDICTED: ATP-binding cassette sub-family A member 13 isoform X6 [Homo sapiens]
gi|119620095	109696	0.04	solute carrier family 4, sodium bicarbonate cotransporter, member 5, isoform CRA_b [Homo sapiens]
gi|1923268	121146	0.04	AP-3 complex beta3A subunit [Homo sapiens]
gi|9790143	50300	0.09	P3 protein isoform 1 precursor [Homo sapiens]
gi|767915110	74789	0.06	PREDICTED: sodium/calcium exchanger 1 isoform X10 [Homo sapiens]

ST 5-4: Immune complex proteins identified

Accession	Mass	emPAI	Description
gi|20146101	29134	0.35	EMMPRIN [Homo sapiens]
gi|11526609	4177	1.54	Ig heavy chain, partial [Homo sapiens]
gi|312273829	5398	1.1	TCR, partial [Homo sapiens]
gi|58221613	12853	0.39	anti-tetanus toxoid immunoglobulin heavy chain variable region [Homo sapiens]
gi|197115768	7786	0.7	immunoglobulin lambda chain variable region [Homo sapiens]
gi|15777368	12168	0.42	immunoglobulin mu heavy chain variable region [Homo sapiens]
gi|62999492	13061	0.38	immunoglobulin gamma heavy chain variable region [Homo sapiens]

gi|15722933	6474	0.89	immunoglobulin lambda chain variable region [Homo sapiens]
gi|3212402	1673	6.85	Chain C, The Structure Of An Intermediate In Class Ii Mhc Maturation: Clip Bound To Hla-dr3
gi|42760403	13053	0.38	immunoglobulin lambda-1 variable region [Homo sapiens]
gi|281185535	11546	0.44	anti-HIV immunoglobulin light chain variable region [Homo sapiens]
gi|219539	25902	0.18	nonspecific cross-reacting antigen [Homo sapiens]
gi|897557	177528	0.03	TIAM1 protein [Homo sapiens]
gi|371447513	13673	0.37	immunoglobulin G heavy chain variable region, partial [Homo sapiens]
gi|323431585	15902	0.31	immunoglobulin variable region [Homo sapiens]
gi|1633624	20982	0.23	HLA-G, partial [Homo sapiens]
gi|270054249	12186	0.42	immunoglobulin heavy chain variable region [Homo sapiens]
gi|323431159	15045	0.33	immunoglobulin variable region [Homo sapiens]
gi|22255307	10042	0.52	pituitary gland specific factor 1b [Homo sapiens]
gi|4323680	12747	0.39	immunoglobulin heavy chain variable region [Homo sapiens]
gi|323432798	14869	0.33	immunoglobulin variable region [Homo sapiens]
gi|161727636	16631	0.29	T cell receptor beta variable 20 [Homo sapiens]

ST 5-5: GPCRs and G proteins identified

Accession	Mass	emPAI	Description
gi|13569962	22157	0.79	ras-related protein Rab-1B [Homo sapiens]
gi|119620329	28129	0.36	RAB1A, member RAS oncogene family, isoform CRA_f [Homo sapiens]
gi|19923231	23534	2.01	ras-related protein Rab-6A isoform a [Homo sapiens]
gi|16933567	23653	0.73	ras-related protein Rab-8A [Homo sapiens]
gi|16758368	23912	0.72	ras-related protein Rab-14 [Rattus norvegicus]
gi|110591381	19753	1.97	Chain A, The Crystal Structure Of Human Neuronal Rab6b In Its Inactive Gdp-bound Form
gi|1174149	23447	1.09	small GTP binding protein Rab7 [Homo sapiens]
gi|508285	23553	1.51	Rab5c-like protein, similar to Canis familiaris Rab5c protein, PIR Accession Number S38625 [Homo sapiens]
gi|19923262	23644	0.73	ras-related protein Rab-5A isoform 1 [Homo sapiens]
gi|3126878	73512	0.35	M4 protein deletion mutant [Homo sapiens]
gi|4506413	20974	0.85	ras-related protein Rap-1A precursor [Homo sapiens]
gi|763130	24559	0.7	YPT3 [Homo sapiens]
gi|51036603	8001	1.82	guanine nucleotide-binding protein G(I)/G(S)/G(O) subunit gamma-12 precursor [Homo sapiens]
gi|183182	40437	0.24	guanine nucleotide-binding regulatory protein alpha-inhibitory subunit [Homo sapiens]
gi|190875	21323	0.5	ras-like protein [Homo sapiens]
gi|6808528	19737	0.24	Rab6-like protein [Homo sapiens]

gi|83753568	21521	0.49	Chain A, Crystal Structure Of Human Rab18 In Complex With Gppnhp
gi|4506405	23394	0.74	ras-related protein Ral-B [Homo sapiens]
gi|20147713	23971	0.72	Ras family small GTP binding protein RALA [Homo sapiens]
gi|306785	37320	0.12	G protein beta subunit [Homo sapiens]
gi|311697329	3564	1.93	KRAS protein [Homo sapiens]
gi|186764	21457	0.22	K-ras oncogene protein [Homo sapiens]
gi|4139784	24393	0.19	Chain A, Canine Gdp-Ran Q69l Mutant
gi|10190714	21841	0.22	ras-related protein Rab-22A [Homo sapiens]
gi|21703367	22471	0.21	GTP-binding protein Di-Ras2 [Homo sapiens]
gi|30749373	20607	0.23	Chain A, Crystal Structure Of A Constitutively Activated Rhoa Mutant (Q63l)
gi|21928356	37181	0.12	seven transmembrane helix receptor [Homo sapiens]
gi|219867	44452	0.1	HM74 [Homo sapiens]
gi|62088744	29577	0.16	regulator of G-protein signalling 11 isoform 1 variant [Homo sapiens]
gi|433720	145291	0.03	CDC25 [Homo sapiens]
gi|3292965	1071	15.8	m1 muscarinic acetylcholine receptor protein [Homo sapiens]
gi|119581051	52736	0.09	Rap guanine nucleotide exchange factor (GEF)-like 1, isoform CRA_c [Homo sapiens]
gi|122920033	54912	0.08	Chain A, Crystal Structure Of Rhogef Protein Asef
gi|6005794	19246	0.25	PRA1 family protein 2 [Homo sapiens]

gi|3327166	141499	0.03	KIAA0676 protein [Homo sapiens]
gi|4505187	14010	0.36	C-X-C motif chemokine 9 precursor [Homo sapiens]
gi|19702127	186116	0.02	P-Rex1 protein [Homo sapiens]
gi|768024595	49427	0.09	PREDICTED: ral-GDS-related protein isoform X1 [Homo sapiens]

ST 5-6: Chaperone proteins detected

Accession	Mass	emPAI	Description
gi|119602173	57697	0.35	heat shock protein 90kDa alpha (cytosolic), class A member 1, isoform CRA_b [Homo sapiens]
gi|1136741	58465	0.08	KIAA0002 [Homo sapiens]
gi|671527	60292	0.08	gamma subunit of CCT chaperonin [Homo sapiens]
gi|5453607	59329	0.08	T-complex protein 1 subunit eta isoform a [Homo sapiens]

ST 5-7: Other receptors identified

Accession	Mass	emPAI	Description
gi|19743813	88357	0.28	integrin beta-1 isoform 1A precursor [Homo sapiens]
gi|124942	129214	0.11	RecName: Full=Integrin alpha-2; AltName: Full=CD49 antigen-like family member B; AltName: Full=Collagen receptor; AltName: Full=Platelet membrane glycoprotein Ia; Short=GPIa; AltName: Full=VLA-2 subunit alpha; AltName: CD_antigen=CD49b; Flags: Precu
gi|291621647	26154	0.64	membrane-associated progesterone receptor component 2 [Homo sapiens]

gi|767927470	56504	0.17	PREDICTED: transferrin receptor protein 1 isoform X1 [Homo sapiens]
gi|62087318	166422	0.03	protein tyrosine phosphatase, receptor type, D isoform 4 precursor variant [Homo sapiens]
gi|119612685	544418	0.01	ryanodine receptor 3, isoform CRA_d, partial [Homo sapiens]
gi|41406086	89594	0.05	semaphorin-3D precursor [Homo sapiens]
gi|1632816	17317	0.64	C-Type lectin [Homo sapiens]
gi|30410880	125355	0.04	CD163 molecule [Homo sapiens]
gi|2337920	29827	0.16	syntaxin 7 [Homo sapiens]
gi|339570	64498	0.07	TGF-beta type II receptor [Homo sapiens]

ST 5-8: Enzymes detected

Accession	Mass	emPAI	Description
gi|22209028	31786	0.32	Thioredoxin-related transmembrane protein 1 [Homo sapiens]
gi|7243107	48042	0.1	KIAA1363 protein [Homo sapiens]
gi|1617312	72592	0.13	UDP-GalNAc:polypeptide N-acetylgalactosaminyltransferase (GalNAc-T3) [Homo sapiens]
gi|152149137	11017	0.47	Chain A, Crystal Structure Of Pdz Domain Of Synaptojanin-2 Binding Protein
gi|4826932	40738	0.11	peptidyl-prolyl cis-trans isomerase D [Homo sapiens]

gi|4506529	63485	0.07	rhodopsin kinase [Homo sapiens]
gi|641389703	64465	0.07	Chain A, Phosphatidylinositol 4-kinase Iii Beta-pik93 In A Complex With Rab11a-gtp Gammas
gi|58082081	84205	0.05	phosphoinositide 3-kinase regulatory subunit 6 isoform 1 [Homo sapiens]
gi|118573093	124985	0.04	RecName: Full=Ovochymase-1; Flags: Precursor [Homo sapiens]
gi|4885583	158076	0.03	rho-associated protein kinase 1 [Homo sapiens]
gi|1572645	9693	0.54	protein tyrosine phosphatase PEP, partial [Homo sapiens]

ST 5-9: Other membrane proteins identified

Accession	Mass	emPAI	Description
gi|119594185	36338	0.27	thioredoxin domain containing 14, isoform CRA_c [Homo sapiens]
gi|2465729	24642	0.19	TFAR15 [Homo sapiens]
gi|20521764	207178	0.02	KIAA1096 protein [Homo sapiens]
gi|33340133	79767	0.06	La binding protein 1 [Homo sapiens]
gi|46094081	125420	0.04	arf-GAP with SH3 domain, ANK repeat and PH domain-containing protein 1 isoform 1 [Homo sapiens]
gi|119600030	44772	0.1	GRAM domain containing 1C, isoform CRA_d [Homo sapiens]
gi|349587565	40057	0.12	Chain A, The Dodecameric Human Ruvbl1:ruvbl2 Complex With Truncated Domains Ii

gi|530411601	84186	0.05	PREDICTED: AP-4 complex accessory subunit tepsin isoform X2 [Homo sapiens]
gi|13195721	95398	0.05	KIAA1133 protein [Homo sapiens]

APPENDIX D: TABLES OF LIPIDS IDENTIFIED BY HIGH THROUGHPUT LIPIDOMICS OF FOB, HOS AND 143B CELL LINES

Table 1: Ceramides

Lipid Ion	FOB	HOS	143B
Cer(d18:1/10:0)+H	0.002 ± 0.000	0.001 ± 0.000	0.001 ± 0.000
Cer(d18:0/12:0)+H	0.002 ± 0.000	0.002 ± 0.000	0.001 ± 0.000
	0.000 ± 0.000	0.000 ± 0.000	0.000 ± 0.000
Cer(d18:1/13:0)+H	0.001 ± 0.000	0.001 ± 0.000	0.001 ± 0.001
Cer(d18:0/14:0)+H	0.002 ± 0.000	0.001 ± 0.000	0.003 ± 0.001
Cer(d18:1/14:0)+H	0.027 ± 0.006	0.006 ± 0.000	0.003 ± 0.001
Cer(d17:1/16:0)+H	0.006 ± 0.001	0.001 ± 0.000	0.002 ± 0.001
Cer(d18:0/16:0)+H	0.003 ± 0.001	0.001 ± 0.000	0.017 ± 0.015
Cer(d18:1/16:0)+H	0.162 ± 0.047	0.027 ± 0.001	0.022 ± 0.012
Cer(d34:1)+H	0.002 ± 0.000	0.001 ± 0.000	0.001 ± 0.001
Cer(d18:2/16:0)+H	0.016 ± 0.005	0.003 ± 0.000	0.001 ± 0.001
Cer(d18:0/17:0)+H	0.001 ± 0.000	0.001 ± 0.000	0.000 ± 0.000
Cer(d18:1/17:0)+H	0.009 ± 0.002	0.002 ± 0.000	0.001 ± 0.001
Cer(d18:0/18:0)+H	0.003 ± 0.000	0.004 ± 0.000	0.002 ± 0.001
Cer(d18:1/18:0)+H	0.021 ± 0.004	0.008 ± 0.000	0.002 ± 0.001
Cer(d36:1)+H	0.002 ± 0.000	0.001 ± 0.000	0.000 ± 0.000
Cer(d18:2/18:0)+H	0.002 ± 0.001	0.000 ± 0.000	0.001 ± 0.001
Cer(d18:0/20:0)+H	0.002 ± 0.000	0.002 ± 0.000	0.001 ± 0.000
Cer(d18:1/20:0)+H	0.007 ± 0.001	0.003 ± 0.000	0.001 ± 0.000
Cer(d38:1)+H	0.001 ± 0.000	0.001 ± 0.000	0.000 ± 0.000
Cer(d17:1/22:0)+H	0.003 ± 0.000	0.001 ± 0.000	0.000 ± 0.000
Cer(d40:0)+H	0.001 ± 0.001	0.000 ± 0.000	0.007 ± 0.006
Cer(d18:0/22:0)+H	0.005 ± 0.001	0.010 ± 0.001	0.007 ± 0.003
Cer(d18:0/22:1)+H	0.001 ± 0.000	0.001 ± 0.000	0.005 ± 0.004
Cer(d18:1/22:0)+H	0.055 ± 0.014	0.016 ± 0.001	0.006 ± 0.003
Cer(d18:2/22:0)+H	0.014 ± 0.005	0.003 ± 0.000	0.001 ± 0.000

Cer(d18:0/23:0)+H	0.001 ± 0.000	0.001 ± 0.000	0.001 ± 0.000
Cer(d18:0/23:1)+H	0.001 ± 0.000	0.001 ± 0.000	0.002 ± 0.001
Cer(d18:1/23:0)+H	0.013 ± 0.003	0.003 ± 0.000	0.002 ± 0.000
Cer(d18:2/23:0)+H	0.012 ± 0.003	0.002 ± 0.000	0.034 ± 0.033
Cer(d18:0/24:0)+H	0.006 ± 0.001	0.022 ± 0.002	0.037 ± 0.020
Cer(d18:1/24:0)+H	0.001 ± 0.000	0.000 ± 0.000	0.012 ± 0.012
Cer(d18:0/24:1)+H	0.008 ± 0.002	0.011 ± 0.001	0.040 ± 0.020
Cer(d18:1/24:0)+H	0.101 ± 0.028	0.051 ± 0.004	0.047 ± 0.008
Cer(d18:1/24:1)+H	0.145 ± 0.049	0.038 ± 0.006	0.020 ± 0.010
Cer(d18:2/24:0)+H	0.007 ± 0.002	0.001 ± 0.000	0.002 ± 0.001
Cer(d18:2/24:1)+H	0.038 ± 0.011	0.008 ± 0.001	0.002 ± 0.001
Cer(d18:1/24:2)+H	0.002 ± 0.000	0.003 ± 0.000	0.002 ± 0.000
Cer(d18:1/24:3)+H	0.010 ± 0.001	0.007 ± 0.000	0.002 ± 0.000
Cer(d18:0/25:0)+H	0.001 ± 0.000	0.001 ± 0.000	0.001 ± 0.000
Cer(d18:0/25:1)+H	0.000 ± 0.000	0.000 ± 0.000	0.002 ± 0.001
Cer(d18:1/25:0)+H	0.004 ± 0.001	0.002 ± 0.000	0.002 ± 0.000
Cer(d18:1/25:1)+H	0.006 ± 0.002	0.002 ± 0.000	0.001 ± 0.000
Cer(d18:2/25:1)+H	0.004 ± 0.001	0.001 ± 0.000	0.009 ± 0.009
Cer(d18:0/26:0)+H	0.001 ± 0.000	0.005 ± 0.001	0.014 ± 0.002
Cer(d18:0/26:1)+H	0.001 ± 0.000	0.001 ± 0.000	0.013 ± 0.007
Cer(d18:1/26:0)+H	0.007 ± 0.002	0.006 ± 0.001	0.010 ± 0.005
Cer(d18:2/26:0)+H	0.001 ± 0.000	0.001 ± 0.000	0.006 ± 0.005
Cer(d18:1/26:1)+H	0.017 ± 0.006	0.005 ± 0.000	0.008 ± 0.003
Cer(d18:2/26:1)+H	0.009 ± 0.003	0.002 ± 0.000	0.001 ± 0.000
Cer(d18:1/26:3)+H	0.002 ± 0.001	0.000 ± 0.000	0.000 ± 0.000
Cer(d20:0/25:0)+H	0.001 ± 0.000	0.002 ± 0.001	0.001 ± 0.000
Cer(d18:1/27:0)+H	0.000 ± 0.000	0.001 ± 0.001	0.001 ± 0.000
Cer(d20:0/26:0)+H	0.001 ± 0.000	0.003 ± 0.002	0.001 ± 0.000
Cer(d18:0/28:1)+H	0.000 ± 0.000	0.000 ± 0.000	0.001 ± 0.000
Cer(d18:1/28:0)+H	0.001 ± 0.000	0.002 ± 0.001	0.001 ± 0.000
Cer(d18:1/28:1)+H	0.000 ± 0.000	0.000 ± 0.000	0.000 ± 0.000

Cer(d22:1/24:1)+H	0.000 ± 0.000	0.000 ± 0.000	0.000 ± 0.000
Cer(d22:0/25:0)+H	0.001 ± 0.000	0.003 ± 0.002	0.000 ± 0.000
Cer(d20:1/27:0)+H	0.000 ± 0.000	0.001 ± 0.001	0.000 ± 0.000
Cer(d22:1/25:1)+H	0.000 ± 0.000	0.000 ± 0.000	0.000 ± 0.000
Cer(d24:0/24:0)+H	0.001 ± 0.000	0.005 ± 0.004	0.001 ± 0.000
Cer(d20:1/28:0)+H	0.000 ± 0.000	0.002 ± 0.002	0.000 ± 0.000
Cer(d20:2/28:0)+H	0.000 ± 0.000	0.001 ± 0.001	0.000 ± 0.000
Cer(d25:0/24:0)+H	0.000 ± 0.000	0.003 ± 0.002	0.000 ± 0.000
Cer(d22:1/27:0)+H	0.000 ± 0.000	0.001 ± 0.001	0.000 ± 0.000
Cer(d24:0/26:0)+H	0.001 ± 0.000	0.003 ± 0.003	0.000 ± 0.000
Cer(d22:1/28:0)+H	0.000 ± 0.000	0.002 ± 0.001	0.000 ± 0.000
Cer(d25:0/26:0)+H	0.000 ± 0.000	0.001 ± 0.001	0.000 ± 0.000
Cer(d22:1/29:0)+H	0.000 ± 0.000	0.001 ± 0.001	0.000 ± 0.000
Cer(d22:1/30:0)+H	0.000 ± 0.000	0.001 ± 0.001	0.000 ± 0.000
Cer(d25:0/28:0)+H	0.000 ± 0.000	0.000 ± 0.000	0.000 ± 0.000
CerG1(d18:0/14:0)+H	0.001 ± 0.000	0.000 ± 0.000	0.002 ± 0.001
CerG1(d18:1/14:0)+H	0.021 ± 0.007	0.001 ± 0.000	0.002 ± 0.000
CerG1(d17:1/16:0)+H	0.008 ± 0.002	0.001 ± 0.000	0.013 ± 0.012
CerG1(d18:0/16:0)+H	0.027 ± 0.007	0.013 ± 0.001	0.048 ± 0.027
CerG1(d18:1/16:0)+H	0.446 ± 0.116	0.047 ± 0.007	0.043 ± 0.020
CerG1(d18:2/16:0)+H	0.007 ± 0.002	0.002 ± 0.000	0.002 ± 0.000
CerG1(d18:1/17:0)+H	0.018 ± 0.004	0.002 ± 0.000	0.002 ± 0.001
CerG1(d18:1/18:0)+H	0.029 ± 0.004	0.011 ± 0.000	0.002 ± 0.001
CerG1(d18:0/20:0)+H	0.001 ± 0.000	0.002 ± 0.000	0.001 ± 0.001
CerG1(d18:1/20:0)+H	0.009 ± 0.001	0.005 ± 0.000	0.005 ± 0.004
CerG1(d18:0/22:0)+H	0.006 ± 0.002	0.008 ± 0.000	0.012 ± 0.005
CerG1(d18:1/22:0)+H	0.083 ± 0.018	0.020 ± 0.001	0.007 ± 0.003
CerG1(d18:1/22:1)+H	0.012 ± 0.002	0.003 ± 0.000	0.001 ± 0.000
CerG1(d18:0/23:0)+H	0.001 ± 0.000	0.000 ± 0.000	0.003 ± 0.003
CerG1(d18:1/23:0)+H	0.024 ± 0.007	0.003 ± 0.000	0.003 ± 0.001
CerG1(d18:1/23:1)+H	0.010 ± 0.003	0.002 ± 0.000	0.014 ± 0.014

CerG1(d18:0/24:0)+H	0.007 ± 0.002	0.005 ± 0.000	0.018 ± 0.001
CerG1(d18:0/24:1)+H	0.005 ± 0.001	0.005 ± 0.000	0.060 ± 0.051
CerG1(d18:1/24:0)+H	0.286 ± 0.110	0.031 ± 0.002	0.065 ± 0.005
CerG1(d18:1/24:1)+H	0.140 ± 0.048	0.024 ± 0.003	0.021 ± 0.008
CerG1(d18:2/24:1)+H	0.021 ± 0.006	0.005 ± 0.001	0.002 ± 0.001
CerG1(d18:0/25:0)+H	0.000 ± 0.000	0.000 ± 0.000	0.000 ± 0.000
CerG1(d18:1/25:0)+H	0.002 ± 0.001	0.000 ± 0.000	0.001 ± 0.000
CerG1(d18:1/25:1)+H	0.007 ± 0.002	0.001 ± 0.000	0.002 ± 0.001
CerG1(d18:0/26:0)+H	0.000 ± 0.000	0.000 ± 0.000	0.002 ± 0.000
CerG1(d18:0/26:1)+H	0.001 ± 0.000	0.000 ± 0.000	0.008 ± 0.006
CerG1(d18:1/26:0)+H	0.012 ± 0.005	0.002 ± 0.000	0.012 ± 0.002
CerG1(d18:1/26:1)+H	0.023 ± 0.010	0.002 ± 0.000	0.005 ± 0.003
CerG1(d44:4)+H	0.002 ± 0.000	0.000 ± 0.000	0.000 ± 0.000
CerG1(d46:1)+H	0.000 ± 0.000	0.000 ± 0.000	0.006 ± 0.006
CerG2(d18:1/16:0)+H	0.028 ± 0.010	0.008 ± 0.004	0.006 ± 0.003
CerG2(d34:2)+H	0.002 ± 0.001	0.002 ± 0.000	0.002 ± 0.002
CerG2(d18:1/22:0)+H	0.010 ± 0.002	0.007 ± 0.000	0.002 ± 0.001
CerG2(d18:1/22:1)+H	0.002 ± 0.000	0.002 ± 0.000	0.000 ± 0.000
CerG2(d18:1/23:0)+H	0.002 ± 0.001	0.001 ± 0.000	0.000 ± 0.000
CerG2(d18:1/23:1)+H	0.002 ± 0.001	0.001 ± 0.000	0.001 ± 0.001
CerG2(d18:0/24:1)+H	0.001 ± 0.000	0.001 ± 0.000	0.009 ± 0.007
CerG2(d18:1/24:0)+H	0.018 ± 0.007	0.004 ± 0.000	0.012 ± 0.002
CerG2(d18:1/24:1)+H	0.018 ± 0.005	0.009 ± 0.001	0.006 ± 0.003
CerG2(d18:2/24:1)+H	0.004 ± 0.001	0.002 ± 0.000	0.001 ± 0.000
CerG2(d18:1/25:0)+H	0.001 ± 0.000	0.000 ± 0.000	0.000 ± 0.000
CerG2(d43:2)+H	0.001 ± 0.000	0.000 ± 0.000	0.001 ± 0.001
CerG2(d18:1/26:0)+H	0.001 ± 0.000	0.000 ± 0.000	0.002 ± 0.000
CerG2(d18:1/26:1)+H	0.002 ± 0.001	0.001 ± 0.000	0.001 ± 0.000
CerG3(d18:1/14:0)+H	0.001 ± 0.000	0.000 ± 0.000	0.001 ± 0.001
CerG3(d18:1/16:0)+H	0.015 ± 0.004	0.002 ± 0.000	0.001 ± 0.000
CerG3(d18:1/22:0)+H	0.005 ± 0.001	0.001 ± 0.000	0.000 ± 0.000

CerG3(d18:1/23:0)+H	0.001 ± 0.000	0.000 ± 0.000	0.000 ± 0.000
CerG3(d18:1/24:0)+H	0.008 ± 0.003	0.001 ± 0.000	0.001 ± 0.000
CerG3(d18:1/24:1)+H	0.010 ± 0.003	0.002 ± 0.000	0.000 ± 0.000
CerG3(d18:2/24:1)+H	0.002 ± 0.001	0.000 ± 0.000	0.000 ± 0.000
CerG3(d18:1/26:0)+H	0.001 ± 0.000	0.000 ± 0.000	0.000 ± 0.000
CerG3(d18:1/26:1)+H	0.001 ± 0.000	0.000 ± 0.000	0.373 ± 0.373

Table 2: Cholesterol Esters

Lipid Ion	FOB	HOS	143B
ChE(18:1)+NH4	0.047 ± 0.012	0.013 ± 0.001	0.007 ± 0.002
ChE(18:2)+NH4	0.030 ± 0.006	0.006 ± 0.001	0.005 ± 0.001
ChE(20:1)+NH4	0.005 ± 0.002	0.003 ± 0.000	0.001 ± 0.000
ChE(20:2)+NH4	0.014 ± 0.006	0.010 ± 0.001	0.001 ± 0.000
ChE(20:3)+NH4	0.043 ± 0.011	0.031 ± 0.003	0.002 ± 0.000
ChE(20:4)+NH4	0.075 ± 0.012	0.052 ± 0.005	0.007 ± 0.001
ChE(20:5)+NH4	0.030 ± 0.007	0.022 ± 0.002	0.003 ± 0.001
ChE(22:1)+NH4	0.002 ± 0.001	0.002 ± 0.000	0.000 ± 0.000
ChE(22:2)+NH4	0.005 ± 0.002	0.004 ± 0.001	0.000 ± 0.000
ChE(22:3)+NH4	0.015 ± 0.005	0.024 ± 0.004	0.001 ± 0.000
ChE(22:4)+NH4	0.031 ± 0.005	0.174 ± 0.018	0.001 ± 0.000
ChE(22:5)+NH4	0.079 ± 0.019	0.125 ± 0.009	0.005 ± 0.001
ChE(22:6)+NH4	0.325 ± 0.121	0.430 ± 0.067	0.032 ± 0.009
ChE(24:1)+NH4	0.005 ± 0.002	0.002 ± 0.000	0.002 ± 0.001
ChE(24:3)+NH4	0.014 ± 0.006	0.016 ± 0.003	0.001 ± 0.000
ChE(24:4)+NH4	0.025 ± 0.008	0.073 ± 0.013	0.001 ± 0.000
ChE(24:5)+NH4	0.042 ± 0.015	0.135 ± 0.020	0.002 ± 0.001
ChE(24:6)+NH4	0.074 ± 0.032	0.127 ± 0.021	0.003 ± 0.001
ChE(26:0)+NH4	0.001 ± 0.000	0.000 ± 0.000	0.004 ± 0.001
ChE(26:1)+NH4	0.010 ± 0.005	0.001 ± 0.000	0.008 ± 0.002

ChE(26:2)+NH4	0.009 ± 0.005	0.004 ± 0.001	0.006 ± 0.001
ChE(26:3)+NH4	0.020 ± 0.009	0.011 ± 0.001	0.002 ± 0.000
ChE(26:4)+NH4	0.036 ± 0.016	0.028 ± 0.004	0.002 ± 0.000
ChE(26:5)+NH4	0.119 ± 0.050	0.100 ± 0.019	0.004 ± 0.001
ChE(26:6)+NH4	0.193 ± 0.088	0.076 ± 0.012	0.005 ± 0.001
ChE(28:1)+NH4	0.001 ± 0.001	0.000 ± 0.000	0.003 ± 0.001
ChE(28:2)+NH4	0.002 ± 0.001	0.000 ± 0.000	0.001 ± 0.000
ChE(28:3)+NH4	0.003 ± 0.002	0.001 ± 0.000	0.001 ± 0.000
ChE(28:4)+NH4	0.006 ± 0.003	0.003 ± 0.000	0.000 ± 0.000
ChE(28:5)+NH4	0.031 ± 0.014	0.028 ± 0.004	0.001 ± 0.000
ChE(28:6)+NH4	0.059 ± 0.028	0.017 ± 0.002	0.002 ± 0.000
ChE(30:1)+NH4	0.000 ± 0.000	0.000 ± 0.000	0.001 ± 0.000
ChE(30:3)+NH4	0.001 ± 0.000	0.000 ± 0.000	0.000 ± 0.000
ChE(30:4)+NH4	0.001 ± 0.001	0.001 ± 0.000	0.000 ± 0.000
ChE(30:5)+NH4	0.007 ± 0.003	0.010 ± 0.001	0.001 ± 0.000
ChE(30:6)+NH4	0.025 ± 0.012	0.010 ± 0.001	0.002 ± 0.000
ChE(32:5)+NH4	0.002 ± 0.001	0.001 ± 0.000	0.001 ± 0.000
ChE(32:6)+NH4	0.007 ± 0.003	0.003 ± 0.000	0.002 ± 0.000

Table 3: Cardiolipin

Lipid Ion	FOB	HOS	143B
CL(14:0/16:0/16:0/16:0)-H	0.000 ± 0.000	0.001 ± 0.000	0.000 ± 0.000
CL(14:0/16:0/16:1/16:0)-H	0.000 ± 0.000	0.003 ± 0.000	0.001 ± 0.000
CL(14:0/14:0/18:1/16:1)-H	0.000 ± 0.000	0.001 ± 0.000	0.002 ± 0.000
CL(14:0/16:1/16:1/16:1)-H	0.001 ± 0.000	0.000 ± 0.000	0.002 ± 0.000
CL(16:0/16:0/16:0/16:0)-H	0.000 ± 0.000	0.003 ± 0.000	0.000 ± 0.000
CL(14:0/16:0/16:0/18:1)-H	0.000 ± 0.000	0.013 ± 0.003	0.002 ± 0.001
CL(14:0/18:1/16:0/16:1)-H	0.001 ± 0.000	0.006 ± 0.001	0.006 ± 0.001
CL(14:0/16:1/16:1/18:1)-H	0.003 ± 0.001	0.001 ± 0.000	0.008 ± 0.002
CL(16:1/16:1/16:1/16:1)-H	0.003 ± 0.002	0.000 ± 0.000	0.004 ± 0.001

CL(15:0/16:0/16:0/18:1)-H	0.000 ± 0.000	0.004 ± 0.001	0.000 ± 0.000
CL(14:0/15:0/18:1/18:1)-H	0.000 ± 0.000	0.003 ± 0.001	0.001 ± 0.000
CL(17:1/14:0/18:1/16:1)-H	0.001 ± 0.000	0.001 ± 0.000	0.001 ± 0.000
CL(17:1/16:1/16:1/16:1)-H	0.001 ± 0.001	0.000 ± 0.000	0.001 ± 0.000
CL(16:0/16:0/16:0/18:0)-H	0.000 ± 0.000	0.002 ± 0.000	0.000 ± 0.000
CL(18:1/16:0/16:0/16:0)-H	0.000 ± 0.000	0.050 ± 0.007	0.002 ± 0.001
CL(14:0/18:1/16:0/18:1)-H	0.003 ± 0.001	0.050 ± 0.010	0.013 ± 0.003
CL(18:1/16:1/16:0/16:1)-H	0.006 ± 0.003	0.009 ± 0.002	0.021 ± 0.006
CL(16:1/16:1/16:1/18:1)-H	0.013 ± 0.006	0.004 ± 0.001	0.023 ± 0.006
CL(18:3/14:0/16:0/18:1)-H	0.000 ± 0.000	0.003 ± 0.000	0.001 ± 0.000
CL(18:2/16:1/16:1/16:1)-H	0.004 ± 0.002	0.002 ± 0.000	0.005 ± 0.001
CL(12:2/18:1/18:1/18:1)-H	0.000 ± 0.000	0.001 ± 0.000	0.001 ± 0.000
CL(22:5/14:0/16:1/14:0)-H	0.001 ± 0.000	0.000 ± 0.000	0.002 ± 0.000
CL(18:4/16:1/16:1/16:1)-H	0.001 ± 0.000	0.000 ± 0.000	0.001 ± 0.000
CL(17:0/16:0/16:0/18:1)-H	0.000 ± 0.000	0.006 ± 0.001	0.000 ± 0.000
CL(18:1/16:0/18:1/15:0)-H	0.001 ± 0.000	0.021 ± 0.004	0.001 ± 0.000
CL(17:1/16:0/16:1/18:1)-H	0.002 ± 0.000	0.005 ± 0.001	0.003 ± 0.001
CL(17:1/16:1/16:1/18:1)-H	0.004 ± 0.002	0.003 ± 0.000	0.004 ± 0.001
CL(17:1/16:1/18:2/16:1)-H	0.001 ± 0.001	0.001 ± 0.000	0.001 ± 0.000
CL(16:0/16:0/16:0/20:0)-H	0.000 ± 0.000	0.002 ± 0.000	0.000 ± 0.000
CL(18:1/16:0/18:0/16:0)-H	0.000 ± 0.000	0.029 ± 0.005	0.001 ± 0.000
CL(18:1/16:0/16:0/18:1)-H	0.005 ± 0.001	0.297 ± 0.046	0.026 ± 0.006
CL(18:1/16:0/16:1/18:1)-H	0.011 ± 0.003	0.069 ± 0.014	0.036 ± 0.008
CL(18:1/16:1/18:2/16:0)-H	0.029 ± 0.011	0.019 ± 0.003	0.063 ± 0.018
CL(18:3/16:0/16:0/18:1)-H	0.001 ± 0.000	0.004 ± 0.001	0.001 ± 0.000
CL(18:3/18:1/16:0/16:0)-H	0.000 ± 0.000	0.008 ± 0.001	0.001 ± 0.000
CL(18:2/16:1/18:1/16:1)-H	0.019 ± 0.008	0.013 ± 0.003	0.027 ± 0.007
CL(20:4/16:0/14:0/18:1)-H	0.001 ± 0.000	0.010 ± 0.002	0.002 ± 0.000
CL(18:2/16:1/18:2/16:1)-H	0.004 ± 0.002	0.003 ± 0.001	0.003 ± 0.001
CL(18:4/16:0/16:1/18:1)-H	0.002 ± 0.001	0.002 ± 0.001	0.004 ± 0.001
CL(20:4/16:1/16:1/16:1)-H	0.001 ± 0.001	0.000 ± 0.000	0.001 ± 0.000

CL(18:4/16:1/16:1/18:1)-H	0.003 ± 0.002	0.001 ± 0.000	0.005 ± 0.001
CL(18:4/16:1/18:2/16:1)-H	0.001 ± 0.001	0.000 ± 0.000	0.001 ± 0.000
CL(17:0/18:1/18:1/16:0)-H	0.001 ± 0.000	0.023 ± 0.004	0.001 ± 0.000
CL(17:1/18:1/16:0/18:1)-H	0.002 ± 0.000	0.018 ± 0.004	0.004 ± 0.001
CL(17:1/18:1/16:1/18:1)-H	0.006 ± 0.002	0.008 ± 0.002	0.009 ± 0.002
CL(18:1/15:1/18:1/18:1)-H	0.000 ± 0.000	0.001 ± 0.000	0.000 ± 0.000
CL(17:1/16:1/18:2/18:1)-H	0.005 ± 0.002	0.006 ± 0.001	0.004 ± 0.001
CL(18:3/18:1/15:0/18:1)-H	0.000 ± 0.000	0.005 ± 0.001	0.000 ± 0.000
CL(17:1/16:1/18:2/18:2)-H	0.001 ± 0.000	0.002 ± 0.000	0.000 ± 0.000
CL(17:1/16:1/16:1/20:4)-H	0.001 ± 0.000	0.001 ± 0.000	0.001 ± 0.000
CL(18:1/16:0/18:0/18:0)-H	0.001 ± 0.001	0.001 ± 0.000	0.005 ± 0.001
CL(18:1/16:0/18:0/18:1)-H	0.002 ± 0.000	0.095 ± 0.017	0.004 ± 0.001
CL(18:1/16:0/18:1/18:1)-H	0.009 ± 0.002	0.238 ± 0.036	0.022 ± 0.005
CL(18:1/16:1/18:1/18:1)-H	0.029 ± 0.009	0.055 ± 0.011	0.056 ± 0.013
CL(18:3/18:1/16:0/18:0)-H	0.000 ± 0.000	0.007 ± 0.001	0.000 ± 0.000
CL(18:2/18:1/16:1/18:1)-H	0.032 ± 0.009	0.041 ± 0.007	0.056 ± 0.015
CL(18:3/18:1/16:0/18:1)-H	0.001 ± 0.000	0.039 ± 0.005	0.006 ± 0.001
CL(18:2/16:1/18:1/18:2)-H	0.016 ± 0.005	0.025 ± 0.005	0.014 ± 0.004
CL(18:2/18:2/16:1/18:1)-H	0.003 ± 0.001	0.017 ± 0.003	0.007 ± 0.001
CL(18:2/18:2/18:2/16:1)-H	0.003 ± 0.001	0.005 ± 0.001	0.002 ± 0.001
CL(20:4/16:1/16:1/18:1)-H	0.004 ± 0.001	0.003 ± 0.000	0.003 ± 0.001
CL(20:4/16:1/18:1/16:1)-H	0.008 ± 0.003	0.005 ± 0.001	0.011 ± 0.002
CL(22:5/16:1/16:1/16:1)-H	0.001 ± 0.000	0.001 ± 0.000	0.001 ± 0.000
CL(18:2/20:4/16:1/16:1)-H	0.005 ± 0.002	0.003 ± 0.001	0.006 ± 0.001
CL(20:5/16:1/16:1/18:2)-H	0.001 ± 0.000	0.001 ± 0.000	0.001 ± 0.000
CL(17:0/18:1/18:0/18:1)-H	0.000 ± 0.000	0.005 ± 0.001	0.000 ± 0.000
CL(17:0/18:1/18:1/18:1)-H	0.001 ± 0.000	0.011 ± 0.002	0.001 ± 0.000
CL(17:1/18:1/18:1/18:1)-H	0.005 ± 0.001	0.008 ± 0.001	0.005 ± 0.001
CL(17:1/18:1/18:2/18:1)-H	0.005 ± 0.001	0.010 ± 0.002	0.005 ± 0.001
CL(17:0/20:4/16:0/18:1)-H	0.000 ± 0.000	0.005 ± 0.001	0.000 ± 0.000
CL(17:1/18:1/18:2/18:2)-H	0.003 ± 0.001	0.006 ± 0.001	0.001 ± 0.000

CL(17:0/18:2/18:2/18:2)-H	0.001 ± 0.000	0.001 ± 0.000	0.001 ± 0.000
CL(17:1/20:4/16:0/18:1)-H	0.001 ± 0.000	0.004 ± 0.001	0.001 ± 0.000
CL(17:1/18:2/18:2/18:2)-H	0.001 ± 0.000	0.001 ± 0.000	0.001 ± 0.000
CL(17:1/20:4/16:1/18:1)-H	0.002 ± 0.001	0.002 ± 0.000	0.002 ± 0.000
CL(17:1/16:1/20:4/18:2)-H	0.001 ± 0.000	0.001 ± 0.000	0.001 ± 0.000
CL(16:0/18:0/18:0/20:0)-H	0.000 ± 0.000	0.002 ± 0.000	0.001 ± 0.000
CL(18:4/18:2/18:2/18:2)-H	0.001 ± 0.000	0.001 ± 0.000	0.000 ± 0.000
CL(18:1/18:0/18:0/18:1)-H	0.005 ± 0.002	0.002 ± 0.000	0.013 ± 0.003
CL(18:1/18:0/18:1/18:1)-H	0.002 ± 0.000	0.037 ± 0.007	0.002 ± 0.001
CL(18:1/18:1/18:1/18:1)-H	0.012 ± 0.002	0.058 ± 0.009	0.016 ± 0.004
CL(18:2/18:1/18:1/18:1)-H	0.021 ± 0.002	0.038 ± 0.008	0.027 ± 0.006
CL(20:4/16:0/18:0/18:1)-H	0.001 ± 0.000	0.021 ± 0.003	0.001 ± 0.000
CL(18:2/18:1/18:1/18:2)-H	0.020 ± 0.001	0.042 ± 0.007	0.017 ± 0.004
CL(20:4/16:0/18:1/18:1)-H	0.002 ± 0.001	0.031 ± 0.004	0.005 ± 0.001
CL(18:2/18:2/18:2/18:1)-H	0.009 ± 0.001	0.021 ± 0.004	0.005 ± 0.001
CL(18:2/18:1/18:2/18:2)-H	0.008 ± 0.002	0.015 ± 0.003	0.012 ± 0.002
CL(18:2/18:1/20:4/16:1)-H	0.002 ± 0.000	0.004 ± 0.001	0.001 ± 0.000
CL(18:2/20:4/16:1/18:1)-H	0.009 ± 0.002	0.010 ± 0.001	0.009 ± 0.002
CL(18:2/16:1/16:1/22:5)-H	0.002 ± 0.000	0.002 ± 0.000	0.001 ± 0.000
CL(18:2/16:1/20:4/18:2)-H	0.004 ± 0.001	0.006 ± 0.001	0.003 ± 0.001
CL(19:1/18:1/18:1/18:1)-H	0.000 ± 0.000	0.001 ± 0.000	0.001 ± 0.000
CL(19:1/18:1/18:2/18:1)-H	0.001 ± 0.000	0.002 ± 0.000	0.001 ± 0.000
CL(19:1/18:1/18:2/18:2)-H	0.001 ± 0.000	0.003 ± 0.001	0.001 ± 0.000
CL(17:0/18:1/20:4/18:1)-H	0.000 ± 0.000	0.002 ± 0.000	0.000 ± 0.000
CL(17:1/18:1/18:1/20:4)-H	0.000 ± 0.000	0.002 ± 0.000	0.001 ± 0.000
CL(17:1/18:1/20:4/18:1)-H	0.001 ± 0.000	0.002 ± 0.000	0.001 ± 0.000
CL(17:1/18:1/18:2/20:4)-H	0.001 ± 0.000	0.002 ± 0.001	0.001 ± 0.000
CL(17:1/18:2/18:2/20:4)-H	0.001 ± 0.000	0.001 ± 0.000	0.000 ± 0.000
CL(18:1/18:0/18:0/20:0)-H	0.029 ± 0.008	0.009 ± 0.002	0.021 ± 0.004
CL(18:2/18:2/18:2/20:4)-H	0.002 ± 0.000	0.001 ± 0.000	0.000 ± 0.000
CL(20:5/18:2/18:2/18:2)-H	0.001 ± 0.000	0.001 ± 0.000	0.000 ± 0.000

CL(18:1/16:0/16:0/24:1)-H	0.001 ± 0.001	0.001 ± 0.000	0.003 ± 0.001
CL(22:2/16:0/18:0/18:1)-H	0.009 ± 0.003	0.005 ± 0.001	0.010 ± 0.002
CL(20:4/18:0/18:0/18:0)-H	0.009 ± 0.002	0.008 ± 0.001	0.007 ± 0.001
CL(18:1/18:1/18:1/20:1)-H	0.001 ± 0.000	0.003 ± 0.001	0.001 ± 0.000
CL(18:1/16:0/20:1/20:3)-H	0.000 ± 0.000	0.005 ± 0.001	0.000 ± 0.000
CL(18:1/18:0/18:0/20:4)-H	0.000 ± 0.000	0.003 ± 0.000	0.000 ± 0.000
CL(20:4/18:1/18:0/18:1)-H	0.001 ± 0.000	0.009 ± 0.001	0.001 ± 0.000
CL(18:2/18:1/20:3/18:1)-H	0.005 ± 0.000	0.014 ± 0.003	0.003 ± 0.001
CL(20:4/18:1/18:1/18:1)-H	0.004 ± 0.001	0.011 ± 0.001	0.004 ± 0.001
CL(18:2/18:1/20:4/18:1)-H	0.002 ± 0.000	0.004 ± 0.001	0.001 ± 0.000
CL(18:2/20:4/18:1/18:1)-H	0.006 ± 0.000	0.011 ± 0.002	0.005 ± 0.001
CL(18:2/18:1/18:2/20:4)-H	0.006 ± 0.001	0.009 ± 0.002	0.003 ± 0.001
CL(18:2/18:1/20:4/18:2)-H	0.006 ± 0.000	0.011 ± 0.002	0.004 ± 0.001
CL(23:0/16:0/18:1/18:1)-H	0.002 ± 0.001	0.002 ± 0.001	0.003 ± 0.001
CL(21:0/20:4/16:0/18:0)-H	0.005 ± 0.000	0.006 ± 0.001	0.003 ± 0.001
CL(20:5/18:1/20:4/18:1)-H	0.000 ± 0.000	0.001 ± 0.000	0.000 ± 0.000
CL(18:2/18:2/18:2/22:6)-H	0.001 ± 0.000	0.001 ± 0.000	0.000 ± 0.000
CL(18:4/22:6/20:4/16:1)-H	0.001 ± 0.001	0.001 ± 0.000	0.002 ± 0.000
CL(18:1/18:0/20:1/20:1)-H	0.005 ± 0.001	0.002 ± 0.000	0.002 ± 0.000
CL(18:1/16:0/18:1/24:1)-H	0.000 ± 0.000	0.001 ± 0.000	0.000 ± 0.000
CL(22:3/18:0/18:0/18:1)-H	0.011 ± 0.002	0.004 ± 0.001	0.005 ± 0.000
CL(22:1/18:1/18:1/18:1)-H	0.000 ± 0.000	0.001 ± 0.000	0.000 ± 0.000
CL(20:4/18:0/18:1/20:0)-H	0.015 ± 0.003	0.010 ± 0.002	0.010 ± 0.002
CL(22:3/18:1/18:1/18:1)-H	0.000 ± 0.000	0.001 ± 0.000	0.000 ± 0.000
CL(20:2/18:0/18:1/20:4)-H	0.004 ± 0.001	0.002 ± 0.001	0.003 ± 0.000
CL(22:5/18:0/18:1/18:1)-H	0.000 ± 0.000	0.003 ± 0.001	0.000 ± 0.000
CL(22:5/18:1/18:1/18:1)-H	0.001 ± 0.000	0.004 ± 0.001	0.000 ± 0.000
CL(23:0/18:0/18:0/18:1)-H	0.001 ± 0.000	0.000 ± 0.000	0.001 ± 0.000
CL(20:5/20:4/20:4/18:1)-H	0.000 ± 0.000	0.005 ± 0.001	0.001 ± 0.000
CL(22:2/18:0/18:1/20:4)-H	0.024 ± 0.006	0.034 ± 0.005	0.005 ± 0.001
CL(22:3/18:0/18:1/20:4)-H	0.006 ± 0.002	0.004 ± 0.001	0.004 ± 0.001

CL(23:0/18:0/18:0/20:3)-H	0.002 ± 0.001	0.002 ± 0.001	0.001 ± 0.000
CL(23:1/18:0/18:0/20:4)-H	0.002 ± 0.000	0.002 ± 0.000	0.001 ± 0.000
CL(21:0/18:0/18:0/22:6)-H	0.005 ± 0.001	0.006 ± 0.001	0.005 ± 0.001
CL(22:2/18:0/20:4/20:4)-H	0.007 ± 0.001	0.007 ± 0.001	0.001 ± 0.000
CL(22:6/18:1/22:6/18:1)-H	0.000 ± 0.000	0.002 ± 0.000	0.000 ± 0.000
CL(22:6/20:4/20:4/18:1)-H	0.001 ± 0.000	0.001 ± 0.000	0.001 ± 0.000
CL(20:4/18:0/20:4/22:0)-H	0.003 ± 0.001	0.004 ± 0.001	0.002 ± 0.000
CL(23:0/18:0/18:0/22:4)-H	0.002 ± 0.000	0.001 ± 0.000	0.001 ± 0.000
CL(23:1/18:0/18:0/22:6)-H	0.003 ± 0.001	0.002 ± 0.001	0.002 ± 0.000

Table 4: Diacyglycerols

Lipid Ion	FOB	HOS	143B
DG(16:0/14:0)+NH4	0.004 ± 0.001	0.006 ± 0.000	0.027 ± 0.004
DG(16:1/14:0)+NH4	0.001 ± 0.001	0.000 ± 0.000	0.006 ± 0.001
DG(16:0/16:0)+NH4	0.017 ± 0.004	0.038 ± 0.003	0.143 ± 0.028
DG(18:1/14:0)+NH4	0.043 ± 0.014	0.025 ± 0.002	0.171 ± 0.025
DG(17:1/16:0)+NH4	0.010 ± 0.002	0.008 ± 0.001	0.009 ± 0.002
DG(18:0/16:0)+NH4	0.013 ± 0.004	0.046 ± 0.003	0.102 ± 0.021
DG(16:0/18:1)+NH4	0.222 ± 0.061	0.214 ± 0.016	0.756 ± 0.152
DG(16:1/18:1)+NH4	0.108 ± 0.042	0.023 ± 0.001	0.156 ± 0.024
DG(16:0/18:2)+NH4	0.041 ± 0.019	0.031 ± 0.002	0.045 ± 0.010
DG(19:1/16:0)+NH4	0.008 ± 0.001	0.007 ± 0.000	0.008 ± 0.002
DG(17:1/18:1)+NH4	0.018 ± 0.005	0.007 ± 0.001	0.014 ± 0.004
DG(18:0/18:0)+NH4	0.013 ± 0.009	0.005 ± 0.001	0.029 ± 0.017
DG(18:0/18:1)+NH4	0.072 ± 0.017	0.068 ± 0.003	0.239 ± 0.057

DG(18:1/18:1)+NH4	0.270	±	0.082	0.130	±	0.018	0.639	±	0.128
DG(18:1/18:2)+NH4	0.055	±	0.014	0.025	±	0.002	0.043	±	0.013
DG(18:2/18:2)+NH4	0.015	±	0.005	0.007	±	0.003	0.001	±	0.001
DG(16:0/20:4)+NH4	0.032	±	0.003	0.026	±	0.002	0.007	±	0.001
DG(19:1/18:1)+NH4	0.006	±	0.002	0.003	±	0.000	0.006	±	0.001
DG(16:0/22:0)+NH4	0.001	±	0.000	0.001	±	0.000	0.004	±	0.001
DG(20:0/18:1)+NH4	0.002	±	0.001	0.002	±	0.000	0.020	±	0.006
DG(20:1/18:1)+NH4	0.012	±	0.004	0.007	±	0.001	0.066	±	0.017
DG(18:1/20:2)+NH4	0.032	±	0.007	0.015	±	0.001	0.017	±	0.003
DG(18:0/20:3)+NH4	0.033	±	0.007	0.014	±	0.001	0.009	±	0.002
DG(18:1/20:3)+NH4	0.019	±	0.004	0.010	±	0.001	0.005	±	0.001
DG(18:0/20:4)+NH4	0.131	±	0.002	0.127	±	0.003	0.041	±	0.009
DG(18:1/20:4)+NH4	0.074	±	0.007	0.035	±	0.004	0.022	±	0.003
DG(18:0/20:5)+NH4	0.012	±	0.003	0.008	±	0.001	0.004	±	0.001
DG(16:0/22:6)+NH4	0.027	±	0.004	0.021	±	0.003	0.011	±	0.002
DG(16:1/22:6)+NH4	0.010	±	0.003	0.001	±	0.000	0.002	±	0.000
DG(26:0/14:0)+NH4	0.001	±	0.000	0.001	±	0.000	0.013	±	0.003
DG(16:0/24:1)+NH4	0.000	±	0.000	0.001	±	0.000	0.014	±	0.005
DG(18:1/22:1)+NH4	0.002	±	0.001	0.002	±	0.000	0.017	±	0.005
DG(18:1/22:2)+NH4	0.005	±	0.000	0.001	±	0.000	0.005	±	0.001
DG(18:0/22:4)+NH4	0.006	±	0.001	0.006	±	0.000	0.004	±	0.001
DG(18:0/22:5)+NH4	0.014	±	0.001	0.012	±	0.000	0.020	±	0.005

DG(18:1/22:5)+NH4	0.014 ± 0.002	0.007 ± 0.001	0.009 ± 0.002
DG(18:0/22:6)+NH4	0.021 ± 0.005	0.018 ± 0.002	0.022 ± 0.005
DG(18:1/22:6)+NH4	0.040 ± 0.007	0.013 ± 0.002	0.012 ± 0.002
DG(25:0/16:0)+NH4	0.000 ± 0.000	0.000 ± 0.000	0.001 ± 0.000
DG(26:0/16:0)+NH4	0.001 ± 0.000	0.002 ± 0.000	0.037 ± 0.009
DG(26:1/16:0)+NH4	0.001 ± 0.000	0.001 ± 0.000	0.041 ± 0.012
DG(26:1/16:1)+NH4	0.002 ± 0.001	0.001 ± 0.000	0.034 ± 0.010
DG(27:1/16:0)+NH4	0.000 ± 0.000	0.000 ± 0.000	0.002 ± 0.000
DG(28:0/16:0)+NH4	0.000 ± 0.000	0.001 ± 0.000	0.011 ± 0.002
DG(28:1/16:0)+NH4	0.001 ± 0.000	0.000 ± 0.000	0.016 ± 0.005
DG(26:1/18:1)+NH4	0.002 ± 0.001	0.001 ± 0.000	0.075 ± 0.022
DG(30:0/16:0)+NH4	0.000 ± 0.000	0.001 ± 0.000	0.003 ± 0.001
DG(30:1/16:0)+NH4	0.000 ± 0.000	0.001 ± 0.001	0.027 ± 0.014
DG(28:1/18:1)+NH4	0.000 ± 0.000	0.001 ± 0.000	0.026 ± 0.008
DG(29:1/18:1)+NH4	0.000 ± 0.000	0.000 ± 0.000	0.003 ± 0.001
DG(32:1/16:0)+NH4	0.004 ± 0.000	0.007 ± 0.001	0.014 ± 0.004
DG(30:1/18:1)+NH4	0.001 ± 0.000	0.001 ± 0.001	0.013 ± 0.003
DG(31:1/18:1)+NH4	0.000 ± 0.000	0.000 ± 0.000	0.001 ± 0.000
DG(32:1/18:1)+NH4	0.001 ± 0.000	0.001 ± 0.000	0.008 ± 0.002

TABLE 5: LYSOPHOSPHATIDYLCHOLINE

Lipid Ion	FOB	HOS	143B
LPC(16:0)+H	0.004 ± 0.001	0.004 ± 0.001	0.005 ± 0.002

LPC(16:0e)+H	0.001 ± 0.000	0.001 ± 0.000	0.001 ± 0.000
LPC(16:0p)+H	0.001 ± 0.000	0.000 ± 0.000	0.000 ± 0.000
LPC(16:1)+H	0.000 ± 0.000	0.000 ± 0.000	0.000 ± 0.000
LPC(18:0)+H	0.007 ± 0.000	0.005 ± 0.001	0.003 ± 0.001
LPC(18:0e)+H	0.001 ± 0.000	0.001 ± 0.000	0.001 ± 0.000
LPC(18:0p)+H	0.001 ± 0.000	0.001 ± 0.000	0.001 ± 0.000
LPC(18:1)+H	0.005 ± 0.001	0.004 ± 0.001	0.005 ± 0.001
LPC(18:1p)+H	0.000 ± 0.000	0.000 ± 0.000	0.000 ± 0.000
LPC(20:0)+H	0.000 ± 0.000	0.000 ± 0.000	0.000 ± 0.000
LPC(20:0p)+H	0.001 ± 0.000	0.000 ± 0.000	0.000 ± 0.000
LPC(20:1)+H	0.000 ± 0.000	0.000 ± 0.000	0.000 ± 0.000
LPC(20:3)+H	0.000 ± 0.000	0.000 ± 0.000	0.000 ± 0.000
LPC(22:0)+H	0.000 ± 0.000	0.000 ± 0.000	0.000 ± 0.000
LPC(24:0)+H	0.001 ± 0.000	0.000 ± 0.000	0.000 ± 0.000
LPC(24:1)+H	0.000 ± 0.000	0.000 ± 0.000	0.000 ± 0.000
LPC(26:0)+H	0.006 ± 0.000	0.007 ± 0.000	0.003 ± 0.001
LPC(26:1)+H	0.001 ± 0.000	0.000 ± 0.000	0.002 ± 0.000
LPC(28:0)+H	0.337 ± 0.093	0.160 ± 0.011	0.046 ± 0.011
LPC(28:1)+H	0.022 ± 0.002	0.013 ± 0.001	0.007 ± 0.002
LPC(30:0)+H	0.000 ± 0.000	0.000 ± 0.000	0.000 ± 0.000

Table 6: Phosphatidylcholines

Lipid Ion	FOB	HOS	143B
PC(11:0/16:0)+H	0.001 ± 0.000	0.001 ± 0.000	0.002 ± 0.000
PC(28:0)+H	0.038 ± 0.017	0.027 ± 0.004	0.090 ± 0.022
PC(14:0e/14:0)+H	0.350 ± 0.095	0.166 ± 0.011	0.048 ± 0.011
PC(14:0p/14:0)+H	0.009 ± 0.001	0.003 ± 0.000	0.001 ± 0.000
PC(29:0)+H	0.017 ± 0.005	0.019 ± 0.003	0.009 ± 0.002
PC(16:0/13:0)+H	0.004 ± 0.001	0.002 ± 0.000	0.002 ± 0.001
PC(11:0/18:1)+H	0.024 ± 0.007	0.010 ± 0.004	0.027 ± 0.005

PC(30:0)+H	0.367 ± 0.117	0.390 ± 0.037	0.531 ± 0.075
PC(30:0e)+H	0.101 ± 0.012	0.074 ± 0.005	0.139 ± 0.029
PC(16:0p/14:0)+H	0.063 ± 0.005	0.042 ± 0.003	0.039 ± 0.009
PC(14:0p/16:0)+H	0.024 ± 0.006	0.026 ± 0.001	0.024 ± 0.005
PC(30:1)+H	0.196 ± 0.085	0.080 ± 0.009	0.237 ± 0.058
PC(16:0/14:1)+H	0.005 ± 0.001	0.003 ± 0.000	0.003 ± 0.001
PC(30:1e)+H	0.079 ± 0.005	0.048 ± 0.004	0.046 ± 0.012
PC(14:0p/16:1)+H	0.005 ± 0.001	0.003 ± 0.000	0.002 ± 0.000
PC(30:2)+H	0.008 ± 0.004	0.002 ± 0.000	0.005 ± 0.001
PC(16:1/14:1)+H	0.001 ± 0.000	0.000 ± 0.000	0.000 ± 0.000
PC(30:2e)+H	0.008 ± 0.002	0.007 ± 0.001	0.002 ± 0.000
PC(18:1/12:2)+H	0.003 ± 0.001	0.002 ± 0.000	0.006 ± 0.001
PC(31:0)+H	0.073 ± 0.003	0.100 ± 0.010	0.037 ± 0.008
PC(18:0/13:0)+H	0.002 ± 0.001	0.007 ± 0.001	0.003 ± 0.000
PC(17:1/14:0)+H	0.044 ± 0.013	0.027 ± 0.004	0.018 ± 0.005
PC(32:0)+H	0.232 ± 0.116	0.476 ± 0.014	0.379 ± 0.030
PC(32:0e)+H	0.219 ± 0.071	0.173 ± 0.017	0.347 ± 0.050
PC(16:0p/16:0)+H	0.064 ± 0.013	0.097 ± 0.007	0.059 ± 0.009
PC(16:0/16:1)+H	1.930 ± 0.546	1.129 ± 0.314	1.390 ± 0.158
PC(16:1p/16:0)+H	0.011 ± 0.003	0.006 ± 0.001	0.007 ± 0.003
PC(32:1p)+H	0.047 ± 0.015	0.056 ± 0.005	0.044 ± 0.009
PC(32:2)+H	0.484 ± 0.229	0.083 ± 0.014	0.165 ± 0.030
PC(18:1/14:1)+H	0.016 ± 0.004	0.004 ± 0.001	0.005 ± 0.001
PC(14:0p/18:3)+H	0.004 ± 0.000	0.003 ± 0.000	0.003 ± 0.001
PC(18:4/14:0)+H	0.007 ± 0.004	0.004 ± 0.000	0.009 ± 0.004
PC(32:4e)+H	0.077 ± 0.042	0.020 ± 0.001	0.000 ± 0.000
PC(12:0p/20:5)+H	0.000 ± 0.000	0.000 ± 0.000	0.000 ± 0.000
PC(33:0)+H	0.024 ± 0.001	0.054 ± 0.004	0.011 ± 0.002
PC(33:1)+H	0.432 ± 0.086	0.318 ± 0.031	0.145 ± 0.029
PC(17:1/16:1)+H	0.046 ± 0.017	0.012 ± 0.002	0.016 ± 0.004
PC(34:0)+H	0.132 ± 0.018	0.497 ± 0.010	0.188 ± 0.034

PC(34:0e)+H	0.099 ± 0.029	0.111 ± 0.009	0.157 ± 0.031
PC(16:0p/18:0)+H	0.630 ± 0.142	0.403 ± 0.052	0.745 ± 0.106
PC(34:1)+H	2.954 ± 0.501	1.987 ± 0.116	1.631 ± 0.200
PC(16:0p/18:1)+H	0.104 ± 0.026	0.069 ± 0.005	0.097 ± 0.017
PC(34:2)+H	2.005 ± 0.678	0.930 ± 0.093	1.072 ± 0.151
PC(16:1p/18:1)+H	0.009 ± 0.002	0.007 ± 0.000	0.005 ± 0.000
PC(34:3)+H	0.174 ± 0.064	0.042 ± 0.007	0.045 ± 0.012
PC(16:0/18:3)+H	0.004 ± 0.000	0.004 ± 0.000	0.001 ± 0.000
PC(34:4)+H	0.036 ± 0.012	0.009 ± 0.001	0.004 ± 0.001
PC(18:4/16:0)+H	0.043 ± 0.011	0.018 ± 0.004	0.009 ± 0.001
PC(14:0/20:5)+H	0.004 ± 0.001	0.001 ± 0.000	0.000 ± 0.000
PC(34:6e)+H	0.023 ± 0.005	0.009 ± 0.001	0.000 ± 0.000
PC(35:0)+H	0.002 ± 0.000	0.012 ± 0.001	0.001 ± 0.000
PC(17:0/18:1)+H	0.085 ± 0.019	0.051 ± 0.006	0.044 ± 0.008
PC(35:1)+H	0.191 ± 0.027	0.132 ± 0.013	0.070 ± 0.014
PC(17:1/18:1)+H	0.235 ± 0.065	0.116 ± 0.014	0.130 ± 0.028
PC(36:0)+H	0.007 ± 0.000	0.029 ± 0.002	0.013 ± 0.003
PC(36:0e)+H	0.012 ± 0.004	0.016 ± 0.001	0.015 ± 0.004
PC(16:0/20:1)+H	1.061 ± 0.171	0.546 ± 0.048	0.622 ± 0.098
PC(36:1e)+H	0.048 ± 0.017	0.043 ± 0.004	0.215 ± 0.047
PC(18:0p/18:1)+H	0.110 ± 0.035	0.051 ± 0.009	0.114 ± 0.023
PC(20:1p/16:0)+H	0.017 ± 0.006	0.015 ± 0.002	0.027 ± 0.006
PC(18:1p/18:0)+H	0.010 ± 0.004	0.011 ± 0.001	0.030 ± 0.008
PC(18:1/18:1)+H	1.718 ± 0.417	0.677 ± 0.054	1.091 ± 0.156
PC(16:1p/20:1)+H	0.018 ± 0.005	0.018 ± 0.002	0.014 ± 0.003
PC(18:2p/18:0)+H	0.026 ± 0.008	0.013 ± 0.002	0.011 ± 0.002
PC(36:2p)+H	0.033 ± 0.010	0.022 ± 0.002	0.028 ± 0.005
PC(36:3)+H	0.528 ± 0.113	0.273 ± 0.028	0.171 ± 0.024
PC(36:4)+H	0.394 ± 0.056	0.239 ± 0.012	0.024 ± 0.003
PC(18:1/18:3)+H	0.036 ± 0.005	0.022 ± 0.001	0.008 ± 0.001
PC(36:4e)+H	0.147 ± 0.005	0.127 ± 0.010	0.022 ± 0.004

PC(16:0p/20:4)+H	0.075 ± 0.002	0.050 ± 0.003	0.006 ± 0.002
PC(36:5)+H	0.094 ± 0.025	0.032 ± 0.007	0.007 ± 0.002
PC(18:4/18:1)+H	0.034 ± 0.006	0.011 ± 0.002	0.007 ± 0.001
PC(14:0/22:5)+H	0.003 ± 0.000	0.003 ± 0.000	0.001 ± 0.001
PC(36:6)+H	0.013 ± 0.002	0.004 ± 0.001	0.003 ± 0.001
PC(22:2/14:4)+H	0.005 ± 0.001	0.002 ± 0.000	0.001 ± 0.000
PC(16:1/21:0)+H	0.006 ± 0.002	0.001 ± 0.000	0.003 ± 0.001
PC(19:1/18:1)+H	0.073 ± 0.019	0.049 ± 0.008	0.056 ± 0.012
PC(15:0/22:4)+H	0.011 ± 0.001	0.013 ± 0.001	0.008 ± 0.002
PC(37:5)+H	0.020 ± 0.004	0.008 ± 0.002	0.001 ± 0.000
PC(17:0/20:5)+H	0.003 ± 0.001	0.004 ± 0.001	0.001 ± 0.000
PC(38:0e)+H	0.007 ± 0.002	0.005 ± 0.000	0.006 ± 0.002
PC(20:0/18:1)+H	0.000 ± 0.000	0.000 ± 0.000	0.000 ± 0.000
PC(38:1e)+H	0.009 ± 0.003	0.008 ± 0.001	0.036 ± 0.009
PC(20:1p/18:0)+H	0.006 ± 0.002	0.003 ± 0.000	0.011 ± 0.002
PC(20:1/18:1)+H	0.142 ± 0.049	0.077 ± 0.017	0.184 ± 0.027
PC(38:2e)+H	0.004 ± 0.002	0.001 ± 0.000	0.007 ± 0.002
PC(38:3)+H	0.196 ± 0.038	0.070 ± 0.009	0.056 ± 0.012
PC(38:3e)+H	0.006 ± 0.002	0.004 ± 0.000	0.005 ± 0.001
PC(38:4)+H	0.186 ± 0.042	0.062 ± 0.007	0.026 ± 0.006
PC(38:4e)+H	0.075 ± 0.011	0.068 ± 0.006	0.009 ± 0.002
PC(18:0/20:5)+H	0.040 ± 0.006	0.015 ± 0.002	0.006 ± 0.002
PC(38:5)+H	0.428 ± 0.041	0.238 ± 0.017	0.034 ± 0.005
PC(16:0/22:6)+H	0.141 ± 0.029	0.085 ± 0.012	0.034 ± 0.009
PC(38:6e)+H	0.147 ± 0.026	0.086 ± 0.008	0.024 ± 0.005
PC(38:7)+H	0.039 ± 0.013	0.008 ± 0.002	0.006 ± 0.002
PC(39:2)+H	0.005 ± 0.002	0.004 ± 0.000	0.007 ± 0.001
PC(40:0)+H	0.001 ± 0.000	0.001 ± 0.000	0.008 ± 0.002
PC(40:1)+H	0.004 ± 0.002	0.004 ± 0.001	0.026 ± 0.007
PC(40:2)+H	0.016 ± 0.006	0.012 ± 0.002	0.046 ± 0.011
PC(40:3)+H	0.014 ± 0.004	0.010 ± 0.001	0.014 ± 0.003

PC(40:4)+H	0.026 ± 0.005	0.018 ± 0.002	0.009 ± 0.002
PC(18:0/22:5)+H	0.048 ± 0.002	0.042 ± 0.004	0.012 ± 0.003
PC(40:5e)+H	0.040 ± 0.003	0.019 ± 0.002	0.006 ± 0.001
PC(18:0/22:6)+H	0.083 ± 0.011	0.055 ± 0.005	0.010 ± 0.002
PC(40:6e)+H	0.045 ± 0.009	0.029 ± 0.003	0.009 ± 0.002
PC(18:1/22:6)+H	0.127 ± 0.030	0.067 ± 0.010	0.039 ± 0.011
PC(18:1/23:0)+H	0.001 ± 0.001	0.000 ± 0.000	0.003 ± 0.001
PC(31:0/10:2)+H	0.001 ± 0.001	0.001 ± 0.000	0.002 ± 0.001
PC(18:1/23:1)+H	0.002 ± 0.001	0.000 ± 0.000	0.003 ± 0.001
PC(26:0/16:0)+H	0.001 ± 0.000	0.001 ± 0.000	0.019 ± 0.006
PC(42:1)+H	0.006 ± 0.002	0.003 ± 0.000	0.036 ± 0.003
PC(42:2)+H	0.011 ± 0.005	0.005 ± 0.001	0.055 ± 0.015
PC(42:3)+H	0.007 ± 0.003	0.006 ± 0.001	0.016 ± 0.004
PC(18:2p/24:1)+H	0.005 ± 0.001	0.002 ± 0.000	0.001 ± 0.000
PC(27:1/16:0)+H	0.001 ± 0.000	0.000 ± 0.000	0.003 ± 0.001
PC(25:1/18:1)+H	0.001 ± 0.001	0.000 ± 0.000	0.005 ± 0.001
PC(44:0)+H	0.000 ± 0.000	0.001 ± 0.000	0.011 ± 0.003
PC(44:1)+H	0.003 ± 0.001	0.002 ± 0.000	0.055 ± 0.014
PC(44:2)+H	0.006 ± 0.003	0.003 ± 0.000	0.065 ± 0.018
PC(44:3)+H	0.006 ± 0.003	0.003 ± 0.001	0.020 ± 0.003
PC(29:0/16:0)+H	0.000 ± 0.000	0.000 ± 0.000	0.000 ± 0.000
PC(27:0/18:1)+H	0.000 ± 0.000	0.000 ± 0.000	0.003 ± 0.001
PC(45:2)+H	0.000 ± 0.000	0.000 ± 0.000	0.003 ± 0.001
PC(46:1)+H	0.000 ± 0.000	0.000 ± 0.000	0.023 ± 0.009
PC(46:2)+H	0.001 ± 0.000	0.001 ± 0.000	0.028 ± 0.007
PC(31:1/16:0)+H	0.000 ± 0.000	0.000 ± 0.000	0.001 ± 0.000
PC(47:2)+H	0.000 ± 0.000	0.000 ± 0.000	0.003 ± 0.001
PC(48:1)+H	0.000 ± 0.000	0.000 ± 0.000	0.007 ± 0.002
PC(48:2)+H	0.000 ± 0.000	0.000 ± 0.000	0.015 ± 0.004
PC(50:2)+H	0.000 ± 0.000	0.000 ± 0.000	0.008 ± 0.002

Table 7: Phosphatidylethanolamines

Lipid Ion	FOB	HOS	143B
PE(26:0)+H	0.004 ± 0.001	0.002 ± 0.000	0.001 ± 0.000
PE(12:0p/16:0)+H	0.028 ± 0.001	0.015 ± 0.001	0.002 ± 0.001
PE(16:0/14:0)+H	0.009 ± 0.005	0.011 ± 0.001	0.029 ± 0.005
PE(16:0p/14:0)+H	0.007 ± 0.002	0.012 ± 0.000	0.002 ± 0.000
PE(16:1/14:0)+H	0.012 ± 0.005	0.003 ± 0.000	0.015 ± 0.005
PE(12:0p/18:1)+H	0.034 ± 0.003	0.019 ± 0.001	0.011 ± 0.002
PE(12:0p/18:2)+H	0.003 ± 0.002	0.003 ± 0.000	0.001 ± 0.000
PE(16:0/16:0)+H	0.035 ± 0.007	0.057 ± 0.004	0.054 ± 0.011
PE(16:0p/16:0)+H	0.034 ± 0.013	0.115 ± 0.007	0.011 ± 0.002
PE(16:0/16:1)+H	0.362 ± 0.097	0.133 ± 0.055	0.385 ± 0.064
PE(16:0p/16:1)+H	0.077 ± 0.020	0.048 ± 0.010	0.137 ± 0.025
PE(16:1/16:1)+H	0.039 ± 0.017	0.006 ± 0.002	0.039 ± 0.010
PE(12:0p/20:4)+H	0.126 ± 0.057	0.063 ± 0.000	0.005 ± 0.001
PE(12:0p/20:5)+H	0.009 ± 0.001	0.003 ± 0.000	0.001 ± 0.000
PE(18:0p/15:0)+H	0.003 ± 0.001	0.012 ± 0.001	0.000 ± 0.000
PE(17:1/16:0)+H	0.086 ± 0.028	0.045 ± 0.002	0.043 ± 0.008
PE(16:0p/17:1)+H	0.030 ± 0.009	0.019 ± 0.001	0.019 ± 0.003
PE(18:0/16:0)+H	0.029 ± 0.009	0.109 ± 0.005	0.036 ± 0.007
PE(18:0p/16:0)+H	0.029 ± 0.010	0.090 ± 0.005	0.010 ± 0.002
PE(16:0/18:1)+H	1.620 ± 0.426	0.980 ± 0.041	1.720 ± 0.294
PE(16:0p/18:1)+H	0.698 ± 0.238	0.318 ± 0.017	0.706 ± 0.136
PE(16:1/18:1)+H	1.018 ± 0.258	0.165 ± 0.023	0.550 ± 0.076
PE(18:1p/16:1)+H	0.054 ± 0.018	0.029 ± 0.001	0.045 ± 0.008
PE(16:0p/18:2)+H	0.046 ± 0.013	0.047 ± 0.002	0.035 ± 0.002
PE(12:0p/22:4)+H	0.018 ± 0.011	0.005 ± 0.000	0.001 ± 0.000
PE(14:0p/20:4)+H	0.085 ± 0.023	0.041 ± 0.002	0.005 ± 0.001
PE(12:0p/22:5)+H	0.013 ± 0.007	0.004 ± 0.000	0.002 ± 0.001
PE(14:0p/20:5)+H	0.011 ± 0.002	0.004 ± 0.001	0.001 ± 0.000

PE(12:0p/22:6)+H	0.044 ± 0.004	0.021 ± 0.000	0.004 ± 0.001
PE(17:0/18:1)+H	0.249 ± 0.065	0.138 ± 0.014	0.151 ± 0.037
PE(16:0p/19:1)+H	0.033 ± 0.012	0.021 ± 0.001	0.030 ± 0.006
PE(17:1/18:1)+H	0.237 ± 0.055	0.068 ± 0.006	0.079 ± 0.011
PE(18:1p/17:1)+H	0.017 ± 0.006	0.013 ± 0.000	0.007 ± 0.000
PE(16:0p/20:0)+H	0.004 ± 0.002	0.020 ± 0.001	0.004 ± 0.001
PE(18:0/18:1)+H	3.323 ± 0.877	1.100 ± 0.067	2.016 ± 0.418
PE(18:0p/18:1)+H	0.162 ± 0.057	0.122 ± 0.008	0.438 ± 0.087
PE(18:1/18:1)+H	2.676 ± 0.873	0.958 ± 0.063	1.975 ± 0.262
PE(18:1p/18:1)+H	0.285 ± 0.087	0.135 ± 0.010	0.211 ± 0.041
PE(18:0p/18:2)+H	0.062 ± 0.024	0.045 ± 0.002	0.086 ± 0.015
PE(18:1/18:2)+H	0.406 ± 0.114	0.268 ± 0.006	0.244 ± 0.064
PE(18:1p/18:2)+H	0.120 ± 0.020	0.136 ± 0.003	0.055 ± 0.010
PE(16:0p/20:3)+H	0.082 ± 0.025	0.048 ± 0.004	0.099 ± 0.019
PE(16:0/20:4)+H	0.486 ± 0.022	0.598 ± 0.013	0.228 ± 0.032
PE(16:0p/20:4)+H	1.985 ± 0.307	2.331 ± 0.071	0.878 ± 0.187
PE(16:1/20:4)+H	0.078 ± 0.027	0.017 ± 0.003	0.019 ± 0.005
PE(16:0/20:5)+H	0.043 ± 0.010	0.024 ± 0.002	0.027 ± 0.007
PE(14:0p/22:5)+H	0.053 ± 0.023	0.029 ± 0.011	0.004 ± 0.001
PE(16:0p/20:5)+H	0.271 ± 0.080	0.137 ± 0.013	0.130 ± 0.023
PE(16:1/20:5)+H	0.007 ± 0.003	0.001 ± 0.000	0.002 ± 0.000
PE(14:0p/22:6)+H	0.060 ± 0.005	0.013 ± 0.001	0.003 ± 0.001
PE(18:0p/19:1)+H	1.613 ± 0.376	1.280 ± 0.038	1.459 ± 0.282
PE(17:0/20:4)+H	0.109 ± 0.004	0.151 ± 0.009	0.031 ± 0.006
PE(17:1/20:4)+H	0.039 ± 0.010	0.036 ± 0.002	0.006 ± 0.001
PE(17:1/20:5)+H	0.009 ± 0.003	0.004 ± 0.000	0.000 ± 0.000
PE(20:0/18:1)+H	0.052 ± 0.017	0.024 ± 0.004	0.039 ± 0.013
PE(16:0p/22:1)+H	0.021 ± 0.009	0.017 ± 0.002	0.088 ± 0.022
PE(20:1/18:1)+H	0.115 ± 0.041	0.060 ± 0.007	0.120 ± 0.047
PE(16:0p/22:2)+H	0.020 ± 0.008	0.008 ± 0.001	0.025 ± 0.005
PE(18:0/20:3)+H	0.570 ± 0.149	0.173 ± 0.007	0.114 ± 0.025

PE(18:0p/20:3)+H	0.021 ± 0.009	0.012 ± 0.001	0.042 ± 0.011
PE(18:0/20:4)+H	5.322 ± 0.402	4.656 ± 0.069	1.319 ± 0.275
PE(38:4e)+H	0.052 ± 0.009	0.080 ± 0.004	0.027 ± 0.006
PE(16:0p/22:4)+H	0.351 ± 0.017	0.483 ± 0.029	0.143 ± 0.029
PE(18:0p/20:4)+H	0.923 ± 0.172	1.398 ± 0.062	0.506 ± 0.100
PE(18:1/20:4)+H	1.579 ± 0.187	0.930 ± 0.040	0.537 ± 0.099
PE(18:0/20:5)+H	0.540 ± 0.132	0.274 ± 0.010	0.233 ± 0.041
PE(18:1p/20:4)+H	2.288 ± 0.208	1.734 ± 0.064	0.852 ± 0.149
PE(18:0p/20:5)+H	0.172 ± 0.054	0.168 ± 0.011	0.088 ± 0.012
PE(16:1/22:5)+H	0.001 ± 0.000	0.000 ± 0.000	0.003 ± 0.001
PE(38:6)+H	0.158 ± 0.051	0.054 ± 0.005	0.071 ± 0.019
PE(16:0/22:6)+H	0.271 ± 0.032	0.195 ± 0.004	0.086 ± 0.015
PE(18:1p/20:5)+H	0.166 ± 0.038	0.079 ± 0.002	0.031 ± 0.004
PE(16:0p/22:6)+H	2.735 ± 0.870	1.121 ± 0.080	0.699 ± 0.135
PE(16:1/22:6)+H	0.051 ± 0.022	0.009 ± 0.000	0.019 ± 0.004
PE(16:1p/22:6)+H	0.038 ± 0.011	0.006 ± 0.002	0.002 ± 0.001
PE(17:0/22:6)+H	0.021 ± 0.004	0.034 ± 0.003	0.020 ± 0.006
PE(18:1/22:0)+H	0.083 ± 0.031	0.013 ± 0.001	0.038 ± 0.011
PE(18:0p/22:1)+H	0.007 ± 0.002	0.003 ± 0.000	0.024 ± 0.004
PE(18:1/22:1)+H	0.082 ± 0.026	0.031 ± 0.003	0.052 ± 0.013
PE(18:1p/22:1)+H	0.008 ± 0.004	0.003 ± 0.000	0.013 ± 0.003
PE(18:0p/22:3)+H	0.018 ± 0.006	0.014 ± 0.001	0.018 ± 0.005
PE(18:0/22:4)+H	0.179 ± 0.022	0.217 ± 0.000	0.109 ± 0.022
PE(20:0/20:4)+H	0.024 ± 0.002	0.021 ± 0.001	0.014 ± 0.004
PE(18:0p/22:4)+H	0.118 ± 0.011	0.214 ± 0.017	0.072 ± 0.018
PE(20:0p/20:4)+H	0.063 ± 0.004	0.031 ± 0.002	0.016 ± 0.004
PE(18:0/22:5)+H	0.326 ± 0.020	0.270 ± 0.016	0.339 ± 0.081
PE(40:5e)+H	0.027 ± 0.003	0.027 ± 0.001	0.010 ± 0.002
PE(40:5p)+H	0.201 ± 0.011	0.216 ± 0.008	0.095 ± 0.020
PE(18:0p/22:5)+H	0.451 ± 0.032	0.371 ± 0.032	0.325 ± 0.064
PE(18:0/22:6)+H	0.758 ± 0.168	0.698 ± 0.050	0.483 ± 0.077

PE(18:1p/22:5)+H	0.375 ± 0.039	0.179 ± 0.012	0.123 ± 0.027
PE(18:0p/22:6)+H	1.018 ± 0.292	0.733 ± 0.060	0.347 ± 0.071
PE(18:1/22:6)+H	0.570 ± 0.151	0.357 ± 0.021	0.208 ± 0.038
PE(18:1p/22:6)+H	1.223 ± 0.369	0.532 ± 0.045	0.184 ± 0.042
PE(18:2/22:6)+H	0.016 ± 0.005	0.008 ± 0.001	0.004 ± 0.001
PE(18:2p/22:6)+H	0.014 ± 0.006	0.002 ± 0.001	0.000 ± 0.000
PE(18:1/24:0)+H	0.097 ± 0.040	0.009 ± 0.001	0.063 ± 0.013
PE(20:4/22:6)+H	0.007 ± 0.002	0.004 ± 0.001	0.004 ± 0.001
PE(18:0p/24:1)+H	0.002 ± 0.000	0.000 ± 0.000	0.002 ± 0.001
PE(18:1/24:1)+H	0.079 ± 0.032	0.008 ± 0.001	0.051 ± 0.010
PE(22:0/20:4)+H	0.012 ± 0.003	0.004 ± 0.000	0.008 ± 0.002
PE(20:0p/22:5)+H	0.021 ± 0.003	0.021 ± 0.002	0.013 ± 0.003
PE(20:1p/22:5)+H	0.021 ± 0.004	0.017 ± 0.002	0.006 ± 0.002
PE(20:0p/22:6)+H	0.037 ± 0.010	0.010 ± 0.001	0.007 ± 0.002
PE(25:0/18:1)+H	0.005 ± 0.002	0.000 ± 0.000	0.004 ± 0.001
PE(43:2)+H	0.008 ± 0.003	0.001 ± 0.000	0.003 ± 0.001
PE(26:0/18:1)+H	0.022 ± 0.010	0.002 ± 0.000	0.050 ± 0.015
PE(26:1/18:1)+H	0.037 ± 0.015	0.002 ± 0.000	0.043 ± 0.014
PE(44:2)+H	0.002 ± 0.001	0.000 ± 0.000	0.003 ± 0.001
PE(44:3)+H	0.003 ± 0.001	0.000 ± 0.000	0.001 ± 0.000
PE(24:0/20:4)+H	0.016 ± 0.006	0.003 ± 0.000	0.017 ± 0.005
PE(24:1/20:4)+H	0.011 ± 0.005	0.003 ± 0.000	0.020 ± 0.005
PE(28:1/18:1)+H	0.001 ± 0.000	0.000 ± 0.000	0.011 ± 0.003
PE(26:0/20:4)+H	0.002 ± 0.001	0.000 ± 0.000	0.007 ± 0.001
PE(24:0/22:6)+H	0.007 ± 0.003	0.005 ± 0.001	0.020 ± 0.005
PE(24:1/22:6)+H	0.003 ± 0.001	0.001 ± 0.000	0.003 ± 0.001
PE(48:5)+H	0.001 ± 0.000	0.000 ± 0.000	0.003 ± 0.001

Table 8: Lysophosphatidylethanolamines

Lipid Ion	FOB	HOS	143B
LPE(20:4)-H	0.005 ± 0.001	0.005 ± 0.001	0.001 ± 0.000
LPE(22:5)-H	0.002 ± 0.000	0.001 ± 0.000	0.000 ± 0.000
LPE(22:6)-H	0.004 ± 0.001	0.002 ± 0.000	0.001 ± 0.000
LPE(24:1)-H	0.000 ± 0.000	0.000 ± 0.000	0.001 ± 0.000

Table 9: Phosphatidylinositols

Lipid Ion	FOB	HOS	143B
PI(16:0/14:1)-H	0.000 ± 0.000	0.000 ± 0.000	0.003 ± 0.001
PI(16:0/16:0)-H	0.004 ± 0.002	0.008 ± 0.002	0.013 ± 0.005
PI(18:1/14:1)-H	0.006 ± 0.003	0.001 ± 0.000	0.014 ± 0.003
PI(17:1/16:0)-H	0.008 ± 0.002	0.005 ± 0.001	0.005 ± 0.001
PI(18:0/16:0)-H	0.004 ± 0.001	0.011 ± 0.001	0.015 ± 0.003
PI(16:0/18:1)-H	0.552 ± 0.207	0.432 ± 0.108	0.885 ± 0.156
PI(16:0e/18:1)-H	0.003 ± 0.001	0.005 ± 0.002	0.006 ± 0.001
PI(18:0/17:0)-H	0.001 ± 0.001	0.001 ± 0.000	0.001 ± 0.000
PI(17:0/18:1)-H	0.007 ± 0.002	0.005 ± 0.000	0.008 ± 0.002
PI(18:0/18:0)-H	0.003 ± 0.001	0.002 ± 0.000	0.006 ± 0.001
PI(18:0/18:1)-H	0.317 ± 0.112	0.214 ± 0.045	0.802 ± 0.179
PI(18:0e/18:1)-H	0.000 ± 0.000	0.000 ± 0.000	0.003 ± 0.001
PI(18:0p/18:1)-H	0.001 ± 0.000	0.001 ± 0.000	0.002 ± 0.001
PI(18:1/18:1)-H	1.107 ± 0.432	0.595 ± 0.178	2.352 ± 0.411
PI(18:1/18:3)-H	0.006 ± 0.001	0.007 ± 0.001	0.000 ± 0.000
PI(16:0e/20:4)-H	0.000 ± 0.000	0.004 ± 0.001	0.001 ± 0.000
PI(16:1/20:4)-H	0.005 ± 0.000	0.002 ± 0.000	0.001 ± 0.000

PI(16:0/20:5)-H	0.002	±	0.001	0.001	±	0.000	0.001	± 0.000
PI(19:1/18:0)-H	0.005	±	0.002	0.005	±	0.001	0.012	± 0.005
PI(17:0/20:2)-H	0.004	±	0.001	0.002	±	0.000	0.008	± 0.002
PI(19:1/18:2)-H	0.014	±	0.004	0.002	±	0.001	0.005	± 0.001
PI(17:0/20:3)-H	0.025	±	0.010	0.015	±	0.005	0.010	± 0.002
PI(17:1/20:4)-H	0.006	±	0.002	0.007	±	0.001	0.000	± 0.000
PI(18:0/20:0)-H	0.002	±	0.001	0.001	±	0.000	0.002	± 0.000
PI(18:0/20:1)-H	0.001	±	0.001	0.003	±	0.001	0.009	± 0.002
PI(18:0p/20:1)-H	0.000	±	0.000	0.000	±	0.000	0.001	± 0.000
PI(18:0/20:4)-H	2.434	±	0.120	4.080	±	1.119	0.612	± 0.117
PI(18:0/20:5)-H	0.027	±	0.004	0.022	±	0.003	0.006	± 0.001
PI(19:1/20:1)-H	0.000	±	0.000	0.000	±	0.000	0.002	± 0.001
PI(19:1/20:2)-H	0.001	±	0.000	0.002	±	0.000	0.004	± 0.001
PI(19:1/20:3)-H	0.010	±	0.003	0.007	±	0.002	0.004	± 0.001
PI(19:0/20:4)-H	0.007	±	0.001	0.009	±	0.002	0.001	± 0.000
PI(18:0/22:1)-H	0.002	±	0.001	0.002	±	0.001	0.005	± 0.001
PI(18:0/22:3)-H	0.036	±	0.019	0.019	±	0.006	0.019	± 0.005
PI(20:0/20:4)-H	0.003	±	0.001	0.004	±	0.002	0.002	± 0.000
PI(18:0/24:1)-H	0.000	±	0.000	0.002	±	0.000	0.002	± 0.001
PI(18:1/24:2)-H	0.001	±	0.000	0.001	±	0.000	0.003	± 0.001
PI(22:4/20:4)-H	0.001	±	0.000	0.006	±	0.001	0.001	± 0.000
PI(26:0/18:1)-H	0.000	±	0.000	0.001	±	0.000	0.002	± 0.001
PI(26:1/18:1)-H	0.000	±	0.000	0.000	±	0.000	0.001	± 0.000

Table 10: Phosphatidylglycerols

Lipid Ion	FOB			HOS			143B		
PG(12:0/14:0)-H	0.003	±	0.000	0.003	±	0.000	0.001	±	0.000
PG(15:0/14:0)-H	0.000	±	0.000	0.001	±	0.000	0.000	±	0.000
PG(16:0/14:0)-H	0.001	±	0.000	0.025	±	0.002	0.003	±	0.001

PG(16:1/14:0)-H	0.010	±	0.001	0.006	±	0.000	0.002	±	0.000
PG(15:0/16:0)-H	0.000	±	0.000	0.006	±	0.001	0.000	±	0.000
PG(16:0/16:0)-H	0.104	±	0.042	0.081	±	0.009	0.014	±	0.002
PG(16:0/16:1)-H	0.005	±	0.005	0.000	±	0.000	0.007	±	0.002
PG(18:1/14:0)-H	0.020	±	0.001	0.021	±	0.002	0.009	±	0.002
PG(16:0/17:0)-H	0.000	±	0.000	0.004	±	0.000	0.000	±	0.000
PG(17:1/16:0)-H	0.019	±	0.004	0.003	±	0.001	0.004	±	0.001
PG(18:0/16:0)-H	0.032	±	0.010	0.035	±	0.003	0.012	±	0.002
PG(16:0/18:1)-H	0.053	±	0.010	0.405	±	0.051	0.141	±	0.031
PG(16:1/18:1)-H	0.021	±	0.012	0.000	±	0.000	0.021	±	0.007
PG(16:1/18:2)-H	0.004	±	0.002	0.001	±	0.000	0.001	±	0.000
PG(19:1/16:0)-H	0.016	±	0.002	0.014	±	0.001	0.004	±	0.001
PG(17:1/18:0)-H	0.028	±	0.007	0.018	±	0.002	0.006	±	0.001
PG(17:1/18:1)-H	0.010	±	0.003	0.008	±	0.001	0.002	±	0.001
PG(18:0/18:1)-H	0.155	±	0.043	0.115	±	0.012	0.060	±	0.011
PG(18:1/18:1)-H	0.078	±	0.041	0.020	±	0.002	0.098	±	0.023
PG(18:1/18:2)-H	0.004	±	0.002	0.004	±	0.001	0.002	±	0.001
PG(16:0/20:3)-H	0.002	±	0.001	0.001	±	0.000	0.000	±	0.000
PG(16:0/20:4)-H	0.002	±	0.000	0.002	±	0.000	0.001	±	0.000
PG(14:0/22:6)-H	0.001	±	0.001	0.000	±	0.000	0.001	±	0.000
PG(20:1/18:1)-H	0.002	±	0.001	0.001	±	0.000	0.003	±	0.001
PG(18:1/20:2)-H	0.015	±	0.008	0.003	±	0.001	0.006	±	0.001
PG(16:0/22:4)-H	0.003	±	0.001	0.003	±	0.001	0.000	±	0.000
PG(18:0/20:4)-H	0.003	±	0.001	0.004	±	0.000	0.001	±	0.000
PG(18:1/20:4)-H	0.001	±	0.000	0.002	±	0.000	0.000	±	0.000
PG(18:1/20:5)-H	0.007	±	0.001	0.002	±	0.000	0.000	±	0.000
PG(16:0/22:6)-H	0.022	±	0.010	0.007	±	0.002	0.011	±	0.004
PG(16:1/22:6)-H	0.019	±	0.008	0.003	±	0.000	0.004	±	0.002
PG(20:2/20:2)-H	0.006	±	0.003	0.002	±	0.000	0.000	±	0.000
PG(18:1/22:4)-H	0.007	±	0.003	0.005	±	0.001	0.000	±	0.000
PG(18:0/22:6)-H	0.002	±	0.001	0.004	±	0.001	0.001	±	0.000

PG(18:1/22:6)-H	0.247	±	0.108	0.072	±	0.011	0.076	±	0.024
PG(18:2/22:6)-H	0.032	±	0.008	0.012	±	0.002	0.002	±	0.000
PG(20:4/22:6)-H	0.019	±	0.006	0.009	±	0.002	0.001	±	0.000
PG(20:5/22:6)-H	0.004	±	0.001	0.001	±	0.000	0.000	±	0.000
PG(20:2/22:6)-H	0.013	±	0.003	0.005	±	0.000	0.001	±	0.000
PG(20:3/22:6)-H	0.023	±	0.004	0.006	±	0.001	0.000	±	0.000
PG(22:4/22:6)-H	0.014	±	0.003	0.009	±	0.001	0.000	±	0.000
PG(22:5/22:6)-H	0.026	±	0.007	0.012	±	0.002	0.002	±	0.000
PG(22:6/22:6)-H	0.109	±	0.031	0.068	±	0.008	0.011	±	0.003

Table 11: Phosphatidylserines

Lipid Ion	FOB			HOS			143B		
PS(12:0/14:0)-H	0.007	±	0.004	0.002	±	0.000	0.001	±	0.000
PS(16:0/14:0)-H	0.005	±	0.004	0.003	±	0.001	0.002	±	0.001
PS(16:0/14:1)-H	0.033	±	0.033	0.000	±	0.000	0.002	±	0.001
PS(16:0/16:0)-H	0.012	±	0.006	0.012	±	0.002	0.004	±	0.002
PS(16:1/16:1)-H	0.006	±	0.005	0.000	±	0.000	0.001	±	0.001
PS(16:1/17:0)-H	0.029	±	0.017	0.035	±	0.015	0.001	±	0.000
PS(18:0/16:0)-H	0.023	±	0.005	0.033	±	0.008	0.004	±	0.001
PS(16:0e/18:1)-H	0.005	±	0.003	0.003	±	0.001	0.009	±	0.002
PS(16:1/18:2)-H	0.002	±	0.000	0.000	±	0.000	0.002	±	0.000
PS(18:0/18:0)-H	0.005	±	0.002	0.003	±	0.001	0.000	±	0.000
PS(18:0e/18:1)-H	0.072	±	0.067	0.008	±	0.001	0.017	±	0.003
PS(18:1/18:1)-H	0.105	±	0.059	0.142	±	0.030	0.217	±	0.040
PS(18:0/18:3)-H	0.044	±	0.029	0.006	±	0.001	0.001	±	0.001
PS(16:0/20:3)-H	0.013	±	0.002	0.009	±	0.001	0.013	±	0.002
PS(16:0/20:4)-H	0.006	±	0.003	0.006	±	0.000	0.003	±	0.001
PS(16:1/20:3)-H	0.011	±	0.006	0.013	±	0.004	0.012	±	0.001
PS(16:0/22:0)-H	0.003	±	0.001	0.002	±	0.001	0.000	±	0.000
PS(18:1/20:2)-H	0.037	±	0.016	0.020	±	0.003	0.010	±	0.002

PS(18:0/20:3)-H	0.013	±	0.005	0.004	±	0.001	0.002	±	0.001
PS(18:1/20:3)-H	0.010	±	0.005	0.012	±	0.002	0.008	±	0.001
PS(18:0/20:4)-H	0.050	±	0.025	0.049	±	0.006	0.032	±	0.004
PS(18:1/20:4)-H	0.011	±	0.006	0.013	±	0.002	0.011	±	0.002
PS(20:3/18:2)-H	0.009	±	0.003	0.012	±	0.002	0.006	±	0.001
PS(19:0/20:3)-H	0.005	±	0.003	0.007	±	0.002	0.003	±	0.001
PS(17:0/22:4)-H	0.017	±	0.008	0.033	±	0.008	0.008	±	0.002
PS(17:0/22:5)-H	0.006	±	0.004	0.009	±	0.002	0.004	±	0.001
PS(16:0/24:0)-H	0.001	±	0.001	0.002	±	0.000	0.000	±	0.000
PS(20:2/20:2)-H	0.004	±	0.003	0.007	±	0.001	0.005	±	0.001
PS(18:1/22:4)-H	0.122	±	0.092	0.151	±	0.036	0.352	±	0.104
PS(18:0/22:5)-H	0.009	±	0.006	0.028	±	0.004	0.003	±	0.000
PS(18:1/22:5)-H	0.022	±	0.015	0.027	±	0.001	0.110	±	0.024
PS(20:3/20:3)-H	0.009	±	0.005	0.005	±	0.001	0.002	±	0.000
PS(20:0/22:5)-H	0.006	±	0.004	0.010	±	0.002	0.016	±	0.002
PS(25:0/18:1)-H	0.001	±	0.001	0.001	±	0.000	0.002	±	0.000
PS(25:1/18:1)-H	0.002	±	0.002	0.001	±	0.000	0.002	±	0.000
PS(26:0/18:1)-H	0.003	±	0.003	0.002	±	0.000	0.015	±	0.003
PS(24:0/20:4)-H	0.006	±	0.005	0.003	±	0.001	0.005	±	0.001
PS(24:1/20:4)-H	0.002	±	0.002	0.002	±	0.000	0.002	±	0.000
PS(27:1/18:1)-H	0.000	±	0.000	0.000	±	0.000	0.001	±	0.000
PS(28:0/18:1)-H	0.000	±	0.000	0.000	±	0.000	0.001	±	0.000
PS(28:1/18:1)-H	0.002	±	0.002	0.003	±	0.000	0.010	±	0.002
PS(24:0/22:5)-H	0.000	±	0.000	0.001	±	0.000	0.001	±	0.000
PS(30:1/18:1)-H	0.000	±	0.000	0.000	±	0.000	0.002	±	0.000

Table 12: Sphingomyelines

LipiD Ion	FOB			HOS			143B		
SM(d30:0)+H	0.000	±	0.000	0.001	±	0.000	0.001	±	0.000
SM(d30:1)+H	0.003	±	0.001	0.001	±	0.000	0.001	±	0.000

SM(d31:1)+H	0.005	±	0.002	0.001	±	0.000	0.001	± 0.000
SM(d32:0)+H	0.047	±	0.014	0.053	±	0.004	0.069	± 0.018
SM(d32:1)+H	0.367	±	0.130	0.119	±	0.015	0.102	± 0.028
SM(d32:2)+H	0.008	±	0.003	0.002	±	0.000	0.001	± 0.000
SM(d33:1)+H	0.196	±	0.055	0.103	±	0.011	0.089	± 0.024
SM(d33:2)+H	0.002	±	0.000	0.001	±	0.000	0.000	± 0.000
SM(d33:5)+H	0.007	±	0.001	0.004	±	0.000	0.002	± 0.000
SM(d34:0)+H	0.570	±	0.070	1.439	±	0.056	1.423	± 0.227
SM(d18:1/16:0)+H	4.483	±	0.850	3.217	±	0.235	2.031	± 0.334
SM(d18:1/16:1)+H	0.383	±	0.114	0.161	±	0.008	0.126	± 0.029
SM(d18:2/16:1)+H	0.003	±	0.001	0.005	±	0.000	0.003	± 0.000
SM(d34:4)+H	0.050	±	0.016	0.017	±	0.003	0.015	± 0.004
SM(d35:1)+H	0.193	±	0.015	0.163	±	0.006	0.028	± 0.006
SM(d35:2)+H	0.014	±	0.002	0.008	±	0.001	0.002	± 0.000
SM(d35:4)+H	0.017	±	0.003	0.011	±	0.001	0.007	± 0.001
SM(d36:0)+H	0.023	±	0.002	0.190	±	0.006	0.029	± 0.006
SM(d36:1)+H	0.157	±	0.010	0.366	±	0.016	0.020	± 0.002
SM(d36:2)+H	0.061	±	0.003	0.105	±	0.011	0.008	± 0.002
SM(d18:2/18:1)+H	0.012	±	0.002	0.025	±	0.002	0.016	± 0.001
SM(d18:1/18:3)+H	0.157	±	0.015	0.111	±	0.004	0.043	± 0.005
SM(d36:5)+H	0.038	±	0.011	0.018	±	0.001	0.011	± 0.002
SM(d18:1/19:0)+H	0.003	±	0.000	0.000	±	0.000	0.000	± 0.000
SM(d37:4)+H	0.005	±	0.002	0.005	±	0.000	0.000	± 0.000
SM(d37:5)+H	0.001	±	0.000	0.001	±	0.000	0.000	± 0.000
SM(d37:6)+H	0.018	±	0.005	0.007	±	0.000	0.002	± 0.000
SM(d38:0)+H	0.005	±	0.000	0.035	±	0.002	0.005	± 0.002
SM(d38:1)+H	0.058	±	0.002	0.149	±	0.005	0.016	± 0.003
SM(d38:2)+H	0.009	±	0.001	0.020	±	0.001	0.001	± 0.000
SM(d38:3)+H	0.001	±	0.000	0.008	±	0.001	0.001	± 0.000
SM(d18:1/21:0)+H	0.003	±	0.001	0.000	±	0.000	0.000	± 0.000
SM(d39:1)+H	0.015	±	0.001	0.020	±	0.002	0.003	± 0.001

SM(d39:4)+H	0.000	±	0.000	0.001	±	0.000	0.003	±	0.001
SM(d40:0)+H	0.013	±	0.002	0.080	±	0.005	0.046	±	0.012
SM(d40:1)+H	0.011	±	0.002	0.047	±	0.003	0.014	±	0.004
SM(d18:1/22:0)+H	0.301	±	0.062	0.507	±	0.044	0.171	±	0.040
SM(d40:2)+H	0.098	±	0.020	0.179	±	0.017	0.030	±	0.006
SM(d40:4)+H	0.002	±	0.001	0.006	±	0.000	0.000	±	0.000
SM(d40:6)+H	0.004	±	0.002	0.003	±	0.000	0.013	±	0.003
SM(d18:0/23:0)+H	0.002	±	0.000	0.001	±	0.000	0.002	±	0.000
SM(d41:0)+H	0.001	±	0.000	0.005	±	0.000	0.005	±	0.001
SM(d18:1/23:0)+H	0.031	±	0.006	0.004	±	0.000	0.004	±	0.000
SM(d41:1)+H	0.004	±	0.001	0.025	±	0.002	0.006	±	0.001
SM(d41:1)+H	0.046	±	0.010	0.042	±	0.003	0.028	±	0.006
SM(d41:2)+H	0.110	±	0.028	0.119	±	0.013	0.040	±	0.011
SM(d41:3)+H	0.013	±	0.003	0.016	±	0.002	0.001	±	0.000
SM(d42:0)+H	0.010	±	0.002	0.031	±	0.002	0.108	±	0.031
SM(d42:1)+H	0.040	±	0.012	0.190	±	0.021	0.312	±	0.082
SM(d18:1/24:0)+H	0.472	±	0.155	0.371	±	0.032	0.707	±	0.177
SM(d18:1/24:1)+H	0.936	±	0.245	1.457	±	0.139	0.888	±	0.196
SM(d18:0/24:2)+H	0.049	±	0.020	0.005	±	0.001	0.016	±	0.005
SM(d18:1/24:2)+H	0.216	±	0.044	0.256	±	0.014	0.057	±	0.010
SM(d18:0/24:3)+H	0.002	±	0.001	0.010	±	0.001	0.005	±	0.001
SM(d18:1/24:3)+H	0.043	±	0.007	0.071	±	0.003	0.016	±	0.003
SM(d42:5)+H	0.003	±	0.001	0.076	±	0.005	0.000	±	0.000
SM(d42:5)+H	0.010	±	0.001	0.014	±	0.000	0.001	±	0.000
SM(d42:6)+H	0.000	±	0.000	0.013	±	0.001	0.000	±	0.000
SM(d42:6)+H	0.000	±	0.000	0.020	±	0.001	0.000	±	0.000
SM(d42:7)+H	0.000	±	0.000	0.003	±	0.000	0.000	±	0.000
SM(d18:1/25:0)+H	0.003	±	0.000	0.001	±	0.000	0.000	±	0.000
SM(d43:1)+H	0.007	±	0.002	0.004	±	0.000	0.012	±	0.003
SM(d43:2)+H	0.025	±	0.008	0.022	±	0.003	0.018	±	0.005
SM(d18:1/25:3)+H	0.000	±	0.000	0.002	±	0.000	0.000	±	0.000

SM(d43:4)+H	0.005	±	0.001	0.004	±	0.001	0.003	±	0.001
SM(d43:5)+H	0.012	±	0.002	0.015	±	0.001	0.003	±	0.000
SM(d44:0)+H	0.000	±	0.000	0.001	±	0.000	0.005	±	0.002
SM(d44:1)+H	0.010	±	0.004	0.006	±	0.000	0.039	±	0.009
SM(d44:2)+H	0.000	±	0.000	0.004	±	0.000	0.003	±	0.001
SM(d18:1/26:1)+H	0.047	±	0.017	0.030	±	0.005	0.097	±	0.030
SM(d44:3)+H	0.038	±	0.014	0.035	±	0.003	0.016	±	0.004
SM(d18:2/26:1)+H	0.001	±	0.000	0.003	±	0.000	0.011	±	0.003
SM(d44:4)+H	0.000	±	0.000	0.006	±	0.000	0.000	±	0.000
SM(d18:1/26:3)+H	0.053	±	0.019	0.048	±	0.005	0.062	±	0.011
SM(d44:5)+H	0.003	±	0.000	0.042	±	0.009	0.000	±	0.000
SM(d18:1/26:4)+H	0.113	±	0.021	0.121	±	0.004	0.050	±	0.006
SM(d44:6)+H	0.021	±	0.004	0.014	±	0.000	0.003	±	0.000
SM(d44:7)+H	0.002	±	0.000	0.013	±	0.001	0.000	±	0.000
SM(d44:8)+H	0.000	±	0.000	0.005	±	0.000	0.000	±	0.000
SM(d18:1/27:0)+H	0.003	±	0.001	0.000	±	0.000	0.001	±	0.000
SM(d18:1/27:1)+H	0.002	±	0.001	0.000	±	0.000	0.000	±	0.000
SM(d45:6)+H	0.013	±	0.002	0.003	±	0.000	0.003	±	0.000
SM(d18:1/28:0)+H	0.005	±	0.001	0.001	±	0.000	0.001	±	0.000
SM(d46:3)+H	0.000	±	0.000	0.000	±	0.000	0.000	±	0.000
SM(d46:4)+H	0.001	±	0.000	0.000	±	0.000	0.003	±	0.001
SM(d46:5)+H	0.004	±	0.001	0.003	±	0.000	0.008	±	0.002
SM(d46:6)+H	0.004	±	0.001	0.005	±	0.000	0.001	±	0.000
SM(d46:7)+H	0.001	±	0.000	0.001	±	0.000	0.000	±	0.000
SM(d18:1/30:0)+H	0.013	±	0.005	0.002	±	0.000	0.005	±	0.001
SM(d48:1)+H	0.007	±	0.002	0.008	±	0.001	0.003	±	0.001
SM(d48:2)+H	0.002	±	0.001	0.000	±	0.000	0.000	±	0.000
SM(d18:1/30:1)+H	0.008	±	0.003	0.002	±	0.000	0.002	±	0.000
SM(d17:0/32:1)+H	0.038	±	0.013	0.006	±	0.000	0.015	±	0.004
SM(d17:0/32:2)+H	0.003	±	0.001	0.001	±	0.000	0.001	±	0.000
SM(d18:1/32:0)+H	0.002	±	0.001	0.000	±	0.000	0.001	±	0.000

SM(d50:1)+H	0.009	±	0.002	0.004	±	0.000	0.001	±	0.000
SM(d50:2)+H	0.001	±	0.000	0.000	±	0.000	0.000	±	0.000
SM(d18:1/32:1)+H	0.001	±	0.000	0.000	±	0.000	0.001	±	0.000
SM(d56:2)+H	0.014	±	0.001	0.003	±	0.000	0.004	±	0.001
SM(d56:3)+H	0.011	±	0.002	0.002	±	0.000	0.004	±	0.001
SM(d56:4)+H	0.007	±	0.001	0.001	±	0.000	0.002	±	0.000

Table 13: Triacylglycerols

Lipid Ion	FOB			HOS			143B		
TG(8:0/8:0/8:0)+NH4	0.004	±	0.002	0.002	±	0.000	0.001	±	0.000
TG(8:0/8:0/10:0)+NH4	0.009	±	0.005	0.003	±	0.001	0.002	±	0.000
TG(8:0/10:0/10:0)+NH4	0.009	±	0.004	0.003	±	0.001	0.001	±	0.001
TG(8:0/12:0/14:0)+NH4	0.004	±	0.002	0.002	±	0.000	0.001	±	0.000
TG(10:0/12:0/14:0)+NH4	0.006	±	0.003	0.002	±	0.000	0.001	±	0.000
TG(4:0/16:0/16:0)+NH4	0.002	±	0.000	0.001	±	0.000	0.001	±	0.000
TG(12:0/12:0/14:0)+NH4	0.004	±	0.001	0.002	±	0.000	0.001	±	0.000
TG(12:0/14:0/14:0)+NH4	0.005	±	0.001	0.002	±	0.000	0.001	±	0.000
TG(16:1/12:0/12:0)+NH4	0.001	±	0.001	0.003	±	0.001	0.001	±	0.001
TG(16:0/12:0/14:0)+NH4	0.007	±	0.001	0.004	±	0.000	0.002	±	0.000
TG(14:0e/14:0/14:0)+NH4	0.001	±	0.000	0.004	±	0.000	0.002	±	0.000
TG(16:0/10:3/16:0)+NH4	0.026	±	0.005	0.012	±	0.001	0.006	±	0.001
TG(16:0/13:0/14:0)+NH4	0.007	±	0.002	0.007	±	0.001	0.003	±	0.001
TG(15:0/13:0/16:0)+NH4	0.002	±	0.000	0.002	±	0.000	0.001	±	0.000
TG(16:0/14:0/14:0)+NH4	0.021	±	0.005	0.020	±	0.003	0.010	±	0.003
TG(12:0e/16:0/16:0)+NH4	0.015	±	0.001	0.024	±	0.001	0.012	±	0.001
TG(16:1/14:0/14:0)+NH4	0.019	±	0.009	0.022	±	0.009	0.011	±	0.005
TG(15:0/14:0/16:0)+NH4	0.015	±	0.004	0.018	±	0.005	0.009	±	0.003
TG(15:0/14:0/16:1)+NH4	0.020	±	0.016	0.037	±	0.018	0.018	±	0.009

TG(12:0e/16:0/17:1)+NH4	0.002	±	0.000	0.006	±	0.000	0.003	±	0.000
TG(16:0/14:0/16:0)+NH4	0.081	±	0.015	0.038	±	0.010	0.019	±	0.006
TG(16:0e/14:0/16:0)+NH4	0.012	±	0.001	0.018	±	0.001	0.009	±	0.001
TG(14:0p/16:0/16:0)+NH4	0.029	±	0.002	0.062	±	0.002	0.031	±	0.002
TG(16:0/14:0/16:1)+NH4	0.055	±	0.018	0.051	±	0.009	0.027	±	0.007
TG(16:1/14:0/16:1)+NH4	0.017	±	0.005	0.009	±	0.005	0.005	±	0.003
TG(12:0p/16:1/18:1)+NH4	0.000	±	0.000	0.000	±	0.000	0.000	±	0.000
TG(15:0/16:0/16:0)+NH4	0.035	±	0.008	0.068	±	0.011	0.035	±	0.009
TG(15:0/16:0/16:1)+NH4	0.047	±	0.011	0.065	±	0.012	0.033	±	0.009
TG(16:1/14:0/17:1)+NH4	0.015	±	0.003	0.016	±	0.006	0.008	±	0.004
TG(16:0/16:0/16:0)+NH4	0.186	±	0.025	0.102	±	0.018	0.053	±	0.014
TG(16:0e/16:0/16:0)+NH4	0.008	±	0.003	0.015	±	0.001	0.008	±	0.001
TG(16:0p/16:0/16:0)+NH4	0.018	±	0.006	0.024	±	0.003	0.012	±	0.001
TG(16:0/16:0/16:1)+NH4	0.184	±	0.051	0.124	±	0.018	0.063	±	0.015
TG(20:1p/14:0/14:0)+NH4	0.008	±	0.001	0.016	±	0.001	0.008	±	0.001
TG(16:1/14:0/18:1)+NH4	0.082	±	0.024	0.059	±	0.008	0.030	±	0.007
TG(12:0p/18:1/18:1)+NH4	0.000	±	0.000	0.000	±	0.000	0.000	±	0.000
TG(16:1/16:1/16:1)+NH4	0.017	±	0.005	0.010	±	0.002	0.005	±	0.002
TG(16:0/16:0/17:0)+NH4	0.050	±	0.009	0.036	±	0.003	0.018	±	0.004
TG(15:0/16:0/18:1)+NH4	0.072	±	0.015	0.064	±	0.011	0.033	±	0.009
TG(15:0/16:1/18:1)+NH4	0.040	±	0.010	0.039	±	0.011	0.020	±	0.007
TG(16:1/16:1/17:1)+NH4	0.009	±	0.002	0.008	±	0.002	0.004	±	0.001
TG(18:0/16:0/16:0)+NH4	0.150	±	0.027	0.091	±	0.043	0.045	±	0.021
TG(18:0e/16:0/16:0)+NH4	0.011	±	0.004	0.026	±	0.002	0.013	±	0.001
TG(16:0/16:0/18:1)+NH4	0.455	±	0.123	0.267	±	0.022	0.135	±	0.022
TG(16:0e/16:0/18:1)+NH4	0.032	±	0.012	0.062	±	0.008	0.031	±	0.002
TG(18:0p/16:0/16:1)+NH4	0.019	±	0.006	0.029	±	0.003	0.014	±	0.001
TG(16:0/16:1/18:1)+NH4	0.366	±	0.113	0.188	±	0.015	0.094	±	0.013
TG(16:1/16:1/18:1)+NH4	0.095	±	0.032	0.043	±	0.004	0.022	±	0.004
TG(18:0/16:0/17:0)+NH4	0.024	±	0.004	0.018	±	0.001	0.009	±	0.001
TG(16:0/17:0/18:1)+NH4	0.070	±	0.016	0.049	±	0.005	0.025	±	0.005

TG(20:1p/15:0/16:0)+NH4	0.006	±	0.002	0.011	±	0.001	0.005	±	0.000
TG(16:0/17:1/18:1)+NH4	0.088	±	0.025	0.054	±	0.005	0.027	±	0.005
TG(16:1/17:1/18:1)+NH4	0.032	±	0.009	0.019	±	0.003	0.010	±	0.002
TG(20:0/16:0/16:0)+NH4	0.097	±	0.010	0.048	±	0.005	0.025	±	0.005
TG(18:0/16:0/18:0)+NH4	0.068	±	0.017	0.101	±	0.009	0.050	±	0.002
TG(18:0e/16:0/18:0)+NH4	0.006	±	0.002	0.017	±	0.001	0.009	±	0.001
TG(18:0/16:0/18:1)+NH4	0.340	±	0.089	0.264	±	0.025	0.130	±	0.006
TG(18:0e/16:0/18:1)+NH4	0.029	±	0.010	0.073	±	0.008	0.036	±	0.003
TG(16:0/18:1/18:1)+NH4	0.655	±	0.193	0.406	±	0.030	0.205	±	0.032
TG(16:0e/18:1/18:1)+NH4	0.041	±	0.014	0.074	±	0.012	0.036	±	0.004
TG(20:0p/16:1/16:1)+NH4	0.010	±	0.003	0.017	±	0.002	0.008	±	0.000
TG(16:1/18:1/18:1)+NH4	0.325	±	0.112	0.159	±	0.021	0.080	±	0.014
TG(16:1/18:1/18:2)+NH4	0.090	±	0.023	0.055	±	0.003	0.028	±	0.004
TG(16:0/16:0/20:4)+NH4	0.019	±	0.002	0.016	±	0.001	0.008	±	0.000
TG(16:1/16:1/20:3)+NH4	0.015	±	0.004	0.006	±	0.000	0.003	±	0.000
TG(16:0/14:0/22:6)+NH4	0.004	±	0.001	0.001	±	0.000	0.001	±	0.000
TG(19:1/16:0/18:0)+NH4	0.030	±	0.007	0.027	±	0.004	0.013	±	0.002
TG(19:1/16:0/18:1)+NH4	0.066	±	0.017	0.042	±	0.003	0.021	±	0.002
TG(18:1/17:1/18:1)+NH4	0.054	±	0.016	0.030	±	0.002	0.015	±	0.002
TG(18:1/17:1/18:2)+NH4	0.022	±	0.006	0.011	±	0.001	0.006	±	0.000
TG(15:0/18:1/20:5)+NH4	0.030	±	0.006	0.012	±	0.001	0.006	±	0.001
TG(18:0/18:0/18:0)+NH4	0.032	±	0.008	0.032	±	0.003	0.016	±	0.002
TG(20:0e/16:0/18:0)+NH4	0.003	±	0.001	0.003	±	0.000	0.001	±	0.000
TG(20:0/16:0/18:1)+NH4	0.241	±	0.048	0.105	±	0.011	0.054	±	0.011
TG(18:0/18:0/18:1)+NH4	0.064	±	0.020	0.075	±	0.003	0.038	±	0.003
TG(20:0e/16:0/18:1)+NH4	0.007	±	0.003	0.014	±	0.001	0.007	±	0.001
TG(18:0/18:1/18:1)+NH4	0.321	±	0.091	0.194	±	0.014	0.097	±	0.008
TG(16:0e/18:1/20:1)+NH4	0.011	±	0.004	0.023	±	0.003	0.011	±	0.001
TG(18:1/18:1/18:1)+NH4	0.425	±	0.115	0.293	±	0.028	0.149	±	0.028
TG(16:0e/18:1/20:2)+NH4	0.012	±	0.004	0.017	±	0.003	0.009	±	0.001
TG(18:1/18:1/18:2)+NH4	0.151	±	0.036	0.108	±	0.004	0.054	±	0.007

TG(18:1/18:2/18:2)+NH4	0.036	±	0.008	0.045	±	0.003	0.022	±	0.003
TG(18:1/18:1/18:3)+NH4	0.067	±	0.008	0.043	±	0.004	0.021	±	0.001
TG(18:2/18:2/18:2)+NH4	0.035	±	0.010	0.029	±	0.004	0.015	±	0.002
TG(16:0/16:0/22:6)+NH4	0.026	±	0.007	0.009	±	0.001	0.004	±	0.000
TG(16:0/16:1/22:6)+NH4	0.022	±	0.006	0.006	±	0.001	0.003	±	0.000
TG(15:0/16:0/24:0)+NH4	0.009	±	0.002	0.008	±	0.002	0.004	±	0.001
TG(16:0/16:0/23:1)+NH4	0.013	±	0.002	0.013	±	0.002	0.007	±	0.002
TG(19:1/18:0/18:1)+NH4	0.027	±	0.004	0.016	±	0.001	0.008	±	0.001
TG(19:1/18:1/18:1)+NH4	0.024	±	0.008	0.013	±	0.001	0.006	±	0.000
TG(19:1/18:1/18:2)+NH4	0.027	±	0.007	0.012	±	0.001	0.006	±	0.001
TG(18:1/17:1/20:3)+NH4	0.019	±	0.004	0.009	±	0.001	0.005	±	0.000
TG(16:0/16:0/24:0)+NH4	0.018	±	0.005	0.014	±	0.004	0.007	±	0.003
TG(16:0e/16:0/24:0)+NH4	0.002	±	0.001	0.001	±	0.000	0.000	±	0.000
TG(16:0/16:0/24:1)+NH4	0.013	±	0.004	0.015	±	0.002	0.007	±	0.002
TG(18:0e/16:0/22:1)+NH4	0.006	±	0.003	0.005	±	0.001	0.003	±	0.000
TG(18:0/18:1/20:1)+NH4	0.033	±	0.010	0.028	±	0.002	0.014	±	0.002
TG(20:0e/18:1/18:1)+NH4	0.006	±	0.002	0.008	±	0.001	0.004	±	0.000
TG(20:1/18:1/18:1)+NH4	0.082	±	0.025	0.044	±	0.004	0.022	±	0.002
TG(16:0e/18:1/22:2)+NH4	0.006	±	0.002	0.006	±	0.001	0.003	±	0.000
TG(18:1/18:1/20:2)+NH4	0.082	±	0.023	0.036	±	0.003	0.018	±	0.001
TG(18:1/18:1/20:3)+NH4	0.065	±	0.011	0.032	±	0.001	0.016	±	0.001
TG(16:0e/18:1/22:4)+NH4	0.008	±	0.001	0.005	±	0.000	0.003	±	0.000
TG(18:1/18:1/20:4)+NH4	0.050	±	0.010	0.036	±	0.007	0.018	±	0.002
TG(18:0/16:0/22:6)+NH4	0.012	±	0.004	0.007	±	0.001	0.003	±	0.000
TG(16:0/18:1/22:6)+NH4	0.066	±	0.014	0.022	±	0.003	0.011	±	0.001
TG(16:1/18:1/22:6)+NH4	0.038	±	0.007	0.010	±	0.002	0.005	±	0.000
TG(25:0/16:0/16:0)+NH4	0.008	±	0.001	0.006	±	0.001	0.003	±	0.001
TG(25:0/16:0/16:1)+NH4	0.007	±	0.001	0.008	±	0.002	0.004	±	0.001
TG(25:1/16:0/16:1)+NH4	0.010	±	0.002	0.008	±	0.001	0.004	±	0.001
TG(18:1/18:1/21:1)+NH4	0.090	±	0.018	0.050	±	0.005	0.025	±	0.005
TG(18:1/18:2/21:1)+NH4	0.048	±	0.009	0.023	±	0.001	0.012	±	0.001

TG(26:0/16:0/16:0)+NH4	0.008	±	0.001	0.006	±	0.002	0.003	±	0.001
TG(26:1/16:0/16:0)+NH4	0.011	±	0.003	0.009	±	0.001	0.005	±	0.001
TG(18:0e/16:0/24:1)+NH4	0.004	±	0.002	0.002	±	0.000	0.001	±	0.000
TG(18:0p/16:0/24:1)+NH4	0.006	±	0.003	0.004	±	0.000	0.002	±	0.000
TG(16:0/18:1/24:1)+NH4	0.026	±	0.005	0.020	±	0.001	0.010	±	0.001
TG(18:0p/18:1/22:1)+NH4	0.003	±	0.001	0.003	±	0.000	0.001	±	0.000
TG(16:1/18:1/24:1)+NH4	0.018	±	0.007	0.012	±	0.001	0.006	±	0.001
TG(18:1/18:1/22:2)+NH4	0.024	±	0.006	0.011	±	0.001	0.006	±	0.000
TG(18:1/18:1/22:3)+NH4	0.073	±	0.014	0.023	±	0.001	0.012	±	0.001
TG(18:1/18:1/22:4)+NH4	0.059	±	0.008	0.035	±	0.003	0.017	±	0.001
TG(18:1/18:1/22:5)+NH4	0.028	±	0.005	0.013	±	0.002	0.006	±	0.001
TG(18:1/18:1/22:6)+NH4	0.048	±	0.006	0.017	±	0.002	0.008	±	0.001
TG(18:1/20:4/20:4)+NH4	0.019	±	0.002	0.006	±	0.001	0.003	±	0.000
TG(27:0/16:0/16:0)+NH4	0.004	±	0.001	0.002	±	0.000	0.001	±	0.000
TG(27:1/16:0/16:0)+NH4	0.003	±	0.001	0.003	±	0.001	0.002	±	0.001
TG(25:1/16:0/18:1)+NH4	0.006	±	0.001	0.004	±	0.001	0.002	±	0.001
TG(25:1/16:1/18:1)+NH4	0.006	±	0.001	0.003	±	0.001	0.001	±	0.000
TG(26:1/16:0/18:0)+NH4	0.007	±	0.003	0.004	±	0.001	0.002	±	0.001
TG(26:1/16:0/18:1)+NH4	0.017	±	0.005	0.009	±	0.002	0.005	±	0.001
TG(18:1/18:1/24:1)+NH4	0.423	±	0.043	0.225	±	0.025	0.114	±	0.020
TG(26:1/16:1/18:1)+NH4	0.027	±	0.006	0.019	±	0.001	0.010	±	0.001
TG(18:1/18:1/24:2)+NH4	0.015	±	0.004	0.008	±	0.002	0.004	±	0.000
TG(20:0/18:1/22:6)+NH4	0.021	±	0.004	0.011	±	0.001	0.005	±	0.001
TG(27:1/16:0/18:1)+NH4	0.003	±	0.001	0.002	±	0.001	0.001	±	0.000
TG(25:1/18:1/18:1)+NH4	0.002	±	0.001	0.001	±	0.000	0.001	±	0.000
TG(28:0/16:0/18:0)+NH4	0.000	±	0.000	0.001	±	0.000	0.000	±	0.000
TG(28:0/16:0/18:1)+NH4	0.002	±	0.001	0.001	±	0.000	0.001	±	0.000
TG(28:1/16:0/18:1)+NH4	0.006	±	0.002	0.003	±	0.000	0.002	±	0.000
TG(26:1/18:1/18:1)+NH4	0.008	±	0.004	0.003	±	0.000	0.002	±	0.000
TG(26:1/18:1/18:2)+NH4	0.005	±	0.002	0.002	±	0.000	0.001	±	0.000
TG(18:1/20:4/24:0)+NH4	0.002	±	0.001	0.001	±	0.000	0.000	±	0.000

TG(29:0/16:0/18:1)+NH4	0.002	±	0.001	0.001	±	0.000	0.001	±	0.000
TG(29:1/16:0/18:1)+NH4	0.001	±	0.000	0.001	±	0.001	0.001	±	0.000
TG(27:1/18:1/18:1)+NH4	0.001	±	0.000	0.000	±	0.000	0.000	±	0.000
TG(30:0/16:0/18:1)+NH4	0.000	±	0.000	0.000	±	0.000	0.000	±	0.000
TG(30:1/16:0/18:1)+NH4	0.001	±	0.000	0.001	±	0.000	0.000	±	0.000
TG(28:1/18:1/18:1)+NH4	0.002	±	0.001	0.001	±	0.000	0.000	±	0.000
TG(26:1/18:1/20:2)+NH4	0.001	±	0.000	0.001	±	0.000	0.000	±	0.000
TG(29:1/18:0/18:1)+NH4	0.002	±	0.001	0.001	±	0.000	0.000	±	0.000
TG(29:1/18:1/18:1)+NH4	0.000	±	0.000	0.000	±	0.000	0.000	±	0.000
TG(30:0/18:0/18:1)+NH4	0.000	±	0.000	0.000	±	0.000	0.000	±	0.000
TG(30:0/18:1/18:1)+NH4	0.000	±	0.000	0.000	±	0.000	0.000	±	0.000
TG(30:1/18:1/18:1)+NH4	0.000	±	0.000	0.000	±	0.000	0.000	±	0.000
TG(28:1/18:1/20:2)+NH4	0.000	±	0.000	0.000	±	0.000	0.000	±	0.000
TG(26:0/18:1/24:0)+NH4	0.000	±	0.000	0.000	±	0.000	0.000	±	0.000
TG(26:1/18:1/24:0)+NH4	0.000	±	0.000	0.000	±	0.000	0.000	±	0.000
TG(26:1/18:1/24:1)+NH4	0.000	±	0.000	0.000	±	0.000	0.000	±	0.000
TG(26:1/18:1/24:2)+NH4	0.000	±	0.000	0.000	±	0.000	0.000	±	0.000
TG(28:0/18:1/24:1)+NH4	0.000	±	0.000	0.000	±	0.000	0.000	±	0.000
TG(28:1/18:1/24:1)+NH4	0.000	±	0.000	0.000	±	0.000	0.000	±	0.000
TG(28:1/22:1/22:1)+NH4	0.000	±	0.000	0.000	±	0.000	0.000	±	0.000

Table 14: Phosphatidic Acids

Lipid Ion	FOB			HOS			143B		
PA(16:1/18:1)-H	0.004	±	0.002	0.000	±	0.000	0.001	±	0.001
PA(18:0/18:1)-H	0.011	±	0.003	0.005	±	0.001	0.006	±	0.003
PA(26:0/18:1)-H	0.000	±	0.000	0.000	±	0.000	0.001	±	0.000
PA(24:0/23:0)-H	0.009	±	0.003	0.006	±	0.001	0.013	±	0.003
PA(24:1/23:0)-H	0.025	±	0.008	0.005	±	0.001	0.006	±	0.001
PA(24:1/23:1)-H	0.021	±	0.005	0.006	±	0.000	0.002	±	0.001

Table 15: Monoacylglycerols

Lipid Ion	FOB			HOS			143B		
MG(30:0)+H	0.000	±	0.000	0.000	±	0.000	0.003	±	0.000
MG(32:0)+H	0.003	±	0.001	0.005	±	0.000	0.032	±	0.006
MG(32:1)+H	0.001	±	0.001	0.001	±	0.000	0.007	±	0.002
MG(34:0)+H	0.002	±	0.001	0.009	±	0.000	0.029	±	0.006
MG(36:0)+H	0.000	±	0.000	0.001	±	0.000	0.006	±	0.002
MG(36:1)+H	0.002	±	0.001	0.002	±	0.000	0.026	±	0.007
MG(38:1)+H	0.001	±	0.000	0.001	±	0.000	0.012	±	0.004

Table 16: Fold Change in Lipids

Lipid Ion	p-Value			log10(Fold Change)		
	HOS vs FOB	143B vs HOS	FOB vs 143B	HOS vs FOB	143B vs HOS	FOB vs 143B
Cer(d18:1/10:0)+H	0.05	0.05	0.05	0.20	0.32	-0.52
Cer(d18:0/12:0)+H	0.10	0.05	0.05	0.13	0.31	-0.45
Cer(d18:1/13:0)+H	0.05	0.05	0.05	0.22	0.19	-0.41
Cer(d18:0/14:0)+H	0.05	0.05	0.35	0.38	-0.49	0.11
Cer(d18:1/14:0)+H	0.05	0.05	0.05	0.64	0.16	-0.80
Cer(d17:1/16:0)+H	0.05	0.20	0.05	0.74	0.12	-0.85
Cer(d18:0/16:0)+H	0.05	0.05	0.65	0.44	-0.42	-0.02
Cer(d18:1/16:0)+H	0.05	0.35	0.05	0.78	-0.15	-0.64
Cer(d34:1)+H	0.05	0.05	0.05	0.24	0.14	-0.38
Cer(d18:2/16:0)+H	0.05	0.05	0.05	0.67	0.21	-0.89
Cer(d18:0/17:0)+H	0.05	0.05	0.05	0.24	0.47	-0.71
Cer(d18:1/17:0)+H	0.05	0.05	0.05	0.75	0.70	-1.45
Cer(d18:0/18:0)+H	0.05	0.05	0.10	-0.16	0.36	-0.20

Cer(d18:1/18:0)+H	0.05	0.05	0.05	0.40	0.48	-0.88
Cer(d36:1)+H	0.05	0.10	0.05	0.19	0.23	-0.42
Cer(d18:2/18:0)+H	0.20	0.10	0.10	0.73	0.63	-1.36
Cer(d18:0/20:0)+H	0.20	0.10	0.10	-0.08	0.24	-0.16
Cer(d18:1/20:0)+H	0.05	0.05	0.05	0.36	0.44	-0.80
Cer(d38:1)+H	0.05	0.05	0.05	0.19	0.21	-0.40
Cer(d17:1/22:0)+H	0.05	0.05	0.05	0.55	0.34	-0.89
Cer(d40:0)+H	0.50	0.80	0.80	0.53	-0.65	0.13
Cer(d18:0/22:0)+H	0.05	0.35	0.05	-0.35	-0.10	0.45
Cer(d18:0/22:1)+H	0.05	0.65	0.20	0.11	-0.02	-0.09
Cer(d18:1/22:0)+H	0.05	0.05	0.05	0.53	0.22	-0.75
Cer(d18:2/22:0)+H	0.05	0.05	0.05	0.71	0.38	-1.09
Cer(d18:0/23:0)+H	0.50	0.50	0.50	-0.04	-0.02	0.06
Cer(d18:0/23:1)+H	0.05	0.50	0.20	0.14	0.03	-0.18
Cer(d18:1/23:0)+H	0.05	0.50	0.05	0.59	0.08	-0.68
Cer(d18:2/23:0)+H	0.05	0.05	0.05	0.68	0.34	-1.02
Cer(d18:0/24:0)+H	0.05	0.05	0.05	-0.59	-0.50	1.09
Cer(d18:1/24:0)+H	0.10	0.50	0.10	0.69	0.08	-0.78
Cer(d18:0/24:1)+H	0.10	0.05	0.05	-0.17	-0.37	0.53
Cer(d18:1/24:0)+H	0.20	0.35	0.20	0.29	-0.05	-0.25
Cer(d18:1/24:1)+H	0.10	0.50	0.10	0.58	0.02	-0.60
Cer(d18:2/24:0)+H	0.05	0.10	0.05	0.70	0.20	-0.90
Cer(d18:2/24:1)+H	0.05	0.05	0.05	0.66	0.40	-1.07
Cer(d18:1/24:2)+H	0.05	0.05	0.20	-0.34	0.20	0.14
Cer(d18:1/24:3)+H	0.05	0.05	0.05	0.20	0.62	-0.82
Cer(d18:0/25:0)+H	0.20	0.20	0.05	-0.30	-0.12	0.42
Cer(d18:0/25:1)+H	0.65	0.05	0.05	-0.06	-0.32	0.37
Cer(d18:1/25:0)+H	0.10	0.20	0.20	0.37	-0.15	-0.22

Cer(d18:1/25:1)+H	0.05	0.20	0.05	0.62	0.13	-0.75
Cer(d18:2/25:1)+H	0.05	0.05	0.05	0.47	0.40	-0.87
Cer(d18:0/26:0)+H	0.05	0.05	0.05	-0.55	-0.55	1.10
Cer(d18:0/26:1)+H	0.05	0.05	0.05	-0.40	-0.75	1.15
Cer(d18:1/26:0)+H	0.35	0.05	0.05	0.04	-0.48	0.43
Cer(d18:2/26:0)+H	0.50	0.80	0.50	-0.14	0.05	0.08
Cer(d18:1/26:1)+H	0.10	0.05	0.35	0.56	-0.42	-0.14
Cer(d18:2/26:1)+H	0.05	0.20	0.05	0.69	0.14	-0.83
Cer(d18:1/26:3)+H	0.05	0.05	0.05	0.87	1.16	-2.03
Cer(d20:0/25:0)+H	0.65	0.65	0.50	-0.43	0.41	0.02
Cer(d18:1/27:0)+H	0.50	0.50	0.20	-0.44	0.34	0.09
Cer(d20:0/26:0)+H	0.35	0.35	0.50	-0.54	0.51	0.04
Cer(d18:0/28:1)+H	0.05	0.05	0.05	#NAME?	-0.67	Inf
Cer(d18:1/28:0)+H	0.10	0.65	0.10	-0.59	0.21	0.38
Cer(d18:1/28:1)+H	0.35	0.05	0.05	0.22	-0.58	0.36
Cer(d22:1/24:1)+H	0.10	0.35	0.50	-0.66	0.42	0.24
Cer(d22:0/25:0)+H	0.65	0.50	0.35	-0.71	0.80	-0.09
Cer(d20:1/27:0)+H	0.65	0.35	0.80	-0.64	0.61	0.03
Cer(d22:1/25:1)+H	0.35	0.50	0.40	-0.95	0.78	0.17
Cer(d24:0/24:0)+H	0.20	0.20	0.65	-0.79	0.87	-0.07
Cer(d20:1/28:0)+H	0.20	0.20	0.50	-0.70	0.69	0.02
Cer(d20:2/28:0)+H	0.65	0.20	0.35	-0.31	0.31	-0.01
Cer(d25:0/24:0)+H	0.20	0.20	0.35	-0.85	0.95	-0.10
Cer(d22:1/27:0)+H	0.80	0.50	0.50	-0.90	1.00	-0.11
Cer(d24:0/26:0)+H	0.35	0.05	0.10	-0.74	1.00	-0.26
Cer(d22:1/28:0)+H	0.20	0.20	0.35	-0.74	0.93	-0.18
Cer(d25:0/26:0)+H	0.35	0.20	0.35	-0.91	1.20	-0.29
Cer(d22:1/29:0)+H	0.05	0.05	0.20	-1.20	1.44	-0.24

Cer(d22:1/30:0)+H	0.20	0.20	0.35	-0.81	0.84	-0.03
Cer(d25:0/28:0)+H	0.60	0.20	0.20	-0.93	Inf	#NAME?
CerG1(d18:0/14:0)+H	0.10	0.20	0.35	0.60	-0.30	-0.30
CerG1(d18:1/14:0)+H	0.05	0.05	0.05	1.17	-0.31	-0.86
CerG1(d17:1/16:0)+H	0.05	0.80	0.05	0.90	-0.09	-0.81
CerG1(d18:0/16:0)+H	0.10	0.05	0.50	0.32	-0.32	0.00
CerG1(d18:1/16:0)+H	0.05	0.10	0.05	0.98	-0.21	-0.77
CerG1(d18:2/16:0)+H	0.05	0.05	0.20	0.66	-0.28	-0.38
CerG1(d18:1/17:0)+H	0.05	0.05	0.05	0.97	0.45	-1.42
CerG1(d18:1/18:0)+H	0.05	0.05	0.05	0.42	0.60	-1.02
CerG1(d18:0/20:0)+H	0.05	0.05	0.20	-0.32	0.44	-0.12
CerG1(d18:1/20:0)+H	0.05	0.05	0.05	0.28	0.52	-0.80
CerG1(d18:0/22:0)+H	0.50	0.80	0.50	-0.07	-0.05	0.12
CerG1(d18:1/22:0)+H	0.05	0.20	0.05	0.61	0.16	-0.77
CerG1(d18:1/22:1)+H	0.05	0.05	0.05	0.58	0.60	-1.18
CerG1(d18:0/23:0)+H	0.05	0.10	0.35	0.35	-0.22	-0.14
CerG1(d18:1/23:0)+H	0.05	0.20	0.05	0.88	-0.24	-0.64
CerG1(d18:1/23:1)+H	0.05	0.05	0.05	0.80	0.50	-1.30
CerG1(d18:0/24:0)+H	0.35	0.05	0.05	0.15	-0.74	0.59
CerG1(d18:0/24:1)+H	0.35	0.05	0.05	-0.01	-0.38	0.39
CerG1(d18:1/24:0)+H	0.05	0.05	0.20	0.96	-0.50	-0.46
CerG1(d18:1/24:1)+H	0.05	0.10	0.10	0.77	-0.21	-0.56
CerG1(d18:2/24:1)+H	0.05	0.20	0.05	0.60	0.15	-0.75
CerG1(d18:0/25:0)+H	0.35	0.05	0.20	0.17	-0.34	0.16
CerG1(d18:1/25:0)+H	0.05	0.05	0.10	0.87	-0.36	-0.51
CerG1(d18:1/25:1)+H	0.05	0.20	0.05	0.94	-0.17	-0.77
CerG1(d18:0/26:0)+H	0.35	0.05	0.05	0.12	-0.96	0.83
CerG1(d18:0/26:1)+H	0.05	0.05	0.20	0.48	-0.68	0.20

CerG1(d18:1/26:0)+H	0.05	0.05	0.50	0.83	-0.85	0.02
CerG1(d18:1/26:1)+H	0.05	0.05	0.35	0.99	-0.64	-0.35
CerG1(d44:4)+H	0.05	0.05	0.05	0.54	1.14	-1.68
CerG1(d46:1)+H	0.20	0.05	0.50	0.29	-0.46	0.16
CerG2(d18:1/16:0)+H	0.20	0.35	0.20	0.54	-0.17	-0.37
CerG2(d34:2)+H	0.80	0.05	0.05	0.04	1.72	-1.75
CerG2(d18:1/22:0)+H	0.35	0.05	0.10	0.13	0.27	-0.40
CerG2(d18:1/22:1)+H	0.10	0.05	0.05	-0.05	1.21	-1.16
CerG2(d18:1/23:0)+H	0.05	0.65	0.10	0.49	-0.03	-0.46
CerG2(d18:1/23:1)+H	0.05	0.05	0.05	0.47	0.41	-0.88
CerG2(d18:0/24:1)+H	0.50	0.05	0.10	0.08	-0.42	0.35
CerG2(d18:1/24:0)+H	0.05	0.05	0.50	0.63	-0.58	-0.05
CerG2(d18:1/24:1)+H	0.35	0.35	0.20	0.31	-0.06	-0.25
CerG2(d18:2/24:1)+H	0.35	0.05	0.05	0.22	0.62	-0.83
CerG2(d18:1/25:0)+H	0.05	0.05	0.35	0.82	-0.59	-0.23
CerG2(d43:2)+H	0.35	0.50	0.20	0.44	0.03	-0.46
CerG2(d18:1/26:0)+H	0.20	0.05	0.10	0.68	-1.02	0.34
CerG2(d18:1/26:1)+H	0.10	0.05	0.35	0.58	-0.45	-0.13
CerG3(d18:1/14:0)+H	0.05	0.05	0.05	1.71	Inf	#NAME?
CerG3(d18:1/16:0)+H	0.05	0.35	0.05	0.99	0.08	-1.07
CerG3(d18:1/22:0)+H	0.05	0.05	0.05	0.68	0.80	-1.48
CerG3(d18:1/23:0)+H	0.05	0.60	0.05	1.84	0.05	-1.88
CerG3(d18:1/24:0)+H	0.05	0.50	0.05	1.13	-0.06	-1.07
CerG3(d18:1/24:1)+H	0.05	0.05	0.05	0.81	0.32	-1.13
CerG3(d18:2/24:1)+H	0.05	0.20	0.05	1.39	Inf	#NAME?
CerG3(d18:1/26:0)+H	0.05	0.05	0.10	Inf	#NAME?	-0.90
CerG3(d18:1/26:1)+H	0.05	0.05	0.05	1.74	-0.62	-1.12
ChE(18:1)+NH4	0.05	0.10	0.05	0.57	0.23	-0.79

ChE(18:2)+NH4	0.05	0.65	0.05	0.71	0.04	-0.75
ChE(20:1)+NH4	0.35	0.05	0.10	0.22	0.57	-0.79
ChE(20:2)+NH4	0.35	0.05	0.05	0.14	1.24	-1.38
ChE(20:3)+NH4	0.35	0.05	0.05	0.14	1.23	-1.37
ChE(20:4)+NH4	0.10	0.05	0.05	0.16	0.87	-1.02
ChE(20:5)+NH4	0.35	0.05	0.05	0.12	0.92	-1.04
ChE(22:1)+NH4	0.50	0.05	0.35	-0.13	0.68	-0.55
ChE(22:2)+NH4	0.35	0.05	0.05	0.06	1.06	-1.12
ChE(22:3)+NH4	0.10	0.05	0.05	-0.20	1.53	-1.33
ChE(22:4)+NH4	0.05	0.05	0.05	-0.75	2.20	-1.45
ChE(22:5)+NH4	0.05	0.05	0.05	-0.20	1.43	-1.23
ChE(22:6)+NH4	0.50	0.05	0.05	-0.12	1.13	-1.01
ChE(24:1)+NH4	0.35	0.50	0.35	0.43	-0.07	-0.36
ChE(24:3)+NH4	0.65	0.05	0.05	-0.03	1.20	-1.17
ChE(24:4)+NH4	0.05	0.05	0.05	-0.47	1.78	-1.32
ChE(24:5)+NH4	0.05	0.05	0.05	-0.50	1.79	-1.28
ChE(24:6)+NH4	0.20	0.05	0.05	-0.23	1.62	-1.39
ChE(26:0)+NH4	0.35	0.05	0.05	0.91	-1.64	0.73
ChE(26:1)+NH4	0.35	0.05	0.35	0.83	-0.73	-0.10
ChE(26:2)+NH4	0.35	0.20	0.35	0.33	-0.16	-0.17
ChE(26:3)+NH4	0.35	0.05	0.20	0.27	0.68	-0.94
ChE(26:4)+NH4	0.35	0.05	0.05	0.12	1.15	-1.27
ChE(26:5)+NH4	0.35	0.05	0.05	0.08	1.44	-1.52
ChE(26:6)+NH4	0.35	0.05	0.05	0.41	1.16	-1.57
ChE(28:1)+NH4	0.35	0.05	0.20	1.06	-1.41	0.35
ChE(28:2)+NH4	0.35	0.05	0.35	0.85	-0.68	-0.18
ChE(28:3)+NH4	0.35	0.20	0.35	0.65	0.12	-0.77
ChE(28:4)+NH4	0.35	0.05	0.10	0.30	0.84	-1.14

ChE(28:5)+NH4	0.35	0.05	0.05	0.04	1.50	-1.54
ChE(28:6)+NH4	0.35	0.05	0.05	0.55	1.05	-1.59
ChE(30:1)+NH4	0.50	0.05	0.05	Inf	#NAME?	1.07
ChE(30:3)+NH4	0.20	0.05	0.50	Inf	#NAME?	-0.15
ChE(30:4)+NH4	0.35	0.05	0.35	0.26	0.34	-0.60
ChE(30:5)+NH4	0.35	0.05	0.20	-0.18	1.10	-0.92
ChE(30:6)+NH4	0.35	0.05	0.20	0.42	0.68	-1.09
ChE(32:5)+NH4	0.50	0.05	0.35	0.13	0.35	-0.48
ChE(32:6)+NH4	0.35	0.10	0.35	0.35	0.18	-0.53
CL(14:0/16:0/16:0/16:0)-H	0.05	0.05	0.20	#NAME?	1.15	Inf
CL(14:0/16:0/16:1/16:0)-H	0.05	0.05	0.05	#NAME?	0.48	Inf
CL(14:0/14:0/18:1/16:1)-H	0.05	0.05	0.05	-0.49	-0.31	0.80
CL(14:0/16:1/16:1/16:1)-H	0.20	0.05	0.05	Inf	#NAME?	0.48
CL(16:0/16:0/16:0/16:0)-H	0.05	0.05	0.20	#NAME?	1.56	Inf
CL(14:0/16:0/16:0/18:1)-H	0.05	0.05	0.05	-1.72	0.74	0.97
CL(14:0/18:1/16:0/16:1)-H	0.05	0.35	0.05	-0.72	0.03	0.70
CL(14:0/16:1/16:1/18:1)-H	0.35	0.05	0.05	0.35	-0.80	0.45
CL(16:1/16:1/16:1/16:1)-H	0.35	0.05	0.20	0.82	-0.98	0.15
CL(15:0/16:0/16:0/18:1)-H	0.05	0.05	0.10	-2.00	1.44	0.55
CL(14:0/15:0/18:1/18:1)-H	0.05	0.05	0.20	-1.08	0.69	0.39
CL(17:1/14:0/18:1/16:1)-H	0.35	0.10	0.35	0.10	-0.27	0.17
CL(17:1/16:1/16:1/16:1)-H	0.35	0.05	0.50	0.50	-0.45	-0.05
CL(16:0/16:0/16:0/18:0)-H	0.05	0.05	1.00	#NAME?	Inf	NaN
CL(18:1/16:0/16:0/16:0)-H	0.05	0.05	0.05	-2.02	1.30	0.72
CL(14:0/18:1/16:0/18:1)-H	0.05	0.05	0.05	-1.21	0.58	0.63
CL(18:1/16:1/16:0/16:1)-H	0.35	0.05	0.05	-0.14	-0.36	0.50
CL(16:1/16:1/16:1/18:1)-H	0.35	0.05	0.20	0.46	-0.72	0.26
CL(18:3/14:0/16:0/18:1)-H	0.05	0.05	0.05	#NAME?	0.73	Inf

CL(18:2/16:1/16:1/16:1)-H	0.35	0.05	0.65	0.41	-0.47	0.05
CL(12:2/18:1/18:1/18:1)-H	0.05	0.20	0.05	-1.20	0.13	1.07
CL(22:5/14:0/16:1/14:0)-H	0.25	0.05	0.10	0.76	-1.12	0.36
CL(18:4/16:1/16:1/16:1)-H	0.20	0.05	0.35	Inf	#NAME?	0.13
CL(17:0/16:0/16:0/18:1)-H	0.05	0.05	0.05	#NAME?	1.68	Inf
CL(18:1/16:0/18:1/15:0)-H	0.05	0.05	0.35	-1.43	1.26	0.16
CL(17:1/16:0/16:1/18:1)-H	0.05	0.10	0.20	-0.40	0.22	0.18
CL(17:1/16:1/16:1/18:1)-H	0.35	0.10	0.65	0.19	-0.23	0.04
CL(17:1/16:1/18:2/16:1)-H	0.35	0.65	0.50	0.17	0.00	-0.17
CL(16:0/16:0/16:0/20:0)-H	0.05	0.05	0.05	#NAME?	0.69	Inf
CL(18:1/16:0/18:0/16:0)-H	0.05	0.05	0.05	-2.05	1.53	0.51
CL(18:1/16:0/16:0/18:1)-H	0.05	0.05	0.05	-1.79	1.06	0.73
CL(18:1/16:0/16:1/18:1)-H	0.05	0.10	0.05	-0.82	0.29	0.53
CL(18:1/16:1/18:2/16:0)-H	0.35	0.05	0.10	0.18	-0.53	0.34
CL(18:3/16:0/16:0/18:1)-H	0.05	0.05	0.35	-0.55	0.62	-0.07
CL(18:3/18:1/16:0/16:0)-H	0.05	0.05	0.05	#NAME?	1.03	Inf
CL(18:2/16:1/18:1/16:1)-H	0.35	0.10	0.35	0.15	-0.30	0.15
CL(20:4/16:0/14:0/18:1)-H	0.05	0.05	0.05	-1.20	0.60	0.60
CL(18:2/16:1/18:2/16:1)-H	0.50	0.65	0.50	0.08	0.01	-0.08
CL(18:4/16:0/16:1/18:1)-H	0.35	0.10	0.05	-0.09	-0.29	0.38
CL(20:4/16:1/16:1/16:1)-H	0.35	0.05	0.35	0.53	-0.34	-0.18
CL(18:4/16:1/16:1/18:1)-H	0.35	0.05	0.35	0.52	-0.71	0.19
CL(18:4/16:1/18:2/16:1)-H	0.35	0.05	0.65	0.46	-0.46	0.00
CL(17:0/18:1/18:1/16:0)-H	0.05	0.05	0.20	-1.41	1.23	0.18
CL(17:1/18:1/16:0/18:1)-H	0.05	0.05	0.20	-0.94	0.68	0.26
CL(17:1/18:1/16:1/18:1)-H	0.35	0.35	0.35	-0.08	-0.07	0.16
CL(18:1/15:1/18:1/18:1)-H	0.05	0.05	1.00	#NAME?	Inf	NaN
CL(17:1/16:1/18:2/18:1)-H	0.50	0.20	0.50	-0.07	0.15	-0.08

CL(18:3/18:1/15:0/18:1)-H	0.05	0.05	0.05	#NAME?	1.22	Inf
CL(17:1/16:1/18:2/18:2)-H	0.35	0.05	0.20	-0.17	0.59	-0.41
CL(17:1/16:1/16:1/20:4)-H	0.35	0.20	0.65	0.15	-0.17	0.02
CL(18:1/16:0/18:0/18:0)-H	0.35	0.05	0.05	0.11	-0.67	0.57
CL(18:1/16:0/18:0/18:1)-H	0.05	0.05	0.05	-1.74	1.38	0.36
CL(18:1/16:0/18:1/18:1)-H	0.05	0.05	0.05	-1.43	1.03	0.40
CL(18:1/16:1/18:1/18:1)-H	0.10	0.65	0.10	-0.28	-0.01	0.29
CL(18:3/18:1/16:0/18:0)-H	0.05	0.05	0.05	-1.59	1.14	0.46
CL(18:2/18:1/16:1/18:1)-H	0.35	0.35	0.10	-0.10	-0.13	0.24
CL(18:3/18:1/16:0/18:1)-H	0.05	0.05	0.05	-1.50	0.80	0.69
CL(18:2/16:1/18:1/18:2)-H	0.10	0.10	0.50	-0.20	0.26	-0.05
CL(18:2/18:2/16:1/18:1)-H	0.05	0.05	0.05	-0.75	0.38	0.36
CL(18:2/18:2/18:2/16:1)-H	0.35	0.05	0.20	-0.20	0.41	-0.21
CL(20:4/16:1/16:1/18:1)-H	0.35	0.35	0.50	0.20	-0.10	-0.10
CL(20:4/16:1/18:1/16:1)-H	0.35	0.05	0.35	0.18	-0.33	0.15
CL(22:5/16:1/16:1/16:1)-H	0.20	0.35	0.20	0.25	-0.07	-0.18
CL(18:2/20:4/16:1/16:1)-H	0.35	0.10	0.50	0.15	-0.24	0.09
CL(20:5/16:1/16:1/18:2)-H	0.50	0.50	0.50	0.08	0.02	-0.10
CL(17:0/18:1/18:0/18:1)-H	0.05	0.05	0.50	-1.39	1.39	0.00
CL(17:0/18:1/18:1/18:1)-H	0.05	0.05	0.35	-0.89	0.95	-0.07
CL(17:1/18:1/18:1/18:1)-H	0.10	0.20	0.35	-0.22	0.17	0.06
CL(17:1/18:1/18:2/18:1)-H	0.05	0.10	0.50	-0.29	0.26	0.03
CL(17:0/20:4/16:0/18:1)-H	0.05	0.05	0.20	-1.46	1.14	0.32
CL(17:1/18:1/18:2/18:2)-H	0.05	0.05	0.10	-0.31	0.64	-0.32
CL(17:0/18:2/18:2/18:2)-H	0.35	0.20	0.50	-0.11	0.15	-0.04
CL(17:1/20:4/16:0/18:1)-H	0.05	0.05	0.20	-0.81	0.65	0.17
CL(17:1/18:2/18:2/18:2)-H	0.50	0.10	0.10	0.06	0.29	-0.35
CL(17:1/20:4/16:1/18:1)-H	0.50	0.50	0.35	-0.05	-0.04	0.09

CL(17:1/16:1/20:4/18:2)-H	0.50	0.20	0.50	-0.05	0.16	-0.11
CL(16:0/18:0/18:0/20:0)-H	0.05	0.05	0.10	-0.69	0.43	0.25
CL(18:4/18:2/18:2/18:2)-H	0.20	0.05	0.20	-0.24	0.48	-0.24
CL(18:1/18:0/18:0/18:1)-H	0.35	0.05	0.05	0.49	-0.86	0.37
CL(18:1/18:0/18:1/18:1)-H	0.05	0.05	0.50	-1.19	1.20	-0.01
CL(18:1/18:1/18:1/18:1)-H	0.05	0.05	0.20	-0.68	0.57	0.11
CL(18:2/18:1/18:1/18:1)-H	0.05	0.35	0.35	-0.25	0.15	0.10
CL(20:4/16:0/18:0/18:1)-H	0.05	0.05	0.05	-1.62	1.23	0.39
CL(18:2/18:1/18:1/18:2)-H	0.05	0.05	0.35	-0.32	0.39	-0.07
CL(20:4/16:0/18:1/18:1)-H	0.05	0.05	0.05	-1.11	0.76	0.34
CL(18:2/18:2/18:2/18:1)-H	0.05	0.05	0.05	-0.35	0.62	-0.28
CL(18:2/18:1/18:2/18:2)-H	0.10	0.35	0.35	-0.27	0.11	0.16
CL(18:2/18:1/20:4/16:1)-H	0.10	0.05	0.05	-0.27	0.68	-0.40
CL(18:2/20:4/16:1/18:1)-H	0.50	0.35	0.50	-0.07	0.03	0.04
CL(18:2/16:1/16:1/22:5)-H	0.50	0.05	0.10	0.06	0.34	-0.40
CL(18:2/16:1/20:4/18:2)-H	0.20	0.05	0.35	-0.22	0.33	-0.12
CL(19:1/18:1/18:1/18:1)-H	0.05	0.05	0.50	-0.44	0.36	0.08
CL(19:1/18:1/18:2/18:1)-H	0.05	0.10	0.35	-0.41	0.30	0.11
CL(19:1/18:1/18:2/18:2)-H	0.05	0.05	0.05	-0.48	0.69	-0.21
CL(17:0/18:1/20:4/18:1)-H	0.05	0.05	0.50	-1.04	1.07	-0.03
CL(17:1/18:1/18:1/20:4)-H	0.10	0.05	0.35	-0.54	0.42	0.11
CL(17:1/18:1/20:4/18:1)-H	0.10	0.20	0.35	-0.28	0.19	0.09
CL(17:1/18:1/18:2/20:4)-H	0.10	0.10	0.50	-0.26	0.26	0.00
CL(17:1/18:2/18:2/20:4)-H	0.05	0.05	0.10	-0.36	0.68	-0.33
CL(18:1/18:0/18:0/20:0)-H	0.05	0.05	0.35	0.51	-0.38	-0.13
CL(18:2/18:2/18:2/20:4)-H	0.35	0.05	0.05	0.11	0.53	-0.64
CL(20:5/18:2/18:2/18:2)-H	0.20	0.05	0.05	-0.24	0.69	-0.45
CL(18:1/16:0/16:0/24:1)-H	0.35	0.05	0.20	0.39	-0.74	0.35

CL(22:2/16:0/18:0/18:1)-H	0.35	0.05	0.50	0.29	-0.32	0.03
CL(20:4/18:0/18:0/18:0)-H	0.50	0.35	0.20	0.04	0.06	-0.11
CL(18:1/18:1/18:1/20:1)-H	0.05	0.05	0.35	-0.72	0.78	-0.06
CL(18:1/16:0/20:1/20:3)-H	0.05	0.05	0.20	-1.01	1.15	-0.14
CL(18:1/18:0/18:0/20:4)-H	0.05	0.05	0.05	#NAME?	1.45	Inf
CL(20:4/18:1/18:0/18:1)-H	0.05	0.05	0.35	-1.18	1.12	0.06
CL(18:2/18:1/20:3/18:1)-H	0.05	0.05	0.05	-0.48	0.74	-0.27
CL(20:4/18:1/18:1/18:1)-H	0.05	0.05	0.50	-0.50	0.45	0.05
CL(18:2/18:1/20:4/18:1)-H	0.05	0.05	0.05	-0.21	0.64	-0.43
CL(18:2/20:4/18:1/18:1)-H	0.05	0.05	0.50	-0.23	0.30	-0.07
CL(18:2/18:1/18:2/20:4)-H	0.10	0.05	0.05	-0.19	0.52	-0.33
CL(18:2/18:1/20:4/18:2)-H	0.05	0.05	0.05	-0.31	0.48	-0.18
CL(23:0/16:0/18:1/18:1)-H	0.65	0.20	0.35	0.10	-0.20	0.10
CL(21:0/20:4/16:0/18:0)-H	0.35	0.10	0.05	-0.07	0.38	-0.30
CL(20:5/18:1/20:4/18:1)-H	0.05	0.05	1.00	#NAME?	Inf	NaN
CL(18:2/18:2/18:2/22:6)-H	0.10	0.05	0.05	-0.17	0.57	-0.40
CL(18:4/22:6/20:4/16:1)-H	0.20	0.05	0.35	0.38	-0.48	0.10
CL(18:1/18:0/20:1/20:1)-H	0.05	0.20	0.05	0.44	-0.11	-0.34
CL(18:1/16:0/18:1/24:1)-H	0.05	0.05	1.00	#NAME?	Inf	NaN
CL(22:3/18:0/18:0/18:1)-H	0.05	0.10	0.05	0.42	-0.10	-0.32
CL(22:1/18:1/18:1/18:1)-H	0.05	0.05	1.00	#NAME?	Inf	NaN
CL(20:4/18:0/18:1/20:0)-H	0.20	0.65	0.20	0.17	-0.01	-0.16
CL(22:3/18:1/18:1/18:1)-H	0.05	0.05	0.10	-1.87	1.30	0.58
CL(20:2/18:0/18:1/20:4)-H	0.10	0.35	0.35	0.25	-0.14	-0.11
CL(22:5/18:0/18:1/18:1)-H	0.05	0.05	0.35	-1.37	1.68	-0.32
CL(22:5/18:1/18:1/18:1)-H	0.05	0.05	0.05	-0.73	1.33	-0.60
CL(23:0/18:0/18:0/18:1)-H	0.10	0.20	0.10	0.51	-0.23	-0.27
CL(20:5/20:4/20:4/18:1)-H	0.05	0.05	0.10	-1.00	0.67	0.33

CL(22:2/18:0/18:1/20:4)-H	0.20	0.05	0.05	-0.14	0.85	-0.71
CL(22:3/18:0/18:1/20:4)-H	0.35	0.50	0.35	0.16	0.04	-0.20
CL(23:0/18:0/18:0/20:3)-H	0.50	0.10	0.35	0.00	0.32	-0.32
CL(23:1/18:0/18:0/20:4)-H	0.20	0.05	0.05	-0.07	0.39	-0.32
CL(21:0/18:0/18:0/22:6)-H	0.20	0.35	0.50	-0.14	0.11	0.02
CL(22:2/18:0/20:4/20:4)-H	0.50	0.05	0.05	0.00	0.96	-0.95
CL(22:6/18:1/22:6/18:1)-H	0.05	0.05	0.05	#NAME?	1.16	Inf
CL(22:6/20:4/20:4/18:1)-H	0.20	0.20	0.35	-0.10	0.17	-0.07
CL(20:4/18:0/20:4/22:0)-H	0.35	0.05	0.05	-0.07	0.32	-0.25
CL(23:0/18:0/18:0/22:4)-H	0.20	0.20	0.20	0.04	0.25	-0.29
CL(23:1/18:0/18:0/22:6)-H	0.35	0.50	0.35	0.12	-0.04	-0.08
DG(16:0/14:0)+NH4	0.05	0.05	0.05	-0.21	-0.66	0.87
DG(16:1/14:0)+NH4	0.05	0.05	0.05	Inf	#NAME?	0.72
DG(16:0/16:0)+NH4	0.05	0.05	0.05	-0.34	-0.57	0.92
DG(18:1/14:0)+NH4	0.35	0.05	0.05	0.23	-0.84	0.60
DG(17:1/16:0)+NH4	0.35	0.50	0.50	0.11	-0.08	-0.03
DG(18:0/16:0)+NH4	0.05	0.05	0.05	-0.54	-0.35	0.88
DG(16:0/18:1)+NH4	0.35	0.05	0.05	0.02	-0.55	0.53
DG(16:1/18:1)+NH4	0.05	0.05	0.35	0.66	-0.82	0.16
DG(16:0/18:2)+NH4	0.80	0.35	0.35	0.12	-0.16	0.03
DG(19:1/16:0)+NH4	0.35	0.50	0.65	0.04	-0.05	0.00
DG(17:1/18:1)+NH4	0.10	0.20	0.20	0.42	-0.31	-0.11
DG(18:0/18:0)+NH4	0.50	0.05	0.20	0.37	-0.73	0.36
DG(18:0/18:1)+NH4	0.35	0.05	0.05	0.02	-0.55	0.52
DG(18:1/18:1)+NH4	0.20	0.05	0.05	0.32	-0.69	0.37
DG(18:1/18:2)+NH4	0.05	0.05	0.50	0.34	-0.23	-0.11
DG(18:2/18:2)+NH4	0.10	0.10	0.05	0.37	0.70	-1.07
DG(16:0/20:4)+NH4	0.10	0.05	0.05	0.09	0.58	-0.67

DG(19:1/18:1)+NH4	0.35	0.05	0.35	0.32	-0.38	0.05
DG(16:0/22:0)+NH4	0.20	0.05	0.05	-0.05	-0.75	0.80
DG(20:0/18:1)+NH4	0.50	0.05	0.05	-0.10	-0.90	1.01
DG(20:1/18:1)+NH4	0.35	0.05	0.05	0.25	-0.98	0.73
DG(18:1/20:2)+NH4	0.05	0.35	0.10	0.34	-0.06	-0.28
DG(18:0/20:3)+NH4	0.05	0.10	0.05	0.38	0.18	-0.56
DG(18:1/20:3)+NH4	0.05	0.05	0.05	0.30	0.25	-0.56
DG(18:0/20:4)+NH4	0.20	0.05	0.05	0.01	0.49	-0.51
DG(18:1/20:4)+NH4	0.05	0.05	0.05	0.32	0.20	-0.52
DG(18:0/20:5)+NH4	0.35	0.05	0.05	0.17	0.29	-0.46
DG(16:0/22:6)+NH4	0.20	0.05	0.05	0.11	0.29	-0.40
DG(16:1/22:6)+NH4	0.05	0.10	0.05	0.97	-0.27	-0.69
DG(26:0/14:0)+NH4	0.65	0.05	0.05	0.00	-1.09	1.09
DG(16:0/24:1)+NH4	0.05	0.05	0.05	-0.65	-0.99	1.64
DG(18:1/22:1)+NH4	0.35	0.05	0.05	0.17	-1.01	0.84
DG(18:1/22:2)+NH4	0.05	0.05	0.65	0.61	-0.66	0.06
DG(18:0/22:4)+NH4	0.50	0.10	0.20	-0.02	0.18	-0.16
DG(18:0/22:5)+NH4	0.05	0.10	0.35	0.06	-0.23	0.17
DG(18:1/22:5)+NH4	0.05	0.35	0.10	0.28	-0.06	-0.22
DG(18:0/22:6)+NH4	0.35	0.35	0.50	0.06	-0.08	0.02
DG(18:1/22:6)+NH4	0.05	0.50	0.05	0.49	0.04	-0.53
DG(25:0/16:0)+NH4	0.50	0.05	0.10	0.06	-0.41	0.35
DG(26:0/16:0)+NH4	0.10	0.05	0.05	-0.31	-1.24	1.55
DG(26:1/16:0)+NH4	0.20	0.05	0.05	-0.22	-1.46	1.68
DG(26:1/16:1)+NH4	0.35	0.05	0.05	0.26	-1.55	1.29
DG(27:1/16:0)+NH4	0.80	0.05	0.05	0.01	-1.09	1.08
DG(28:0/16:0)+NH4	0.05	0.05	0.05	-0.55	-1.26	1.81
DG(28:1/16:0)+NH4	0.65	0.05	0.05	0.40	-1.75	1.35

DG(26:1/18:1)+NH4	0.35	0.05	0.05	0.33	-1.86	1.54
DG(30:0/16:0)+NH4	0.05	0.05	0.05	-0.54	-0.70	1.24
DG(30:1/16:0)+NH4	0.80	0.05	0.05	-0.53	-1.42	1.94
DG(28:1/18:1)+NH4	0.10	0.05	0.05	-0.41	-1.48	1.89
DG(29:1/18:1)+NH4	0.35	0.05	0.05	0.19	-1.40	1.21
DG(32:1/16:0)+NH4	0.05	0.05	0.05	-0.26	-0.29	0.55
DG(30:1/18:1)+NH4	0.50	0.05	0.05	-0.12	-1.01	1.13
DG(31:1/18:1)+NH4	0.20	0.05	0.05	Inf	#NAME?	1.07
DG(32:1/18:1)+NH4	0.05	0.05	0.05	-0.35	-0.74	1.09
LPC(16:0)+H	0.65	0.50	0.65	0.03	-0.10	0.08
LPC(16:0e)+H	0.35	0.20	0.50	0.11	-0.14	0.03
LPC(16:0p)+H	0.20	0.50	0.35	0.17	-0.04	-0.12
LPC(16:1)+H	0.50	0.20	0.65	0.59	-0.50	-0.10
LPC(18:0)+H	0.05	0.20	0.05	0.20	0.21	-0.41
LPC(18:0e)+H	0.35	0.20	0.50	-0.05	0.11	-0.06
LPC(18:0p)+H	0.35	0.65	0.20	0.12	0.00	-0.13
LPC(18:1)+H	0.20	0.20	0.50	0.14	-0.16	0.02
LPC(18:1p)+H	0.35	0.35	0.20	0.14	0.06	-0.20
LPC(20:0)+H	0.05	0.50	0.05	0.31	0.04	-0.35
LPC(20:0p)+H	0.10	0.10	0.50	0.50	-0.45	-0.05
LPC(20:1)+H	0.35	0.20	0.50	0.02	-0.15	0.13
LPC(20:3)+H	0.20	0.35	0.20	0.25	0.08	-0.34
LPC(22:0)+H	0.05	0.05	0.05	0.87	-0.38	-0.48
LPC(24:0)+H	0.05	0.05	0.50	1.02	-0.92	-0.09
LPC(24:1)+H	0.10	0.05	0.65	0.88	-0.92	0.04
LPC(26:0)+H	0.50	0.05	0.05	-0.01	0.39	-0.38
LPC(26:1)+H	0.10	0.05	0.20	0.88	-1.17	0.29
LPC(28:0)+H	0.05	0.05	0.05	0.32	0.54	-0.86

LPC(28:1)+H	0.05	0.05	0.05	0.22	0.27	-0.49
LPC(30:0)+H	0.05	0.05	0.05	0.39	-1.25	0.86
PC(11:0/16:0)+H	0.35	0.05	0.05	-0.01	-0.47	0.48
PC(28:0)+H	0.35	0.05	0.10	0.15	-0.52	0.37
PC(14:0e/14:0)+H	0.05	0.05	0.05	0.32	0.54	-0.87
PC(14:0p/14:0)+H	0.05	0.10	0.05	0.55	0.26	-0.81
PC(29:0)+H	0.50	0.05	0.20	-0.04	0.31	-0.27
PC(16:0/13:0)+H	0.35	0.35	0.20	0.23	0.03	-0.27
PC(11:0/18:1)+H	0.10	0.05	0.50	0.39	-0.45	0.06
PC(30:0)+H	0.80	0.10	0.20	-0.03	-0.13	0.16
PC(30:0e)+H	0.10	0.05	0.20	0.13	-0.27	0.14
PC(16:0p/14:0)+H	0.05	0.50	0.05	0.18	0.02	-0.20
PC(14:0p/16:0)+H	0.80	0.35	0.65	-0.02	0.02	0.00
PC(30:1)+H	0.35	0.05	0.50	0.39	-0.47	0.08
PC(16:0/14:1)+H	0.35	0.50	0.35	0.23	-0.03	-0.20
PC(30:1e)+H	0.05	0.35	0.05	0.21	0.02	-0.23
PC(14:0p/16:1)+H	0.10	0.05	0.05	0.22	0.21	-0.43
PC(30:2)+H	0.35	0.05	0.35	0.72	-0.50	-0.22
PC(16:1/14:1)+H	0.10	0.05	0.35	0.93	-0.59	-0.34
PC(30:2e)+H	0.65	0.05	0.05	0.04	0.63	-0.67
PC(18:1/12:2)+H	0.35	0.05	0.10	0.10	-0.45	0.35
PC(31:0)+H	0.05	0.05	0.05	-0.13	0.43	-0.30
PC(18:0/13:0)+H	0.05	0.05	0.50	-0.51	0.42	0.09
PC(17:1/14:0)+H	0.35	0.20	0.10	0.21	0.17	-0.38
PC(32:0)+H	0.05	0.05	0.20	-0.31	0.10	0.21
PC(32:0e)+H	0.35	0.05	0.10	0.10	-0.30	0.20
PC(16:0p/16:0)+H	0.05	0.05	0.50	-0.18	0.22	-0.04
PC(16:0/16:1)+H	0.20	0.35	0.35	0.23	-0.09	-0.14

PC(16:1p/16:0)+H	0.10	0.50	0.20	0.30	-0.06	-0.24
PC(32:1p)+H	0.35	0.20	0.50	-0.07	0.10	-0.03
PC(32:2)+H	0.20	0.10	0.35	0.77	-0.30	-0.47
PC(18:1/14:1)+H	0.05	0.20	0.05	0.57	-0.12	-0.45
PC(14:0p/18:3)+H	0.05	0.50	0.05	0.17	0.03	-0.20
PC(18:4/14:0)+H	0.35	0.35	0.35	0.20	-0.34	0.14
PC(32:4e)+H	0.05	0.05	0.05	0.58	1.69	-2.27
PC(12:0p/20:5)+H	0.05	0.05	0.05	0.51	0.45	-0.96
PC(33:0)+H	0.05	0.05	0.05	-0.34	0.71	-0.37
PC(33:1)+H	0.35	0.05	0.05	0.13	0.34	-0.47
PC(17:1/16:1)+H	0.10	0.20	0.20	0.60	-0.14	-0.46
PC(34:0)+H	0.05	0.05	0.05	-0.58	0.42	0.15
PC(34:0e)+H	0.65	0.10	0.20	-0.05	-0.15	0.20
PC(16:0p/18:0)+H	0.20	0.05	0.50	0.19	-0.27	0.07
PC(34:1)+H	0.10	0.20	0.05	0.17	0.09	-0.26
PC(16:0p/18:1)+H	0.35	0.10	0.50	0.18	-0.15	-0.03
PC(34:2)+H	0.35	0.35	0.35	0.33	-0.06	-0.27
PC(16:1p/18:1)+H	0.35	0.05	0.10	0.11	0.10	-0.20
PC(34:3)+H	0.10	0.50	0.10	0.62	-0.03	-0.59
PC(16:0/18:3)+H	0.35	0.05	0.05	-0.01	0.53	-0.52
PC(34:4)+H	0.05	0.05	0.05	0.59	0.42	-1.01
PC(18:4/16:0)+H	0.05	0.05	0.05	0.38	0.32	-0.69
PC(14:0/20:5)+H	0.05	0.05	0.05	0.81	0.32	-1.13
PC(34:6e)+H	0.05	0.05	0.05	0.43	1.58	-2.00
PC(35:0)+H	0.05	0.05	0.05	-0.86	1.19	-0.34
PC(17:0/18:1)+H	0.20	0.35	0.10	0.23	0.06	-0.29
PC(35:1)+H	0.10	0.05	0.05	0.16	0.27	-0.44
PC(17:1/18:1)+H	0.20	0.50	0.20	0.31	-0.05	-0.26

PC(36:0)+H	0.05	0.05	0.05	-0.64	0.36	0.28
PC(36:0e)+H	0.20	0.35	0.50	-0.12	0.04	0.08
PC(16:0/20:1)+H	0.05	0.50	0.10	0.29	-0.06	-0.23
PC(36:1e)+H	0.35	0.05	0.05	0.05	-0.70	0.65
PC(18:0p/18:1)+H	0.35	0.05	0.50	0.33	-0.35	0.02
PC(20:1p/16:0)+H	0.35	0.05	0.35	0.07	-0.27	0.20
PC(18:1p/18:0)+H	0.65	0.05	0.05	-0.03	-0.43	0.46
PC(18:1/18:1)+H	0.05	0.05	0.20	0.40	-0.21	-0.20
PC(16:1p/20:1)+H	0.50	0.20	0.35	0.00	0.12	-0.12
PC(18:2p/18:0)+H	0.35	0.35	0.20	0.28	0.09	-0.37
PC(36:2p)+H	0.35	0.20	0.35	0.18	-0.11	-0.07
PC(36:3)+H	0.10	0.05	0.05	0.29	0.20	-0.49
PC(36:4)+H	0.05	0.05	0.05	0.22	1.00	-1.22
PC(18:1/18:3)+H	0.05	0.05	0.05	0.22	0.44	-0.66
PC(36:4e)+H	0.10	0.05	0.05	0.06	0.76	-0.82
PC(16:0p/20:4)+H	0.05	0.05	0.05	0.18	0.90	-1.08
PC(36:5)+H	0.10	0.05	0.05	0.47	0.65	-1.12
PC(18:4/18:1)+H	0.05	0.05	0.05	0.47	0.19	-0.66
PC(14:0/22:5)+H	0.35	0.05	0.05	0.04	0.42	-0.45
PC(36:6)+H	0.05	0.20	0.05	0.46	0.18	-0.64
PC(22:2/14:4)+H	0.10	0.05	0.05	0.41	0.43	-0.83
PC(16:1/21:0)+H	0.05	0.05	0.35	0.85	-0.54	-0.31
PC(19:1/18:1)+H	0.35	0.50	0.35	0.17	-0.05	-0.12
PC(15:0/22:4)+H	0.05	0.05	0.05	-0.07	0.24	-0.17
PC(37:5)+H	0.05	0.05	0.05	0.40	0.99	-1.39
PC(17:0/20:5)+H	0.50	0.05	0.10	-0.07	0.44	-0.37
PC(38:0e)+H	0.35	0.35	0.65	0.11	-0.10	-0.01
PC(20:0/18:1)+H	0.05	0.05	0.05	-0.47	-0.65	1.12

PC(38:1e)+H	0.35	0.05	0.05	0.04	-0.64	0.60
PC(20:1p/18:0)+H	0.35	0.05	0.20	0.24	-0.49	0.24
PC(20:1/18:1)+H	0.35	0.05	0.50	0.26	-0.38	0.11
PC(38:2e)+H	0.35	0.05	0.20	0.44	-0.71	0.27
PC(38:3)+H	0.05	0.20	0.05	0.45	0.09	-0.54
PC(38:3e)+H	0.35	0.35	0.50	0.20	-0.14	-0.06
PC(38:4)+H	0.05	0.05	0.05	0.48	0.38	-0.86
PC(38:4e)+H	0.35	0.05	0.05	0.04	0.90	-0.94
PC(18:0/20:5)+H	0.05	0.05	0.05	0.43	0.37	-0.81
PC(38:5)+H	0.05	0.05	0.05	0.25	0.85	-1.10
PC(16:0/22:6)+H	0.10	0.05	0.05	0.22	0.40	-0.62
PC(38:6e)+H	0.10	0.05	0.05	0.23	0.55	-0.78
PC(38:7)+H	0.05	0.20	0.05	0.66	0.15	-0.81
PC(39:2)+H	0.35	0.05	0.35	0.13	-0.29	0.16
PC(40:0)+H	0.35	0.05	0.05	0.03	-1.03	0.99
PC(40:1)+H	0.35	0.05	0.05	-0.02	-0.77	0.79
PC(40:2)+H	0.35	0.05	0.05	0.11	-0.57	0.46
PC(40:3)+H	0.35	0.10	0.50	0.15	-0.17	0.02
PC(40:4)+H	0.20	0.05	0.05	0.16	0.30	-0.46
PC(18:0/22:5)+H	0.20	0.05	0.05	0.06	0.53	-0.59
PC(40:5e)+H	0.05	0.05	0.05	0.33	0.52	-0.85
PC(18:0/22:6)+H	0.10	0.05	0.05	0.18	0.72	-0.90
PC(40:6e)+H	0.20	0.05	0.05	0.18	0.53	-0.72
PC(18:1/22:6)+H	0.10	0.20	0.05	0.28	0.24	-0.52
PC(18:1/23:0)+H	0.05	0.05	0.10	1.14	-1.51	0.37
PC(31:0/10:2)+H	0.35	0.05	0.20	0.24	-0.53	0.29
PC(18:1/23:1)+H	0.05	0.05	0.50	1.24	-1.34	0.10
PC(26:0/16:0)+H	0.35	0.05	0.05	0.08	-1.33	1.25

PC(42:1)+H	0.35	0.05	0.05	0.35	-1.14	0.79
PC(42:2)+H	0.35	0.05	0.05	0.31	-1.02	0.71
PC(42:3)+H	0.35	0.05	0.10	0.11	-0.45	0.34
PC(18:2p/24:1)+H	0.05	0.10	0.05	0.52	0.25	-0.77
PC(27:1/16:0)+H	0.35	0.05	0.05	0.37	-1.13	0.75
PC(25:1/18:1)+H	0.35	0.05	0.05	0.48	-1.05	0.57
PC(44:0)+H	0.20	0.05	0.05	-0.17	-1.31	1.48
PC(44:1)+H	0.35	0.05	0.05	0.28	-1.52	1.24
PC(44:2)+H	0.35	0.05	0.05	0.39	-1.41	1.02
PC(44:3)+H	0.35	0.05	0.05	0.33	-0.88	0.55
PC(29:0/16:0)+H	0.50	0.05	0.05	Inf	#NAME?	2.25
PC(27:0/18:1)+H	0.35	0.05	0.05	0.27	-1.57	1.30
PC(45:2)+H	0.35	0.05	0.05	0.41	-1.25	0.84
PC(46:1)+H	0.35	0.05	0.05	0.07	-1.77	1.70
PC(46:2)+H	0.35	0.05	0.05	0.25	-1.68	1.43
PC(31:1/16:0)+H	1.00	0.05	0.05	NaN	#NAME?	Inf
PC(47:2)+H	0.35	0.05	0.05	0.27	-1.78	1.50
PC(48:1)+H	0.80	0.05	0.05	0.10	-2.08	1.98
PC(48:2)+H	0.35	0.05	0.05	0.12	-2.24	2.11
PC(50:2)+H	0.05	0.05	0.05	#NAME?	-2.74	Inf
PE(26:0)+H	0.05	0.05	0.05	0.24	0.41	-0.65
PE(12:0p/16:0)+H	0.05	0.05	0.05	0.26	0.97	-1.23
PE(16:0/14:0)+H	0.35	0.05	0.05	-0.11	-0.42	0.53
PE(16:0p/14:0)+H	0.05	0.05	0.05	-0.23	0.85	-0.62
PE(16:1/14:0)+H	0.35	0.05	0.50	0.60	-0.68	0.08
PE(12:0p/18:1)+H	0.05	0.05	0.05	0.27	0.24	-0.50
PE(12:0p/18:2)+H	0.35	0.05	0.05	-0.04	0.76	-0.72
PE(16:0/16:0)+H	0.05	0.50	0.10	-0.21	0.02	0.19

PE(16:0p/16:0)+H	0.05	0.05	0.35	-0.53	1.02	-0.49
PE(16:0/16:1)+H	0.10	0.05	0.50	0.43	-0.46	0.03
PE(16:0p/16:1)+H	0.35	0.05	0.05	0.21	-0.46	0.25
PE(16:1/16:1)+H	0.10	0.05	0.50	0.83	-0.84	0.01
PE(12:0p/20:4)+H	0.05	0.05	0.05	0.30	1.07	-1.37
PE(12:0p/20:5)+H	0.05	0.05	0.05	0.41	0.62	-1.03
PE(18:0p/15:0)+H	0.05	0.05	0.05	-0.59	1.80	-1.21
PE(17:1/16:0)+H	0.35	0.35	0.20	0.28	0.02	-0.30
PE(16:0p/17:1)+H	0.35	0.35	0.35	0.20	0.00	-0.20
PE(18:0/16:0)+H	0.05	0.05	0.50	-0.58	0.48	0.09
PE(18:0p/16:0)+H	0.05	0.05	0.10	-0.49	0.93	-0.45
PE(16:0/18:1)+H	0.35	0.05	0.50	0.22	-0.24	0.03
PE(16:0p/18:1)+H	0.35	0.05	0.50	0.34	-0.35	0.00
PE(16:1/18:1)+H	0.05	0.05	0.10	0.79	-0.52	-0.27
PE(18:1p/16:1)+H	0.35	0.05	0.35	0.27	-0.19	-0.08
PE(16:0p/18:2)+H	0.80	0.05	0.35	-0.02	0.13	-0.11
PE(12:0p/22:4)+H	0.05	0.05	0.05	0.54	0.68	-1.22
PE(14:0p/20:4)+H	0.05	0.05	0.05	0.32	0.88	-1.20
PE(12:0p/22:5)+H	0.05	0.05	0.05	0.52	0.22	-0.74
PE(14:0p/20:5)+H	0.05	0.05	0.05	0.42	0.81	-1.22
PE(12:0p/22:6)+H	0.05	0.05	0.05	0.33	0.76	-1.09
PE(17:0/18:1)+H	0.20	0.65	0.20	0.26	-0.04	-0.22
PE(16:0p/19:1)+H	0.35	0.10	0.35	0.21	-0.16	-0.05
PE(17:1/18:1)+H	0.05	0.20	0.05	0.54	-0.07	-0.48
PE(18:1p/17:1)+H	0.35	0.05	0.20	0.10	0.25	-0.35
PE(16:0p/20:0)+H	0.05	0.05	0.50	-0.69	0.71	-0.02
PE(18:0/18:1)+H	0.05	0.05	0.20	0.48	-0.26	-0.22
PE(18:0p/18:1)+H	0.35	0.05	0.05	0.12	-0.55	0.43

PE(18:1/18:1)+H	0.10	0.05	0.35	0.45	-0.31	-0.13
PE(18:1p/18:1)+H	0.35	0.05	0.35	0.32	-0.19	-0.13
PE(18:0p/18:2)+H	0.35	0.05	0.50	0.14	-0.28	0.14
PE(18:1/18:2)+H	0.35	0.35	0.20	0.18	0.04	-0.22
PE(18:1p/18:2)+H	0.35	0.05	0.05	-0.06	0.40	-0.34
PE(16:0p/20:3)+H	0.35	0.05	0.35	0.23	-0.31	0.08
PE(16:0/20:4)+H	0.05	0.05	0.05	-0.09	0.42	-0.33
PE(16:0p/20:4)+H	0.20	0.05	0.05	-0.07	0.42	-0.35
PE(16:1/20:4)+H	0.05	0.50	0.10	0.66	-0.04	-0.62
PE(16:0/20:5)+H	0.20	0.65	0.20	0.25	-0.04	-0.21
PE(14:0p/22:5)+H	0.20	0.05	0.05	0.26	0.84	-1.09
PE(16:0p/20:5)+H	0.20	0.50	0.20	0.30	0.02	-0.32
PE(16:1/20:5)+H	0.10	0.05	0.35	1.03	-0.53	-0.49
PE(14:0p/22:6)+H	0.05	0.05	0.05	0.67	0.65	-1.32
PE(18:0p/19:1)+H	0.35	0.35	0.50	0.10	-0.06	-0.04
PE(17:0/20:4)+H	0.05	0.05	0.05	-0.14	0.69	-0.54
PE(17:1/20:4)+H	0.35	0.05	0.05	0.03	0.79	-0.82
PE(17:1/20:5)+H	0.35	0.05	0.05	0.38	0.94	-1.32
PE(20:0/18:1)+H	0.35	0.20	0.35	0.34	-0.22	-0.12
PE(16:0p/22:1)+H	0.50	0.05	0.05	0.09	-0.71	0.62
PE(20:1/18:1)+H	0.35	0.10	0.50	0.29	-0.30	0.02
PE(16:0p/22:2)+H	0.35	0.05	0.50	0.37	-0.47	0.10
PE(18:0/20:3)+H	0.05	0.10	0.05	0.52	0.18	-0.70
PE(18:0p/20:3)+H	0.35	0.05	0.20	0.25	-0.55	0.30
PE(18:0/20:4)+H	0.20	0.05	0.05	0.06	0.55	-0.61
PE(38:4e)+H	0.05	0.05	0.10	-0.19	0.47	-0.29
PE(16:0p/22:4)+H	0.05	0.05	0.05	-0.14	0.53	-0.39
PE(18:0p/20:4)+H	0.05	0.05	0.10	-0.18	0.44	-0.26

PE(18:1/20:4)+H	0.05	0.05	0.05	0.23	0.24	-0.47
PE(18:0/20:5)+H	0.10	0.20	0.10	0.29	0.07	-0.37
PE(18:1p/20:4)+H	0.05	0.05	0.05	0.12	0.31	-0.43
PE(18:0p/20:5)+H	0.35	0.05	0.35	0.01	0.28	-0.29
PE(16:1/22:5)+H	0.35	0.05	0.05	0.32	-1.02	0.70
PE(38:6)+H	0.10	0.35	0.20	0.47	-0.12	-0.35
PE(16:0/22:6)+H	0.05	0.05	0.05	0.14	0.36	-0.50
PE(18:1p/20:5)+H	0.05	0.05	0.05	0.32	0.40	-0.72
PE(16:0p/22:6)+H	0.35	0.05	0.05	0.39	0.21	-0.59
PE(16:1/22:6)+H	0.35	0.05	0.35	0.77	-0.33	-0.44
PE(16:1p/22:6)+H	0.05	0.10	0.05	0.80	0.48	-1.28
PE(17:0/22:6)+H	0.05	0.05	0.50	-0.20	0.23	-0.03
PE(18:1/22:0)+H	0.05	0.05	0.35	0.81	-0.47	-0.34
PE(18:0p/22:1)+H	0.35	0.05	0.05	0.33	-0.89	0.56
PE(18:1/22:1)+H	0.10	0.10	0.35	0.42	-0.22	-0.20
PE(18:1p/22:1)+H	0.35	0.05	0.35	0.48	-0.68	0.20
PE(18:0p/22:3)+H	0.35	0.35	0.50	0.11	-0.09	-0.02
PE(18:0/22:4)+H	0.35	0.05	0.05	-0.08	0.30	-0.22
PE(20:0/20:4)+H	0.35	0.20	0.10	0.05	0.19	-0.24
PE(18:0p/22:4)+H	0.05	0.05	0.05	-0.26	0.47	-0.22
PE(20:0p/20:4)+H	0.05	0.05	0.05	0.31	0.29	-0.61
PE(18:0/22:5)+H	0.10	0.35	0.50	0.08	-0.10	0.02
PE(40:5e)+H	0.80	0.05	0.05	0.01	0.41	-0.42
PE(40:5p)+H	0.20	0.05	0.05	-0.03	0.36	-0.33
PE(18:0p/22:5)+H	0.10	0.50	0.10	0.08	0.06	-0.14
PE(18:0/22:6)+H	0.50	0.05	0.20	0.04	0.16	-0.20
PE(18:1p/22:5)+H	0.05	0.10	0.05	0.32	0.16	-0.48
PE(18:0p/22:6)+H	0.35	0.05	0.10	0.14	0.32	-0.47

PE(18:1/22:6)+H	0.35	0.05	0.05	0.20	0.23	-0.44
PE(18:1p/22:6)+H	0.10	0.05	0.05	0.36	0.46	-0.82
PE(18:2/22:6)+H	0.20	0.05	0.05	0.31	0.29	-0.60
PE(18:2p/22:6)+H	0.10	0.20	0.05	0.92	0.89	-1.82
PE(18:1/24:0)+H	0.05	0.05	0.35	1.02	-0.83	-0.19
PE(20:4/22:6)+H	0.10	0.50	0.20	0.26	-0.04	-0.23
PE(18:0p/24:1)+H	0.05	0.05	0.50	0.87	-0.87	-0.01
PE(18:1/24:1)+H	0.05	0.05	0.35	1.00	-0.80	-0.19
PE(22:0/20:4)+H	0.05	0.10	0.20	0.45	-0.28	-0.17
PE(20:0p/22:5)+H	0.35	0.05	0.10	0.01	0.21	-0.23
PE(20:1p/22:5)+H	0.20	0.05	0.05	0.10	0.42	-0.52
PE(20:0p/22:6)+H	0.05	0.20	0.05	0.55	0.16	-0.71
PE(25:0/18:1)+H	0.05	0.05	0.35	1.16	-1.06	-0.10
PE(43:2)+H	0.05	0.05	0.35	1.07	-0.70	-0.36
PE(26:0/18:1)+H	0.05	0.05	0.20	1.07	-1.43	0.36
PE(26:1/18:1)+H	0.05	0.05	0.50	1.23	-1.30	0.07
PE(44:2)+H	0.35	0.05	0.50	0.92	-1.03	0.11
PE(44:3)+H	0.05	0.05	0.20	1.06	-0.43	-0.63
PE(24:0/20:4)+H	0.05	0.05	0.50	0.81	-0.82	0.01
PE(24:1/20:4)+H	0.10	0.05	0.20	0.65	-0.90	0.25
PE(28:1/18:1)+H	0.35	0.05	0.05	1.19	-2.26	1.06
PE(26:0/20:4)+H	0.05	0.05	0.05	1.01	-1.51	0.51
PE(24:0/22:6)+H	0.35	0.05	0.10	0.21	-0.65	0.44
PE(24:1/22:6)+H	0.35	0.05	0.50	0.46	-0.52	0.06
PE(48:5)+H	0.05	0.05	0.05	0.48	-1.23	0.76
LPE(20:4)-H	0.50	0.05	0.05	0.04	0.94	-0.97
LPE(22:5)-H	0.10	0.05	0.05	0.23	0.39	-0.62
LPE(22:6)-H	0.05	0.05	0.05	0.33	0.48	-0.81

LPE(24:1)-H	0.05	0.05	0.65	1.68	-1.72	0.05
PEt(14:0/14:0)-H	0.05	0.10	0.05	-0.37	-0.30	0.68
PEt(16:0/14:0)-H	0.05	0.20	0.05	-0.18	-0.11	0.30
PEt(16:1/14:0)-H	0.35	0.05	0.35	0.63	-0.50	-0.14
PEt(16:0/16:0)-H	0.05	0.35	0.05	-0.58	0.11	0.47
PEt(16:0/16:1)-H	0.35	0.10	0.10	0.07	0.20	-0.27
PEt(16:0/18:1)-H	0.05	0.05	0.05	-1.46	0.79	0.68
PEt(16:1/18:1)-H	0.05	0.80	0.35	0.27	-0.19	-0.07
PI(16:0/14:1)-H	1.00	0.05	0.05	NaN	#NAME?	Inf
PI(16:0/16:0)-H	0.10	0.20	0.10	-0.29	-0.24	0.53
PI(18:1/14:1)-H	0.35	0.05	0.05	0.94	-1.29	0.34
PI(17:1/16:0)-H	0.35	0.50	0.35	0.16	0.02	-0.19
PI(18:0/16:0)-H	0.05	0.20	0.05	-0.47	-0.13	0.60
PI(16:0/18:1)-H	0.50	0.05	0.20	0.11	-0.31	0.20
PI(16:0e/18:1)-H	0.50	0.20	0.20	-0.12	-0.09	0.21
PI(18:0/17:0)-H	0.65	0.35	0.50	0.11	-0.13	0.02
PI(17:0/18:1)-H	0.35	0.10	0.50	0.17	-0.26	0.10
PI(18:0/18:0)-H	0.35	0.05	0.05	0.11	-0.45	0.33
PI(18:0/18:1)-H	0.35	0.05	0.05	0.17	-0.57	0.40
PI(18:0e/18:1)-H	0.05	0.05	0.05	#NAME?	-0.79	Inf
PI(18:0p/18:1)-H	0.20	0.35	0.05	-0.24	-0.24	0.48
PI(18:1/18:1)-H	0.35	0.05	0.05	0.27	-0.60	0.33
PI(18:1/18:3)-H	0.20	0.05	0.05	-0.08	1.12	-1.04
PI(16:0e/20:4)-H	0.05	0.05	0.05	-1.12	0.48	0.64
PI(16:1/20:4)-H	0.05	0.10	0.05	0.29	0.21	-0.50
PI(16:0/20:5)-H	0.35	0.20	0.35	0.24	-0.11	-0.13
PI(19:1/18:0)-H	0.50	0.10	0.10	0.03	-0.41	0.38
PI(17:0/20:2)-H	0.10	0.05	0.20	0.35	-0.60	0.25

PI(19:1/18:2)-H	0.05	0.05	0.05	0.86	-0.44	-0.42
PI(17:0/20:3)-H	0.35	0.35	0.35	0.23	0.16	-0.40
PI(17:1/20:4)-H	0.35	0.05	0.05	-0.06	1.46	-1.40
PI(18:0/20:0)-H	0.35	0.05	0.35	0.39	-0.34	-0.05
PI(18:0/20:1)-H	0.20	0.05	0.05	-0.41	-0.47	0.89
PI(18:0p/20:1)-H	1.00	0.05	0.05	NaN	#NAME?	Inf
PI(18:0/20:4)-H	0.05	0.05	0.05	-0.22	0.82	-0.60
PI(18:0/20:5)-H	0.20	0.05	0.05	0.09	0.58	-0.66
PI(19:1/20:1)-H	0.05	0.05	0.05	#NAME?	-0.92	Inf
PI(19:1/20:2)-H	0.35	0.05	0.05	-0.13	-0.31	0.44
PI(19:1/20:3)-H	0.35	0.20	0.20	0.14	0.21	-0.35
PI(19:0/20:4)-H	0.20	0.05	0.05	-0.11	0.86	-0.75
PI(18:0/22:1)-H	0.50	0.05	0.05	-0.06	-0.41	0.47
PI(18:0/22:3)-H	0.35	0.65	0.35	0.28	-0.01	-0.28
PI(20:0/20:4)-H	0.65	0.20	0.10	-0.07	0.40	-0.33
PI(18:0/24:1)-H	0.05	0.35	0.05	-1.20	-0.12	1.32
PI(18:1/24:2)-H	0.05	0.05	0.05	-0.30	-0.36	0.66
PI(22:4/20:4)-H	0.05	0.05	0.65	-0.77	0.75	0.02
PI(26:0/18:1)-H	0.05	0.05	0.05	-0.84	-0.37	1.22
PI(26:1/18:1)-H	0.05	0.05	0.05	-0.66	-0.77	1.43
PG(12:0/14:0)-H	0.20	0.05	0.05	0.07	0.35	-0.41
PG(15:0/14:0)-H	0.05	0.05	1.00	#NAME?	Inf	NaN
PG(16:0/14:0)-H	0.05	0.05	0.05	-1.41	0.89	0.51
PG(16:1/14:0)-H	0.05	0.05	0.05	0.20	0.61	-0.80
PG(15:0/16:0)-H	0.05	0.05	1.00	#NAME?	Inf	NaN
PG(16:0/16:0)-H	0.35	0.05	0.05	0.10	0.77	-0.87
PG(16:0/16:1)-H	0.35	0.05	0.35	2.28	-2.44	0.16
PG(18:1/14:0)-H	0.35	0.05	0.05	-0.03	0.38	-0.36

PG(16:0/17:0)-H	0.05	0.05	1.00	#NAME?	Inf	NaN
PG(17:1/16:0)-H	0.05	0.35	0.05	0.76	-0.07	-0.69
PG(18:0/16:0)-H	0.65	0.05	0.10	-0.04	0.46	-0.43
PG(16:0/18:1)-H	0.05	0.05	0.05	-0.88	0.46	0.42
PG(16:1/18:1)-H	0.20	0.05	0.50	1.96	-1.95	0.00
PG(16:1/18:2)-H	0.20	0.50	0.35	0.53	-0.15	-0.39
PG(19:1/16:0)-H	0.35	0.05	0.05	0.06	0.52	-0.59
PG(17:1/18:0)-H	0.35	0.05	0.05	0.18	0.50	-0.68
PG(17:1/18:1)-H	0.35	0.05	0.05	0.11	0.69	-0.80
PG(18:0/18:1)-H	0.35	0.05	0.10	0.13	0.28	-0.41
PG(18:1/18:1)-H	0.35	0.05	0.50	0.59	-0.69	0.10
PG(18:1/18:2)-H	0.35	0.10	0.35	0.07	0.19	-0.26
PG(16:0/20:3)-H	0.50	0.05	0.05	0.12	Inf	#NAME?
PG(16:0/20:4)-H	0.35	0.05	0.05	-0.04	0.52	-0.48
PG(14:0/22:6)-H	0.25	0.05	0.50	0.83	-0.77	-0.07
PG(20:1/18:1)-H	0.35	0.05	0.35	0.43	-0.64	0.22
PG(18:1/20:2)-H	0.35	0.10	0.35	0.64	-0.26	-0.37
PG(16:0/22:4)-H	0.65	0.05	0.05	-0.05	Inf	#NAME?
PG(18:0/20:4)-H	0.10	0.05	0.05	-0.13	0.69	-0.56
PG(18:1/20:4)-H	0.10	0.05	0.05	-0.18	0.82	-0.63
PG(18:1/20:5)-H	0.05	0.05	0.05	0.50	1.00	-1.51
PG(16:0/22:6)-H	0.20	0.35	0.50	0.48	-0.20	-0.28
PG(16:1/22:6)-H	0.20	0.80	0.10	0.76	-0.07	-0.69
PG(20:2/20:2)-H	0.35	0.05	0.05	0.50	0.66	-1.16
PG(18:1/22:4)-H	0.35	0.05	0.05	0.10	1.50	-1.60
PG(18:0/22:6)-H	0.20	0.05	0.20	-0.27	0.88	-0.61
PG(18:1/22:6)-H	0.35	0.65	0.20	0.54	-0.03	-0.51
PG(18:2/22:6)-H	0.05	0.05	0.05	0.41	0.84	-1.25

PG(20:4/22:6)-H	0.05	0.05	0.05	0.34	1.21	-1.55
PG(20:5/22:6)-H	0.05	0.05	0.05	0.62	1.39	-2.01
PG(20:2/22:6)-H	0.05	0.05	0.05	0.43	0.68	-1.11
PG(20:3/22:6)-H	0.05	0.05	0.05	0.61	1.08	-1.68
PG(22:4/22:6)-H	0.20	0.05	0.05	0.18	1.28	-1.46
PG(22:5/22:6)-H	0.05	0.05	0.05	0.33	0.77	-1.10
PG(22:6/22:6)-H	0.35	0.05	0.05	0.20	0.77	-0.98
PS(12:0/14:0)-H	0.35	0.05	0.05	0.47	0.42	-0.89
PS(16:0/14:0)-H	0.50	0.20	0.35	0.28	0.21	-0.49
PS(16:0/14:1)-H	0.50	0.05	0.75	Inf	#NAME?	-1.31
PS(16:0/16:0)-H	0.35	0.05	0.35	0.02	0.42	-0.43
PS(16:1/16:1)-H	0.20	0.05	0.35	Inf	#NAME?	-0.87
PS(16:1/17:0)-H	0.65	0.05	0.05	-0.09	1.39	-1.30
PS(18:0/16:0)-H	0.35	0.05	0.05	-0.15	0.96	-0.81
PS(16:0e/18:1)-H	0.50	0.05	0.20	0.19	-0.40	0.21
PS(16:1/18:2)-H	0.05	0.05	0.50	0.75	-0.70	-0.05
PS(18:0/18:0)-H	0.35	0.05	0.05	0.22	0.84	-1.06
PS(18:0e/18:1)-H	0.50	0.05	0.80	0.96	-0.33	-0.63
PS(18:1/18:1)-H	0.35	0.10	0.10	-0.13	-0.18	0.31
PS(18:0/18:3)-H	0.35	0.05	0.05	0.85	0.72	-1.57
PS(16:0/20:3)-H	0.20	0.05	0.50	0.14	-0.16	0.01
PS(16:0/20:4)-H	0.80	0.05	0.50	0.03	0.23	-0.26
PS(16:1/20:3)-H	0.50	0.65	0.35	-0.07	0.03	0.04
PS(16:0/22:0)-H	0.50	0.05	0.05	0.13	0.89	-1.02
PS(18:1/20:2)-H	0.35	0.05	0.35	0.26	0.33	-0.59
PS(18:0/20:3)-H	0.10	0.10	0.05	0.54	0.27	-0.82
PS(18:1/20:3)-H	0.35	0.20	0.80	-0.05	0.17	-0.12
PS(18:0/20:4)-H	0.35	0.05	0.35	0.01	0.19	-0.20

PS(18:1/20:4)-H	0.50	0.50	0.65	-0.08	0.08	0.00
PS(20:3/18:2)-H	0.20	0.05	0.10	-0.10	0.33	-0.23
PS(19:0/20:3)-H	0.35	0.05	0.50	-0.15	0.35	-0.20
PS(17:0/22:4)-H	0.35	0.05	0.35	-0.29	0.63	-0.34
PS(17:0/22:5)-H	0.35	0.05	0.35	-0.18	0.39	-0.21
PS(16:0/24:0)-H	0.20	0.05	0.50	-0.23	0.74	-0.51
PS(20:2/20:2)-H	0.35	0.20	0.35	-0.18	0.13	0.05
PS(18:1/22:4)-H	0.35	0.05	0.20	-0.09	-0.37	0.46
PS(18:0/22:5)-H	0.05	0.05	0.35	-0.48	1.01	-0.53
PS(18:1/22:5)-H	0.35	0.05	0.05	-0.07	-0.62	0.69
PS(20:3/20:3)-H	0.35	0.05	0.35	0.23	0.44	-0.66
PS(20:0/22:5)-H	0.35	0.10	0.10	-0.21	-0.18	0.40
PS(25:0/18:1)-H	0.65	0.05	0.35	0.21	-0.48	0.27
PS(25:1/18:1)-H	0.80	0.20	0.80	0.23	-0.11	-0.12
PS(26:0/18:1)-H	0.80	0.05	0.05	0.10	-0.79	0.69
PS(24:0/20:4)-H	0.50	0.20	0.80	0.25	-0.22	-0.03
PS(24:1/20:4)-H	0.65	0.35	0.80	0.18	-0.17	-0.01
PS(27:1/18:1)-H	0.35	0.10	0.20	-0.12	-0.25	0.37
PS(28:0/18:1)-H	1.00	0.05	0.05	NaN	#NAME?	Inf
PS(28:1/18:1)-H	0.35	0.05	0.05	-0.15	-0.48	0.63
PS(24:0/22:5)-H	0.05	0.20	0.05	-0.60	-0.21	0.81
PS(30:1/18:1)-H	0.60	0.05	0.05	0.12	-1.25	1.13
SM(d30:0)+H	0.05	0.20	0.10	-0.21	0.09	0.12
SM(d30:1)+H	0.10	0.50	0.10	0.48	-0.09	-0.39
SM(d31:1)+H	0.05	0.35	0.20	0.75	-0.22	-0.53
SM(d32:0)+H	0.65	0.50	0.50	-0.05	-0.11	0.16
SM(d32:1)+H	0.10	0.35	0.10	0.49	0.06	-0.55
SM(d32:2)+H	0.05	0.20	0.05	0.61	0.15	-0.76

SM(d33:1)+H	0.20	0.35	0.10	0.28	0.07	-0.34
SM(d33:2)+H	0.10	0.05	0.05	0.19	0.42	-0.61
SM(d33:5)+H	0.05	0.05	0.05	0.19	0.33	-0.52
SM(d34:0)+H	0.05	0.35	0.05	-0.40	0.00	0.40
SM(d18:1/16:0)+H	0.35	0.05	0.05	0.14	0.20	-0.34
SM(d18:1/16:1)+H	0.05	0.35	0.10	0.38	0.11	-0.48
SM(d18:2/16:1)+H	0.05	0.05	0.35	-0.21	0.23	-0.02
SM(d34:4)+H	0.10	0.20	0.10	0.47	0.07	-0.53
SM(d35:1)+H	0.20	0.05	0.05	0.07	0.76	-0.83
SM(d35:2)+H	0.05	0.05	0.05	0.24	0.70	-0.94
SM(d35:4)+H	0.10	0.05	0.05	0.18	0.20	-0.38
SM(d36:0)+H	0.05	0.05	0.35	-0.92	0.81	0.11
SM(d36:1)+H	0.05	0.05	0.05	-0.37	1.27	-0.90
SM(d36:2)+H	0.05	0.05	0.05	-0.24	1.14	-0.90
SM(d18:2/18:1)+H	0.05	0.05	0.10	-0.33	0.18	0.14
SM(d18:1/18:3)+H	0.05	0.05	0.05	0.15	0.41	-0.56
SM(d36:5)+H	0.10	0.05	0.05	0.32	0.21	-0.53
SM(d18:1/19:0)+H	0.05	1.00	0.05	Inf	NaN	#NAME?
SM(d37:4)+H	0.35	0.05	0.05	0.06	1.02	-1.08
SM(d37:5)+H	0.20	0.05	0.05	0.15	0.93	-1.08
SM(d37:6)+H	0.05	0.05	0.05	0.39	0.66	-1.05
SM(d38:0)+H	0.05	0.05	0.80	-0.83	0.81	0.02
SM(d38:1)+H	0.05	0.05	0.05	-0.41	0.96	-0.55
SM(d38:2)+H	0.05	0.05	0.05	-0.36	1.13	-0.77
SM(d38:3)+H	0.05	0.05	0.35	-0.93	1.02	-0.08
SM(d18:1/21:0)+H	0.05	0.05	0.10	1.54	-0.72	-0.83
SM(d39:1)+H	0.10	0.05	0.05	-0.15	0.85	-0.70
SM(d39:4)+H	0.05	0.05	0.05	#NAME?	-0.70	Inf

SM(d40:0)+H	0.05	0.05	0.05	-0.78	0.24	0.54
SM(d40:1)+H	0.05	0.05	0.50	-0.61	0.54	0.07
SM(d18:1/22:0)+H	0.05	0.05	0.10	-0.23	0.47	-0.24
SM(d40:2)+H	0.05	0.05	0.05	-0.26	0.78	-0.52
SM(d40:4)+H	0.05	0.05	0.05	-0.49	1.74	-1.25
SM(d40:6)+H	0.35	0.05	0.05	0.10	-0.57	0.47
SM(d18:0/23:0)+H	0.05	0.05	0.35	0.35	-0.30	-0.05
SM(d41:0)+H	0.05	0.35	0.05	-0.60	0.04	0.56
SM(d18:1/23:0)+H	0.05	0.35	0.05	0.93	-0.01	-0.92
SM(d41:1)+H	0.05	0.05	0.05	-0.82	0.61	0.21
SM(d41:1)+H	0.35	0.10	0.10	0.05	0.18	-0.22
SM(d41:2)+H	0.65	0.05	0.10	-0.04	0.48	-0.44
SM(d41:3)+H	0.35	0.05	0.05	-0.09	1.08	-0.99
SM(d42:0)+H	0.05	0.05	0.05	-0.50	-0.54	1.04
SM(d42:1)+H	0.05	0.10	0.05	-0.68	-0.21	0.90
SM(d18:1/24:0)+H	0.35	0.05	0.50	0.11	-0.28	0.17
SM(d18:1/24:1)+H	0.10	0.10	0.50	-0.19	0.22	-0.02
SM(d18:0/24:2)+H	0.05	0.05	0.20	0.99	-0.51	-0.49
SM(d18:1/24:2)+H	0.35	0.05	0.05	-0.07	0.65	-0.58
SM(d18:0/24:3)+H	0.05	0.05	0.10	-0.60	0.31	0.28
SM(d18:1/24:3)+H	0.05	0.05	0.05	-0.22	0.65	-0.43
SM(d42:5)+H	0.05	0.05	0.05	-1.46	3.41	-1.95
SM(d42:5)+H	0.05	0.05	0.05	-0.14	1.17	-1.03
SM(d42:6)+H	0.05	0.05	0.05	#NAME?	2.13	Inf
SM(d42:6)+H	0.05	0.05	0.20	-1.66	3.26	-1.60
SM(d42:7)+H	0.05	0.05	0.35	-1.39	1.64	-0.26
SM(d18:1/25:0)+H	0.05	0.05	0.05	0.55	0.79	-1.34
SM(d43:1)+H	0.20	0.05	0.35	0.30	-0.51	0.20

SM(d43:2)+H	0.35	0.20	0.35	0.04	0.10	-0.14
SM(d18:1/25:3)+H	0.05	0.05	0.20	-0.85	1.10	-0.26
SM(d43:4)+H	0.50	0.20	0.20	0.05	0.15	-0.20
SM(d43:5)+H	0.10	0.05	0.05	-0.09	0.76	-0.68
SM(d44:0)+H	0.05	0.05	0.05	-0.53	-0.80	1.33
SM(d44:1)+H	0.35	0.05	0.05	0.26	-0.84	0.59
SM(d44:2)+H	0.05	0.35	0.05	-1.08	0.11	0.97
SM(d18:1/26:1)+H	0.35	0.05	0.10	0.20	-0.52	0.31
SM(d44:3)+H	0.35	0.05	0.35	0.03	0.35	-0.38
SM(d18:2/26:1)+H	0.05	0.05	0.05	-0.74	-0.56	1.30
SM(d44:4)+H	0.05	0.05	0.20	-1.41	Inf	#NAME?
SM(d18:1/26:3)+H	0.35	0.50	0.50	0.05	-0.11	0.07
SM(d44:5)+H	0.05	0.05	0.05	-1.16	2.42	-1.26
SM(d18:1/26:4)+H	0.50	0.05	0.05	-0.03	0.38	-0.35
SM(d44:6)+H	0.20	0.05	0.05	0.16	0.74	-0.91
SM(d44:7)+H	0.05	0.05	0.05	-0.87	Inf	#NAME?
SM(d44:8)+H	0.05	0.05	1.00	#NAME?	Inf	NaN
SM(d18:1/27:0)+H	0.05	0.05	0.10	1.12	-0.43	-0.69
SM(d18:1/27:1)+H	0.05	0.65	0.05	0.70	0.03	-0.72
SM(d45:6)+H	0.05	0.35	0.05	0.70	-0.03	-0.67
SM(d18:1/28:0)+H	0.05	0.10	0.05	0.65	0.21	-0.85
SM(d46:3)+H	1.00	0.05	0.05	NaN	#NAME?	Inf
SM(d46:4)+H	0.35	0.05	0.05	0.42	-0.81	0.39
SM(d46:5)+H	0.35	0.05	0.10	0.15	-0.48	0.33
SM(d46:6)+H	0.80	0.05	0.10	-0.06	0.57	-0.52
SM(d46:7)+H	0.05	0.05	0.05	-0.35	Inf	#NAME?
SM(d18:1/30:0)+H	0.05	0.05	0.20	0.82	-0.37	-0.45
SM(d48:1)+H	0.35	0.05	0.10	-0.08	0.46	-0.38

SM(d48:2)+H	0.05	0.05	0.05	0.88	0.74	-1.62
SM(d18:1/30:1)+H	0.05	0.35	0.05	0.66	-0.06	-0.60
SM(d17:0/32:1)+H	0.05	0.05	0.20	0.80	-0.40	-0.39
SM(d17:0/32:2)+H	0.05	0.35	0.10	0.67	-0.12	-0.55
SM(d18:1/32:0)+H	0.05	0.05	0.35	1.08	-0.64	-0.45
SM(d50:1)+H	0.05	0.05	0.05	0.32	0.48	-0.79
SM(d50:2)+H	0.05	0.50	0.05	0.74	-0.04	-0.70
SM(d18:1/32:1)+H	0.05	0.05	0.35	0.84	-0.46	-0.38
SM(d56:2)+H	0.05	0.50	0.05	0.63	-0.03	-0.60
SM(d56:3)+H	0.05	0.20	0.05	0.66	-0.19	-0.46
SM(d56:4)+H	0.05	0.20	0.05	0.74	-0.12	-0.62
TG(8:0/8:0/8:0)+NH4	0.05	0.05	0.05	0.43	0.29	-0.72
TG(8:0/8:0/10:0)+NH4	0.10	0.10	0.05	0.44	0.29	-0.73
TG(8:0/10:0/10:0)+NH4	0.20	0.20	0.05	0.52	0.27	-0.79
TG(8:0/12:0/14:0)+NH4	0.05	0.05	0.05	0.44	0.31	-0.75
TG(10:0/12:0/14:0)+NH4	0.05	0.05	0.05	0.41	0.30	-0.71
TG(4:0/16:0/16:0)+NH4	0.05	0.05	0.05	0.30	0.30	-0.60
TG(12:0/12:0/14:0)+NH4	0.05	0.05	0.05	0.38	0.29	-0.67
TG(12:0/14:0/14:0)+NH4	0.05	0.05	0.05	0.28	0.30	-0.59
TG(16:1/12:0/12:0)+NH4	0.20	0.20	0.50	-0.45	0.33	0.12
TG(16:0/12:0/14:0)+NH4	0.05	0.05	0.05	0.24	0.30	-0.54
TG(14:0e/14:0/14:0)+NH4	0.05	0.05	0.10	-0.45	0.30	0.15
TG(16:0/10:3/16:0)+NH4	0.05	0.05	0.05	0.33	0.30	-0.63
TG(16:0/13:0/14:0)+NH4	0.50	0.20	0.10	0.01	0.28	-0.29
TG(15:0/13:0/16:0)+NH4	0.20	0.05	0.05	0.12	0.29	-0.42
TG(16:0/14:0/14:0)+NH4	0.50	0.05	0.10	0.00	0.29	-0.29
TG(12:0e/16:0/16:0)+NH4	0.05	0.05	0.05	-0.19	0.30	-0.11
TG(16:1/14:0/14:0)+NH4	0.50	0.20	0.35	-0.06	0.32	-0.26

TG(15:0/14:0/16:0)+NH4	0.35	0.20	0.20	-0.07	0.28	-0.21
TG(15:0/14:0/16:1)+NH4	0.35	0.20	0.65	-0.26	0.32	-0.06
TG(12:0e/16:0/17:1)+NH4	0.05	0.05	0.05	-0.48	0.30	0.18
TG(16:0/14:0/16:0)+NH4	0.05	0.20	0.05	0.33	0.29	-0.62
TG(16:0e/14:0/16:0)+NH4	0.05	0.05	0.10	-0.18	0.30	-0.12
TG(14:0p/16:0/16:0)+NH4	0.05	0.05	0.35	-0.32	0.30	0.02
TG(16:0/14:0/16:1)+NH4	0.50	0.10	0.10	0.03	0.29	-0.32
TG(16:1/14:0/16:1)+NH4	0.20	0.35	0.10	0.26	0.26	-0.52
TG(12:0p/16:1/18:1)+NH4	0.20	1.00	0.20	Inf	NaN	#NAME?
TG(15:0/16:0/16:0)+NH4	0.05	0.05	0.50	-0.29	0.29	0.01
TG(15:0/16:0/16:1)+NH4	0.20	0.10	0.20	-0.14	0.29	-0.15
TG(16:1/14:0/17:1)+NH4	0.50	0.20	0.10	-0.02	0.27	-0.26
TG(16:0/16:0/16:0)+NH4	0.10	0.10	0.05	0.26	0.29	-0.55
TG(16:0e/16:0/16:0)+NH4	0.05	0.05	0.35	-0.25	0.30	-0.05
TG(16:0p/16:0/16:0)+NH4	0.50	0.05	0.35	-0.14	0.31	-0.17
TG(16:0/16:0/16:1)+NH4	0.35	0.05	0.10	0.17	0.29	-0.46
TG(20:1p/14:0/14:0)+NH4	0.05	0.05	0.35	-0.30	0.30	-0.01
TG(16:1/14:0/18:1)+NH4	0.35	0.05	0.10	0.14	0.29	-0.43
TG(12:0p/18:1/18:1)+NH4	0.35	0.25	0.50	-0.31	0.31	0.00
TG(16:1/16:1/16:1)+NH4	0.20	0.10	0.10	0.23	0.29	-0.51
TG(16:0/16:0/17:0)+NH4	0.10	0.05	0.05	0.15	0.29	-0.44
TG(15:0/16:0/18:1)+NH4	0.50	0.05	0.10	0.05	0.29	-0.34
TG(15:0/16:1/18:1)+NH4	0.50	0.10	0.10	0.01	0.29	-0.29
TG(16:1/16:1/17:1)+NH4	0.50	0.10	0.10	0.07	0.29	-0.35
TG(18:0/16:0/16:0)+NH4	0.20	0.20	0.05	0.22	0.30	-0.52
TG(18:0e/16:0/16:0)+NH4	0.05	0.05	0.65	-0.39	0.30	0.08
TG(16:0/16:0/18:1)+NH4	0.35	0.05	0.05	0.23	0.30	-0.53
TG(16:0e/16:0/18:1)+NH4	0.05	0.05	0.35	-0.28	0.31	-0.02

TG(18:0p/16:0/16:1)+NH4	0.10	0.05	0.35	-0.18	0.30	-0.12
TG(16:0/16:1/18:1)+NH4	0.35	0.05	0.05	0.29	0.30	-0.59
TG(16:1/16:1/18:1)+NH4	0.35	0.05	0.05	0.34	0.30	-0.64
TG(18:0/16:0/17:0)+NH4	0.20	0.05	0.05	0.13	0.30	-0.43
TG(16:0/17:0/18:1)+NH4	0.35	0.05	0.05	0.16	0.29	-0.45
TG(20:1p/15:0/16:0)+NH4	0.05	0.05	0.35	-0.25	0.30	-0.05
TG(16:0/17:1/18:1)+NH4	0.35	0.05	0.05	0.21	0.30	-0.51
TG(16:1/17:1/18:1)+NH4	0.35	0.05	0.10	0.21	0.29	-0.50
TG(20:0/16:0/16:0)+NH4	0.05	0.05	0.05	0.30	0.29	-0.59
TG(18:0/16:0/18:0)+NH4	0.20	0.05	0.35	-0.18	0.31	-0.13
TG(18:0e/16:0/18:0)+NH4	0.05	0.05	0.20	-0.48	0.30	0.18
TG(18:0/16:0/18:1)+NH4	0.35	0.05	0.05	0.11	0.31	-0.42
TG(18:0e/16:0/18:1)+NH4	0.05	0.05	0.50	-0.40	0.31	0.10
TG(16:0/18:1/18:1)+NH4	0.35	0.05	0.05	0.21	0.30	-0.50
TG(16:0e/18:1/18:1)+NH4	0.10	0.05	0.35	-0.26	0.31	-0.05
TG(20:0p/16:1/16:1)+NH4	0.05	0.05	0.35	-0.22	0.31	-0.09
TG(16:1/18:1/18:1)+NH4	0.35	0.05	0.10	0.31	0.30	-0.61
TG(16:1/18:1/18:2)+NH4	0.35	0.05	0.05	0.22	0.30	-0.52
TG(16:0/16:0/20:4)+NH4	0.20	0.05	0.05	0.08	0.30	-0.38
TG(16:1/16:1/20:3)+NH4	0.05	0.05	0.05	0.39	0.30	-0.69
TG(16:0/14:0/22:6)+NH4	0.10	0.05	0.05	0.53	0.31	-0.84
TG(19:1/16:0/18:0)+NH4	0.35	0.05	0.10	0.05	0.30	-0.35
TG(19:1/16:0/18:1)+NH4	0.35	0.05	0.05	0.20	0.30	-0.50
TG(18:1/17:1/18:1)+NH4	0.35	0.05	0.05	0.26	0.30	-0.56
TG(18:1/17:1/18:2)+NH4	0.20	0.05	0.05	0.29	0.30	-0.59
TG(15:0/18:1/20:5)+NH4	0.05	0.05	0.05	0.41	0.29	-0.70
TG(18:0/18:0/18:0)+NH4	0.50	0.05	0.10	0.00	0.30	-0.30
TG(20:0e/16:0/18:0)+NH4	0.65	0.05	0.35	-0.06	0.30	-0.25

TG(20:0/16:0/18:1)+NH4	0.05	0.05	0.05	0.36	0.29	-0.65
TG(18:0/18:0/18:1)+NH4	0.65	0.05	0.35	-0.07	0.30	-0.23
TG(20:0e/16:0/18:1)+NH4	0.05	0.05	0.35	-0.30	0.30	-0.01
TG(18:0/18:1/18:1)+NH4	0.35	0.05	0.05	0.22	0.30	-0.52
TG(16:0e/18:1/20:1)+NH4	0.05	0.05	0.80	-0.32	0.31	0.01
TG(18:1/18:1/18:1)+NH4	0.35	0.05	0.10	0.16	0.29	-0.45
TG(16:0e/18:1/20:2)+NH4	0.35	0.05	0.35	-0.17	0.31	-0.14
TG(18:1/18:1/18:2)+NH4	0.35	0.05	0.05	0.15	0.30	-0.44
TG(18:1/18:2/18:2)+NH4	0.35	0.05	0.20	-0.10	0.30	-0.20
TG(18:1/18:1/18:3)+NH4	0.10	0.05	0.05	0.19	0.31	-0.50
TG(18:2/18:2/18:2)+NH4	0.50	0.05	0.05	0.08	0.30	-0.39
TG(16:0/16:0/22:6)+NH4	0.05	0.05	0.05	0.46	0.31	-0.77
TG(16:0/16:1/22:6)+NH4	0.05	0.05	0.05	0.56	0.31	-0.87
TG(15:0/16:0/24:0)+NH4	0.35	0.10	0.05	0.07	0.28	-0.35
TG(16:0/16:0/23:1)+NH4	0.50	0.10	0.10	0.00	0.29	-0.29
TG(19:1/18:0/18:1)+NH4	0.05	0.05	0.05	0.22	0.30	-0.52
TG(19:1/18:1/18:1)+NH4	0.35	0.05	0.05	0.27	0.31	-0.58
TG(19:1/18:1/18:2)+NH4	0.10	0.05	0.05	0.33	0.30	-0.63
TG(18:1/17:1/20:3)+NH4	0.05	0.05	0.05	0.31	0.30	-0.62
TG(16:0/16:0/24:0)+NH4	0.50	0.20	0.05	0.11	0.28	-0.39
TG(16:0e/16:0/24:0)+NH4	0.35	0.05	0.35	0.26	0.30	-0.56
TG(16:0/16:0/24:1)+NH4	0.65	0.05	0.35	-0.04	0.29	-0.25
TG(18:0e/16:0/22:1)+NH4	0.35	0.05	0.35	0.07	0.31	-0.38
TG(18:0/18:1/20:1)+NH4	0.35	0.05	0.20	0.07	0.30	-0.37
TG(20:0e/18:1/18:1)+NH4	0.50	0.05	0.35	-0.12	0.30	-0.18
TG(20:1/18:1/18:1)+NH4	0.35	0.05	0.05	0.27	0.30	-0.57
TG(16:0e/18:1/22:2)+NH4	0.50	0.05	0.35	-0.05	0.31	-0.26
TG(18:1/18:1/20:2)+NH4	0.10	0.05	0.05	0.36	0.30	-0.66

TG(18:1/18:1/20:3)+NH4	0.05	0.05	0.05	0.30	0.30	-0.61
TG(16:0e/18:1/22:4)+NH4	0.05	0.05	0.05	0.17	0.30	-0.48
TG(18:1/18:1/20:4)+NH4	0.20	0.05	0.05	0.14	0.31	-0.45
TG(18:0/16:0/22:6)+NH4	0.35	0.05	0.05	0.25	0.31	-0.56
TG(16:0/18:1/22:6)+NH4	0.05	0.05	0.05	0.47	0.31	-0.78
TG(16:1/18:1/22:6)+NH4	0.05	0.05	0.05	0.59	0.31	-0.90
TG(25:0/16:0/16:0)+NH4	0.20	0.10	0.05	0.14	0.28	-0.43
TG(25:0/16:0/16:1)+NH4	0.50	0.20	0.10	-0.01	0.28	-0.27
TG(25:1/16:0/16:1)+NH4	0.10	0.05	0.05	0.12	0.29	-0.41
TG(18:1/18:1/21:1)+NH4	0.05	0.05	0.05	0.26	0.29	-0.55
TG(18:1/18:2/21:1)+NH4	0.05	0.05	0.05	0.32	0.30	-0.62
TG(26:0/16:0/16:0)+NH4	0.35	0.20	0.05	0.11	0.28	-0.39
TG(26:1/16:0/16:0)+NH4	0.35	0.05	0.10	0.09	0.29	-0.38
TG(18:0e/16:0/24:1)+NH4	0.35	0.05	0.35	0.28	0.30	-0.58
TG(18:0p/16:0/24:1)+NH4	0.35	0.05	0.35	0.21	0.31	-0.51
TG(16:0/18:1/24:1)+NH4	0.20	0.05	0.05	0.13	0.30	-0.42
TG(18:0p/18:1/22:1)+NH4	0.65	0.05	0.35	-0.01	0.31	-0.29
TG(16:1/18:1/24:1)+NH4	0.35	0.05	0.10	0.20	0.30	-0.50
TG(18:1/18:1/22:2)+NH4	0.10	0.05	0.05	0.33	0.31	-0.64
TG(18:1/18:1/22:3)+NH4	0.05	0.05	0.05	0.49	0.30	-0.80
TG(18:1/18:1/22:4)+NH4	0.05	0.05	0.05	0.22	0.30	-0.53
TG(18:1/18:1/22:5)+NH4	0.05	0.05	0.05	0.33	0.31	-0.64
TG(18:1/18:1/22:6)+NH4	0.05	0.05	0.05	0.46	0.30	-0.76
TG(18:1/20:4/20:4)+NH4	0.05	0.05	0.05	0.51	0.31	-0.82
TG(27:0/16:0/16:0)+NH4	0.10	0.05	0.05	0.20	0.29	-0.49
TG(27:1/16:0/16:0)+NH4	0.65	0.20	0.20	-0.04	0.27	-0.23
TG(25:1/16:0/18:1)+NH4	0.10	0.20	0.05	0.17	0.28	-0.45
TG(25:1/16:1/18:1)+NH4	0.05	0.10	0.05	0.37	0.29	-0.66

TG(26:1/16:0/18:0)+NH4	0.35	0.05	0.10	0.19	0.29	-0.48
TG(26:1/16:0/18:1)+NH4	0.35	0.10	0.10	0.27	0.28	-0.55
TG(18:1/18:1/24:1)+NH4	0.05	0.05	0.05	0.27	0.29	-0.57
TG(26:1/16:1/18:1)+NH4	0.20	0.05	0.05	0.16	0.30	-0.45
TG(18:1/18:1/24:2)+NH4	0.10	0.05	0.05	0.28	0.31	-0.59
TG(20:0/18:1/22:6)+NH4	0.05	0.05	0.05	0.30	0.30	-0.60
TG(27:1/16:0/18:1)+NH4	0.10	0.20	0.10	0.22	0.27	-0.50
TG(25:1/18:1/18:1)+NH4	0.35	0.05	0.20	0.30	0.29	-0.59
TG(28:0/16:0/18:0)+NH4	0.50	0.35	0.50	-0.20	0.27	-0.07
TG(28:0/16:0/18:1)+NH4	0.35	0.05	0.35	0.13	0.29	-0.42
TG(28:1/16:0/18:1)+NH4	0.35	0.05	0.10	0.30	0.30	-0.60
TG(26:1/18:1/18:1)+NH4	0.35	0.05	0.10	0.42	0.30	-0.71
TG(26:1/18:1/18:2)+NH4	0.35	0.05	0.05	0.48	0.30	-0.78
TG(18:1/20:4/24:0)+NH4	0.20	0.05	0.05	0.40	0.30	-0.70
TG(29:0/16:0/18:1)+NH4	0.35	0.05	0.35	0.23	0.31	-0.54
TG(29:1/16:0/18:1)+NH4	0.35	0.20	0.35	-0.24	0.32	-0.08
TG(27:1/18:1/18:1)+NH4	0.35	0.05	0.05	0.49	0.30	-0.79
TG(30:0/16:0/18:1)+NH4	0.20	0.20	0.35	-0.22	0.27	-0.06
TG(30:1/16:0/18:1)+NH4	0.50	0.20	0.10	0.13	0.28	-0.41
TG(28:1/18:1/18:1)+NH4	0.35	0.10	0.10	0.28	0.29	-0.57
TG(26:1/18:1/20:2)+NH4	0.35	0.05	0.35	0.23	0.31	-0.54
TG(29:1/18:0/18:1)+NH4	0.35	0.10	0.35	0.32	0.32	-0.64
TG(29:1/18:1/18:1)+NH4	0.05	0.20	0.05	#NAME?	0.26	Inf
TG(30:0/18:0/18:1)+NH4	0.05	0.20	0.05	#NAME?	0.29	Inf
TG(30:0/18:1/18:1)+NH4	0.35	0.10	0.10	0.03	0.28	-0.31
TG(30:1/18:1/18:1)+NH4	0.50	0.20	0.10	0.04	0.28	-0.31
TG(28:1/18:1/20:2)+NH4	0.05	0.20	0.05	#NAME?	0.28	Inf
TG(26:0/18:1/24:0)+NH4	0.05	0.05	0.05	#NAME?	0.30	Inf

TG(26:1/18:1/24:0)+NH4	0.05	0.10	0.05	#NAME?	0.28	Inf
TG(26:1/18:1/24:1)+NH4	1.00	1.00	1.00	NaN	NaN	NaN
TG(26:1/18:1/24:2)+NH4	1.00	1.00	1.00	NaN	NaN	NaN
TG(28:0/18:1/24:1)+NH4	1.00	1.00	1.00	NaN	NaN	NaN
TG(28:1/18:1/24:1)+NH4	1.00	1.00	1.00	NaN	NaN	NaN
TG(28:1/22:1/22:1)+NH4	1.00	1.00	1.00	NaN	NaN	NaN
PA(16:1/18:1)-H	0.05	0.05	0.35	Inf	#NAME?	-0.44
PA(18:0/18:1)-H	0.20	0.50	0.20	0.32	-0.09	-0.23
PA(26:0/18:1)-H	1.00	0.05	0.05	NaN	#NAME?	Inf
PA(24:0/23:0)-H	0.35	0.05	0.20	0.14	-0.32	0.17
PA(24:1/23:0)-H	0.05	0.50	0.05	0.67	-0.03	-0.64
PA(24:1/23:1)-H	0.05	0.05	0.05	0.52	0.48	-1.00
MG(30:0)+H	0.05	0.05	0.05	#NAME?	-0.91	Inf
MG(32:0)+H	0.10	0.05	0.05	-0.23	-0.81	1.04
MG(32:1)+H	0.35	0.05	0.05	0.38	-1.09	0.71
MG(34:0)+H	0.05	0.05	0.05	-0.62	-0.53	1.15
MG(36:0)+H	0.05	0.05	0.05	-0.46	-0.75	1.20
MG(36:1)+H	0.50	0.05	0.05	0.00	-1.08	1.07
MG(38:1)+H	0.35	0.05	0.05	-0.02	-1.05	1.07

Table of 143B lipidome after U73122 (PLC inhibitor) treatment

Table 17: Ceramides in treated 143B cells

Lipid Ion	Ceramides		
Cer(d18:1/10:0)+H	0.000	±	0.000
Cer(d18:0/12:0)+H	0.001	±	0.000
Cer(d18:0/14:0)+H	0.004	±	0.001

Cer(d18:1/14:0)+H	0.007	±	0.000
Cer(d17:1/16:0)+H	0.002	±	0.000
Cer(d18:0/16:0)+H	0.004	±	0.001
Cer(d18:1/16:0)+H	0.073	±	0.006
Cer(d18:2/16:0)+H	0.005	±	0.000
Cer(d18:0/17:0)+H	0.001	±	0.000
Cer(d18:0/18:0)+H	0.006	±	0.002
Cer(d18:1/18:0)+H	0.007	±	0.001
Cer(d18:0/20:0)+H	0.004	±	0.001
Cer(d18:1/20:0)+H	0.002	±	0.000
Cer(d18:0/21:0)+H	0.000	±	0.000
Cer(d18:0/22:0)+H	0.035	±	0.011
Cer(d18:0/22:1)+H	0.003	±	0.001
Cer(d18:1/22:0)+H	0.024	±	0.003
Cer(d18:2/22:0)+H	0.003	±	0.000
Cer(d18:0/23:0)+H	0.005	±	0.001
Cer(d18:1/23:0)+H	0.007	±	0.001
Cer(d18:2/23:0)+H	0.003	±	0.000
Cer(d18:0/24:0)+H	0.093	±	0.033
Cer(d18:0/24:1)+H	0.071	±	0.022
Cer(d18:1/24:0)+H	0.096	±	0.012
Cer(d18:1/24:1)+H	0.088	±	0.011
Cer(d18:1/24:2)+H	0.012	±	0.001
Cer(d18:0/25:0)+H	0.003	±	0.001
Cer(d18:0/25:1)+H	0.003	±	0.001
Cer(d18:1/25:0)+H	0.005	±	0.001
Cer(d18:1/25:1)+H	0.003	±	0.001
Cer(d18:2/25:1)+H	0.001	±	0.000
Cer(d18:1/25:2)+H	0.001	±	0.000
Cer(d18:0/26:0)+H	0.027	±	0.011
Cer(d18:0/26:1)+H	0.020	±	0.007

Cer(d18:1/26:0)+H	0.028	±	0.006
Cer(d18:1/26:1)+H	0.025	±	0.004
Cer(d18:2/26:1)+H	0.004	±	0.001
Cer(d18:0/27:1)+H	0.000	±	0.000
Cer(d18:0/28:0)+H	0.001	±	0.000
Cer(d18:0/28:1)+H	0.001	±	0.000
Cer(d18:1/28:0)+H	0.001	±	0.000
Cer(d18:1/28:1)+H	0.001	±	0.000
CerG1(d18:0/14:0)+H	0.001	±	0.000
CerG1(d18:1/14:0)+H	0.007	±	0.001
CerG1(d17:1/16:0)+H	0.002	±	0.000
CerG1(d18:0/16:0)+H	0.029	±	0.005
CerG1(d18:1/16:0)+H	0.184	±	0.017
CerG1(d18:2/16:0)+H	0.005	±	0.001
CerG1(d34:2)+H	0.001	±	0.000
CerG1(d18:1/17:0)+H	0.001	±	0.000
CerG1(d18:1/18:0)+H	0.007	±	0.001
CerG1(d18:0/22:0)+H	0.012	±	0.004
CerG1(d18:1/22:0)+H	0.025	±	0.004
CerG1(d18:0/23:0)+H	0.001	±	0.000
CerG1(d18:1/23:0)+H	0.009	±	0.002
CerG1(d18:0/24:0)+H	0.017	±	0.004
CerG1(d18:0/24:1)+H	0.014	±	0.003
CerG1(d18:1/24:0)+H	0.161	±	0.029
CerG1(d18:1/24:1)+H	0.087	±	0.016
CerG1(d18:2/24:1)+H	0.007	±	0.002
CerG1(d18:0/25:0)+H	0.000	±	0.000
CerG1(d18:1/25:0)+H	0.001	±	0.000
CerG1(d43:2)+H	0.002	±	0.000
CerG1(d18:0/26:0)+H	0.002	±	0.001
CerG1(d18:0/26:1)+H	0.002	±	0.001

CerG1(d18:1/26:0)+H	0.016	±	0.003
CerG1(d18:1/26:1)+H	0.014	±	0.003
CerG2(d18:1/14:0)+H	0.001	±	0.000
CerG2(d18:1/16:0)+H	0.011	±	0.001
CerG2(d34:2)+H	0.003	±	0.000
CerG2(d18:1/22:0)+H	0.003	±	0.001
CerG2(d18:0/24:1)+H	0.001	±	0.000
CerG2(d18:1/24:0)+H	0.011	±	0.002
CerG2(d18:1/24:1)+H	0.009	±	0.002
CerG2(d18:2/24:0)+H	0.002	±	0.000
CerG2(d18:1/26:0)+H	0.001	±	0.000
CerG2(d18:1/26:1)+H	0.001	±	0.000
CerG3(d18:1/16:0)+H	0.001	±	0.000
CerG3(d18:1/24:0)+H	0.001	±	0.000
Cer(d18:1/12:0)+H	1.332	±	0.235

Table 18: Cholesteryl Esters in treated 143B cells

Lipid Ion	Cholesteryl Esters		
ChE(18:1)+NH4	0.024502	±	0.001227
ChE(18:2)+NH4	0.010048	±	0.000607
ChE(20:2)+NH4	0.003115	±	0.000556
ChE(20:3)+NH4	0.004809	±	0.000382
ChE(20:4)+NH4	0.03015	±	0.002917
ChE(20:5)+NH4	0.005493	±	0.000414
ChE(22:3)+NH4	0.004706	±	0.000582
ChE(22:4)+NH4	0.015999	±	0.001584
ChE(22:5)+NH4	0.057184	±	0.011906
ChE(22:6)+NH4	0.124234	±	0.016162
ChE(24:0)+NH4	0.001126	±	8.53E-05
ChE(24:1)+NH4	0.009209	±	0.000684

ChE(24:2)+NH4	0.004459	±	0.000549
ChE(24:3)+NH4	0.006157	±	0.000763
ChE(24:4)+NH4	0.015306	±	0.002121
ChE(24:5)+NH4	0.021138	±	0.004692
ChE(24:6)+NH4	0.017383	±	0.003211
ChE(26:0)+NH4	0.010886	±	0.000898
ChE(26:1)+NH4	0.03936	±	0.002653
ChE(26:2)+NH4	0.022062	±	0.001273
ChE(26:3)+NH4	0.008532	±	0.000586
ChE(26:4)+NH4	0.01503	±	0.001988
ChE(26:5)+NH4	0.020798	±	0.002724
ChE(26:6)+NH4	0.020606	±	0.003958
ChE(28:0)+NH4	0.001121	±	0.000182
ChE(28:1)+NH4	0.014791	±	0.001597
ChE(28:2)+NH4	0.007167	±	0.000704
ChE(28:3)+NH4	0.002882	±	0.000223
ChE(28:5)+NH4	0.00634	±	0.000857
ChE(28:6)+NH4	0.00549	±	0.000346
ChE(30:1)+NH4	0.005637	±	0.000733
ChE(30:2)+NH4	0.003917	±	0.000442
ChE(30:3)+NH4	0.002172	±	0.000103
ChE(30:4)+NH4	0.002169	±	0.00023
ChE(30:5)+NH4	0.004719	±	0.00051
ChE(30:6)+NH4	0.007527	±	0.000775
ChE(32:1)+NH4	0.001241	±	0.000292
ChE(32:2)+NH4	0.001804	±	0.00027
ChE(32:3)+NH4	0.000978	±	0.000163
ChE(32:4)+NH4	0.001769	±	6.66E-05
ChE(32:5)+NH4	0.005715	±	0.000449
ChE(32:6)+NH4	0.008476	±	0.000995
ChE(34:6)+NH4	0.003752	±	0.000597

Table 19: Cardiolipin in treated 143B cells

Lipid Ion	Cardiolipin
CL(14:0/14:0/14:0/20:1)-H	0.001 ± 0.000
CL(14:0/14:0/18:1/16:1)-H	0.002 ± 0.000
CL(16:1/16:1/16:1/14:0)-H	0.002 ± 0.000
CL(15:0/16:1/16:1/16:1)-H	0.000 ± 0.000
CL(14:0/16:0/18:1/16:0)-H	0.001 ± 0.000
CL(14:0/16:0/16:1/18:1)-H	0.004 ± 0.001
CL(14:0/16:1/16:1/18:1)-H	0.010 ± 0.002
CL(16:1/16:1/16:1/16:1)-H	0.008 ± 0.002
CL(20:2/14:0/15:0/16:0)-H	0.000 ± 0.000
CL(17:1/14:0/18:1/16:1)-H	0.001 ± 0.000
CL(17:1/16:1/16:1/16:1)-H	0.001 ± 0.000
CL(18:1/16:0/16:0/16:0)-H	0.001 ± 0.000
CL(18:1/16:0/16:0/16:1)-H	0.008 ± 0.001
CL(14:0/18:1/16:1/18:1)-H	0.020 ± 0.004
CL(16:1/16:1/16:1/18:1)-H	0.037 ± 0.009
CL(18:2/16:1/16:1/16:1)-H	0.009 ± 0.002
CL(18:4/18:1/14:0/16:1)-H	0.002 ± 0.000
CL(18:4/16:1/16:1/16:1)-H	0.002 ± 0.000
CL(15:0/16:0/18:1/18:1)-H	0.001 ± 0.000
CL(17:1/16:1/18:1/16:0)-H	0.002 ± 0.000
CL(17:1/16:1/18:1/16:1)-H	0.005 ± 0.001
CL(17:1/16:1/18:2/16:1)-H	0.001 ± 0.000
CL(18:1/16:0/16:0/18:1)-H	0.017 ± 0.003
CL(18:1/16:0/16:1/18:1)-H	0.026 ± 0.005
CL(18:1/16:1/16:0/18:2)-H	0.078 ± 0.018
CL(68:4)-2H	0.002 ± 0.000
CL(18:2/16:1/18:1/16:1)-H	0.038 ± 0.007
CL(14:0/16:0/18:1/20:4)-H	0.002 ± 0.000

CL(18:2/16:1/16:1/18:2)-H	0.005	±	0.001
CL(16:1/16:1/20:3/16:1)-H	0.003	±	0.001
CL(14:0/20:4/18:1/16:1)-H	0.004	±	0.001
CL(20:4/16:1/16:1/16:1)-H	0.002	±	0.001
CL(18:4/16:1/18:2/16:1)-H	0.002	±	0.000
CL(17:0/16:0/18:1/18:1)-H	0.001	±	0.000
CL(17:1/16:0/18:1/18:1)-H	0.003	±	0.000
CL(17:1/16:1/18:1/18:1)-H	0.008	±	0.001
CL(17:1/16:1/18:2/18:1)-H	0.005	±	0.001
CL(17:1/16:1/18:2/18:2)-H	0.001	±	0.000
CL(17:1/16:1/20:4/16:1)-H	0.001	±	0.000
CL(18:1/16:0/18:0/18:0)-H	0.006	±	0.001
CL(18:1/16:0/18:0/18:1)-H	0.003	±	0.001
CL(18:1/16:0/18:1/18:1)-H	0.015	±	0.003
CL(18:1/16:1/18:1/18:1)-H	0.059	±	0.010
CL(18:2/18:1/16:1/18:1)-H	0.067	±	0.013
CL(20:4/16:0/18:1/16:0)-H	0.004	±	0.001
CL(18:2/16:1/18:1/18:2)-H	0.019	±	0.003
CL(20:4/16:0/16:1/18:1)-H	0.006	±	0.001
CL(18:2/16:1/18:2/18:2)-H	0.003	±	0.000
CL(20:4/16:1/18:1/16:1)-H	0.006	±	0.001
CL(20:4/16:1/16:1/18:1)-H	0.013	±	0.002
CL(18:2/16:1/16:1/20:4)-H	0.001	±	0.000
CL(18:4/18:2/18:1/16:1)-H	0.008	±	0.001
CL(20:5/16:1/16:1/18:2)-H	0.001	±	0.000
CL(17:0/18:1/18:1/18:1)-H	0.001	±	0.000
CL(17:1/18:1/18:1/18:1)-H	0.004	±	0.001
CL(17:1/18:1/18:1/18:2)-H	0.005	±	0.001
CL(17:1/18:1/18:2/18:2)-H	0.001	±	0.000
CL(17:1/20:4/16:1/18:1)-H	0.002	±	0.000
CL(17:1/16:1/18:2/20:4)-H	0.001	±	0.000

CL(18:2/16:1/16:1/22:6)-H	0.001	±	0.000
CL(18:1/18:0/18:0/18:1)-H	0.012	±	0.002
CL(18:1/18:0/18:1/18:1)-H	0.002	±	0.000
CL(18:1/18:1/18:1/18:1)-H	0.013	±	0.003
CL(18:2/18:1/18:1/18:1)-H	0.029	±	0.005
CL(18:1/16:0/18:1/20:3)-H	0.001	±	0.000
CL(18:2/18:1/18:1/18:2)-H	0.023	±	0.004
CL(20:4/16:0/18:1/18:1)-H	0.004	±	0.001
CL(18:2/16:1/20:3/18:1)-H	0.008	±	0.001
CL(18:2/18:2/18:2/18:1)-H	0.008	±	0.001
CL(20:4/18:1/16:1/18:1)-H	0.012	±	0.002
CL(18:2/18:2/18:2/18:2)-H	0.004	±	0.002
CL(18:2/18:1/20:4/16:1)-H	0.012	±	0.002
CL(18:2/16:1/16:1/22:5)-H	0.002	±	0.000
CL(20:5/18:1/16:1/18:2)-H	0.005	±	0.001
CL(19:1/18:1/18:1/18:1)-H	0.000	±	0.000
CL(19:1/18:1/18:1/18:2)-H	0.001	±	0.000
CL(19:1/18:1/18:2/18:2)-H	0.001	±	0.000
CL(17:1/18:1/20:4/18:1)-H	0.001	±	0.000
CL(17:1/18:1/18:2/20:4)-H	0.001	±	0.000
CL(18:1/18:0/18:0/20:0)-H	0.019	±	0.003
CL(22:5/16:1/18:2/18:2)-H	0.002	±	0.000
CL(18:2/16:1/20:4/20:4)-H	0.001	±	0.000
CL(22:2/16:1/18:0/18:1)-H	0.006	±	0.001
CL(20:4/18:0/18:0/18:1)-H	0.000	±	0.000
CL(18:2/18:1/18:2/20:1)-H	0.002	±	0.000
CL(18:1/18:1/20:3/18:1)-H	0.001	±	0.000
CL(18:2/18:1/20:3/18:1)-H	0.003	±	0.001
CL(20:4/18:1/18:1/18:1)-H	0.004	±	0.001
CL(18:2/16:1/18:1/22:4)-H	0.001	±	0.000
CL(18:2/18:1/20:3/18:2)-H	0.004	±	0.001

CL(18:1/18:1/18:2/20:4)-H	0.006	±	0.001
CL(18:2/18:1/20:4/18:2)-H	0.005	±	0.001
CL(23:1/16:0/18:0/18:1)-H	0.003	±	0.000
CL(18:2/18:2/18:2/22:5)-H	0.000	±	0.000
CL(22:3/18:0/18:0/18:1)-H	0.005	±	0.000
CL(20:4/18:0/18:1/20:0)-H	0.011	±	0.002
CL(22:5/18:0/18:0/18:1)-H	0.002	±	0.001
CL(22:6/18:1/18:1/18:1)-H	0.001	±	0.000
CL(23:0/18:0/18:0/18:1)-H	0.002	±	0.001
CL(22:3/18:0/18:0/20:4)-H	0.008	±	0.001
CL(21:0/18:0/18:0/22:6)-H	0.004	±	0.001
CL(22:3/18:0/18:0/22:5)-H	0.002	±	0.000
CL(23:0/18:0/18:0/22:4)-H	0.002	±	0.000

Table 20: Diacylglycerols in treated 143B cells

Lipid Ion	Diacylglycerol		
DG(16:0/14:0)+NH4	0.027	±	0.002
DG(16:1/14:0)+NH4	0.005	±	0.001
DG(16:0/16:0)+NH4	0.124	±	0.017
DG(18:1/14:0)+NH4	0.150	±	0.004
DG(16:1/16:1)+NH4	0.003	±	0.002
DG(16:0/17:0)+NH4	0.002	±	0.000
DG(17:1/16:0)+NH4	0.014	±	0.002
DG(18:0/16:0)+NH4	0.072	±	0.017
DG(16:0/18:1)+NH4	0.745	±	0.077
DG(16:1/18:1)+NH4	0.106	±	0.005
DG(17:0/18:1)+NH4	0.005	±	0.001
DG(17:1/18:1)+NH4	0.014	±	0.002
DG(18:0/18:0)+NH4	0.006	±	0.001
DG(18:0/18:1)+NH4	0.247	±	0.039
DG(18:1/18:1)+NH4	0.486	±	0.055

DG(18:1/18:2)+NH4	0.039	±	0.005
DG(16:0/20:4)+NH4	0.022	±	0.001
DG(19:1/18:1)+NH4	0.007	±	0.000
DG(16:0/22:1)+NH4	0.017	±	0.004
DG(20:1/18:1)+NH4	0.054	±	0.007
DG(18:1/20:2)+NH4	0.021	±	0.002
DG(18:0/20:3)+NH4	0.014	±	0.002
DG(18:1/20:3)+NH4	0.012	±	0.003
DG(16:0/22:4)+NH4	0.010	±	0.002
DG(18:0/20:4)+NH4	0.089	±	0.007
DG(18:1/20:4)+NH4	0.038	±	0.003
DG(16:0/22:6)+NH4	0.023	±	0.002
DG(16:1/22:6)+NH4	0.005	±	0.001
DG(26:0/14:0)+NH4	0.005	±	0.001
DG(16:0/24:1)+NH4	0.009	±	0.003
DG(18:1/22:1)+NH4	0.012	±	0.003
DG(18:0/22:4)+NH4	0.007	±	0.001
DG(18:0/22:5)+NH4	0.021	±	0.002
DG(18:1/22:5)+NH4	0.012	±	0.002
DG(18:0/22:6)+NH4	0.013	±	0.002
DG(18:1/22:6)+NH4	0.021	±	0.001
DG(26:0/16:0)+NH4	0.019	±	0.005
DG(26:1/16:0)+NH4	0.020	±	0.006
DG(18:1/24:1)+NH4	0.018	±	0.004
DG(27:1/16:0)+NH4	0.002	±	0.000
DG(28:0/16:0)+NH4	0.004	±	0.001
DG(28:1/16:0)+NH4	0.031	±	0.010
DG(26:1/18:1)+NH4	0.039	±	0.011
DG(27:1/18:1)+NH4	0.003	±	0.001
DG(30:1/16:0)+NH4	0.008	±	0.004
DG(28:1/18:1)+NH4	0.010	±	0.003

DG(30:1/18:1)+NH4	0.007 ± 0.001

Table 21: LPC in treated 143B cells

Lipid Ion	LPC
LPC(12:0)+H	0.000 ± 0.000
LPC(14:0)+H	0.000 ± 0.000
LPC(15:0)+H	0.001 ± 0.000
LPC(16:0)+H	0.004 ± 0.000
LPC(16:0e)+H	0.002 ± 0.000
LPC(16:0p)+H	0.001 ± 0.000
LPC(16:1)+H	0.000 ± 0.000
LPC(17:1)+H	0.000 ± 0.000
LPC(18:0)+H	0.005 ± 0.001
LPC(18:0e)+H	0.001 ± 0.000
LPC(18:0p)+H	0.001 ± 0.000
LPC(18:1)+H	0.003 ± 0.000
LPC(18:1p)+H	0.000 ± 0.000
LPC(18:2)+H	0.000 ± 0.000
LPC(19:0)+H	0.000 ± 0.000
LPC(19:1)+H	0.000 ± 0.000
LPC(20:0)+H	0.000 ± 0.000
LPC(20:0e)+H	0.000 ± 0.000
LPC(20:0p)+H	0.001 ± 0.000
LPC(20:1)+H	0.001 ± 0.000
LPC(20:3)+H	0.000 ± 0.000
LPC(20:4)+H	0.000 ± 0.000
LPC(22:0)+H	0.000 ± 0.000
LPC(22:1)+H	0.000 ± 0.000
LPC(22:5)+H	0.000 ± 0.000
LPC(22:6)+H	0.000 ± 0.000

LPC(24:0)+H	0.001	±	0.000
LPC(24:1)+H	0.001	±	0.000
LPC(26:0)+H	0.005	±	0.001
LPC(26:1)+H	0.002	±	0.000
LPC(28:0)+H	0.008	±	0.002
LPC(28:1)+H	0.002	±	0.000

Table 22: PC in treated 143B cells

Lipid Ion	PC		
PC(18:2p/8:0)+H	0.000	±	0.000
PC(28:0)+H	0.132	±	0.028
PC(14:0p/14:0)+H	0.001	±	0.000
PC(16:0/13:0)+H	0.004	±	0.001
PC(11:0/18:1)+H	0.025	±	0.006
PC(30:0)+H	0.580	±	0.082
PC(30:0e)+H	0.181	±	0.032
PC(30:0p)+H	0.032	±	0.004
PC(30:1)+H	0.240	±	0.068
PC(16:0/14:1)+H	0.003	±	0.000
PC(14:0p/16:1)+H	0.002	±	0.000
PC(31:0)+H	0.062	±	0.010
PC(31:1)+H	0.038	±	0.009
PC(32:0)+H	0.318	±	0.017
PC(32:0e)+H	0.332	±	0.043
PC(16:0p/16:0)+H	0.336	±	0.070
PC(32:1)+H	1.650	±	0.181
PC(16:0/16:1)+H	0.009	±	0.001
PC(32:1p)+H	0.051	±	0.007
PC(32:2)+H	0.074	±	0.012
PC(18:1/14:1)+H	0.005	±	0.001

PC(14:0/18:3)+H	0.005	±	0.001
PC(17:1/16:0)+H	0.255	±	0.030
PC(15:0/18:1)+H	0.119	±	0.022
PC(17:1/16:1)+H	0.031	±	0.007
PC(20:0/14:0)+H	0.000	±	0.000
PC(34:0)+H	0.153	±	0.019
PC(34:0e)+H	0.128	±	0.015
PC(34:1)+H	2.077	±	0.190
PC(34:1e)+H	0.811	±	0.103
PC(18:1p/16:0)+H	0.066	±	0.010
PC(16:0p/18:1)+H	0.120	±	0.021
PC(34:2)+H	0.748	±	0.140
PC(16:1/18:1)+H	0.003	±	0.001
PC(34:2e)+H	0.067	±	0.008
PC(16:1p/18:1)+H	0.012	±	0.002
PC(34:3)+H	0.058	±	0.015
PC(34:4)+H	0.013	±	0.002
PC(17:0/18:1)+H	0.045	±	0.003
PC(35:1)+H	0.104	±	0.017
PC(17:1/18:1)+H	0.130	±	0.027
PC(35:2)+H	0.035	±	0.005
PC(15:0/20:3)+H	0.012	±	0.003
PC(36:0e)+H	0.010	±	0.002
PC(36:1)+H	0.918	±	0.121
PC(36:1e)+H	0.224	±	0.045
PC(20:1p/16:0)+H	0.053	±	0.006
PC(18:1p/18:0)+H	0.034	±	0.009
PC(18:1/18:1)+H	1.272	±	0.227
PC(18:2p/18:0)+H	0.022	±	0.003
PC(36:2p)+H	0.030	±	0.004
PC(14:0p/22:2)+H	0.004	±	0.001

PC(36:3)+H	0.293	±	0.028
PC(18:2p/18:1)+H	0.102	±	0.012
PC(36:4)+H	0.158	±	0.018
PC(18:4/18:0)+H	0.013	±	0.004
PC(16:0p/20:4)+H	0.018	±	0.002
PC(14:0p/22:4)+H	0.000	±	0.000
PC(36:5)+H	0.030	±	0.006
PC(14:0/22:6)+H	0.001	±	0.000
PC(16:0/21:1)+H	0.022	±	0.004
PC(19:1/18:1)+H	0.065	±	0.012
PC(15:0/22:4)+H	0.010	±	0.001
PC(20:0/18:1)+H	0.000	±	0.000
PC(38:1e)+H	0.028	±	0.006
PC(38:2)+H	0.221	±	0.038
PC(38:3)+H	0.080	±	0.010
PC(38:4)+H	0.102	±	0.013
PC(38:4e)+H	0.032	±	0.003
PC(38:4p)+H	0.066	±	0.009
PC(38:5)+H	0.183	±	0.020
PC(16:0e/22:5)+H	0.008	±	0.000
PC(38:6)+H	0.097	±	0.015
PC(38:7)+H	0.021	±	0.003
PC(18:1/21:0)+H	0.003	±	0.001
PC(18:1/21:1)+H	0.003	±	0.001
PC(40:0e)+H	0.002	±	0.000
PC(40:1)+H	0.029	±	0.006
PC(40:2)+H	0.056	±	0.010
PC(40:3)+H	0.015	±	0.002
PC(26:1/14:3)+H	0.000	±	0.000
PC(40:4)+H	0.017	±	0.001
PC(18:0/22:5)+H	0.037	±	0.006

PC(40:6)+H	0.045	±	0.005
PC(40:7)+H	0.097	±	0.013
PC(40:8)+H	0.021	±	0.003
PC(18:1/23:0)+H	0.002	±	0.001
PC(18:1/23:1)+H	0.002	±	0.000
PC(20:4/21:1)+H	0.001	±	0.000
PC(42:0)+H	0.015	±	0.005
PC(42:1)+H	0.032	±	0.007
PC(42:2)+H	0.054	±	0.011
PC(42:3)+H	0.016	±	0.003
PC(27:0/16:0)+H	0.001	±	0.000
PC(44:1)+H	0.039	±	0.009
PC(44:2)+H	0.060	±	0.013
PC(44:3)+H	0.019	±	0.006
PC(27:0/18:1)+H	0.002	±	0.001
PC(46:1)+H	0.017	±	0.003
PC(46:2)+H	0.020	±	0.005
PC(46:4)+H	0.004	±	0.001
PC(46:5)+H	0.006	±	0.001
PC(48:2)+H	0.007	±	0.002

Table 23: LPE in treated 143B cells

Lipid Ion	LPE		
LPE(16:0)-H	0.001	±	0.000
LPE(18:1)-H	0.002	±	0.000
LPE(20:4)-H	0.001	±	0.000
LPE(24:0)-H	0.004	±	0.001
LPE(26:1)-H	0.001	±	0.000

Table 24: PE in treated 143B cells

Lipid Ion	PE

PE(16:0/14:0)+H	0.026	±	0.001
PE(30:1)+H	0.013	±	0.002
PE(16:0p/14:1)+H	0.003	±	0.001
PE(16:0/16:0)+H	0.051	±	0.007
PE(16:0p/16:0)+H	0.010	±	0.002
PE(16:0/16:1)+H	0.368	±	0.066
PE(16:0p/16:1)+H	0.173	±	0.024
PE(16:1/16:1)+H	0.026	±	0.005
PE(16:0p/17:1)+H	0.024	±	0.003
PE(18:0p/16:0)+H	0.011	±	0.003
PE(16:0/18:1)+H	1.975	±	0.175
PE(16:0e/18:1)+H	0.049	±	0.006
PE(16:0p/18:1)+H	0.898	±	0.148
PE(16:1/18:1)+H	0.546	±	0.071
PE(18:1p/16:1)+H	0.065	±	0.010
PE(16:0p/18:2)+H	0.066	±	0.007
PE(16:1/18:2)+H	0.025	±	0.012
PE(16:0p/18:3)+H	0.006	±	0.001
PE(14:0/20:4)+H	0.006	±	0.001
PE(16:0p/19:1)+H	0.028	±	0.004
PE(17:1/18:1)+H	0.078	±	0.010
PE(18:0/18:1)+H	1.726	±	0.244
PE(18:0p/18:1)+H	0.417	±	0.081
PE(18:1/18:1)+H	2.064	±	0.226
PE(18:1p/18:1)+H	0.242	±	0.042
PE(18:0p/18:2)+H	0.100	±	0.014
PE(18:1/18:2)+H	0.271	±	0.034
PE(36:3)+H	0.028	±	0.004
PE(16:0p/20:3)+H	0.170	±	0.022
PE(16:0/20:4)+H	0.432	±	0.040
PE(16:0p/20:4)+H	1.134	±	0.557

PE(16:1/20:4)+H	0.027	±	0.005
PE(16:0/20:5)+H	0.029	±	0.004
PE(16:0p/20:5)+H	0.150	±	0.012
PE(16:1/20:5)+H	0.002	±	0.000
PE(16:0p/22:1)+H	0.062	±	0.012
PE(18:1p/20:1)+H	0.025	±	0.007
PE(18:0/20:3)+H	0.175	±	0.034
PE(18:0p/20:3)+H	0.095	±	0.018
PE(18:0/20:4)+H	1.917	±	0.199
PE(16:0p/22:4)+H	0.269	±	0.030
PE(18:0p/20:4)+H	0.699	±	0.079
PE(18:0/20:5)+H	0.173	±	0.020
PE(16:0p/22:5)+H	1.171	±	0.110
PE(18:0p/20:5)+H	0.127	±	0.022
PE(16:0/22:6)+H	0.112	±	0.004
PE(18:1p/20:5)+H	0.041	±	0.002
PE(16:1/22:6)+H	0.015	±	0.003
PE(17:0/22:6)+H	0.014	±	0.002
PE(18:0p/22:1)+H	0.011	±	0.007
PE(18:0p/22:2)+H	0.014	±	0.002
PE(18:0p/22:3)+H	0.011	±	0.002
PE(18:0/22:4)+H	0.150	±	0.013
PE(18:0p/22:4)+H	0.077	±	0.009
PE(18:0/22:5)+H	0.318	±	0.032
PE(18:0p/22:5)+H	0.290	±	0.027
PE(18:0/22:6)+H	0.514	±	0.012
PE(18:1p/22:5)+H	0.138	±	0.010
PE(18:1/22:6)+H	0.244	±	0.018
PE(18:1/24:0)+H	0.050	±	0.008
PE(22:0/20:4)+H	0.009	±	0.002
PE(20:0p/22:5)+H	0.014	±	0.002

PE(26:0/18:1)+H	0.030	±	0.006
PE(24:0/20:4)+H	0.028	±	0.008
PE(24:1/20:4)+H	0.029	±	0.005
PE(26:1/20:4)+H	0.016	±	0.002

Table 25: PI in treated 143B cells

Lipid Ion	PI		
PI(16:0/16:1)-H	0.050	±	0.014
PI(18:1/14:1)-H	0.004	±	0.001
PI(17:1/16:0)-H	0.007	±	0.002
PI(18:0/16:0)-H	0.013	±	0.002
PI(16:0/18:1)-H	0.819	±	0.111
PI(16:0e/18:1)-H	0.009	±	0.001
PI(16:1/18:2)-H	0.003	±	0.001
PI(17:0/18:1)-H	0.011	±	0.002
PI(17:1/18:1)-H	0.018	±	0.006
PI(17:0/18:2)-H	0.004	±	0.000
PI(18:0/18:1)-H	0.037	±	0.009
PI(18:0p/18:1)-H	0.003	±	0.002
PI(18:1/18:1)-H	1.542	±	0.302
PI(16:0/20:4)-H	0.119	±	0.017
PI(16:0e/20:4)-H	0.004	±	0.001
PI(16:1/20:4)-H	0.002	±	0.001
PI(19:1/18:0)-H	0.016	±	0.003
PI(17:0/20:4)-H	0.018	±	0.003
PI(18:0/20:1)-H	0.030	±	0.006
PI(18:1/20:3)-H	0.059	±	0.013
PI(18:0/20:4)-H	2.162	±	0.342
PI(18:0e/20:4)-H	0.006	±	0.001
PI(18:0p/20:4)-H	0.008	±	0.002

PI(19:1/20:3)-H	0.007	±	0.004
PI(19:0/20:4)-H	0.005	±	0.001
PI(19:1/20:4)-H	0.007	±	0.001
PI(18:0/22:1)-H	0.004	±	0.001
PI(18:1/22:1)-H	0.006	±	0.002
PI(18:0/22:3)-H	0.032	±	0.006
PI(20:0/20:3)-H	0.001	±	0.000
PI(20:0/20:4)-H	0.005	±	0.001
PI(18:0e/22:5)-H	0.002	±	0.000
PI(20:3/20:4)-H	0.001	±	0.000
PI(18:0/24:2)-H	0.003	±	0.001
PI(18:1/24:2)-H	0.002	±	0.001
PI(22:5/20:4)-H	0.001	±	0.000
PI(26:1/18:0)-H	0.002	±	0.001

Table 26: PI in treated 143B cells

Lipid Ion	PG		
PG(16:1/14:0)-H	0.001	±	0.000
PG(16:0/16:0)-H	0.006	±	0.001
PG(16:0/16:1)-H	0.007	±	0.002
PG(16:1/16:1)-H	0.001	±	0.000
PG(16:0/18:1)-H	0.124	±	0.008
PG(16:1/18:1)-H	0.012	±	0.002
PG(19:1/16:0)-H	0.003	±	0.001
PG(18:0/18:1)-H	0.051	±	0.008
PG(18:1/18:1)-H	0.161	±	0.031
PG(18:1/18:2)-H	0.003	±	0.001
PG(20:1/18:1)-H	0.005	±	0.001
PG(18:1/20:2)-H	0.010	±	0.002
PG(16:0/22:6)-H	0.009	±	0.002

PG(16:1/22:6)-H	0.003	±	0.001
PG(18:1/22:5)-H	0.007	±	0.002
PG(18:1/22:6)-H	0.087	±	0.018
PG(18:2/22:6)-H	0.003	±	0.000
PG(42:9)-H	0.002	±	0.000
PG(22:5/22:6)-H	0.002	±	0.000
PG(22:6/22:6)-H	0.014	±	0.002

Table 27: PS in treated 143B cells

Lipid Ion	PS		
PS(16:0/14:0)-H	0.002	±	0.000
PS(16:0/16:1)-H	0.063	±	0.015
PS(18:0/16:0)-H	0.004	±	0.001
PS(16:0/18:1)-H	0.387	±	0.020
PS(16:0e/18:1)-H	0.014	±	0.003
PS(16:1/18:1)-H	0.043	±	0.005
PS(17:1/18:1)-H	0.010	±	0.002
PS(18:0e/18:1)-H	0.026	±	0.006
PS(18:1/18:2)-H	0.016	±	0.001
PS(16:0/20:4)-H	0.009	±	0.001
PS(19:0/18:1)-H	0.045	±	0.008
PS(17:0/20:4)-H	0.002	±	0.000
PS(18:0/20:1)-H	0.063	±	0.014
PS(18:0/20:2)-H	0.042	±	0.007
PS(18:0/20:3)-H	0.084	±	0.010
PS(18:1/20:2)-H	0.053	±	0.004
PS(18:0/20:4)-H	0.036	±	0.002
PS(18:1/20:3)-H	0.006	±	0.001
PS(18:1/20:4)-H	0.016	±	0.003
PS(18:0/20:5)-H	0.008	±	0.001

PS(18:1/21:0)-H	0.012	±	0.002
PS(19:0/20:3)-H	0.005	±	0.001
PS(17:0/22:5)-H	0.004	±	0.001
PS(18:1/22:1)-H	0.020	±	0.003
PS(18:0/22:5)-H	0.013	±	0.002
PS(18:1/22:5)-H	0.028	±	0.005
PS(20:3/20:3)-H	0.003	±	0.000
PS(18:1/22:6)-H	0.018	±	0.004
PS(18:1/24:1)-H	0.006	±	0.001
PS(20:0/22:4)-H	0.002	±	0.000
PS(20:0/22:6)-H	0.023	±	0.005
PS(25:0/18:1)-H	0.002	±	0.000
PS(26:0/18:1)-H	0.016	±	0.002
PS(26:1/18:1)-H	0.023	±	0.004
PS(26:1/18:2)-H	0.005	±	0.001
PS(24:0/20:3)-H	0.016	±	0.002
PS(24:1/20:3)-H	0.002	±	0.000
PS(24:0/20:4)-H	0.008	±	0.001
PS(28:0/18:1)-H	0.001	±	0.000
PS(28:1/18:1)-H	0.009	±	0.002

Table 28: SM in treated 143B cells

Lipid Ion	SM		
SM(d30:1)+H	0.001	±	0.000
SM(d31:1)+H	0.002	±	0.000
SM(d32:0)+H	0.050	±	0.013
SM(d32:1)+H	0.151	±	0.024
SM(d32:2)+H	0.003	±	0.000
SM(d33:1)+H	0.139	±	0.029
SM(d33:2)+H	0.001	±	0.000

SM(d34:0)+H	1.051	±	0.140
SM(d34:1)+H	2.946	±	0.303
SM(d34:2)+H	0.254	±	0.040
SM(d34:3)+H	0.003	±	0.001
SM(d34:4)+H	0.023	±	0.003
SM(d35:1)+H	0.037	±	0.005
SM(d35:4)+H	0.014	±	0.002
SM(d36:0)+H	0.034	±	0.008
SM(d36:1)+H	0.047	±	0.003
SM(d36:2)+H	0.023	±	0.005
SM(d18:2/18:1)+H	0.011	±	0.001
SM(d36:5)+H	0.024	±	0.003
SM(d38:1)+H	0.024	±	0.003
SM(d38:5)+H	0.007	±	0.001
SM(d39:6)+H	0.004	±	0.001
SM(d40:0)+H	0.031	±	0.007
SM(d40:1)+H	0.245	±	0.035
SM(d40:2)+H	0.048	±	0.006
SM(d41:1)+H	0.038	±	0.007
SM(d41:2)+H	0.053	±	0.009
SM(d42:0)+H	0.040	±	0.008
SM(d42:1)+H	0.735	±	0.122
SM(d18:1/24:1)+H	1.300	±	0.151
SM(d18:0/24:2)+H	0.015	±	0.003
SM(d18:1/24:2)+H	0.002	±	0.000
SM(d42:3)+H	0.177	±	0.022
SM(d18:2/24:1)+H	0.003	±	0.001
SM(d42:4)+H	0.023	±	0.002
SM(d42:5)+H	0.002	±	0.000
SM(d43:1)+H	0.011	±	0.002
SM(d43:2)+H	0.017	±	0.003

SM(d18:1/25:3)+H	0.004	±	0.001
SM(d43:4)+H	0.006	±	0.000
SM(d43:5)+H	0.004	±	0.000
SM(d44:0)+H	0.003	±	0.001
SM(d44:1)+H	0.029	±	0.006
SM(d44:2)+H	0.065	±	0.012
SM(d44:3)+H	0.022	±	0.006
SM(d18:0/26:3)+H	0.004	±	0.001
SM(d18:2/26:2)+H	0.022	±	0.005
SM(d18:1/26:3)+H	0.080	±	0.008
SM(d18:1/26:4)+H	0.083	±	0.004
SM(d44:6)+H	0.005	±	0.000
SM(d18:1/28:0)+H	0.004	±	0.000
SM(d46:4)+H	0.003	±	0.001
SM(d46:5)+H	0.006	±	0.001
SM(d48:2)+H	0.007	±	0.001
SM(d54:3)+H	0.005	±	0.000
SM(d56:4)+H	0.005	±	0.001

Table 29: TG in treated 143B cells

Lipid Ion	TG		
TG(16:0/12:0/14:0)+NH4	0.013	±	0.004
TG(16:1/12:0/14:0)+NH4	0.002	±	0.001
TG(16:0/14:0/14:0)+NH4	0.051	±	0.016
TG(18:0e/12:0/14:0)+NH4	0.012	±	0.003
TG(16:0/14:0/14:1)+NH4	0.038	±	0.013
TG(15:0/14:0/16:0)+NH4	0.005	±	0.002

TG(16:0/14:0/16:0)+NH4	0.162	±	0.082
TG(16:0e/14:0/16:0)+NH4	0.058	±	0.013
TG(16:0/14:0/16:1)+NH4	0.246	±	0.065
TG(16:0e/14:0/16:1)+NH4	0.026	±	0.005
TG(16:1/14:0/16:1)+NH4	0.052	±	0.013
TG(15:0/16:0/16:0)+NH4	0.023	±	0.008
TG(15:0/15:0/17:1)+NH4	0.028	±	0.004
TG(16:1/14:0/17:1)+NH4	0.005	±	0.001
TG(16:0/16:0/16:0)+NH4	0.387	±	0.065
TG(16:0e/16:0/16:0)+NH4	0.155	±	0.024
TG(16:0/14:0/18:1)+NH4	0.930	±	0.132
TG(18:0e/14:0/16:1)+NH4	0.160	±	0.032
TG(16:1/14:0/18:1)+NH4	0.366	±	0.086
TG(16:0e/16:1/16:1)+NH4	0.028	±	0.006
TG(16:1/16:1/16:1)+NH4	0.033	±	0.009
TG(16:0/16:0/17:0)+NH4	0.015	±	0.003
TG(16:0/16:0/17:1)+NH4	0.088	±	0.007
TG(16:0/16:1/17:1)+NH4	0.047	±	0.008
TG(16:1/16:1/17:1)+NH4	0.007	±	0.002
TG(18:0/16:0/16:0)+NH4	0.318	±	0.056
TG(18:0e/16:0/16:0)+NH4	0.130	±	0.027
TG(18:0p/16:0/16:0)+NH4	0.471	±	0.075
TG(16:0/16:0/18:1)+NH4	1.553	±	0.229
TG(18:1p/16:0/16:0)+NH4	0.117	±	0.057
TG(16:0/16:1/18:1)+NH4	1.252	±	0.156
TG(16:1/16:1/18:1)+NH4	0.223	±	0.045
TG(16:1/16:1/18:2)+NH4	0.016	±	0.004
TG(16:0/14:0/20:4)+NH4	0.008	±	0.001
TG(18:0/16:0/17:0)+NH4	0.011	±	0.002
TG(16:0/17:0/18:1)+NH4	0.044	±	0.008
TG(16:0/17:1/18:1)+NH4	0.152	±	0.019

TG(16:1/17:1/18:1)+NH4	0.031	±	0.003
TG(18:0/16:0/18:0)+NH4	0.116	±	0.025
TG(20:0p/16:0/16:0)+NH4	0.322	±	0.054
TG(18:0/16:0/18:1)+NH4	1.105	±	0.169
TG(16:0/18:1/18:1)+NH4	2.362	±	0.336
TG(16:0e/18:1/18:1)+NH4	0.342	±	0.050
TG(18:0p/16:1/18:1)+NH4	0.073	±	0.011
TG(16:1/18:1/18:1)+NH4	0.758	±	0.101
TG(16:1/18:1/18:2)+NH4	0.087	±	0.008
TG(16:0/16:0/20:4)+NH4	0.026	±	0.005
TG(18:1/14:0/20:4)+NH4	0.008	±	0.002
TG(19:1/16:0/18:0)+NH4	0.049	±	0.011
TG(17:0/18:1/18:1)+NH4	0.140	±	0.023
TG(18:1/17:1/18:1)+NH4	0.079	±	0.010
TG(18:1/17:1/18:2)+NH4	0.011	±	0.001
TG(18:0/16:0/20:0)+NH4	0.026	±	0.007
TG(16:0e/16:0/22:0)+NH4	0.016	±	0.003
TG(18:0/18:0/18:1)+NH4	0.267	±	0.061
TG(16:0e/16:0/22:1)+NH4	0.078	±	0.015
TG(18:0/18:1/18:1)+NH4	1.112	±	0.175
TG(18:0e/18:1/18:1)+NH4	0.151	±	0.026
TG(18:0p/18:1/18:1)+NH4	0.083	±	0.013
TG(18:1/18:1/18:1)+NH4	1.257	±	0.187
TG(16:0e/18:1/20:3)+NH4	0.032	±	0.001
TG(16:1/18:1/20:4)+NH4	0.038	±	0.007
TG(16:0/16:0/22:6)+NH4	0.024	±	0.003
TG(16:0/16:1/22:6)+NH4	0.014	±	0.005
TG(16:1/16:1/22:6)+NH4	0.004	±	0.001
TG(18:0/18:1/19:0)+NH4	0.018	±	0.005
TG(19:1/18:0/18:1)+NH4	0.045	±	0.007
TG(19:1/18:1/18:1)+NH4	0.054	±	0.011

TG(19:1/18:1/18:2)+NH4	0.017	±	0.001
TG(26:0/14:0/16:0)+NH4	0.031	±	0.009
TG(26:1/14:0/16:0)+NH4	0.116	±	0.035
TG(16:0e/16:0/24:1)+NH4	0.064	±	0.012
TG(18:1p/19:0/19:0)+NH4	0.062	±	0.012
TG(16:0/18:1/22:1)+NH4	0.246	±	0.049
TG(20:0p/18:1/18:1)+NH4	0.039	±	0.010
TG(20:1/18:1/18:1)+NH4	0.339	±	0.055
TG(18:1/18:1/20:2)+NH4	0.140	±	0.028
TG(16:0e/18:1/22:5)+NH4	0.058	±	0.008
TG(16:1/18:1/22:5)+NH4	0.041	±	0.006
TG(16:0/18:1/22:6)+NH4	0.066	±	0.007
TG(16:0e/18:1/22:6)+NH4	0.043	±	0.006
TG(16:1/18:1/22:6)+NH4	0.023	±	0.003
TG(25:0/16:0/16:1)+NH4	0.012	±	0.003
TG(25:1/16:0/16:1)+NH4	0.022	±	0.004
TG(18:1/18:1/21:1)+NH4	0.019	±	0.002
TG(26:0/16:0/16:0)+NH4	0.051	±	0.012
TG(18:0e/16:0/24:0)+NH4	0.020	±	0.004
TG(26:1/16:0/16:0)+NH4	0.167	±	0.041
TG(18:0e/16:0/24:1)+NH4	0.052	±	0.007
TG(16:0/18:1/24:1)+NH4	0.248	±	0.061
TG(16:0e/18:1/24:1)+NH4	0.056	±	0.011
TG(18:0p/18:1/22:1)+NH4	0.024	±	0.005
TG(18:1/18:1/22:1)+NH4	0.142	±	0.026
TG(18:0/18:1/22:3)+NH4	0.048	±	0.010
TG(18:1/18:1/22:3)+NH4	0.034	±	0.004
TG(18:1/18:1/22:4)+NH4	0.064	±	0.024
TG(18:1/18:1/22:6)+NH4	0.055	±	0.005
TG(18:1/18:2/22:6)+NH4	0.009	±	0.001
TG(27:0/16:0/16:0)+NH4	0.003	±	0.001

TG(27:1/16:0/16:0)+NH4	0.018	±	0.005
TG(25:1/16:0/18:1)+NH4	0.024	±	0.007
TG(18:1/18:1/23:1)+NH4	0.014	±	0.003
TG(26:0/16:0/18:0)+NH4	0.029	±	0.006
TG(26:0/16:0/18:1)+NH4	0.218	±	0.050
TG(18:1/20:4/22:6)+NH4	0.006	±	0.001
TG(26:1/16:0/18:1)+NH4	0.302	±	0.070
TG(18:1/18:1/24:1)+NH4	0.199	±	0.042
TG(18:1/18:1/24:2)+NH4	0.039	±	0.008
TG(20:0/18:1/22:4)+NH4	0.014	±	0.004
TG(20:1/18:1/22:5)+NH4	0.028	±	0.004
TG(20:1/18:1/22:6)+NH4	0.010	±	0.002
TG(29:1/16:0/16:0)+NH4	0.012	±	0.003
TG(27:1/16:0/18:1)+NH4	0.025	±	0.006
TG(25:1/18:1/18:1)+NH4	0.016	±	0.005
TG(28:0/16:0/18:0)+NH4	0.006	±	0.001
TG(26:0/18:0/18:1)+NH4	0.091	±	0.021
TG(18:1/22:5/22:6)+NH4	0.004	±	0.000
TG(26:1/18:0/18:1)+NH4	0.260	±	0.065
TG(26:1/18:1/18:1)+NH4	0.178	±	0.041
TG(26:1/18:1/18:2)+NH4	0.045	±	0.010
TG(18:1/20:3/24:1)+NH4	0.015	±	0.003
TG(29:0/16:0/18:1)+NH4	0.005	±	0.001
TG(29:1/16:0/18:1)+NH4	0.014	±	0.004
TG(27:1/18:1/18:1)+NH4	0.009	±	0.003
TG(30:0/16:0/18:1)+NH4	0.022	±	0.008
TG(28:0/18:1/18:1)+NH4	0.079	±	0.018
TG(20:0e/22:1/22:1)+NH4	0.012	±	0.003
TG(28:1/18:1/18:1)+NH4	0.075	±	0.020
TG(26:1/18:1/20:2)+NH4	0.019	±	0.005
TG(26:1/18:1/20:3)+NH4	0.006	±	0.002

TG(29:1/18:0/18:1)+NH4	0.006	±	0.002
TG(29:1/18:1/18:1)+NH4	0.006	±	0.001
TG(26:0/16:0/24:1)+NH4	0.015	±	0.004
TG(30:0/18:1/18:1)+NH4	0.033	±	0.010
TG(30:1/18:1/18:1)+NH4	0.032	±	0.008
TG(26:1/18:1/22:6)+NH4	0.003	±	0.000
TG(26:0/18:1/24:0)+NH4	0.008	±	0.002
TG(26:0/18:1/24:1)+NH4	0.025	±	0.006
TG(26:1/18:1/24:1)+NH4	0.024	±	0.006
TG(27:1/18:1/24:0)+NH4	0.002	±	0.001
TG(27:1/18:1/24:1)+NH4	0.002	±	0.001
TG(28:0/18:1/24:0)+NH4	0.004	±	0.001
TG(28:1/18:1/24:0)+NH4	0.014	±	0.004
TG(26:1/20:1/24:1)+NH4	0.014	±	0.004
TG(28:1/18:1/24:2)+NH4	0.004	±	0.001
TG(30:1/18:1/24:1)+NH4	0.005	±	0.001

Table 30: PA in treated 143B cells

Lipid Ion	PA		
PA(18:0/16:0)-H	0.004	±	0.001
PA(16:0/18:1)-H	0.012	±	0.001
PA(18:0/18:1)-H	0.005	±	0.000

Table 31: MG in treated 143B cells

Lipid Ion	MG		
MG(32:0)+H	0.034	±	0.000

MG(34:0)+H	0.030	±	0.007
MG(34:1)+H	0.087	±	0.010
MG(36:0)+H	0.003	±	0.001
MG(36:1)+H	0.018	±	0.003
MG(38:0)+H	0.003	±	0.001

Table 31: Fold Change in Lipids in 143B cells with and without U73122 treatment

Lipid Ion	p-Value	log10(Fold Change)
CL(12:2/18:1/18:1/18:1)-H	0.05	2.02
CL(14:0/14:0/14:0/20:1)-H	0.05	-1.74
CL(14:0/14:0/18:1/16:1)-H	0.50	0.02
CL(14:0/15:0/18:1/18:1)-H	0.05	1.82
CL(14:0/16:0/16:0/16:0)-H	0.35	0.79
CL(14:0/16:0/16:0/18:1)-H	0.05	2.36
CL(14:0/16:0/16:1/16:0)-H	0.05	1.98
CL(14:0/16:0/16:1/18:1)-H	0.05	-2.60
CL(14:0/16:0/18:1/16:0)-H	0.05	-2.11
CL(14:0/16:0/18:1/20:4)-H	0.05	-2.28
CL(14:0/16:1/16:1/16:1)-H	0.05	2.20
CL(14:0/16:1/16:1/18:1)-H	0.20	-0.13
CL(14:0/18:1/16:0/16:1)-H	0.05	2.76
CL(14:0/18:1/16:0/18:1)-H	0.05	3.12
CL(14:0/18:1/16:1/18:1)-H	0.05	-3.29
CL(14:0/20:4/18:1/16:1)-H	0.05	-2.56
CL(15:0/16:0/16:0/18:1)-H	0.05	1.15
CL(15:0/16:0/18:1/18:1)-H	0.05	-1.94

CL(15:0/16:1/16:1/16:1)-H	0.05	-1.55
CL(16:0/16:0/16:0/16:0)-H	0.35	0.89
CL(16:0/16:0/16:0/18:0)-H	0.05	#NAME?
CL(16:0/16:0/16:0/20:0)-H	0.05	1.53
CL(16:0/18:0/18:0/20:0)-H	0.05	1.81
CL(16:1/16:1/16:1/14:0)-H	0.05	-2.34
CL(16:1/16:1/16:1/16:1)-H	0.10	-0.27
CL(16:1/16:1/16:1/18:1)-H	0.20	-0.21
CL(16:1/16:1/20:3/16:1)-H	0.05	-2.51
CL(17:0/16:0/16:0/18:1)-H	0.05	1.08
CL(17:0/16:0/18:1/18:1)-H	0.05	-2.05
CL(17:0/18:1/18:0/18:1)-H	0.05	1.30
CL(17:0/18:1/18:1/16:0)-H	0.05	2.14
CL(17:0/18:1/18:1/18:1)-H	0.35	0.11
CL(17:0/18:1/20:4/18:1)-H	0.05	1.25
CL(17:0/18:2/18:2/18:2)-H	0.05	1.89
CL(17:0/20:4/16:0/18:1)-H	0.05	1.56
CL(17:1/14:0/18:1/16:1)-H	0.65	0.03
CL(17:1/16:0/16:1/18:1)-H	0.05	2.49
CL(17:1/16:0/18:1/18:1)-H	0.05	-2.42
CL(17:1/16:1/16:1/16:1)-H	0.20	-0.10
CL(17:1/16:1/16:1/18:1)-H	0.05	2.64
CL(17:1/16:1/16:1/20:4)-H	0.05	2.02
CL(17:1/16:1/18:1/16:0)-H	0.05	-2.39
CL(17:1/16:1/18:1/16:1)-H	0.05	-2.71
CL(17:1/16:1/18:1/18:1)-H	0.05	-2.90
CL(17:1/16:1/18:2/16:1)-H	0.35	-0.09
CL(17:1/16:1/18:2/18:1)-H	0.50	-0.05

CL(17:1/16:1/18:2/18:2)-H	0.20	-0.17
CL(17:1/16:1/18:2/20:4)-H	0.05	-2.02
CL(17:1/16:1/20:4/16:1)-H	0.05	-2.11
CL(17:1/16:1/20:4/18:2)-H	0.05	1.97
CL(17:1/18:1/16:0/18:1)-H	0.05	2.57
CL(17:1/18:1/16:1/18:1)-H	0.05	2.95
CL(17:1/18:1/18:1/18:1)-H	0.20	0.15
CL(17:1/18:1/18:1/18:2)-H	0.05	-2.65
CL(17:1/18:1/18:1/20:4)-H	0.05	1.77
CL(17:1/18:1/18:2/18:1)-H	0.05	2.72
CL(17:1/18:1/18:2/18:2)-H	0.20	0.20
CL(17:1/18:1/18:2/20:4)-H	0.65	0.03
CL(17:1/18:1/20:4/18:1)-H	0.35	0.08
CL(17:1/18:2/18:2/18:2)-H	0.05	1.71
CL(17:1/18:2/18:2/20:4)-H	0.05	1.47
CL(17:1/20:4/16:0/18:1)-H	0.05	1.97
CL(17:1/20:4/16:1/18:1)-H	0.35	0.04
CL(18:1/15:1/18:1/18:1)-H	0.05	#NAME?
CL(18:1/16:0/16:0/16:0)-H	0.10	0.28
CL(18:1/16:0/16:0/16:1)-H	0.05	-2.92
CL(18:1/16:0/16:0/18:1)-H	0.20	0.19
CL(18:1/16:0/16:0/24:1)-H	0.05	2.50
CL(18:1/16:0/16:1/18:1)-H	0.35	0.14
CL(18:1/16:0/18:0/16:0)-H	0.05	1.92
CL(18:1/16:0/18:0/18:0)-H	0.35	-0.08
CL(18:1/16:0/18:0/18:1)-H	0.35	0.09
CL(18:1/16:0/18:1/15:0)-H	0.05	2.06
CL(18:1/16:0/18:1/18:1)-H	0.20	0.17

CL(18:1/16:0/18:1/20:3)-H	0.05	-1.99
CL(18:1/16:0/18:1/24:1)-H	0.05	#NAME?
CL(18:1/16:0/20:1/20:3)-H	0.05	1.51
CL(18:1/16:1/16:0/16:1)-H	0.05	3.31
CL(18:1/16:1/16:0/18:2)-H	0.05	-3.89
CL(18:1/16:1/18:1/18:1)-H	0.50	-0.02
CL(18:1/16:1/18:2/16:0)-H	0.05	3.80
CL(18:1/18:0/18:0/18:1)-H	0.50	0.04
CL(18:1/18:0/18:0/20:0)-H	0.50	0.04
CL(18:1/18:0/18:0/20:4)-H	0.05	0.96
CL(18:1/18:0/18:1/18:1)-H	0.50	0.09
CL(18:1/18:0/20:1/20:1)-H	0.05	2.36
CL(18:1/18:1/18:1/18:1)-H	0.35	0.09
CL(18:1/18:1/18:1/20:1)-H	0.05	1.70
CL(18:1/18:1/18:2/20:4)-H	0.05	-2.79
CL(18:1/18:1/20:3/18:1)-H	0.05	-1.80
CL(18:2/16:1/16:1/16:1)-H	0.10	-0.25
CL(18:2/16:1/16:1/18:2)-H	0.05	-2.74
CL(18:2/16:1/16:1/20:4)-H	0.05	-2.15
CL(18:2/16:1/16:1/22:5)-H	0.10	-0.36
CL(18:2/16:1/16:1/22:6)-H	0.05	-1.82
CL(18:2/16:1/18:1/16:1)-H	0.20	-0.15
CL(18:2/16:1/18:1/18:2)-H	0.20	-0.15
CL(18:2/16:1/18:1/22:4)-H	0.05	-2.05
CL(18:2/16:1/18:2/16:1)-H	0.05	2.50
CL(18:2/16:1/18:2/18:2)-H	0.05	-2.41
CL(18:2/16:1/20:3/18:1)-H	0.05	-2.88
CL(18:2/16:1/20:4/18:2)-H	0.05	2.48

CL(18:2/16:1/20:4/20:4)-H	0.05	-1.95
CL(18:2/18:1/16:1/18:1)-H	0.35	-0.08
CL(18:2/18:1/18:1/18:1)-H	0.50	-0.03
CL(18:2/18:1/18:1/18:2)-H	0.20	-0.12
CL(18:2/18:1/18:2/18:2)-H	0.05	3.07
CL(18:2/18:1/18:2/20:1)-H	0.05	-2.24
CL(18:2/18:1/18:2/20:4)-H	0.05	2.43
CL(18:2/18:1/20:3/18:1)-H	0.35	-0.04
CL(18:2/18:1/20:3/18:2)-H	0.05	-2.56
CL(18:2/18:1/20:4/16:1)-H	0.05	-1.20
CL(18:2/18:1/20:4/18:1)-H	0.05	1.96
CL(18:2/18:1/20:4/18:2)-H	0.20	-0.10
CL(18:2/18:2/16:1/18:1)-H	0.05	2.84
CL(18:2/18:2/18:2/16:1)-H	0.05	2.27
CL(18:2/18:2/18:2/18:1)-H	0.10	-0.23
CL(18:2/18:2/18:2/18:2)-H	0.05	-2.65
CL(18:2/18:2/18:2/20:4)-H	0.05	1.63
CL(18:2/18:2/18:2/22:5)-H	0.05	-1.59
CL(18:2/18:2/18:2/22:6)-H	0.05	1.43
CL(18:2/20:4/16:1/16:1)-H	0.05	2.78
CL(18:2/20:4/16:1/18:1)-H	0.05	2.97
CL(18:2/20:4/18:1/18:1)-H	0.05	2.73
CL(18:3/14:0/16:0/18:1)-H	0.05	1.71
CL(18:3/16:0/16:0/18:1)-H	0.05	2.02
CL(18:3/18:1/15:0/18:1)-H	0.05	1.47
CL(18:3/18:1/16:0/16:0)-H	0.05	1.86
CL(18:3/18:1/16:0/18:0)-H	0.05	1.70
CL(18:3/18:1/16:0/18:1)-H	0.05	2.79

CL(18:4/16:0/16:1/18:1)-H	0.05	2.57
CL(18:4/16:1/16:1/16:1)-H	0.10	-0.27
CL(18:4/16:1/16:1/18:1)-H	0.05	2.72
CL(18:4/16:1/18:2/16:1)-H	0.10	-0.30
CL(18:4/18:1/14:0/16:1)-H	0.05	-2.34
CL(18:4/18:2/18:1/16:1)-H	0.05	-2.90
CL(18:4/18:2/18:2/18:2)-H	0.05	1.60
CL(18:4/22:6/20:4/16:1)-H	0.05	2.27
CL(19:1/18:1/18:1/18:1)-H	0.20	0.15
CL(19:1/18:1/18:1/18:2)-H	0.05	-1.89
CL(19:1/18:1/18:2/18:1)-H	0.05	2.00
CL(19:1/18:1/18:2/18:2)-H	0.50	-0.03
CL(20:2/14:0/15:0/16:0)-H	0.05	-1.58
CL(20:2/18:0/18:1/20:4)-H	0.05	2.44
CL(20:4/16:0/14:0/18:1)-H	0.05	2.38
CL(20:4/16:0/16:1/18:1)-H	0.05	-2.75
CL(20:4/16:0/18:0/18:1)-H	0.05	2.10
CL(20:4/16:0/18:1/16:0)-H	0.05	-2.64
CL(20:4/16:0/18:1/18:1)-H	0.20	0.10
CL(20:4/16:1/16:1/16:1)-H	0.10	-0.34
CL(20:4/16:1/16:1/18:1)-H	0.05	-0.62
CL(20:4/16:1/18:1/16:1)-H	0.05	0.27
CL(20:4/18:0/18:0/18:0)-H	0.05	2.85
CL(20:4/18:0/18:0/18:1)-H	0.05	-1.55
CL(20:4/18:0/18:1/20:0)-H	0.35	-0.06
CL(20:4/18:0/20:4/22:0)-H	0.05	2.28
CL(20:4/18:1/16:1/18:1)-H	0.05	-3.06
CL(20:4/18:1/18:0/18:1)-H	0.05	1.85

CL(20:4/18:1/18:1/18:1)-H	0.50	0.02
CL(20:5/16:1/16:1/18:2)-H	0.10	-0.22
CL(20:5/18:1/16:1/18:2)-H	0.05	-2.67
CL(20:5/18:1/20:4/18:1)-H	0.05	#NAME?
CL(20:5/18:2/18:2/18:2)-H	0.05	1.30
CL(20:5/20:4/20:4/18:1)-H	0.05	2.00
CL(21:0/18:0/18:0/22:6)-H	0.50	0.09
CL(21:0/20:4/16:0/18:0)-H	0.05	2.42
CL(22:1/18:1/18:1/18:1)-H	0.05	#NAME?
CL(22:2/16:0/18:0/18:1)-H	0.05	3.00
CL(22:2/16:1/18:0/18:1)-H	0.05	-2.80
CL(22:2/18:0/18:1/20:4)-H	0.05	2.67
CL(22:2/18:0/20:4/20:4)-H	0.05	1.88
CL(22:3/18:0/18:0/18:1)-H	0.50	0.01
CL(22:3/18:0/18:0/20:4)-H	0.05	-2.91
CL(22:3/18:0/18:0/22:5)-H	0.05	-2.38
CL(22:3/18:0/18:1/20:4)-H	0.05	2.59
CL(22:3/18:1/18:1/18:1)-H	0.05	0.87
CL(22:5/14:0/16:1/14:0)-H	0.05	2.23
CL(22:5/16:1/16:1/16:1)-H	0.05	1.95
CL(22:5/16:1/18:2/18:2)-H	0.05	-2.29
CL(22:5/18:0/18:0/18:1)-H	0.05	-2.21
CL(22:5/18:0/18:1/18:1)-H	0.05	0.85
CL(22:5/18:1/18:1/18:1)-H	0.05	1.24
CL(22:6/18:1/18:1/18:1)-H	0.05	-1.79
CL(22:6/18:1/22:6/18:1)-H	0.05	1.08
CL(22:6/20:4/20:4/18:1)-H	0.05	1.86
CL(23:0/16:0/18:1/18:1)-H	0.05	2.49

CL(23:0/18:0/18:0/18:1)-H	0.05	-0.51
CL(23:0/18:0/18:0/20:3)-H	0.05	2.05
CL(23:0/18:0/18:0/22:4)-H	0.05	-0.33
CL(23:1/16:0/18:0/18:1)-H	0.05	-2.47
CL(23:1/18:0/18:0/20:4)-H	0.05	1.96
CL(23:1/18:0/18:0/22:6)-H	0.05	2.38
CL(68:4)-2H	0.05	-2.19
Cer(d17:1/16:0)+H	0.05	-0.33
Cer(d17:1/22:0)+H	0.05	1.56
Cer(d18:0/12:0)+H	0.10	0.14
Cer(d18:0/14:0)+H	0.10	-0.28
Cer(d18:0/16:0)+H	0.10	-0.24
Cer(d18:0/17:0)+H	0.05	-0.70
Cer(d18:0/18:0)+H	0.05	-0.49
Cer(d18:0/20:0)+H	0.05	-0.52
Cer(d18:0/21:0)+H	0.05	-1.65
Cer(d18:0/22:0)+H	0.05	-0.44
Cer(d18:0/22:1)+H	0.05	-0.56
Cer(d18:0/23:0)+H	0.05	-0.55
Cer(d18:0/23:1)+H	0.05	1.85
Cer(d18:0/24:0)+H	0.50	-0.12
Cer(d18:0/24:1)+H	0.05	-0.44
Cer(d18:0/25:0)+H	0.20	-0.28
Cer(d18:0/25:1)+H	0.05	-0.53
Cer(d18:0/26:0)+H	0.35	-0.16
Cer(d18:0/26:1)+H	0.10	-0.38
Cer(d18:0/27:1)+H	0.05	-1.24
Cer(d18:0/28:0)+H	0.05	-1.79

Cer(d18:0/28:1)+H	0.10	-0.34
Cer(d18:1/10:0)+H	0.05	0.36
Cer(d18:1/13:0)+H	0.05	1.77
Cer(d18:1/14:0)+H	0.05	-0.21
Cer(d18:1/16:0)+H	0.05	-0.29
Cer(d18:1/17:0)+H	0.05	1.51
Cer(d18:1/18:0)+H	0.05	-0.40
Cer(d18:1/20:0)+H	0.05	-0.32
Cer(d18:1/22:0)+H	0.05	-0.40
Cer(d18:1/23:0)+H	0.05	-0.39
Cer(d18:1/24:0)+H	0.05	-3.03
Cer(d18:1/24:1)+H	0.05	-0.39
Cer(d18:1/24:2)+H	0.05	-0.75
Cer(d18:1/24:3)+H	0.05	2.20
Cer(d18:1/25:0)+H	0.05	-0.31
Cer(d18:1/25:1)+H	0.05	-0.48
Cer(d18:1/25:2)+H	0.05	-1.94
Cer(d18:1/26:0)+H	0.20	-0.19
Cer(d18:1/26:1)+H	0.05	-0.30
Cer(d18:1/26:3)+H	0.05	0.36
Cer(d18:1/27:0)+H	0.05	1.58
Cer(d18:1/28:0)+H	0.20	0.15
Cer(d18:1/28:1)+H	0.35	-0.03
Cer(d18:2/16:0)+H	0.05	-0.42
Cer(d18:2/18:0)+H	0.35	0.95
Cer(d18:2/22:0)+H	0.05	-0.46
Cer(d18:2/23:0)+H	0.05	-0.42
Cer(d18:2/24:0)+H	0.05	1.94

Cer(d18:2/24:1)+H	0.05	2.51
Cer(d18:2/25:1)+H	0.35	-0.02
Cer(d18:2/26:0)+H	0.05	1.83
Cer(d18:2/26:1)+H	0.05	-0.46
Cer(d20:0/25:0)+H	0.05	1.81
Cer(d20:0/26:0)+H	0.05	1.99
Cer(d20:1/27:0)+H	0.05	1.37
Cer(d20:1/28:0)+H	0.05	1.65
Cer(d20:2/28:0)+H	0.05	1.66
Cer(d22:0/25:0)+H	0.05	1.66
Cer(d22:1/24:1)+H	0.05	1.21
Cer(d22:1/25:1)+H	0.35	0.75
Cer(d22:1/27:0)+H	0.05	1.15
Cer(d22:1/28:0)+H	0.05	1.30
Cer(d22:1/29:0)+H	0.05	0.49
Cer(d22:1/30:0)+H	0.05	1.08
Cer(d24:0/24:0)+H	0.05	1.82
Cer(d24:0/26:0)+H	0.05	1.51
Cer(d25:0/24:0)+H	0.05	1.46
Cer(d25:0/26:0)+H	0.05	0.78
Cer(d25:0/28:0)+H	0.05	#NAME?
Cer(d34:1)+H	0.05	1.83
Cer(d36:1)+H	0.05	1.90
Cer(d38:1)+H	0.05	1.72
Cer(d40:0)+H	0.05	2.07
CerG1(d17:1/16:0)+H	0.10	-0.27
CerG1(d18:0/14:0)+H	0.65	-0.03
CerG1(d18:0/16:0)+H	0.50	-0.03

CerG1(d18:0/20:0)+H	0.05	1.79
CerG1(d18:0/22:0)+H	0.20	-0.13
CerG1(d18:0/23:0)+H	0.20	-0.19
CerG1(d18:0/24:0)+H	0.20	0.20
CerG1(d18:0/24:1)+H	0.35	-0.07
CerG1(d18:0/25:0)+H	0.50	-0.04
CerG1(d18:0/26:0)+H	0.35	0.06
CerG1(d18:0/26:1)+H	0.20	-0.19
CerG1(d18:1/14:0)+H	0.05	-0.38
CerG1(d18:1/16:0)+H	0.05	-0.39
CerG1(d18:1/17:0)+H	0.10	-0.24
CerG1(d18:1/18:0)+H	0.05	-0.39
CerG1(d18:1/20:0)+H	0.05	2.13
CerG1(d18:1/22:0)+H	0.10	-0.25
CerG1(d18:1/22:1)+H	0.05	1.89
CerG1(d18:1/23:0)+H	0.10	-0.24
CerG1(d18:1/23:1)+H	0.05	1.71
CerG1(d18:1/24:0)+H	0.10	-0.21
CerG1(d18:1/24:1)+H	0.10	-0.35
CerG1(d18:1/25:0)+H	0.35	-0.13
CerG1(d18:1/25:1)+H	0.05	2.07
CerG1(d18:1/26:0)+H	0.20	-0.08
CerG1(d18:1/26:1)+H	0.20	-0.13
CerG1(d18:2/16:0)+H	0.10	-0.26
CerG1(d18:2/24:1)+H	0.10	-0.30
CerG1(d34:2)+H	0.05	-2.02
CerG1(d43:2)+H	0.05	-2.21
CerG1(d44:4)+H	0.05	0.51

CerG1(d46:1)+H	0.05	1.48
CerG2(d18:0/24:1)+H	0.10	0.24
CerG2(d18:1/14:0)+H	0.05	-1.71
CerG2(d18:1/16:0)+H	0.50	0.04
CerG2(d18:1/22:0)+H	0.50	0.05
CerG2(d18:1/22:1)+H	0.05	1.07
CerG2(d18:1/23:0)+H	0.05	1.84
CerG2(d18:1/23:1)+H	0.05	1.46
CerG2(d18:1/24:0)+H	0.35	0.16
CerG2(d18:1/24:1)+H	0.50	0.06
CerG2(d18:1/25:0)+H	0.05	1.76
CerG2(d18:1/26:0)+H	0.35	0.19
CerG2(d18:1/26:1)+H	0.10	0.28
CerG2(d18:2/24:0)+H	0.05	-2.28
CerG2(d18:2/24:1)+H	0.05	1.75
CerG2(d34:2)+H	0.05	-1.99
CerG2(d43:2)+H	0.05	1.56
CerG3(d18:1/14:0)+H	0.05	#NAME?
CerG3(d18:1/16:0)+H	0.35	0.04
CerG3(d18:1/22:0)+H	0.05	1.22
CerG3(d18:1/23:0)+H	0.35	0.17
CerG3(d18:1/24:0)+H	0.50	-0.02
CerG3(d18:1/24:1)+H	0.05	1.89
CerG3(d18:1/26:0)+H	0.05	0.85
CerG3(d18:1/26:1)+H	0.05	0.93
CerG3(d18:2/24:1)+H	0.05	#NAME?
ChE(18:1)+NH4	0.05	-0.52
ChE(18:2)+NH4	0.05	-0.27

ChE(20:1)+NH4	0.05	1.86
ChE(20:2)+NH4	0.05	-0.72
ChE(20:3)+NH4	0.05	-0.42
ChE(20:4)+NH4	0.05	-0.63
ChE(20:5)+NH4	0.05	-0.31
ChE(22:1)+NH4	0.05	1.64
ChE(22:2)+NH4	0.05	1.56
ChE(22:3)+NH4	0.05	-0.82
ChE(22:4)+NH4	0.05	-1.17
ChE(22:5)+NH4	0.05	-1.09
ChE(22:6)+NH4	0.05	-0.59
ChE(24:0)+NH4	0.05	-2.05
ChE(24:1)+NH4	0.05	-0.64
ChE(24:2)+NH4	0.05	-2.65
ChE(24:3)+NH4	0.05	-0.80
ChE(24:4)+NH4	0.05	-1.11
ChE(24:5)+NH4	0.05	-0.98
ChE(24:6)+NH4	0.05	-0.76
ChE(26:0)+NH4	0.05	-0.42
ChE(26:1)+NH4	0.05	-0.70
ChE(26:2)+NH4	0.05	-0.55
ChE(26:3)+NH4	0.05	-0.56
ChE(26:4)+NH4	0.05	-0.89
ChE(26:5)+NH4	0.05	-0.76
ChE(26:6)+NH4	0.05	-0.60
ChE(28:0)+NH4	0.05	-2.05
ChE(28:1)+NH4	0.05	-0.77
ChE(28:2)+NH4	0.05	-0.75

ChE(28:3)+NH4	0.05	-0.71
ChE(28:4)+NH4	0.05	1.62
ChE(28:5)+NH4	0.05	-0.85
ChE(28:6)+NH4	0.05	-0.56
ChE(30:1)+NH4	0.05	-0.76
ChE(30:2)+NH4	0.05	-2.59
ChE(30:3)+NH4	0.05	-0.78
ChE(30:4)+NH4	0.05	-0.87
ChE(30:5)+NH4	0.05	-0.77
ChE(30:6)+NH4	0.05	-0.57
ChE(32:1)+NH4	0.05	-2.09
ChE(32:2)+NH4	0.05	-2.26
ChE(32:3)+NH4	0.05	-1.99
ChE(32:4)+NH4	0.05	-2.25
ChE(32:5)+NH4	0.05	-0.94
ChE(32:6)+NH4	0.05	-0.64
ChE(34:6)+NH4	0.05	-2.57
DG(16:0/14:0)+NH4	0.65	-0.01
DG(16:0/16:0)+NH4	0.50	0.06
DG(16:0/17:0)+NH4	0.05	-2.34
DG(16:0/18:1)+NH4	0.50	0.01
DG(16:0/18:2)+NH4	0.05	3.65
DG(16:0/20:4)+NH4	0.05	-0.50
DG(16:0/22:0)+NH4	0.05	2.55
DG(16:0/22:1)+NH4	0.05	-3.23
DG(16:0/22:4)+NH4	0.05	-3.01
DG(16:0/22:6)+NH4	0.05	-0.34
DG(16:0/24:1)+NH4	0.20	0.20

DG(16:1/14:0)+NH4	0.35	0.09
DG(16:1/16:1)+NH4	0.05	-2.51
DG(16:1/18:1)+NH4	0.05	0.17
DG(16:1/22:6)+NH4	0.05	-0.41
DG(17:0/18:1)+NH4	0.05	-2.71
DG(17:1/16:0)+NH4	0.10	-0.17
DG(17:1/18:1)+NH4	0.50	0.00
DG(18:0/16:0)+NH4	0.20	0.15
DG(18:0/18:0)+NH4	0.10	0.70
DG(18:0/18:1)+NH4	0.50	-0.01
DG(18:0/20:3)+NH4	0.10	-0.18
DG(18:0/20:4)+NH4	0.05	-0.34
DG(18:0/20:5)+NH4	0.05	2.60
DG(18:0/22:4)+NH4	0.10	-0.23
DG(18:0/22:5)+NH4	0.50	0.00
DG(18:0/22:6)+NH4	0.10	0.23
DG(18:1/14:0)+NH4	0.35	0.06
DG(18:1/18:1)+NH4	0.20	0.12
DG(18:1/18:2)+NH4	0.80	0.04
DG(18:1/20:2)+NH4	0.20	-0.10
DG(18:1/20:3)+NH4	0.05	-0.37
DG(18:1/20:4)+NH4	0.05	-0.23
DG(18:1/22:1)+NH4	0.20	0.17
DG(18:1/22:2)+NH4	0.05	2.73
DG(18:1/22:5)+NH4	0.35	-0.14
DG(18:1/22:6)+NH4	0.05	-0.25
DG(18:1/24:1)+NH4	0.05	-3.26
DG(18:2/18:2)+NH4	0.05	2.12

DG(19:1/16:0)+NH4	0.05	2.89
DG(19:1/18:1)+NH4	0.35	-0.05
DG(20:0/18:1)+NH4	0.05	3.30
DG(20:1/18:1)+NH4	0.35	0.08
DG(25:0/16:0)+NH4	0.05	2.03
DG(26:0/14:0)+NH4	0.05	0.42
DG(26:0/16:0)+NH4	0.10	0.29
DG(26:1/16:0)+NH4	0.10	0.31
DG(26:1/16:1)+NH4	0.05	3.53
DG(26:1/18:1)+NH4	0.10	0.29
DG(27:1/16:0)+NH4	0.35	0.03
DG(27:1/18:1)+NH4	0.05	-2.52
DG(28:0/16:0)+NH4	0.05	0.45
DG(28:1/16:0)+NH4	0.20	-0.27
DG(28:1/18:1)+NH4	0.05	0.42
DG(29:1/18:1)+NH4	0.05	2.43
DG(30:0/16:0)+NH4	0.05	2.46
DG(30:1/16:0)+NH4	0.10	0.53
DG(30:1/18:1)+NH4	0.05	0.28
DG(31:1/18:1)+NH4	0.05	2.03
DG(32:1/16:0)+NH4	0.05	3.14
DG(32:1/18:1)+NH4	0.05	2.88
LPC(12:0)+H	0.05	-1.59
LPC(14:0)+H	0.05	-1.56
LPC(15:0)+H	0.05	-1.92
LPC(16:0)+H	0.50	0.14
LPC(16:0e)+H	0.05	-0.16
LPC(16:0p)+H	0.05	-0.31

LPC(16:1)+H	0.35	0.02
LPC(17:1)+H	0.05	-0.60
LPC(18:0)+H	0.10	-0.26
LPC(18:0e)+H	0.20	-0.12
LPC(18:0p)+H	0.10	-0.15
LPC(18:1)+H	0.20	0.20
LPC(18:1p)+H	0.05	-0.55
LPC(18:2)+H	0.05	-1.04
LPC(19:0)+H	0.05	-1.12
LPC(19:1)+H	0.05	-0.51
LPC(20:0)+H	0.10	-0.30
LPC(20:0e)+H	0.05	-1.29
LPC(20:0p)+H	0.10	-0.21
LPC(20:1)+H	0.20	-0.05
LPC(20:3)+H	0.05	-0.54
LPC(20:4)+H	0.05	-1.49
LPC(22:0)+H	0.05	-0.26
LPC(22:1)+H	0.05	-1.27
LPC(22:5)+H	0.05	-0.52
LPC(22:6)+H	0.05	-0.51
LPC(24:0)+H	0.10	-0.24
LPC(24:1)+H	0.20	-0.12
LPC(26:0)+H	0.10	-0.27
LPC(26:1)+H	0.35	-0.07
LPC(28:0)+H	0.05	0.76
LPC(28:1)+H	0.05	0.66
LPC(30:0)+H	0.05	1.52
LPE(16:0)-H	0.05	-1.84

LPE(18:1)-H	0.05	-2.35
LPE(20:4)-H	0.35	-0.14
LPE(22:5)-H	0.05	1.69
LPE(22:6)-H	0.05	1.75
LPE(24:0)-H	0.05	-2.57
LPE(24:1)-H	0.05	1.73
LPE(26:1)-H	0.05	-2.08
MG(30:0)+H	0.05	2.40
MG(32:0)+H	0.35	-0.02
MG(32:1)+H	0.05	2.86
MG(34:0)+H	0.50	-0.01
MG(34:1)+H	0.05	-3.94
MG(36:0)+H	0.20	0.25
MG(36:1)+H	0.35	0.15
MG(38:0)+H	0.05	-2.53
MG(38:1)+H	0.05	3.08
PA(16:0/18:1)-H	0.05	-3.10
PA(16:1/18:1)-H	0.05	2.16
PA(18:0/16:0)-H	0.05	-2.57
PA(18:0/18:1)-H	0.80	0.07
PA(24:0/23:0)-H	0.05	3.12
PA(24:1/23:0)-H	0.05	2.76
PA(24:1/23:1)-H	0.05	2.33
PA(26:0/18:1)-H	0.05	2.11
PC(11:0/16:0)+H	0.05	2.31
PC(11:0/18:1)+H	0.35	0.03
PC(12:0p/20:5)+H	0.05	0.61
PC(14:0/18:3)+H	0.05	-2.68

PC(14:0/20:5)+H	0.05	1.50
PC(14:0/22:5)+H	0.05	2.05
PC(14:0/22:6)+H	0.05	-1.98
PC(14:0e/14:0)+H	0.05	3.68
PC(14:0p/14:0)+H	0.65	0.03
PC(14:0p/16:0)+H	0.05	3.38
PC(14:0p/16:1)+H	0.65	0.01
PC(14:0p/18:3)+H	0.05	2.44
PC(14:0p/22:2)+H	0.05	-2.61
PC(14:0p/22:4)+H	0.05	-1.63
PC(15:0/18:1)+H	0.05	-4.07
PC(15:0/20:3)+H	0.05	-3.08
PC(15:0/22:4)+H	0.20	-0.13
PC(16:0/13:0)+H	0.10	-0.23
PC(16:0/14:1)+H	0.50	-0.02
PC(16:0/16:1)+H	0.05	2.19
PC(16:0/18:3)+H	0.05	2.12
PC(16:0/20:1)+H	0.05	4.79
PC(16:0/21:1)+H	0.05	-3.34
PC(16:0/22:6)+H	0.05	3.53
PC(16:0e/22:5)+H	0.05	-2.91
PC(16:0p/14:0)+H	0.05	3.60
PC(16:0p/16:0)+H	0.05	-0.76
PC(16:0p/18:0)+H	0.05	4.87
PC(16:0p/18:1)+H	0.35	-0.09
PC(16:0p/20:4)+H	0.05	-0.46
PC(16:1/14:1)+H	0.05	1.61
PC(16:1/18:1)+H	0.05	-2.46

PC(16:1/21:0)+H	0.05	2.43
PC(16:1p/16:0)+H	0.05	2.82
PC(16:1p/18:1)+H	0.05	-0.33
PC(16:1p/20:1)+H	0.05	3.15
PC(17:0/18:1)+H	0.65	-0.01
PC(17:0/20:5)+H	0.05	2.14
PC(17:1/14:0)+H	0.05	3.27
PC(17:1/16:0)+H	0.05	-4.41
PC(17:1/16:1)+H	0.10	-0.28
PC(17:1/18:1)+H	0.50	0.00
PC(18:0/13:0)+H	0.05	2.40
PC(18:0/20:5)+H	0.05	2.80
PC(18:0/22:5)+H	0.05	-0.48
PC(18:0/22:6)+H	0.05	3.02
PC(18:0p/18:1)+H	0.05	4.06
PC(18:1/12:2)+H	0.05	2.76
PC(18:1/14:1)+H	0.65	0.01
PC(18:1/18:1)+H	0.20	-0.07
PC(18:1/18:3)+H	0.05	2.90
PC(18:1/21:0)+H	0.05	-2.54
PC(18:1/21:1)+H	0.05	-2.46
PC(18:1/22:6)+H	0.05	3.59
PC(18:1/23:0)+H	0.20	0.24
PC(18:1/23:1)+H	0.20	0.27
PC(18:1p/16:0)+H	0.05	-3.82
PC(18:1p/18:0)+H	0.35	-0.05
PC(18:2p/18:0)+H	0.05	-0.30
PC(18:2p/18:1)+H	0.05	-4.01

PC(18:2p/24:1)+H	0.05	1.95
PC(18:2p/8:0)+H	0.05	-0.83
PC(18:4/14:0)+H	0.05	2.97
PC(18:4/16:0)+H	0.05	2.94
PC(18:4/18:0)+H	0.05	-3.12
PC(18:4/18:1)+H	0.05	2.87
PC(19:1/18:1)+H	0.35	-0.06
PC(20:0/14:0)+H	0.05	-1.43
PC(20:0/18:1)+H	0.50	0.03
PC(20:1/18:1)+H	0.05	4.26
PC(20:1p/16:0)+H	0.05	-0.29
PC(20:1p/18:0)+H	0.05	3.03
PC(20:4/21:1)+H	0.05	-2.17
PC(22:2/14:4)+H	0.05	1.87
PC(25:1/18:1)+H	0.05	2.66
PC(26:0/16:0)+H	0.05	3.28
PC(26:1/14:3)+H	0.05	-1.54
PC(27:0/16:0)+H	0.05	-1.94
PC(27:0/18:1)+H	0.50	0.08
PC(27:1/16:0)+H	0.05	2.47
PC(28:0)+H	0.20	-0.17
PC(29:0)+H	0.05	2.97
PC(29:0/16:0)+H	0.05	1.61
PC(30:0)+H	0.35	-0.04
PC(30:0e)+H	0.20	-0.12
PC(30:0p)+H	0.05	-3.50
PC(30:1)+H	0.50	0.00
PC(30:1e)+H	0.05	3.66

PC(30:2)+H	0.05	2.67
PC(30:2e)+H	0.05	2.21
PC(31:0)+H	0.10	-0.23
PC(31:0/10:2)+H	0.05	2.39
PC(31:1)+H	0.05	-3.58
PC(31:1/16:0)+H	0.05	2.11
PC(32:0)+H	0.20	0.08
PC(32:0e)+H	0.35	0.02
PC(32:1)+H	0.05	-5.22
PC(32:1p)+H	0.35	-0.06
PC(32:2)+H	0.05	0.35
PC(32:4e)+H	0.05	1.62
PC(33:0)+H	0.05	3.02
PC(33:1)+H	0.05	4.16
PC(34:0)+H	0.20	0.09
PC(34:0e)+H	0.35	0.09
PC(34:1)+H	0.10	-0.11
PC(34:1e)+H	0.05	-4.91
PC(34:2)+H	0.10	0.16
PC(34:2e)+H	0.05	-3.83
PC(34:3)+H	0.50	-0.11
PC(34:4)+H	0.05	-0.56
PC(34:6e)+H	0.05	1.36
PC(35:0)+H	0.05	1.87
PC(35:1)+H	0.10	-0.17
PC(35:2)+H	0.05	-3.54
PC(36:0)+H	0.05	3.11
PC(36:0e)+H	0.20	0.16

PC(36:1)+H	0.05	-4.96
PC(36:1e)+H	0.35	-0.02
PC(36:2p)+H	0.50	-0.02
PC(36:3)+H	0.05	-0.23
PC(36:4)+H	0.05	-0.83
PC(36:4e)+H	0.05	3.35
PC(36:5)+H	0.05	-0.62
PC(36:6)+H	0.05	2.46
PC(37:5)+H	0.05	1.91
PC(38:0e)+H	0.05	2.80
PC(38:1e)+H	0.35	0.11
PC(38:2)+H	0.05	-4.35
PC(38:2e)+H	0.05	2.87
PC(38:3)+H	0.10	-0.15
PC(38:3e)+H	0.05	2.69
PC(38:4)+H	0.05	-0.59
PC(38:4e)+H	0.05	-0.57
PC(38:4p)+H	0.05	-3.82
PC(38:5)+H	0.05	-0.73
PC(38:6)+H	0.05	-3.99
PC(38:6e)+H	0.05	3.38
PC(38:7)+H	0.05	-0.54
PC(39:2)+H	0.05	2.84
PC(40:0)+H	0.05	2.88
PC(40:0e)+H	0.05	-2.33
PC(40:1)+H	0.50	-0.04
PC(40:2)+H	0.20	-0.09
PC(40:3)+H	0.50	-0.02

PC(40:4)+H	0.05	-0.27
PC(40:5e)+H	0.05	2.76
PC(40:6)+H	0.05	-3.65
PC(40:6e)+H	0.05	2.93
PC(40:7)+H	0.05	-3.99
PC(40:8)+H	0.05	-3.32
PC(42:0)+H	0.05	-3.16
PC(42:1)+H	0.50	0.05
PC(42:2)+H	0.50	0.01
PC(42:3)+H	0.50	-0.01
PC(44:0)+H	0.05	3.05
PC(44:1)+H	0.35	0.14
PC(44:2)+H	0.50	0.04
PC(44:3)+H	0.65	0.02
PC(45:2)+H	0.05	2.52
PC(46:1)+H	0.50	0.13
PC(46:2)+H	0.20	0.14
PC(46:4)+H	0.05	-2.59
PC(46:5)+H	0.05	-2.79
PC(47:2)+H	0.05	2.40
PC(48:1)+H	0.05	2.86
PC(48:2)+H	0.10	0.31
PC(50:2)+H	0.05	2.92
PE(12:0p/16:0)+H	0.05	2.22
PE(12:0p/18:1)+H	0.05	3.03
PE(12:0p/18:2)+H	0.05	1.76
PE(12:0p/20:4)+H	0.05	2.73
PE(12:0p/20:5)+H	0.05	1.92

PE(12:0p/22:4)+H	0.05	2.02
PE(12:0p/22:5)+H	0.05	2.37
PE(12:0p/22:6)+H	0.05	2.55
PE(14:0/20:4)+H	0.05	-2.78
PE(14:0p/20:4)+H	0.05	2.73
PE(14:0p/20:5)+H	0.05	1.82
PE(14:0p/22:5)+H	0.05	2.63
PE(14:0p/22:6)+H	0.05	2.46
PE(16:0/14:0)+H	0.35	0.05
PE(16:0/16:0)+H	0.65	0.03
PE(16:0/16:1)+H	0.35	0.02
PE(16:0/18:1)+H	0.50	-0.06
PE(16:0/20:4)+H	0.05	-0.28
PE(16:0/20:5)+H	0.50	-0.03
PE(16:0/22:6)+H	0.05	-0.12
PE(16:0e/18:1)+H	0.05	-3.69
PE(16:0p/14:0)+H	0.05	2.24
PE(16:0p/14:1)+H	0.05	-2.44
PE(16:0p/16:0)+H	0.35	0.05
PE(16:0p/16:1)+H	0.20	-0.10
PE(16:0p/17:1)+H	0.20	-0.10
PE(16:0p/18:1)+H	0.20	-0.10
PE(16:0p/18:2)+H	0.05	-0.27
PE(16:0p/18:3)+H	0.05	-2.77
PE(16:0p/19:1)+H	0.50	0.03
PE(16:0p/20:0)+H	0.05	2.59
PE(16:0p/20:3)+H	0.05	-0.23
PE(16:0p/20:4)+H	0.35	-0.11

PE(16:0p/20:5)+H	0.35	-0.06
PE(16:0p/22:1)+H	0.20	0.15
PE(16:0p/22:2)+H	0.05	3.39
PE(16:0p/22:4)+H	0.05	-0.28
PE(16:0p/22:5)+H	0.05	-5.07
PE(16:0p/22:6)+H	0.05	4.84
PE(16:1/14:0)+H	0.05	3.16
PE(16:1/16:1)+H	0.20	0.18
PE(16:1/18:1)+H	0.50	0.00
PE(16:1/18:2)+H	0.05	-3.40
PE(16:1/20:4)+H	0.20	-0.15
PE(16:1/20:5)+H	0.35	0.10
PE(16:1/22:5)+H	0.05	2.54
PE(16:1/22:6)+H	0.35	0.08
PE(16:1p/22:6)+H	0.05	2.30
PE(17:0/18:1)+H	0.05	4.18
PE(17:0/20:4)+H	0.05	3.49
PE(17:0/22:6)+H	0.35	0.17
PE(17:1/16:0)+H	0.05	3.64
PE(17:1/18:1)+H	0.50	0.00
PE(17:1/20:4)+H	0.05	2.77
PE(17:1/20:5)+H	0.05	1.63
PE(18:0/16:0)+H	0.05	3.55
PE(18:0/18:1)+H	0.35	0.07
PE(18:0/20:3)+H	0.10	-0.19
PE(18:0/20:4)+H	0.20	-0.16
PE(18:0/20:5)+H	0.20	0.13
PE(18:0/22:4)+H	0.10	-0.14

PE(18:0/22:5)+H	0.35	0.03
PE(18:0/22:6)+H	0.65	-0.03
PE(18:0p/15:0)+H	0.05	1.27
PE(18:0p/16:0)+H	0.50	-0.03
PE(18:0p/18:1)+H	0.35	0.02
PE(18:0p/18:2)+H	0.20	-0.06
PE(18:0p/19:1)+H	0.05	5.16
PE(18:0p/20:3)+H	0.10	-0.35
PE(18:0p/20:4)+H	0.10	-0.14
PE(18:0p/20:5)+H	0.10	-0.16
PE(18:0p/22:1)+H	0.20	0.33
PE(18:0p/22:2)+H	0.05	-3.16
PE(18:0p/22:3)+H	0.20	0.18
PE(18:0p/22:4)+H	0.50	-0.03
PE(18:0p/22:5)+H	0.35	0.05
PE(18:0p/22:6)+H	0.05	4.54
PE(18:0p/24:1)+H	0.05	2.32
PE(18:1/18:1)+H	0.50	-0.02
PE(18:1/18:2)+H	0.50	-0.04
PE(18:1/20:4)+H	0.05	4.73
PE(18:1/22:0)+H	0.05	3.58
PE(18:1/22:1)+H	0.05	3.72
PE(18:1/22:6)+H	0.50	-0.07
PE(18:1/24:0)+H	0.35	0.09
PE(18:1/24:1)+H	0.05	3.70
PE(18:1p/16:1)+H	0.20	-0.16
PE(18:1p/17:1)+H	0.05	2.87
PE(18:1p/18:1)+H	0.20	-0.06

PE(18:1p/18:2)+H	0.05	3.74
PE(18:1p/20:1)+H	0.05	-3.39
PE(18:1p/20:4)+H	0.05	4.93
PE(18:1p/20:5)+H	0.05	-0.11
PE(18:1p/22:1)+H	0.05	3.12
PE(18:1p/22:5)+H	0.50	-0.05
PE(18:1p/22:6)+H	0.05	4.27
PE(18:2/22:6)+H	0.05	2.61
PE(18:2p/22:6)+H	0.05	1.33
PE(20:0/18:1)+H	0.05	3.59
PE(20:0/20:4)+H	0.05	3.14
PE(20:0p/20:4)+H	0.05	3.20
PE(20:0p/22:5)+H	0.50	-0.03
PE(20:0p/22:6)+H	0.05	2.85
PE(20:1/18:1)+H	0.05	4.08
PE(20:1p/22:5)+H	0.05	2.80
PE(20:4/22:6)+H	0.05	2.65
PE(22:0/20:4)+H	0.35	-0.06
PE(24:0/20:4)+H	0.20	-0.23
PE(24:0/22:6)+H	0.05	3.31
PE(24:1/20:4)+H	0.10	-0.16
PE(24:1/22:6)+H	0.05	2.51
PE(25:0/18:1)+H	0.05	2.58
PE(26:0)+H	0.05	1.96
PE(26:0/18:1)+H	0.20	0.21
PE(26:0/20:4)+H	0.05	2.87
PE(26:1/18:1)+H	0.05	3.63
PE(26:1/20:4)+H	0.05	-3.20

PE(28:1/18:1)+H	0.05	3.03
PE(30:1)+H	0.05	-3.11
PE(36:3)+H	0.05	-3.45
PE(38:4e)+H	0.05	3.43
PE(38:6)+H	0.05	3.85
PE(40:5e)+H	0.05	3.02
PE(40:5p)+H	0.05	3.98
PE(43:2)+H	0.05	2.53
PE(44:2)+H	0.05	2.51
PE(44:3)+H	0.05	1.89
PE(48:5)+H	0.05	2.46
PEt(14:0/14:0)-H	0.05	2.26
PEt(16:0/14:0)-H	0.05	2.64
PEt(16:0/16:0)-H	0.05	2.40
PEt(16:0/16:1)-H	0.05	2.74
PEt(16:0/18:1)-H	0.05	1.72
PEt(16:1/14:0)-H	0.05	2.43
PEt(16:1/18:1)-H	0.05	2.36
PG(12:0/14:0)-H	0.05	2.12
PG(14:0/22:6)-H	0.05	2.06
PG(15:0/14:0)-H	0.05	#NAME?
PG(15:0/16:0)-H	0.05	#NAME?
PG(16:0/14:0)-H	0.05	2.51
PG(16:0/16:0)-H	0.05	0.39
PG(16:0/16:1)-H	0.50	-0.02
PG(16:0/17:0)-H	0.05	#NAME?
PG(16:0/18:1)-H	0.50	0.06
PG(16:0/20:3)-H	0.05	#NAME?

PG(16:0/20:4)-H	0.05	1.82
PG(16:0/22:4)-H	0.05	#NAME?
PG(16:0/22:6)-H	0.65	0.09
PG(16:1/14:0)-H	0.05	0.47
PG(16:1/16:1)-H	0.05	-2.07
PG(16:1/18:1)-H	0.20	0.24
PG(16:1/18:2)-H	0.05	2.17
PG(16:1/22:6)-H	0.80	0.08
PG(17:1/16:0)-H	0.05	2.59
PG(17:1/18:0)-H	0.05	2.76
PG(17:1/18:1)-H	0.05	2.21
PG(18:0/16:0)-H	0.05	3.08
PG(18:0/18:1)-H	0.35	0.07
PG(18:0/20:4)-H	0.05	1.91
PG(18:0/22:6)-H	0.35	1.75
PG(18:1/14:0)-H	0.05	2.95
PG(18:1/18:1)-H	0.10	-0.22
PG(18:1/18:2)-H	0.50	-0.16
PG(18:1/20:2)-H	0.20	-0.20
PG(18:1/20:4)-H	0.05	1.52
PG(18:1/20:5)-H	0.05	1.33
PG(18:1/22:4)-H	0.05	1.22
PG(18:1/22:5)-H	0.05	-2.86
PG(18:1/22:6)-H	0.50	-0.06
PG(18:2/22:6)-H	0.05	-0.26
PG(19:1/16:0)-H	0.50	0.16
PG(20:1/18:1)-H	0.20	-0.23
PG(20:2/20:2)-H	0.05	1.61

PG(20:2/22:6)-H	0.05	2.00
PG(20:3/22:6)-H	0.05	1.67
PG(20:4/22:6)-H	0.05	1.73
PG(20:5/22:6)-H	0.05	0.58
PG(22:4/22:6)-H	0.05	1.68
PG(22:5/22:6)-H	0.20	-0.06
PG(22:6/22:6)-H	0.50	-0.09
PG(42:9)-H	0.05	-2.19
PI(16:0/14:1)-H	0.05	2.51
PI(16:0/16:0)-H	0.05	3.12
PI(16:0/16:1)-H	0.05	-3.70
PI(16:0/18:1)-H	0.50	0.03
PI(16:0/20:4)-H	0.05	-4.07
PI(16:0/20:5)-H	0.05	2.07
PI(16:0e/18:1)-H	0.10	-0.20
PI(16:0e/20:4)-H	0.05	-0.49
PI(16:1/18:2)-H	0.05	-2.42
PI(16:1/20:4)-H	0.20	-0.18
PI(17:0/18:1)-H	0.35	-0.11
PI(17:0/18:2)-H	0.05	-2.57
PI(17:0/20:2)-H	0.05	2.90
PI(17:0/20:3)-H	0.05	3.01
PI(17:0/20:4)-H	0.05	-3.26
PI(17:1/16:0)-H	0.20	-0.16
PI(17:1/18:1)-H	0.05	-3.24
PI(17:1/20:4)-H	0.05	1.41
PI(18:0/16:0)-H	0.35	0.08
PI(18:0/17:0)-H	0.05	2.14

PI(18:0/18:0)-H	0.05	2.80
PI(18:0/18:1)-H	0.05	1.34
PI(18:0/20:0)-H	0.05	2.24
PI(18:0/20:1)-H	0.05	-0.51
PI(18:0/20:4)-H	0.05	-0.55
PI(18:0/20:5)-H	0.05	2.77
PI(18:0/22:1)-H	0.20	0.14
PI(18:0/22:3)-H	0.10	-0.23
PI(18:0/24:1)-H	0.05	2.37
PI(18:0/24:2)-H	0.05	-2.49
PI(18:0e/18:1)-H	0.05	2.46
PI(18:0e/20:4)-H	0.05	-2.80
PI(18:0e/22:5)-H	0.05	-2.24
PI(18:0p/18:1)-H	0.50	-0.15
PI(18:0p/20:1)-H	0.05	1.84
PI(18:0p/20:4)-H	0.05	-2.89
PI(18:1/14:1)-H	0.05	0.51
PI(18:1/18:1)-H	0.20	0.18
PI(18:1/18:3)-H	0.05	1.70
PI(18:1/20:3)-H	0.05	-3.77
PI(18:1/22:1)-H	0.05	-2.78
PI(18:1/24:2)-H	0.20	0.21
PI(19:0/20:4)-H	0.05	-0.60
PI(19:1/18:0)-H	0.35	-0.13
PI(19:1/18:2)-H	0.05	2.72
PI(19:1/20:1)-H	0.05	2.39
PI(19:1/20:2)-H	0.05	2.60
PI(19:1/20:3)-H	0.50	-0.23

PI(19:1/20:4)-H	0.05	-2.84
PI(20:0/20:3)-H	0.05	-2.00
PI(20:0/20:4)-H	0.05	-0.54
PI(20:3/20:4)-H	0.05	-1.94
PI(22:4/20:4)-H	0.05	2.01
PI(22:5/20:4)-H	0.05	-1.82
PI(26:0/18:1)-H	0.05	2.34
PI(26:1/18:0)-H	0.05	-2.24
PI(26:1/18:1)-H	0.05	2.12
PS(12:0/14:0)-H	0.05	1.93
PS(16:0/14:0)-H	0.35	-0.07
PS(16:0/14:1)-H	0.05	2.21
PS(16:0/16:0)-H	0.05	2.65
PS(16:0/16:1)-H	0.05	-3.80
PS(16:0/18:1)-H	0.05	-4.59
PS(16:0/20:3)-H	0.05	3.11
PS(16:0/20:4)-H	0.05	-0.45
PS(16:0/22:0)-H	0.05	1.44
PS(16:0/24:0)-H	0.05	1.44
PS(16:0e/18:1)-H	0.10	-0.21
PS(16:1/16:1)-H	0.05	1.91
PS(16:1/17:0)-H	0.05	2.16
PS(16:1/18:1)-H	0.05	-3.63
PS(16:1/18:2)-H	0.05	2.22
PS(16:1/20:3)-H	0.05	3.10
PS(17:0/20:4)-H	0.05	-2.19
PS(17:0/22:4)-H	0.05	2.88
PS(17:0/22:5)-H	0.50	0.04

PS(17:1/18:1)-H	0.05	-3.00
PS(18:0/16:0)-H	0.65	0.00
PS(18:0/18:0)-H	0.05	1.67
PS(18:0/18:3)-H	0.05	2.07
PS(18:0/20:1)-H	0.05	-3.80
PS(18:0/20:2)-H	0.05	-3.62
PS(18:0/20:3)-H	0.05	-1.63
PS(18:0/20:4)-H	0.35	-0.06
PS(18:0/20:5)-H	0.05	-2.88
PS(18:0/22:5)-H	0.05	-0.69
PS(18:0e/18:1)-H	0.10	-0.19
PS(18:1/18:1)-H	0.05	4.34
PS(18:1/18:2)-H	0.05	-3.19
PS(18:1/20:2)-H	0.05	-0.75
PS(18:1/20:3)-H	0.20	0.11
PS(18:1/20:4)-H	0.20	-0.17
PS(18:1/21:0)-H	0.05	-3.07
PS(18:1/22:1)-H	0.05	-3.31
PS(18:1/22:4)-H	0.05	4.55
PS(18:1/22:5)-H	0.05	0.60
PS(18:1/22:6)-H	0.05	-3.27
PS(18:1/24:1)-H	0.05	-2.79
PS(19:0/18:1)-H	0.05	-3.65
PS(19:0/20:3)-H	0.20	-0.21
PS(20:0/22:4)-H	0.05	-2.35
PS(20:0/22:5)-H	0.05	3.19
PS(20:0/22:6)-H	0.05	-3.35
PS(20:2/20:2)-H	0.05	2.70

PS(20:3/18:2)-H	0.05	2.74
PS(20:3/20:3)-H	0.05	-0.20
PS(24:0/20:3)-H	0.05	-3.21
PS(24:0/20:4)-H	0.10	-0.19
PS(24:0/22:5)-H	0.05	1.99
PS(24:1/20:3)-H	0.05	-2.24
PS(24:1/20:4)-H	0.05	2.37
PS(25:0/18:1)-H	0.10	-0.17
PS(25:1/18:1)-H	0.05	2.23
PS(26:0/18:1)-H	0.50	-0.04
PS(26:1/18:1)-H	0.05	-3.37
PS(26:1/18:2)-H	0.05	-2.69
PS(27:1/18:1)-H	0.05	1.90
PS(28:0/18:1)-H	0.50	0.04
PS(28:1/18:1)-H	0.35	0.08
PS(30:1/18:1)-H	0.05	2.20
SM(d17:0/32:1)+H	0.05	3.19
SM(d17:0/32:2)+H	0.05	1.92
SM(d18:0/23:0)+H	0.05	2.25
SM(d18:0/24:2)+H	0.50	0.02
SM(d18:0/24:3)+H	0.05	2.68
SM(d18:0/26:3)+H	0.05	-2.56
SM(d18:1/16:0)+H	0.05	5.31
SM(d18:1/16:1)+H	0.05	4.10
SM(d18:1/18:3)+H	0.05	3.63
SM(d18:1/19:0)+H	0.05	#NAME?
SM(d18:1/21:0)+H	0.05	1.66
SM(d18:1/22:0)+H	0.05	4.23

SM(d18:1/23:0)+H	0.05	2.58
SM(d18:1/24:0)+H	0.05	4.85
SM(d18:1/24:1)+H	0.20	-0.17
SM(d18:1/24:2)+H	0.05	1.44
SM(d18:1/24:3)+H	0.05	3.21
SM(d18:1/25:0)+H	0.05	1.18
SM(d18:1/25:3)+H	0.05	-1.53
SM(d18:1/26:1)+H	0.05	3.99
SM(d18:1/26:3)+H	0.20	-0.11
SM(d18:1/26:4)+H	0.05	-0.22
SM(d18:1/27:0)+H	0.05	1.81
SM(d18:1/27:1)+H	0.05	1.60
SM(d18:1/28:0)+H	0.05	-0.77
SM(d18:1/30:0)+H	0.05	2.68
SM(d18:1/30:1)+H	0.05	2.33
SM(d18:1/32:0)+H	0.05	1.77
SM(d18:1/32:1)+H	0.05	1.71
SM(d18:2/16:1)+H	0.05	2.49
SM(d18:2/18:1)+H	0.05	0.18
SM(d18:2/24:1)+H	0.05	-2.46
SM(d18:2/26:1)+H	0.05	3.03
SM(d18:2/26:2)+H	0.05	-3.35
SM(d30:0)+H	0.05	1.71
SM(d30:1)+H	0.80	0.05
SM(d31:1)+H	0.10	-0.17
SM(d32:0)+H	0.20	0.14
SM(d32:1)+H	0.20	-0.17
SM(d32:2)+H	0.10	-0.28

SM(d33:1)+H	0.10	-0.19
SM(d33:2)+H	0.10	-0.29
SM(d33:5)+H	0.05	2.32
SM(d34:0)+H	0.10	0.13
SM(d34:1)+H	0.05	-5.47
SM(d34:2)+H	0.05	-4.40
SM(d34:3)+H	0.05	-2.50
SM(d34:4)+H	0.10	-0.20
SM(d35:1)+H	0.35	-0.11
SM(d35:2)+H	0.05	2.20
SM(d35:4)+H	0.05	-0.31
SM(d36:0)+H	0.35	-0.07
SM(d36:1)+H	0.05	-0.37
SM(d36:2)+H	0.05	-0.48
SM(d36:5)+H	0.05	-0.32
SM(d37:4)+H	0.05	1.65
SM(d37:5)+H	0.05	0.89
SM(d37:6)+H	0.05	2.20
SM(d38:0)+H	0.05	2.73
SM(d38:1)+H	0.10	-0.17
SM(d38:2)+H	0.05	2.17
SM(d38:3)+H	0.05	1.87
SM(d38:5)+H	0.05	-2.85
SM(d39:1)+H	0.05	2.46
SM(d39:4)+H	0.05	2.46
SM(d39:6)+H	0.05	-2.64
SM(d40:0)+H	0.20	0.16
SM(d40:1)+H	0.05	-1.26

SM(d40:2)+H	0.10	-0.21
SM(d40:4)+H	0.35	1.00
SM(d40:6)+H	0.05	3.10
SM(d41:0)+H	0.05	2.67
SM(d41:1)+H	0.05	-0.79
SM(d41:2)+H	0.20	-0.12
SM(d41:3)+H	0.05	2.13
SM(d42:0)+H	0.05	0.43
SM(d42:1)+H	0.05	-0.37
SM(d42:3)+H	0.05	-4.25
SM(d42:4)+H	0.05	-3.36
SM(d42:5)+H	0.05	-1.84
SM(d42:6)+H	0.05	0.98
SM(d42:7)+H	0.05	0.77
SM(d43:1)+H	0.50	0.04
SM(d43:2)+H	0.65	0.01
SM(d43:4)+H	0.05	-0.30
SM(d43:5)+H	0.05	-0.20
SM(d44:0)+H	0.20	0.21
SM(d44:1)+H	0.20	0.12
SM(d44:2)+H	0.05	-1.30
SM(d44:3)+H	0.20	-0.15
SM(d44:4)+H	0.05	#NAME?
SM(d44:5)+H	0.05	1.20
SM(d44:6)+H	0.05	-0.25
SM(d44:7)+H	0.05	#NAME?
SM(d44:8)+H	0.05	#NAME?
SM(d45:6)+H	0.05	2.44

SM(d46:3)+H	0.05	1.61
SM(d46:4)+H	0.35	-0.08
SM(d46:5)+H	0.35	0.13
SM(d46:6)+H	0.05	2.13
SM(d46:7)+H	0.05	#NAME?
SM(d48:1)+H	0.05	2.44
SM(d48:2)+H	0.05	-2.20
SM(d50:1)+H	0.05	2.14
SM(d50:2)+H	0.05	1.47
SM(d54:3)+H	0.05	-2.68
SM(d56:2)+H	0.05	2.56
SM(d56:3)+H	0.05	2.57
SM(d56:4)+H	0.05	-0.48
TG(10:0/12:0/14:0)+NH4	0.05	2.05
TG(12:0/12:0/14:0)+NH4	0.05	1.90
TG(12:0/14:0/14:0)+NH4	0.05	2.07
TG(12:0e/16:0/16:0)+NH4	0.05	3.07
TG(12:0e/16:0/17:1)+NH4	0.05	2.51
TG(12:0p/16:1/18:1)+NH4	0.05	#NAME?
TG(12:0p/18:1/18:1)+NH4	0.35	0.68
TG(14:0e/14:0/14:0)+NH4	0.05	2.27
TG(14:0p/16:0/16:0)+NH4	0.05	3.49
TG(15:0/13:0/16:0)+NH4	0.05	1.89
TG(15:0/14:0/16:0)+NH4	0.20	0.31
TG(15:0/14:0/16:1)+NH4	0.05	3.25
TG(15:0/15:0/17:1)+NH4	0.05	-3.45
TG(15:0/16:0/16:0)+NH4	0.35	0.18
TG(15:0/16:0/16:1)+NH4	0.05	3.52

TG(15:0/16:0/18:1)+NH4	0.05	3.52
TG(15:0/16:0/24:0)+NH4	0.05	2.62
TG(15:0/16:1/18:1)+NH4	0.05	3.30
TG(15:0/18:1/20:5)+NH4	0.05	2.77
TG(16:0/10:3/16:0)+NH4	0.05	2.80
TG(16:0/12:0/14:0)+NH4	0.05	-0.82
TG(16:0/13:0/14:0)+NH4	0.05	2.53
TG(16:0/14:0/14:0)+NH4	0.05	-0.69
TG(16:0/14:0/14:1)+NH4	0.05	-3.58
TG(16:0/14:0/16:0)+NH4	0.35	-0.93
TG(16:0/14:0/16:1)+NH4	0.05	-0.97
TG(16:0/14:0/18:1)+NH4	0.05	-4.97
TG(16:0/14:0/20:4)+NH4	0.05	-2.92
TG(16:0/14:0/22:6)+NH4	0.05	1.76
TG(16:0/16:0/16:0)+NH4	0.05	-0.87
TG(16:0/16:0/16:1)+NH4	0.05	3.80
TG(16:0/16:0/17:0)+NH4	0.35	0.09
TG(16:0/16:0/17:1)+NH4	0.05	-3.94
TG(16:0/16:0/18:1)+NH4	0.05	-1.06
TG(16:0/16:0/20:4)+NH4	0.05	-0.51
TG(16:0/16:0/22:6)+NH4	0.05	-0.75
TG(16:0/16:0/23:1)+NH4	0.05	2.84
TG(16:0/16:0/24:0)+NH4	0.05	2.85
TG(16:0/16:0/24:1)+NH4	0.05	2.87
TG(16:0/16:1/17:1)+NH4	0.05	-3.68
TG(16:0/16:1/18:1)+NH4	0.05	-1.12
TG(16:0/16:1/22:6)+NH4	0.05	-0.68
TG(16:0/17:0/18:1)+NH4	0.10	-0.24

TG(16:0/17:1/18:1)+NH4	0.05	-0.75
TG(16:0/18:1/18:1)+NH4	0.05	-1.06
TG(16:0/18:1/22:1)+NH4	0.05	-4.39
TG(16:0/18:1/22:6)+NH4	0.05	-0.78
TG(16:0/18:1/24:1)+NH4	0.05	-1.40
TG(16:0e/14:0/16:0)+NH4	0.05	-0.81
TG(16:0e/14:0/16:1)+NH4	0.05	-3.42
TG(16:0e/16:0/16:0)+NH4	0.05	-1.31
TG(16:0e/16:0/18:1)+NH4	0.05	3.49
TG(16:0e/16:0/22:0)+NH4	0.05	-3.20
TG(16:0e/16:0/22:1)+NH4	0.05	-3.89
TG(16:0e/16:0/24:0)+NH4	0.05	1.65
TG(16:0e/16:0/24:1)+NH4	0.05	-3.81
TG(16:0e/16:1/16:1)+NH4	0.05	-3.44
TG(16:0e/18:1/18:1)+NH4	0.05	-0.97
TG(16:0e/18:1/20:1)+NH4	0.05	3.05
TG(16:0e/18:1/20:2)+NH4	0.05	2.93
TG(16:0e/18:1/20:3)+NH4	0.05	-3.50
TG(16:0e/18:1/22:2)+NH4	0.05	2.49
TG(16:0e/18:1/22:4)+NH4	0.05	2.43
TG(16:0e/18:1/22:5)+NH4	0.05	-3.77
TG(16:0e/18:1/22:6)+NH4	0.05	-3.63
TG(16:0e/18:1/24:1)+NH4	0.05	-3.75
TG(16:0p/16:0/16:0)+NH4	0.05	3.07
TG(16:1/12:0/12:0)+NH4	0.05	2.07
TG(16:1/12:0/14:0)+NH4	0.05	-2.25
TG(16:1/14:0/14:0)+NH4	0.05	3.02
TG(16:1/14:0/16:1)+NH4	0.05	-1.00

TG(16:1/14:0/17:1)+NH4	0.50	0.20
TG(16:1/14:0/18:1)+NH4	0.05	-1.08
TG(16:1/16:1/16:1)+NH4	0.05	-0.80
TG(16:1/16:1/17:1)+NH4	0.35	-0.22
TG(16:1/16:1/18:1)+NH4	0.05	-1.01
TG(16:1/16:1/18:2)+NH4	0.05	-3.20
TG(16:1/16:1/20:3)+NH4	0.05	2.47
TG(16:1/16:1/22:6)+NH4	0.05	-2.56
TG(16:1/17:1/18:1)+NH4	0.05	-0.50
TG(16:1/18:1/18:1)+NH4	0.05	-0.98
TG(16:1/18:1/18:2)+NH4	0.05	-0.50
TG(16:1/18:1/20:4)+NH4	0.05	-3.58
TG(16:1/18:1/22:5)+NH4	0.05	-3.61
TG(16:1/18:1/22:6)+NH4	0.05	-0.68
TG(16:1/18:1/24:1)+NH4	0.05	2.76
TG(17:0/18:1/18:1)+NH4	0.05	-4.14
TG(18:0/16:0/16:0)+NH4	0.05	-0.85
TG(18:0/16:0/17:0)+NH4	0.20	-0.09
TG(18:0/16:0/18:0)+NH4	0.05	-0.36
TG(18:0/16:0/18:1)+NH4	0.05	-0.93
TG(18:0/16:0/20:0)+NH4	0.05	-3.42
TG(18:0/16:0/22:6)+NH4	0.05	2.53
TG(18:0/18:0/18:0)+NH4	0.05	3.21
TG(18:0/18:0/18:1)+NH4	0.05	-0.85
TG(18:0/18:1/18:1)+NH4	0.05	-1.06
TG(18:0/18:1/19:0)+NH4	0.05	-3.25
TG(18:0/18:1/20:1)+NH4	0.05	3.15
TG(18:0/18:1/22:3)+NH4	0.05	-3.68

TG(18:0e/12:0/14:0)+NH4	0.05	-3.07
TG(18:0e/14:0/16:1)+NH4	0.05	-4.20
TG(18:0e/16:0/16:0)+NH4	0.05	-1.00
TG(18:0e/16:0/18:0)+NH4	0.05	2.93
TG(18:0e/16:0/18:1)+NH4	0.05	3.56
TG(18:0e/16:0/22:1)+NH4	0.05	2.41
TG(18:0e/16:0/24:0)+NH4	0.05	-3.30
TG(18:0e/16:0/24:1)+NH4	0.05	-1.73
TG(18:0e/18:1/18:1)+NH4	0.05	-4.18
TG(18:0p/16:0/16:0)+NH4	0.05	-4.67
TG(18:0p/16:0/16:1)+NH4	0.05	3.16
TG(18:0p/16:0/24:1)+NH4	0.05	2.29
TG(18:0p/16:1/18:1)+NH4	0.05	-3.86
TG(18:0p/18:1/18:1)+NH4	0.05	-3.92
TG(18:0p/18:1/22:1)+NH4	0.05	-1.20
TG(18:1/14:0/20:4)+NH4	0.05	-2.89
TG(18:1/17:1/18:1)+NH4	0.05	-0.73
TG(18:1/17:1/18:2)+NH4	0.05	-0.30
TG(18:1/17:1/20:3)+NH4	0.05	2.66
TG(18:1/18:1/18:1)+NH4	0.05	-0.93
TG(18:1/18:1/18:2)+NH4	0.05	3.74
TG(18:1/18:1/18:3)+NH4	0.05	3.33
TG(18:1/18:1/20:2)+NH4	0.05	-0.89
TG(18:1/18:1/20:3)+NH4	0.05	3.21
TG(18:1/18:1/20:4)+NH4	0.05	3.25
TG(18:1/18:1/21:1)+NH4	0.10	0.13
TG(18:1/18:1/22:1)+NH4	0.05	-4.15
TG(18:1/18:1/22:2)+NH4	0.05	2.75

TG(18:1/18:1/22:3)+NH4	0.05	-0.46
TG(18:1/18:1/22:4)+NH4	0.05	-0.56
TG(18:1/18:1/22:5)+NH4	0.05	2.80
TG(18:1/18:1/22:6)+NH4	0.05	-0.82
TG(18:1/18:1/23:1)+NH4	0.05	-3.14
TG(18:1/18:1/24:1)+NH4	0.05	-0.24
TG(18:1/18:1/24:2)+NH4	0.05	-1.01
TG(18:1/18:2/18:2)+NH4	0.05	3.35
TG(18:1/18:2/21:1)+NH4	0.05	3.06
TG(18:1/18:2/22:6)+NH4	0.05	-2.96
TG(18:1/20:3/24:1)+NH4	0.05	-3.18
TG(18:1/20:4/20:4)+NH4	0.05	2.47
TG(18:1/20:4/22:6)+NH4	0.05	-2.78
TG(18:1/20:4/24:0)+NH4	0.05	1.70
TG(18:1/22:5/22:6)+NH4	0.05	-2.56
TG(18:1p/16:0/16:0)+NH4	0.05	-4.07
TG(18:1p/19:0/19:0)+NH4	0.05	-3.80
TG(18:2/18:2/18:2)+NH4	0.05	3.16
TG(19:1/16:0/18:0)+NH4	0.05	-0.56
TG(19:1/16:0/18:1)+NH4	0.05	3.32
TG(19:1/18:0/18:1)+NH4	0.05	-0.74
TG(19:1/18:1/18:1)+NH4	0.05	-0.92
TG(19:1/18:1/18:2)+NH4	0.05	-0.42
TG(20:0/16:0/16:0)+NH4	0.05	3.39
TG(20:0/16:0/18:1)+NH4	0.05	3.73
TG(20:0/18:1/22:4)+NH4	0.05	-3.16
TG(20:0/18:1/22:6)+NH4	0.05	2.73
TG(20:0e/16:0/18:0)+NH4	0.05	2.16

TG(20:0e/16:0/18:1)+NH4	0.05	2.84
TG(20:0e/18:1/18:1)+NH4	0.05	2.60
TG(20:0e/22:1/22:1)+NH4	0.05	-3.06
TG(20:0p/16:0/16:0)+NH4	0.05	-4.51
TG(20:0p/16:1/16:1)+NH4	0.05	2.91
TG(20:0p/18:1/18:1)+NH4	0.05	-3.59
TG(20:1/18:1/18:1)+NH4	0.05	-1.19
TG(20:1/18:1/22:5)+NH4	0.05	-3.44
TG(20:1/18:1/22:6)+NH4	0.05	-3.02
TG(20:1p/14:0/14:0)+NH4	0.05	2.91
TG(20:1p/15:0/16:0)+NH4	0.05	2.72
TG(25:0/16:0/16:0)+NH4	0.05	2.47
TG(25:0/16:0/16:1)+NH4	0.05	-0.46
TG(25:1/16:0/16:1)+NH4	0.05	-0.74
TG(25:1/16:0/18:1)+NH4	0.05	-1.05
TG(25:1/16:1/18:1)+NH4	0.05	2.14
TG(25:1/18:1/18:1)+NH4	0.05	-1.46
TG(26:0/14:0/16:0)+NH4	0.05	-3.50
TG(26:0/16:0/16:0)+NH4	0.05	-1.18
TG(26:0/16:0/18:0)+NH4	0.05	-3.46
TG(26:0/16:0/18:1)+NH4	0.05	-4.34
TG(26:0/16:0/24:1)+NH4	0.05	-3.16
TG(26:0/18:0/18:1)+NH4	0.05	-3.96
TG(26:0/18:1/24:0)+NH4	0.05	-2.08
TG(26:0/18:1/24:1)+NH4	0.05	-3.40
TG(26:1/14:0/16:0)+NH4	0.05	-4.06
TG(26:1/16:0/16:0)+NH4	0.05	-1.56
TG(26:1/16:0/18:0)+NH4	0.05	2.35

TG(26:1/16:0/18:1)+NH4	0.05	-1.80
TG(26:1/16:1/18:1)+NH4	0.05	2.98
TG(26:1/18:0/18:1)+NH4	0.05	-4.42
TG(26:1/18:1/18:1)+NH4	0.05	-2.04
TG(26:1/18:1/18:2)+NH4	0.05	-1.76
TG(26:1/18:1/20:2)+NH4	0.05	-1.83
TG(26:1/18:1/20:3)+NH4	0.05	-2.78
TG(26:1/18:1/22:6)+NH4	0.05	-2.44
TG(26:1/18:1/24:0)+NH4	0.05	0.91
TG(26:1/18:1/24:1)+NH4	0.05	#NAME?
TG(26:1/18:1/24:2)+NH4	0.05	#NAME?
TG(26:1/20:1/24:1)+NH4	0.05	-3.14
TG(27:0/16:0/16:0)+NH4	0.05	-0.45
TG(27:1/16:0/16:0)+NH4	0.05	-0.98
TG(27:1/16:0/18:1)+NH4	0.05	-1.47
TG(27:1/18:1/18:1)+NH4	0.05	-1.83
TG(27:1/18:1/24:0)+NH4	0.05	-2.37
TG(27:1/18:1/24:1)+NH4	0.05	-2.25
TG(28:0/16:0/18:0)+NH4	0.05	-1.14
TG(28:0/16:0/18:1)+NH4	0.05	1.87
TG(28:0/18:1/18:1)+NH4	0.05	-3.90
TG(28:0/18:1/24:0)+NH4	0.05	-2.56
TG(28:0/18:1/24:1)+NH4	0.05	#NAME?
TG(28:1/16:0/18:1)+NH4	0.05	2.20
TG(28:1/18:1/18:1)+NH4	0.05	-2.25
TG(28:1/18:1/20:2)+NH4	0.05	1.14
TG(28:1/18:1/24:0)+NH4	0.05	-3.14
TG(28:1/18:1/24:1)+NH4	0.05	#NAME?

TG(28:1/18:1/24:2)+NH4	0.05	-2.65
TG(28:1/22:1/22:1)+NH4	0.05	#NAME?
TG(29:0/16:0/18:1)+NH4	0.05	-0.90
TG(29:1/16:0/16:0)+NH4	0.05	-3.08
TG(29:1/16:0/18:1)+NH4	0.05	-1.39
TG(29:1/18:0/18:1)+NH4	0.05	-1.17
TG(29:1/18:1/18:1)+NH4	0.05	-1.72
TG(30:0/16:0/18:1)+NH4	0.05	-2.05
TG(30:0/18:0/18:1)+NH4	0.05	0.96
TG(30:0/18:1/18:1)+NH4	0.05	-2.36
TG(30:1/16:0/18:1)+NH4	0.05	1.56
TG(30:1/18:1/18:1)+NH4	0.05	-2.31
TG(30:1/18:1/24:1)+NH4	0.05	-2.69
TG(4:0/16:0/16:0)+NH4	0.05	1.73
TG(8:0/10:0/10:0)+NH4	0.05	2.15
TG(8:0/12:0/14:0)+NH4	0.05	1.87
TG(8:0/8:0/10:0)+NH4	0.05	2.22
TG(8:0/8:0/8:0)+NH4	0.05	1.92
dMePE(12:0/12:0)-H	0.05	-2.30
dMePE(14:0/14:0)-H	0.05	-1.72
dMePE(16:0/14:0)-H	0.05	-2.78
dMePE(16:0/16:0)-H	0.05	-2.19
dMePE(16:0/16:1)-H	0.05	-4.39
dMePE(16:0/18:1)-H	0.05	-2.91
dMePE(16:1/14:1)-H	0.05	-2.92
dMePE(18:0/18:1)-H	0.05	-2.26
dMePE(18:1/14:0)-H	0.05	-2.34
dMePE(18:1/18:1)-H	0.05	-3.35

dMePE(20:1/18:1)-H	0.05	-3.14

APPENDIX E: SUPPLEMENTARY INFORMATION ASSOCIATED WITH CHAPTER V: ANTI-TUMORIGENIC PROPERTIES OF OMEGA-3 ENDOCANNABINOID EPOXIDES

Supplementary Figure 1: endocannabinoids detected in normal lungs and lungs with OS tumor:

Figure shows the levels of endocannabinoids and endocannabinoid epoxides in lungs of nude mice and lungs of mice with tumor metastasis.

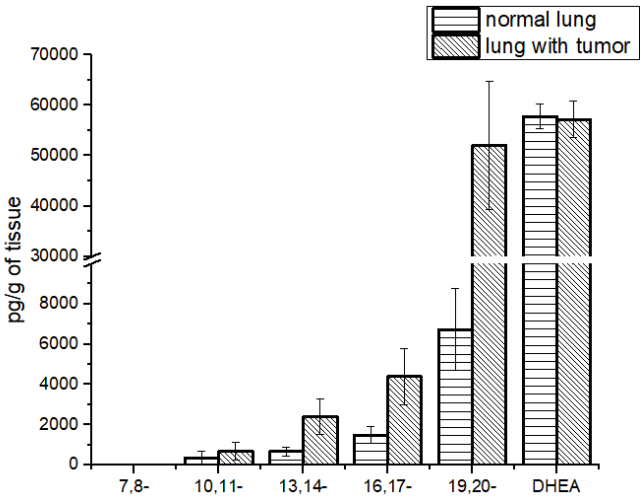

pmol/g	7,8-	10,11-	13,14-	16,17-	19,20	DHEA	EPEA	Anandamide
normal lungs	0	339.36	668.88	1488.34	6722.83	57776.52	2668.96	48571.57
lungs with tumors	0	670.97	2393.41	4382.93	51947.03	57211.73	2755.32	235592.78
error (normal)	0	339.36	230.39	421.43	2042.16	2449.697	196.20	9427.26
error (tumor)	0	447.27	879.65	1395.30	12721.57	3613.3	821.65	63203.15

Supplementary figure 2: endocannabinoids detected in k7m2 murine osteosarcoma cells

Figure shows the levels of endocannabinoid epoxides in K7M2 murine osteosarcoma cell lines with and without LPS stimulation

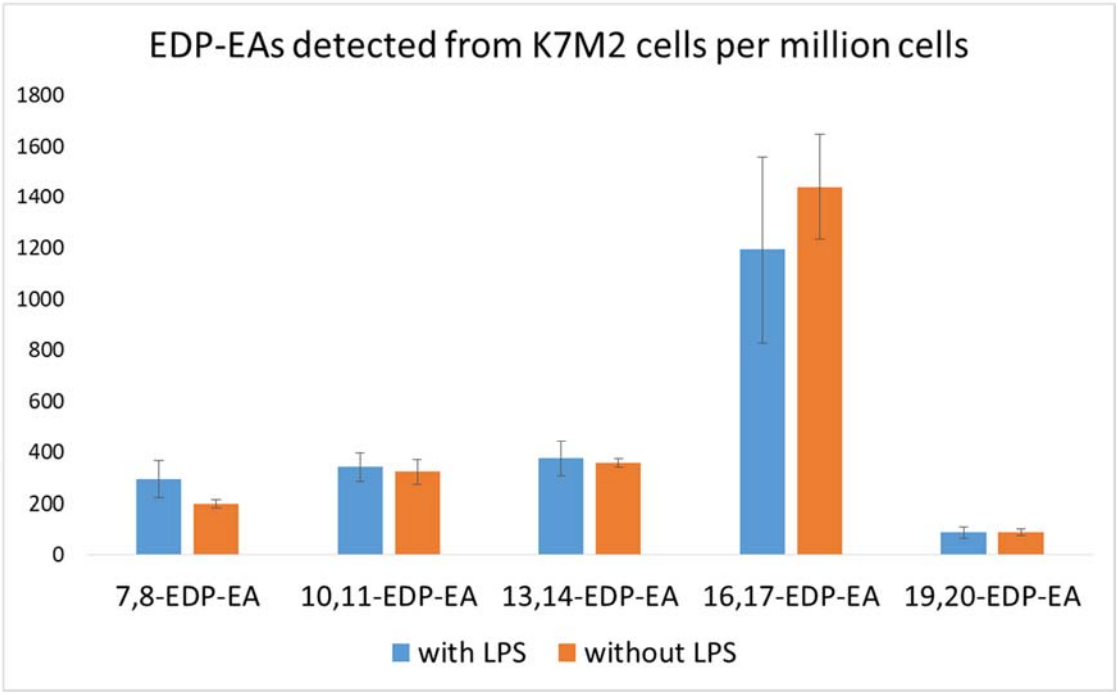

Supplementary figure 3: CTB assay all compounds

Figure shows cell viability of 143B cells in presence of various endogenous endocannabinoid epoxides

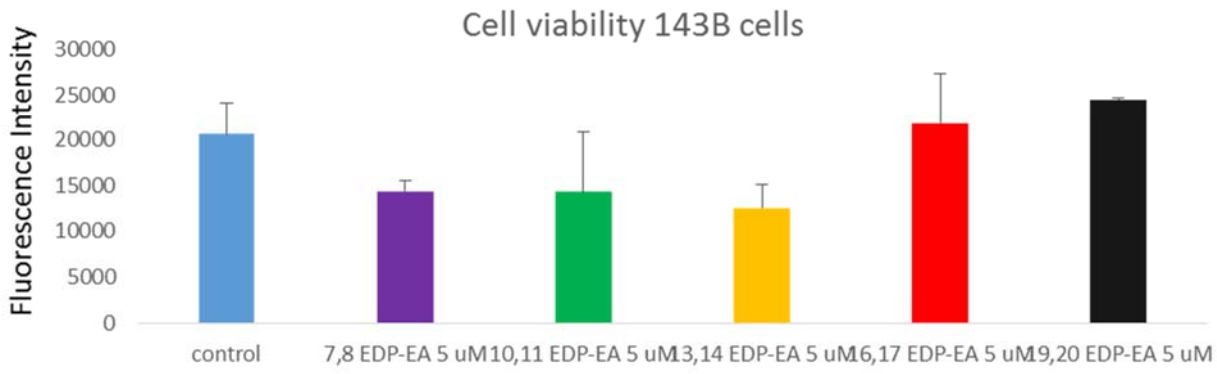

Table 1: Apoptosis assay with parent compounds

Apoptosis measured by Annexin V/ PI binding by parent omega-3 fatty acids and endocannabinoids

Treatment	HOS	MG63	143B
AA	5.07 ± 0.75%	3.8 ± 1.06%	5.12 ± 1.29%
AEA	4.89 ± 0.72%	4.17 ± 1.28%	6.17 ± 1.77%
DHA	5.08 ± 0.62%	3.78 ± 0.07%	4.12 ± 0.35%
DHEA	6.18 ± 0.28%	4.43 ± 0.31%	6.94 ± 0.63%
control	6.47± 0.1%	2.54 ± 0.12%	5.43 ± 0.1%

Table 2: Apoptosis assay HOS cells with Cb1 and cb2 antagonists

Apoptosis measured by Annexin V/ PI binding by endogenous endocannabinoid epoxides

	7,8-EDP-EA	10,11-EDP-EA	13,14-EDP-EA
TREATED	17.1 ± 0.5%	31.1 ± 2.3%	19.6 ± 3.5%
With CB1 antagonist	12.3 ± 1.2%	12.3 ± 2.8%	17.2 ± 1.3%
With CB2 antagonist	15.3 ± 0.7%	14.3 ± 1.3%	14.4 ± 0.1%

Table 3: Apoptosis assay 143B cells with Cb1 and cb2 antagonists

Apoptosis measured by Annexin V/ PI binding by endogenous endocannabinoid epoxides

	7,8-EDP-EA	10,11-EDP-EA	13,14-EDP-EA
12.5 uM compound	8.75 ±0.15%	17.92 ± 3.32%	9.95 ± 1.88%
+CB1 antagonist	14.60 ± 1.82%	7.44 ± 2.19%	13.03 ± 3.63%
+ Cb2 antagonist	10.12 ± 1.36%	10.9 ± 0.08%	9.2 ± 0.80%

controls	Negative control	Positive control	CB1 antagonist	CB2 antagonist
% apoptosis	0.03	4.26	5.66	5.88

Table 4: Apoptosis assay MG63 cells with Cb1 and cb2 antagonists

Apoptosis measured by Annexin V/ PI binding by endogenous endocannabinoid epoxides

	7,8-EDP-EA	10,11-EDP-EA	13,14-EDP-EA
TREATED	16.4 ± 1.4%	26.6 ± 3.5%	16.9 ± 2.3%
With CB1 antagonist	17.4 ± 0.9%	23.2 ± 5%	14.3 ± 0.7%
With CB2 antagonist	18.7 ± 1.8%	19.4 ± 2.5%	21.0 ± 7.0%
With both CB1 and CB2 antagonist	15.1 ± 0.6%	16.6 ± 2.3%	24.2 ± 0.6%

controls	Negative control	Positive control	CB1 antagonist	CB2 antagonist
% apoptosis	0.03	5.8	4.3	5.1

Supplementary figure 4: Scratch assay 143B cells

Wound healing measured over 10 hours by endogenous endocannabinoid epoxides

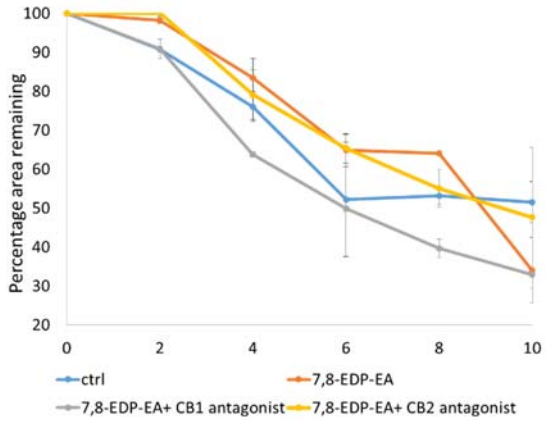

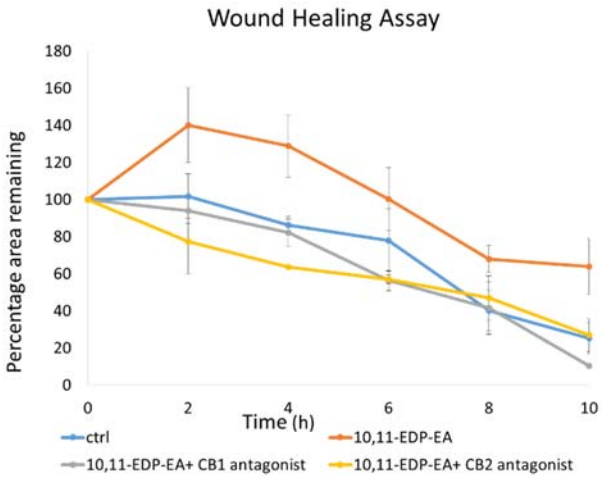

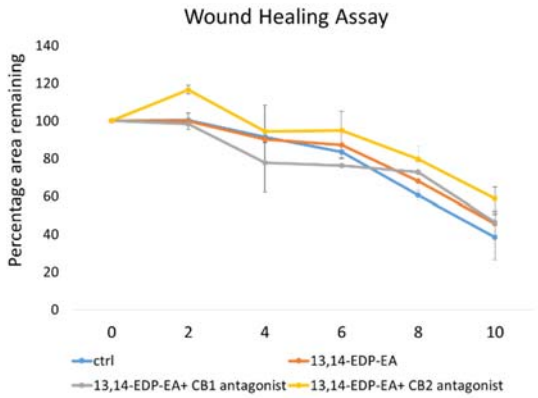

Supplementary figure 5: Scratch assay MG63 cells

Wound healing measured over 10 hours by endogenous endocannabinoid epoxides

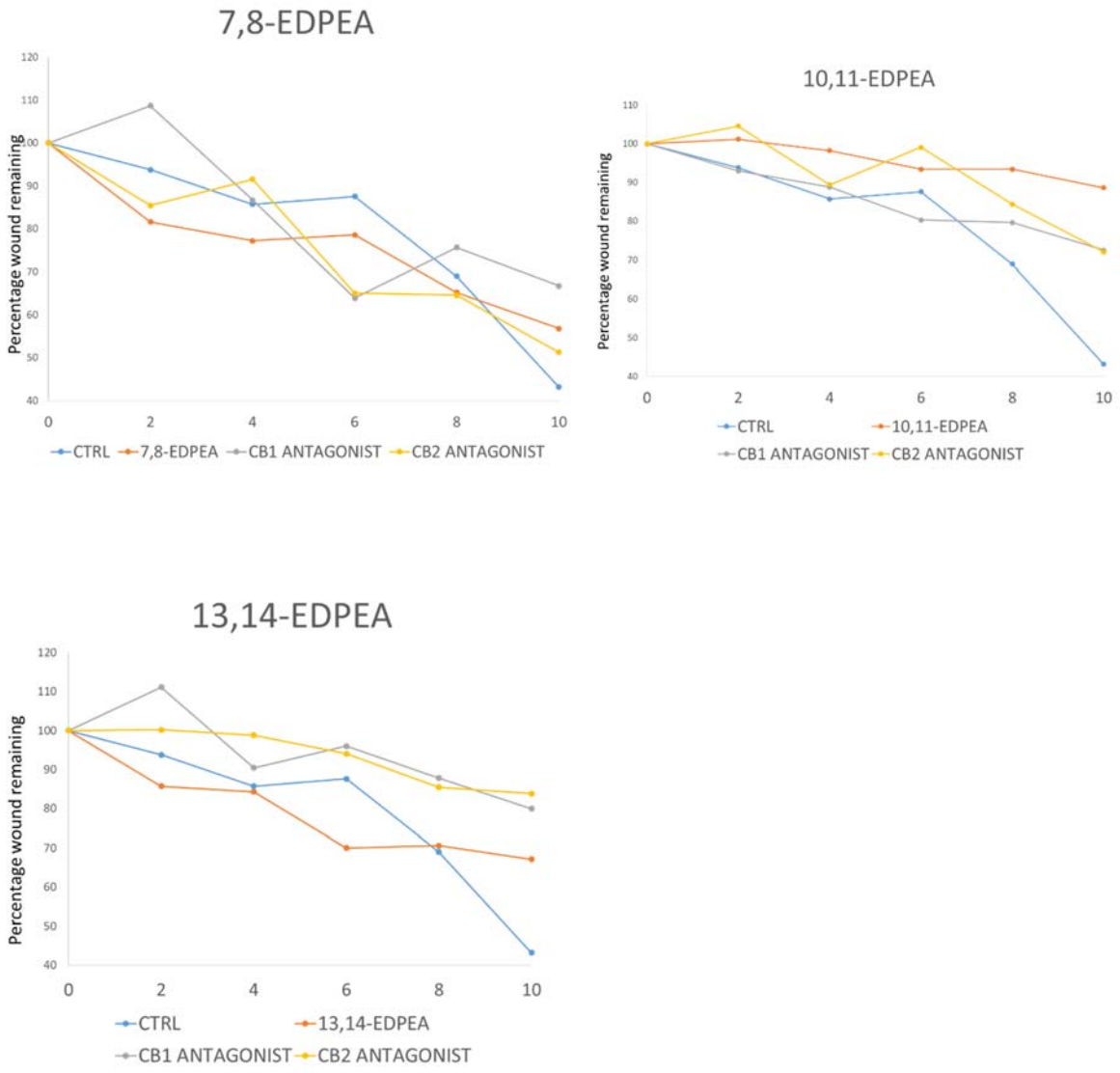

Supplementary figure 6: Scratch assay HOS cells

Wound healing measured over 10 hours by endogenous endocannabinoid epoxides

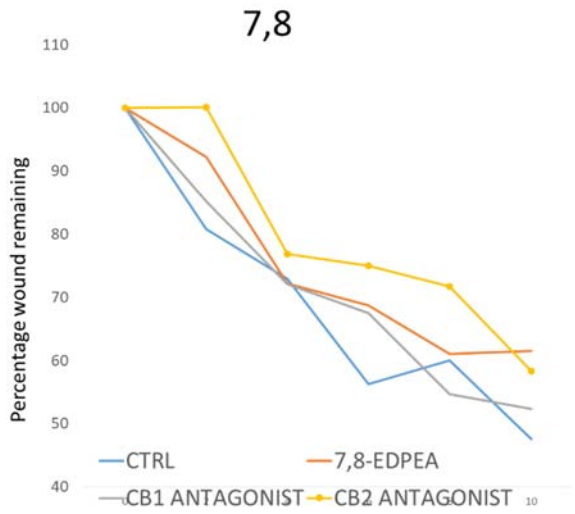

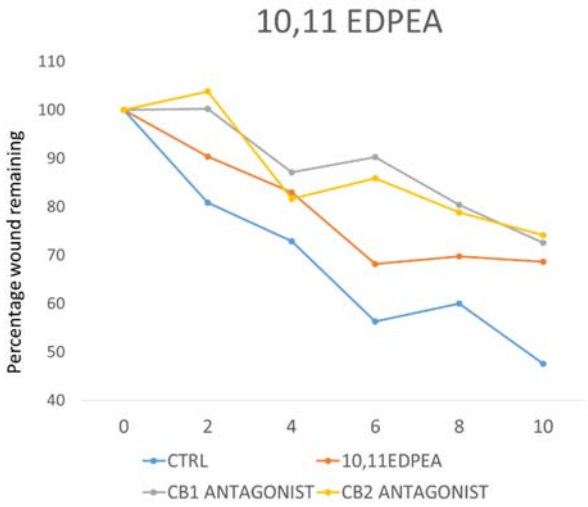

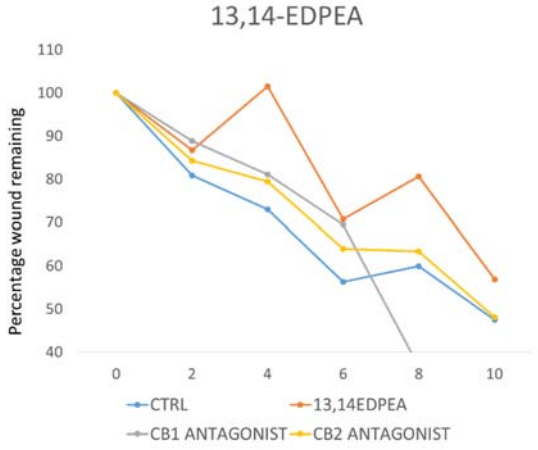

Supplementary figure 7: sEH hydrolysis of amide modified derivatives

Hydrolysis of amide derivatives of endocannabinoid epoxides by soluble epoxide hydrolase (sEH)

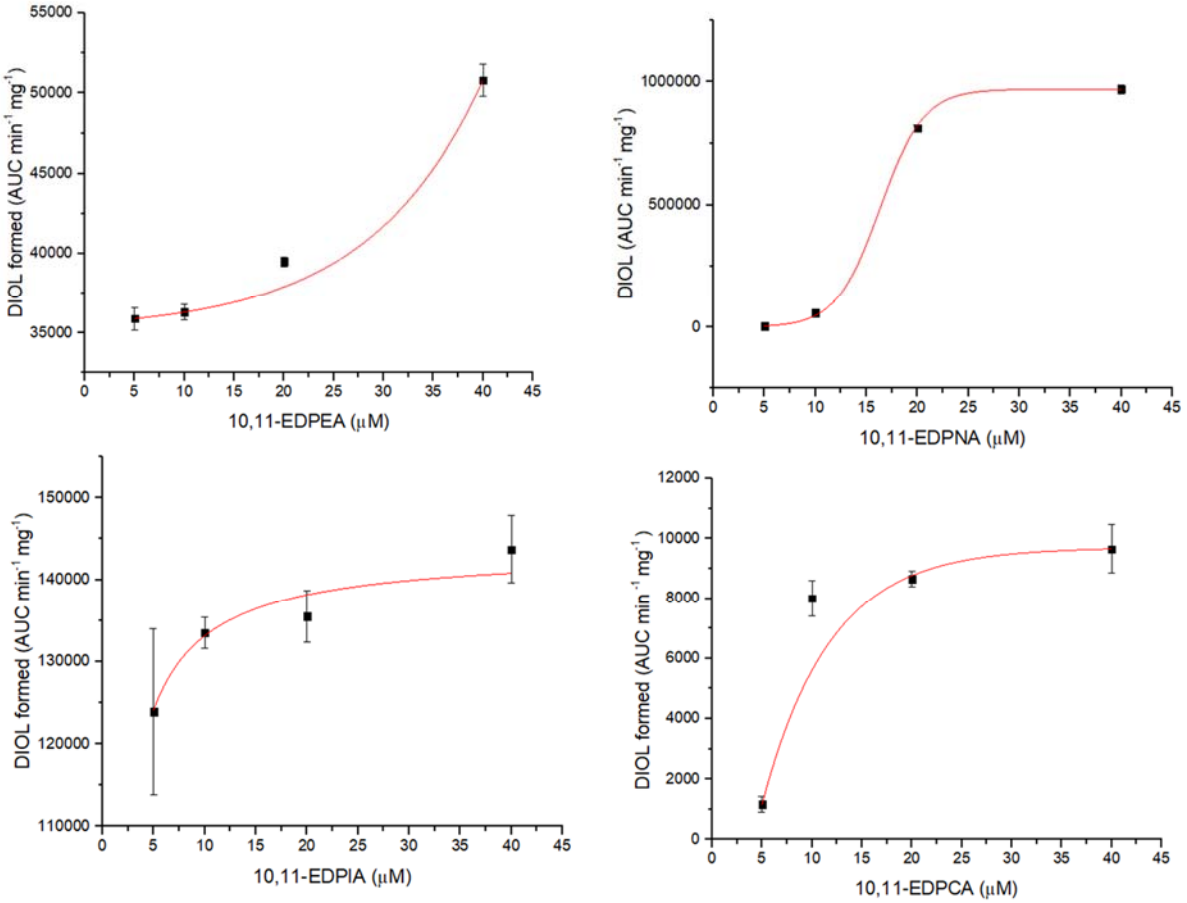

Supplementary figure 8: CTB assay with HUVEC cells

Figure shows cell viability of HUVEC cells in presence of various amide derivatives of 10,11-EDPEA

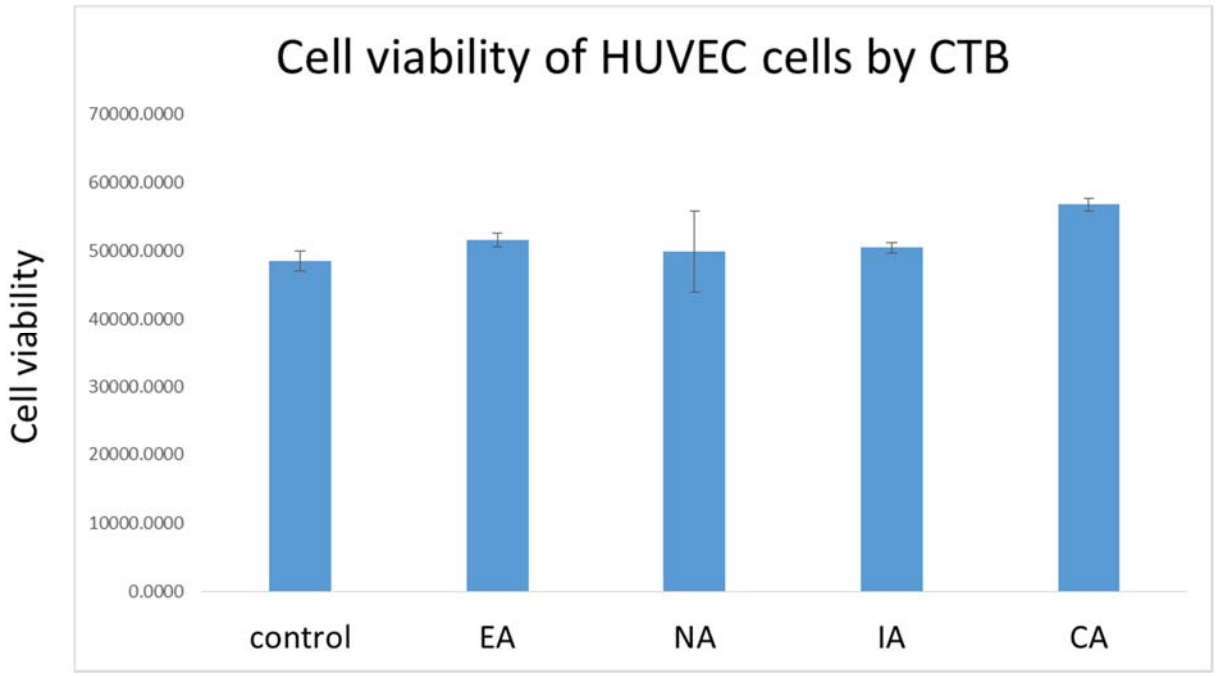

Supplementary figure 9: PCR of cannabinoid receptors in cell lines

Figure shows CB1 and CB2 receptor expression by PCR. Delta Ct values are inversely related to expression levels.

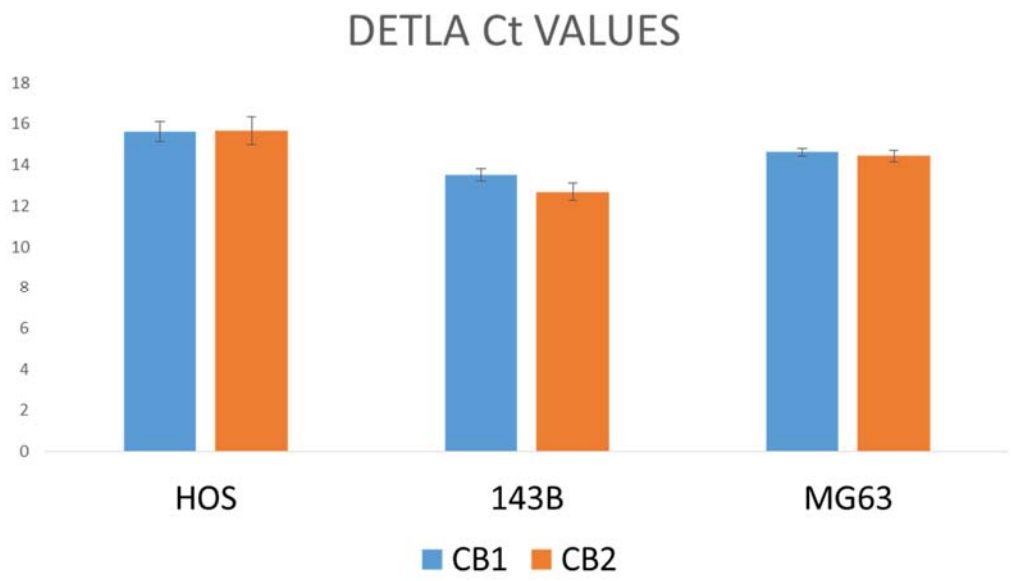

Supplementary Figure 10: Presto Tango assay showing receptor activation of cannabinoid receptors 1 and 2 (CNR1 and CNR2)

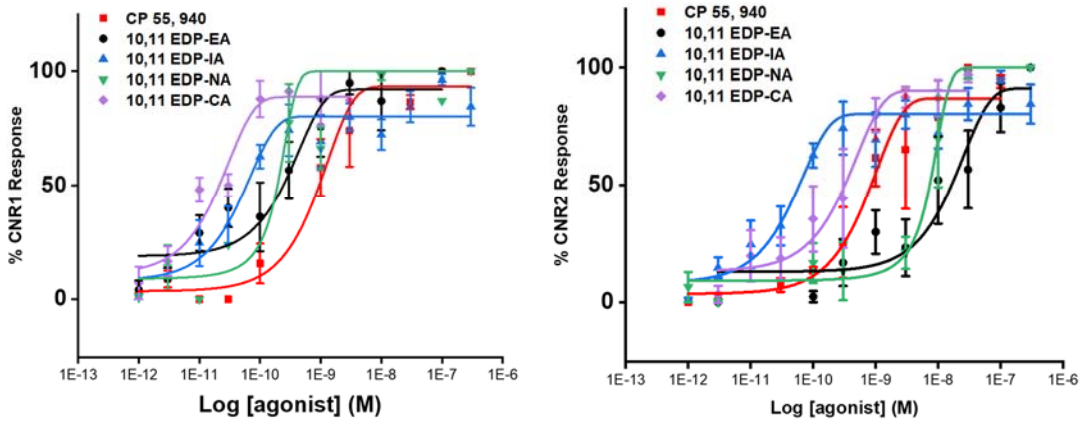

	CNR2	CNR1
Compound	**EC_{50} (nM)**	**EC_{50} (nM)**
CP 55 940	**1.73**	**0.9**
10,11 EDP-EA	**22.5**	**0.43**
10,11 EDP-IA	**0.08**	**0.07**
10,11 EDP-NA	**7.3**	**0.19**
10,11 EDP-CA	**0.46**	**0.03**